1215

TRANSPORTATION RESEARCH RECORD

Pavement Management and Rehabilitation

TRANSPORTATION RESEARCH BOARD
NATIONAL RESEARCH COUNCIL
WASHINGTON, D.C. 1989

Transportation Research Record 1215
Price: $42.00

mode
1 highway transportation

subject areas
12 planning
24 pavement design and performance
40 maintenance

TRB Publications Staff

Director of Publications: Nancy A. Ackerman
Senior Editor: Edythe T. Crump
Associate Editors: Naomi C. Kassabian
Ruth S. Pitt
Alison G. Tobias
Production Editor: Kieran P. O'Leary
Graphics Coordinator: Karen L. White
Office Manager: Phyllis D. Barber
Production Assistant: Betty L. Hawkins

Printed in the United States of America

Library of Congress Cataloging-in-Publication Data
National Research Council. Transportation Research Board.

Pavement management and rehabilitation.
p. cm.—(Transportation research record, ISSN 0361-1981 ; 1215)
Papers from the 68th annual meeting of the Transportation Research Board.
ISBN 0-309-04819-2
1. Pavements—Maintenance and repair. 2. Pavements—Maintenance and repair—Management—Data processing. 3. Pavements—Performance. I. National Research Council (U.S.). Transportation Research Board. Meeting (68th : 1989 : Washington, D.C.) II. Series.
TE7.H5 no. 1215
[TE250]
388 s—dc20
[625.7'6] 90-31269
CIP

Transportation Research Board publications are available by ordering directly from TRB. They may also be obtained on a regular basis through organizational or individual affiliation with TRB; affiliates or library subscribers are eligible for substantial discounts. For further information, write to the Transportation Research Board, National Research Council, 2101 Constitution Avenue, N.W., Washington, D.C. 20418.

Transportation Research Record 1215

Contents

Foreword

Pavements are one of the largest concerns in any transportation department. The search for effective designs, efficient management techniques, and economic restoration and repair procedures never ends. The papers in this Record, which present recent research in these areas, should be of use to transportation officials, designers, planners, and engineers.

Design guidelines for pavements are discussed in several papers. One study examines the performance and costs of nearly 25 years of experience with AASHO-designed pavements in Louisiana, and two papers examine the implementation of AASHTO design guidelines and the remaining life factor.

Pavement life cycle costs and deterioration are considered in five papers that cover topics ranging from economics of various structures and loadings to computer modeling of deterioration rate. Other studies examine vehicle classification and weigh-in-motion systems that can provide valuable data to pavement designers and planners.

Pavement surface characteristics are an important factor in pavement safety and can be a reflection of structural performance. Skid resistance, roughness, pavement microtexture, and ride quality are explored in five papers in this Record.

Computerized pavement management systems, which can help a highway department get the best returns from its pavement investments, are described in three papers. Two other papers describe technological tools that are available to help detect and analyze pavement damage.

Asphalt overlays and the crack and seat method are each discussed in three papers. Other aspects of the repair/rehabilitation process covered in the Record include concrete pavement restoration techniques, such as dowels in PCC pavement repair, pressure relief joints, and rehabilitation performance and cost effectiveness.

Models for Predicting Pavement Deterioration

K. P. GEORGE, A. S. RAJAGOPAL, AND L. K. LIM

The measurement and prediction of pavement performance is a critical element of any pavement management system (PMS). Pavement condition rating (PCR), a composite statistic derived from functional and structural conditions, is used as a measure of serviceability. After a review of the various types of prediction models, the authors concluded that an empirical-mechanistic model is best suited, with a systematic database that includes the structural information, traffic volume, and condition data for each "homogeneous" section of the road. Pavements with an asphalt concrete surface are grouped into three categories (pavements with no overlay, pavements with overlay, and composite pavements), and prediction equations are developed for each of them. The equations are validated by comparing them with several existing models, both empirically and mechanistically based. In all three prediction models, age is by far the most significant predictor of serviceability. The traffic volume and weight expressed in terms of equivalent single-axle loads (*ESALs*) and the structural makeup of the pavement described by the composite structural number play only a secondary role in forecasting performance of pavements.

Over the past two decades considerable emphasis has been directed toward rationalizing planning in the area of pavement maintenance and rehabilitation. Planning at the project level deals with issues relating to the design of proper treatments for particular deficiencies and the impacts of traffic and environmental factors on pavement structures. Network-level planning, the backbone of a pavement management system (PMS), addresses the need for trade-offs in project selection, including viewing the benefits and costs of each in relation to all other potentially competing projects.

Modeling pavement performance is an essential activity of a pavement management system. The models play a crucial role in several aspects of the PMS, including financial planning and budgeting as well as pavement design and life-cycle economic analysis. First, models are used in PMSs to predict when maintenance will be required for individual road sections and how to prioritize competing maintenance requirements. Second, by virtue of its prediction capability, the model enables the owner agency to estimate long-range funding requirements for pavement preservation and to analyze the consequences of different budgets on the condition of the pavement network. Third, because the models attempt to relate the influence of pavement exposure variables to pavement distresses or to a combined performance index, they can be used for design as well as the life-cycle economic evaluation.

Department of Civil Engineering, University of Mississippi, University, Miss. 38677.

Several approaches employed for their development include regression analysis using field performance data, mechanistic modeling based on pavement response parameters, and models that combine both field data and response parameters, which are aptly called mechanistic-empirical models. An excellent summary and comparison of several models of the first type appear in Hajek et al. (*1*). Although these models currently serve a crucial role in expediting pavement management decisions, future endeavors should be directed toward developing physically based deterioration mechanisms.

The research reported in this paper is part of a program to develop a pavement management system for 2,000 lane-miles of roads in northern Mississippi. Employing the condition data of the road system, the authors developed performance equations for three categories of pavements: flexible pavements with no overlay, flexible pavements with overlay, and composite pavements (asphalt concrete surface over a rigid base). Several equation forms are attempted. As a basic principle, the form of the equation is selected on the basis of whether it adheres to the boundary conditions or other physical principles that govern the deterioration of the pavement family. With the equation form chosen, multiple regression analysis, using the SAS program, is employed for developing pavement deterioration equations.

REVIEW OF PERFORMANCE PREDICTION MODELS

Performance is a broad, general term describing how pavement conditions change or how pavements serve their intended function with accumulating use. What should be included in a performance evaluation depends to a large measure on whether one's interest lies in project-level or network-level activities. Various approaches have been used in quantifying the performance measure. The pavement serviceability index (PSI), coined in connection with the AASHO Road Test (*2*), pavement condition index (0–100 scale), and pavement quality index (0–10 scale), are but a few of many existing measures. The performance indicator developed by the authors is designated a pavement condition rating (*PCR*, 0–100 scale), which is a composite index derived from monitoring data—pavement roughness or roughness rating (*RR*) and distress rating (*DR*)—in accordance with the following relation:

$$PCR = RR^{0.6}\, DR^{0.4} \quad (1)$$

The equipment and procedure that determine pavement roughness employing the AASHO concept of slope variance (in turn, present serviceability rating) and that quantify the

density and severity of distresses facilitating the calculation of distress rating are described elsewhere (*3*).

Performance prediction models may be categorized into two kinds: deterministic and probabilistic. Deterministic models include primary response, structural performance, functional performance, and damage models. All of the preceding models may be either empirical, implying they are developed from regression analysis, or mechanistic-empirical correlations. For the latter type, a combination of mechanistic and empirical parameters enter the prediction model. In the damage models, damage—an abstract number (0–1 scale)—is being predicted; a typical example is the pioneering equation of the AASHO Road Test (*2*).

Probabilistic models include Markov chain (MC) models and survivor curves (*4,5*). Knowing the "before" condition or state of pavement in probabilistic form, one can employ the Markov process to predict the "after" state, again in probabilistic forms, for as many time steps as are desired. The evolution is governed by a characteristic transition rule, otherwise known as transition probability matrix in MC theory. Survivor curves describe pavement deterioration in the form of a cumulative distribution, which subsequently can be employed to develop a transition probability matrix. The principal advantage of probabilistic predictions lies in their ability to recognize and accommodate uncertainties in design/analysis leading to reliability-based designs.

DEVELOPMENT OF A PAVEMENT DETERIORATION MODEL

Pavements are complex physical structures responding in a complex way to the influences of numerous environmental and load-related variables and their interactions. A prediction model, therefore, should consider the evolution of various distresses and how they may be affected by both routine and planned maintenance. Such an approach is so highly complex that a compromise procedure combining a strong empirical base and a mechanistic approach is adopted to achieve a reliable model. The empirical base includes time-series pavement condition data compiled on pavements exposed to different environmental and loading conditions. With regard to mechanistic principles, interactions between traffic loading and pavement strength parameters, between loading and pavement deflections, and so on are carefully observed and included when significant. These considerations dictated the model form and provided guidance in the selection of independent variables (parameters) for inclusion in the prediction model.

Model Variables

The empirical-mechanistic model alluded to earlier requires a variety of data on factors that affect the rate of deterioration; these include traffic loads, pavement layer thicknesses, materials, subgrade strength, environmental factors, and construction technique, to name a few. The historical component of the PMS database provided this segment of information; the condition data (*PCR*) were compiled from the 1986 and 1988 pavement condition surveys.

The task of predicting the responses of pavements to a battery of interrelated variables is a complex problem that can be accomplished only by resorting to a number of assumptions and simplifications. A brief discussion of these simplifications and a listing of the independent variables (factors) follow.

Ideally, data collection would consist of complete histories, or sample functions, of *PCR* versus time for roads belonging to a particular family of pavements. It would also be convenient for data to be collected from roads put into use at the same time, so that their ages would be identical. The pavement survey data available in this study do not conform to this pattern, since the roads included in the survey were placed into service at different times whereas the survey data were collected at a single point in time (Figure 1a). The transformation into *PCR* versus age data is shown in Figure 1b.

A preliminary analysis of the data confirmed the contention that the rate of deterioration varies from pavement to pavement, and possibly the best strategy would be to attempt to determine a single relationship for a family of pavements having similar characteristics. The data dictated that five categories of pavements be recognized in the analysis: flexible pavements with no overlay, flexible pavements with one or more overlays, composite pavements, jointed concrete pavements, and continuously reinforced concrete pavements. Only the first three categories are included in this study.

The selection of independent variables for the prediction equations is based on experience suggesting that the predic-

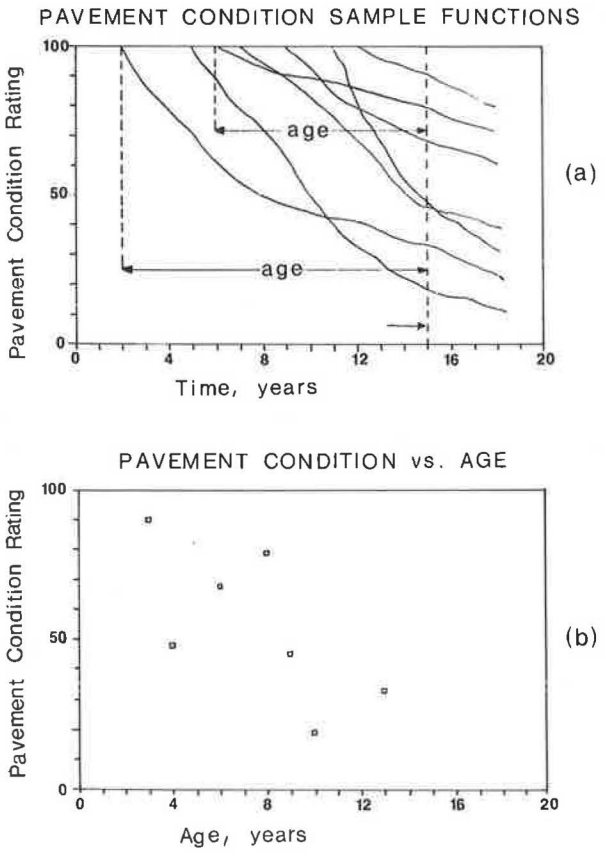

FIGURE 1 Transformation of one-time pavement survey data to *PCR* versus age (adaptation *4*).

tion of pavement condition depends on the following factors:

1. Period during which the pavement has been in service, age of the pavement (Age, years);
2. Traffic volume and weight, which are expressed in terms of yearly equivalent single-axle loads (*ESAL*s);
3. Thickness of last overlay, T, in inches;
4. Strength and condition of pavement structure represented by modified structural number (*SNC*). The American Association of State Highway Officials (AASHO) structural number, modified to account for subgrade support, is designated as modified structural number (*6*):

$$SNC = \Sigma a_i h_i + SN_g \quad (2)$$

where

a_i = material layer coefficients,

h_i = layer thicknesses (in.),

SN_g = subgrade contribution, and

$$= 3.51 \log CBR - 0.85 (\log CBR)^2 - 1.43 \quad (3)$$

in which CBR = in situ California bearing ratio of subgrade (percent).

5. Surface deflection/Benkelman beam deflection under 18-kip axle load DEF, mm. The empirical equations employed for deflection calculation are due to Paterson (*6*):

For granular base pavements,

$$DEF = 6.5\ SNC^{-1.6} \quad (4)$$

For cement-treated base pavements,

$$DEF = 3.5\ SNC^{-1.6} \quad (5)$$

6. Construction quality (*CQ*). For want of quantitative data, this factor could not be included in the analysis.

The performance equation of each pavement category has been derived from a statistical analysis of road condition trends observed at two discrete times on in-service highways in Mississippi. The data included 54, 193, and 135 observations, respectively, for flexible pavements with no overlay, flexible pavements with overlay, and composite pavements. The ranges of variables of the database are given in Table 1. The causative factors, such as traffic volume, surface deflection, and modified structural number, are obtained directly from the PMS database or are calculated employing the structural data relating to each pavement section.

Data Analysis

After the factors affecting pavement deterioration have been identified, one wishes to derive a regression equation (i.e., a statistical transform) that can be used to make future predictions of pavement condition. SAS version 5 is capable of handling three types of regression analysis: regular, nonlinear, and stepwise. The latter method was employed initially, without much success. Nonlinear analysis, however, resulted in physically based equations reported in this paper.

Several different models were constructed and evaluated. The evaluation was based on rational formulation and behavior of the model and on its statistical parameters. Primarily owing to the large scatter of data points, several equation forms appear to fit the data with more or less the same correlation coefficient. Exponential and power functions of both concave and convex shapes, including an S-shape (sigmoidal), were explored. The criterion that dictated the selection of a particular model for a pavement family was its ability to satisfy the initial and possibly the end-of-life boundary conditions, in addition to yielding a reasonably low standard error of estimate.

The best-fit model for the performance prediction of flexible pavement with no overlay is presented in Equation 6.

$$PCR(t) = 90 - a\,[\exp(\text{Age}^b) - 1] \log\left[\frac{ESAL}{SNC^c}\right] \quad (6)$$

with $a = 0.6349$; $b = 0.4203$; and $c = 2.7062$.

$$R^2 = 1 - \frac{\Sigma(y - \hat{y})^2}{\Sigma(y - \bar{y})^2} = 0.75$$

where $PCR(t)$ = pavement condition rating at time t.

TABLE 1 RANGES OF VALUES OF MAIN PARAMETERS IN EMPIRICAL DATA BASE

	Range of Each Parameter, Flexible Pavement		
Parameter	No Overlay	Overlay	Composite Pavement
Number of data points	54	193	135
Thickness of AC surface, inches (T)	NA	1.0–8.0	2.0–5.0
Modified structural number (*SNC*)	2.5–7.7	1.1–8.2	NA
Yearly equivalent single axle load (*ESAL*)	1,055–104,965	1,191–809,289	4,331–119,696
Age since construction or last overlay, years	1–16	1–10	1–10
Pavement condition rating (*PCR*)	59–89	62–89	52–89
Year of *PCR* survey	1986–1988	1986–1988	1986–1988

Similar equations are developed for flexible pavement with overlay and composite pavements. Respectively, those equations are:

$$PCR_{(t)} = 90 - a[\exp(\text{Age}^b) - 1] \log\left[\frac{ESAL}{SNC^{c*}\ T}\right] \quad (7)$$

with $a = 0.8122$, $b = 0.3390$, and $c = 0.8082$.

$$PCR_{(t)} = 90 - a\left[\exp\left(\frac{\text{Age}}{T}\right)^b - 1\right] \log [ESAL] \quad (8)$$

with $a = 1.7661$ and $b = 0.2826$. All other symbols are explained in the previous sections.

Model Evaluation

The prediction model of Equation 6 was statistically significant with an R^2 of 0.75. Models for the other two types, flexible pavements with overlay and composite pavements, exhibited R^2s of 0.76 and 0.70, respectively. Table 2 lists the regression constants and their standard errors of estimate in Equations 6, 7, and 8. The relatively small standard errors of the regression coefficients suggest that the relation is satisfactory and can be advantageously used for predicting pavement performance.

As a further verification of the model, a plot of measured versus calculated *PCR* is presented in Figure 2. The residuals, differences between the predicted and observed *PCR* values, were normally distributed.

Despite the fact that *PCR* is influenced by three factors (age, traffic, and *SNC*), the evolution of serviceability, with time suppressing the other two variables, would be of interest in the overall evaluation of a specific family of pavements. The scattergram of the 54 data points and the trend line, along with the 95 percent confidence levels for average values of traffic and *SNC* ($ADT = 3000$, $SNC = 3.0$), are presented in Figure 3. The trend line conforms to the traditional "concave down" shape subscribing to slow deterioration during the early life followed by a period in which the rate of deterioration surges significantly. Typically, one-half of pavement deterioration (and an even higher proportion of maintenance costs) is concentrated in the final third of the design life (approximately 15 years) of the pavement.

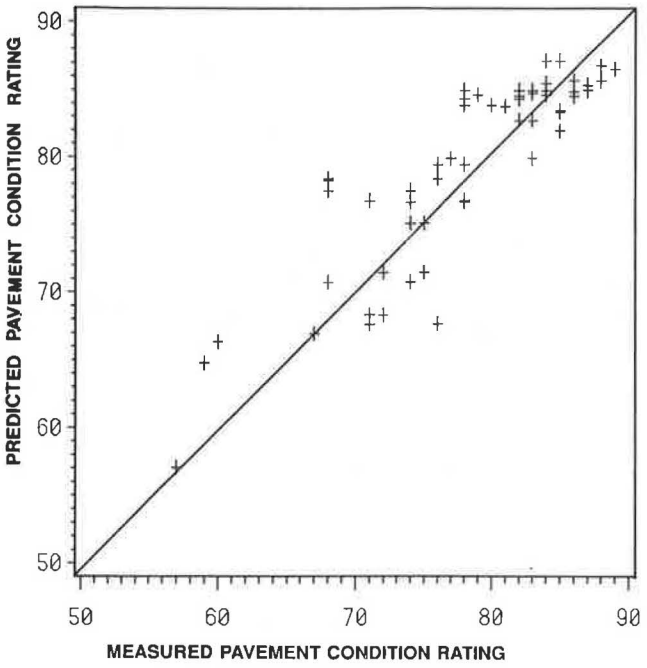

FIGURE 2 Measured versus prediction (Equation 6) pavement condition rating (*PCR*). Flexible pavement with no overlay.

The initial boundary condition is satisfied in that the trend lines pass through the 90-*PCR* point, signifying that a new pavement would start with a *PCR* of 90. The authors believe that the increasing rate of deterioration, beyond approximately 10 years of service, is reasonable provided the pavement in question does not undergo heavy maintenance or rehabilitation activities. The "more-than-normal" *PCR* drop during the first year can be attributed to the "breaking in" of the pavement structure by the traffic and environmental loads.

To evaluate the authors' model, the performance histories predicted by five other models (*1*) are compared with the one

TABLE 2 STATISTICAL PARAMETERS OF *PCR* PREDICTION MODELS

Type of Pavement	Regression Coefficient	Standard Error of estimate, %	R^2
Flexible Original	a = 0.6349	17.1	0.75
	b = 0.4203	5.6	
	c = 2.7062	21.4	
Flexible Overlay	a = 0.8122	7.4	0.76
	b = 0.3390	3.2	
	c = 0.8082	38.8	
Composite	a = 1.7661	3.0	0.69
	b = 0.2826	6.0	

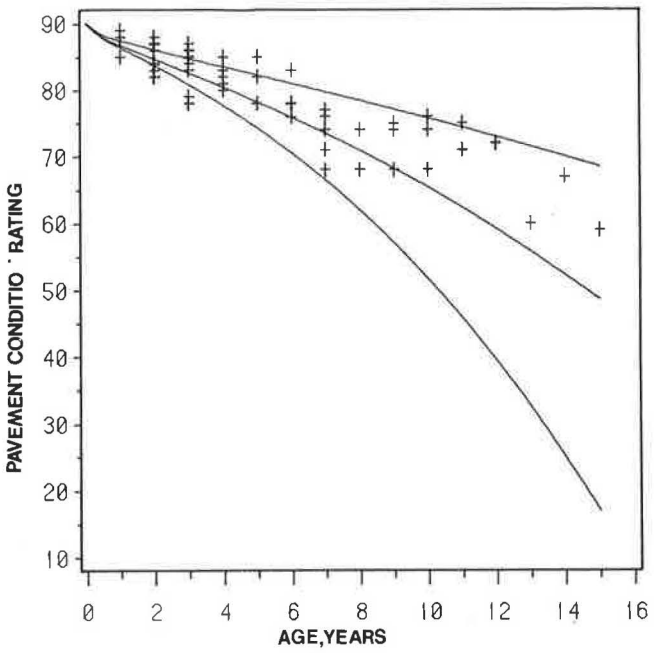

FIGURE 3 Scattergram of pavement condition data with age. Predicted *PCR* (*ADT* = 3000, and *SNC* = 3.0) using Equation 6 and corresponding 95 percent confidence limits.

developed herein (Equation 6), as shown in Figure 4. The performance history observed by Hajek et al. (*1*) is also plotted in the figure. It is gratifying to note that the proposed model is in good agreement, especially with the observed points, despite some difference in regard to curvature of the models elsewhere (*1*).

Significance of Causal Factors

The prediction equation recognizes three causal factors in defining pavement performance. They are age (years since original construction or last overlay), yearly traffic (*ESAL*), and composite structural number, with age being the most significant factor. That the yearly *ESAL* and structural number are of only minor importance can clearly be seen from Figures 5 and 6, where each of these factors is varied over a moderate range and the corresponding *PCR* changes are investigated. The changes in *PCR* after 15 years of service, owing to variations of *ESAL* and *SNC*, amount to only 9 and 8 points, respectively.

The question now arises of why age is so significant in predicting pavement deterioration. In fact, the data suggest that age alone can account for a substantial portion of the decline in serviceability. Age is significant because it is a common factor in the estimation of both cumulative traffic loads and environmental loads over the life-cycle period. For example, cumulative traffic is the product of yearly *ESAL* and age of pavement. Between the two, *ESAL* would be the weakest link in the cumulative traffic computation because several questionable input parameters (for example, the sample traffic count, the growth factor, the truck factor) enter the daily (or yearly) *ESAL* estimation. In contrast, age can be determined precisely for any pavement and, by virtue of its accuracy, would be expected to be a better predictor. The same argument also holds well for environmental loads. The environmental loads include thermal effects, subgrade movements in expansive clays if applicable, freeze-thaw effects, and bitumen aging, which are difficult to quantify. Age, however, can be a surrogate for the cumulative effect of these detrimental factors. Simply put, age plays a pivotal role in predicting pavement deterioration.

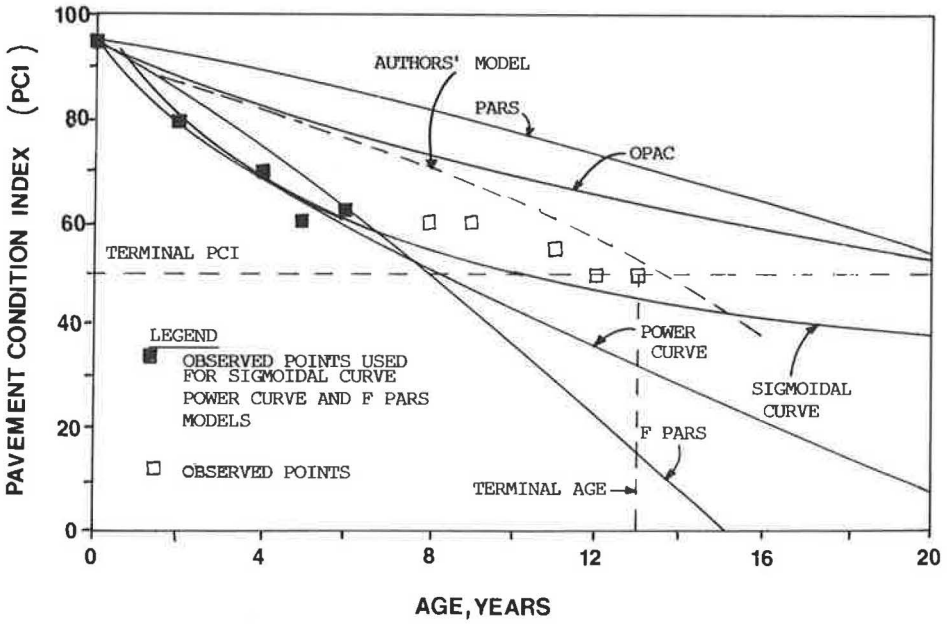

FIGURE 4 Model comparisons. Explanation: OPAC model (mechanistically derived), authors' model (Equation 6); PARS model (empirical, pavement classes); power curve (empirical-site-specific); sigmoidal curve (empirical, site-specific); factored PARS model (Bayesian approach, site-specific) (adaptation *1*).

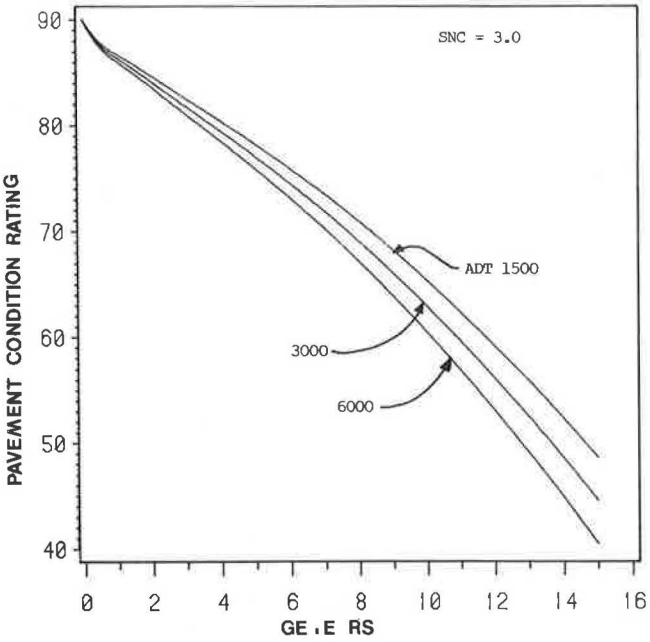

FIGURE 5 Effect of traffic on *PCR* as predicted by Equation 6. Flexible pavements with no overlay, structural number = 3.0.

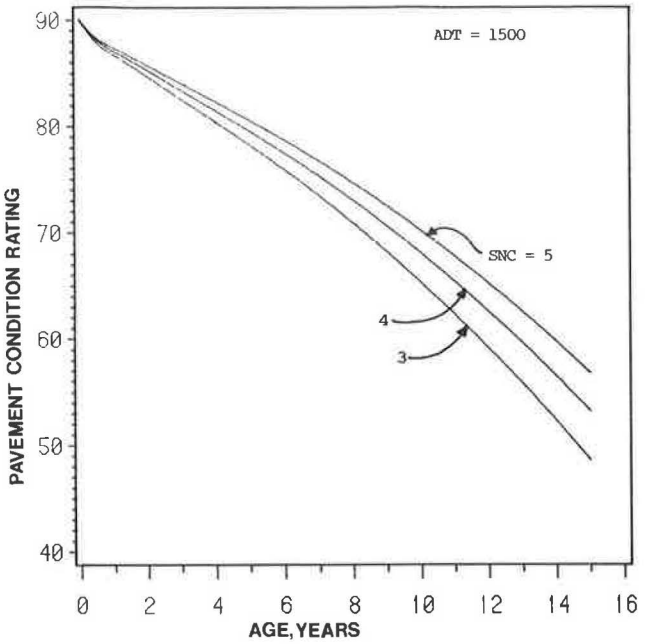

FIGURE 6 Effect of structural number on *PCR* as predicted by Equation 6. Flexible pavements with no overlay, *ADT* = 1500.

A question now arises of why traffic appears as a distinct entity in the equations (Equations 6, 7, and 8) whereas the environmental effects do not. The environmental factors of a specified region, north Mississippi, for example, can be assumed to be uniform, causing approximately the same ΔPCR in a wide range of pavement structures; age alone, therefore, can be a predictor of climate-related deterioration. Yearly traffic of the pavement network, however, ranges over two orders of magnitude (see Table 1), justifying the presence of traffic term in the equation.

Structural number, a mechanistic parameter in the equation, emerges, and rightly so, as a factor influencing the deterioration of flexible pavements without and with overlay. Composite and overlaid pavement equations include asphalt surface thickness as well. Besides their direct influence on the mechanistic parameters—for example, stress, strain, and deflection and, in turn, on performance—their computational accuracy could well be another reason for its significance in the performance model.

Had those pavements been proportioned in accordance with any one of the numerous design models, the structural number would be expected to increase with yearly *ESAL*. Only because of the collinearity between the loading and strength, the *ESAL*-structural number interaction term is coined as a ratio (see Equations 6–8), which accentuates the serviceability loss because the logarithm of this ratio always assumes values greater than 1.

Three Prediction Models Compared

The performance prediction equations for the three families of pavements are graphed with age, keeping traffic and *SNC* constant (see Figure 7). As can be noted, the flexible original pavement trend line conforms to the more traditional "concave down" shape, whereas the composite family follows a slightly "convex down" path, with the overlay family exhibiting hardly any curvature at all. The convex down shape or exponential decay of *PCR* with age has been reported by other researchers as well (see Figure 4 and Keddy [7]). A cursory examination of the distress data reveals that the composite pavements generally undergo premature (early) reflection cracking, with a concomitant abrupt *PCR* decrease setting the stage for exponential decay. Another noteworthy observation is that all the three families of pavements attain an assumed threshold (*PCR* = 55) in about 12 to 15 years. Similar life cycles have been reported by other researchers; for example, a survey of in-service flexible pavements in Ohio estimates them to last 14 years on the average. Hajek et al. (*1*) and Sharaf et al. (*8*) report that 3-in. overlays performed satisfactorily for 12 and 15 years, respectively. In summary, the authors believe that the serviceability trends, in accordance with Equations 6, 7, and 8, are reasonable and should serve well in predicting pavement condition at the project and/or network levels.

SUMMARY

Employing historical information and monitoring data over a 2-year period on some 2,000 miles of roads, empirical-mechanistic predictive models have been developed. Preliminary investigation of the data (pavement with asphalt surfacing) suggested a three-group classification based on deterioration rate. The groups are flexible pavements with no overlay, flexible pavements with one or more overlay(s), and composite pavements. One model for each pavement family was developed. Of the three causal factors identified in each model, age (life cycle in years) indeed correlates strongly with serviceability decline. As formulated, age is a surrogate for

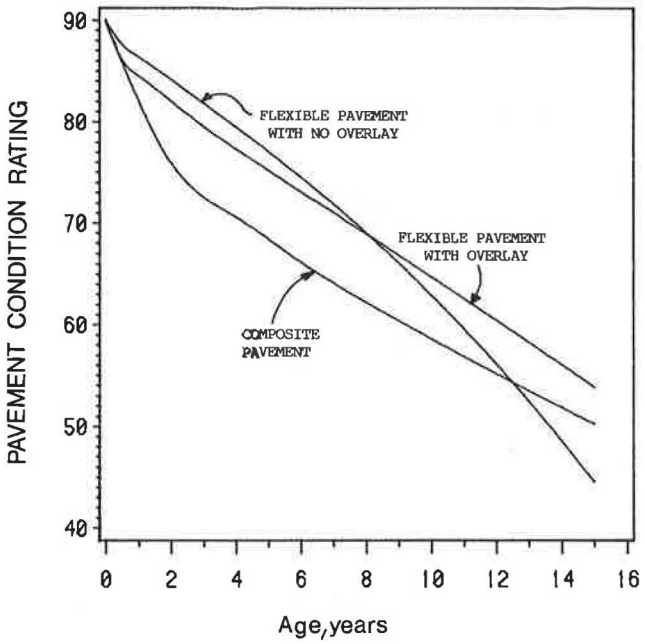

FIGURE 7 Pavement deterioration curves of three families of pavements. *ADT* = 3000; flexible pavement with no overlay, *SNC* = 3.0; flexible pavement with overlay, *SNC* = 3.0, *T* = 2 in.; composite pavement, *T* = 2 in.

both cumulative traffic and environmental loads. The composite structural number (the AASHO structural number modified to account for the subgrade support) shows a weak correlation to serviceability loss. The trends predicted by the respective models exhibit varied shapes: concave down for flexible pavements with no overlay, convex down for composite pavements, and neither concave nor convex curvature for overlaid pavements. Finally, the models are validated by comparing them with those developed (by other researchers) employing field performance data.

ACKNOWLEDGMENT

This report is a part of the study entitled "Pavement Management Information System" conducted by the Department of Civil Engineering, The University of Mississippi, in cooperation with the Mississippi State Highway Department and the U.S. Department of Transportation, Federal Highway Administration. The authors wish to acknowledge the excellent cooperation and assistance received from the Department personnel.

REFERENCES

1. J. J. Hajek, W. A. Phang, A. Prakash, and G. A. Wrong. Performance Prediction for Pavement Management. *Proc., North American Pavement Management Conference*, Toronto, Ontario, Canada, Vol. 1, 1985.
2. *AASHO Road Test—Report 61E*. HRB, National Research Council, Washington, D.C., 1962.
3. *Pavement Distress Manual—PMIS Report No. 1*. Civil Engineering Department, University of Mississippi, University, Miss., 1986.
4. J. V. Carnahan, W. J. Davis, M. Y. Shahin, P. L. Keene, and M. I. Wu. Optimal Maintenance Decisions for Pavement Management. *Journal of Transportation Engineering*, ASCE, Vol. 113, No. 5, 1987, pp. 554–572.
5. R. L. Lytton. Concepts of Pavement Performance Prediction Modeling. *Proc., North American Conference on Managing Pavements*, Toronto, Canada, Vol. 2, 1987.
6. W. D. O. Paterson. Applicability of Structural Parameters to Prediction of Pavement Performance. The 1986 International Conference on Bearing Capacity of Roads and Airfields, Plymouth, England, 1986.
7. J. M. Keddy. Effective Pavement Management Through Good Inventory. *Proc., North American Pavement Management Conference*, Toronto, Ontario, Canada, Vol. 1, 1985.
8. E. A. Sharaf, E. Reichelt, M. Y. Shahin, and K. C. Sinha. Development of a Methodology to Estimate Pavement Maintenance and Repair Costs for Different Ranges of Pavement Condition Index. In *Transportation Research Record 1123*, TRB, National Research Council, Washington, D.C., 1987, pp. 30–39.

Publication of this paper sponsored by Committee on Pavement Management Systems.

Life-Cycle, Cost, and Loading Characteristics of AASHO-Designed Rigid and Flexible Pavements in Louisiana (1965–1989)

WILLIAM H. TEMPLE AND DEBORAH A. BOLEWARE

This report represents a study undertaken to determine the life cycle, load characteristics, and associated costs of a representative sample of the oldest rigid and flexible pavements designed in Louisiana (1963–1967) using the AASHO Guide for Design of Pavement Structures. Project selection resulted in a sampling of two classes of roads designed and constructed during this period—Interstate route jointed concrete pavements and secondary route asphaltic concrete pavements. An index, termed the Load Rate Index, was developed to compare actual and designed rates of equivalent single-axle loading (*EAL*) at any point in the life of a pavement. The total accumulated *EAL* was also compared with the total designed *EAL*. The typical jointed concrete pavement had not reached end of life by its 20th year (1989), having carried its design *EAL*. The effects of factors of safety used in the original design were removed by relating design *EAL* to actual section thickness. The typical flexible pavement in the sample reached end of life within 14 years. The performance of these pavements was characterized by cracking and settlement within the cement-treated bases. Total project costs (construction plus maintenance) prior to end of life were expressed in terms of cost per mile, per *EAL* (\$*EAL*-mile), to represent pavement value or return on investment for each route class. It is concluded that expressions of pavement value to be incorporated into Louisiana's pavement management system should include the rate and quantity of designed load actually carried before end of life.

The purpose of this study was to select and evaluate a representative sample of rigid and flexible pavements from the original population of projects designed and constructed between 1963 and 1967 using the Louisiana—AASHO Design Guide for Pavements (*1,2*). It was hoped that, by studying the life-cycle and associated costs of the sampled pavements, a general indication of design adequacy could be formulated and that some of the basic information needed to characterize pavement types for life-cycle cost studies could also be obtained.

One data element of particular interest was the accumulated, equivalent 18-kip, single-axle loads (*EAL*s) as compared with original design estimates, both in terms of magnitude and rate of accumulation.

The sampling of jointed portland cement concrete pavements resulted in mostly Interstate route projects reflecting the typical type of rigid pavement designed during this period in Louisiana. The sample of asphaltic concrete pavement designs resulted in a set of pavements that could be described as secondary class routes or rural collector roads.

All of the project information collected during the study, including accumulated *EAL*, pavement age, condition, and associated costs, represents information available at the end of the 1987 calendar year. Actual *EAL*s carried by the Interstate concrete pavements and their ages have been updated through 1989.

Louisiana Transportation Research Center, P.O. Box 94245, Baton Rouge, La. 70804-9245.

PROJECT SELECTION

The group of projects most representative of rigid pavement construction typically consisted of 10 in. of jointed concrete with a 58.5-ft joint spacing constructed over a 6-in. base of either untreated granular material, cement-treated granular material (sand-clay-gravel), or cement-stabilized soil. This sample of jointed concrete was developed by selecting all available designs that exceeded one mile in length, for which construction costs could be determined, and that represented normal mainline section design. A smaller number of jointed concrete projects, 8 or 9 in. thick, with 20-ft joint spacing was also included to represent non-Interstate construction. Altogether, 22 concrete projects were selected for evaluation; 15 represented Interstate construction, and 7 represented U.S. route or state route construction.

Flexible pavements selected for evaluation were typically 3.0- to 5.0-in. asphalt concrete with an 8.5-in., cement-treated base course. Again, all available projects representing this type of design were selected for evaluation, resulting in 22 sample pavements. The base courses were constructed by stabilizing in place either sand-clay-gravel or select soils with portland cement.

PAVEMENT DESIGN CONSIDERATIONS

Concrete pavements in the study were constructed using a 5.8-sack, river gravel mix that was designed to provide a minimum of 3,600 psi compressive strength at 28 days. No routine measurements were made of flexural strength; however, a conservative value of 450 psi was used in design to provide a factor of safety.

Published conversions of compressive to flexural strength indicate the following relationships (*3*):

$$\text{flexural psi} = (7 \text{ to } 10)\ (\text{compressive, psi})^{0.5}$$

Using the conversion, a factor of between 7 and 10 is multiplied by the square root of the compressive strength. Applying the formula to 3,600 psi results in values of flexural strength of between 420 and 600 psi. Measured values of flexural strength (third point loading) for the 5.8-sack, gravel aggregate concrete described are typically around 550 psi. The concrete used at the AASHO Road Test had a higher strength (690 psi) as a result of a higher cement factor and the use of dolomitic limestone as the coarse aggregate.

Summary statistics that involve "design *EAL*" in this report are provided across a range of flexural strengths to illustrate the sensitivity of design *EAL* (from the design guide) for a given thickness of concrete to variation in 28-day flexural strength. The values selected for this purpose are 450, 550, and 600 psi.

The modulus of subgrade reaction (composite *K*-value) used in the original designs was typically set at 120 for both cement-treated and granular subbases. Recommended design thickness was rounded upward to the next higher inch, and Interstate route pavements were specified to be a minimum of 10 in. thick. For the purposes of this study, values referred to as "design *EAL*" represent the *EAL*s that a 10-in. concrete pavement should, according to the AASHO design relationship, be able to carry. This was done to provide continuity between pavement section, performance, and *EAL* by effectively removing the factors of safety from the design data analysis.

The Louisiana-AASHO design for flexible pavements required a regional factor of 1.5 for projects constructed in northern Louisiana (above the 31st parallel) and 1.0 for those constructed below that line. The effect of the 1.5 regional factor was "factored out" of the data analysis in this study by relating design *EAL* to the actual structural number specified for construction. This process therefore allowed all of the asphaltic concrete pavements to be represented by the same basic design relationships.

LIFE CYCLE AND PERFORMANCE

The number of years between opening to traffic and structural overlay or rehabilitation was determined for each project that reached end of life. This was accomplished using a Louisiana Department of Transportation and Development (DOTD) computer file named Record of Control Units and Jobs (RCUJ). The file lists each construction project undertaken within specified project limits. For those projects where no action was indicated, a field condition survey was conducted to determine the condition of each pavement section.

The results of the 1987 project life survey indicated that out of a sample of 22 jointed concrete pavements, 19 had not reached end of life and the average age of the surviving projects was 17.5 years. Of the three concrete projects that were considered to have reached end of life, one had been resurfaced. The other two pavements had not been scheduled for overlay but contained frequent joint spalling and blowups and, therefore, were considered to be at end of life. None of the 10-in. jointed concrete pavements constructed on Interstate routes fell into the end-of-life group. An update in 1989 indicated that these pavements had not reached end of life at an average age of 20 years.

A survey of the flexible pavement projects indicated that, out of a sample of 22 pavements, 17 had reached end of life and the average age of the projects overlaid or reconstructed was 14.2 years. The condition of the five surviving, asphaltic concrete over cement-treated base pavements provided a clue to the probable mode of failure of this group. The performance of this group was characterized by a loss in serviceability due to transverse and longitudinal block cracking, which was heavily spalled in the wheel paths occasionally having required patching. Pavement ride was adversely affected by depressions that occurred along transverse cracks and by occasional buckling, somewhat similar to blowups that occur on jointed concrete pavements. This mode of failure is characteristic of this type of pavement in Louisiana and is thought to be principally related to performance of the cement-treated base course.

Table 1 contains a summary of the life cycle and the number of projects reaching end of life for each pavement type. Within the rigid pavement group, the surviving projects are considered to be representative of performance as they represent 86 percent of the sample. Within the flexible pavement group, the projects that reached end of life are considered representative as they make up 77 percent of that sample.

TRAFFIC LOAD

The magnitude and rate of application of traffic *EAL* are among the most difficult design factors to predict correctly over an extended design period and are often overlooked in analyses of project life-cycle cost. In historical studies of specific paving projects, it seems reasonable to include *EAL* as a factor that contributes to performance, where this type of information is available.

Estimates of actual accumulated *EAL* were calculated from traffic classification data and traffic volume data provided by the department's Traffic and Planning Section. Past research studies have indicated that this method provides reasonable results compared to similar data obtained from Weigh-in-Motion and vehicle classification studies (*3*).

The variable of traffic loading was evaluated from two perspectives: (1) the rate of accumulation of *EAL* and (2) the ratio of actual to design *EAL* over the life of each project. An index termed the Load Rate Index (*LRI*) was developed to compare actual to design rates of loading at any stage in the life of a pavement:

$$LRI = \frac{Yd\ (EAL \text{ actual})}{Ya\ (EAL \text{ design})}$$

where

Yd = design period in years,
Ya = current age in years,
EAL actual = current accumulated EAL, and
EAL design = designed total EAL.

Using a design period of 20 years, the relationship can be

TABLE 1 PROJECT LIFE CYCLE (1987)

	End of Life		Survivors	
	Sample %	Age (yrs)	Sample %	Age (yrs)
Rigid (22 projects)	13.64	17.97	86.36	17.54 *
(std)		(1.34)		(1.94)
Flexible (22 projects)	77.27	14.16 *	22.73	17.58
(std)		(4.18)		(0.80)

* This group is considered to be representative of each respective pavement type.

(std) = sample standard deviation

TABLE 2 PROJECT LOAD DATA

	Concrete Flexural Strength (psi)	Load Rate Index (LRI)	Actual EAL / Design EAL
Rigid (Survivors) (std) (1989)	450	2.61 (0.65)	2.58 (0.60)
	550	1.35 (0.34)	1.33 (0.31)
	600	1.00 (0.25)	0.98 (0.23)
Flexible (End of Life) (std) (1987)		1.11 (0.88)	0.79 (0.58)

These values are considered to represent each respective pavement type. (Thin pavements are not included.)

(std) = sample standard deviation

expressed as

$$LRI = \frac{20\ (EAL\ \text{actual})}{Ya\ (EAL\ \text{design})}$$

$LRI = 1.0$, indicates actual loading rate is as designed;
$LRI < 1.0$, actual loading rate is less than designed; and
$LRI > 1.0$, actual loading rate is greater than designed.

Tables 2, 4, and 5 contain the *LRI* values that characterize the rigid and flexible pavements in the study. All values of actual load carried for the rigid survivors were calculated as of 1989. The data indicate a higher than anticipated rate of loading for the 10-in. Interstate pavements and generally a lower than anticipated rate for most of the 8-in. and 9-in. concrete pavements. The thinner concrete pavements were found to occur primarily in urban areas where automobile and pickup trucks comprised a majority of the traffic volume. The typical flexible pavement (Table 2) was loaded at a rate closer to the rate envisioned in the original pavement designs. Figures 1 and 2 depict the project frequency distribution of *LRI* for projects considered to represent each pavement type.

The actual accumulated *EAL* carried prior to end of life is an important indicator of the performance of any pavement. A simple ratio of actual-to-design accumulated *EAL* is provided in Table 2 for this purpose. It can be seen that, even at a concrete flexural strength of 600 psi, the 10-in. Interstate

TABLE 3 INTERSTATE PROJECTS—TOTAL LOAD AND AGE (1989)

PROJECT NUMBER	LIFE CYCLE as of 1989	ACTUAL LOAD 1989
450-04-13	22.92	27,963,900
450-05-04	20.17	20,278,032
450-06-01	16.75	24,365,979
451-06-21	20.08	20,883,251
451-06-22	21.08	19,677,409
451-07-03	21.08	16,132,426
451-07-07	20.50	15,817,774
451-07-09	19.17	12,362,491
454-01-07	18.33	24,701,277
454-02-01	19.25	18,342,650
454-02-05	18.42	18,016,512
454-02-06	21.00	16,947,768
454-02-07	18.33	14,624,318
454-02-08	20.00	14,895,236
454-02-09	20.00	15,104,098
Averages	19.81	18,674,208

pavements have carried their design *EAL*. The magnitudes of estimated *EAL* as of 1989 are listed in Table 3 for the 15 Interstate pavements along with years of service. The data indicate an average total *EAL* of 18.7 $\times$ 10^6 carried at an average age of 19.8 years. Table 4 contains a listing of traffic loading characteristics by project.

The sample representing flexible pavement construction typically carried less than their design load (79 percent) prior to end of life. This effect is thought to be due to the absence of a factor of safety in the design procedure and to surface roughness caused by the performance of the cement-treated bases used in most of the pavements in the sample. In general, if these pavements had performed for 5 additional years and had carried an additional 21 percent designed load, they would have met minimum design load expectations. Table 5 contains a listing of traffic loading characteristics by project.

These findings closely parallel the results of a 1979 research study entitled "Performance Evaluation of Louisiana's AASHO Satellite Test Sections" (*4*), in which the life cycle and *EAL* of a sample of rigid and flexible pavements were investigated. The projects in the 1979 study were not actually designed using the AASHO procedure; therefore, design *EAL* had to be backcalculated from pavement thickness information. In the study it was concluded that the typical flexible pavement reached end of life in 13 years and carried less than the designed *EAL*.

The design adjustments made as a result of these findings provided a more realistic link between the flexible pavement materials design coefficients for asphaltic concrete (c = 0.44 lowered to c = 0.40) and the specified Marshall properties. The effect of these changes could possibly have extended the life of the flexible pavements in the current study had the adjusted design values been used back in the mid-1960s. For example, the effect would have been to add approximately 1 in. of asphaltic concrete to the 5.0-in. A.C./8.5-in. C.T.B. pavements in this study.

COST DATA

Project cost information was obtained by examination of the final estimate data for construction projects, which also included any changes in planned quantities or materials. Maintenance costs were available on computer file and were cross-referenced to original construction project limits using log-mile as a location identifier. Construction costs, which make up a majority of the total project costs, were not adjusted forward or backward to reflect the time change in dollars since most projects were constructed during the same time period.

Construction costs reflect the cost of only the pavement section itself—surface, base, and subbase for a 24-ft-wide

TABLE 4 PROJECT LIFE CYCLE AND LOAD DATA RIGID (SURVIVORS)

PROJECT NUMBER	CONCRETE THICKNESS (inches)	LIFE CYCLE (years)	ACTUAL EAL / DESIGN EAL	LOAD RATE INDEX
052-30-06	8.0" PCCP	19.42	0.06	0.06
424-04-04	8.0" PCCP	21.00	1.06	0.77
055-30-03	9.0" PCCP	22.42	0.11	0.12
062-01-09	9.0" PCCP	14.50	1.23	1.38
450-04-13	10.0" PCCP	22.92	2.00	1.74
450-05-04	10.0" PCCP	20.17	1.45	1.44
450-06-01	10.0" PCCP	16.75	1.74	2.08
451-06-21	10.0" PCCP	20.08	1.49	1.49
451-06-22	10.0" PCCP	21.08	1.41	1.33
451-07-03	10.0" PCCP	21.08	1.15	1.09
451-07-07	10.0" PCCP	20.50	1.13	1.10
451-07-09	10.0" PCCP	19.17	0.88	0.92
454-01-07	10.0" PCCP	18.33	1.76	1.92
454-02-01	10.0" PCCP	19.25	1.31	1.36
454-02-05	10.0" PCCP	18.42	1.29	1.40
454-02-06	10.0" PCCP	21.00	1.21	1.15
454-02-07	10.0" PCCP	18.33	1.04	1.14
454-02-08	10.0" PCCP	20.00	1.06	1.06
454-02-09	10.0" PCCP	20.00	1.08	1.08

TABLE 5 PROJECT LIFE CYCLE AND LOAD DATA FLEXIBLE (END OF LIFE)

PROJECT NUMBER	ASPHALT THICKNESS	LIFE CYCLE (years)	ACTUAL EAL / DESIGN EAL	LOAD RATE INDEX
058-02-06	3.0" AC	12.25	1.22	1.99
859-12-05	3.0" AC	17.33	0.35	0.40
070-02-10	3.5" AC	14.17	0.66	0.93
071-02-01	3.5" AC	15.25	2.08	2.73
071-03-01	3.5" AC	16.00	1.48	1.86
156-03-07	3.5" AC	22.33	0.64	0.57
173-01-17	3.5" AC	10.25	0.36	0.71
177-01-06	3.5" AC	21.00	1.04	0.99
224-02-16	3.5" AC	14.42	0.63	0.88
228-06-12	3.5" AC	13.92	0.06	0.08
414-02-02	3.5" AC	9.17	0.14	0.30
414-03-04	3.5" AC	7.08	0.06	0.17
005-07-34	4.5" AC	9.00	0.22	0.49
028-02-13	5.0" AC	10.33	1.63	3.15
034-04-08	5.0" AC	17.58	0.89	1.01
034-05-14	5.0" AC	14.50	1.08	1.49
805-15-03	5.0" AC	16.08	0.89	1.11

pavement section—expressed as cost per mile. Maintenance cost data include that of all maintenance work undertaken within the original project limits but do not include the cost of a structural overlay for those projects that reached end of life and were subsequently resurfaced.

Calculations were made of maintenance cost expressed as a percentage of total cost (maintenance plus construction) to provide an indication of the relative magnitude of maintenance expenditures. This information, included in Table 6, indicates that approximately 7 to 9 percent of the total project cost is represented by maintenance expenditures, for both rigid and flexible pavements in this study.

PAVEMENT VALUE

The value of a pavement system to an agency can be expressed in terms of total cost (at some identifiable point in time) per total *EAL* carried to that point. This measure of the return on an investment is a necessary recognition of the fact that pavement systems that are designed to carry a large total *EAL* during their life span will be relatively move expensive to construct. The identifiable time for calculation of total cost per *EAL*-mile for the flexible pavement sample in this study was selected to be end of life. A majority of the rigid pavements sampled did not reach end of life; however, since these pavements have carried more than the total *EAL* designed, the cost per *EAL*-mile statistic has meaning as an index of current value to the agency.

The total project cost per *EAL*-mile calculation can be accomplished using a variety of methods, since costs and loads vary with number of lanes. Table 7 contains six formulas for calculating this information, depending on the number of lanes (two or four) and on whether cost and load data are based on critical (design) lane only, direction (roadway), or total project data per mile. The critical lane approach was selected for this study because design loads typically are calculated on the basis of the critical or design lane.

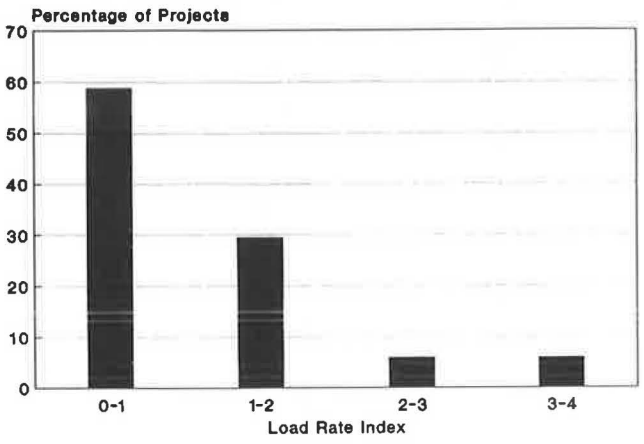

FIGURE 1 Load Rate Index for flexible pavements (end of life).

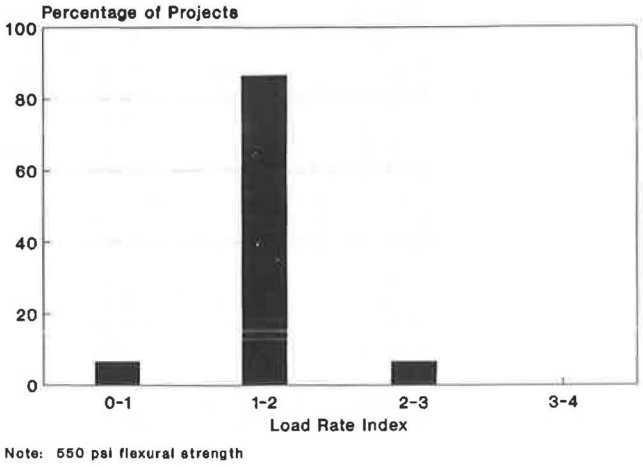

FIGURE 2 Load Rate Index for rigid pavements (survivors—10-in. pavements).

TABLE 6 PROJECT COST DATA

	Interstate Rigid (Survivors)	Secondary Flexible (End of Life)
Construction ($/mile)	134,040.81	70,222.28
Maintenance ($/mile)	7,601.18	5,234.21
Total ($/mile)	141,641.99	75,456.48
Maintenance / Total (%)	7.24	8.60
$ / EAL-mile (critical lane)*	0.01	0.12

* Note: The cost per unit load data should not be used to compare the two pavement types since they represent different road classes.

TABLE 7 FORMULAS FOR COMPUTATION OF TOTAL COST/*EAL*-MILE

Number of Lanes	Critical (Design) Lane	Directional Roadway	Project Basis
2	$\frac{\text{Total Cost / 2}}{\Sigma \text{ Actual EAL}}$	$\frac{\text{Total Cost / 2}}{\Sigma \text{ Actual EAL}}$	$\frac{\text{Total Cost}}{2 * \Sigma \text{ Actual EAL}}$
4	$\frac{\text{Total Cost / 2}}{0.9 * \Sigma \text{ Actual EAL}}$	$\frac{\text{Total Cost}}{\Sigma \text{ Actual EAL}}$	$\frac{2 * \text{Total Cost}}{2 * \Sigma \text{ Actual EAL}}$

Total Cost = Cost for 24' width per mile

The costs per unit load data provided are not appropriate methods for comparing the two types of pavement presented since they represent quite different classes of road. Unit load costs will always be relatively higher for lower-class roads because of the lower total load carried by these systems and because of the relationship between section thickness and design load (i.e., much more total *EAL* carried for an increasingly smaller additional pavement thickness).

The best use of cost per unit load data is to compare the value of pavements within the same road class that are subjected to similar total applications of *EAL*. This process could have been used, for instance, to compare flexible and rigid pavement systems on Interstate routes. However, there was an insufficient number of full-depth asphaltic concrete pavements of similar age on Interstates to permit such a comparison in this study. Eventually, as the pavement management system of the Louisiana DOTD matures, it is expected that an improved database will be available for determination of relative pavement value.

Figures 3 and 4 provide three-dimensional bar charts of project distribution considering "cost per unit load" as an indicator of relative value and the quantity "*EAL* carried/*EAL* designed" as a general indicator of design adequacy. The pavement management process within an agency can utilize project analyses such as these to determine the expected norm for a route class and to identify individual pavements within that class that vary significantly from the norm.

It becomes obvious from such examples that pavement value analysis methods utilizing life-cycle costing techniques that do not account for the actual *EAL* carried by a pavement may not necessarily represent the true value of the system to the agency.

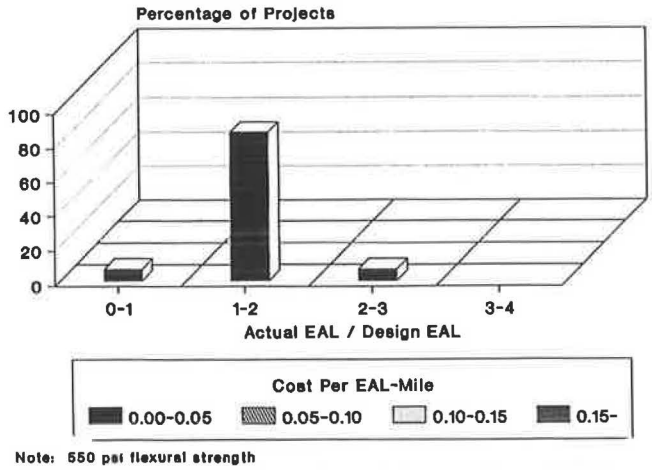

FIGURE 3 Load-cost characteristics for representative rigid pavements (sample percent).

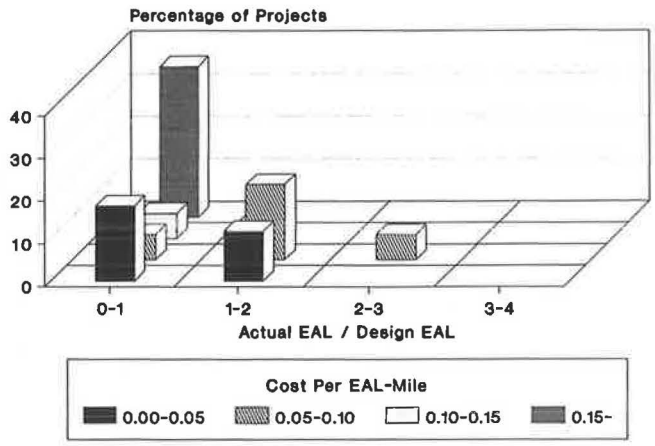

FIGURE 4 Load-cost characteristics for representative flexible pavements (sample percent).

CONCLUSIONS

An expression of the value of a pavement system to a transportation agency should ideally contain some index of the amount of total designed *EAL* carried prior to end of life. While it may be appropriate to assume that design loading rates and actual loading rates are equal for theoretical life-cycle analyses, this assumption can be misleading when evaluating actual project data.

One such indicator of relative pavement value is total cost (per mile) over the life of a pavement, expressed as a ratio of *EAL* carried prior to end of life ($/*EAL*-mile). This index will be incorporated into Louisiana's Pavement Management System as an indicator of relative performance.

The 10-in. jointed concrete pavements constructed on Interstate using early Louisiana—AASHO designs have carried their designed *EAL* and are continuing to perform after 20 years of service as of 1989. The analysis used to arrive at this conclusion effectively removed the factors of safety used in the original design procedure by associating design *EAL* with the final designed slab thickness.

The typical asphaltic concrete pavements with cement-treated bases (3.0- to 5.0-in. A.C./8.5-in. C.T.B.), designed for secondary class routes during the same period (1963–1967), were correctly designed in terms of expected rate of loading. The pavements reached end of life after approximately 14 years of service. Cracking and surface distortion associated with the performance of the cement-treated bases are believed to be the cause of the loss in serviceability.

REFERENCES

1. *AASHO Interim Guide for the Design of Flexible Pavement Structures*. American Association of State Highway Officials, Washington, D.C., Oct. 1961.
2. *AASHO Interim Guide for the Design of Rigid Pavement Structures*. American Association of State Highway Officials, Washington, D.C., April 1962.
3. W. H. Temple and S. C. Shah. *Louisiana Experimental Base Project*. Report FHWA/LA-87/192. Louisiana Transportation Research Center, Baton Rouge, Dec. 1987.
4. W. H. Temple. *Performance Evaluation of Louisiana's AASHO Satellite Test Sections*. Report FHWA/LA-79/122. Research and Development Sections, Louisiana Department of Transportation and Development, Baton Rouge, July 1979.

Publication of this paper sponsored by Committee on Pavement Management Systems.

Implementation of the 1986 AASHTO Guide at the City and County Levels

MICHAEL S. MAMLOUK, JOE O. CANO, AND EQUBAL CHARANIA

Many cities and counties have not yet implemented the 1986 AASHTO Guide, mostly because of its sophistication and wide scope. This paper provides guidelines and recommendations to narrow the scope of the guide to match the local conditions. The paper summarizes the main steps recommended by the guide for the design and rehabilitation of flexible pavements. The paper discusses some of the obstacles that might face design engineers at the city and county levels due to budget and equipment limitations. Local designers need training to adopt the mechanistic concepts of the guide, such as the use of nondestructive testing data and of resilient modulus values, the choice of reliability levels, and the use of life-cycle cost analysis. Engineering judgment and previous experience are still needed to implement the guide properly, especially during the transition between the old and new guides. The experience of the City of Phoenix in implementing the 1986 AASHTO Guide is presented.

Although the new AASHTO Guide was published in 1986, many cities and counties across the nation are still using the old version of the AASHTO Guide (1981) with or without some modifications in the design of their flexible pavements. The scope of the old guide is quite limited and does not cover all facets of pavement design and rehabilitation.

The *AASHTO Guide for Design of Pavement Structures* has been published by the American Association of State Highway and Transportation Officials in an effort to update the pavement design process (*1*). Although the new guide is still based on data obtained at the AASHTO Road Test in the late 1950s and early 1960s, the scope of the guide has been largely extended to cover many areas and applications in pavement design and rehabilitation. New mechanistic-empirical approaches have been introduced to provide better prediction of pavement life and performance. Among the new elements that the guide incorporates are the use of the reliability approach, of nondestructive testing (NDT) in pavement evaluation, of resilient modulus in material characterization, and of overlay design procedure. In fact, the new AASHTO Guide is considered one of the most comprehensive and rational handbooks currently available in the literature.

The new AASHTO Guide, however, is not the "ultimate" goal in pavement design and rehabilitation. In several design steps engineering judgment is still needed, and some assumptions have to be made. In addition, the large-volume guide and its sophisticated nature intimidate many design engineers and technicians and prevent them from fully using the available new concepts.

The objective of this paper is to assist city and county personnel in incorporating the 1986 AASHTO Guide in the design and rehabilitation of asphalt pavements. The paper sets guidelines to simplify the AASHTO Guide and reduce its scope to match local conditions. The paper discusses specific design parameters, nondestructive testing, lab testing, and computer programming that need to be considered for proper implementation of the guide. Obstacles and problems associated with use of the guide are also addressed.

The AASHTO Guide covers many areas, ranging from low-volume roads to rigid pavements. The scope of this paper is limited to design and rehabilitation of asphalt pavements.

MAIN DIFFERENCES BETWEEN NEW AND OLD GUIDES

The main differences between the 1986 version of the AASHTO Guide and previous versions, as far as flexible pavements are concerned, are as follows:

1. Consideration of the reliability concept,
2. Use of elastic (resilient) modulus in material characterization,
3. Consideration of drainage condition,
4. Consideration of the effect of frost heave, swelling soils, and thaw-weakening on pavement performance,
5. Use of NDT in pavement evaluation, and
6. Use of life-cycle cost analysis in determining the most cost-effective construction/rehabilitation strategy.

Both soil support value and regional factor have been deleted from the new guide and substituted by the effective roadbed soil resilient modulus. The following sections present the main design parameters and methods of pavement evaluation that characterize the new guide.

Reliability

The reliability of a pavement design-performance process is the probability that a pavement section designed using the process will perform satisfactorily for the traffic and the environmental conditions of the design period.

The selection of an appropriate level of reliability for the design of a particular facility depends primarily upon the projected level of usage and the consequences (risk) associated

M. S. Mamlouk, Department of Civil Engineering and Center for Advanced Research in Transportation, Arizona State University, Tempe, Ariz. 85287. J. O. Cano and E. Charania, Materials Section, City of Phoenix, Phoenix, Ariz. 85034.

with constructing an initially thinner pavement structure. In general, larger reliability values increase the required pavement thickness and its associated initial cost, and decrease the future distress-related costs (maintenance, rehabilitation, user-delay, etc.).

The reliability level varies from 50 percent to 99.9 percent. The guide recommends a set of wide ranges of reliability for various road classes. Depending on local experience and needs, cities and counties should specify more specific ranges of reliability.

When considering reliability in stage construction or "planned rehabilitation" design alternatives, it is important to consider the effects of compound reliability. The overall reliability is the product of reliabilities of all stages.

Another parameter associated with reliability is the overall standard deviation (S_o). The selection of the overall standard deviation is dependent on the variability of various factors associated with the performance prediction model, such as future traffic, soil modulus, and so forth. Obviously, the larger the variability of various performance factors, the larger the overall standard deviation and the larger the required pavement thickness. According to AASHTO, an approximate range of S_o is 0.40 to 0.50 for flexible pavements.

Traffic Analysis

Similar to that of the old AASHTO Guide, the design procedure is based on the cumulative expected 18-kip, equivalent single-axle load (ESAL) during the design (performance) period in the design lane. To convert mixed traffic into 18-kip ESAL units, the AASHTO equivalency factors can be used. Note that the load equivalency factors have been extended in the new guide to include heavier loads, more axles, and terminal serviceability levels up to 3.0 (see AASHTO, Appendix D). If the cumulative two-directional, 18-kip ESAL expected on the road is known, the designer must factor the design traffic by directions and then by lanes to calculate the axle repetitions in the design lane (W_{18}).

Effective Roadbed Soil Resilient Modulus

The basis for material characterization in the 1986 AASHTO Guide is the elastic or resilient modulus. The roadbed soil resilient modulus can either be measured in the lab using the AASHTO T274 test procedure on representative samples or backcalculated from nondestructive deflection measurements.

Figure 1 shows the laboratory device used to determine the resilient modulus of soils and unbound base and subbase materials. The device is commercially available for between $35,000 and $70,000, depending on whether it is driven by compressed air or electrohydraulic power. The compressed air-driven device can be assembled locally from its basic components.

In both lab testing and backcalculation cases, it is important to determine the elastic (resilient) modulus of the roadbed soil in the different seasons of the year, such as the wet and dry seasons. In addition to determining the seasonal moduli, it is also necessary to determine the length of time in each season during which the different moduli are effective. The effective roadbed soil resilient modulus can be determined using the procedure presented in the guide if the different moduli of the roadbed soil and the time interval associated with each modulus are known.

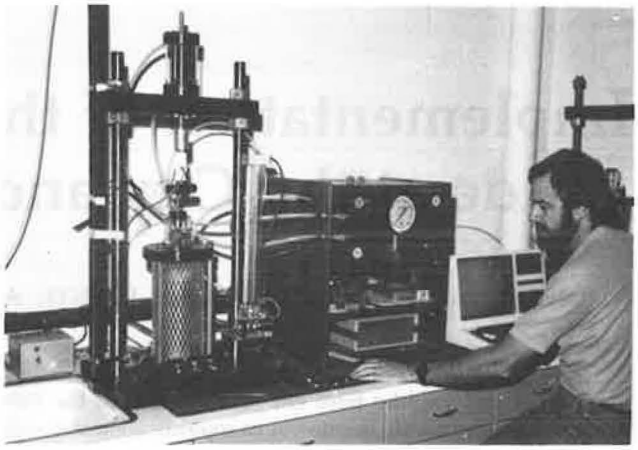

FIGURE 1 Triaxial resilient modulus machine for soils and unbound base and subbase materials.

Serviceability

The serviceability concept in the new AASHTO Guide, similar to that in the old AASHTO Guide, is still the basis of evaluating the condition of the pavement.

Structural Layer Coefficients

The new guide followed the concept of the old guide in assigning a structural layer coefficient (a_i) to each layer material in the pavement structure in order to convert actual layer thicknesses into structural number (SN). The resilient modulus has been recommended as the parameter to be used in assigning layer coefficients to both stabilized and destabilized materials. Direct lab measurement of resilient modulus can be performed using AASHTO Method T274 for subbase and unbound granular materials and ASTM D4123 for asphalt concrete and other stabilized materials (Figure 2). Layer moduli can also be backcalculated from the NDT data.

Research and field studies indicate that many factors influence the layer coefficients; thus previous experience might be used to assign the layer coefficients. For example, the layer coefficient may vary with thickness, underlying support, position in the pavement structure, and so on.

One figure was added to the new guide to convert the resilient modulus of asphalt concrete to its layer coefficient a_i. Four other charts were adopted from the old guide to convert various material properties to the layer coefficients a_2 and a_3 of granular bases and subbases as well as cement- and bituminous-treated bases. These charts, however, have to be used with caution since the correlations among various material properties might not be very accurate, as discussed later.

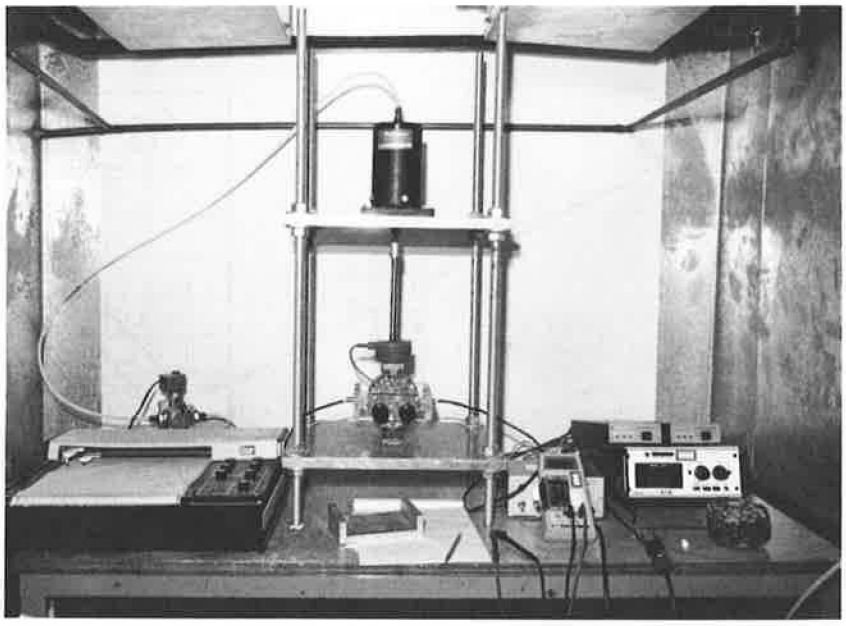

FIGURE 2 Diametral resilient modulus machine for asphalt concrete and other stabilized materials.

Structural Number and Drainage Conditions

Similar to that of the old guide, the structural number (SN) adopted is an index number that may be converted to thickness of various flexible pavement layers through use of the structural layer coefficients. The new guide, however, introduced drainage coefficients (m_2 and m_3) to modify the layer coefficients of bases and subbases, depending on the expected level of drainage in the pavement section. The guide includes a table showing the value of the drainage coefficients if both quality of drainage and percent of time when pavement is approaching saturation are known.

Design of New Pavements

The basic equation and nomograph used to design the required structural number above subgrade, subbase, and base are shown in Figure 3. It can be seen that new parameters have been introduced in the design process instead of those in the old guide, such as the reliability factor (R), overall standard deviation (S_o) and resilient modulus (M_r). Note also that the designer has the ability to design for different design serviceability losses ΔPSI where ΔPSI is the difference between the initial serviceability and the terminal serviceability. Therefore, the designer is not limited to a terminal serviceability of 2.0 or 2.5, as is the case in the old guide. Using Figure 3, the structural number above each layer can be obtained and the thicknesses of various layers can be determined.

Effect of Seasonal Variation on Performance

Improvements in the new guide have been made to adjust designs as a function of environment (e.g., frost heave, swelling soils, and thaw-weakening). If one or more of these environmental conditions are applicable, a graph of serviceability loss versus time needs to be developed under the local conditions, as shown in Figure 4. The serviceability loss due to environment must be added to that resulting from cumulative axle loads. An iteration process is needed to predict the pavement performance period under both traffic loads and environmental conditions.

Structural Evaluation of Existing Pavements

The new guide recommends the use of NDT devices such as the Falling Weight Deflectometer (FWD) or Dynaflect to evaluate the structural capability of existing pavements.

The inverse problem of determining material properties from the response of the pavement structure to surface loading is not a straightforward process. The AASHTO Guide includes two methods: backcalculation of layer moduli (NDT Method 1) and prediction of subgrade modulus (NDT Method 2). Method 1 (backcalculation) can be used with all types of loading devices, while Method 2 is applicable only to the FWD. Using the backcalculation technique, it is necessary to employ iterative schemes based on the fact that surface deflections remote from the loaded area are primarily governed by the stiffness of the deeper layers.

Several mainframe and microcomputer programs are available to backcalculate the layer moduli if the load, surface deflections, layer thicknesses, and Poisson's ratios are known. Some of the available backcalculation programs are BISDEF, ELSDEF, CHEVDEF, and MODCOMP2.

Typically, many NDT readings would be available for each pavement section. For a uniform pavement section, only a few backcalculation processes are needed. The question that arises is which NDT readings to use in backcalculation out of the many available data. Two methods are usually used: to select a "representative" reading or to use the average of all

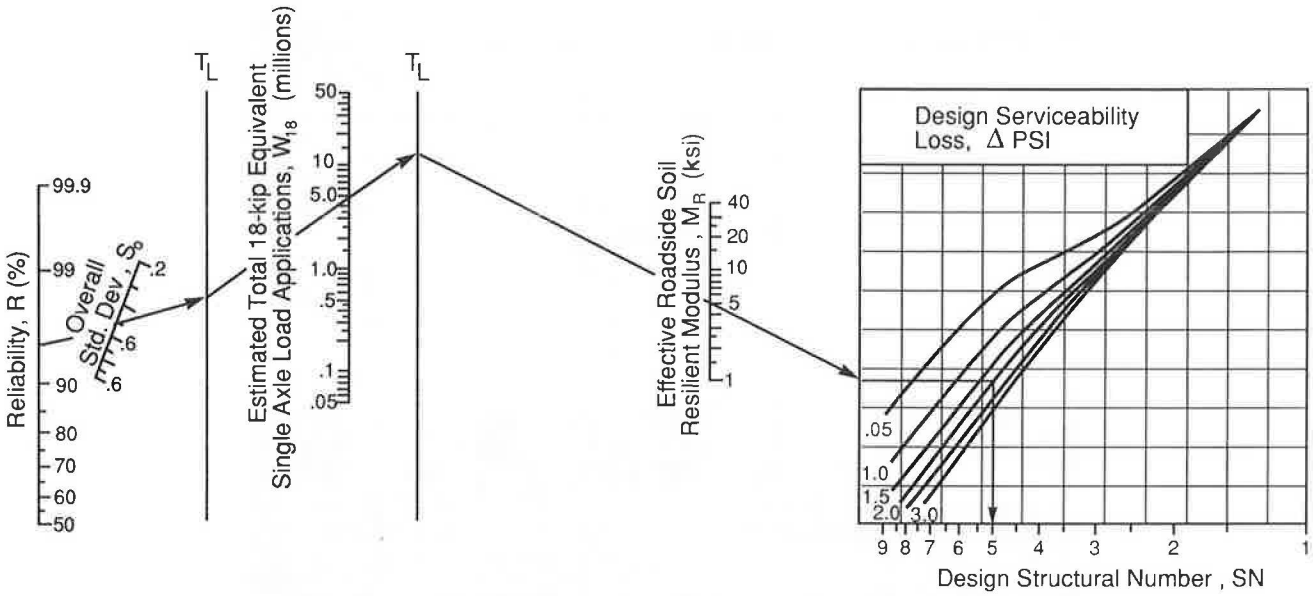

FIGURE 3 Design chart for flexible pavements based on using mean values for each input (AASHTO, Fig. II, 3.1).

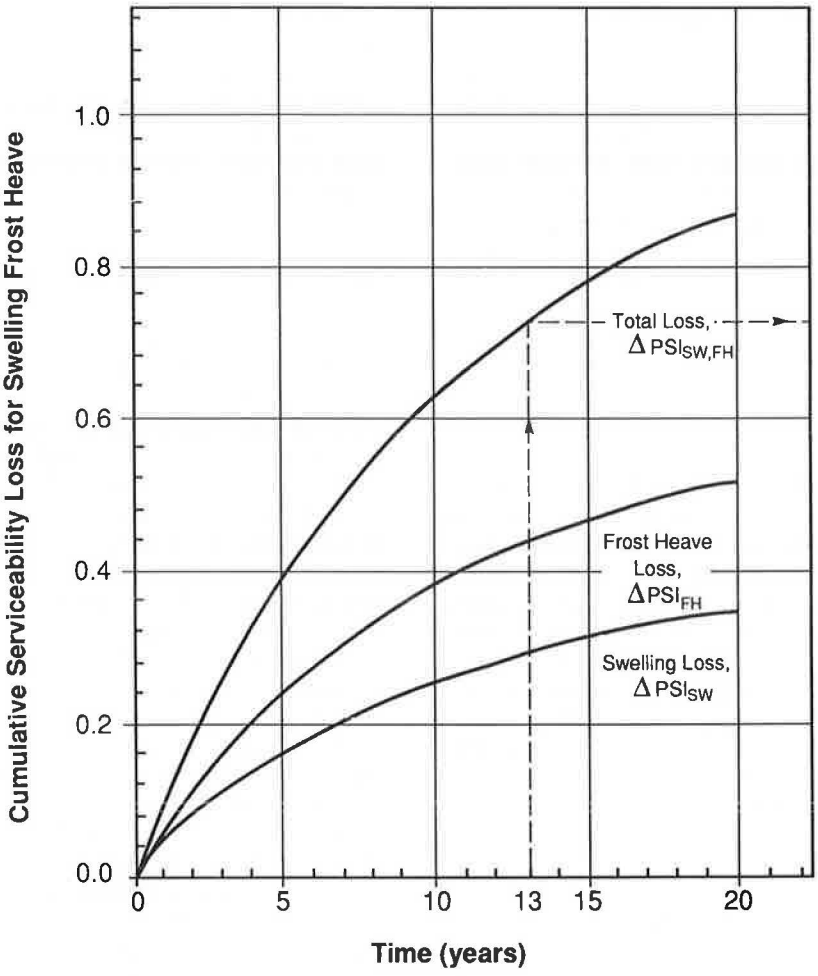

FIGURE 4 Conceptual example of the environmental serviceability loss versus time graph that may be developed for a specific location (AASHTO, Fig. II, 2.2).

readings for each geophone. The first method is recommended since the latter might result in an unreasonable deflection basin. Note that the less uniform the pavement section is, the more backcalculations would be needed. In this case, the designer should satisfy the weak spots as well as possible depending on the amount of reliability needed.

Resilient modulus lab testing can also be performed to verify the results of nondestructive testing.

Since asphalt is highly temperature-susceptible, it is important to correct (normalize) either the NDT readings or the backcalculated moduli of asphalt-bound layers to a standard temperature. The AASHTO Guide includes two procedures for correcting either the first deflection reading at the load center or the moduli of asphalt-bound layers. Correcting the deflection reading seems to be more empirical and applicable to plate-loading devices such as the FWD.

Once the layer moduli of the existing pavement structures are determined, the designer can determine the type of rehabilitation needed; if overlay is needed, its thickness can be determined.

Overlay Design

The procedure of overlay design consists of seven steps, as summarized below:

1. The rehabilitation project has to be subdivided into statistically homogenous pavement units possessing uniform pavement cross-section, subgrade support, construction histories, and subsequent pavement conditions.
2. Figure 5 shows the relationship between serviceability/structural number and traffic. The cumulative 18-kip ESAL repetitions (y) that will be applied in the design lane along the pavement section during its design life need to be estimated.
3. The material properties of existing pavement layers, subgrade, and overlay need to be evaluated. The NDT readings can be used to obtain the elastic moduli of the existing pavement layers and subgrade as discussed earlier. Limited destructive testing/sampling is encouraged to provide spot verification of the backcalculated moduli.

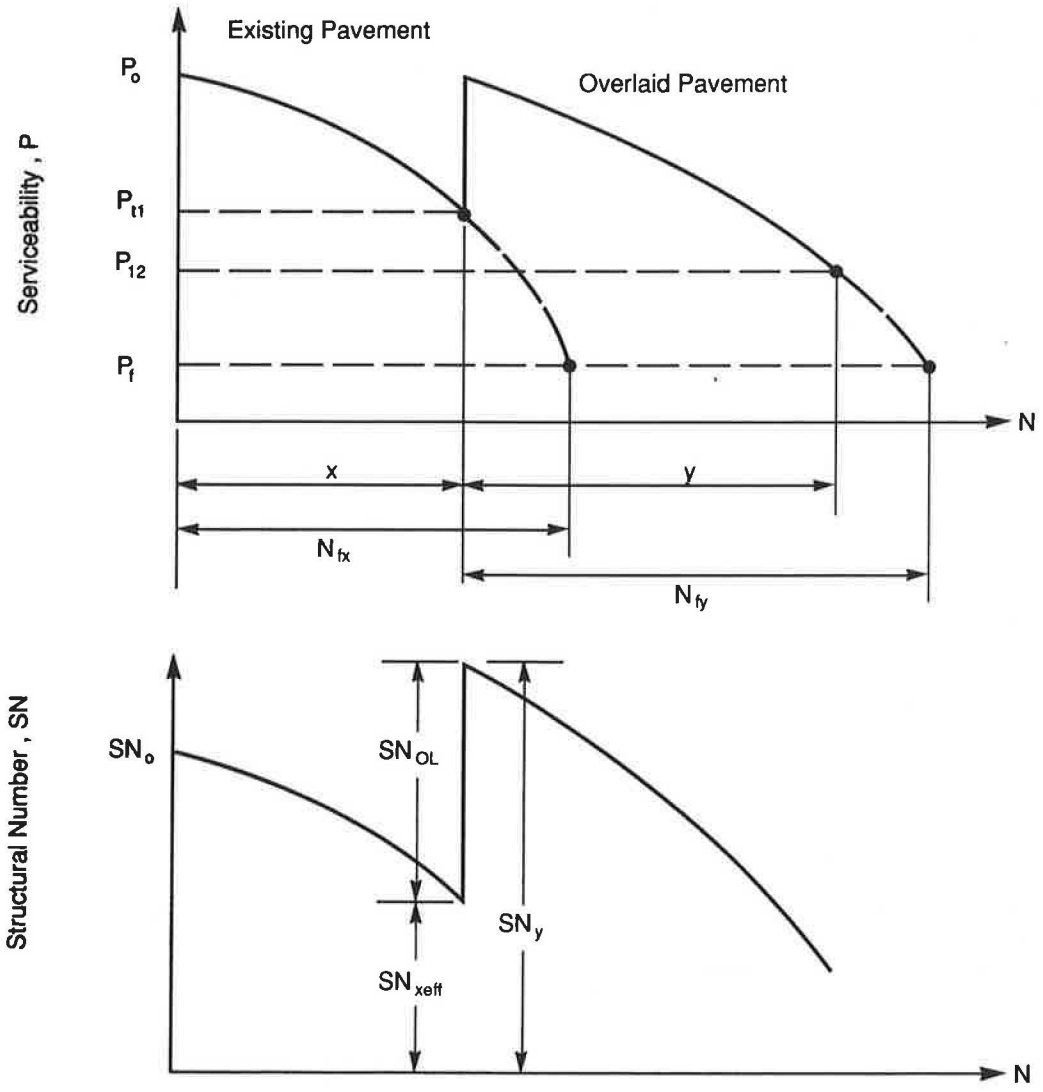

FIGURE 5 Relationship between serviceability-structural number and traffic (AASHTO, Fig. III, 5.1).

4. The effective (in situ) structural number (SN_{xeff}) needs to be determined as follows:

$$SN_{xeff} = a_1D_1 + a_2D_2m_2 + a_3D_3m_3$$

where

a_1, a_2, and a_3 are the layer coefficients of surface, base, and subbase;

D_1, D_2, and D_3 are the layer thicknesses; and

m_2 and m_3 are the drainage coefficients.

5. The required structural number of the overlaid pavement (SN_y) is determined according to the procedure used for the design of new pavements shown in Figure 3.

6. The remaining life factor (F_{RL}) is an adjustment factor applied to the effective structural number (SN_{xeff}) to reflect a more realistic assessment of the weighted effective capacity during the overlay period. This factor is dependent upon the remaining life factor (percent) of the existing pavement before overlay (R_{Lx}) and the remaining life factor (percent) of the overlaid pavement system after the overlay traffic has been reached (R_{Ly}). As a consequence, both of these values (R_{Lx} and R_{Ly}) must be determined.

Five possible methods are available in the guide to determine R_{Lx}, depending on the available data. R_{Ly} can be determined by knowing both the expected 18-kip ESAL applications on the overlay until failure using Figure 3 and the expected 18-kip ESAL applications on the overlay until the time of the next overlay.

7. The required overlay thickness, h_o, is determined from:

$$h_{ol} = \frac{SN_y - F_{RL}\,SN_{xeff}}{a_{ol}}$$

where

SN_y = structural number of overlaid pavement (Step 5),
F_{RL} = remaining life factor (Step 6),
SN_{xeff} = effective (in situ) structural number (Step 4), and
a_{ol} = structural coefficient of the overlay material.

Life-Cycle Cost Analysis

Information has been added in the new AASHTO Guide relative to economic analysis and economic comparisons of alternate designs based on life-cycle costs. The objective of the life-cycle cost analysis is to achieve the maximum economy within a project. For example, should the pavement be designed to last for 10 years and then overlaid afterward or for only 7 years before the next overlay (see Figure 6)? Obviously, the first strategy (10-year life) requires larger pavement thickness and consequently larger initial construction costs than the second strategy (7-year life). On the other hand, the second strategy will require earlier resurfacing, earlier traffic control during resurfacing, and more frequent time delays for users, and it may entail more maintenance costs. The choice between these two alternatives and others should depend not only on the initial construction cost but on all costs (and benefits) that are involved in provision of the pavement during the analysis period.

There are several methods of economic analysis that can be used to compare alternatives. One of the common methods is the present worth method; it compares alternatives after discounting all future costs to their present worth using an appropriate discount rate.

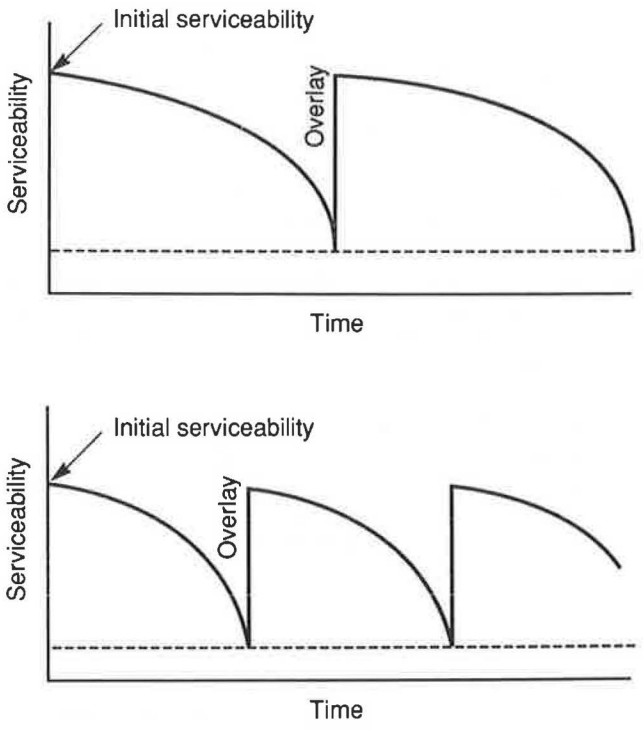

FIGURE 6 Performance curves for two initial pavement structural sections and subsequent overlay strategy alternatives.

OBSTACLES FACING SMALL AGENCIES AND POSSIBLE SOLUTIONS

Several obstacles exist that make implementation of the new AASHTO Guide difficult for some highway agencies, especially at the city and county levels. Some of these obstacles are discussed in the following sections.

Nondestructive Testing (NDT) Equipment

Some highway agencies at the city and county levels do not own any NDT devices, while others own Benkelman beams or Dynaflects. Obviously, Benkelman beams are obsolete, while Dynaflects apply light loads with a specific frequency that do not match the load applied by heavy trucks. Very few cities or counties, if any, own FWDs.

The fact that FWD devices are not available should not prevent cities and counties from using the concepts in the new AASHTO Guide. The Dynaflect results, if available, can still be used to backcalculate the layer moduli with reasonable accuracy. Typical material properties and correlation from previous experience can also be used in lieu of NDT.

Laboratory Resilient Modulus Testing

The new AASHTO Guide calls for some asphalt concrete, base/subbase, and subgrade resilient modulus testing accord-

ing to ASTM D4123 and AASHTO T274 procedures. Since these tests are very sophisticated and require a great deal of experience, most cities and counties do not have the test equipment or the personnel qualified to perform these tests.

One of the solutions to this problem is to contract some tests on typical local materials to commercial labs. Correlations provided in the guide or other correlations developed by research agencies can also be used to estimate the material modulus from the results of other commonly used tests, such as *CBR* and *R*-value tests.

It should be noted, however, that the correlations available in the AASHTO Guide and in other references between the resilient modulus and other material properties are generally poor. The main reason for these poor correlations is that each test measures a specific material property, and different properties of the same material may not be well correlated. For example, Marshall stability and flow values are empirical parameters related to the resistance of the asphalt concrete material to deformation under certain temperature and loading conditions, while the diametral resilient modulus (ASTM D4123) is a measure of the elastic stiffness of the material under different conditions. Likewise, the *CBR* value is an empirical measure of the ratio of penetration resistance of the soil to that of a standard rock material under specific conditions, while the triaxial resilient modulus (AASHTO T274) is a measure of the elastic stiffness under certain confining and deviator stresses. Trying to correlate these properties may be like trying to correlate the color of a material with its strength. In a few cases, reasonable correlations might be obtained, but in most cases the correlations would be poor.

Backcalculation of Moduli

There is no "closed-form" solution to calculate the layer moduli of a multilayer pavement system if the surface deflections and layer thicknesses are known. Therefore, an inverse or "backcalculation" process is commonly used in which initial layer moduli are assumed and an iteration process is used to adjust these moduli until the computed deflections match the measured deflections. This process is an "ill-conditioned" problem in which no unique solution is guaranteed. Thus, any error in deflection measurements or in load and system modeling (i.e., static load, linear elastic isotropic behavior, and assumed Poisson's ratio) is magnified and reflected in the results. Also, self-compensation among layer moduli may develop, which may result in several possible solutions.

Another problem with backcalculation of moduli is the assumption of a homogeneous semi-infinite subgrade in some cases or a bedrock (or rigid layer) at a specific depth. Actual conditions in the field may not exactly match one of these two extreme cases. The stiffness of the subgrade material usually increases with depth, with no consistent trend. Thus, the backcalculation process results in an "equivalent subgrade modulus" if a semi-infinite subgrade is assumed or an "equivalent subgrade/bedrock modulus" if a bedrock is assumed at a specific depth. This difference between the actual and the idealized backcalculation cases explains the disagreement found between the laboratory-obtained subgrade modulus and the backcalculated subgrade modulus in many cases. The lab modulus represents the subgrade modulus at a specific depth, while the backcalculated modulus represents a weighted average subgrade modulus. These two moduli may not necessarily be the same in most cases.

Until the problems associated with backcalculation are solved, the design engineer should use the backcalculation results as rough estimates and may modify them if they are unreasonable.

Need for Training and Engineering Judgment

The transition between the old and new guides is not expected to be sudden. Design personnel must practice use of the new guide and design a number of projects using both guides to understand the difference between the two design concepts.

It should be noted that the pavement design process is in a continuously evolving process. Some problems still exist that are beyond the ability of current pavement literature. For example, the resilient modulus is not always well correlated to other material properties, the backcalculation process is not always accurate, and temperature correction is not very accurate. Therefore, the new guide should not be treated as a "black box" or a "cookbook" that can be applied without thinking. Engineering judgment and previous experience are always needed to guarantee sound engineering designs.

CITY OF PHOENIX EXPERIENCE

A study has been performed by the authors at Arizona State University for the City of Phoenix to simplify the 1986 AASHTO Guide for its direct use by city personnel. The City of Phoenix covers a large road network ranging from principal arteries to local streets. Previously, the city's personnel followed the old (1981) version of the AASHTO Guide in the design of city streets (*2*).

The study included selection of typical flexible pavement sites, Dynaflect testing, material sample acquisition, laboratory resilient modulus testing, and backcalculation of layer moduli. A report simplifying the AASHTO Guide for local use and a final report presenting the study results have been prepared (*3,4*).

The first step in the study was to consider specific conditions in Phoenix, such as the following:

1. No freeze or thaw develops;
2. Swelling of soils is neglected;
3. The Dynaflect is currently the only available deflection device;
4. Resilient modulus equipment for asphalt concrete and soil is not available; and
5. The in situ moisture content of the subgrade is close to the optimum moisture content and is fairly constant throughout the year unless an external problem exists, such as a leaking irrigation ditch or broken water line.

Computer Programming

Four microcomputer programs have been developed to solve several AASHTO equations using the Lotus spreadsheet program. These computer programs can be used to determine the required structural number, the cumulative ESAL until

failure, and the required overlay without the need for nomographs.

Development of NDT and Backcalculation Strategy

A strategy was developed for using the available Dynaflect to evaluate the structural condition of existing pavements. Two computer programs were recommended to backcalculate the moduli: CHEVDEF (mainframe) and ELSDEF (microcomputer) (*5*). Typical pavement sections have been tested, and moduli have been estimated. A set of rules and guidelines has been developed to be followed by city personnel in running the programs.

Resilient Modulus Soil Testing

Eight soil samples were tested for resilient modulus at Arizona State University, according to the AASHTO T274-82 test procedure. City personnel provided the disturbed soils, which were taken from five bore holes at 75th Avenue (B-5, B-7, B-9, B-12, and B-15). Five samples (one from each bore hole) were compacted in the lab, matching 95 percent of the maximum dry density (AASHTO T99) and the optimum moisture content. Each sample was compacted in ten layers to guarantee uniform density. After the test was completed, both density and moisture content were determined in the lab to compare the actual with the target values. The other three samples were taken from bore holes B-5, B-9, and B-15 and were compacted in a saturated condition to match the density and the moisture content of the *R*-value test samples. Figure 7 shows a typical example of test results.

Lab Moduli Versus Backcalculated Moduli and *R* Values

To determine the laboratory resilient modulus corresponding to the in situ condition, the octahedral normal stress and octahedral shear stress (*6*) in the field were computed using the Chevron program (*7*) at the top of the subgrade due to a load of 9000 lb. By matching both octahedral normal and shear stresses in the lab and field, the resilient modulus in the lab can be determined. Table 1 shows the lab moduli, backcalculated moduli, and *R* values. Note that the backcalculated moduli are in the in situ condition, while *R* values are at the saturated condition. No good correlations could be derived, mostly because of the small number of observations and because the resilient modulus and the *R* value are different and uncorrelated parameters.

Development of Typical Design Parameters for City of Phoenix

The 1986 AASHTO Guide includes a wide range of design parameters to cover all climatic, traffic, and material conditions. In this study, specific ranges of design parameters applicable to the City of Phoenix were recommended mostly through the experience of city personnel. Among these parameters

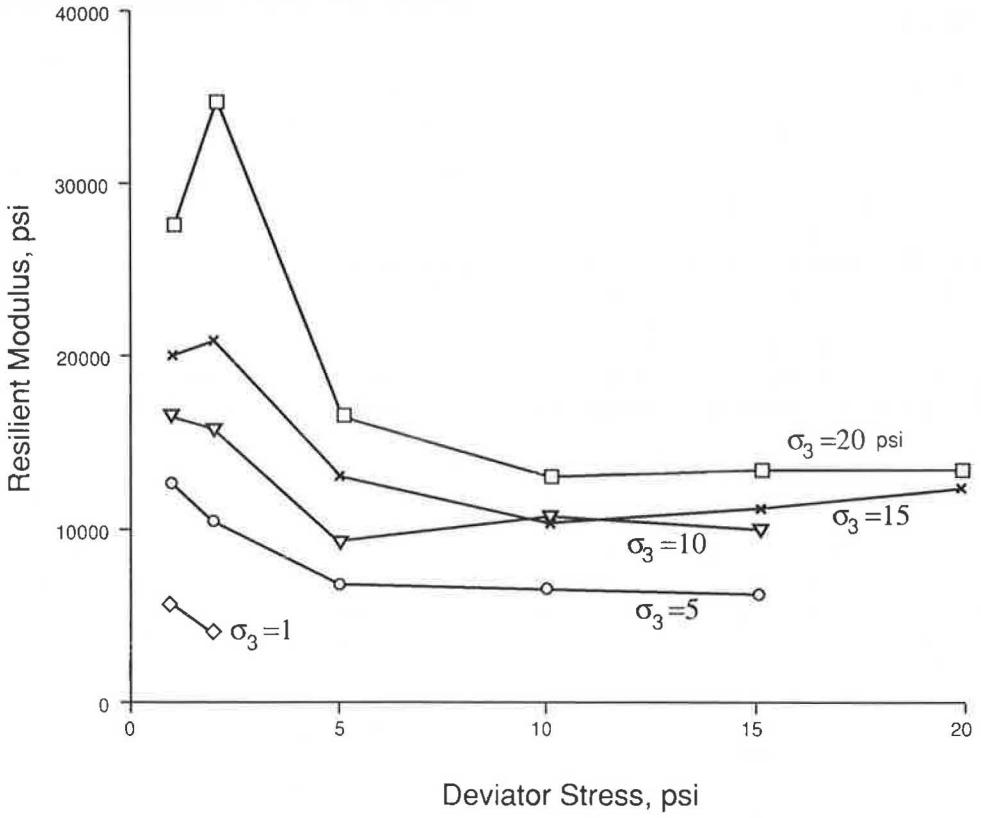

FIGURE 7 Typical resilient modulus test results on subgrade materials according to AASHTO T274 procedure.

TABLE 1 COMPARISON BETWEEN SUBGRADE LAB MODULI, BACKCALCULATED MODULI, AND *R* VALUES

Boring No.	Material Type	Condition	Lab E(ksi)	Back-calculated E(ksi)	R-Value
5	SM	In-Situ	25	19	--
		Saturated	21	--	55
7	SM	In-Situ	24	23	--
		Saturated	--	--	24
9	SM	In-Situ	16	30	--
		Saturated	25	--	38
12	ML	In-Situ	8	19	--
		Saturated	--	--	17
15	ML	In-Situ	11	19	--
		Saturated	8	--	47

are reliability levels, overall standard deviation, lane distribution factors, structural layer coefficients, drainage condition coefficients, and minimum layer thicknesses, as discussed in the following paragraphs.

Reliability

To reduce the amount of risk in pavement performance, the City of Phoenix recommends the use of reliability levels of 95 percent for principal arteries, 90–95 percent for collectors, and 80 percent for local streets. Continuous monitoring of pavement conditions, together with the use of pavement management programs, is recommended for further optimization and refinement of these reliability levels. In addition, the City of Phoenix recommends, based on historical experience, a typical standard deviation of 0.4 for flexible pavements.

Traffic Analysis

The average daily traffic (ADT) for the design period is predicted by the city Streets and Traffic Department. The classification of vehicles is obtained from the weigh studies conducted by the Arizona Department of Transportation.

Effective Roadbed Soil Resilient Modulus

Based on historical data, it was found that the in situ moisture content of subgrade materials in Phoenix does not significantly change from one season to another; it remains fairly close to the optimum moisture content. In addition, the rainy season in Phoenix is very short. Therefore, it was recommended that the effective roadbed soil resilient modulus could be assumed to be equal to the resilient modulus measured at any time of the year. Following this recommendation significantly reduces the effort made in determining the effective modulus throughout the year.

It was also recommended that there is no current need for the city to acquire costly resilient modulus machines or an FWD device. In the future, when these devices are better established and less expensive, the city might consider obtaining them and training its personnel for their use.

Structural Layer Coefficients

If the elastic modulus and/or other material properties are known, the charts in the AASHTO Guide can be used to estimate the structural layer coefficients a_1, a_2, and a_3 for surface, base, and subbase materials, respectively. If no previous data are available, the City of Phoenix recommends the following structural coefficients:

Pavement Component	*Structural Coefficient*	*Range*
Plant-mixed asphalt concrete and recycled AC:		
3 in. or less	0.40	0.40–0.44
4 in. or more	0.42	0.40–0.44
Cement-treated base	0.27	0.15–0.29
Aggregate base	0.12	0.08–0.14
Select material	0.11	0.05–0.12

Drainage Coefficients

In Phoenix, the typical time during which pavement is exposed to moisture levels approaching saturation is less than 1 percent. Also, the quality of drainage varies from "excellent" to "good." Therefore, the m_2 and m_3 values vary from 1.25 to 1.40, as recommended by the AASHTO Guide.

Minimum Layer Thicknesses

Considering the specific climatic conditions and stop-and-go traffic in the city streets, the following are provided as min-

imum practical thicknesses for various pavement courses. (Note that in a CTB design 5-in. minimum aggregate base thickness is required.)

Pavement Component	*Minimum Thickness (in.)*
Major Streets	
Asphaltic concrete	5
Cement-treated base (CTB)	6
Aggregate base	4
Select material	4
All Other Streets	
Asphaltic concrete	2
Cement-treated base (CTB)	6
Aggregate base	4

Impact of the Use of the 1986 AASHTO Guide in Phoenix

On the basis of the preceding investigations, the City of Phoenix adopted the 1986 AASHTO Guide for the design of city's streets in August 1988. Since then a number of streets have been designed using this new design procedure. For the initial period pavement designs of the streets using both the new AASHTO 1986 and the old AASHTO 1981 procedures are being carried out. It has been determined that both designs are comparable for streets with coarse sand and gravel subgrades. For streets with silt and clay subgrades, however, the new designs result in a reduction in the required pavement thickness of approximately 15 to 20 percent. This difference is due mainly to the use of a rather conservative resistance R value to characterize the subgrade material when the old guide was used, whereas the soil modulus backcalculated from the Dynaflect test was used in the new guide. This indicates that the new guide may provide some saving in the initial cost of pavement materials when compared to the old guide as previously used by the city.

Also, since the new guide is based on more rational concepts than the old guide, it is believed that the new guide will provide better prediction of pavement performance than did the old guide.

CONCLUSIONS

Cities and counties that currently follow the old version of the AASHTO Guide can gradually adopt the 1986 guide for the design and rehabilitation of their streets. This paper provides guidelines and recommendations to simplify the task of design personnel in adopting the guide. Specific conditions that are locally applicable should be considered in order to reduce the scope of the guide. Training is needed by local designers to adopt concepts of the guide, such as use of NDT data, use of resilient modulus values, choice of reliability levels, and use of life-cycle cost analysis. Engineering judgment and previous experience are still needed to overcome obstacles that might arise at city and county levels.

ACKNOWLEDGMENTS

The authors would like to thank City of Phoenix personnel Syn Anderson and Dong-Chie Wong for their valuable input and assistance during the course of the project. The City of Phoenix is also acknowledged for its financial support of this study. Sincere thanks go to Masood Mirza, who performed the resilient modulus tests. Finally, thanks also go to the Center for Advanced Research in Transportation and the Department of Civil Engineering at Arizona State University for making their facilities available for this study.

REFERENCES

1. *AASHTO Guide for Design of Pavement Structures*. American Association of State Highway and Transportation Officials, Washington, D.C., 1986.
2. *City of Phoenix Pavement Design*. City of Phoenix Materials Division, Phoenix, Ariz., Jan. 1985.
3. M. S. Mamlouk. *Simplified AASHTO Design Method of Flexible Pavements for City of Phoenix*. Report, Contract 47961, P-875518, submitted to City of Phoenix, Materials Division, June 1988.
4. M. S. Mamlouk. *Pavement Evaluation Study*. Final Report, Contract 47961, P-875518, submitted to City of Phoenix, Materials Division, July 1988.
5. A. J. Bush III. *Nondestructive Testing for Light Aircraft Pavements*. Phase II. U.S. Army Corps of Engineers, U.S. Army Engineer Waterways Experiment Station, Vicksburg, Miss., Nov. 1980.
6. R. D. Holtz and W. D. Kovacs. *An Introduction to Geotechnical Engineering*. Prentice-Hall, Inc., Englewood Cliffs, N.J., 1981.
7. J. Michelow. *Analysis of Stress and Displacements in N-Layered Elastic System Under a Load Uniformly Distributed on a Circular Area*. California Research Corp., Richmond, Calif., Sept. 1963.

Publication of this paper sponsored by Committee on Pavement Management Systems.

Implications of Life-Cycle Performance Specifications

DEMETRES A. VLATAS AND ROGER E. SMITH

The professional, managerial, and legal implications of using life-cycle performance specifications are presented. Changes in the roles of the parties using life-cycle performance specifications are discussed. Life-cycle performance specifications are a cost-effective means of procuring highway pavements that will provide satisfactory service over their design life. This approach can improve quality, reduce costs, and expedite the construction process. The basis of the process is the development of models of expected performance. These models will be used to predict whether the pavement will perform as required over the life of the project. Tests are performed at the end of construction to determine whether the expected performance is likely to be achieved. Adjustments in payment can be made, based on the performance model predictions. The ramifications of adopting life-cycle performance specifications are discussed.

People want more for their money—better quality for the same amount or less. Life-cycle performance specifications have been proposed as a means of accomplishing this objective in highway pavement construction. Normally, highway pavements are constructed using prescriptive specifications. Prescriptive specifications define what is to be done, when and how it will be done, who will do it, and the materials to be used. Performance specifications can be either end-result specifications or life-cycle specifications. An end-result specification defines the desired properties of the component or project at the end of construction by means of a set of defined criteria. If the criteria are met at that point, the component or project is acceptable. A minimum acceptable level of roughness in a new pavement is becoming a common end-result specification in the pavement industry. Life-cycle performance specifications define the function of the component, facility, or pavement: what it is to be used for, what it must be able to do, the period of that performance, and an acceptable range of performance parameters that must be met during the life cycle or period of performance.

A major pitfall in using prescriptive specifications is that under the Spearin Doctrine (United States v. Spearin, 248 U.S. 132 [1918]), which is the prevailing law in forty-nine states and for federal construction, it is implied that the owner warrants the adequacy of the plans and specifications to the contractor. Where the component, facility, or project is constructed according to those plans and specifications, the owner has no recourse against the contractor over the quality of workmanship expected, even if the constructed product is unacceptable or will not function.

Department of Civil Engineering, Texas A&M University, College Station, Tex. 77843.

Owners can avoid the implied warranty by specifying the properties desired with an end-result specification. By doing so, however, they lose control of the design. For example, end-result specifications are frequently used for air-conditioning and heating systems, where a set of desired performance criteria is furnished to the contractor, who is free to find a system that will meet those criteria. On a competitively bid, fixed-price contract, the contractor will undoubtedly find the system that will meet the specified performance requirements at the least cost to the contractor and to the owner. In these situations, it is imperative that owners properly define their minimum acceptable requirements, because they are rarely given more than they request.

With an end-result specification, performance is measured at the time of acceptance. After acceptance, the responsibility of the contractor for the performance of the system or component is limited to what was agreed upon in the contract, or to warranties provided by law. Moreover, if the system ceases to perform as specified, the period in which the owner can look to the manufacturer for relief is generally limited to the warranty period in the contract.

Life-cycle performance specifications have been proposed as means of enabling owners to ensure that acceptable performance is obtained over the intended useful life of the system, component, or facility. There are many difficulties associated with developing and using life-cycle performance specifications. One difficulty is how to ensure performance over a design life of 20 or more years. Others lie in establishing the acceptance criteria and, last, the testing procedures to be used to determine whether the criteria have been met.

NEED FOR PERFORMANCE SPECIFICATIONS

Owners may want to adopt a life-cycle performance specification approach for the following reasons:

1. To shift the risk of performance to the contractor. It is implied that the owner who provides plans and specifications to a contractor warrants the adequacy of the plans and specifications. This is commonly referred to as the "Spearin Doctrine." After construction is completed, if the project does not work, or does not work as desired, the contractor cannot be held accountable. By specifying performance, it becomes the contractor's responsibility to ensure performance.
2. To obtain the most cost-effective design. By specifying performance, the owner will receive competitive bids that will meet the performance requirements. The owner will thus have the performance he or she specified at the lowest cost.

3. To spend more time defining objectives and needs. Owners will devote their time to defining their objectives and needs, rather than on design and writing specifications addressing materials and procedures for the contractor to follow.

4. To select from the best thinking of several designers. The contractors can engage different designers to develop the best way of providing the specified performance at lowest cost. The owner will have the benefit of the thinking of several designers, rather than only one.

DRAWBACKS TO OWNERS

Loss of Control Over Design

While owners can avoid the implied warranty by specifying performance, they lose control of the design. The contractor is furnished a set of desired performance criteria and is free to find a system that will meet those criteria. On a competitively bid, fixed-price contract, the contractor will undoubtedly find the system that will meet the specified performance requirements at the least cost to the contractor and to the owner. It is imperative, in these situations, that owners properly define their minimum acceptable requirements, because the materials selection, structural design, and construction techniques are the responsibility of the contractor.

No Guarantee of Performance After Acceptance

With an end-result specification, performance is measured at the time of acceptance. Life-cycle performance specifications have been proposed as a means of enabling owners to ensure that acceptable performance is obtained over the intended useful life of the system, component, or facility. In the pavement area, with a long life and a volatile environment in which contractors come and go over the expected life of the pavement, the expected method of determining the life-cycle performance would be the use of predictive models. If the pavement properties at the end of the construction are placed in the model and the projected life is equal to or greater than required, based on a predetermined reliability level, the pavement would be acceptable.

Implementation Difficulties

There are several major difficulties associated with developing and using life-cycle performance specifications. One is in the area of contractor selection. Other major problems center on the development of procedures to ensure performance over a design life of 20 years or more, establishment of the acceptance criteria, and finally the testing procedures and equipment to be used to determine whether the criteria have been met.

Higher Design Costs

It must be stressed that owners will not avoid the cost of design; indeed, their costs may be higher for the following reasons.

- Owners will still have to go through the process of scope definition, specification preparation, criteria selection and definition, identification of testing procedures and methods, and possibly development of testing equipment, with either in-house staff or an outside engineering firm.
- The contractor will include the cost of design in the bid. Owners will pay for the cost of design and for the contractor's usual markup for overhead and profit attributable to the cost of design.
- Owners may have to pay for the cost of conceptual design for all bidders. Some contractors may be reluctant to bid competitively on performance specification work where they may have to bear the cost of initial or conceptual designs. A possible solution is to have the client pay for the expense of the conceptual design for all bidders. If this happens, owners will be obliged to develop a procedure to screen potential bidders to limit their bid list significantly and, thereby, limit their costs. The U.S. Department of Defense does this now in aircraft procurement competitions. However, this may prove difficult to do in public works where laws dictate that bids must be accepted from all responsible and responsive bidders.

NEW ROLES

If, with life-cycle performance specifications, the contractor determines what the final product will be, what are the roles of the owner, engineer, or designer?

Role of the Owner

Owners commission the work to be performed. They decide the scope of the work and specify the performance required. They must also define how the required performance will be measured.

Role of the Contractor

Contractors must now become the designers and optimizers. They must still develop the lowest price bid or they will not get the job. But they must now determine whether they can provide the performance specified and do it by the least costly means of accomplishing the work. It will be up to the contractor to decide how best to accomplish the work, the materials to be used, and whether it will be possible to meet the performance requirements within the cost parameters necessary to win the bid.

Role of the Engineer

An engineer may continue to work for the client, where his or her new role will be to determine when, where, and how to use life-cycle performance specifications for a project; or an engineer may work with or for a contractor in developing the design to meet the performance requirements specified.

Engineer for the Owner

The owner's engineer will not design that portion of the project to be procured by means of life-cycle performance spec-

ifications. Instead, he or she will have to determine what the owner really needs, envision the performance required, establish the criteria by which achievement of performance will be determined, identify models or predictors of desired performance, and develop acceptance procedures (tests, testing criteria, and testing procedures) to establish whether the performance criteria established for the predictors have been met. Another major task facing the owner's engineer will be the determination of predictors of long-term performance. This will involve a major long-term testing program examining many different roadway surfaces, designs, bases, and material components and the mix of such components under different environmental conditions. The engineer will then establish the performance requirements to be furnished to potential contractors for bidding purposes. In addition to furnishing this information to the contractors, the engineer will have to develop criteria to be used to select the best proposal. These criteria must also be shared with the contractors so that they may know the standards against which they are to be judged.

Engineer for the Contractor

The engineer's client may no longer be the owner. The contractor's engineer will do the design, as the owner's engineer did before. Because of the partnership with the contractor, however, it is expected that constructability will be incorporated into the design, as well as innovative concepts based upon a value engineering approach to design necessitated by competitive bidding. The engineer may also face conflicts of still owing a duty to the owner, even while working for the contractor. The contractor's demands on the engineer may affect decisions in critical areas of design. Engineers will have to make their decisions based upon their best professional judgment.

CONTRACTOR SELECTION PROCESS

The contractor's bid will include the cost of the work and the contractor's design. The owner's engineer will have to evaluate the designs to determine which are acceptable. The criteria for design evaluation must be included in the Invitation for Bids so the contractors will know what they must do to prepare an acceptable design. Designs that are unacceptable will be excluded from further consideration. The remaining bids can then be evaluated on the basis of cost. Since all of the remaining designs are acceptable, the low bidder would appear to be the obvious selection. Appearances, however, may be deceiving. The low bidder of all of the acceptable designs may not be the most cost-effective. The designs may not be equivalent; some will be better than others. Some of the better designs will cost more than some of the lesser designs. What will be needed will be a means to evaluate the designs on a comparable basis, since one design may give a longer performance prediction than another one that costs less. Unit costs are routinely used in prescriptive specifications; a cost per year of service standard could be applied, with some minimum life required.

DEFINING AND ENSURING PERFORMANCE

A major task in developing life-cycle performance specifications is devising what will be considered an acceptable product and ensuring that it is achieved. The simplest approach is to define required performance and require a warranty to cover the design life. For a flexible pavement, an example might be that the pavement would not reach a PSI of less than 2.5, develop ruts greater than ½ in., or develop fatigue cracking over more than 3 percent of the traveled surface in fewer than 5 million equivalent single-axle loads. There is no assurance, however, that the contractor will still be in business after 12 or 13 years, should problems develop at that time.

Another approach is to develop models that predict the performance of the pavement. These models must then reliably predict performance based on properties that can be measured at the end of construction. These could include a measure of built-in defects, such as PSI; as well as properties used in the predictive equation, such as a measure of strength; items that indicate durability, such as air voids; items that indicate environmental effects, such as temperature susceptibility; and so on. At the end of construction, the owner would measure these properties and use them in the model to determine if the desired life is predicted. If it is, then the pavement is accepted. This approach differs from the end-result specification in that any combination of the measured variable in the predictive model that indicates satisfactory performance is acceptable. The concept of using a predictive model requires that reliable performance of pavements be established on the basis of parameters that can be measured at the end of construction. The variance must also be established so that the owner can specify the life and define the level of reliability desired.

A warranty, however, is only as good as the entity standing behind it. It is apparent that the time span during which a contractor can be held accountable is limited. With a design life of 20 or 25 years, who is to say that the contractor will still be in business when something goes awry? A large equipment manufacturer might possibly have more staying power than the contractor; but again, nothing is certain. An insurance policy to pay for any needed repairs might be prohibitively expensive, and the cost of the premium for such a policy would be passed on by the contractor to the owner. A lump sum amount might be retained from the contract amount, placed in escrow at project completion, and invested to provide funds in the event of needed repairs. The profit margin in pavement construction, however, has historically been relatively low, and the cost of added retainment would probably be passed on to the owner.

To make life-cycle performance specifications work, it is necessary to incorporate the concepts of control theory into the specification. Control always begins with an objective (*1*, p. 12). The objective must be measurable, if possible. Development of a control strategy includes the establishment of the following components:

- Predictors of results. It is often possible, by means of analysis or experience, to say that a particular result or objective will come to pass if something happens, or fails to happen. If it does not rain in the Midwest in May and June, then the corn crop will be 60 percent of normal in September; if an

NFC team wins the Superbowl, the stock market will go up for the remainder of the year; and so forth.

- Par. Par is the measurable value established for each objective that indicates whether the objective is achieved or not. In golf, for example, par is the number of strokes necessary to get the ball into the cup for each hole. In highway construction, it may be that a particular test value is obtained when concrete is tested, in situ. If the test value is less than what is considered acceptable, then the concrete is considered to be below par. This test may be conducted in several different locations and possibly at several different times. The values obtained would be compared against a standard—the par for that test in the context of that particular project.
- Assignment of responsibility to achieve par.

Scope definition of a project establishes the functions that a facility or highway is to perform. The better the definition of the scope, the better the design and the better the plans and specifications.

It has been shown that most savings in a project are made as a result of changes during the design period. It is difficult to value-engineer a project during design. Performance specifications and competitive bidding can be used to achieve similar results. The contractors will develop novel means of achieving the desired performance, and because they are bidding against each other, the price of achieving the performance will be low.

NO FREE LUNCH

Contractors will not prepare designs to meet performance specifications at no cost to the owner. The contractor's costs incurred in preparing the bids will be charged to the owner in the bid price of the successful bidder. The design costs of the unsuccessful contractors will be paid by other owners in the form of higher overhead costs.

INSPECTION AND TESTING

Who Does the Testing?

Testing can be performed by the owner (or the owner's agents), by the contractor, or by an independent testing laboratory.

Cost of Testing Equipment

The cost of testing equipment may be the determining factor in who is to do the testing. If the equipment cost is so high that it would be unlikely that one contractor would be willing to purchase it, or that a group of contractors would each be willing to purchase such equipment on a one-time basis, the owner or an independent testing agency would need to conduct the tests. Leasing the equipment may be possible, but the leasing company would obviously want to be sure of having enough business to justify their expenditure.

DUTY TO INFORM—WARN

After the results of tests during construction, does the owner have a duty to tell the contractor that the contractor's final product will not be acceptable? Does the answer depend on the stage at which the tests were conducted—that is, at a point where it is too late to make changes or one where changes to make the product conform can easily be made? Where the owner had knowledge that would have made a significant difference in the contractor's actions and, hence, the end result had the owner passed that knowledge on to the contractor, will the owner be estopped from raising the issue that the product will not meet the specification?

Duties are created by

- Contractual agreement,
- Gratuitously volunteering to undertake, and
- Operation of law, a requirement of statute.

In this instance, the owner may or may not undertake a contractual duty to keep the contractor informed of the quality and/or status of the work as it progresses. A court could find an implied duty on the part of the owner to tell the contractor if the product is unsatisfactory before the contractor proceeded too far. The question of whether the owner is correct or not may arise. In this discussion, "correct" refers to the interpretation and conclusions drawn from the test results, rather than to the values obtained in the test results. If the owner mistakenly tells the contractor that, based on the tests, the work is unacceptable, then the contractor may have a cause of action against the owner for negligently interfering with the conduct of the work.

CONVERSION TO PRESCRIPTIVE

The contractor has the ultimate responsibility for the final product when dealing with an end-result or performance specification. The specification defines the quality, which is defined as what is specified. In a prescriptive specification format, the contractor agrees to provide the material specified and workmanship of journeyman quality. Within a performance specification, the only testing required is at project completion, when a determination is made that the work performs or does not perform as specified. Testing by the owner prior to completion may result in undesirable legal consequences. If the owner tests during construction and the contractor does not meet the required performance stipulated in the contract, two consequences may result. The contractor may argue against having to meet the necessary performance standards because the owner knew that it was not performing acceptably and did nothing about it. The argument is that the owner's inaction constituted a waiver of the requirement. The obverse of this position is that if the owner advises the contractor of the deficiencies and then, human nature being what it is, offers advice on how to correct the situation, the contractor will argue that this action constituted a conversion of the performance specification into a prescriptive specification. The conversion from performance specification into prescriptive specification shifts the risk of failure to perform as desired from the contractor to the owner. Requiring testing by the contractor during construction or by an independent testing

organization, with results to be provided to the owner, would not alter the preceding scenarios, since the contractor could still argue, convincingly, that the owner had knowledge that the performance requirement was not being met and that this constituted a waiver, or that the owner told the contractor what to do and that this constituted a conversion to a prescriptive specification. The better approach would be to tell the contractor what tests the owner will conduct at completion and to allow the contractor to run these tests if desired prior to testing by the owner.

Does this mean that no testing should be completed during construction? No, it indicates that testing during construction is the contractor's responsibility. Assuming that the pavement will be judged acceptable, or nonacceptable, based on test results used with the performance model, the contractor must ensure the achievement of the desired test results. This means that the contractor must be able to conduct tests during the materials selection, design, and construction phases that will reliably predict the end desired inputs to the performance model. This is the contractor's only means of ensuring that the final product will be acceptable.

PAYMENT FOR PERFORMANCE

Payment for work done under a performance specification may be an issue. Under conventional procedures, payment is made for work in place. With a performance specification, the work is not accepted until it is tested and the performance criteria have been met. This could create a cash flow problem for a contractor, so it may be necessary to provide for advanced payments rather than progress payments. Advanced payment is an alternative form of project financing instead of payment for work completed. Advanced payments are advances of money by the owner to the contractor before, in anticipation of, or for the purpose of complete performance under the contract. These advanced payments would be liquidated from payments due the contractor incident to the performance of the contract. Advanced payments differ from partial, progress, or other payments based on costs incurred by the contractor as work progresses. Controls are necessary to avoid abuses of an advanced payment clause in the contract.

ACCEPTABILITY

When using performance specifications, acceptability is dependent upon test results; and test results often vary. The contract should define in advance what is acceptable. What is acceptable may be stated as a value with upper and lower bounds. These bounds will constitute a minimum acceptable value and should be based on reliability concepts.

HANDLING NONPERFORMANCE

One of the major objections to using an end-result specification is that large quantities of material may be found to be defective and the cost of correction is high (*2*). The contract should define what will happen if the minimum acceptable test value is not achieved; for example, the section will be torn out and replaced; or remedial action will be permitted or not permitted or will be required, depending on whether the expected final result will exceed the minimum acceptable value. The cost of such additional work would be borne by the contractor. The cost of additional testing may also be assessed to the contractor by the owner. An alternative might be to reduce payment to the contractor because the pavement will not last as long as was envisioned when the contract was executed. The reduction in payment to which the contractor would be entitled would be established in the contract as a schedule for payment. There is a concern that the contractor may view the payment penalty as the cost of a license to avoid meeting the performance requirement.

PERSPECTIVES

The ultimate performance specification is a design-build contract. Some contractors may not want to bid competitively on jobs that approach being design-build in character. This is partly because they must pay an engineering firm to prepare an initial design as a basis upon which to prepare their bids.

Potentially Higher Overhead Costs

If the contractor is not the low bidder, then the expense of the design is added to overhead costs and must be recovered on other successful bids. The higher overhead costs will mean greater difficulty in winning other jobs. Moreover, the added expense of design is then borne, not by the original intended client, but by others.

Ethical Problems for Engineers

The creative contractor may decide to ask an engineer to work on the design on a contingent fee basis, with the understanding that the engineer will be engaged to complete the detailed design if the contractor has the low bid. The engineer receives no compensation if the contractor's bid is not low. This raises the issue of whether engineers are engaged in competitive bidding. Moreover, the contractor may ask several engineers to submit conceptual designs in order to price them and select the design that will give the lowest cost. The design cost has now been passed on to the engineers. This also raises the question of whether the engineers must limit the submission of their design to one contractor or can submit it to several in the hope that one combination of their design and the contractor's cost will be the winning combination.

Supervision and Control of Design

When contractors assume the design function, they either undertake to perform the design process in-house, subcontract it to an engineer subcontractor, or conduct it through a joint venture with an engineering firm. Contractors who propose to use the engineer as a subcontractor may then request design proposals from several design firms, selecting the design that they believe will provide the specified performance in combination with what they consider will be the lowest price.

CONCLUSIONS

Use of performance specifications can offer owners significant benefits, but not without significant costs. There will be changes in the way owners do business. There may be drastic changes in the composition of engineering staffs and functions. The process of procurement will shift from one of single-stage competitive bidding to one of double-stage competitive bidding. The cost of the engineering staff may increase as the size of the staff decreases. The educational and experience levels of the engineering staff may be significantly different. Fewer but more experienced and better qualified engineers will be needed to specify what needs to be done, while those whose function was primarily design may no longer be needed. They will be replaced by people who can define performance requirements and specify performance criteria and the means of measuring their achievement, and who will test the performance. The contract cost will appear to increase because the contractor has been asked to do the design. The contractor will have to hire engineers or contract with a design firm to be able to bid the work. The number of engineers may not be different, but the people who employ them will be. Owners will attain their objective, performance, at the lowest contract cost. The question remains of whether owners, contractors, and engineers are ready and willing to undergo a significant revolution in the way they do business, with all the accompanying dislocations to people and institutions, in order to achieve performance at lowest contract cost. If it is necessary to remain competitive in the marketplace, industry will do it. Change is inevitable. The more rapid the change, the more painful the dislocations. Tough-minded management, however, will seek and adopt those means that they perceive will enable them to achieve their goals, without regard to dislocations. Tough-minded management will ask whether they can achieve the performance they desire at the lowest total cost by means of performance specifications. If the answer is in the affirmative, the revolution will begin.

REFERENCES

1. W. H. Newman. *Constructive Control*. Prentice-Hall, Inc., Englewood Cliffs, N.J., 1975.
2. D. S. Gendell and A. Masuda. Highway Specifications: Link to Quality. *ASCE Journal of Professional Issues in Engineering*, Vol. 114, No. 1, Jan. 1988, pp. 17–26.

Publication of this paper sponsored by Committee on Pavement-Management Systems.

Cost Allocation Implications of Flexible Pavement Deterioration Models

L. R. RILETT, B. G. HUTCHINSON, AND R. C. G. HAAS

This paper explores the implications of flexible pavement deterioration models that allow the separation of highway pavement life-cycle costs into joint and common costs and the allocation of the joint costs to various vehicle classes on the basis of their pavement damage characteristics. The Ontario flexible pavement deterioration model is used to calculate the joint and common cost portions of pavement costs for a range of traffic loadings and pavement strategies. These calculations show that the portion of pavement costs attributed to traffic varied from one-quarter to one-third, with the remainder being attributed to environmental degradation. The analyses show that there are substantial economies of scale with respect to traffic loadings and that joint costs per ESAL-kilometer decreased significantly with increased traffic loadings. Large differences in the joint costs per vehicle-kilometer occur between the different truck types, while the joint costs per tonne-kilometer are more uniform. The main weakness of the Ontario model seems to be in the prediction of the performance of overlaid pavements.

Public policy makers and their advisors have addressed the problem of the equitable allocation of the costs of providing highway service to various types of users for some 30 years. The principal emphasis has been on the allocation of pavement costs, although bridge and traffic capacity costs have been examined in recent years.

Wong and Markow (*1*) have listed three equity concepts that might be used as a basis for the pricing of highway services:

1. The received benefit-equity concept where user charges are proportional to the benefits received by users;
2. The occasioned cost equity concept where costs are assigned to users on the basis of the costs occasioned by each class of user; and
3. A method that assigns costs on the basis of the ability to pay of each class of user.

The most commonly accepted method is the cost-occasioned approach in which various types of users are assigned the average costs to the highway agency of their trips. The challenge with this approach is to identify a relatively simple responsibility measure that captures the costs occasioned by the passage of different vehicle types and that allows the joint costs of pavement damage to be allocated to different vehicle classes.

Three broad groups of agency costs may be identified:

1. Uniquely occasioned, or long-term separable costs, which may clearly be assigned to a particular vehicle class, with truck climbing lanes providing an example;
2. Common costs that cannot reasonably be assigned separately to any vehicle class, with right-of-way costs representing one example; and
3. Joint costs, which are the costs occasioned by all vehicle types but for which a responsibility measure may be identified.

The focus of this paper is the allocation of flexible pavement life-cycle costs to a set of highway users. The principal issue is to identify that portion of pavement life-cycle costs that are joint costs, and should therefore be allocated to vehicles causing the damage, and that portion that should be classed as common costs and allocated to all vehicle classes. Joint pavement costs are due to load-associated pavement deterioration, while common pavement costs are due to environment-associated pavement deterioration. The technical basis for such allocation is a pavement deterioration model, and one developed by the Ministry of Transportation Ontario (*2,3*) is used for illustrative purposes.

The next section of this paper briefly describes the nature and requirements of pavement deterioration models, with particular emphasis on the Ontario flexible pavement model. The third part of the paper illustrates the variation in the portions of the joint costs of pavements assigned to traffic for a variety of traffic conditions and pavement thicknesses. The penultimate section of the paper examines the implications of these variations in joint costs for the pavement costs occasioned by representative vehicle types using the Ontario highway system. The final section of the paper explores the weaknesses of the Ontario deterioration model and outlines the questions on pavement deterioration that should be addressed by the Strategic Highway Research Program (SHRP) long-term pavement performance monitoring experiments.

PAVEMENT DETERIORATION MODELS: THE ONTARIO EXAMPLE

A major study on pavement damage functions for cost allocation, conducted for the Federal Highway Administration

L. R. Rilett, Department of Civil Engineering, University of Waterloo, Waterloo, Ontario, Canada. Current affiliation: Northwestern University, 313-1940 Sherman Ave., Evanston, Ill. 60201. B. G. Hutchinson and R. C. G. Haas, Department of Civil Engineering, University of Waterloo, Waterloo, Ontario, Canada, N2L 3G1.

(FHWA) (*4*), has identified the following major types of pavement deterioration:

1. Surface distress associated with:
   a. Fatigue cracking,
   b. Low-temperature cracking,
   c. Rutting,
   d. Raveling,
   e. Bleeding or flushing, and
   f. Roughness due to differential subgrade volume change;
2. Reduction in surface friction (skid resistance); and
3. Reduction in serviceability (i.e., increased roughness).

Various models for predicting these types of deterioration have been developed during the past two or three decades, as summarized in the FHWA study (*4*). Of primary interest to this paper are those that involve the third type, reduction in serviceability, because they represent the primary operating function for a pavement and because they can be directly related to vehicle operating costs. In addition, as described by Haas et al. (*5*), it is necessary for cost allocation purposes that such models be capable of identifying the fractions of total deterioration due to environmental factors and to traffic load-associated factors. Comparisons are shown between the FHWA study models and the Ontario (OPAC) models, both of which have the ability to separate environmental and traffic load-associated deterioration, by Haas et al. (*5*).

The Ontario model was chosen for illustrative purposes in this paper mainly because it has been calibrated to field observations of performance and because overlays can be considered.

The Ontario flexible pavement deterioration model was derived from the load-associated flexible pavement deterioration observed at the AASHO Road Test, the load and environment-associated pavement deterioration recorded at a longer-term road test at Brampton, Ontario, and some theoretical analyses.

Figure 1 illustrates the broad structure of the Ontario flexible pavement deterioration estimation model. Alternative pavement strategies are first converted into equivalent granular thicknesses using layer equivalencies based on the behavior of layered elastic systems and field observations. The deflection at the surface of the subgrade under the equivalent granular thickness is then calculated for a standard dual-tire load (40kN).

A relationship was established between this theoretically estimated subgrade deflection and the number of standard axle load repetitions to failure observed at the AASHO Road Test; Figure 2 illustrates the family of functions developed. Step 3 of the Ontario method uses this relationship and the equivalent single-axle load (ESAL) pattern expected at a pavement site to estimate the RCI (riding comfort index) loss due to traffic loads. A 0–10 scale is used for the RCI, and it is therefore equivalent to twice the Present Serviceability Index (PSI) used in the United States.

Figure 1 illustrates that the next step of the procedure is to estimate the RCI loss due to the environment. RCI loss functions versus number of years in service for different magnitudes of subgrade deflection were developed from an integration of the experience at the AASHO and Brampton Road Tests, and Figure 3 illustrates the family of functions.

The RCI losses due to load and environment are then added

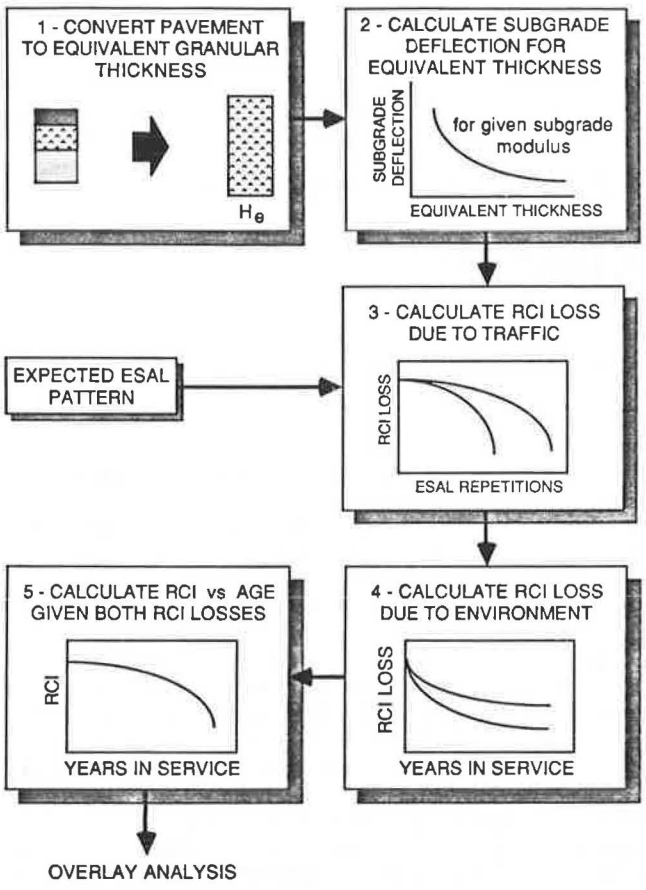

FIGURE 1 Ontario flexible pavement deterioration model.

to estimate the RCI versus age history of given pavement strategy. When a minimum acceptable level of RCI is reached, the pavement is overlaid and the performance of the resurfaced pavement is estimated in a similar way. The layer equivalencies of the asphalt surface and granular layers are discounted according to their condition when the resurfacing occurs. These layer equivalency discounts are substantial, and the equivalent granular thickness of the resurfaced pavement is normally significantly less than that of the original pavement. Figure 4 illustrates the adjustment factors for surface and granular layers.

APPLICATIONS OF THE ONTARIO DETERIORATION MODEL

The implications of the Ontario flexible pavement deterioration model for cost allocation are best illustrated by an example. Consider the pavement requirements for a 20-year analysis period for a four-lane divided highway to be constructed on a subgrade with a modulus of elasticity of 34.5 MPa (5,000 psi). Typical RCI values used in Ontario for primary highways are 8.5 for new pavements, 7.5 after an overlay, and 5.5 as a minimum acceptable or failure level.

The Ontario deterioration equations have been rearranged and an iterative process used to calculate the equivalent granular thickness of pavement required to produce a given initial pavement life for initial and final RCIs, a subgrade modulus, and a user-specified cumulative ESAL loading.

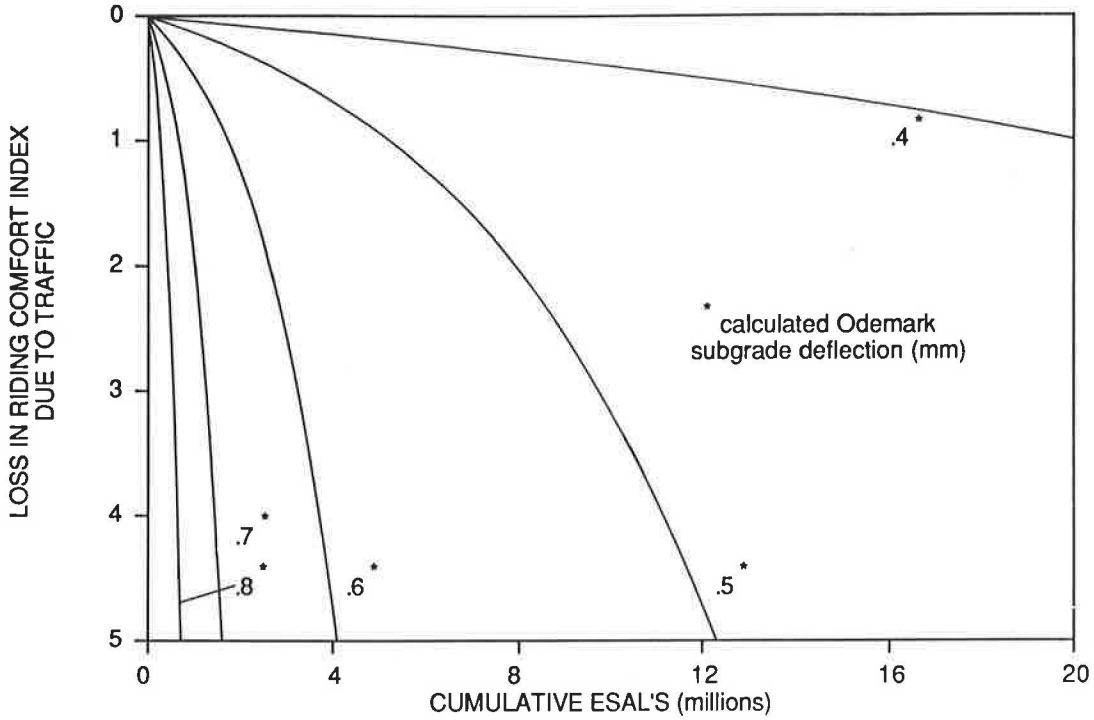

FIGURE 2 Load-associated RCI loss versus cumulative ESALs.

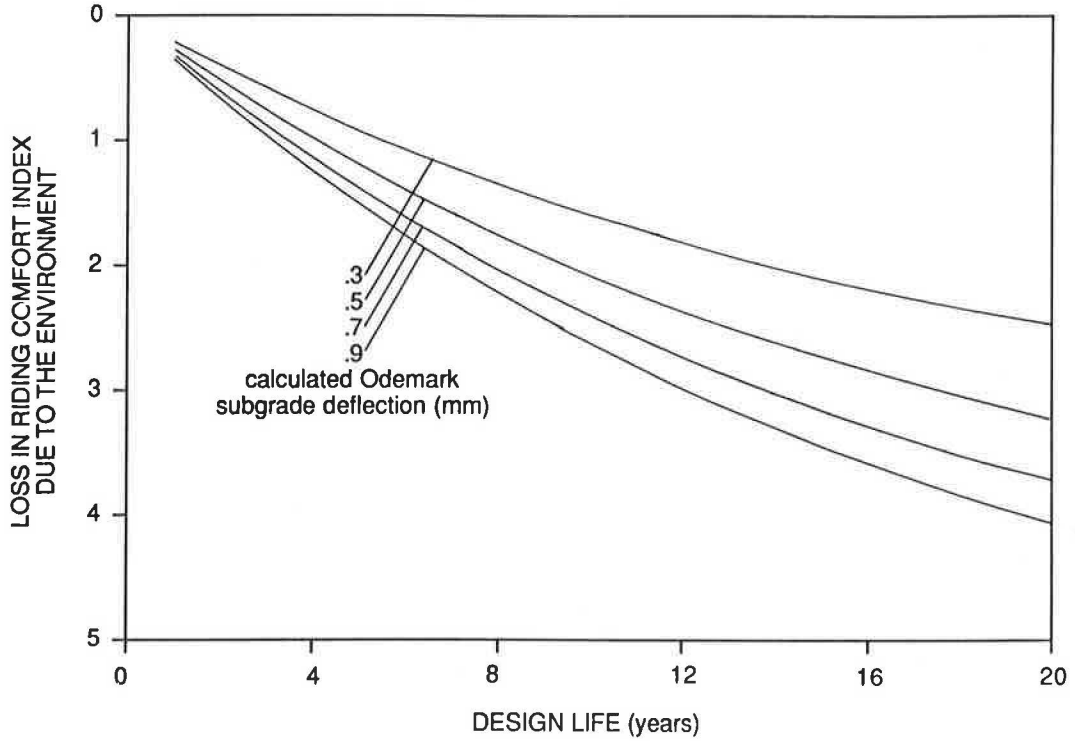

FIGURE 3 Environment-associated RCI loss versus years in service.

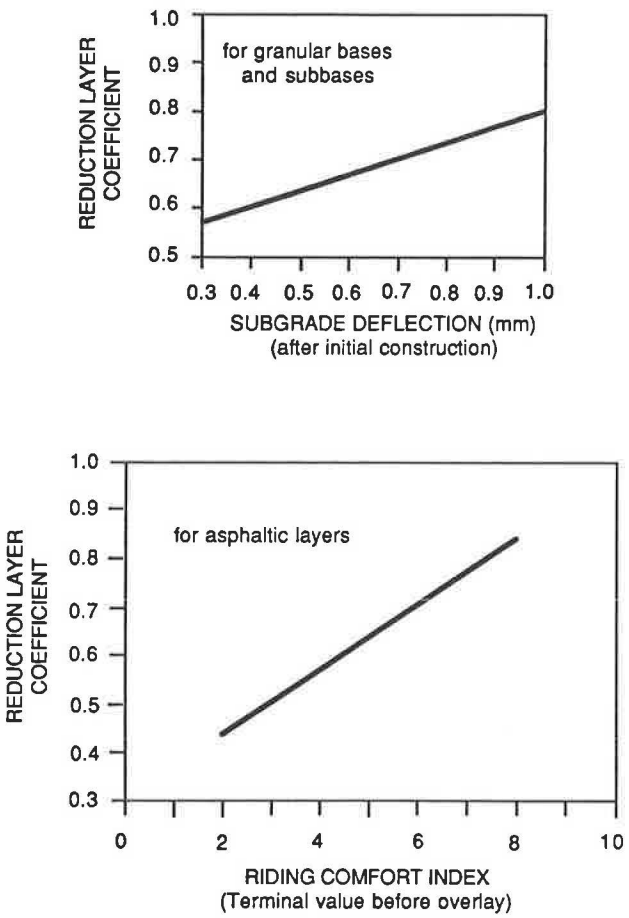

FIGURE 4 Layer coefficient reduction factors.

Figure 5 illustrates the relationships between equivalent granular thickness, cumulative ESALs in the design lane, and years to failure of the initial pavement. The lower function shows that the equivalent granular thickness required to provide a 6-year initial life would increase from about 400 mm at 1 million ESALs to about 680 mm at a cumulative ESAL loading over the 6-year period of 20 million.

The rate of change of this function exhibits the well-known economies of scale characteristics that exist in highway pavements with respect to traffic loadings. Subsequent ESALs require less additional pavement thickness to give the same service life as the earlier ESALs. For example, for a 10-year initial pavement life, an increase in cumulative ESALs from 5 million to 10 million would require an additional granular thickness of 70 mm, while an increase from 15 million to 20 million would require only an additional 30 mm.

Inspection of the functions in Figure 5 shows that the granular thickness required to increase service life for a given cumulative ESAL magnitude increases at an growing rate. This effect may be detected from the increased spacing between the functions as the initial design life increases from 6 to 16 years.

Analyses similar to those carried out for Figure 5 would show that the required pavement thickness decreases as the initial RCI increases, the RCI at failure decreases, and the subgrade strength increases.

Figure 6 illustrates the portion of the RCI loss of an initial pavement that may be assigned to environmental degradation as a function of the cumulative ESAL loading and the life of the initial pavement. The function closest to the origin is for an initial ESAL loading of 250,000 per year, while the fourth function is for an initial ESAL loading of 2 million per year, both of which increase at 2 percent per year.

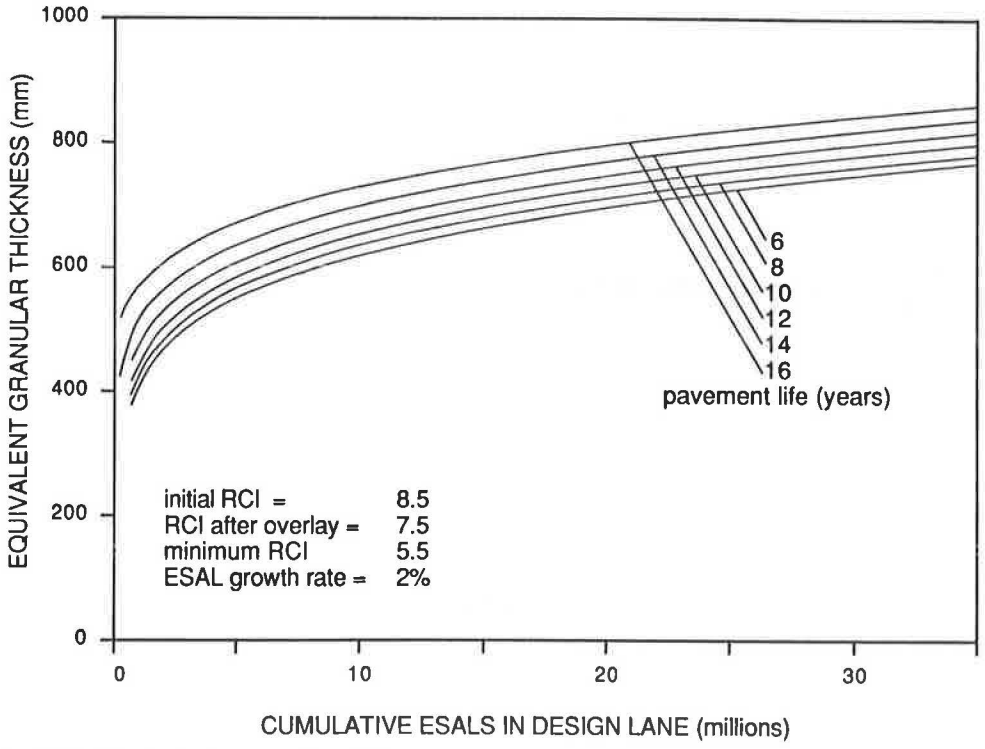

FIGURE 5 Equivalent granular thickness versus design ESALs for different pavement lives.

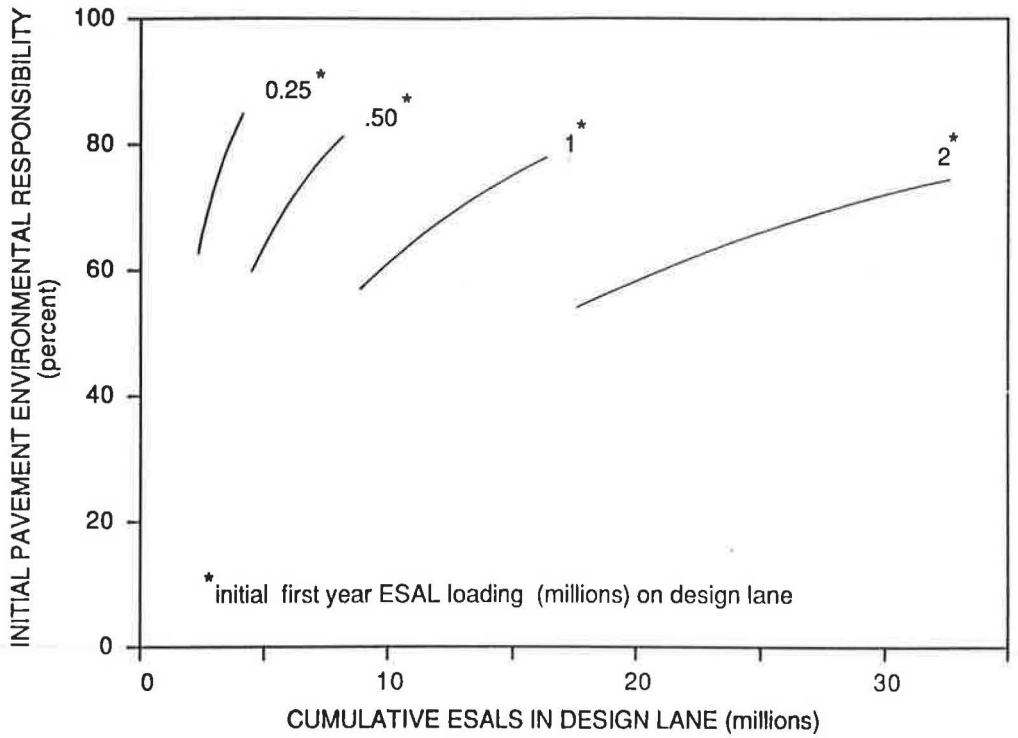

FIGURE 6 Environmental responsibility for initial pavement cost.

The diagram illustrates that the portion of RCI loss assigned to environmental degradation increases with increasing life of the initial pavement but at a decreasing rate. For example, with a traffic loading of 250,000 ESALs per year, this portion increases from 0.62 for an initial pavement life of 8 years to 0.85 for an initial pavement life of 14 years. The diagram also shows that the portion of RCI loss assigned to environmental degradation decreases with increasing traffic loading.

Figures 7 and 8 illustrate similar information for the overlays required to extend the combined initial pavement plus overlay life to 20 years where the overlaid pavement has been assigned an initial RCI of 7.5. There are some important differences in pavement behavior illustrated in Figures 7 and 8 compared with that shown in Figures 5 and 6, respectively. Figure 7 shows that the overlay thickness required to extend the service life to 20 years increases at an increasing rate with decreasing initial pavement life. For example, for the 250,000 ESALs per year traffic loading, an overlay thickness of about 520 mm (equivalent granular basis) would be required for an initial pavement life of 14 years, and this would increase to 750 mm if the initial pavement life were only 8 years. Figure 8 illustrates that the portion of the RCI overlay loss allocated to environmental degradation increases significantly over that shown in Figure 6 for the initial pavement, and this is due primarily to the assumption of an initial RCI of 7.5 for the overlaid pavement.

COST CHARACTERISTICS

Figure 9 illustrates the present worth of the initial pavement and overlay costs required to provide a 20-year service life as a function of the initial pavement life and traffic loadings. The parameters used for this analysis are as follows (*6*):

- Asphalt concrete = $538 per millimeter thickness per kilometer length and 3.75-m lanes;
- Base/subbase = $390 per millimeter thickness;
- Equivalent granular = $400 per millimeter thickness; and
- Discount rate = 4 per annum (long-term difference between market rate and inflation).

The initial traffic loadings used for the economic analyses illustrated in Figure 9 were 250,000, 500,000, 1 million, and 2 million ESALs per year, with an annual growth rate of 2 percent compounded. Assuming an average ESAL per truck of 1,300 days of truck movement, 20 percent trucks, and a lane distribution factor of 0.8, these traffic loadings would correspond to a one-way initial AADT range of 5,200 to 42,000. While Figure 9 includes only pavement costs (i.e., shoulders, drainage, etc., are not included), it clearly shows three major trends:

1. The total cost is not sensitive to initial pavement life; there is a minimum at 12 years, but it is only marginally lower than for other initial lives.
2. The traffic-related cost decreases with increasing initial pavement life because the environmental portion of the initial pavement costs increases with increasing initial pavement life and these initial pavement costs represent the bulk of the life-cycle costs.
3. The traffic-related portion of the total cost ranges from about one-third at lower traffic volumes to one-quarter at the higher traffic volumes.

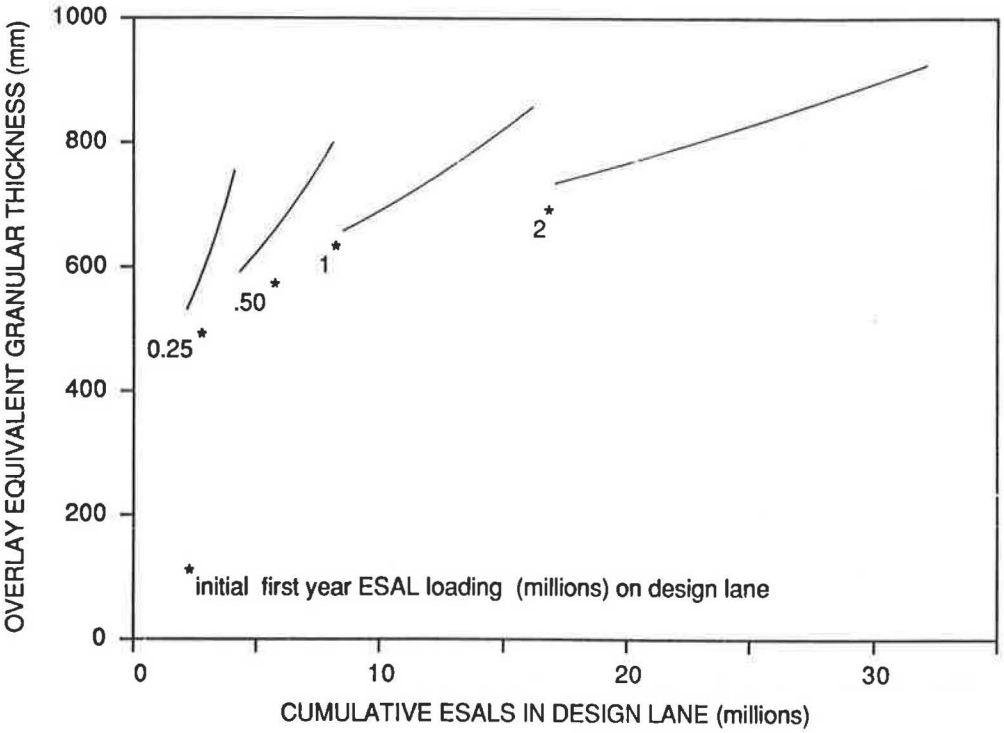

FIGURE 7 Equivalent granular thickness of overlays for different traffic load intensities.

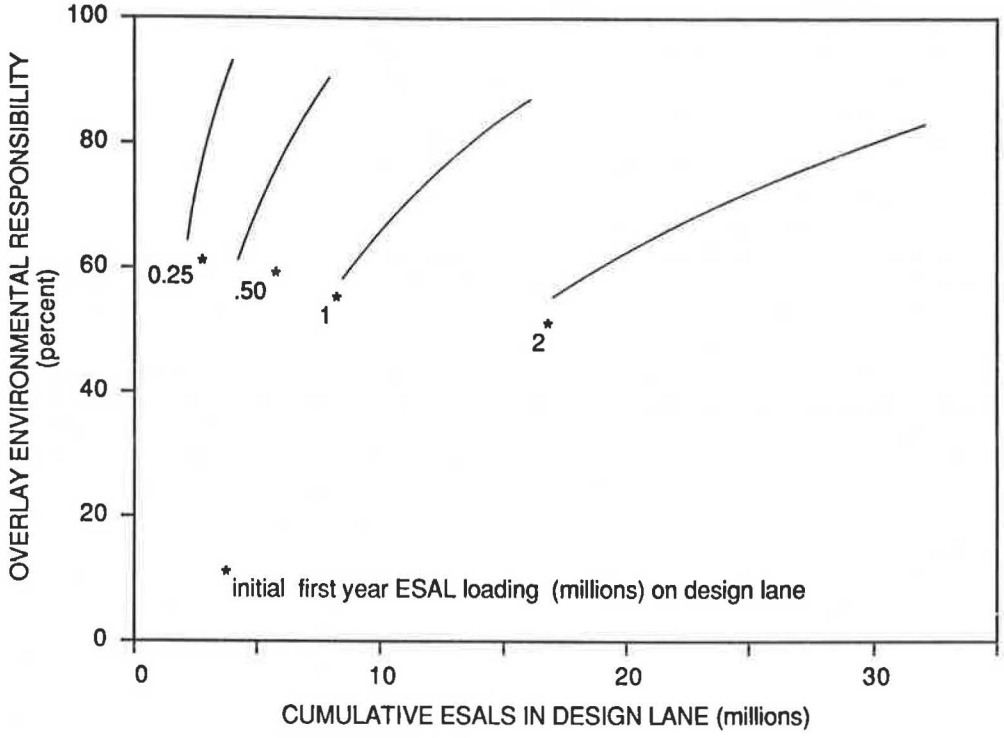

FIGURE 8 Environmental responsibility for overlay cost.

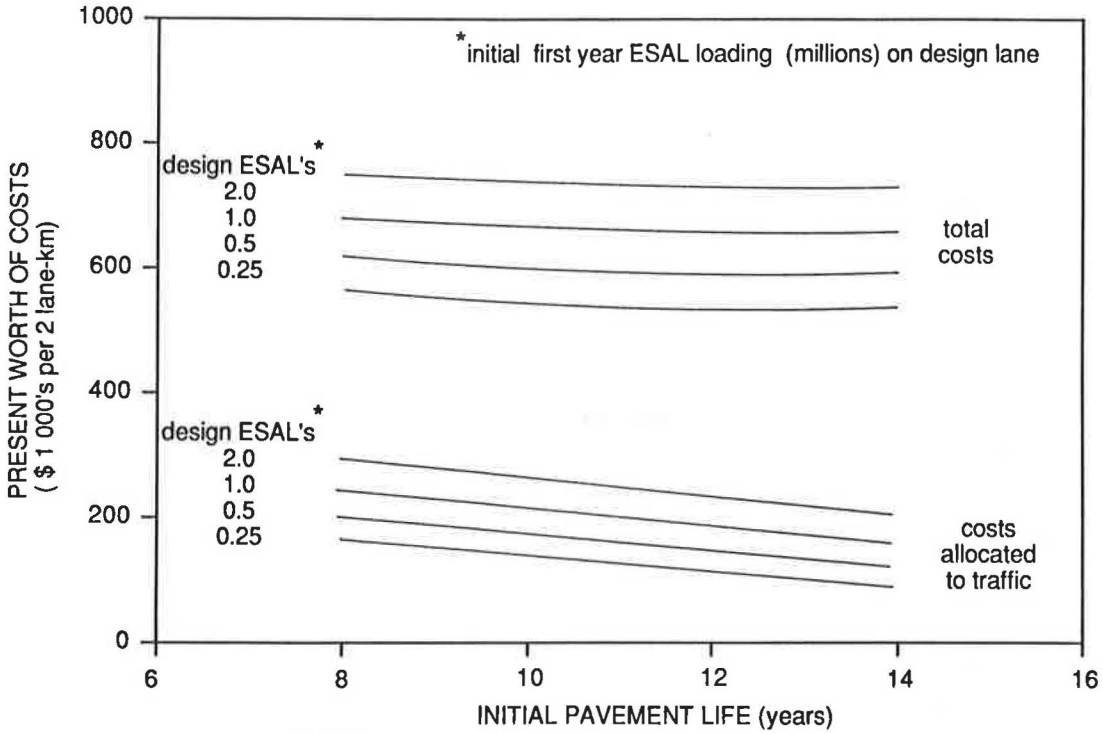

FIGURE 9 Present worth of initial pavement plus overlay costs.

These trends are all consistent with observations from the deterioration-related graphs (Figures 5 to 8). It might also be noted in Figure 9 that the increase of either total cost or traffic-related cost, for any initial pavement life, increases approximately uniformly for each doubling of traffic loads. In effect, this becomes a surrogate for pavement thickness and, similar to Figure 5, illustrates the economies of scale that exist for pavements with respect to traffic loading.

The joint costs in dollars per ESAL-kilometer were calculated by dividing the present worths of the traffic-related life-cycle costs by the present worths of the ESAL versus time profile specified for the design. This approach was taken as it was argued that the consumption of pavement RCI by vehicles has a time base similar to that of pavement costs. This approach is particularly important for situations in which annual traffic loads are increasing.

Figure 10 illustrates the joint costs in dollars per ESAL-kilometer as a function of the cumulative ESALs and the initial pavement life, for the same conditions as in Figure 9. For example, at the lower traffic volume, 250,000 ESALs per year initially, the joint cost would be about 2.6 cents per ESAL-kilometer for an initial pavement life of 10 years. This would drop to about 0.6 cents per ESAL-kilometer for the higher volume of 2×10^6 ESALs per year initially and an initial pavement life of 10 years. While the cost per ESAL-kilometer drops significantly with increasing traffic, the total cost of the pavement would, of course, be higher. Again, it illustrates the economies of scale for thicker pavements and higher traffic volumes. The degree to which these joint costs are actually being met by taxation revenues was not a part of this study.

Figure 11 shows the joint costs as a function of cumulative ESALs for a minor highway (i.e., minimum RCI of 4.5 and initial traffic loadings of 75,000, 150,000, and 300,000 ESALs per year, increasing at 2 percent per year). In this case the joint costs, particularly at the lower rates, are substantially higher than those shown in Figure 10, as might be expected.

ENVIRONMENTAL VERSUS TRAFFIC ALLOCATION OF DETERIORATION

The foregoing sections show that if a deterioration model exists with the capability of separating the contributions of traffic and environment, then the life-cycle costs attributable to traffic can be calculated. In the Ontario method ESALs are the variable used to predict load-associated deterioration and may therefore be used as the responsibility measure for joint costs.

For the particular deterioration model used in the sample allocation, the following major points emerge:

1. The absolute required pavement thickness always increases with increasing cumulative ESALs, but the rate of change decreases. This illustrates an economy of scale in that a small extra thickness can carry substantially more traffic loads.
2. The portion of deterioration due to environmental factors is generally greater than that due to traffic loads. Moreover, this portion increases with increasing life of the pavement but at a decreasing rate.
3. For a fixed life cycle (say, 20 years) the overlay thickness required increases at an increasing rate, as the initial pavement service life becomes shorter. This means that the portion of the deterioration of the resurfaced pavement due to environmental factors increases significantly compared with the initial pavement.

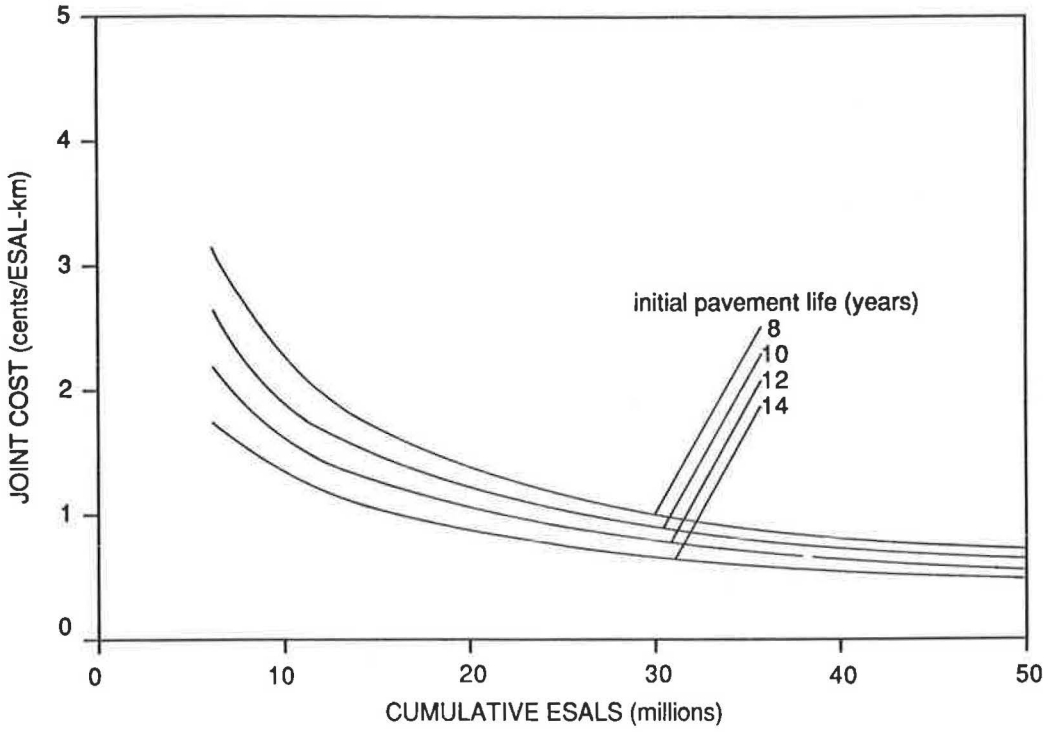

FIGURE 10 Joint costs for a primary highway.

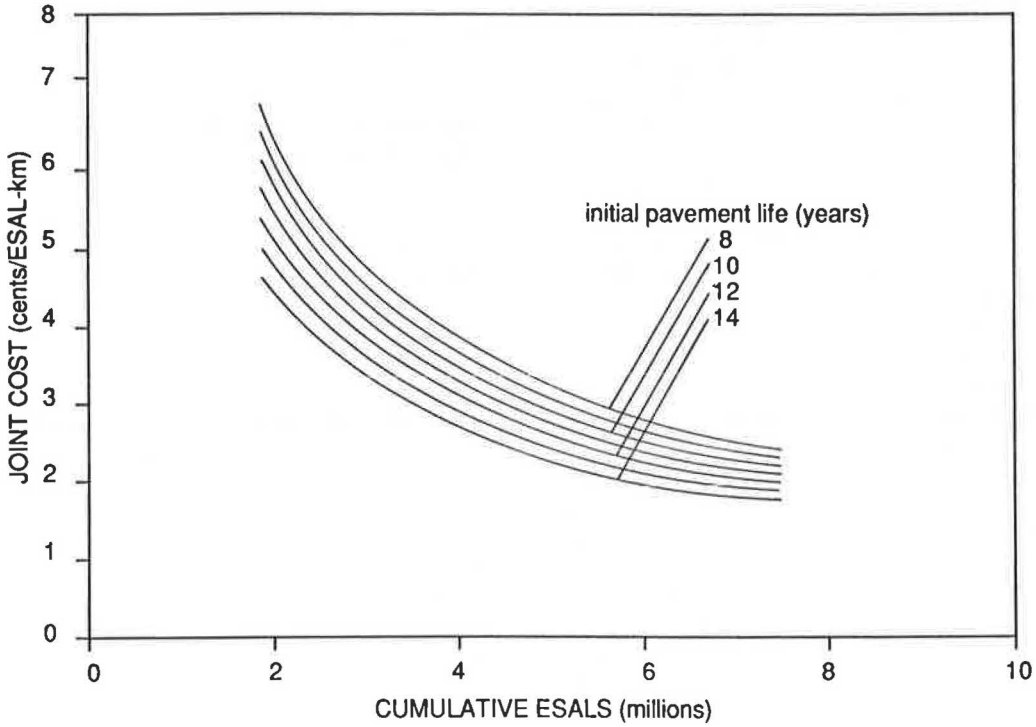

FIGURE 11 Joint costs for a secondary highway.

4. The traffic-related portion of total pavement costs behaves in a manner consistent with the deterioration model behavior summarized in items 1 to 3 above. In relative terms, it ranges from about one-third of the total at lower traffic volumes to about one-quarter of the total at higher traffic volumes.

The basic question is whether the foregoing results are reasonable, both in an absolute and in a relative or trend sense. First, the economy of scale observation (i.e., small extra thickness to handle significantly more traffic loads) is consistent with both pavement design theory and practice. Second, the observation that environmental factors contribute more to deterioration than do traffic factors, but at a decreasing rate with longer pavement lives, is quite consistent with observations from areas with more severe climates (i.e., most of the northern United States and much of Canada). For example, Karan et al. (*7*) illustrated that deterioration models developed from a comprehensive long-term pavement performance database in Alberta reflected traffic loads as quite a minor factor.

While pavements in more severe climates may well have to be designed primarily for environmental factors (i.e., they are "overdesigned" for traffic loading, per se), it would be dangerous to extrapolate this too far. For example, if a pavement were designed only for environmental factors and an unexpected increase in traffic loads occurred, then very rapid deterioration would likely occur (see the initial portion of the Figure 5 functions). Moreover, existing models such as OPAC assume that environmental and load-associated deterioration is separable right to the end of the service life. In reality, the interaction between traffic and environment may be the dominant factor in deterioration as the pavement becomes older.

The observation that overlay thickness required to reach a given life cycle increases, at an increasing rate, as the initial pavement life decreases is due largely to the high "penalty" represented by the layer equivalency adjustment factors (Figure 4). It is questionable whether this is reasonable. Whether joint costs allocated to traffic loads should be more or less than one-quarter to one-third of the total from the Ontario example in this paper depends on the validity of the deterioration models. In general, they seem reasonable for Ontario's conditions, particularly in the conventional ranges of pavement thicknesses and traffic. For extremes, some caution in their use (where extrapolation occurs) would be wise. Also, the results of this paper point out that the joint costs obviously depend on the nature or form of the deterioration models used. These must be applicable or calibrated to local conditions if a cost allocation study is to be meaningful.

REPRESENTATIVE ONTARIO VEHICLE TYPES

Figure 12 shows four typical vehicles currently used in the transport of goods in Ontario; these were analyzed for loaded conditions using typical cargoes. The vehicles were loaded with cargo until one of the axle weights reached the Ontario limits. The three-axle straight truck and the 3-S4/2B belly-axled semitrailer were loaded with gravel (17,000 N/m^3), while the 3-S2 tractor semitrailer and the 3-S2-S2 B-train double transport were loaded with medium-density (5,000 N/m^3) cargo.

The most commonly used damage functions are those developed by AASHTO from the AASHO Road Test data collected in the early 1960s (*8*). Response-based load equivalency functions (LEFs) were also developed by Rilett and Hutchinson (*9*) from pavement surface deflection data collected at a number of instrumented test sites in Canada by the Canroad Transportation Research Corporation (*10*). For the most part these are significantly higher than those recommended by AASHTO.

Both sets of LEF factors have been used to calculate LEFs for the different truck types and unloaded, partially loaded, and fully loaded conditions; these are shown in Table 1. It was assumed that the steering axle (single tire) had twice the damage associated with it as a dual-tire single axle with the same loading (*10*). The LEFs based on the Waterloo analysis for the empty configurations are approximately 4 to 5 times higher than those of AASHTO. For the half-loaded and loaded condition, this ratio is approximately 3 to 4 and 1.5 to 2, respectively.

ALLOCATION TO VEHICLE TYPES

If a road were to be constructed for an initial design lane ESAL loading of 250,000 ESALs per year, with a 12-year initial life and an 8-year overlay life (minimum total cost), the price per ESAL-kilometer would be approximately 2.2 cents. Table 2 lists the cost per kilometer that each vehicle would be charged for the use of the pavement for this section of roadway. The fully loaded 3-S4/2B has the highest LEF and would pay about 23 cents per kilometer based on the Waterloo factors and 17 cents per kilometer using the AASHTO functions.

To examine the infrastructure impact efficiency of different truck types, the costs per tonne-kilometer have been calculated and are summarized in Table 3. This allows a comparison of the pavement costs allocated across truck types. If the LEF functions developed by Rilett and Hutchinson (*9*) were used, then the costs allocated to a gravel carrier would be 54 cents per tonne-kilometer for the 3-S5/2B and 64 cents per tonne-kilometer for the three-axle truck. If these costs were combined with the transportation costs, then the greater economic efficiency of the larger truck would be clearly evident.

IMPLICATIONS FOR SHRP

The Long-Term Pavement Performance (LTPP) study in the Strategic Highway Research Program (SHRP) is directed toward providing data on the long-term performance of various pavement structures under a wide range of climatic conditions, traffic loads, subgrade soils, and other factors.

Specific stated objectives of the LTPP study that are of particular importance to cost allocation are those concerned with evaluating the long-term effects of environmental and traffic load effects, and their interactions, on pavement deterioration and service life. Two other objectives of major importance concern reevaluation of the load equivalency factors developed from the AASHO Road Test, and evaluation of the load-carrying capacity of a pavement at the end of its service life.

If reasonably reliable models can in fact be developed from the LTPP study, then a basis exists for establishing equitable

3-Axle Straight Truck

	tare = 8 619 kg	cargo density = 17 000 N/m^3	GVM = 24 686 kg
	Payload:	8 034 kg (half full)	16 068 kg (full)

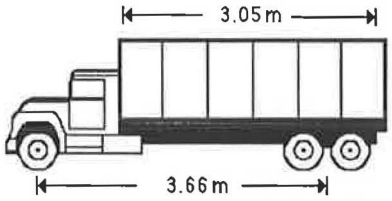

3-S2

tractor	tare = 8 200 kg		
semi-trailer	tare = 6 300 kg	cargo density = 1 000 N/m^3	GVM = 39 220 kg
	Payload:	12 360 kg (half full)	24 720 kg (full)

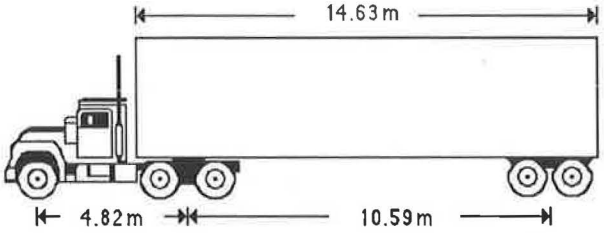

3-S5/2B

tractor	tare = 8 200 kg		
semi-trailer	tare = 8 300 kg	cargo density = 17 000 N/m^3	GVM = 58 740 kg
	Payload:	21 120 kg (half full)	42 240 kg (full)

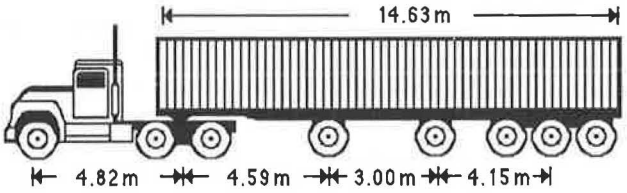

3-S2-S2

tractor	tare = 8 200 kg		
1st semi-trailer	tare = 6 000 kg	cargo density = 17 000 N/m^3	
2nd semi-trailer	tare = 4 300 kg		GVM = 45 836 kg
	Payload:	13 433 kg (half full)	26 866 kg (full)

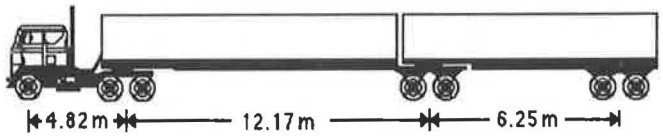

FIGURE 12 Representative Ontario trucks.

cost allocation policies. This would include an ability to capture the increasing effect of traffic loads on pavement deterioration (i.e., through modeling the interaction between environment and traffic) as the pavement ages. The premise is that traffic has a more severe effect on older pavements, both through this interaction and because of the increase in dynamic load effects (*11*).

The implication for cost allocation is that there could be a real benefit (i.e., cost saving) in paying for better roads as opposed to paying only for their rehabilitation in advanced states of deterioration. This would be in addition to the substantial agency savings on investment costs plus vehicle operating cost savings realized by early rehabilitation (*12*).

Because only a limited number of pavement deterioration models exist that separately identify traffic load- and environment-associated contributions, and because these are gen-

TABLE 1 LOAD EQUIVALENCY FUNCTIONS FOR REPRESENTATIVE TRUCKS

TRUCK TYPE	Loading Empty	Half	Full
3 AXLE	0.54 (0.07)	1.88 (0.62)	4.66 (3.03)
3-S2	0.99 (0.20)	2.60 (0.80)	6.34 (3.74)
3-S4/2B	1.12 (0.23)	3.67 (1.21)	10.40 (7.80)
3-S2-S2	1.03 (0.25)	2.45 (0.62)	5.40 (2.54)

the upper entries in each cell are LEFs calculated from LEF functions reported by Rilett & Hutchinson and those in parentheses are calulated from the AASHTO functions

TABLE 2 JOINT PAVEMENT COSTS PER VEHICLE-KILOMETER

TRUCK TYPE	Loading Empty	Half	Full
3 AXLE	1.19 (0.15)	4.14 (1.36)	10.25 (6.67)
3-S2	2.18 (0.44)	5.72 (1.76)	13.95 (8.23)
3-S4/2B	2.46 (0.51)	8.07 (2.66)	22.88 (17.16)
3-S2-S2	2.27 (0.55)	5.39 (1.36)	11.88 (5.59)

entries are cents per kilometer; the upper entries are calculated from LEF functions reported by Rilett and Hutchinson and the lower entries are the costs calculated from the AASHTO LEF functions

TABLE 3 JOINT PAVEMENT COSTS PER TONNE-KILOMETER

TRUCK TYPE	Loading Half	Full
3 AXLE	0.51 (0.17)	0.64 (0.41)
3-S2	0.46 (0.14)	0.56 (0.33)
3-S4/2B	0.38 (0.13)	0.54 (0.41)
3-S2-S2	0.40 (0.10)	0.44 (0.21)

entries are cents per kilometer; the upper entries are calculated from LEF functions reported by Rilett and Hutchinson and the lower entries are the costs calculated from the AASHTO LEF functions

erally limited to a regional set of conditions, the models eventually developed from the LTPP study in SHRP should be able finally to establish the comprehensive technical basis needed for equitable cost allocation.

CONCLUDING REMARKS

Flexible pavement deterioration models that incorporate both load-associated and environment-associated deterioration components allow long-term pavement life-cycle costs to be split into joint and common costs. Joint pavement costs may then be allocated to vehicle classes using an ESAL-kilometer responsibility measure, and common costs may be allocated in proportion to the number of vehicles in each class.

The Ontario flexible pavement deterioration model exhibits the characteristics typical of many deterioration models. There are economies of scale in pavement thickness with respect to increasing traffic loads for a given initial pavement life. However, pavement thickness increases at an increasing rate with increases in the initial pavement life.

Use of the Ontario pavement deterioration model for cost allocation for a representative primary highway pavement section suggested that the portion of pavement costs allocated to environmental degradation and, therefore, to common costs varies between 55 and 88 percent, depending on the intensity of the traffic loading and the length of the initial pavement life chosen. For example, for a pavement experiencing 250,000 ESALs per year, the portion allocated to environmental degradation increases from about 62 percent for an initial design life of 8 years to 84 percent for a design life of 16 years. With a pavement experiencing 2 million ESALs per year, the portion allocated to environmental degradation increases from 55 percent for a design life of 8 years to 72 percent for a design life of 16 years.

Analysis of the performance of overlays showed similar trends but with higher portions of the overlay costs being allocated to environmental degradation. These higher allocations to environmental degradation reflect the larger reductions in strength of the original pavement layers assigned by the Ontario method and the use of an initial RCI of 7.5 for the overlaid pavement.

Analysis of the total life-cycle pavement costs for given traffic loadings showed that they were relatively insensitive to the initial design life selected, with a fairly weak minimum occurring at about 12 years. The joint cost allocated to traffic varied from about 1.8 cents per ESAL-kilometer at a traffic loading of 250,000 ESALs per year to 0.5 cent per ESAL-kilometer for a traffic loading of 2 million ESALs per year.

Analysis of representative Ontario vehicle types showed that the fully loaded tonne-kilometer joint cost varied from 0.64 cents per tonne-kilometer for a three-axle gravel truck to 0.44 cents per tonne-kilometer for a B-train double transporting medium-density cargo.

The results of the cost allocation calculations presented in this paper are critically dependent upon the structure and integrity of the pavement deterioration model used. While the Ontario method seems to capture the performance of initial pavements, there is some question about the performance prediction of pavements with overlays. This is a critical issue in many jurisdictions, because the systems are mature

and most of the pavement work involves rehabilitation and resurfacing.

ACKNOWLEDGMENTS

The work on which this paper is based was funded by the Natural Sciences and Engineering Research Council of Canada, and this support is gratefully acknowledged.

REFERENCES

1. T. F. Wong and M. J. Markow. *Allocation of Life-Cycle Highway Pavement Costs*. Report FHWA/RD-83/030. FHWA, U.S. Department of Transportation, 1984.
2. N. Kamel. Developing Structural Design Models for Ontario Pavements. In *Transportation Research Record 521*, TRB, National Research Council, Washington, D.C., 1974, pp. 60–72.
3. F. W. Jung, R. Kher, and W. A. Phang. *A Performance Prediction Subsystem-Flexible Pavement*. RR 200. Ontario Ministry of Transportation and Communications, Toronto, Ontario, Canada, 1975.
4. J. B. Rauhut, R. L. Lytton, and M. I. Darter. *Pavement Damage Functions for Cost Allocation*. Report FHWA/RD-84/108. FHWA, U.S. Department of Transportation, June 1984.
5. R. Haas, M. Van Aerde, and R. Penner. *Vehicle Operating Costs and Pavement Damage Functions for Highway Cost Allocation*. Prepared for the CTRF-RTAC Workshop on Highway Finance, Toronto, Ontario, Canada, 1985.
6. R. Haas and T. Papagiannakis. *Impacts of Heavy Vehicles on Urban Pavements*. Paper prepared for the Annual Conference of the Roads and Transportation Association of Canada, Saskatoon, Saskatchewan, Canada, 1987.
7. M. A. Karan, T. J. Christison, A. Cheetham, and G. Berdahl. Development and Implementation of Alberta's Pavement Information and Needs System (PINS). In *Transportation Research Record 938*, TRB, National Research Council, Washington, D.C., 1983, pp. 11–20.
8. *AASHTO Guide for the Design of Flexible Pavements*. American Association of State Highway and Transportation Officials, Washington, D.C., 1986.
9. L. R. Rilett, and B. G. Hutchinson. LEF Functions from Canroad Pavement Load-Deflection Data. In *Transportation Research Record 1196*, TRB, National Research Council, Washington, D.C., 1988, pp. 170–178.
10. J. T. Christison. *Pavement Response to Heavy Vehicle Test Program: Part 1—Data Summary Report*. Canroad Transportation Research Corporation, Ottawa, Ontario, Canada, 1986.
11. A. T. Papagiannakis, R. C. G. Haas, J. H. F. Woodroofe, and P. A. LeBlanc. Impact of Roughness-Induced Dynamic Loads on Flexible Pavement Distress and Performance. *Proc., First International Symposium on Surface Characteristics*, State College, Pa., June 1988.
12. R. Haas. The Long Term Effects of Spending Decisions on Paved Roads. *Proc., Eurasphalt Congress*, Berlin, West Germany, May 1984.

Publication of this paper sponsored by Committee on Pavement Management Systems.

Application of the Microeconomic Concepts of Production and Cost Functions to the Analysis of Highway Maintenance Efficiency

HONG-JER CHEN AND JOSSEF PERL

Annual national highway maintenance expenditures increased from $6 billion in 1975 to $15 billion in 1983 and are still increasing each year. Maintenance needs for the highway system are increasing as well, but the funds available for highway maintenance have been decreasing in real terms. The result is a growing gap between highway maintenance needs and available resources and an urgent need to improve the productivity and cost efficiency of highway maintenance operations. In this paper, a microeconomic-based approach for analyzing the allocation of aggregate resources (labor and equipment) and the characteristics of production in highway maintenance operations is presented. The proposed methodologies allow determination of the maximum quantity of any given maintenance activity that can be accomplished with given quantities of labor and equipment, identification of basic characteristics of the production process of a given maintenance activity, determination of the optimal (cost minimizing) combination of labor and equipment needed to perform a given level of maintenance activity, and estimation of the minimum cost of accomplishing any given amount of a specified maintenance activity. The validity of the results and the practical usefulness of the proposed methodology are limited, due primarily to data limitations. Recommendations regarding the needed highway maintenance data base are discussed. The microeconomic concepts of production and cost functions seem to provide a promising theoretical basis for analyzing the productivity and cost efficiency of highway maintenance operations.

National annual highway maintenance expenditures increased from $6 billion in 1975 to $15 billion in 1983 (*1*), and are still increasing each year. Along with the increase in unit maintenance cost, the maintenance needs for the highway system are increasing as well. Growing lane-miles, more complex highway appurtenance, and aging contribute to greater maintenance needs. At the same time, the funds available for highway maintenance have been decreasing in real terms. Highway user revenues from gasoline tax decreased by 7 percent between 1975 and 1979 (*2*). These changes have resulted in a growing gap between highway maintenance needs and available resources, and have led to an urgent need to improve the productivity and cost-efficiency of highway maintenance operations.

H.-J. Chen, New York State Department of Transportation, 1220 Washington Avenue, Albany, N.Y. 12232. J. Perl, Department of Civil Engineering, University of Maryland, College Park, Md. 20742.

No previous study has attempted to analyze the allocation of resources and productivity in highway maintenance operations based on microeconomic theory. Several studies have previously been undertaken to identify highway maintenance research needs and/or to empirically address maintenance productivity. The FHWA has sponsored comprehensive research projects in all aspects of highway maintenance (*2,3*). Recently, the Strategic Highway Research Program (SHRP) identified highway maintenance as one of the six main research areas (*4*). Two early studies conducted for the Louisiana Department of Highways (*5,6*) and the City of Los Angeles (*7*) investigated the relationship between productivity and crew size. A value engineering study on bituminous patching was conducted by a group of four state DOTs to determine the unit cost associated with various combinations of labor, equipment, and materials (*8*). More recently, Sanderson and Sinha (*9*) proposed a monitoring procedure for identifying the high unit cost of some maintenance activities. Several studies attempted to develop regression models for estimating maintenance cost. The early models included explanatory variables such as traffic volume, surface width, and surface condition (*10*). McNeil and Hendrickson (*11*) proposed linear and nonlinear models that represented pavement age and equivalent axle load applications. Sharaf et al. (*12*) proposed a model in which the explanatory variables were equivalent axle load applications and climate zone.

The main objective of this study is to present a microeconomic-based approach for analyzing the allocation of aggregate resources (labor and equipment) and the characteristics of production in highway maintenance operations. The focus is on proposing a methodology based on the microeconomic concepts of production and cost functions that makes it possible to

1. Determine the maximum quantity of any given maintenance activity that can be accomplished with given quantities of labor and equipment;
2. Identify basic characteristic of the production process of a given maintenance activity;
3. Determine the optimal (cost-minimizing) combination of labor and equipment needed to perform a given level of maintenance activity; and
4. Estimate the minimum cost of accomplishing any given amount of a specified maintenance activity.

It should be emphasized that the focus of this study is on proposing a methodology, not on providing accurate empirical results.

At this time, the validity of the results and the practical usefulness of the proposed methodology are limited primarily because of data limitations. These limitations are identified and stated in the paper. Specific suggestions regarding the needed database for highway maintenance are discussed in the last section. However, an effort is made to show that the microeconomic theory of production and cost functions provides a promising theoretical basis for analyzing the productivity and cost efficiency of highway maintenance operations.

The next section provides a brief overview of the microeconomic concepts of production and cost functions in the context of highway maintenance operations. Next is an analysis that applies these concepts to real-life highway maintenance data. The final section summarizes the conclusion of the study and discusses its major recommendations.

MICROECONOMIC CONCEPTS

A production function represents the relationship between quantities of input factors (production factors) and the maximum level of output that can be produced, given those quantities. Common output measures of highway maintenance activities are tons of materials applied or lane-miles of highway maintenance. A maintenance activity can be viewed as a production process in which raw material is being "transformed" into material in place. Consequently, in applying the concept of production function to highway maintenance activities, material is not viewed as a production factor. The input factor in highway maintenance operations can be classified into two aggregate categories: labor and equipment. Quantities of labor and equipment inputs are commonly measured in man-hours and equipment-hours, respectively.

The production function of any given highway maintenance activity may be written as follows:

$$Z = f(L,E) = a_0 L^{a_1} E^{a_2} \tag{1}$$

where

Z = quantity of output,
L = quantity of labor,
E = quantity of equipment, and
a_0, a_1, a_2 = parameters.

Equation 1 provides a common form of a production function known as a Cobb-Douglas function. Other common forms are presented and analyzed in the next section.

Based on a production function, several characteristics of the production process can be derived. The *marginal product* (MP) of any given input factor is the change in output from a unit change in the quantity of that input factor, keeping the quantities of all other input factors unchanged. The *rate of technical substitution* (RTS) between two input factors is the amount by which one input factor can be reduced when there is a unit increase in the amount of the other factor such that the output quantity is kept unchanged. The return to scale represents the behavior of output quantity relative to a proportional change in the quantities of all input factors. Consider a proportional change by a factor K_1 in the quantities of all input factors, resulting in a change of output quantity by a factor K_2. Depending on the relationship between K_1 and K_2, the return to scale may be decreasing ($K_2 < K_1$), constant ($K_2 = K_1$), or increasing ($K_2 > K_1$). As is shown in the next section, these characteristics of the production process may provide important guidelines for the management of highway maintenance operations. Assuming that the prices of labor and equipment inputs remain constant during the analysis period, and are independent of the quantities used, the total expenditures on labor and equipment can be expressed as

$$C = h_L \cdot L + h_E \cdot E \tag{2}$$

where

C = total expenditures on labor and equipment and
h_L,h_E = unit prices of labor and equipment.

A *cost function* provides the minimum cost of producing any given level of output. The *average cost* is the ratio of total cost and output quantity. A cost function can be derived by minimizing Equation 2 subject to the constraint on production, as specified by the production function of Equation 1. This constitutes a constraint minimization problem that can be solved using the method of Lagrange multipliers, as illustrated below:

$$A = h_L \cdot L + h_E \cdot E - \lambda(a_0 \cdot L^{a_1} \cdot E^{a_2} - Z) \tag{3}$$

where A is the "Lagrangian" and is known as the Lagrange multiplier. The first-order conditions for the Lagrangian of Equation 3 result in the following set of simultaneous equations:

$$\frac{\partial A}{\partial L} = h_L + \frac{\lambda^{a_1}}{L} \cdot Z = 0 \tag{4a}$$

$$\frac{\partial A}{\partial E} = h_E + \frac{\lambda^{a_2}}{E} \cdot Z = 0 \tag{4b}$$

$$\frac{\partial A}{\partial \lambda} = a_0 L^{a_1} E^{a_2} - Z = 0 \tag{4c}$$

Solving the simultaneous Equations 4a through 4c provides the optimal (minimum cost) quantities of labor and equipment inputs (L^*, E^*) needed to produce a given quantity of output Z.

$$L^* = a_0^{-1/p} a_1^{a_2/p} a_2^{-a_2/p} h_L^{-a_2/p} h_E^{a_2/p} \cdot Z^{1/p} = \alpha \cdot Z^{1/p} \tag{5a}$$

$$E^* = a_0^{-1/p} a_1^{-a_1/p} a_2^{a_1/p} h_L^{a_1/p} h_E^{-a_1/p} \cdot Z^{1/p} = \beta \cdot Z^{1/p} \tag{5b}$$

where $p = a_1 + a_2$, and α, β are constants, as implied by Equations 5a and 5b, respectively. Substituting the optimal quantities of labor (L^*) and equipment (E^*) in the expenditures, Equation 2 yields the cost function shown below:

$$TC(Z) = p \cdot a_0^{-1/p} (h_L/a_1)^{a_1/p} (h_E/a_2)^{a_2/p} \cdot Z^{1/p} - \gamma \cdot Z^{1/p} \tag{6}$$

where

$TC(Z)$ = total cost of producing output quantity Z and
γ = constant.

Dividing the total cost by the quantity of output provides the average cost (unit cost):

$$AC(Z) = \frac{TC(Z)}{Z} = \gamma \cdot Z^{(1/p - 1)}$$

where $AC(Z)$ = average cost (unit cost) at output level Z.

ANALYSIS

The practical application of the microeconomic theory of production and cost functions involves two types of difficulties: (1) difficulties associated with the availability of adequate data and (2) difficulties related to the assumptions of the theory. The difficulties associated with the availability of adequate data are acute in pavement maintenance operations where little previous work has been done in applying microeconomic analysis methods. The estimation of a production function such as that discussed in the previous section requires homogeneous cross-sectional data on total output level (ton, lane-miles, etc.) and the associated aggregate quantities of labor and equipment, for individual maintenance activities. At this time, there is a little uniformity among state highway agencies in the collection of pavement maintenance data. There are significant differences in the maintenance activities for which data are collected, the types of data collected for each activity, and the units in which the data are represented (*13*).

Even when adequate data are available, there are some practical difficulties associated with the assumptions of the microeconomic theory of production and cost functions. First, the theory assumes homogeneous input factors. Clearly, in the context of pavement maintenance operations, each of the aggregate factors represents a large variety of specific input factors. For an individual maintenance activity, there are multiple types of equipment and employees of different categories. The homogeneity assumption may be satisfied more closely when the production function is estimated at the district level within a given state than when it is estimated at the statewide level. Second, in estimating a production function on cross-sectional data, it is assumed that the data represent the maximum level of output that can be accomplished with the employed combination of input factors. Since some inefficiencies in current pavement maintenance practices can be expected, it is likely that the data represent some points that are not on the "true" production functions. It should be stated that the difficulties associated with the theoretical assumptions are not specific to highway maintenance and are encountered in any application of these concepts. Nevertheless, when appropriate data are available, some useful important approximate results can still be obtained.

The data for this study come from a recent compilation of highway maintenance data produced for the Maryland State Highway Administration (*13*). As part of this data compilation effort, one state provided a uniform cross-sectional data set at the district level. The study uses these data for estimating the production functions. The purpose of the following analysis is twofold: (1) to illustrate the process of developing production functions for pavement maintenance activities and the use of these functions for obtaining information on the characteristics of various maintenance activities and (2) to illustrate the use of production functions for analyzing the productivity of resources and the cost efficiency of highway pavement maintenance operations.

The overall analysis consists of two phases. In the first phase, production functions (models) are estimated for five selected maintenance activities: hand patching, machine patching, concrete patching, joint/crack sealing, and seal coating. For each activity, eight different common forms of production models are estimated and evaluated. Based on this evaluation, "valid" production models are identified for use in the second phase. The second phase demonstrates how estimated production functions can be used for analyzing the productivity of resources and the cost efficiencies of highway pavement maintenance operations. This analysis is conducted at the state level. For each maintenance activity, five states are selected and the productivity of labor and equipment resources in each state is evaluated as discussed below.

Given a production function for a specific maintenance activity estimated in phase 1, the unit prices for labor and equipment, and the actual quantity of output for that activity at the selected state, the "optimal" quantities of labor and equipment are computed mathematically, as illustrated in the previous section. These "optimal" quantities provide target values of the most productive utilization of the two resources. The productivity of the two resources in performing the activity under consideration at the selected state are assessed by comparing the "optimal" and actual quantities of the resources used. Following the discussion of the previous section, the optimal quantities of labor and equipment are substituted in the expenditure function to determine the cost function for the state. Based on the cost function, the minimum unit cost (average cost) of producing the given level of output in the state is computed. The state's cost efficiency is assessed by comparing the "optimal" and actual unit costs.

The estimation district-level data are presented in the appendix (*13*). The data include 12 observations for hand patching, 24 for machine patching, 10 for concrete patching, 11 for joint/crack sealing, and 14 for seal coating. For each activity, the data include annual production, annual man-hours used, annual workdays, and standard equipment fleet size. Total equipment-hours are obtained by multiplying the annual work hours (based on eight work hours per day) by the standard equipment fleet size. Eight different production functions are estimated for each activity: linear, Cobb-Douglas, exponential, semilog linear, quadratic, translog, constant elasticity of substitution (C.E.S.), and modified C.E.S. (M.C.E.S.). The mathematical forms of these production models and their characteristics are shown in Table 1. The estimation is performed by multiple linear regression, where the nonlinear functions are linearized using the appropriate transformations.

The evaluation of the estimated production functions is conducted in two stages. The first stage validates the calibrated functions relative to the characteristics of the production functions specified in Table 1. The validation criteria are as follows:

1. The marginal products of labor and equipment should be non-negative.
2. The second partial derivative of output with respect to the quantities of labor and equipment should be negative, as implied by the law of diminishing returns.
3. The second partial derivative of labor quantity relative to equipment quantity should be non-negative. The second stage of the evaluation constitutes a statistical evaluation with regard to the overall statistical significance of the model (F-test), the statistical significance of individual coefficients (T-test), the expected signs of individual coefficients, and the proportion of variations explained by the model (R^2).

The "valid" calibrated production models are shown in Table 2. Only ten of the forty models have been accepted

TABLE 1 MATHEMATICAL FORMS OF PRODUCTION MODELS AND THEIR CHARACTERISTICS

Model	Function	$MP_L = \frac{\partial Z}{\partial L}$	$MP_E = \frac{\partial Z}{\partial E}$	$\frac{\partial^2 Z}{\partial L^2}$
Linear	$Z = a_0 + a_1 \cdot L + a_2 \cdot E$	a_1	a_2	0
Cobb-Douglas	$Z = a_0 \cdot L^{a_1} \cdot E^{a_2}$	$a_0 a_1 L^{a_1 - 1} \cdot E^{a_2}$	$a_0 a_2 L^{a_1} \cdot E^{a_2 - 1}$	$a_0 a_1 (a_1 - 1) L^{a_1 - 2} \cdot E^{a_2}$
Exponential	$Z = a_0 \cdot a_1^L \cdot a_2^E$	$a_0 \log a_1 \cdot a_1^L \cdot a_2^E$	$a_0 \log a_2 \cdot a_1^L \cdot a_2^E$	$a_0 \cdot (\log a_1)^2 \cdot a_1^L \cdot a_2^E$
Semilog Linear	$Z = a_0 + a_1 \log L + a_2 \log E$	$\frac{a_1}{L}$	$\frac{a_2}{E}$	$-\frac{a_1}{L^2}$
Quadratic	$Z = a_0 + a_1 L + a_2 E + b_1 L^2 + b_2 LE + b_3 E^2$	$a_1 + 2b_1 L + b_2 E$	$a_2 + b_2 L + 2b_3 E$	$2b_1$
Translog	$\log Z = a_0 + a_1 \log L + a_2 \log E + b_1 (\log L)^2 + b_3 (\log E)^2 + b_2 (\log L)(\log E)$	$\frac{Z}{L} \cdot (a_1 + 2b_1 \log L + b_2 \log E)$	$\frac{Z}{E} \cdot (a_2 + b_2 \log L + 2b_3 \log E)$	$\frac{Z}{L^2}(d^2 - d + 2b_1)$ $d = a_1 + 2b_1 \log L + b_2 \log E$
C.E.S.	$Z^{-\rho} = a_1 \cdot L^{-\rho} + a_2 \cdot E^{-\rho}$	$a_1 \cdot \left(\frac{Z}{L}\right)^{\rho+1}$	$a_2 \cdot \left(\frac{Z}{E}\right)^{\rho+1}$	$\frac{a_1 (\rho+1) Z^{\rho+1} \cdot (a_1 Z^{\rho} - L^{\rho})}{L^{2\rho+2}}$
Modified C.E.S.	$Z^{-\rho} = a_0 + a_1 L^{-\rho} + a_2 E^{-\rho}$	$a_1 \cdot \left(\frac{Z}{L}\right)^{\rho+1}$	$a_2 \cdot \left(\frac{Z}{E}\right)^{\rho+1}$	$\frac{a_1 (\rho+1) Z^{\rho+1} \cdot (a_1 Z^{\rho} - L^{\rho})}{L^{2\rho+2}}$

based on the preceding evaluation process. The relatively low quality of the calibration results can be attributed to three basic factors. First is the inadequacy of the estimation data in terms of both the size and quality of the data set. The estimation data were not readily available in the required form and had to be manipulated based on certain assumptions. Second, owing to data limitations, the input factors are defined at the highest level of aggregation, which most likely results in a significant violation of the homogeneity assumption. Third, given the level of aggregation used, there is a significant degree of multicollinearity between the two independent variables, which leads to inaccurate partial coefficients. In highway maintenance operations, one may expect a relatively high correlation between total labor and total equipment because a substantial portion of labor crews are equipment operators. The remedies for the multicollinearity problem are discussed in the next section.

Table 2 shows better calibration results for machine and concrete patching than for hand patching. In all the models for machine patching and concrete patching, the partial coefficient of equipment quantity has the correct sign. This may result from better equipment data. The equipment fleet sizes for machine patching and concrete patching are larger and less variable than those for hand patching. Consequently, the errors associated with the manipulation of equipment data as well as the errors in recording equipment data may be less significant. The superiority of the calibration results of concrete patching over other activities may be attributed to the routine and less variable nature of that activity. No "valid" model for joint/crack sealing was obtained. One possible explanation for the difficulty of calibrating a production model for joint/crack sealing with the available data is that the available unit of output (100 feet of joint or crack) does not reflect actual surface conditions. Joints or cracks that need sealing may have different widths, depths, and severities of damage. A more appropriate unit of output may be the quantity of sealant applied.

Table 3 shows the following three characteristics of each activity, based on the calibrated production models: (1) marginal products of labor (MP_L) and equipment (MP_E), (2) rate of technical substitution between the quantities of labor and equipment (RTS_{EL}), and (3) return to scale. These characteristics are computed at the average level of output from the estimation data. It can be noticed that the values are highly sensitive to the type of production model used. Not all the values presented in Table 3 are "valid." This can be attributed to the three basic reasons for estimation difficulties discussed earlier. The results of Table 3 show that for hand patching, the marginal products of labor at the average level of output, obtained from the translog and quadratic models, are 0.48 and 0.55, respectively. From the translog model, an additional man-hour in hand patching would result in an additional 0.48 ton of hand patching output. The results also indicate that hand patching has a large range of increasing return to scale. This implies that hand patching is often more efficient when done in large-scale operations. Again, it should be recognized that this conclusion is based on the estimated production functions and may not be highly accurate, given the low accuracy of the estimation results.

The results of Table 3 show that the marginal product of labor in machine patching is larger than that in hand patching. Machine patching is the leveling and patching of a roadway

TABLE 2 CALIBRATED PRODUCTION MODEL

Activity	Model	Calibrated Production Model
Hand Patching	Quadratic	$Z = -1395 + 0.34L + 0.009E - 0.000082L^2 + 0.00022L \cdot E - 0.00015E^2$ (0.91) (0.02) (-1.7) (1.66) (-1.7) $R^2=0.71$
	Translog	$\log Z = -19.2 + 1.84\log L + 2.69\log E - 6.24(\log L)^2 + 12.8(\log L)(\log E) - 6.77(\log E)^2$ (0.23) (0.31) (-2.05) (2.13) (-2.20) $R^2=0.86$
Machine Patching	Translog	$\log Z = -71.3 - 37.7\log L + 52.8\log E - 2.56(\log L)^2 + 8.85(\log L)(\log E) - 6.98(\log E)^2$ (-1.38) (1.64) (-0.45) (0.69) (-0.94) $R^2=0.52$
Concrete Patching	Linear	$Z = -22 + 0.14L + 0.02E$ (1.00) (0.22) $R^2=0.59$
	Cobb-Douglas	$Z = 0.00065 \cdot L^{0.87} \cdot E^{0.91}$ (1.78) (1.28) $R^2=0.92$
	Exponential	$\log Z = -0.23 + 0.0015L + 0.0022E$ (0.55) (1.29) $R^2=0.76$
	Quadratic	$Z = -11.8 + 0.13L + 0.02E - 0.001L^2 + 0.002L \cdot E - 0.00046E^2$ (0.20) (0.05) (-1.58) (2.30) (-2.51) $R^2=0.88$
	Translog	$\log Z = -12 - 22.6\log L + 23.3\log E - 4.34(\log L)^2 + 11.2(\log L)(\log E) - 6.69(\log E)^2$ (-1.33) (1.31) (-1.47) (1.43) (-1.38) $R^2=0.95$
	C.E.S.	$Z^{0.9} = 0.15L^{0.9} + 0.008E^{0.9}$ (0.99) (0.08) $R^2=0.74$
	M.C.E.S.	$Z^{-0.25} = -0.36 + 2.96L^{-0.25} + 0.9E^{-0.25}$ (6.11) (1.01) $R^2=0.97$

surface with bituminous mix, using paving machines. The large marginal product of labor in machine patching may result from the fact that additional labor increases the utilization of machines. The calibration results indicate that there are no scale economies in machine patching, which implies that machine patching may be done more efficiently with a relatively large number of small-scale operations than with a small number of large-scale operations. Concrete patching is more "labor-intensive" than either hand patching or machine patching. Maintenance work on concrete pavement usually requires more labor input than do similar activities in asphalt pavements. This may explain the relatively low marginal product of labor obtained for concrete patching. The results show significant variability in the rate of technical substitution in concrete patching, depending on the production model used. The average rate of technical substitution is 6.4, which means that every additional man-hour may allow the reduction of six equipment-hours without affecting the level of output.

Because of the three basic reasons for the expected low accuracy of the calibration results stated earlier, the values of Table 3 are most likely not highly accurate. The preceding discussion, however, illustrates the potential usefulness of accurate production models in enabling the derivation of important characteristics of the production processes of various highway maintenance activities, thereby providing important managerial guidelines.

The second phase of the analysis uses the calibrated production functions of Table 2 to determine the "optimal" quantities of labor and equipment for producing the reported level of output and the "optimal" unit cost (average cost), in each

TABLE 3 CHARACTERISTICS OF PRODUCTION PROCESSES, BASED ON CALIBRATED MODELS

Activity	Acceptable Model	MP_L	MP_E	RTS_{EL}	Return to Scale
Hand Patching	Quadratic	0.55	-0.30	-	$1<K_1<6.67$, increasing $K_1=6.67$, constant $K_1>6.67$, decreasing
	Translog	0.43	-0.31	-	$1<K_1<2.57$, increasing $K_1=2.57$, constant $K_1>2.57$, decreasing
Machine Patching	Translog	2.00	-1.30	-	$1<K_1<\infty$, decreasing
Concrete Patching	Linear	0.14	0.02	-7	$1<K_1<\infty$, increasing
	Cobb-Douglas	0.061	0.034	-1.79	$1<K_1<\infty$, increasing
	Exponential	0.018	0.028	-0.67	$1<K_1<\infty$, decreasing
	Quadratic	0.85	0.26	-3.27	$1<K_1<1.5$, increasing $K_1=1.5$, constant $K_1>1.5$, decreasing
	Translog	-0.12	0.20	-	$1<K_1<\infty$, decreasing
	C.E.S.	0.12	0.006	-19.7	$1<K_1<\infty$, constant
	M.C.E.S.	0.22	0.035	-6.28	$1<K_1<\infty$, increasing

one of the selected five states. The "optimal" values are compared with the actual values reported by the states to assess the productivity of the two aggregate resources and the cost efficiency for each state. For illustration purposes, the results of this phase of the analysis are presented only for concrete patching. Tables 4 and 5 present comparisons of the "optimal" and actual quantities of labor and equipment and the values of unit cost, for the five selected states, based on the M.C.E.S. and Cobb-Douglas production functions, respectively.

The low accuracy of the calibration results not withstanding, the results of Table 4 and 5 show some significant differences between the "optimal" quantities of labor and equipment and the actual reported quantities. In general, the "optimal" quantities of labor and equipment are lower than the actual reported quantities, indicating a potential for gains in both labor and equipment productivities. The results also show that in some states, the unit cost of concrete patching may be reduced. As before, because of the relatively low accuracy of the calibrated production models, some of the results of Tables 4 and 5 that show "optimal" unit cost values that are higher than the corresponding actual values are invalid. With more accurate and disaggregate data and more reliable production functions, however, this type of analysis can provide important information regarding the productivity and cost efficiency of various highway maintenance activities, as well as guidelines for improving both the productivity of resources and the cost efficiency of these activities at the state and/or district levels.

CONCLUSIONS AND RECOMMENDATIONS

The microeconomic theory of production and cost functions provides a promising theoretical basis for analyzing the productivity and cost efficiency of highway maintenance operations. This theory may provide (1) guidelines on the approximate quantities of input resources needed to produce any given quantity of highway maintenance, (2) estimates of minimum unit costs for performing various quantities of maintenance operations, and (3) characteristics of the production process of various maintenance activities (e.g., marginal prod-

TABLE 4 A COMPARISON OF OPTIMAL AND ACTUAL VALUES OF LABOR QUANTITY, EQUIPMENT QUANTITY, AND UNIT COST FOR CONCRETE PATCHING, BASED ON M.C.E.S. PRODUCTION MODEL

State		Labor	Equipment	Unit Cost[b]
1	Optimal	3,179	1,554	41.2
	Actual	8,610	8,610	118
	% Difference[a]	171%	454%	186%
2	Optimal	360.4	362.0	.679
	Actual	295.8	443.7	621
	% Difference[a]	22%	22%	9%
3	Optimal	1,540	1,392	124
	Actual	5,840	3,504	432
	% Difference[a]	279%	152%	248%
4	Optimal	205	50.7	611
	Actual	37.5	19.0	147
	% Difference[a]	447%	167%	316%
5	Optimal	1,514	2,662	78.8
	Actual	3,336	5,156	169
	% Difference[a]	120%	94%	115%

[a] % Difference is the greater value minus the smaller value and then divided by the smaller value of the "optimal" and "actual".
[b] Includes the costs of labor and equipment only.

TABLE 5 A COMPARISON OF OPTIMAL AND ACTUAL VALUES OF LABOR QUANTITY, EQUIPMENT QUANTITY, AND UNIT COST FOR CONCRETE PATCHING, BASED ON COBB-DOUGLAS PRODUCTION MODEL

State		Labor	Equipment	Unit Cost[b]
1	Optimal	4,299	5,425	79.1
	Actual	8,610	8,610	118
	% Difference[a]	100%	59%	99%
2	Optimal	211.2	651.8	590
	Actual	295.8	443.7	621
	% Difference[a]	40%	47%	5%
3	Optimal	1,202	3,254	142
	Actual	5,840	3,504	432
	% Difference[a]	386%	8%	204%
4	Optimal	204	109	823
	Actual	37.5	19.0	147
	% Difference[a]	444%	167%	460%
5	Optimal	1,010	6,266	80.4
	Actual	3,336	5,156	169
	% Difference[a]	230%	22%	110%

[a] % Difference is the greater value minus the smaller value and then divided by the smaller value of the "optimal" and "actual".
[b] Includes the costs of labor and equipment only.

ucts, scale economies). As illustrated by the discussion of the previous section, these guidelines and characteristics can provide highly useful information for the management of highway maintenance operations.

The validity and quality of the results that can be obtained based on the proposed microeconomic approach depend on the availability of adequate data. The development of a uniform structure of a database for highway maintenance is needed. This will enable the collection of data at the state or district level, which will be consistent with the requirements of a microeconomic analysis. Research on the appropriate measures of inputs and outputs in various highway maintenance activities is also needed. Input factors should be defined at more disaggregate levels than that used in this study. The definition of labor input may be disaggregated by classifying maintenance labor into its major categories (i.e., foreman, equipment operator, truck driver, manual laborer, and flagman). Equipment classification may be more difficult. A possible classification may consist of material hauling equipment, crew cab, traffic handling devices, other major equipment, and small tools.

The definition of appropriate output measures in highway maintenance operations is a difficult issue that requires a great deal of study. In general, the volume (or weight) of the materials being processed is a better measure than the surface area being treated. Ideally, not only the quantity but also the quality of maintenance should be represented. This may require the estimation of different production functions for different quality standards. Highway maintenance activities may also be performed using alternative materials. Since different kinds of materials may imply different relationships between the quantities of input factors and the level of output, different production functions may have to be estimated for different materials. The need to determine the maximum quantity of output of any given maintenance activity that can be accomplished from any given combination of disaggregate resources with a given material (such as to achieve a prespecified quality standard) may imply that the data for the development of production functions should be collected from designated highway segments, under controlled conditions, as proposed recently in the SHRP program (*4*).

APPENDIX Estimation District-Level Data

Activity	Fiscal Year	District	Z	L (Man-Hr.)	E (Equi-Hr)
Hand	1984-1985	1	5638	29676	26580
		2	7194	35993	22212
		3	2003	10538	9474
		4	837	8789	8989
		5	3354	24618	22984
		6	4199	20601	19197
		7	2824	19077	16201
		8	2087	11616	7305
		9	2937	14440	11918
		10	2844	12288	10610
		11	2536	14972	9105
		12	6406	24737	17672
Patching Z (ton) Equip. Size = 4	1985-1986	1	3137	18963	17387
		2	5179	28670	19274
		3	1026	5465	4516
		4	886	8094	7081
		5	2430	19331	18127
		6	4218	18133	16978
		7	2821	17358	14870
		8	1409	9056	5986
		9	2220	11813	10025
		10	2435	10700	9760
		11	3294	15894	9594
		12	12050	26329	17800
Machine Patching Z (ton) Equip. Size =13	1984-1985	1	15995	13707	13893
		2	39820	23984	28488
		3	31893	19097	24580
		4	32257	53610	58912
		5	23472	21395	26135
		6	19933	20895	24554
		7	16432	15066	21389
		8	42732	34130	36114
		9	44591	39036	45144
		10	45068	29800	33539
		11	32095	12063	17682
		12	22300	10552	13151

APPENDIX Estimation District-Level Data

Activity	Fiscal Year	District	Z	L (Man-Hr.)	E (Equi-Hr)
Machine Patching Z (ton) Equip. Size =13	1985-1986	1	27165	20488	19846
		2	58547	32570	37040
		3	30090	22261	21694
		4	46112	58195	59751
		5	41048	30487	35284
		6	26016	26337	29534
		7	23480	18826	23003
		8	52688	40161	40093
		9	42760	34600	38094
		10	71371	47880	48948
		11	53711	19893	25794
		12	60933	22434	25547
Concrete Patching Z(Cu.Yd.) Equip. Size =11	1984-1985	1	1	57	99.4
		2	7	365	627
		4	187	1246	1837
		5	46	343	616
		7	53	372	913
		8	26	952	1062
	1985-1986	4	295	1097	1705
		5	50	765	1848
		10	1	56	88
		12	0.1	7	77
Joint/ Crack Sealing Z (Ft.) Equip. Size =10	1984-1985	1	20800	440	810
		2	17200	631	705
		4	7500	40	40
		11	700	100	160
		12	10000	8	40
	1985-1986	1	6300	136	240
		4	22000	120	160
		5	171700	332	440
		6	100	8	80
		8	4500	192	240
		11	12000	352	480
Seal Coating Z (ton) Equip. Size =13	1984-1985	1	7963	5135	5110
		2	144	151	196
		4	2422	1730	1430
		5	4105	2609	2522
		6	7001	3997	2900
		8	607	695	1145
		10	123	151	208
		12	10	75	104
	1985-1986	1	15362	8859	9142
		2	11801	6719	7768
		4	6505	3836	2532
		5	1074	1061	956
		6	7565	4521	3932
		9	5125	3420	3924

ACKNOWLEDGMENTS

The authors wish to thank Matthew W. Witczak and Paul Schonfeld for their useful comments.

REFERENCES

1. *Special Report 202: America's Highways Accelerating the Search for Innovation*. TRB, National Research Council, Washington, D.C., 1984, pp. 97–106.
2. *Highway Maintenance Research Needs 1980*. Report RD-81-502. Office of Research and Development, FHWA, U.S. Department of Transportation, 1981, pp. 1–23.
3. *Highway Maintenance Research Needs*. FHWA Report RD-75-511. TRB, National Research Council, Washington, D.C., 1975, pp. 1–7.
4. *Strategic Highway Research Program, Research Plans*. NCHRP Project 20-20. TRB, National Research Council, Washington, D.C., 1986, pp. 1–6.
5. *Louisiana Highway Maintenance Research Project*. Report IV. Roy Jorgensen Associates, Inc., 1968, pp. 39–49.
6. *Louisiana Highway Maintenance Research Project*. Report VII. Roy Jorgensen Associates, Inc., 1969, pp. 14–19.
7. L. C. Jones. *Special Report 100: Approach to Maintenance Management*. HRB, National Research Council, Washington, D.C., 1968, pp. 108–111.
8. *Optimizing Maintenance Activities, Bituminous Patching*. FHWA Report TS-78-220. Arkansas DOT, Oregon DOT, Pennsylvania DOT, and Utah DOT; FHWA, U.S. Department of Transportation, 1978.
9. V. A. Sanderson and K. C. Sinha. *Development and Use of a Management Information System to Identify Areas of Routine Maintenance Productivity Improvement*. Report IN-JHRP-84-11. FHWA, U.S. Department of Transportation, 1984.
10. M. J. Betz. Highway Maintenance Costs A Consideration for Developing Areas. In *Highway Research Record 94*, HRB, National Research Council, Washington, D.C., 1965, pp. 12–17.
11. S. McNeil and C. Hendrickson. Prediction of Pavement Maintenance Expenditure by Using Statistical Cost Function. In *Transportation Research Record 846*, TRB, National Research Council, Washington, D.C., 1986, pp. 71–76.
12. E. A. Sharaf, K. C. Sinha, R. C. Whitmire, and E. J. Yoder. Field Investigation of Resource Requirements for State Highway Routine Maintenance Activities. In *Transportation Research Record 943*, TRB, National Research Council, Washington, D.C., 1983, pp. 24–27.
13. J. Perl, H. J. Chen, and M. W. Mirza. *Pavement Maintenance: Review and Compilation of Existing Data*. FHWA/MO-88/08. Prepared for the Maryland State Highway Administration, Maryland Department of Transportation, Baltimore, 1987.

Publication of this paper sponsored by Committee on Pavement Management Systems.

An Examination of the AASHTO Remaining Life Factor

ROBERT P. ELLIOTT

The 1986 AASHTO Pavement Design Guide introduced a remaining life factor that is applied in the design of pavement overlays. An examination of the remaining life concept was made to determine its practicality. The examination revealed inconsistencies in overlay designs determined using the AASHTO remaining life factor. Further investigation revealed that the remaining life factor should have a value of 1.0 for all overlay situations. As a result, it is recommended that the AASHTO overlay design approach be revised to exclude remaining life considerations.

The 1986 AASHTO Pavement Design Guide (*1*) introduced a remaining life concept that is applied in the design of overlays. The concept is based on the rationale that the structural capacity of a pavement decreases with load applications. For a pavement that has been overlaid, the structural capacity of the original pavement is a function of the loads applied before overlay as well as those applied after overlay. As presented by AASHTO, the remaining life concept requires that overlay thicknesses be selected considering both the "remaining" life of the pavement at the time of overlay and the expected "remaining" life when the next overlay will be applied.

For flexible pavement overlay design, the remaining life concept is applied using the equation:

$$SNol = SNn - Frl * SNeff \quad (1)$$

where

- $SNol$ = required structural number for the overlay;
- SNn = total structural number required, based on traffic soils, etc.;
- Frl = remaining life factor, a function of pavement condition prior to overlay and the condition predicted at the end of the design traffic; and
- $SNeff$ = the effective structural number of the existing pavement at the time of overlay.

The remaining life factor (Frl) is determined using the graph shown as Figure 1. In using the graph, RLx is the remaining life factor of the existing pavement at the time of overlay, and RLy is the anticipated future remaining life of the overlaid pavement when it will be overlaid. Concern has been expressed regarding the Frl concept. Of particular concern is the fact that at low values of RLx and RLy, the general slope of the Frl curve reverses. This investigation was initiated to study the concept and to establish a rationale for this slope reversal.

The investigation demonstrated inconsistencies in overlay designs using the AASHTO remaining life concept and suggests that for consistent designs Frl should be 1.0 for all values of remaining life.

Department of Civil Engineering, University of Arkansas, 4190 Bell Engineering Center, Fayetteville 72701.

CONCEPT OF REMAINING LIFE

The AASHTO remaining life concept is discussed in detail elsewhere (*2*). The following abbreviated discussion is presented for those not familiar with that document.

The remaining life concept was developed to be used in a structural deficiency approach to overlay design. In the structural deficiency approach, the structural requirement for the overlay ($SNol$) is determined as the difference between the structure needed to support future (design) traffic (SNn) and the structural capacity of the existing pavement ($SNeff$). Frl was added to the basic structural deficiency equation to account for future structural damage to the existing pavement.

The fundamentals of remaining life are illustrated in Figure 2 using the flexible pavement structural number as the measure of structural capacity. The serviceability of a pavement decreases with time and traffic from an initial value, Po. Without rehabilitation, the serviceability would eventually reach a "failure" level, Pf. The total number of traffic applications to "failure" is shown as Nf.

At some point prior to failure, however, an overlay is placed. The traffic applications to that point are x. The remaining life (RLx) is defined as the additional applications that could have been applied to "failure" expressed as a fraction of the total possible applications. That is:

$$RLx = (Nf - x)/Nf \quad (2)$$

The structural capacity of the pavement decreases similarly from SNo to SNf. At the time of overlay, the pavement structural capacity is SNx. A pavement condition factor (Cx) can be defined as:

$$Cx = SNx/SNo \quad (3)$$

Since SNx is also the effective structural capacity ($SNeff$) of the pavement at the time of overlay, $SNeff$ can be expressed as a function of Cx and SNo.

$$SNeff = Cx * SNo \quad (4)$$

For the AASHTO Guide, a relationship between Cx and RLx was developed using the AASHTO flexible pavement design equation. Cx and RLx values were computed for various designs based on present serviceable indices at "failure" (Pf) of 1.5 to 2.5. These produced a "best-fit" relationship:

$$Cx = RLx^{0.165} \quad (5)$$

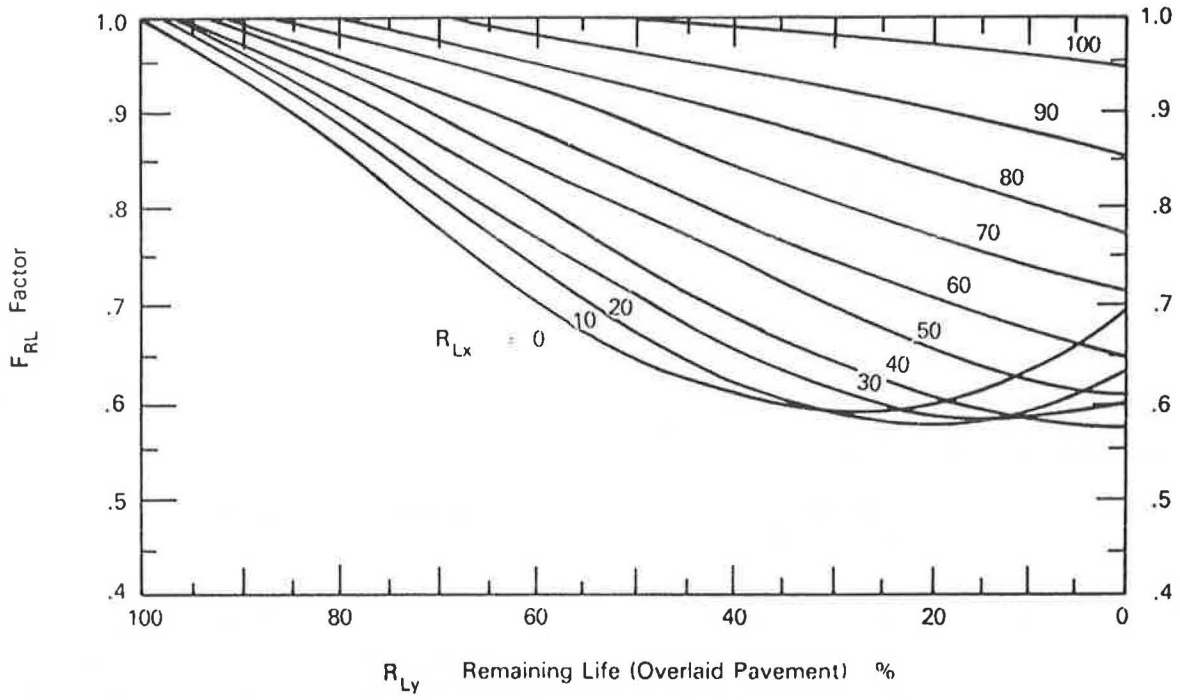

FIGURE 1 AASHTO remaining life factor curves (*1*).

A first step in this investigation was to attempt to reproduce this relationship. *Cx* and *RLx* values were computed for structural numbers ranging from 6.0 to 2.5, with *Pf* equal to 1.5 and 1.0. As shown in Figure 3, these values fit the AASHTO relationship reasonably well.

The AASHTO remaining life concept, however, does not use the "best-fit" relationship. Although the *Cx* values produced by the relationship were viewed as being realistic to *RLx* values as low as 0.005, the relationship was abandoned because *Cx* goes to zero at "failure" (*RLx* = zero). A modified relationship was used by AASHTO. The modified relationship (*2*) is:

$$Cx = 1 - 0.7 * e^{-(RLx + 0.85)^2} \quad (6)$$

The best-fit and modified relationships are compared in Figure 4. In addition to *Cx* not going to zero at "failure," the modified relationship provides a *Cx* value for a negative remaining life. Although the meaning of a negative remaining life is not clear, this feature of the modified relationship is a necessary (although perhaps erroneous) part of the AASHTO application of remaining life.

APPLICATION OF REMAINING LIFE TO OVERLAYS

The reduction in structural capacity of the overlaid pavement is similar to that shown in Figure 2. Thus, if *SNn* and *y* were used in place of the *SNo* and *x* used previously, the structural capacity of the overlaid pavement after *y* load applications would be:

$$SNy = Cy * SNn \quad (7)$$

Without the remaining life factor (*Frl*), *SNn* is *SNol* + *SNeff*. Thus, Equation 7 can be written:

$$SNy = Cy * SNol + Cy * SNeff \quad (8)$$

AASHTO (*2*) argued that this equation is incorrect since the existing pavement (*SNeff*) would lose structural capacity at a greater rate than would the overlay (*SNol*). To "correct" the equation, AASHTO stated that *Cy* * *SNeff* should be replaced by a similar function that includes the original (new) structural number of the existing pavement (*SNo*) and a condition factor (*Cyx*) that is a function of the traffic applications (or remaining life) both before and after the overlay. That is:

$$Cyx = f(RLx, RLy) \quad (9)$$

and

$$SNy = Cy * SNol + Cyx * SNo \quad (10)$$

From these, AASHTO developed a relationship for *Frl* in terms of *Cyx*, *Cx*, and *Cy*:

$$Frl = Cyx/(Cx * Cy) \quad (11)$$

At this point, it should be noted that Equation 8 already included *SNo* and a function of the traffic before and after overlay (*Cx* * *Cy*). Using Equation 4, *SNeff* in Equation 8 may be replaced by *Cx* * *SNo*, resulting in:

$$SNy = Cy * SNol + Cx * Cy * SNo \quad (12)$$

Nevertheless, the introduction of *Cyx* might be viewed as an advance since *Cx* * *Cy* specifies the structural loss relationship for the existing pavement, while *Cyx* does not. Yet,

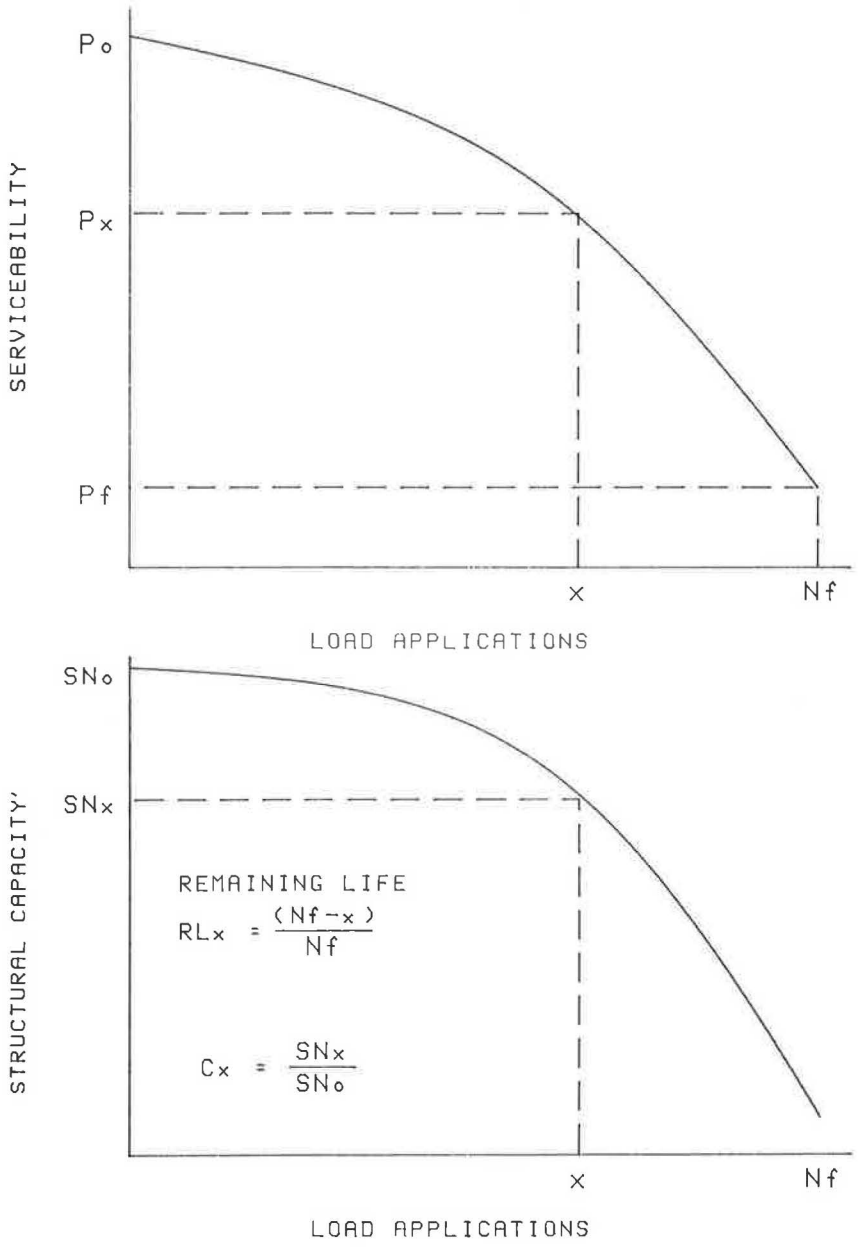

FIGURE 2 Illustration of the remaining life concept.

in order to apply *Frl*, it was necessary to assume an arbitrary relationship (Equation 13, below).

REMAINING LIFE FACTOR CURVES

The second step in the current investigation was to verify the remaining life factor curves (Figure 1). These curves were developed using Equations 6 and 11. However, because *Cxy* is a function of *RLx* and *RLy*, AASHTO has to assume a relationship between the two in order to apply Equation 6. It was assumed that the combined remaining life (*RLxy*) would be equal to the remaining life at the time of overlay (*RLx*) minus the damage done (*dy*) during the period of overlay. That is:

$$RLxy = RLx - dy \tag{13}$$

Since *dy* is $1 - RLy$, this equation may be written:

$$RLxy = RLx + RLy - 1 \tag{14}$$

Initially, this assumption seems reasonable. However, it produces an uneasiness that grows with further reflection. By subtracting the full damage done after overlay, there seems to be no accounting for the reduction in the rate of damage that results from the lower load stresses due to the overlay. Also, because both *RLx* and *RLy* generally will be less than 0.5, the combined remaining life will be negative. A negative remaining life has no meaning. Finally, because the condition

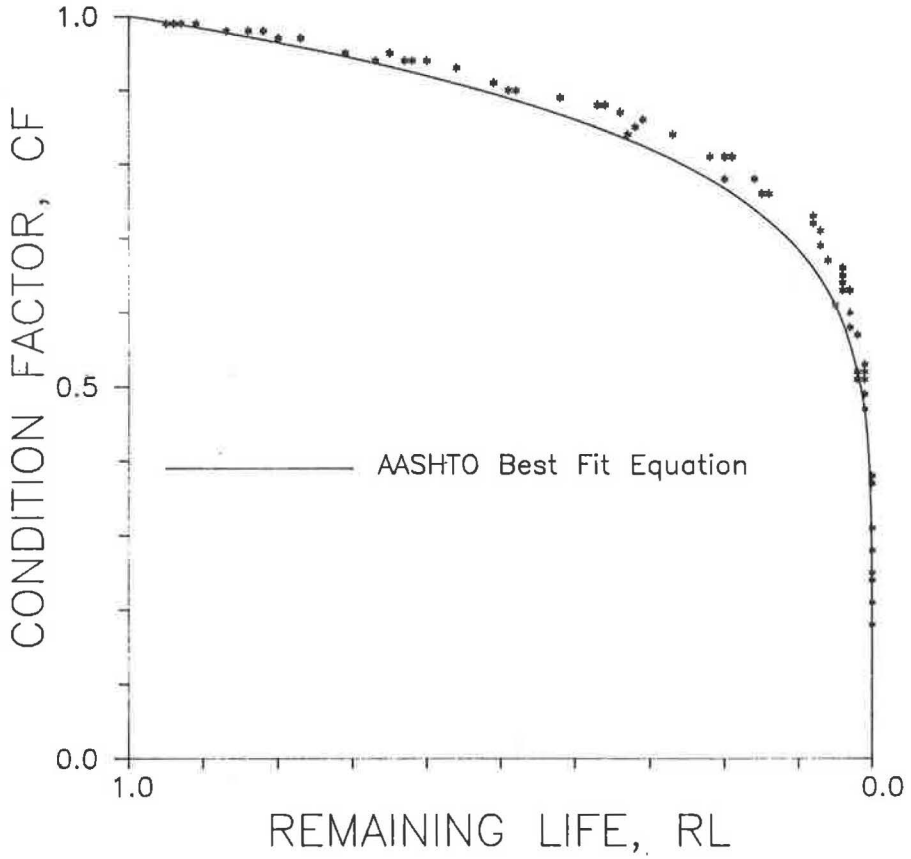

FIGURE 3 Comparison of values from this investigations with the AASHTO "best-fit" equation.

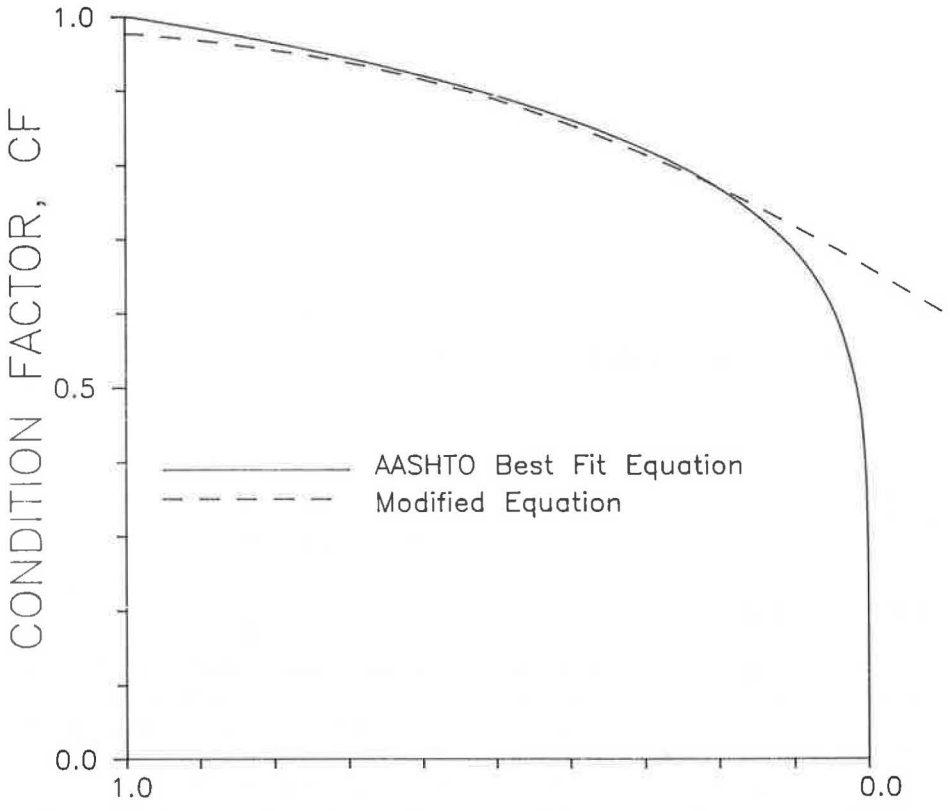

FIGURE 4 Comparison of the AASHTO "best-fit" and modified equations.

TABLE 1 OVERLAY COMPUTATIONS USING REMAINING LIFE FACTORS

Design ESAL = 5,000,000 SNeff = 4.5

Terminal PSI	Required SNn	RLy	RLx = 0.0 Frl	RLx = 0.0 SNol	RLx = 0.2 Frl	RLx = 0.2 SNol	RLx = 0.4 Frl	RLx = 0.4 SNol
3.5	6.65	.904	.988	2.20	.999	2.15	1.00	2.15
3.25	6.02	.904	.945	1.77	.967	1.67	.987	1.58
3.00	5.59	.827	.881	1.63	.919	1.45	.955	1.29
2.50	5.03	.603	.711	1.83	.773	1.55	.848	1.21
2.25	4.84	.465	.633	1.99	.689	1.74	.776	1.35
2.00	4.69	.317	.589	2.04	.616	1.92	.703	1.53
1.75	4.57	.167	.605	1.85	.576	1.98	.642	1.68
1.60	4.50	.062	.665	1.51	.578	1.90	.615	1.73
1.55	4.48	.029	.694	1.36	.586	1.84	.610	1.74

factor relationship itself (Equation 6) is assumed, this assumption (Equation 13) results in a compounding of assumptions.

Nevertheless, application of this assumption together with Equations 6 and 11 verified the mathematical accuracy of Figure 1, including the slope reversals at the lower values of *RLx* and *RLy*.

INCONSISTENCIES IN APPLICATION

The third step in the current investigation involved application of the *Frl* factors to a hypothetical design situation to see if reasonable values and trends were produced. The design situation selected involved a design traffic ESAL of 5 million and an effective structural number for the existing pavement (*SNeff*) of 4.5. The required overlay structural numbers (*SNol*s) were determined for terminal Present Serviceability Indices (PSIs) ranging from 3.5 to 1.55. The remaining life of the existing pavement (*RLx*) was also varied, using the values 0.0, 0.2, and 0.4.

The total structural number required (*SNn*) and remaining life of the overlay (*RLy*) were computed using the AASHTO design equation (*1*) with a "failure" PSI of 1.5. A reliability to 50 percent and subgrade resilient modulus of 3,000 psi were used to reduce the equation to the original AASHO Road Test equation and eliminate any potential effects resulting from assumptions involved in adding reliability and subgrade modulus to the equation. To assure accuracy in application, the *Frl* values were calculated in lieu of being taken from Figure 1.

The results of the analyses are listed in Table 1 and displayed graphically in Figure 5. The slope reversals seen in Figure 5 clearly illustrate an inconsistency. The major inconsistency, however, is the general negative slope of the curves between terminal PSIs of 2.0 to 3.0. For a given design situation, design to a lower terminal PSI should result in a lower required structural number. This is correctly illustrated by the trend of the *SNn* values in Table 1. However, after *Frl* is applied to establish the overlay requirement, the general trend for *SNol* is reversed.

Quite obviously, something is wrong with the AASHTO remaining life approach.

MODIFICATION OF THE REMAINING LIFE APPROACH

The final step in the investigation was to identify the problem with the concept and to develop a recommended correction. The apparent source of the problem is in the compounding of assumptions: first, with the modification of the *Cx-RLx* relationship (Equations 5 and 6) and, second, with the combined remaining life relationship (Equation 14).

As an alternative to Equation 14, the following development is suggested. The curve in Figure 6 represents some as yet undefined relationship between *C* and *RL*. At some point (*x*), the pavement is overlaid and the existing pavement values are *Cx* and *RLx*. After the overlay, *C* of the existing pavement will continue to decline from *Cx*, but *RL* will now be 100. This is represented on Figure 6 by the revised *RL* scale.

At the time of the second resurfacing (*y*), the respective values are *Cyx* and *RLy*. A simple scale transformation of *RLy* from the revised scale to the original scale shows that:

$$RLxy = RLx * RLy \quad (15)$$

This equation for *RLxy* eliminates the need for a negative remaining life. The philosophy behind it is similar to the concept of the man who each day walks halfway to his destination. He never arrives. As long as the pavement is overlaid prior to "failure," "failure" is not reached in any component. The existing damage condition remains in the existing materials and progresses. However, the overlay is designed to slow the rate of additional damage, so that the "failure" condition is reached for the entire pavement.

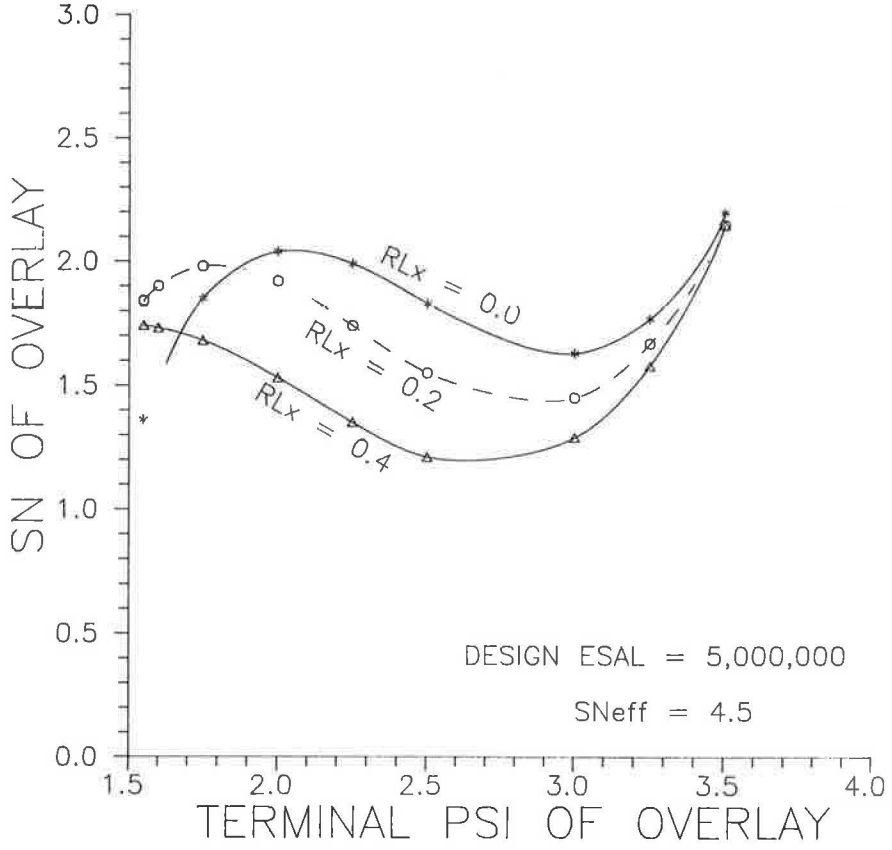

FIGURE 5 Results of overlay analyses using the AASHTO remaining life factor.

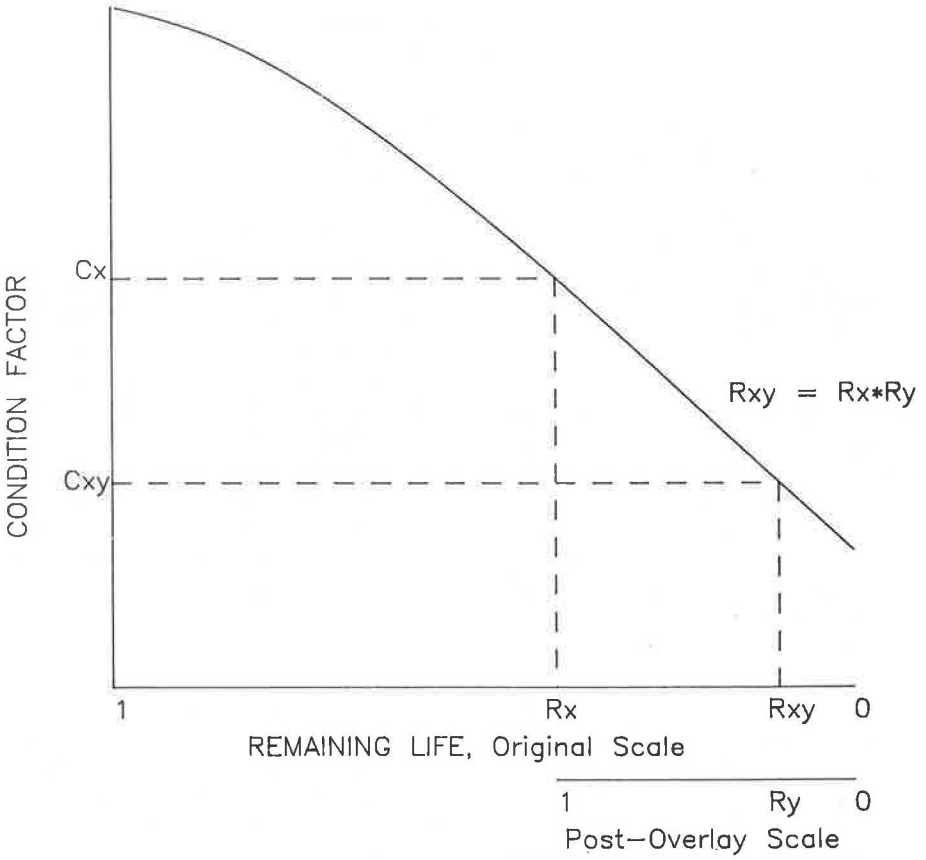

FIGURE 6 Modified approach for determining *Cxy*.

Equations 15 and 11 were used to determine *Frl* values with both the original *C-RL* relationship (Equation 5) and the modified version (Equation 6). With the original relationship, *Frl* is always 1.0:

$$Frl = (RLxy)^{.165}/(RLx^{.165} * RLy^{.165}$$

$$= (RLx * RLy)^{.165}/(RLX * RLY)^{.165} = 1.0 \qquad (16)$$

With the modified AASHTO relationship (Equation 6), the equation is more complicated. However, except for very low values of both *RLx* and *RLy*, *Frl* is generally about 1.0. At very low *RL* values, *Frl* becomes greater than 1.0. (At *RLx* and *RLy* equal to 0.0, *Frl* is 1.5.)

OTHER DIFFICULTIES

Inconsistency in application is not the only difficulty with the AASHTO remaining life concept. Other difficulties need to be recognized and researched. The first of these is the application of the AASHTO Road Test performance equation to establish a remaining life-condition relationship.

The Road Test equation is an empirical relationship selected to provide a means of predicting the performance of the research pavements at the Road Test. It is not a theoretical or fundamental performance relationship and may, in fact, not even be the "best-fit" prediction relationship. It is simply the best relationship found by the researchers involved in the Road Test using the analytic tools that were available at that time. To apply the equation in the fashion used relative to remaining life represents a very significant extrapolation beyond the data and original intent of the equation.

Second, as it is being applied, the remaining life concept assumes that all materials will experience damage and structural loss at the same rate. It is conceivable that at "failure" a stabilized layer will be reduced to the equivalency of a granular layer while a granular layer may experience little loss.

The third difficulty is with the reliance on structural number. Many pavement engineers and researchers have expressed concern with the structural number approach to pavement design since it was first introduced. The structural number approach assumes that each incremental thickness of a material provides an equal contribution to the structural capacity of the pavement regardless of the total thickness or total pavement configuration. Several studies have shown that this assumption is erroneous (*3–6*).

These difficulties are mentioned not to suggest abandonment of the AASHTO overlay approach but to remind the pavement design community of their existence, so that the procedures do not become "etched in stone." Additional thought and research in these areas are needed.

CONCLUSION AND RECOMMENDATION

This investigation has demonstrated that the AASHTO remaining life concept produced inconsistent overlay design thicknesses. The cause of the inconsistencies appears to be due to a compounding of assumptions used to produce the remaining life factor (*Frl*) curves (Figure 1). An alternative approach developed as a part of this investigation found that the appropriate value for *Frl* is 1.0. As a result, it is recommended that the AASHTO overlay design approach be revised to exclude remaining life considerations.

ACKNOWLEDGMENTS

This paper is based on a project entitled "Development of a Flexible Pavement Overlay Design Procedure Utilizing Nondestructive Testing Data," which is being conducted by the Arkansas Highway and Transportation Research Center, University of Arkansas. The project is sponsored by the Arkansas State Highway and Transportation Department and the U.S. Department of Transportation, Federal Highway Administration.

REFERENCES

1. *AASHTO Guide for Design of Pavement Structures*. American Association of State Highway and Transportation Officials, Washington, D.C., 1986.
2. *Remaining Life Considerations in Overlay Design*. Appendix CC, Vol. 2, AASHTO Guide for Design of Pavement Structures. American Association of State Highway and Transportation Officials, Washington, D.C., 1986.
3. M. Gomez and M. Thompson. *Structural Coefficients and Thickness Equivalency Ratios*. Transportation Engineering Series 38. University of Illinois, Urbana-Champaign, 1983.
4. H. D. Dunn, Jr. *A Study of Four Stabilized Base Courses*. Ph.D. dissertation. Department of Civil Engineering, Pennsylvania State University, University Park, 1974.
5. R. P. Elliott. *Rehabilitated AASH(T)O Road Test—Analysis of Performance Data Reported in Illinois Physical Research Report 76*. QIP-101. National Asphalt Pavement Association, Riverdale, Md., 1981.
6. M. C. Wang and T. D. Larson. Performance Evaluation of Bituminous Concrete Pavements at the Pennsylvania State Test Track. In *Transportation Research Record 632*, TRB, National Research Council, Washington, D.C., 1977, pp. 21–27.

Publication of this paper sponsored by Committee on Pavement Management Systems.

Application of HDM3 Pavement Deterioration Model in Saskatchewan Pavement Management Information System

P. Bein, J. B. Cox, R. W. Chursinoff, G. H. Heiman, and G. A. Huber

Performance models for roughness progression, rutting, spot sealing, cracking, and patching have been developed for the Saskatchewan Pavement Management Information System using the World Bank's HDM3 model. A correlation between the Saskatchewan Riding Comfort Index and the International Roughness Index was developed. To separate the environmental effects from traffic effects on roughness, 396 km of asphalt pavements that had appreciably different axle loadings on adjacent lanes were examined. The models have been evaluated using 1976–1987 roughness data and recent maintenance records for the entire paved provincial highway network and 1987 condition survey results from 1,909 km of roads. A modified rut-depth model retains pavement age as the most significant variable. Cracking and potholing do not develop to a state critically affecting roughness and were excluded from the model. Regression analyses revealed that the last term in the HDM3 model explains most of the roughness deterioration observed in the field. This is due to grouping of pavement types for model development, which tends to enhance the collinearity between pavement strength and loading data. The age and cumulative axle loading variables were halved because the pavements are frozen half of the time. The calibrated environmental factors $m = 0.035$ for the arid south and $m = 0.050$ for the humid north of Saskatchewan agree with validations of HDM3 by others. Roughness deterioration becomes faster with more advanced age of all pavements, but the increase is relatively small for resealed full-depth and asphalt concrete pavements. Thin asphalt mixes laid directly over subgrade deteriorate most rapidly of all pavement types and faster in the northern than in the southern climatic zones. Maintenance models show similar trends.

Saskatchewan Highways and Transportation (SHT) have 24,000 km of paved roads under their jurisdiction. A pavement management information system (PMIS) was developed on the principles of life-cycle costing of highway investment decisions (*1*). The consideration of user costs and their dependence on road conditions had been one of the main premises of the SHT philosophy. The HDM3 version of the roughness progression submodel in the World Bank's Highway Design and Maintenance Standards Model was evaluated and was found suitable for the PMIS. Although HDM3 has been verified with data from a wide range of climatic regions, no attempts have been made to adapt or calibrate the pavement deterioration model for climatic conditions typical of the Canadian Prairies. This paper reports on the research that has been performed to develop a set of pavement performance models for the PMIS.

P. Bein and J. B. Cox, N.D. Lea International Ltd., Transportation and Management Consultants, 1455 West Georgia Street, Vancouver, British Columbia, V6G 2T3 Canada. R. W. Chursinoff and G. H. Heiman, Saskatchewan Highways and Transportation, Regina, Saskatchewan. G. A. Huber, The Asphalt Institute, Minneapolis, Minn.

HDM3 PAVEMENT DETERIORATION MODELS

The HDM3 model for roughness progression attributes the total loss of rideability to structural, surface condition, age, and environmental factors. Mechanistic principles have guided the general form and combination of parameters in the relationships, so that the models can be transferred to other conditions with a suitable local calibration. The relationships have been derived from road condition data observed over a 5-year period on 116 in-service sections of flexible pavements. The sample covers a wide range of pavement types, maintenance status, strengths, traffic loadings, and age that were selected according to a composite factorial experimental design (*2*). Other empirical studies from climates ranging from arid to humid, and from tropical to temperate freezing, were used to validate the HDM3 models and to determine the effects of environment and materials across regions. The validation was limited by the availability of roughness time-series and by differences in measures of condition adopted in the empirical studies. For temperate freezing climates, the models may require reformulation.

The model has a number of pragmatically important features for the Saskatchewan PMIS. First, it facilitates life-cycle cost evaluation of pavement projects by concentrating on pavement roughness, which determines riding quality and the economic benefits from maintenance and rehabilitation (*3*). Second, the roughness is measured in International Roughness Index (IRI) units, which are time-stable and transferable. The provincial Riding Comfort Index (RCI) scale is largely subjective and depends on the variability of response-type roughness-measuring equipment used in the RCI surveys. Third, the model has an incremental form, which is compatible with

the annual condition surveys and the PMIS analysis. Fourth, the use of calibration constants in each term facilitates adaptations of the model to the Saskatchewan environment and to local construction and maintenance practices.

Roughness Progression Model

The roughness progression model in HDM3 contains six terms, as follows:

$$\Delta RI = 134 e^{mt} MSNK^{-5.0} \Delta NE4 + 0.114 \Delta RDS + 0.0066 \Delta CRX + 0.003 h \Delta PAT + 0.160 \Delta POT + mRI_t \Delta t \quad (1)$$

where

ΔRI = increase in roughness over time period Δt (m/km *IRI*);
RI_t = roughness at time t (m/km *IRI*);
m = environmental factor;
t = average age of pavement or overlay (years);
Δt = incremental time period of analysis (years);
ΔRDS = increase in rut-depth standard deviation of both wheelpaths (mm);
ΔCRX = increase in indexed area of cracking (percent);
ΔPAT = increase in area of surface patching (percent);
ΔPOT = increase in the total volume of potholes (m^3/lane km);
$\Delta NE4$ = incremental number of equivalent standard-axle loads (ESALs) in period Δt (million ESALs/lane);
$MSNK$ = $1 + MSN - 0.000758\ H\ CRX$;
h = average deviation of patch from original surface profile (mm);
MSN = modified structural number of pavement strength; and
H = thickness of cracked layer (mm).

The first two terms relate to structural factors; the third, fourth, and fifth terms take account of the effects of surface condition; and the sixth term reflects the impact of environment (climate and subgrade factors) and of the present roughness. All terms are affected by maintenance.

Rutting Progression and Other Models

The roughness progression due to traffic loadings and pavement strength is significantly influenced by the longitudinal variation in rut depth (*2*). The HDM3 model predicts the rut depth caused by the accumulated plastic deformation from traffic on asphalt pavements with granular or cemented nonbituminous base construction. In full-depth asphalt concrete pavements, deformation develops by a different mechanism and requires a different model. The mean rut depth was found to increase sharply initially and thereafter at a lower rate in the Brazilian study. The model developed from the data relates the mean rut depth to average compaction of the base course layer, the modified structural number, and the cumulative traffic loading, with effects also from cracking, rainfall, deflection, and rehabilitation status as follows:

$$RDM = K t^{0.166} MSN^{-0.502} COMP^{-2.30} NE4^{ERM} \quad (2)$$

where

RDM = mean rut depth in both wheelpaths (mm);
K = calibration constant for local conditions;
ERM = $0.0902 + 0.0384\ DEF - 0.009\ RH + 0.00158\ MMP\ MCRX$;
t = age of pavement since construction or most recent overlay (years);
$COMP$ = average level of compaction in unbound layers expressed as fraction of nominal specifications;
DEF = Benkelman beam maximum deflection under 80-kN axle load (mm);
$MCRX$ = weighted area of cracking (percent [weight for 3-mm-wide cracking = 2.0, for narrow 1-mm cracking = 1.0]);
MMP = mean monthly precipitation (m);
$NE4$ = cumulative number of ESALs/lane (relative load damage power of 4);
RH = 0 if original surfacing, = 1 if an overlay; and
MSN = modified structural number of pavement strength.

The variation of rut depth was found to be strongly related to the mean rut depth as follows:

$$RDS = k 2.06 RDM^{0.532} MSN^{-0.422} COMP^{-1.66} NE4^{ERS} \quad (3)$$

where

RDS = standard deviation of rut depth in both wheelpaths (mm);
k = calibration constant for local conditions;
ERS = $-0.009\ RH + 0.00116\ MMP\ MCRX$;

and other variables are as in Equation 2.

HDM3 also contains models for initiation and progression of cracking, raveling, and potholing. These distress models, however, are of lesser significance for the PMIS since their impact on roughness is relatively small. A sufficiently detailed database does not yet exist to permit calibration of these relationships to Saskatchewan conditions.

Validation of HDM3 Approach

HDM3 approach to pavement deterioration was evaluated early in the PMIS development for applicability to Saskatchewan (*4*). Accurate RCI-IRI correlations were not available at that time, condition data were limited, and the HDM3 model was an earlier edition but the same as Equations 1, 2, and 3 in principle. The HDM3 mean rut-depth model was found to be a reasonable predictor for a sample of five Saskatchewan asphalt concrete pavements constructed without mix problems. A sample of 396 km of pavements with significantly different axle loadings but similar structure in both lanes was selected from the provincial highway network. The objective of the analysis was to estimate the relative contribution of various terms in the HDM3 model to roughness deterioration. The traffic-related terms in the HDM3 roughness deterioration model were found to be small. Environment and maintenance affect the variability of the roughness

results to a much greater degree. In the preliminary analysis an increase in roughness by 2.5 percent per year was detected owing to a combination of environmental and maintenance factors in Saskatchewan. This increase should be compared with 1 percent (environmental effect only) observed in the drier Tunisian climate and 2 percent in the tropical Brazilian climate. This finding concurs with those of other studies in Canada that found that age, and not traffic, was the major variable affecting pavement deterioration (*5,6*). It also concurs with the measurement of actual pavement distress in Ontario where the predominant failure modes were related to the environment and not to traffic (*7*).

CALIBRATION OF THE HDM3 PAVEMENT PERFORMANCE MODELS

Data Gathering and Preparation

Preparation of data for PMIS model development and calibration involved compilation of the construction history, highway inventory, maintenance, traffic, RCI, environmental, and condition survey data into a Model Development File residing on an SHT mainframe facility. The modified structural number was calculated, and each piece of road was assigned to a pavement model group. Twelve years of historical RCI data, from 1976 to 1987, and annual ESAL data from 1960 to 1986 were also appended to each record. A correlation between RCI and IRI scales was developed to make using the HDM3 model possible with Saskatchewan roughness data.

Correlation of Roughness Scales

Saskatchewan RCI scale ranges from 0 (an "unpassable" pavement) to 10 (the smoothest pavement possible). The IRI scale is expressed in meters per kilometer. In North America the roughest highways are likely to be 5 or 6 m/km IRI, and a new pavement typically has an IRI of 1 to 2 m/km. The correlation shown in Figure 1 was developed in order to use historical RCI data for model development, and to use current RCI data to operate the modified HDM3 models in the PMIS. It compares reasonably well with the World Bank's formula (*2*).

Pavement Model Groups

Because each highway cannot realistically have its own performance models, groups of similar pavements were set up. The SHT pavements have been designed for a specific design life or built with a standard cross section. Staged C and D pavements are 50 mm and 20 mm of asphaltic mix, respectively, laid directly on the subgrade and provided with gravel shoulder surface. These thin pavements comprise half of the paved SHT network. For pavement model groupings in the PMIS (Table 1), original surfacing consists of full-depth asphalt concrete, asphalt concrete on granular base, double seals, and cold mix on granular base. Reseals, overlays, and recycled pavements add five pavement groups encountered in the network.

Modified Structural Number

The HDM3 model uses the modified structural number (*MSN*) to indicate pavement strength, including a contribution from the subgrade dependent on its *CBR* value. Analysis of the *MSN* in the Brazilian study produced a high correlation with pavement performance. Compared with pavements designed by conventional methods, actual in situ strengths of Saskatchewan pavements increase more quickly with design axle loadings and are more consistent with the range of traffic loadings to which each pavement type is used and with an economic pavement design (*8,9*). The modified structural number was calculated as follows (*2*):

$$MSN = \sum_{i=1}^{n} a_i t_i/25.4 + 3.51 \log_{10} CBR - 0.85(\log_{10} CBR)^2 - 1.43 \quad (4)$$

where

MSN = modified structural number including subgrade contribution;
n = number of pavement layers, including subbase, base, surface, and overlays;
a_i = strength coefficient of pavement layer i;
t_i = thickness of pavement layer i (mm); and
CBR = in situ California Bearing Ratio of subgrade, percent.

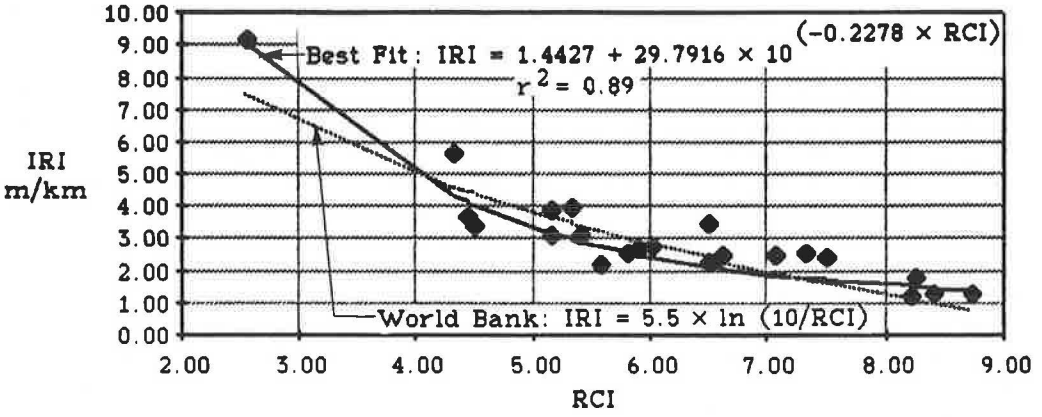

FIGURE 1 Roughness scale correlation.

TABLE 1 SASKATCHEWAN PAVEMENT MODEL GROUPS

Pavement Model Group	Pavement Description
01	Asphalt Concrete (AC) on Granular Base
02	Full Depth Asphalt Concrete (FDAC)
03	Double Seal (DS) on Granular Base
04	Cold Mix on Granular Base, DS or Subgrade,
06	Staged C
07	Staged D
20	Reseal on AC, or on AC Overlay
21	Reseal on FDAC
22	AC Overlay on AC, FDAC, DS, or on Cold Mix
23	Reseal on DS
24	Recycled AC or Recycled FDAC

Pavement Condition Survey

In 1987, 1,909 km of highways were surveyed. SHT collects surface condition data with a minivan towing a Portable Universal Roughness Device (PURD). This unit collects roughness information as well as surface distress and rutting data. Visual rating is accomplished with keyboards used to register observed surface distresses. An on-board computer records information gathered at 50-m intervals. The data collection vehicle is driven at 40 km/h centered in the outside driving lane. A driver and a passenger each operate a keyboard. They must view both lanes of the road surface and determine the severity and extent of surface defects within the 50 m immediately in front of them.

Climatic Zones

The province has been subdivided into four climatic zones for PMIS (Figure 2 and Table 2). Most of the provincial highways are located in climate zones A, B, and C. The climate of Saskatchewan varies from semiarid in the southwest, to dry subhumid in the center, and moist subhumid in the northeast. Negative Thornthwaite Index values in the southwest indicate a negative balance of rainfall to evaporation. Environmental zones follow the general shape of the Thornthwaite Index contours and the pedological soil zones. Soil zones were chosen as the basis of classification because soil types are a reflection of climate.

Pavement performance varies from good in the arid southwest to poor in humid northeast Saskatchewan. Thin pavements, which rely mainly on their subgrade strength for good performance, are particularly sensitive to climate, as is reflected in higher maintenance costs in the wetter zones. Freezing and thawing of subgrades have more impact on a thin pavement than any other climatic factors. Specific weather events or particular seasonal conditions can cause large differences in the performance of thin pavements. The thicker, conventional pavements tend to be less susceptible to climate. Full-depth asphaltic concrete pavements are more susceptible than standard pavements because of their thinner cover over the subgrade.

Subgrades

Subgrades markedly affect the thin pavements, and they also contribute to the strength of conventional pavements. A soaked CBR value is used for pavement design and as a general description of subgrade supportability. Subgrade shear strength varies along and across the highway because of variations in soil types, water contents, and stress history, creating a broad range of shear strengths on the provincial highway system. Modification of the highway subgrade to a design standard reduces some of these variations and provides a preferred soil type in the upper layer. CBR was grouped for the PMIS into four ranges, and each range was assigned a mean value.

Maintenance Data

Maintenance quantities are generally reported as one value for the entire reporting section of road. The data on maintenance quantities contained in the Maintenance Management Information System were distributed along each piece of road in the Model Development File using the actual manual records prepared by the district maintenance engineers, if available. The process consisted of dividing the maintenance cost by its reporting section length, then multiplying by the length of the piece of road in the Model Development File.

Rut Mean Depth and Standard Deviation Analysis

The 1987 PURD survey data were used in developing the rutting models. An attempt was made to calibrate Equation 2 by identifying the exponents in a linear multiple regression analysis. As data on indexed cracking and compaction index are not available in SHT files, assumptions were made in order to calculate the *ERM* exponent. Deflection was calculated from a Benkelman beam deflection—*MSN* relationship. The regressions found were poor, and the following model was tested instead:

$$RDM = t^A * MSN^B * NE4^C * D * e \quad (5)$$

where A, B, C, D are model parameters, e is the error term, and other symbols are as in Equation 2. The multiple regression was run with intercept and without, but the intercept term D was not found to be significantly different than 1.0 and was dropped for simplicity. The resulting equations violated boundary conditions and predicted unreasonable rut depths for two reasons. First, the observed rut depths in Saskatchewan are often masked by the effect of routine maintenance activities, particularly on thin pavements. Second, rut depths appear fairly independent of the modified structural number and only weakly dependent on the cumulative standard axle loading. There is a well-defined rut progression during the first few years of a pavement's life, but afterward the relationship between rut depth, *MSN*, and *NE4* is not clear.

Consequently, rut depth was assumed to be independent of *MSN*. Two subsets of data were isolated for each pavement model group. The first subset contained low rut-depth observations at low levels of *NE4*. The second subset contained high rut-depth observations at high *NE4*. Mean *RDM*, *t*, and *NE4* were calculated for each subset. The mean values defined a set of two equations that were solved for the two unknowns A and C. There was no a priori reason for rut model differences between the climatic zones, and one set of parameters was developed for the entire province. Model groups 01 and

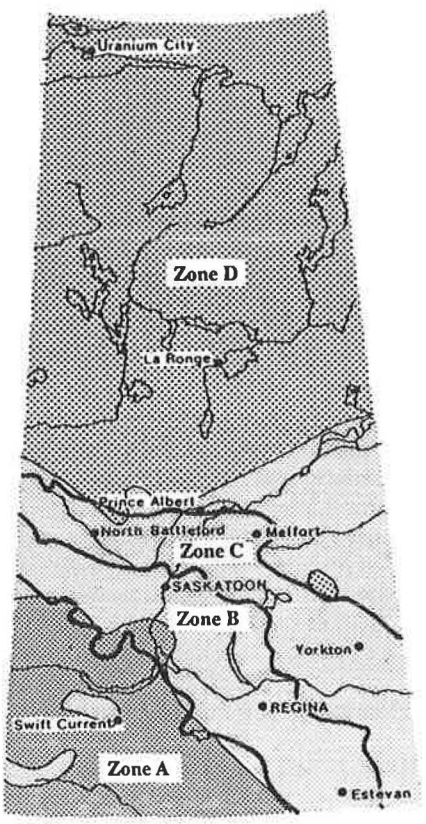

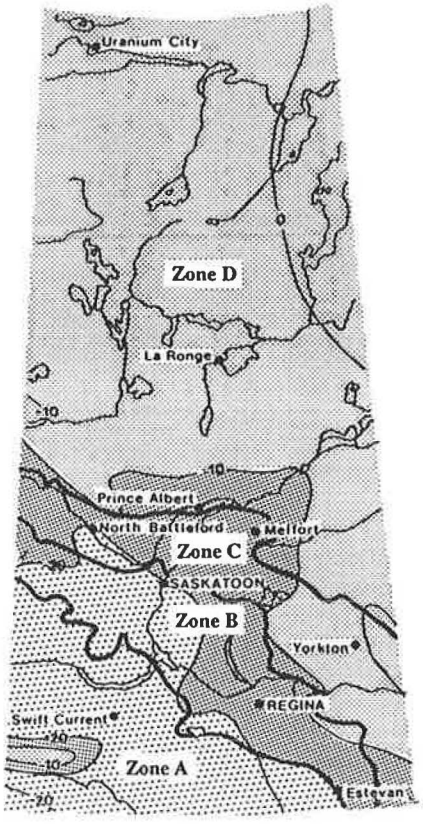

CLIMATIC TYPES

Koeppen's modified classification

- Cold Snowy Forest (moist Short cool summer
- Cold Forest (moist) Cool summer
- Cold Steppe (semi-arid)

MOISTURE REGIONS

Thornthwaite's 1948 classification

- Moist Subhumid
- Dry Subhumid
- Semiarid

Source: Saskatchewan Atlas

FIGURE 2 Climatic zones of Saskatchewan.

TABLE 2 CLIMATIC ZONES IN SASKATCHEWAN

	CLIMATE ZONE			
	A	B	C	D
Predominant Soil Type	Brown	Dark Brown	Black	Forest
Mean Annual Snowfall (mm)	900	1050	1150	1270
Mean Annual Rainfall (mm)	300	340	380	410
Thornthwaite Moisture Index	-20	-15	-10	-10
Mean January Daily Temp. (°C)	-12	-17.5	-20	-22.5
Mean July Daily Temp. (°C)	18.5	17.5	16.5	15.5
Mean Annual Frost Free Days	100	90	80	70
Mean Annual Hours of Sunshine	1300	1300	1250	1200

02 were merged, as were 03, 04, 06, and 23. No data were available for groups 07, 20, 21, and 24, and rut-depth models for these were adopted by analogy to other model groups. Typical rut-depth progression curves are shown in Figure 3, and data underlying the developed models are summarized in Table 3. Thin pavements rut the fastest, and overlays or reseals on asphalt concrete are the slowest to develop rutting. One rut-depth standard deviation model was derived for all pavements:

$$RDS = 0.5 * RDM \tag{6}$$

where 0.5 is a network average of the coefficient of variation of mean rut depth, *RDM*.

Roughness Progression Analysis

Data for evaluation of the cracking, patching, and potholing terms were not available. The terms were omitted because they are not dependent on time in Saskatchewan. Maintenance is routine, and any cracked area is sealed before it is able to progress. At the time of rehabilitation, the cracking, patching, and potholing affect only a small fraction of the surface area. The PMIS system will make use of cracking and patching parameters for project selection along with roughness; therefore, it is not critical that these terms be reflected in the roughness progression equation. With the *RDS* variable substituted by Equation 6, Equation 1 becomes the following:

$$\Delta RI = 134\, e^{mt}\,(MSN + 1)^{-5.0}\,\Delta NE4 + 0.057\,\Delta RDS + mRI,\Delta t \tag{7}$$

Pavements and subgrades in Saskatchewan can remain frozen for 6 months per year. Traffic has no apparent effect on structural deterioration during this period. For this reason, the time and traffic variables were halved in Equation 7. The following model was fitted using SAS mainframe regression analysis package:

$$DRI = a + b * \Delta RI + e \tag{8}$$

where

a and b = model parameters;
DRI and ΔRI = the observed and the predicted roughness increments (in IRI m/km units), respectively; and
e = the error term.

Only the regressions with intercept $a = 0$ produced predictive models in agreement with the professional judgment of SHT engineers. The R^2 measure of fit is not defined for regressions without an intercept, and for this reason the general version of the model was run parallel to the no-intercept model in

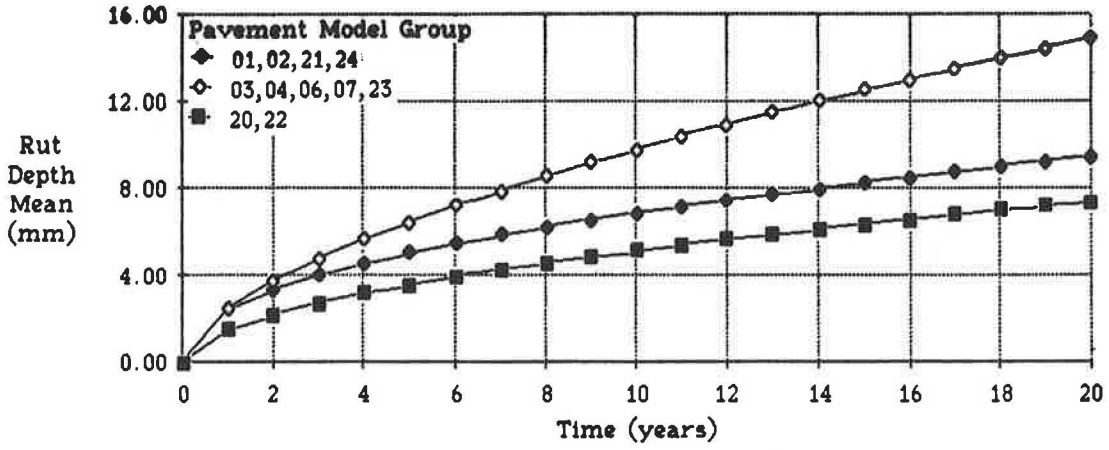

FIGURE 3 Typical mean rut depth progression curves.

TABLE 3 SUMMARY OF DATA FOR THE MEAN RUT DEPTH MODELS

Pavement Model Group	Sample Size, km	RDM, mm			t, years			MSN			NE4, 10^6 ESAL		
		mean	st.dev.	range	mean	st.dev	range	mean	st.dev.	range	mean	st.dev.	range
01	490	5.4	2.5	1-24	16.0	6.6	2-27	3.94	0.84	1.77-7.17	1.15	0.75	0.06-4.73
02	33	4.2	1.3	1-8	14.5	2.2	8-16	4.80	0.64	3.51-5.90	1.51	0.47	0.39-2.07
03	75	5.1	2.6	1-12	5.8	1.7	4-11	2.02	0.42	1.07-3.26	0.35	0.34	0.14-1.07
04	130	5.6	2.7	1-17	5.6	2.7	1-17	2.05	0.62	1.04-3.70	0.41	0.18	0.09-1.59
06	266	7.3	2.9	2-26	9.2	4.1	2-21	1.56	0.42	0.61-2.78	0.29	0.18	0.03-0.63
22	284	4.2	1.7	1-13	10.5	6.1	2-27	5.04	1.12	1.12-8.54	1.46	1.11	0.00-4.56
23	176	6.2	2.1	1-14	8.3	2.6	4-15	2.28	0.63	1.32-4.44	0.28	0.16	0.13-0.81

order to monitor R^2. The observed increment *DRI* was calculated as the difference between the 1987 roughness reading and the starting roughness value immediately following construction or overlay, whichever was latest. Overlaid pieces of road provided one *DRI* record for each subhistory determined between two consecutive overlays. For roughness histories starting prior to 1976, average starting roughness levels were calculated from post-1976 data. Records were weighted by the number of 50-m lengths contained in each piece of road in the Model Development File. The extraction of roughness subhistories and other data transformations were facilitated by a structured programming language built into the SAS package.

The model was analyzed with different values of the environmental factor m. Each climate zone was considered separately, but there were no significant differences and data were lumped for zones A and B, and C and D. The best R^2 and root mean square error of predictions were obtained with $m = 0.035$ for climate zones A and B, and $m = 0.050$ for C and D, consistent with Paterson (*2*). All combinations of terms in Equation 7 were tried, but ΔRI containing only the last term fitted the observed data best. The second-best fits resulted when the rutting term was excluded or, occasionally, when the first term was excluded. This leads to a conclusion that the structural variables are accounted for by the age variable and by the grouping of pavements into model types. Model grouping classifies pavements by general levels of both strength and traffic. The age variable is collinear with cumulative axle loads, which in turn govern pavement thickness design and subsequent overlays.

The data to which the models were fitted are summarized in Table 4. The results of the best regressions are shown in Table 5. All results are significant at the 0.0001 level or better, partly because of the large number of 50-m lengths of road in the sample. However, for model groups 04 and 23, which show large scatter in data, the model slope was assumed from group 03. Group 22 model for climates A and B did not agree with the expert judgment of surfacing and maintenance engineers at SHT and was therefore assumed to be as pavement model 01. Models for groups 21 and 24, for which no field data were available, were assumed from groups 20 and 01, respectively. Typical roughness progression curves based on the models are presented in Figures 4 to 6. The roughness levels in year 0 are network average starting values. The rate of change of slope is increasing toward the more advanced age of pavements, but the increase is relatively small for resealed

TABLE 4 SUMMARY OF DATA FOR ROUGHNESS PROGRESSION MODELS

Pavement Model Group	Sample Size, km	RI, m/km			t, years			MSN			NE4, 10^6 ESAL		
		mean	st.dev.	range	mean	st.dev	range	mean	st.dev.	range	mean	st.dev.	range
01	1696	0.59	0.50	0.01-4.60	15.0	5.8	2-27	3.41	0.79	0.50-7.00	1.15	1.05	0.01-11.63
02	599	0.60	0.45	0.02-3.40	15.2	3.2	5-23	3.81	0.58	2.08-7.00	1.06	0.74	0.14-5.40
03	241	0.28	0.25	0.02-1.61	6.8	3.2	2-15	1.91	0.45	1.01-3.13	0.28	0.21	0.05-0.89
04	409	0.35	0.36	0.03-3.33	15.1	6.0	2-25	2.12	0.59	0.50-3.97	0.35	0.16	0.01-0.76
06	748	0.53	0.46	0.03-5.10	8.8	4.4	2-18	1.19	0.40	0.50-2.83	0.18	0.14	0.01-0.57
07	5748	0.92	0.69	0.02-8.62	14.8	5.5	2-27	0.82	0.26	0.50-1.70	0.14	0.08	0.01-0.55
20	901	0.65	0.46	0.02-4.18	20.2	5.5	4-27	3.24	0.63	1.10-6.16	1.30	0.76	0.01-6.36
22	588	0.57	0.54	0.02-4.32	10.9	5.5	2-23	4.29	0.90	1.10-7.00	1.25	1.05	0.06-6.27
23	484	0.39	0.45	0.02-4.39	8.2	3.5	2-24	1.90	0.47	0.82-3.37	0.23	0.14	0.05-1.14

TABLE 5 REGRESSION RESULTS FOR ROUGHNESS PROGRESSION MODELS

Pavement Model Group	Climate A+B				Climate C+D			
	Sample Size, km	Model Slope b	% Coefficient of Variation of Prediction	R^2	Sample Size km	Model Slope b	% Coefficient of Variation of Prediction	R^2
01	898	0.99	54	0.57	790	0.61	57	0.58
02	271	0.96	61	0.51	328	0.67	54	0.55
03	60	0.87	62	0.35	181	0.73	85	0.14
04	206	0.50	108	0.03	203	0.34	100	0.03
06	381	1.09	66	0.33	367	0.96	73	0.36
07	3420	0.93	64	0.19	2328	0.84	68	0.27
20	507	0.76	50	0.57	394	0.48	52	0.46
22	306	1.35	49	0.59	282	0.66	73	0.48
23	196	0.70	88	0.06	288	0.83	110	0.10

Note: R^2 is taken from a corresponding regression model with intercept $a \neq 0$

full-depth and asphalt concrete pavements. Models shown in Figure 4 differ insignificantly between the climate zones and are represented by one curve for all climates. Resealed asphalt concrete deteriorates the most slowly because more rapidly deteriorating roads receive an overlay and become model group 22. Staged C and D pavements show the highest rates of deterioration (Figure 5), and the northern climate is more detrimental to most of the pavements (Figure 6) than the southern climate.

Maintenance Quantity—Age Relationships

Functions of hand patching, machine patching, deep patching, spot sealing, cumulative cracking, and patching quantities versus age are required to predict maintenance costs and trigger appropriate rehabilitation and maintenance treatments in the PMIS simulation of long-term strategies. The functions have been derived from scatterplots of network data versus age for each pavement model group. The data were lumped beause

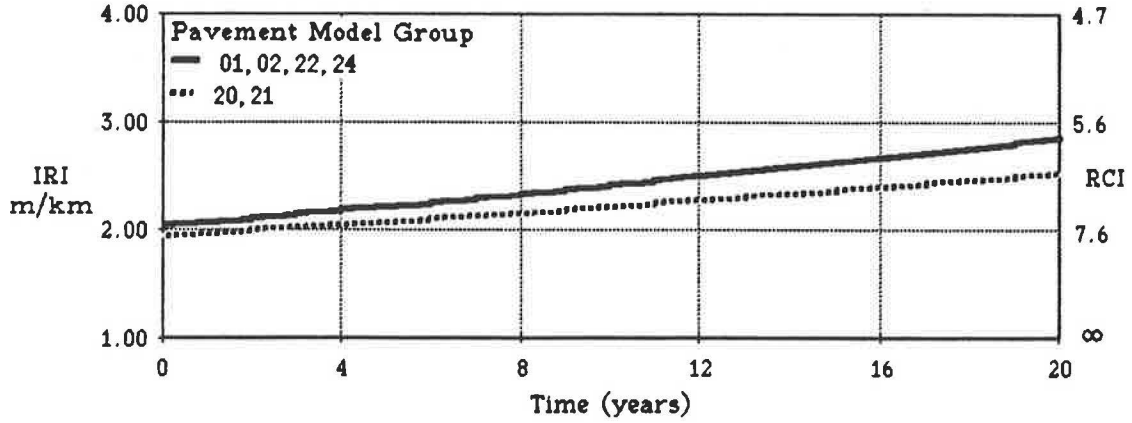

FIGURE 4 Roughness progression of asphalt concrete and full depth asphalt concrete pavements.

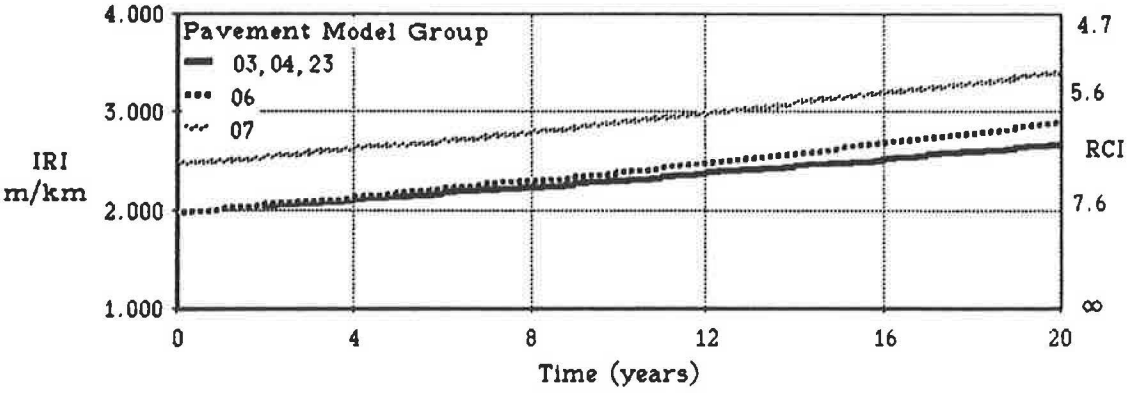

FIGURE 5 Roughness progression in climate Zones A and B.

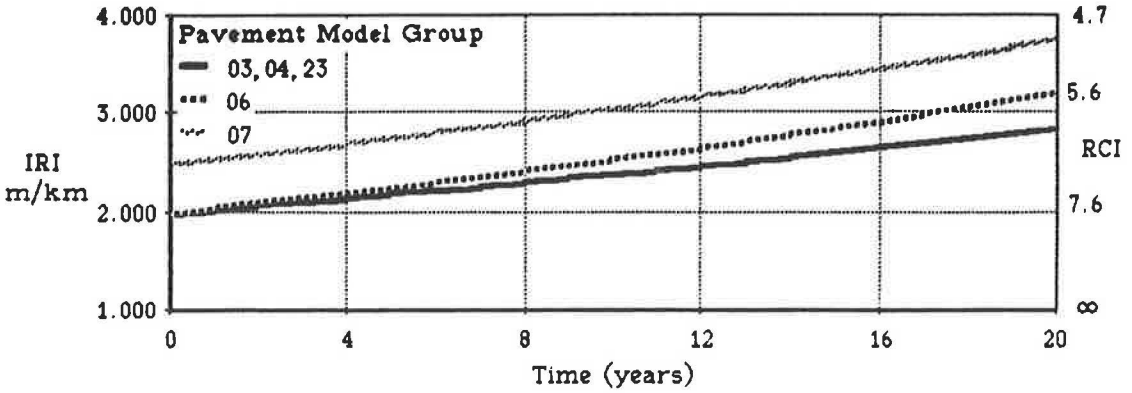

FIGURE 6 Roughness progression in climate Zones C and D.

there were no sufficient data for some climatic zones. For model groups 20, 21, and 24, the function parameters were interpolated from other models. The functions are of a "hinged" form, and the time to initiation and between initiation and the "hinge" were provided through the expert opinion of SHT engineers. The initial slope and the slope after the "hinge" year were estimated from the network sample data.

Hand patching quantities are least on the full-depth asphalt concrete (groups 02 and 21), highest on the staged D (group 07) surfaces, and intermediate on the other original surface types. Little increase in hand patching quantities with age were evident, except in the wetter C and D climatic zones for all surface types except the staged C and D surfaces (Figure 7). Machine patching quantities are least on overlays, highest on the staged C and staged D surfaces, and intermediate on the other original surface types. Machine patching quantities are highest on staged C and D pavements in the northern climate zones (Figure 8). Spot sealing quantities are least on the original asphalt concrete hot mix or overlay surfaces, most on the sealed surfaces, and significant on the cold mix, staged

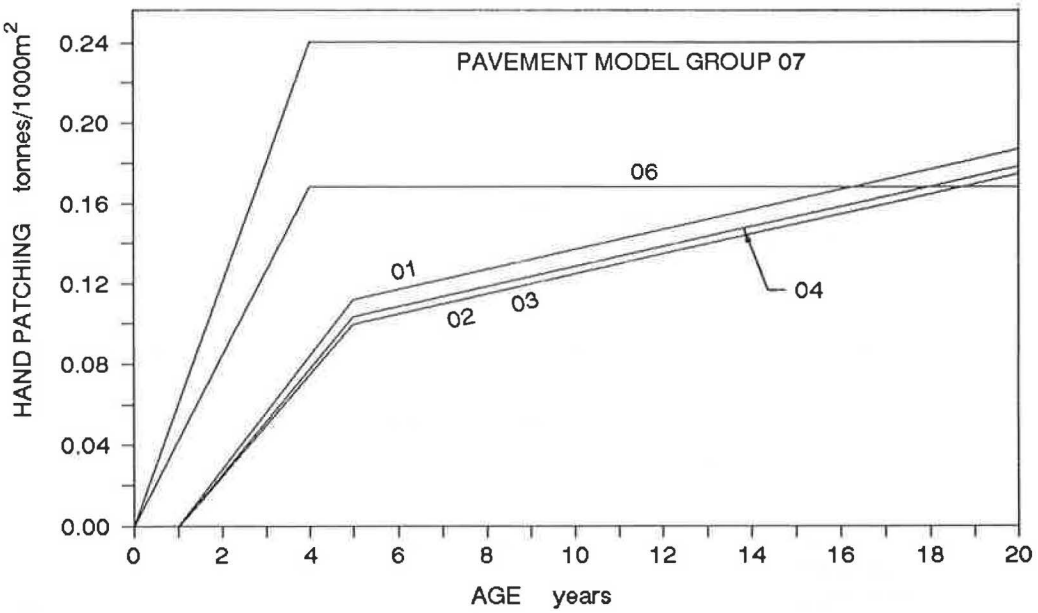

FIGURE 7 Hand patching progression of original pavements in climate Zones C and D.

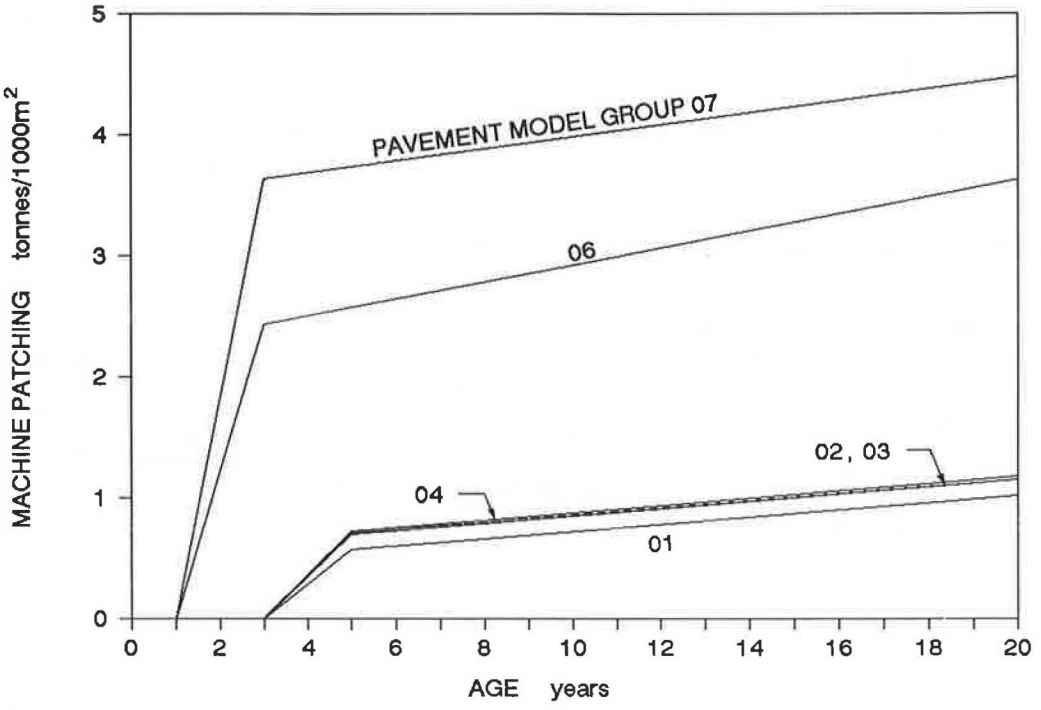

FIGURE 8 Machine patching progression of original pavements in climate Zones C and D.

C and staged D. A slight increase in spot sealing quantities with age was evident in the wetter C and D climate zones.

Deep patching data and cumulative cracking and patching were lumped across all climate zones. Deep patching increases very little with age and is least on the original asphalt concrete hot mix, reseals, or overlays; highest on the staged C and D surfaces. The initial cumulative cracking and patching are least on the cold mix and overlays, highest on the double seal and staged D surfaces. The rate of accumulation of cracking and patching following the "hinge" year is highest on the original and resealed full-depth asphalt concrete pavements.

CONCLUSIONS

A set of pavement performance models has been developed using an approach from the HDM3 model modified for Saskatchewan data, local conditions, and requirements of the pavement management system. The development has been successful because the HDM3 relationships are based on mechanistic principles of pavement behavior and are structured in a way that facilitates local adaptation. Variables relating to pavement structural properties and structural loading as well as to age, maintenance, and environmental factors are included in the models. Models for rutting, roughness progression, and maintenance quantities versus age have been specified for all generic groups of flexible pavements and four climatic zones of Saskatchewan. The rutting model from HDM3 is accurate for pavements without asphalt mix problems, but data are not available to operate the model at present. A modified model was developed showing that age is the most significant independent variable because modified structural number and cumulative axle loading are correlated. The model predicts correctly that thin pavements rut the most quickly, and overlays or reseals on asphalt concrete are the slowest to rut.

In the roughness model, terms relating to environmental deterioration are responsible for the largest part of IRI increase. Cracking and potholing terms were judged the least important, as routine maintenance in Saskatchewan does not allow these distress modes to develop to a state critically affecting roughness. Because the pavements are frozen half the time, the age and cumulative axle loading variables were halved for the IRI progression model. The environmental factor m = 0.035 for the arid south and m = 0.050 for humid north agree with validations of the HDM3 model by others. Roughness deterioration increases toward the more advanced age of all pavements, but the rate of increase is relatively small for resealed full-depth and asphalt concrete pavements. Staged C and D pavements deteriorate the most rapidly of all pavement types. Thin pavements deteriorate more quickly in the northern climatic zones. Maintenance models also show a steeper increase in maintenance quantities with age than in the southern parts of the province.

ACKNOWLEDGMENT

Research reported in this paper has been initiated and sponsored by the Saskatchewan Highways and Transportation.

REFERENCES

1. J. B. Cox, G. H. Heiman, G. A. Huber, M. U. Hassan, and R. A. Deighton. An Integrated Approach to the Development of a Pavement Management System for Saskatchewan. Presented at the Second North American Conference on Managing Pavements, Toronto, Ontario, Canada, 1987.
2. W. D. O. Paterson. *Road Deterioration and Maintenance Effects: Models for Planning and Management*. Highway Design and Maintenance Standards Series. John Hopkins, Baltimore and London, 1987.
3. P. Bein. *Adapting HDM3 User-Cost Model to Saskatchewan Pavement Management Information System*. A paper presented at 68th Annual Meeting of the Transportation Research Board, Washington, D.C., 1989.
4. P. Bein, J. B. Cox, G. H. Heiman, G. A. Huber, and R. W. Chursinoff. Evaluation of Traffic and Environmental Deterioration of Saskatchewan Pavements. *Proc., Roads and Transportation Association of Canada, Annual Meeting*, Halifax, Nova Scotia, Canada, 1988.
5. E. B. Wilkins. Report on the Interim Analysis of Pavement Evaluation Data. *Proc., Canadian Good Roads Association*, Ottawa, Ontario, Canada, 1963.
6. M. A. Karan, J. J. Christison, A. Cheetham, and G. Berdahl. Development and Implementation of Alberta's Pavement Information and Needs System. In *Transportation Research Record 938*, TRB, National Research Council, Washington, D.C., 1983, pp. 11–20.
7. J. J. Hajek and W. A. Phang. Moving from Subjective to Objective Evaluation of Pavement Performance. *Proc., Roads and Transportation Association of Canada, Annual Meeting*, Toronto, Ontario, Canada, 1986.
8. B. C. Martin and F. W. Jamieson. *Maintenance Costs of Oil Treatments vs. Traffic, Subgrade Material and Environment*. Internal Report. Saskatchewan Highways and Transportation, Maintenance Branch, Regina, Canada, Jan. 1983.
9. J. B. Cox and J. Rolt. An Integrated Approach to Pavement Design Based on HDM III Pavement Performance and Vehicle Operating Cost Relationships. *Proc., 13th Australian Road Research Board Conference*, Adelaide, 1986.

Publication of this paper sponsored by Committee on Pavement Management Systems.

A Transferable Causal Model for Predicting Roughness Progression in Flexible Pavements

WILLIAM D. O. PATERSON

An empirical model of roughness progression is developed that differs in form from traditional performance and pavement design models, which attribute roughness changes only to structural factors, and from correlative models, which have often been unable to distinguish any causative factors other than age or environment. The incremental change in roughness is modeled through three groups of components, dealing with structural, surface distress, and environment-age-condition factors, respectively. The formulation and components were estimated statistically from field data of a very comprehensive factorial of in-service pavements in the major Brazil-United Nations Development Program (UNDP) road costs study. It was evident from the data that road roughness develops through multiple mechanisms, and the model resulting from detailed nonlinear statistical analysis shows that significant deterioration can occur even in the absence of structural weakness. This has important implications for pavement and rehabilitation design. Roughness progression follows a generally accelerating trend, with the rate of progression depending initially upon the rate of traffic loading relative to the pavement strength and on the environmental coefficient, and then rising more rapidly once surface defects such as cracking, potholing, and patching occur. Across-country and across-climate studies on independent data sets have quantified the macroclimatic effects and shown the model to be highly transferable.

Predicting the progression of roughness over the life cycle of a road pavement is one of the most important performance predictions for pavement management, pavement design, and road pricing. Vehicle operating costs increase by 2 to 6 percent per m/km IRI (International Roughness Index) of roughness. (The relation of IRI to other roughness scales is given elsewhere (*1*), and 1 m/km IRI equals 63.36 in. per mile, or approximately −0.5 serviceability index units.) Riding comfort targets and performance criteria in design methods and management systems are usually related to roughess. In road pricing studies, road damage is usually defined primarily by roughness, and the relative impacts of traffic and nontraffic factors influence the allocation of costs among users.

The accuracy required of the predictions is demanding, when it is considered that roughness generally increases at rates of less than 3 to 5 percent (about 0.1 m/km IRI) per year on high-standard roads and by double those rates on low-standard roads. The precision of common methods for monitoring roughness is either of the same order or worse (*2*). Thus, the impact on decisions regarding maintenance timing can be appreciable, and the development of empirical models from monitoring data is difficult.

This paper summarizes the empirical development of a roughness progression prediction model to meet these various requirements with a fundamental basis that permits its transfer to a wide range of climates and countries. It was developed as part of a wider analysis of road deterioration under the major World Bank collaborative study on highway design and maintenance standards, and is the main deterioration function of the resulting HDM-III computer model (*3*), which simulates pavement and user life-cycle costs.

The World Bank, 1818 H Street, N.W., Washington, D.C. 20433.

Previous Approaches

Previous model forms for characterizing roughness progression are given in Table 1 (*4–14*). The two models that have been predominant for a decade or more relate roughness progression entirely to structural effects, the interaction between traffic loading and pavement strength. These are, first, the serviceability model (*5*) derived under accelerated controlled trafficking at the 1959–60 AASHO Road Test and, second, the British RTIM2 model (*6*) derived from 4-year monitoring of a network sample in a 1971–75 Kenya study, as summarized by models 1 and 2 in Table 1. The models differ in form (the AASHTO model being convex, the RTIM2 model being linear), in the level of initial roughness, and in the influence of roughness on the subsequent progression rate. They also differ in the rate of roughness progression predicted for pavements of similar strength. The rates predicted from the RTIM2 model are slower and approximately equivalent to those for pavements 60 percent stronger (after correction for subgrade strength) in the AASHTO model. However, the differences (presumed to be environmental) are not represented by a uniform regional factor applying to cumulative traffic as recommended in the AASHTO model, and the factor is at least five times smaller than the regional factor recommended (*5*) for a semiarid region (0.3–1.5).

The 1982 modification of the AASHTO model by Lytton and others (*7*) to an S-shaped function (convex-concave) (model 3 in Table 1) appears to have been influenced by the fact that serviceability is a nonlinear bounded function of roughness, tending to zero at high roughness levels but never being negative (*1*). It is considered to apply to cases in which the contributing modes of distress stabilize over time, such as rutting due to densification or where defects are repaired by maintenance.

TABLE 1 SELECTED PREVIOUS MODEL FORMS FOR CHARACTERIZING ROUGHNESS PROGRESSION

MODEL FORMS	SOURCE AND COMMENT
Traffic Models	
1. $g_t = (p_o - p_t)/(p_o - p_r) = (N_t/\rho)^{\beta}$	AASHTO (5) from 1959 -60 Road Test, Illinois.
2. $R_t = R_o + s(S)\ N_t$	RTIM2 Model (6) from 1971-75 Kenya-TRRL Road Costs Study.
3. $g_t = \exp[-(\rho/N_t)^{\beta}]$	USA (Lytton et al. 1982 (7)): S-shaped curve of slope ρ and curvature ß.
Time-related Models	
4. $\Delta R_t = a\ R_t\ \Delta t - b$	Arizona, USA (Way and Eisenberg 1980 (8)).
5. $R_t = R_o + a\ t^b$	Australia (Potter 1982 (9)).
6. $\Delta R_t/R \simeq 7\%$ per year	Canada (Cheetham and Christison 1981 (10)).
7, 20 - 30% per year	Spain, Belgium (Lucas and Viano 1979 (11)).
Interactive time, traffic or distress	
7. $R_t = a + b\ t + c\ f(S, \log N_t)$	Brazil (Queiroz 1981 (12)).
8. $\frac{\Delta R_t}{R_t} = \max(a\ CX^b, c)\ \Delta t$	Great Britain (Jordan et al. 1987 (13)).
9. $t = f[p_o, \text{var RD}, RD^{2.5}, (C+P)^{0.5}]$	(Uzan and Lytton 1982 (14)).

Note: g = damage function; p = serviceability index; N_t = cumulative number ESAs; R = roughness; S = pavement strength parameter; t = age of pavement since rehabilitation; CX = area of cracking; RD = rut depth; C+P = area of cracking plus patching. ρ, ß are functions, and a, b are constants estimated empirically through research. The detailed formulations are listed in Appendix A of (4).

Source: After Paterson (4).

In sharp contrast to these models, a number of studies evaluating field data from in-service roads have been unable to determine any structural effects and have related roughness progression only to time or age (models 4 to 6 in Table 1). The correlation approach tends to be confounded by the inherent correlation of pavement strength to traffic loading brought about in the design process, and thus strong cross-sectional ranges of loading relative to strength are needed for structural effects to be determined by statistical methods. A significant influence of environment on the time-rate of progression was found in the Arizona study (*8*), with rates ranging from 2 percent per year in arid nonfreezing areas to 8 percent per year in freezing areas. The Australian study (*9*) reported about 2 percent per year for a semiarid climate, and other North American and European studies reported about 7 percent per year (*10,11*).

Very few have been able to quantify interacting effects of traffic and time, or of distress, on roughness. An age-traffic effect in Brazil was identified with a model in a simple log-linear form (model 7). A British study reported a strong link with area of cracking (model 8), and an American mechanistic model included rutting, cracking, and patching (model 9).

There is reasonably consistent agreement that the trend of roughness is generally convex over time or traffic, with the rate of progression increasing toward the end of the pavement life or as the roughness level increases. The degree of convexity, however, varies greatly across the studies—from nil in linear models to high for those reporting high percentage rates of increase. In some cases, the high rates appear to be associated with high levels of surface distress.

With few exceptions, the earlier models for predicting roughness progression treated roughness as an independent mode of distress, attempting to correlate it directly to primary factors, such as traffic loading and pavement strength or age, throughout the life of the pavement. Lacking in them was a clear mechanistic association between roughness and other modes of distress, such as cracking, potholing, and rutting, which themselves cause changes in roughness. The acceler-

ation of roughness progression toward the end of the pavement life due to such defects was often implicit in the models but not an explicit function of the defects. While there is a need for aggregate models that simply relate roughness (or a performance index, such as serviceability) to primary factors, such models are inadequate for policy evaluation and management in two important respects.

First is the need to evaluate maintenance effects. Many maintenance activities repair or modify surface defects, usch as cracking, raveling, potholes, and depressions, with a negligible impact on pavement strength but with significant impacts on both current roughness and the rate of roughness progression. Thus, aggregate models provide no explicit mechanisms by which the effects of such maintenance upon roughness can be evaluated, especially in the short term.

Second is the recognition of variations in the behavior of road pavements, arising from both the mechanistic differences of pavements that fall within one strength group and also from the inherently stochastic nature of properties and behavior within one pavement and across similar pavements. For example, two pavements in the same general strength group and under similar traffic may probably crack at different times and, as the cracking influences roughness, so the roughness progression rates would differ.

Last, there is a need to incorporate traffic-related and time-related effects concurrently, recognizing that both should be included in a model of roughness progression.

Empirical Base

The empirical base chosen for developing the statistical models was the Brazil-UNDP-World Bank Road Costs Study (*15*) because it incorporates a very comprehensive set of parallel time-series data on roughness, cracking, raveling, rut depth, maintenance, traffic loading, and rainfall, for a broad, experimentally designed factorial of flexible pavement types and traffic volumes, on in-service roads, as outlined elsewhere (*4*). In particular, it is known that the roughness measurements were all calibrated to a reliable profile reference, so that the trends over the 5-year study period were free from long-term systematic bias. (See Figure 1.)

The characteristics and scope of the data available are illustrated in Figure 2 and Table 2. These show the changes of roughness on the 380 subsections of the Brazil-UNDP study, as determined from 3,149 measurements and aggregated by the smoothing technique just described. A number of important characteristics are evident from the figure in which, for the sake of clarity, the data represent just a 30-percent sample (one from each fully independent pavement) and the trends are simplified to straight lines. First, the initial roughness was clearly not a constant value for the study pavements, as had been adopted in the AASHTO and Kenya-TRRL formulations, but varied between about 1.0 and 3.5 m/km IRI for asphalt pavements and between 1.3 and 7.3 m/km IRI for surface treatment pavements. Second, the rate of increase of roughness was not a unique function of age in the sample. Some young pavements showed early rapid deterioration, while others showed negligible deterioration rates even at ages of 12 to 20 years, and still others showed a late rapid deterioration. Negative trends resulted from either minor maintenance or a combination of measurement errors; these latter were handled statistically and not excluded because such errors may also have affected apparently "good" data.

The average annual rates of roughness progression, as indicated in the table, were 5.2 percent for asphalt pavements, 4.8 percent for surface treatments, and 6.7 percent for cement-stabilized base pavements. The rates ranged from nil to maxima in the order of 22 to 29 percent per year, which are less than the maximum rates of about 46 percent per year noted in a British study (*13*). The higher rates tended to be associated with high levels of cracking, as shown in Figure 3. For uncracked pavements the rate averaged about 4 percent per year and was similar for all pavement types, while for cracked pavements the rates tended to be higher for those pavements in which the cracked layer was thicker, especially for cement-stabilized bases. It is evident that the study encompassed a broad range of circumstances, including, for example, a range of pavement age from new to 23 years, of traffic loading from 100 to 1.7 million ESAL per lane per year and up to a maximum of 17 million cumulative ESAL, and of pavement modified structural number from 2.1 to 8.7.

COMPONENT INCREMENTAL MODEL

Principles

The basic hypothesis used in developing a comprehensive roughness progression prediction model was that the various

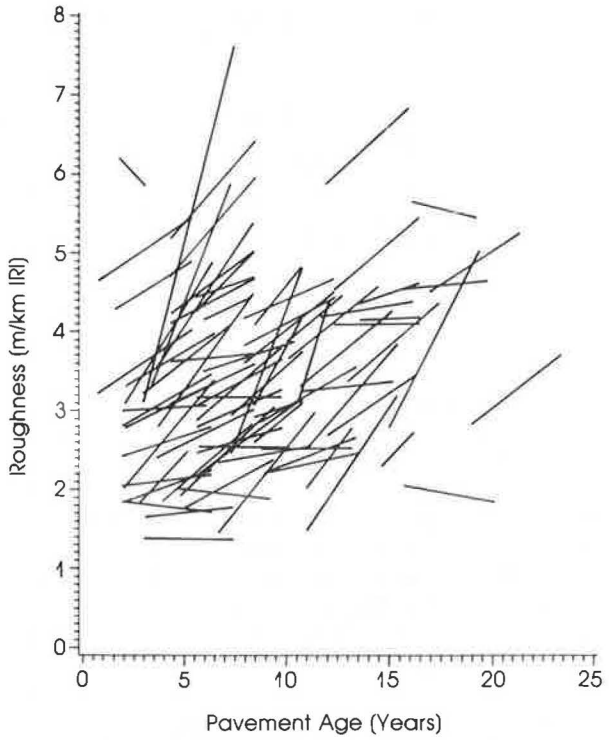

Note: Trends simplified to linear approximation for clarity. Sample shown is one subsection from each of 116 independent sections.
Source: Brazil-UNDP study data.

FIGURE 1 Sample of diverse roughness trends observed in Brazil-UNDP Road Costs Study.

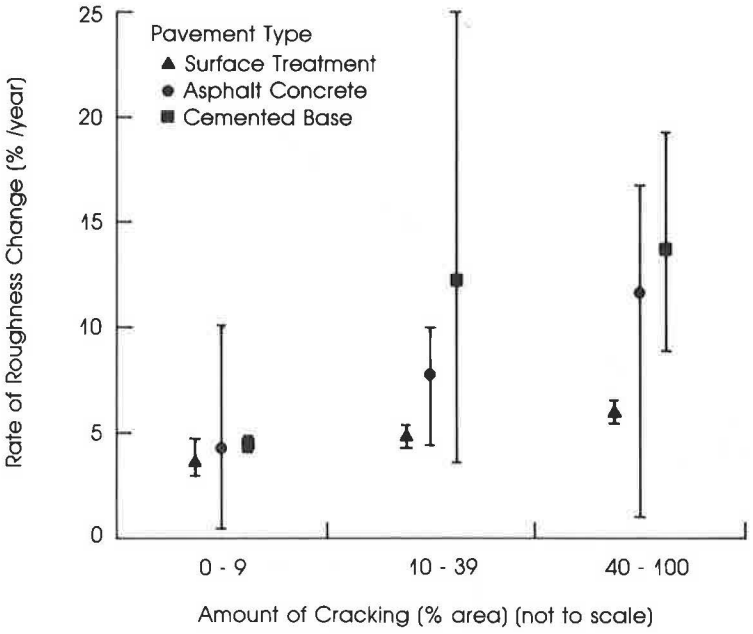

Note: Indexed amount of cracking weights wide cracking twice as much as narrow cracking. Data are group-means of 30 groups representing 4-year trends of 361 subsections.
Source: Brazil-UNDP study data.

FIGURE 2 Influence of cracking on the rate of roughness progression observed in Brazil.

TABLE 2 INFERENCE SPACE OF ROUGHNESS AND OTHER DATA FROM BRAZIL-UNDP ROAD COSTS STUDY

Observed Parameter	Unit	Asphalt and asphalt overlays			Surface treatment, granular base			Cemented base		
		Mean	Min	Max	Mean	Min	Max	Mean	Min	Max
Roughness progression										
- rate	%/yr	5.16	0	25.6	4.77	0	28.9	6.71	0	21.5
- increment	IRI	0.65	-0.50	7.36	0.58	-1.97	4.20	0.81	-0.08	3.09
- average	IRI	2.67	1.13	8.85	3.44	1.68	7.35	3.18	1.66	5.07
- initial	IRI	1.80	1.02	3.46	2.67	1.31	7.28	2.15	1.23	4.11
- final	IRI	2.98	0.93	9.91	3.75	1.37	9.35	3.63	1.86	5.95
Modified structural number	-	4.82	2.08	8.69	3.76	2.04	5.51	3.96	2.18	6.21
Benkelman deflection	mm	0.68	0.19	1.88	0.70	0.26	2.02	0.41	0.13	1.03
Age (average)	yr	7.09	2.15	20.8	8.33	2.43	18.87	9.83	3.46	17.3
Traffic loading										
- annual per lane	MESA/yr	0.35	.0001	1.68	0.09	.0009	0.55	0.20	0.014	0.48
- increment	MESA	1.40	.0006	7.55	0.39	.0039	2.41	0.83	0.02	1.90
- avg. cumulative	MESA	1.78	.0009	13.0	0.53	.0035	3.88	1.50	0.09	2.61
Cracking										
- average	%	15.1	0.	97.4	8.8	0	67.8	21.7	0	93.9
- increment	%	20.3	-22.5	89.6	13.4	-8	99.3	29.0	-38.4	88.6
Patching										
- increment	%	4.3	-3.3	84.6	5.8	-1.3	86.0	4.2	0	38.4
Rut depth - increment of standard deviation	mm	0.90	-0.22	9.68	0.89	0	8.73	0.50	0	4.88
Number of subsections		156			145			60		
Rainfall	mm/yr	1,040 - 1,800			1,040 - 1,800			1,040 - 1,800		

Note: Min - Minimum, Max - maximum.
Source: Author's analysis of data from Brazil-UNDP study (15).

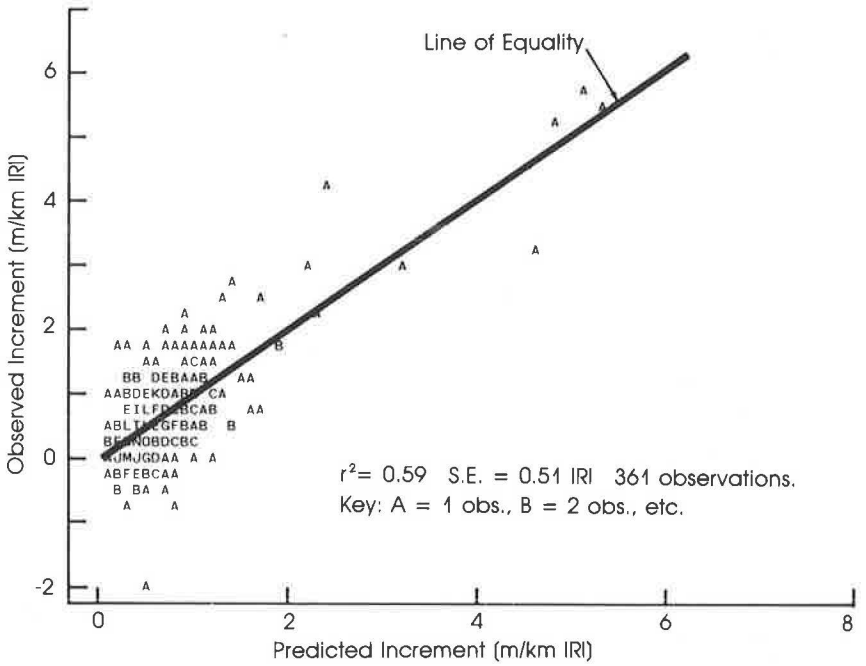

Source: Estimation of Equation (2) on Brazil-UNDP study data.

FIGURE 3 Goodness-of-fit of component incremental model of roughness on original Brazil data.

mechanisms giving rise to roughness changes should be represented by separate components within the model. In broad terms, it was considered that these fell into three groups, according approximately to the parameters involved, the source depth within the pavement, and the resulting waveband of roughness, as follows.

Structural deformation, resulting from plastic deformation in the pavement materials under the shear stresses imposed by traffic loading, commonly appears as rutting in the wheelpaths. Rut depth alone will not give rise to roughness if the depth is uniform; instead, it is the variation of rut depth that relates to roughness as deviations in the longitudinal profile. These variations will therefore be a function of the uniformity of construction and environment of the pavement layers, and particularly of the subgrade.

Superficial defects such as potholes, patches, raveling, cracking or shoving, humps, and localized depressions are generally associated with shallow-seated distress originating in either the surfacing or base of the pavement. These defects typically range in size from less than 0.3 m up to about 2 m in diameter, with a corresponding waveband of about 0.1 to 5 m wavelengths.

The environmental factors that influence roughness through nonstructural effects include primarily temperature and moisture fluctuations, but also foundation movements such as subsidence, which cause volume changes or distortions in the pavement. Daily thermal expansion and contraction movements are a function of the diurnal temperature range, which is often large in desert climates; the effects of seasonal moisture movements depend upon the effectiveness of drainage and the shrinkage properties of the material; and in freezing climates, the combined volume/roughness effects of temperature and moisture are particularly severe.

The model was therefore structured as follows:

$$\Delta R_t = f_1 \text{ (strength, condition, } \Delta\text{traffic, environment)} + f_2 \text{ (}\Delta\text{surface condition, } \Delta\text{maintenance)} + f_3 \text{ (condition, environment, } \Delta\text{time)} + \text{measurement error.} \quad (1)$$

This shows an additive combination of the three major components in the increment of roughness and provides at the same time for such interactions as may prove significant. During the course of analysis, many formulations of the terms comprising each component were tested, and the final choice was determined with respect to statistical significance and engineering reasonableness, ensuring that the model was mathematically integratable.

Empirical Model and Accuracy

After preliminary evaluation using linear regression techniques, the final statistical development of the model was made using a nonlinear least-squares regression technique. While the basic form of the model became evident in the early stages, many variants were examined in order to avoid the adverse effects of correlations between the explanatory parameters, to review alternatives to the parameters, and finally to ensure that the model was integratable and fundamentally consistent with trends of absolute roughness [details

are given elsewhere (*4*)]. The model, as estimated on the Brazilian data, was as follows:

$$\Delta RI_t = 134\, e^{0.023\, t}\, SNCK^{-5.0}\, \Delta NE_4 + 0.114\, \Delta RDS + 0.0066\, \Delta CRX + 0.010\, \Delta PAT + Z_{pot} + 0.023\, RI_t\, \Delta t \quad (2)$$

where

ΔRI_t = increase in roughness over time period t (m/km IRI);
RI_t = roughness at time t (m/km IRI);
ΔRDS = increase in rut depth standard deviation of both wheelpaths (mm);
ΔCRT = increase in area of indexed cracking (percent; see note below);
ΔPAT = increase in area of surface patching (percent);
Δt = incremental time period of analysis (years);
ΔNE_4 = incremental number of equivalent axle loads in period t (million ESA/lane);
$SNCK$ = $1 + SNC - 0.0000758\, H\, CRX$;
SNC = modified structural number of pavement strength;
t = age of pavement or overlay (years);
H = thickness of cracked layer (mm);
CRX = area of cracking (percent); and
Z_{pot} = dummy intercepts estimated for sections with potholing.

Note: Indexed cracking is the weighted area given by CRX = (4 × area of Class 4 + 3 × area of Class 3 + 2 × area of Class 2 + 1 × area of Class 1 cracking)/10.

The model fitted all pavement types without significant class differences, and detailed statistics of the parameter estimates and goodness of fit of the model are given in Table 3, under model A(2). In this final version, which is preferred to the unconstrained model A(1), the value of the γ-exponent of *SNC* has been constrained slightly to take account of strong effects present in the absolute (nonincremental) roughness data [see Paterson (*4*) for detailed discussion]. The robustness of the formulation is evident from the generally strong significance of the individual coefficients. It is also evident from the relatively strong contributions made by the individual components to the overall goodness of fit of the model, as shown by the Type II sums of squared errors presented in Table 4. With the model simplified to its underlying five-component form, the fit (by linear regression) improves to $r^2 = 0.75$, whereas the original fit of $r^2 = 0.59$ represented the variances due to all eleven parameters involved.

The goodness of fit that was achieved is shown as a scattergram of predicted and observed values in Figure 3. This shows that the model fitted the data well, over the wide range of roughness increments observed up to 7 m/km IRI, and that the prediction error of about 0.5 m/km IRI is rather uniform throughout the range. Thus small increments are predicted as accurately as large increments, in absolute terms. This corresponds to an error in an annual prediction of roughness that is of the order of only 0.12 m/km IRI, which is a highly acceptable result, especially given the diverse nature of the conditions studied.

Although the prediction error is small in absolute terms, it is apparent from Figure 3 that errors for the smaller increments can be large in relative terms and of a similar order to the increments being observed. However, about one-half of the apparent error derives from the observation measurement errors (*2,4*), a fact readily appreciated from the number of observed increments falling below the zero ordinate. Also, the residual errors were not correlated to any of the primary parameters. Thus the error component due to lack of fit of the model formulation itself was only about one-half of the values cited in the previous paragraph. The model prediction error, net of any measurement errors, is thus very small, amounting to only about 0.06 m/km IRI (4 in./mile IRI, 0.03 PSI, or 50 mm/km BI) per year.

Examples of the fit of model predictions to the observed roughness trends are shown in Figure 4 for a diverse range of sections, roughness levels, and ages. In each case, both traffic lanes, CS and SC, are depicted for one pair of subsections; the solid lines represent the prediction using condition and traffic data for each observation date, and the broken lines represent the observed roughness trend without smoothing. As the model estimation was based on the increment over the whole period, the predicted and observed trends should give similar total increments. It is apparent that the model fits the data of observed trends very well for a variety of flexible and semirigid pavements, and that the model was remarkably strong in representing the wide variety of conditions in the database.

Engineering Implications

The various components of the incremental model make differing contributions to the total roughness change predicted under different situations. In the statistical estimation, they all made generally similar contributions to the model fit, though with slightly less coming from the rut-depth and patching terms (as shown by the Type II errors in Table 4). The factors that were found to have statistically significant impacts on roughness progression included rut-depth variation, pavement strength, cracking, and traffic loading in the structural deformation component; cracking, patching, and potholing in the surface defects component; and roughness and time in the environment-age component. Among the variables that were not significant were mean rut depth, age, and deflection in the structural component; raveling and narrow cracking in the surface defects; and pavement strength, age, and rainfall in the nontraffic or environmentally related term.

The primary structural deformation term has a conceptual origin in the AASHTO performance model, incorporating traffic loading and pavement strength; but it also includes interactions with cracking and the environment-age variables. Cracking is seen to accelerate the roughness progression by causing a drop in the apparent strength (*SNCK*), which is the most severe for pavements in which the cracked layer(s) is thick and constitutes a major portion of the pavement's structural capacity. Thus this term distinguishes between the performances of two pavements that have similar modified structural number and traffic loading but different thickness of bound layer. The effects of pavement strength and traffic loading on pavement performance are determined by the exponent of the net pavement strength parameter, *SNCK*. The γ-value of 5.0 is very similar to the values found in rutting progression and the AASHTO and TRRL-Kenya performance studies. This deformation term has a strong impact on

TABLE 3 ESTIMATION OF COMPONENT INCREMENTAL ROUGHNESS PREDICTION MODELS.

Model A: $\Delta RI_t = b\, e^{m\,t}\, SNCK^{-\gamma}\, \Delta NE_t + \Sigma a_i\, \Delta SD_{it} + m\, RI_t\, \Delta t$;
and $SNCK = 1 + SNC - c\, H\, CRX$.

Model B: $\Delta RI_t = \Sigma a_i\, \Delta SD_{it} + m\, RI_t\, \Delta t$.

Parameter coefficient	Parameter estimates[1] for given model form		
	A(1) unconstrained	A(2) constrained[2]	B constrained
m	0.0227	0.0230	0.0284
	(6.4)	(6.5)	(8.4)
b	37.7	134	-
	(2.8)	(2.8)	-
γ	4.11	5.0	-
	(16.9)	(-)	-
$c(x10^3)$	0.0887	0.0758	-
	(7.0)	(6.5)	-
a(ΔRDS)	0.114	0.114	0.129
	(4.4)	(4.4)	(4.8)
a(ΔCRX)	0.0066	0.0066	0.0057
	(6.1)	(6.1)	(5.2)
a(ΔPAT)	0.0100	0.0099	0.0117
	(3.9)	(3.9)	(4.4)
Standard error	0.5141	0.5145	0.5385
r^2	0.589	0.588	0.551
Number of observations	361	361	361

1/ t - statistics are given in parentheses; (-) indicates constraint of the parameter; - indicates not included in the model.

2/ This constraint equated the coefficient γ to the value of the unconstrained estimate for the aggregate level model, i.e., $\gamma = 5.0$.

Note: ΔSD_i comprised ΔRDS_i, ΔCRX_i; and ΔPAT_i as the only significant distress variables.

Source: Author's computations from data of Brazil-UNDP Study (15). Method nonlinear least-squares regression.

predictions, especially when the traffic loading is very heavy relative to the structural number and when cracking significantly reduces the structural capacity.

The second term of the structural component, the relation to rut-depth variation, is important because it provides a strong empirical quantification of the link with roughness. The coefficient is statistically well determined and robust, varying little in value over a range of model variants, including those in which the other structural term was omitted. Other forms of rut-depth parameters, including a quadratic function and mean value, were significantly inferior to the linear, standard deviation parameter. The value 0.11 can be compared with 0.14 from a study in Southern Africa, and with 0.15 to 0.25 from the AASHO Road Test [see Paterson (*4*)].

Cracking was found to contribute a small but significant amount of roughness progression in the additive term, which supplements the effects found in the rut-depth variation and structural deformation terms. It is included independently of patching and becomes negative when patching is applied to repair cracking. The term comprises the fractional extent of cracking, weighted for severity so that wide, spalling cracks dominate the effect. The mechanisms inducing roughness here are the effects of spalling and unevenness generated across cracked blocks of surfacing and the birdbath-type of depression that often results from localized deformation in the base as a result of surface cracking. A 60 percent increment in the area of cracking, which is equivalent to full cracking in both wheelpaths, contributes about 0.4 m/km IRI of increase in roughness. Worse consequences result when the cracking is unrepaired and leads to potholing.

The patching term in the model refers to surface patching that, in the study, comprised either replacement of a distressed area of thin surfacing by cold bituminous mix or a superficial patch of fine slurry seal (5-mm maximum size

TABLE 4 RELATIVE CONTRIBUTIONS AND SIGNIFICANCE OF INDIVIDUAL COMPONENTS IN THE INCREMENTAL ROUGHNESS MODEL

Model component	Model terms	Sequential effects Type I SS(%)	Sequential effects F-value	Individual effects Type II SS(%)	Individual effects F-value
Structural	e^{mt} SNCK^{-5} ΔNE_4	40	401	10	36.5
Age-environment	m R Δt	41	435	13	45.6
Rut depth s.d.	ΔRDSD	3	36	5	19.2
Cracking	ΔCRX	6	59	11	38.1
Patching	ΔPAT	5	59	4	15.6
Potholing	Zpot	5	30	25	29.8
Total		100			

Notes: Determined by general linear least-squares regression of the component terms above, based on Equation (2) where m = 0.023. Parameters are defined with Equation (2).
Type I SS (sums of squares) is the incremental improvement in error SS for consecutive additions of further terms, expressed here as a percentage of the model SS(276.6). Type II SS are the reduction of error SS due to adding the relevant term into the model after all others have been included; it is independent of sequence and is expressed as a percentage of the error SS(93.3). The fit for the linear combination of components is r^2 = 0.748.

Source: Author, on data from Brazil-UNDP study (15).

aggregate). The coefficient indicates that surface patching increased the roughness by 0.01 m/km IRI per percentage of area patching, which, after deducting the decrease due to repaired cracking, is equivalent to the effect of an average protrusion (either positive or negative) of 2 to 5 mm, which is in the same order as the height of the patches. Independent data from a Kenya network survey indicate a coefficient of 0.08 m/km IRI per percentage area for patch protrusions of 15 to 25 mm. In general, the coefficient could thus be replaced by 0.003 H_p, where H_p is the average patch protrusion, in millimeters.

The last term of the surface distress component represents pothole and other major surface profile deviations. As potholes were usually repaired immediately during the study on both high- and low-maintenance sections, and as open potholes were avoided in the roughness measurement when they were present, direct statisitcal estimation of the effect of potholes on roughness was not possible. In the model estimation, dummy intercept terms were estimated for five subsections that had significant defects, amounting to about 2.1 m/km of IRI on the four subsections in section 112, which was cited as having "100 percent wide cracking, potholes and patches," and about 1.2 m/km IRI on subsection 022 SEM CS, which showed shoving distress due to an overfilled soft asphalt mix. A separate simulation study was used to derive the roughness-pothole effect (*4*), so that the following substitution could be made in the model:

$$Z_{pot} \simeq 0.16\ \Delta VPOT \text{ (m/km IRI)}$$

where $\Delta VPOT$ equals the increment in volume of open potholes, in m^3/lane/km.

The final component in the model, referred to as the environment-age component, represents a uniform annual percentage increase in roughness independent of traffic loading. The component indicates that an average of 2.3 percent annual increase in roughness was estimated to occur that could not be attributed to traffic, either as the equivalent axle loading or as the number of all vehicle axles. The rate amounts to a total roughness increase of 22 percent over 10 years or 50 percent over 20 years. The coefficient is well determined, and its value increases if the roughness increments are constrained to be non-negative or if the structural deformation function is omitted, as shown in Table 3. Considerable effort was made to find other factors influencing the value of the coefficient, but it was found to be independent of pavement age (the S-curve phenomenon), pavement type or strength, and traffic volume, for example. The value is almost certainly influenced by the pavement environment; but no significant, sensible effect of climate could be determined within the fairly homogeneous climate of the Brazil study area, using either the Thornthwaite Moisture Index, which ranged from 10 to 100 in the study region, or the mean annual precipitation, which ranged from 1,040 to 1,790 mm per year. Instead, further work at the macroclimatic level, applying the model to data in widely different climates and countries, has established that the coefficient does vary with climate over a range of about 0.005 in arid climates to 0.10 to 0.20 in freezing wet climates, as shown in Table 5 (*4*).

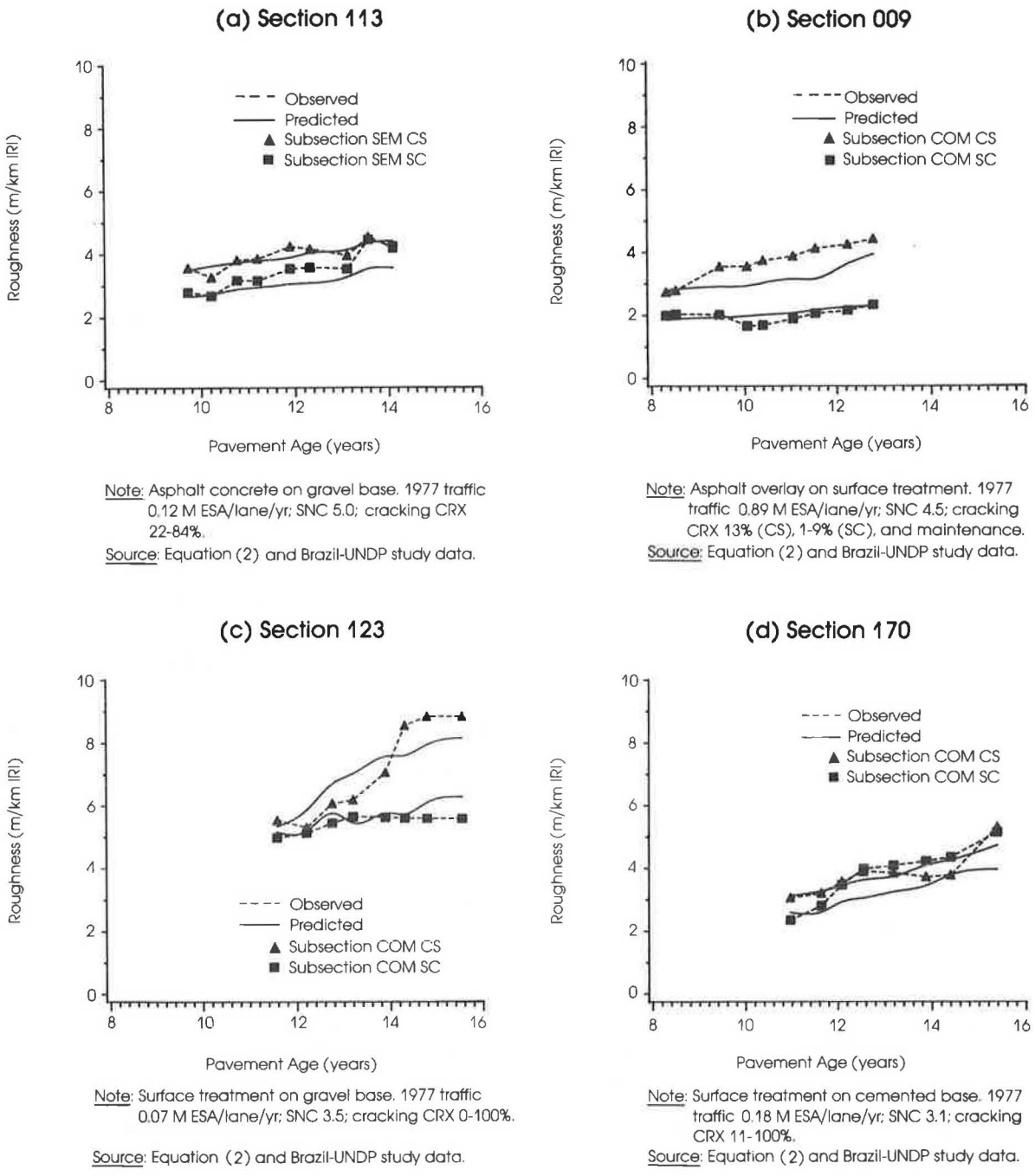

FIGURE 4 Sample comparison of predicted and observed roughness trends in Brazil data.

It was noted during the modeling that traditional model forms, such as the traffic-related models of Table 1, fitted the observed data very poorly, and no sensible estimates of their coefficients could be achieved. This was due mainly to the shortcomings of the traditional forms, as discussed earlier, and in part to the inherent collinearity that exists between various parameters, for example, between traffic loading and pavement strength, roughness, age and surface distress, and so forth. Also, many interactions were investigated, in combinations and powers of parameters and in substitutions, with negligible improvement on the final model presented in Equation 2.

The Brazilian model given by Equation 2 was then generalized, in light of this discussion, to give the following general version:

$$\Delta RI_t = 134\, e^{m\,\prime}\, SNCK^{-5.0}\, \Delta NE_4 + 0.114\, \Delta RDS + 0.0066\, \Delta CRX + 0.003\, H_p\, \Delta PAT + 0.16\, \Delta VPOT + m\, RI_t\, \Delta t \quad (3)$$

TABLE 5 RECOMMENDED VALUES OF ENVIRONMENTAL COEFFICIENT M IN ROUGHNESS PROGRESSION MODEL FOR VARIOUS CLIMATES

Moisture classification	Moisture index[2]	Temperature classification[1]		
		Tropical nonfreezing	Subtropical nonfreezing	Temperate freezing
Arid	-100 to 61	0.005	0.010	0.025
Semiarid	-60 to -21	0.010	0.016	0.035
Subhumid	-20 to +19	0.020	0.030	0.065
Humid, wet	20 to 100	0.025	0.040	0.10-0.23

Source: Author's recommendation based on evaluations of model in several countries and regions (3).

[1] Tentative definition of these classes: Tropical includes warm temperatures 15 to 40°C and small range; Subtropical includes warm, high range (5 to 50°C) and cool, moderate range (-5 to 30°C); Temperate freezing includes climates with annual pavement freezing.

[2] Thornthwaite's Moisture Index.

where

m = environmental coefficient, as given in Table 5;
$\Delta VPOT$ = increment in volume of open potholes (m^3/lane/km);
H_p = average rectified protrusion of patch repairs above or below surrounding surface (mm);

and other parameters are as defined for Equation 2.

The parameter coefficients have been found to transfer well to other circumstances, through a detailed validation exercise in which the model was applied to data from seven countries or regions with climates and characteristics widely different from those in the Brazil study, as described elsewhere (*4*). These areas included Arizona, Colorado, Illinois (the AASHO Road Test), and Texas in the United States, Kenya (two), South Africa, and Tunisia. Thus, the values of the coefficient m, presented in Table 5, were derived from climates ranging from arid- to humid-nonfreezing and from arid- to humid-freezing, but did not include regions of very high rainfall (i.e., more than 2,500 mm per year).

Predictions and Damage Causes

Examples of the predictions of roughness progression given by the incremental model of Equation 3, using distress data generated by empirical models (*3*,*4*), are presented in Figure 5. Two pavement strengths are shown, with six levels of traffic loading on each and minimal maintenance of patching all potholes. The curves show clearly differing trends that reflect the impacts of the different traffic loadings and surface distress on roughness. At extremely low, negligible traffic levels, roughness nevertheless increases because of the effects represented in the environment-age component; the rate of increase depends on the environment coefficient m and the initial roughness level. At higher traffic levels, the rates of roughness progression are both higher and also changing more rapidly due to the impact of surface distress.

All the curves have a generally convex shape, with the rate of roughness progression increasing as the levels of roughness and surface distress increase. The rates reach about 10 percent per year in the case of normal design (e.g., 100,000 ESA per year for SNC 3) and 20 percent per year for the overloading/underdesign cases (e.g., five times more traffic), which are plausible in relation to most other reported studies.

The differing contributions made by the various causes of roughness are illustrated in Figure 6 for one pavement under light, medium, and heavy traffic loadings (representing long-term, medium, and short-term design life cases, respectively). For this example, no maintenance is being applied, so the effects of potholing are evident. Under the light loading case in chart a, very little damage derives from the deformation or distress components. In the medium design case in chart b, the contributions from deformation, surface distress, and environment are more or less similar. In the case of overloading shown in chart c, the deformation component dominates the performance. In each case, the roughness in the first several years of the pavement's life increases slowly and almost linearly at a rate that depends on the design standard and the environment. The rate increases after cracking begins and becomes very rapid if potholing is allowed to progress in the absence of maintenance. Thus the consequence of short-term designs or overloading can be seen to be a very rapid disintegration in the later phase of the pavement's life, an almost L-shaped function, but one that is controllable by timely maintenance.

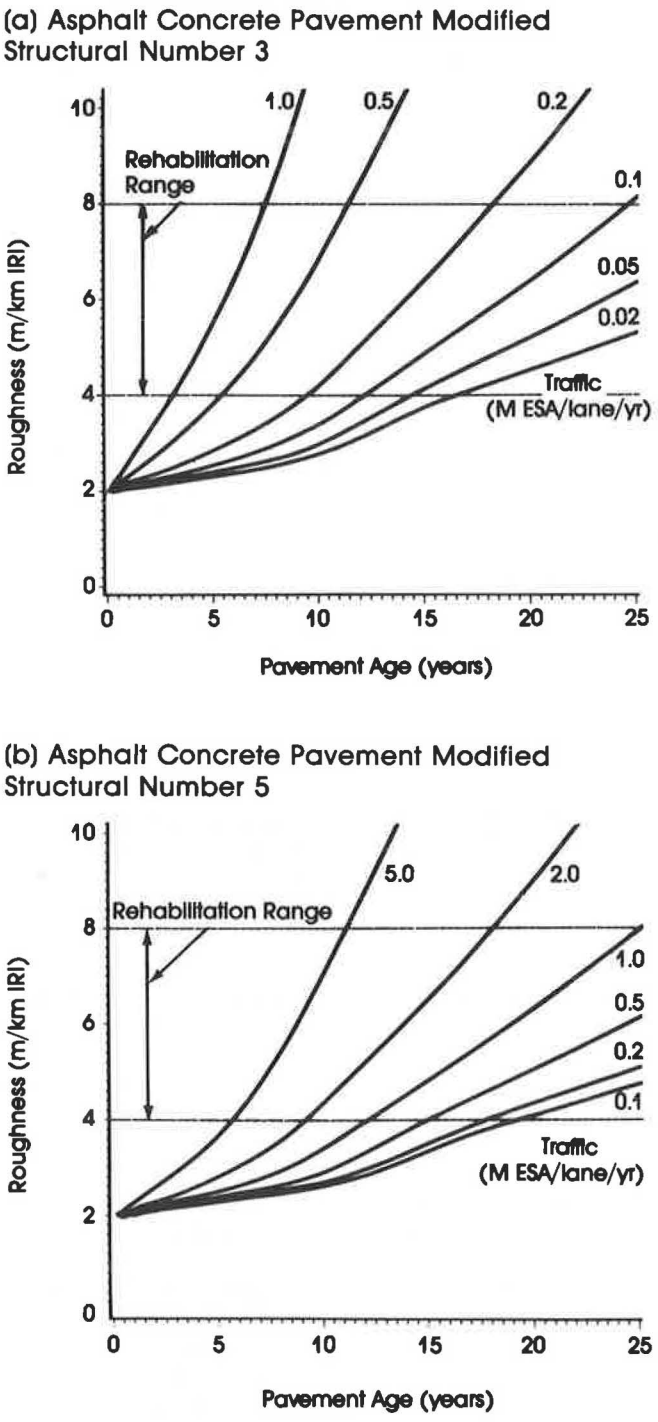

Note: Maintenance comprised patching of all potholes in the year in which they appeared.
Source: Equation (3) applied through Road Deterioration and Maintenance Submodel of HDM-III.

FIGURE 5 Roughness progression prediction curves for a maintenance policy of patching all potholes.

(a) Light Loading, or Longterm Design Pavement

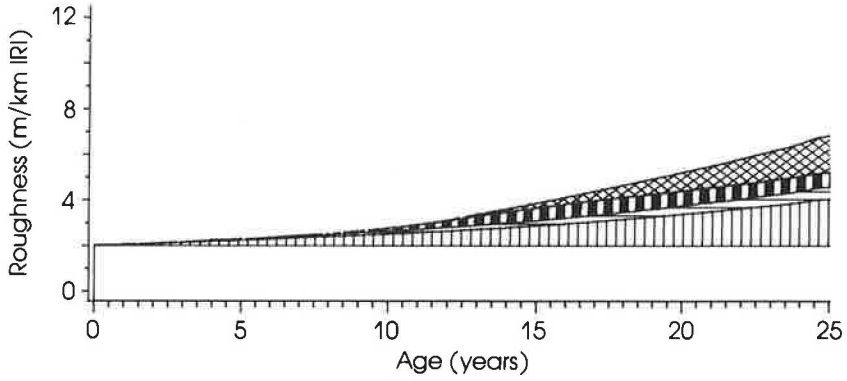

(b) Medium Loading, or Medium-term Design Pavement

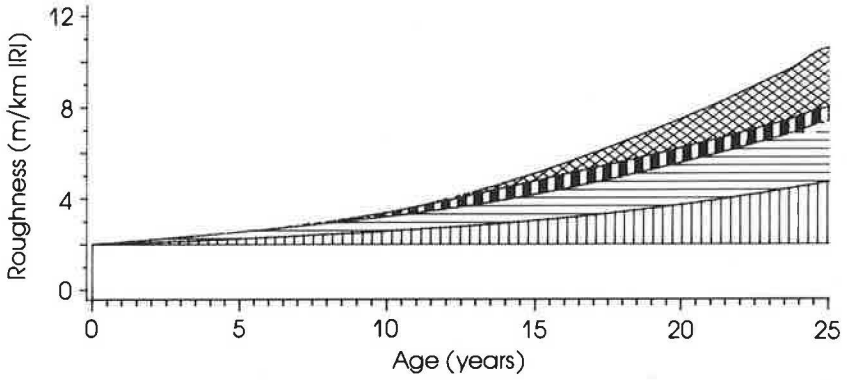

(c) Heavy Loading, or Shortterm Design Pavement

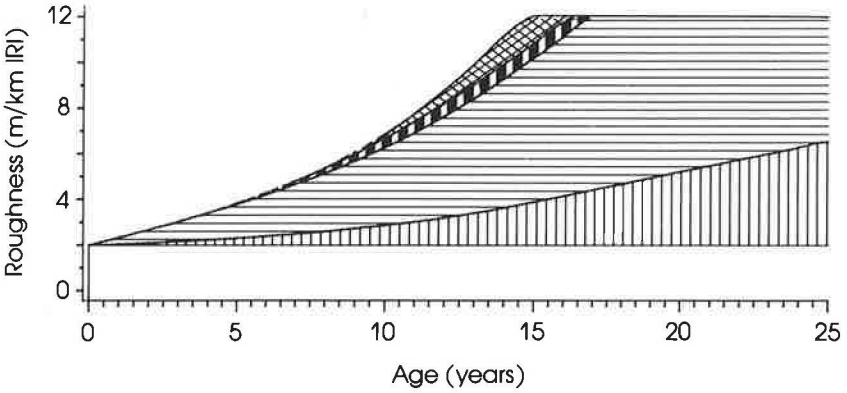

Potholing Cracking and Patching Deformation Environment-Age.

Note: Surface treatment on granular base pavement, SNC 3, with traffic loading of (a) 0.02, (b) 0.10, and (c) 0.50, million ESA/lane/year, respectively.
Source: Equation (2) applied through Road Deterioration and Maintenance submodel of HDM-III.

FIGURE 6 Illustration of component sources of roughness damage under different levels of traffic loading as predicted by model.

INFLUENCES OF TRAFFIC, TIME, AND STRENGTH

Traffic Loading and Pavement Age

The empirical evidence of the dual effects of traffic and time that supports the model is revealing and instructive. Figure 7 presents all the roughness trends observed in the Brazil-UNDP Study for two groups of pavements, each falling in a common flexible pavement strength category. The examples shown are asphalt concrete pavements with modified structural numbers rounding to 5 (a), and rounding to 7 (b). The roughness trends are presented as the increase of roughness since construction or rehabilitation, which normalizes the data across different pavements. The trends are shown against cumulative equivalent standard axle loadings in the left-hand charts and against age in the right-hand charts.

If roughness progression were a function only of traffic loading and pavement strength, as indicated by the traffic-related models, then all the trends in the cumulative loading charts would tend to be coincident within a reasonably narrow band. Instead, a broad scatter is noted, with some extremely rapid rates of progression at low levels of cumulative ESA and some extremely low rates at high levels of cumulative ESA. By way of comparison, the AASHTO predictions fall at about the center of the scatter, giving rates of 1 m/km IRI roughness increment per 1.3 million ESA and per 8 million ESA, respectively, for modified structural numbers 5 and 7.

On the other hand, the same trends appear much more closely grouped when depicted in relation to pavement age,

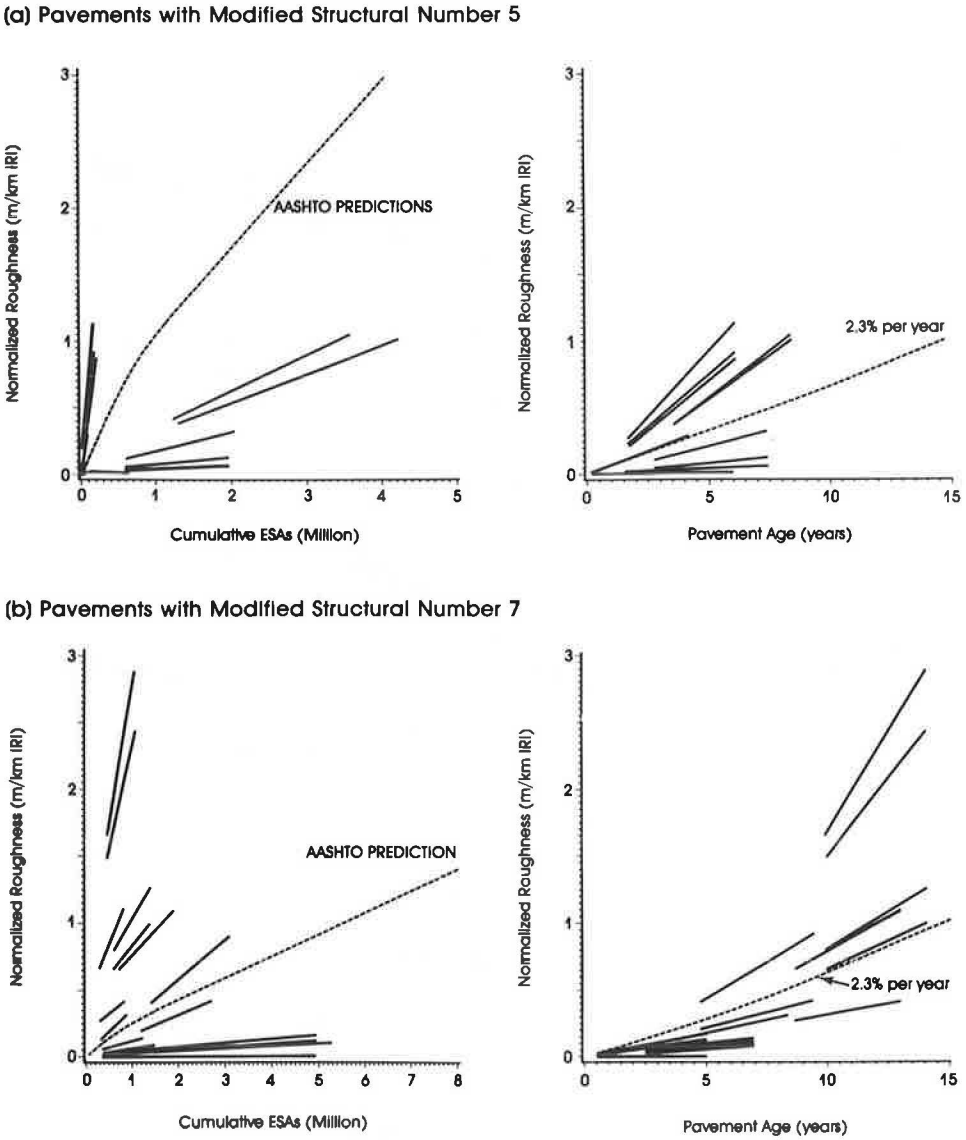

Note: Normalized roughness = RI(t) - RI(0). Trends shown as straight lines for clarity. Each group comprises pavements with SNC values rounding to the nominal value, e.g., 4.5 to 3.5 for SNC 5.
Source: Brazil-UNDP study data.

FIGURE 7 Comparing effects of traffic loading and aging on roughness progression observed in Brazil.

as seen in the age charts. The trends cover a range of about 1 to 3 percent growth per year and can be compared with the statistically estimated overall trend of 2.3 percent per year shown on the charts. The correlation is not perfect because both traffic and age are influencing the roughness, but the improvement over the correlation with traffic is clear.

The evidence is thus compelling that aging effects were strong in the data and explain a sizeable proportion of the roughness trends observed. Similar effects were evident on surface treatment pavements, although the patterns were less pronounced. Thus it is imperative that predictive models include both traffic and aging effects if they are to be reliable and applicable for the wide range of circumstances usually extant in a road network. In the case of the data illustrated in the figure, for example, the range of traffic flows in the SNC 7 pavement category was from as low as 1,000 ESA per year to as high as 2 million ESA per year, per lane.

Strength Parameter

The modified structural number was clearly the strongest predictor of the strength parameters tested in the roughness progression models. The Benkelman beam surface deflection, which is moderately correlated with the modified structural number, was not statistically significant in the deformation term of the component incremental model but did yield a fair alternative to *SNC* in a model of absolute roughness (*4*). Although the modified structural number itself has deficiencies as a strength parameter (because it is a thickness index that is somewhat insensitive to material properties and layer configuration), no improvement to the *SNC* formulation could be estimated from the data.

One inference is that surface deflection, while being an excellent indicator of relative strength along a nominally homogeneous pavement, is apparently not sufficient as a strength comparator to provide satisfactory predictions of roughness across different pavements and conditions. The reason for this is that material stiffness is not a sufficient indicator of deformation potential across different materials, although it is of course a good indicator for any one material, because deformation depends on the shear strength of the material as well as the induced stresses. Thus surface deflection, which aggregates the material stiffness effects under essentially common stress levels, is inferior to a parameter such as structural number that accounts for both shear strength and induced stress level through the material-layer coefficients utilized in its computation.

The Dynaflect deflection indices of maximum deflection and curvature proved to be yet weaker indicators of roughness progression, although having fair correlations to both the Benkelman beam deflection and structural number; and no statistical models for roughness progression could be found. Apparently, the stiffness derived under the low stress levels induced by this method are even further removed from the deformation behavior of the pavements than those under the heavier loading of the Benkelman beam method. While Falling Weight Deflectometer (FWD) deflection data were not available in the study, available evidence indicates that FWD deflections equal Benkelman beam deflections as a first approximation for equivalent levels of loading (*4*, p. 143).

CONCLUDING COMMENTS

This paper has focused on the conceptual and statistical development of the roughness model and its characteristics. The model advances understanding of roughness progression through identifying and quantifying the different mechanisms or sources of roughness change, namely, structural effects, surface defects, and environmental-aging influences. The scope, size, quality, and factorial design of the database from the Brazil Road Costs study made the analyses feasible, and the combination of mechanistic principles and empirical estimation make the model robust.

The robustness and versatility of the model are best demonstrated by its validity for conditions and environments other than the original Brazilian study, and a detailed evaluation has been made elsewhere (*4*). The estimation of the environmental coefficient (Table 5) and the evaluation of the model's transferability were made on data from major field studies in Arizona, Texas, Illinois, Colorado, Kenya (two), South Africa, and Tunisia, covering a range of climates including dry-nonfreezing, dry-freezing, wet-freezing, and wet-nonfreezing. Thus, the environmental factors given in Table 5 are considered applicable in the United States and elsewhere, at least as a first estimate. Further research may help to define better the environmental categories, particularly for high-rainfall climates (more than 2,000 mm per year).

The model leads to interesting interpretations concerning, *inter alia*, the attribution of damage and cost allocation among users. High-standard pavements (the long-term design case in Figure 6a) suffer small levels of damage, but high proportions of that damage are attributable to non-traffic factors, including the environment (*4*). The impact of different maintenance strategies can be evaluated through the influence of surface defects on the rate of roughness progression. The model is thus useful as a general damage model in addition to its use for predicting roughness progression.

ACKNOWLEDGMENTS

The work was conducted under funding from the United Nations Development Program and the World Bank, with greatly appreciated support from the Government of Brazil and the Brazilian Transport Planning Agency (GEIPOT). The data were collected by GEIPOT and the Texas Research and Development Foundation under the Brazil-UNDP-World Bank road costs study 1976–1981. Special thanks are due to the author's colleagues, Per Fossberg, Thawat Watanatada, and Ashok Dhareshwar, and to consultants Siu-On Lo, Andrew Chesher, and David Newbery for their assistance and interaction.

REFERENCES

1. W. D. O. Paterson. International Roughness Index: Relationship to Other Roughness and Riding Quality Measures. In *Transportation Research Record 1084*, TRB, National Research Council, Washington, D.C., 1986, pp. 49–59.
2. W. D. O. Paterson. *Accuracy of Calibrated Roughness Surveys, Measuring Road Roughness and Its Effects on user Cost and Comfort*. Special rep. STP 884. American Society for Testing and Materials, Philadelphia, 1985, pp. 66–88.

3. T. Watanatada, C. G. Harral, W. D. O. Paterson, A. Dhareshwar, A. Bhandari, and K. Tsunokawa. *The Highway Design and Maintenance Standards Model*. Johns Hopkins University Press for World Bank, Baltimore, Md., 2 vols., 1987, 280 p. and 391 p.
4. W. D. O. Paterson. *Road Deterioration and Maintenance Effects: Models for Planning and Management*. Johns Hopkins University Press for World Bank, Baltimore, Md., 1987, 454 pp.
5. *AASHTO Interim Guide for Design of Pavement Structures, 1972*. Association of State Highway and Transportation Officials, Washington, D.C., 1981.
6. L. Parsley and R. Robinson. *The TRRL Road Investment Model for Developing Countries (RTIM2)*. Laboratory Report 1057. Transport and Road Research Laboratory, Crowthorne, England, 1982.
7. R. L. Lytton, C. H. Michalek, and T. Scullion. The Texas Flexible Pavement System. *Proc., Fifth International Conference on Structural Design of Asphalt Pavements*. University of Michigan and the Delft University of Technology, Ann Arbor, Vol. 1, 1982.
8. G. B. Way and J. Eisenberg. *Pavement Management System for Arizona Phase II: Verification of Performance Prediction Models and Development of Data Base*. Arizona Department of Transportation, Phoenix, 1980.
9. D. W. Potter. *The Development of Road Roughness with Time—An Investigation*. Internal Report AIR 346-1. Australia Road Research Board, Melbourne, 1982, 78 pp.
10. A. Cheetham and T. J. Christison. *The Development of RCI Prediction Models for Primary Highways in the Province of Alberta*. Department of Transportation, City of Edmonton, Alberta, Canada, 1981.
11. J. Lucas and A. Viano. Systematic Measurement of Surface Evenness on the Road Network. *Bulletin de Liaison* 101, Laboratoire des Ponts et Chaussées, Paris, 1979.
12. C. A. V. Queiroz. *Performance Prediction Models for Pavement Management in Brazil*. Ph.D. dissertation. University of Texas, Austin, 1981.
13. P. G. Jordan, B. W. Ferne, and D. R. C. Cooper. An Integrated System for the Evaluation of Road Pavements. *Proc., Sixth International Conference on Structural Design of Asphalt Pavements*. University of Michigan, Ann Arbor, Vol. 1, 1987, pp. 607–617.
14. J. Uzan and R. L. Lytton. Structural Design of Flexible Pavements: A Simple Predictive System. In *Transportation Research Record 888*, TRB, National Research Council, Washington, D.C., 1982, pp. 56–63.
15. *Research on the Interrelationships Between Costs of Highway Construction, Maintenance and Utilization (PICR)*. Final Report, 12 vols. Empresa Brasileira de Planejamento de Transportes (GEIPOT), Ministry of Transport, Brasilia, 1982.

The views expressed are the author's and are not necessarily attributable to the World Bank or its agencies.

Publication of this paper sponsored by Committee on Pavement Management Systems.

Integrating Expert Systems in Existing Pavement Management Systems on Microcomputers

HOSIN LEE AND VINCE GALDIERO

The expert system technology is having an increasing role in the continuing development of new pavement management applications for the state and local highway agencies. In recent years, several prototype expert systems have been developed in the pavement management area. Expert systems were often developed as stand-alone systems without considering the existing pavement management systems (PMSs). This paper discusses a concept of integrating an expert system in existing pavement management systems. The expert system components should be combined with the existing pavement management system to make it more intelligent and friendly. Merging an expert system technology into the pavement management system will lead to a complete system capable of managing a large base of complex pavement-related data in an integrated way. This paper presents an expert system that can be integrated into the existing pavement management systems on microcomputers. This expert system is developed to enhance the existing PMS, not to replace it.

Pavement management problems involve empirical knowledge, but many existing pavement management systems (PMSs) use complex procedural algorithmic routines without fully incorporating human expertise. Recently, a number of excellent expert system developments in the pavement management area have been presented at the several workshops and conferences (*1–5*). The expert system technology is having an increasing role in the continuing development of new pavement management applications for state and local highway agencies.

The expert systems developed generally provide interactive input mode through the computer terminal and display conclusions on the screen after completing expert system consultation. The user manually enters all the data items as requested by the expert system, and these inputs and expert system consultation results are not often saved for later analysis or database queries. The expert system's ability to use and propagate the information flow of the existing PMS is critical for the acceptance of the expert system by the user.

Several expert systems were designed for use by state highway engineers with extensive data processing capabilities. For example, the EXpert system for Pavement Evaluation And Rehabilitation (EXPEAR), which was designed for high-type conventional concrete pavements, possesses extensive capabilities for storage and retrieval of input data, as well as output of pavement performance and cost analysis results (*3*).

This paper discusses a pavement management expert system (PMES) that was designed for a local community. The PMES was developed to support the existing PMS. Basic pavement inventory data can automatically be extracted from the pavement databases, and the PMES asks only for the information that is not available from the pavement database. The recommendation by the PMES is then automatically saved in the pavement database to be later utilized by the PMS. The PMES can further provide a detailed description of how to apply the recommended rehabilitation and maintenance strategy for the particular pavement section.

KNOWLEDGE- AND DATA-BASED SYSTEMS

Expert systems have often been developed as stand-alone systems without considering the use of existing application programs and databases. However, the increasing number of applications of expert systems in engineering require algorithmic routines and data processing capabilities (*6*). Consequently, it becomes necessary to develop an interface to connect an expert system with these existing conventional environments, including database management systems (DBMSs).

The concept of knowledge and database systems has been discussed in numerous workshops and textbooks (*7–10*). A knowledge or database system can be defined as "a system for developing applications requiring knowledge-directed processing of shared information" (*7*). The interaction between knowledge-based systems and data-based systems can be organized from "loose" to "tight" coupling of the expert system with a DBMS (*8*).

The tight coupling approach usually requires a sophisticated mechanism for a completely integrated system, such as an intelligent database system and an internal expert system database. A loosely coupled, expert system–database management system concept is more flexible. This concept allows an expert system to be connected to the existing systems as one of the application programs. The conceptual architecture of the PMES is shown in Figure 1. As shown in that figure, the expert system is just an extension of the existing system to provide the deductive inferencing search and explanation capabilities.

Recently, the necessity of integrating the expert systems and the existing database management technologies has been

H. Lee, Department of Civil and Environmental Engineering, Washington State University, Pullman, Washington 99164. V. Galdiero, Pavement Services, Inc., 2171 Jericho Turnpike, Commack, N.Y. 11725.

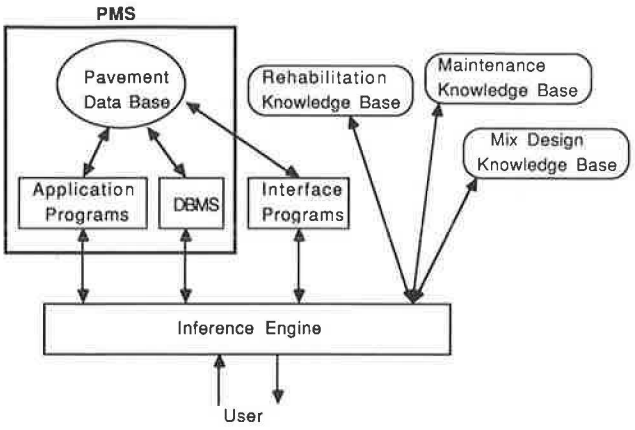

FIGURE 1 Conceptual architecture of PMES.

widely recognized, and the concept has been implemented in several expert system building tools. These tools, also referred to as shells, are now commercially available for microcomputers. Out of sixty commercially available expert system shells (*11*), eleven microcomputer-based expert-system shells were evaluated on the basis of their integration capabilities with conventional programming environments (*12*).

Only five shells have been reported to offer database management system interfacing. One of these shells, called INSIGHT 2+, was used to develop the PMES. This shell provides the integration capabilities through the special Pascal language DBPAS and its database extensions. The interface programs were written using DBPAS for accessing and manipulating the dBase III Plus database files.

DBPAS and its database extensions have somewhat limited data-base interface capabilities. For instance, a maximum of ten variables can be passed between the expert system environment and the interface programs, and a maximum of four database files can be open at the same time. INSIGHT 2+ may not be capable of serving as a shell for the large-scale expert system for the state agency that would require a large pavement database. The compilation and execution times for large knowledge bases could be prohibitively long for practical use by any state highway agency.

EXPERT SYSTEMS FOR A SMALL COMMUNITY

The Town of Huntington, New York, is located on the north shore of Long Island, 50 miles east of New York City. The town highway department is responsible for maintaining approximately 790 miles of two-lane roadways. The majority of this mileage can be classified as low-volume roadways with average daily traffic volume of fewer than 400 vehicles per day.

In 1984, through the efforts of the highway engineer, a PMS was developed by the in-house staff. The PMS developed was a modified version of a system used in Cherry Hill, New Jersey. The system, a manual one, was used by Huntington to produce a road program for the next construction season. The PMS was capable of identifying only two types of treatments, overlay or reconstruction, based upon an aggregate pavement condition rating score.

In 1987, after 3 years of use of the PMS, the town realized that the system needed to be enhanced to include a greater range of treatment options and identification of the appropriate treatment based on factors other than just an aggregate pavement condition rating value. The town highway department hired the firm of Pavement Services, Inc., to develop software for a new PMS. The development of the entire software package has been planned over three phases. A brief description of each phase follows.

Phase I—Current Network Needs

1. Identify the framework and data requirements for the PMS;
2. Collect and interpret the data;
3. Define broad-based maintenance and rehabilitation options; and
4. Assess overall network needs.

Phase II—Project Selection and Optimization

1. Identify potential projects;
2. Develop feasible maintenance alternatives;
3. Test each alternative using an economic analysis;
4. Select the optimum treatment; and
5. Establish a logical priority for taking action.

Phase III—Network Level Programming

1. Develop a long-range program;
2. Input budget and/or condition-level constraints;
3. Evaluate the effectiveness of each program;
4. Suggest a series of potential alternative programs; and
5. Select the final overall program.

Data collection and development of the Phase I module began during the summer of 1988. A new pavement condition survey form was first developed for the town. The new survey form is much more detailed and comprehensive than the one previously used by the town. A condition survey has been completed using the new form during Phase I.

The project is now in the second phase to identify feasible maintenance and rehabilitation alternatives. The improvements in the survey form should allow the town to use the individual distress items instead of an aggregated pavement rating score. During discussions with the town highway department with regard to the general framework of the PMS package, an interest was shown in the possible development of an expert system to aid department personnel in determining the most appropriate strategy for each pavement section.

The highway department was interested in an expert system for the following reasons: (a) lack of pavement management expertise in the town, (b) limited resources available for development, (c) fast prototyping of the system for initial acceptance, and (d) ease of modifying the system because of changing administrative policies.

DEVELOPMENT OF A PAVEMENT MANAGEMENT EXPERT SYSTEM

The Pavement Management Expert System (PMES) is being developed during the second phase of the project for the town of Huntington. The PMES is to determine the most appropriate rehabilitation and maintenance strategy for each pavement section based on condition survey data and other factors. The PMES is linked to the pavement database through the interface program written in the DBPAS language for which data had been previously collected and saved by the prototype PMS developed in dBASE III Plus.

Given the present condition of a pavement, the most appropriate rehabilitation or maintenance strategy is recommended by the PMES after all other subjective factors are fully considered. The basic pavement inventory data, such as distress condition survey, will automatically be extracted from the existing pavement database through the interface program named GetProgram, written in DBPAS.

The GetProgram can be called from a decision rule written in INSIGHT 2+. The simplified rule to access the pavement database using GetProgram is shown in Figure 2. This rule asks the user to provide the road name, then calls the GetProgram. The GetProgram searches through the pavement database to locate the pavement section requested by the user and returns the condition survey data to the knowledge base. Using distress information obtained from the database, an initial decision on whether to rehabilitate the pavement section will be made. A simple example of a decision rule for rehabilitation is shown in Figure 3.

The user will be asked only about other judgmental factors that are not currently available from the database, such as geometric design requirements, administrative information, pavement history, and so forth, to arrive at the final recommendation. This final recommendation is then automatically saved in the pavement database to be utilized later by the PMS. An example of the decision rule for a pavement recycling strategy is given in Figure 4. This rule utilizes the program called SaveProgram written in DBPAS to save the recommendation

PMES can further provide a detailed description of how best to apply the recommended rehabilitation and maintenance strategy for the particular pavement section. Thus the user does not have to look for additional reference materials regarding the specific application procedure.

For example, it can assist in determining the portions of reclaimed asphalt pavement and aggregate materials that are allowed in order to obtain a combined aggregate gradation that meets the specification requirement for recycling hot-mix design. A decision rule to determine optimum proportions

```
RULE        For Accessing Data Base
IF          Get the Pavement Data
AND ASK     Road Name
AND CALL    GetProgram
SEND        Road Name
RETURN      Distress Data
THEN        Have Distress Data
```

FIGURE 2 A rule to access pavement database.

```
RULE        For Rehabilitation
IF          Have Distress Data
AND         Rutting Area = Extensive
AND         Rutting Level = Severe
THEN        Evaluate for Rehabilitation
```

FIGURE 3 A sample decision rule for rehabilitation.

interactively is shown in Figure 5. A small GradProgram was written to conduct a gradation test against the specification.

After the gradation test is satisfied, another decision rule can be activated to compute the asphalt content needed for hot-mix recycling based upon the California Kerosene Equivalent formula, as shown in Figure 6.

A final recommendation can be displayed with all the necessary information at the end of consultation with the PMES. A sample recommendation display is shown in Figure 7. This DISPLAY function can be used to provide explanatory information for any technical jargon or ambiguous word for the user in the middle of the expert system consultation.

Any application program can be run from the PMES using the ACTIVATE function. The program should exist as an .EXE or .COM file. The parameter data can be passed via memory or a disk file. The rule shown in Figure 8 activates the program dBASE.EXE, and the COMMAND function is used to specify the program "PMS" that dBASE.EXE program will use. This ACTIVATE function will allow the PMES to access instantly any application program in the middle of an expert system consultation.

CONCLUSIONS

Pavement management is an appropriate application area of an expert system because pavement management problems require sound engineering knowledge provided by a human expert. An expert system can also provide explanatory information on the technical jargon and decision flow to make the existing PMS more friendly to the user.

The PMES is being developed for the local government, which is not capable of predicting the pavement performance and conducting life-cycle cost analysis. The running speed and the maximum number of rules allowed for the expert system shell are not constraints for developing a system for the small community.

In expert system applications in the pavement management area, it becomes necessary to integrate an expert system into the existing PMS. The inability of an expert system to inter-

```
RULE        For Recycling
IF          Evaluate for Rehabilitation
AND         Sufficient Pavement Thickness
AND NOT     Too Many Manhole Covers
THEN        Pavement Recycling Recommended
AND         Strategy := Recycling
AND         CALL SaveProgram
SEND        Strategy
```

FIGURE 4 A sample decision rule for pavement recycling.

```
RULE        For Gradation Test
IF          Have Aggregate Proportion
AND         CALL GradProgram
SEND        Initial Proportions
RETURN      Combined Proportions
THEN        Gradation Test Satisfied
DISPLAY     Gradation Test
```

FIGURE 5 A rule to determine aggregate proportions.

```
RULE        For Asphalt Content Required
IF          Gradation Test Satisfied
AND         CALL GetProgram
RETURN      Sieve8
RETURN      Sieve200
THEN        Asphalt Content Recommended
AND         AsphaltNeed:=0.035*Sieve8+0.045*Sieve200
AND         Asphalt:=AsphaltNeed-AsphaltReclaimed
DISPLAY     Final Recommendation
```

FIGURE 6 A rule to compute asphalt content needed.

```
DISPLAY          Final Recommendation

[Road Name] Is recommended for Recycling with
preliminary specifications as follow:
Reclaimed Asphalt Pavement Proportion is [RAP]
Reclaimed Aggregate Material Proportion is [RAM]
New Aggregate Material Proportion is [NEW]
Recommended Asphalt Content is [Asphalt]
```

FIGURE 7 A final recommendation display.

```
RULE            For Huntington PMS Active
IF              Menu Option IS Run PMS
THEN            PMS Activated
AND ACTIVATE    dBase.exe COMMAND PMS
```

FIGURE 8 A rule to activate external programs.

face with the existing PMS could lead to a low rate of acceptance of an expert system by the user.

In regard to the interface between the PMES and the existing PMS, the user sees the PMES as an extension of the PMS. The PMES can access the database whenever the data are needed. If the data are not available from the database, the PMES will automatically turn to the user for the information. The PMES can be considered an intelligent interface to the PMS.

Merging of an expert system technology into the existing PMS will lead to a complete system capable of managing a large base of complex pavement-related data in an integrated way. The PMES is developed to supplement the existing PMS, not to replace it.

REFERENCES

1. Expert Systems and Information Technology. In *Proc., Second North American Conference on Managing Pavements*, Toronto, Ontario, Canada, Vol. 2, 1987.
2. S. G. Ritchie, C. I. Yeh, J. P. Mahoney, and N. C. Jackson. Development of an Expert System for Pavement Rehabilitation Decision Making. In *Transportation Research Record 1070*, TRB, National Research Council, Washington, D.C., 1986, pp. 96–103.
3. K. T. Hall, J. M. Connor, M. I. Darter, and S. H. Carpenter. Expert System for Concrete Pavement Evaluation and Rehabilitation. In *Transportation Research Record 1207*, TRB, National Research Council, Washington D.C., 1988, pp. 21–29.
4. R. P. Tandon and K. C. Sinha. *An Expert System to Estimate Highway Pavement Routine Maintenance Work Load*. Presented at 67th Annual Meeting of the Transportation Research Board, Washington D.C., 1988.
5. M. L. Maher. *Expert Systems for Civil Engineers: Technology and Application*. ASCE, New York, 1987.
6. *Applications of Artificial Intelligence in Engineering*. (D. Sriram and R. Adey, eds.) Springer-Verlag, London, England, 1986.
7. L. Kerschberg. *Expert Database Systems*. Benjamin/Cummings Publishing Co., Menlo Park, Calif., 1986.
8. G. Gardarin and E. Gelenbe. *New Applications of Data Bases*. Academic Press, London, England, 1984.
9. A. Gupta and B. E. Prasad. *Principles of Expert Systems*. IEEE Press, New York, 1988.
10. J. D. Ullman. *Database and Knowledge-Base Systems*. Computer Science Press, New York, Vol. I, 1988.
11. S. Finnie. Sudden Shower Enriches MIS Turf. *ComputerWorld*, Vol. XXII, No. 41, 1988.
12. K. Petersen. Connecting Expert Systems and Conventional Environments. *AI Expert Magazine*, Vol. 3, No. 5, 1988.

Publication of this paper sponsored by Committee on Pavement Management Systems.

A Prioritization Scheme for the Micro PAVER Pavement Management System

KIERAN J. FEIGHAN, MOHAMED Y. SHAHIN, KUMARES C. SINHA, AND THOMAS D. WHITE

The ultimate aim of any pavement management system is to get an optimal return from the available resources. The culmination of a research effort to improve the prediction, optimization, and budget allocation abilities of the Micro PAVER pavement management system is a prioritization scheme capable of taking in available budget estimates for any number of years and outputting the sections recommended for repair and the type and cost of repair to be applied. The scheme uses as its base the effectiveness/cost ratios obtained from a dynamic programming module. These ratios are then modified by weights that are related to section characteristics by each individual pavement manager. This enables a customized output to be obtained for each database. The available budget for repair is determined as the actual budget less the cost of routine and stopgap repairs on every section. This budget is then allocated to the highest-scoring (in terms of weighted effectiveness/cost ratio) sections until the budget is exhausted. Deterministic Pavement Condition Index (PCI) versus age curves are used to predict each section's condition in the following year, and the process is then repeated. A completed example is included to illustrate the working of the program logic.

There is an ongoing effort to improve the prediction and optimizing capabilities of the Micro PAVER pavement management system (*1,2*). Papers presented and published at past Transportation Research Board (TRB) annual meetings have outlined the progression in thought and development from the early stages of this effort (*3–5*). This paper outlines the logic and use of the prioritization schema developed for use in Micro PAVER. It takes inputs from the new Pavement Condition Index (PCI) prediction models developed at the U.S. Army Construction Engineering Research Laboratory (USA-CERL), both deterministic (*3*) and Markovian probabilistic (*4*). It also uses the outputs from the dynamic programming package developed at USA-CERL (*5–7*) and additionally accepts user inputs of budgets available for as many years as is desired. The output from this program is a list of prioritized sections to be repaired within the given budget in every year desired along with the recommended M&R treatment and the estimated cost for each section. A summary of the previous work performed at USA-CERL is not contained in this paper. There is a brief synopsis in an accompanying paper (*8*), and of course the references quoted above deal with each of the related topics in a detailed way.

K. J. Feighan, ERES International Inc., Champaign, Ill. 61820. M. Y. Shahin, United States Army, Construction Engineering Research Laboratory, Champaign, Ill. 61820. K. C. Sinha and T. D. White, Department of Civil Engineering, Purdue University, West Lafayette, Ind. 47907.

INTRODUCTION TO PRIORITIZATION

There would be no need for prioritization if unlimited financial, temporal, and manpower resources were available. Unfortunately, this is seldom the case. Consequently, decisions must be made as to which sections it is most advantageous to repair and which must be left unrepaired at the moment. In the most common case, pavement managers are constrained by the budget allocated to them. A decision must be made as to which sections it is "best" to repair for this budget.

Of course, the problem lies in deciding upon the definition of "best" or "optimal." Dynamic programming yields an optimal solution for every family/state combination over a given life-cycle length. However, this solution is unconstrained by budgetary restrictions. If it were possible to perform the recommended treatment on every section, this would be a truly network-optimal solution. As this is unrealistic in most cases, further analysis must be performed to determine which sections should be repaired within the given budget to yield a network-optimal solution.

Network Optimality

The issue of network optimality must be discussed before progressing further in the prioritization algorithm. Basically, what needs to be decided is which properties of the network are deemed to be most important by the pavement manager. These properties may include

1. Servicing the most important routes first,
2. Attempting to keep the entire network functionally operational,
3. Placing emphasis on some pavement uses over others,
4. Attempting constantly to improve the overall network condition, and
5. Attempting to maintain a uniform network condition.

Many other possible goals can also be included. It can quickly be seen that some of these goals impinge directly upon one

another, and all cannot be addressed. Some, indeed, are directly contradictory.

Only the pavement manager can decide which properties to emphasize on the particular network that he or she is managing. There is no universal "best" set of goals applicable to all networks. Many factors, including size of network, diversity of users, available budget, age of network, and others, will all bear upon the manager's decisions and priorities. As the Micro PAVER system is designed for implementation on a large range of networks across the United States and abroad, it is doubly obvious that a single set of goals cannot be universally optimal.

Given that this is the case, a tool must be provided that has the flexibility built in to reflect the different priority schemes possible. A set of weighting factors that are user-defined can be used to customize the prioritization scheme for the individual manager. The particular types of weights and categories to be used are discussed subsequently in the specific details of the prioritization program proposed. It is sufficient at this stage to point out the need for such a scheme.

Thus, the skeleton of a prioritization scheme can be glimpsed. It should take inputs of available budget, candidate sections for repair (in the most general network case, all sections are candidates), and a means whereby the optimal attributes that the network should have are represented. Each candidate section is then judged against all others on the basis of how well it can improve or maintain the network attributes if chosen for repair. Sections should be chosen until the available budget is exhausted. With this background in mind, a detailed description of the proposed prioritization plan now follows.

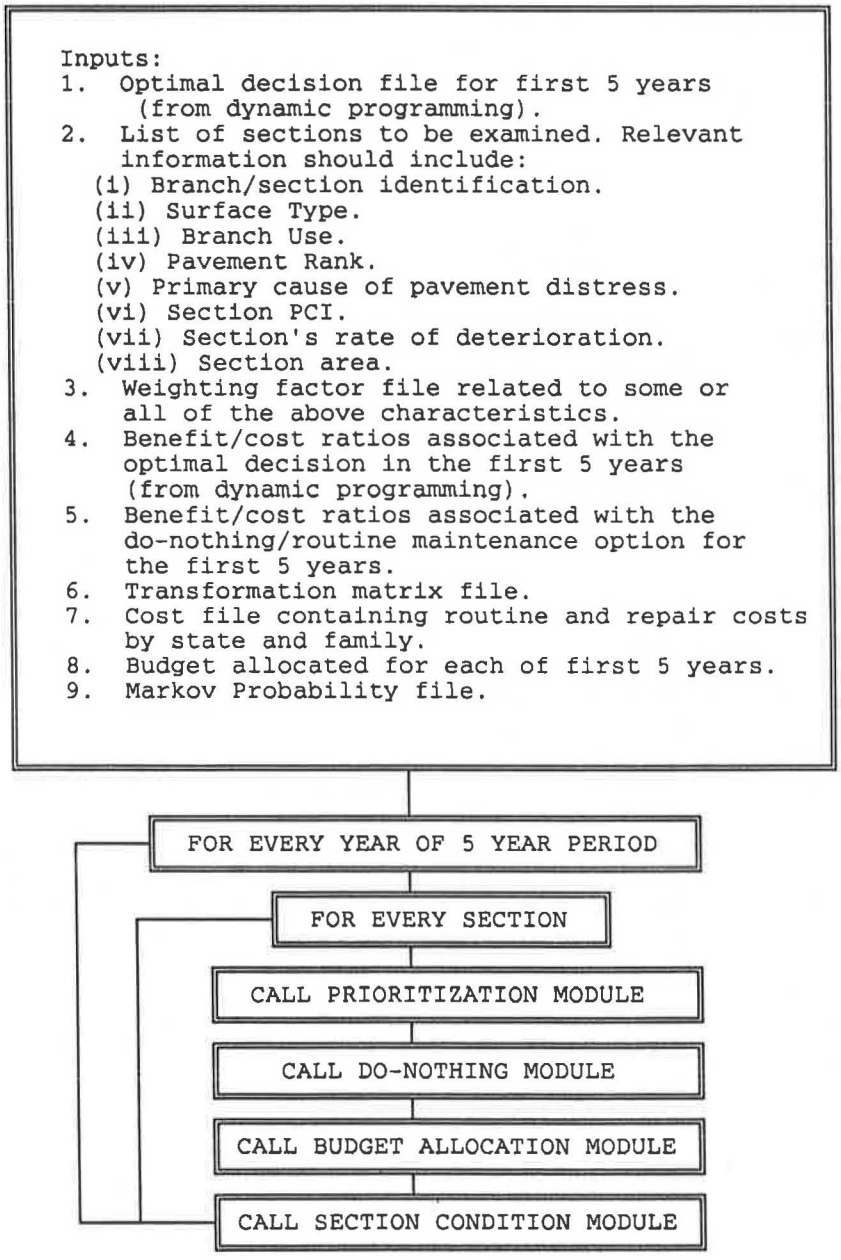

FIGURE 1 Prioritization using dynamic programming.

PRIORITIZATION AND BUDGET ALLOCATION FOR PAVER

The most important step in designing a prioritization program is knowing what type of output is required. In the present case, for the purposes of network planning, it is required that an optimized 5-year plan be output. The plan should consist of a list of sections to be repaired in each of the 5 years for a given annual budget. The annual budget can vary from year to year. Obviously, there will be less confidence in the schedule devised for 5 years before the present time because of the uncertainty in prediction of condition, future costs, and other factors. As the years go by, updated and revised 5-year plans will yield greater confidence in the schedule proposed, just as there is much confidence in the schedule proposed for the first year of the current 5-year plan.

There are a number of tools available, both existing and recently developed, that can be used in constructing a useful prioritization and budget allocation plan. The dynamic programming output (*5*), which contains a list of optimal decisions for every family/state combination in every year of a given life-cycle analysis, is a crucial input to the prioritization scheme. The constrained least squares (LSI) best-fit program (*3*), used to fit predicted PCI versus age curves to the available data, also provides an extremely useful tool.

PRIORITIZATION USING DYNAMIC PROGRAMMING

The overall flowchart outlining this prioritization algorithm is shown in Figure 1. The process consists of four main modules.

1. Prioritization module,
2. Do-nothing/routine maintenance module,
3. Budget allocation module, and
4. Section condition prediction module.

Each of these is described in detail subsequently. Figure 1 also shows all the input data required to allow proper functioning of the prioritization and budget allocation process. While at first glance it may appear that substantial information is required, in fact most of this information has already been provided for the dynamic programming program (*5*).

The optimal decision file contains the optimal decision for every family/state combination considered in dynamic programming for the first 5 years of the life cycle analyzed. This is a direct output from dynamic programming that can be fed straight into prioritization. The list of sections to be evaluated is obviously a user input. The default situation would be to consider all sections in the network; if a manager has earmarked funds for sections with particular characteristics, however, he or she may want to allocate these funds among the qualifying sections only.

The section-related information required is already stored in each network's database and is easily extractable. The use to which each piece of information is put will be outlined in the following module descriptions. The weighting factors used are again user-defined. These weights allow the manager to express the particular goals of the network in a physical way.

The effectiveness/cost ratios for the first 5 years are again direct outputs from dynamic programming. The dynamic programming has also been modified to allow the user to "force" the program to accept routine maintenance as the only viable option in the first few years, the number of years to be determined by the user. Thus, the default budget that calculates the cost and subsequent effectiveness/cost ratio if only routine maintenance is allowed in year 1 can be calculated. This should be the absolute minimum budget allowable. The implications of this approach are discussed further in the do-nothing and budget allocation modules. The transformation matrix, cost, and Markov probability files are all exactly as used in dynamic programming.

The only other input required is the budget allocated for each of the first 5 years. Again, these values must be entered by the pavement manager. It should be possible to enter a number of different combinations of budget values and evaluate their respective impacts upon the overall network condition and upon individual sections. Through playing out these "what-if" scenarios, the manager can seek justification for increased funding or for improved funding in earlier or later years. A description of the four modules constituting the overall program is now presented.

Prioritization Module

An overall flowchart of this module is shown in Figure 2. The first step in the prioritization module is to identify which section is currently being dealt with. Once this is clear, the section characteristics are obtained and the family to which the section belongs is identified. The definition of "family," as used throughout the whole development of the Micro PAVER packages, is a group of sections having common section characteristics (e.g., pavement type, traffic loading, surface thicknesses). On the basis of the section's PCI, the state it belongs to is identified. A state is defined as a 10 PCI-wide bracket in each family. For example, sections having a PCI of 90 to 100 are defined to be in state 1. Thus, it is possible to assign a family/state identification to the section.

The reason for performing this assignment is that the dynamic programming output of effectiveness/cost (E/C) ratio is in terms of family/state combinations. The E/C ratio corresponding to the section's family and state is located. This is a "raw" score, not taking into account any of the section's characteristics, such as branch use, pavement rank, or rate of deterioration. If these characteristics are not considered, all sections in a particular state of a given family will have exactly the same E/C ratio.

If branch use and pavement rank are incorporated into the family definition, then it is still possible that all sections in each state of that family will have the same E/C ratio. To differentiate further between these sections, it is necessary to use another criterion, one that is specifically related to the section's PCI.

The candidate criteria that were considered were

1. Sections with a lower PCI in a state to be repaired first,
2. Sections with a higher PCI in a state to be repaired first,
3. Older sections in a state to be repaired first,
4. Newer sections in a state to be repaired first, and
5. Sections with higher rates of deterioration to be repaired first.

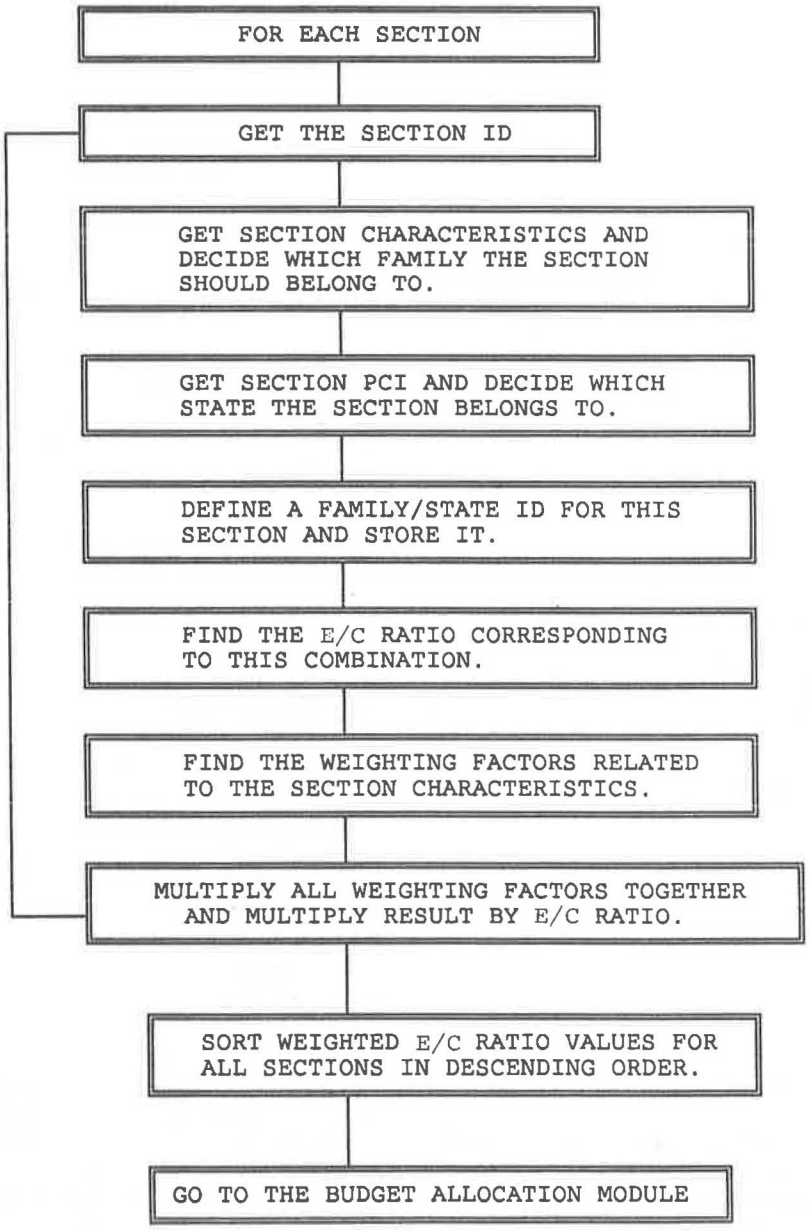

FIGURE 2 Prioritization module.

The justifications for selecting each of these potential criteria follow.

1. Sections with a lower PCI are more likely to transit to the next state, where it will cost more to repair, and thus should be repaired as soon as possible.
2. Life-cycle analysis has shown that preventive maintenance is more cost-effective than after-the-fact repair. Thus, sections with a higher PCI should be repaired first.
3. Older sections are more deserving of repair than newer sections and may be nearer the end of their design life, necessitating major repair if not repaired first.
4. Newer sections usually have higher rates of deterioration than older sections with the same PCI and should be repaired first.
5. Sections with higher rates of deterioration should be repaired first. Using rate of deterioration as a criterion combines the idea of using PCI with that of using age together into a rational decision mechanism. This criterion was chosen as the most suitable.

The weighting factors corresponding to each section's characteristics are then extracted and multiplied by the "raw" effectiveness/cost ratio to give a weighted E/C ratio. This whole process is repeated for every section. All of the candidate sections are then sorted in descending order of weighted E/C ratio. This is the output from the prioritization module, a prioritized list of candidate sections for repair, with prioritization based upon weighted effectiveness/cost ratio.

Routine Maintenance Module

The routine maintenance module is very simple and easily understood. Figure 3 shows a flowchart of the algorithm. The

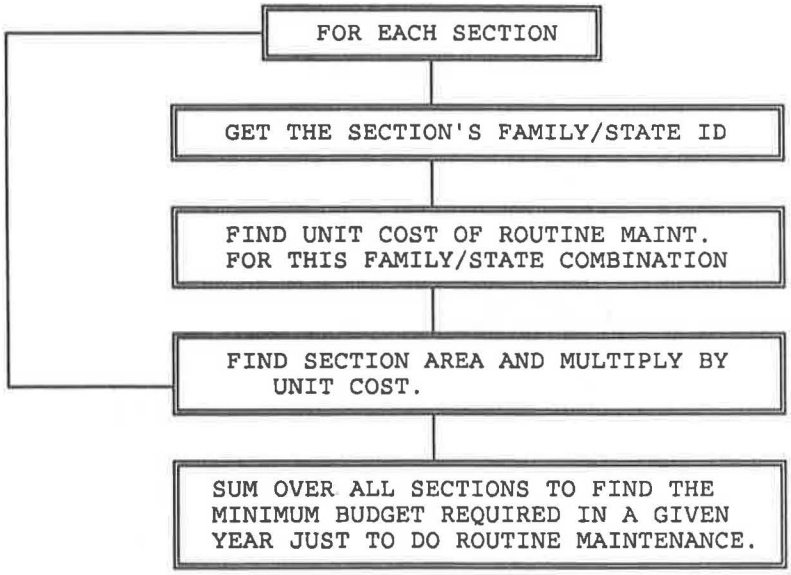

FIGURE 3 Routine maintenance module.

purpose of this module is to determine the absolute minimum budget required just to apply routine maintenance to every section considered. It should be noted that the budget allocated is at least as large as the value obtained from the routine maintenance module; otherwise, many sections will not have any maintenance whatsoever performed. By identifying the surplus of actual budget over minimum allowable budget, it should be possible to calculate how much is actually available for repair activities. Further discussion of this point is contained in the budget allocation module.

Basically, what the routine maintenance module does is locate the unit cost of routine maintenance for each section, multiply this cost by the section area, and sum over all candidate sections. The cost information is contained on a state-by-state basis, so the section's family/state identification is sufficient to locate this cost. The output from this module is the cost of routine maintenance for each section in the given year and the total of these costs over all candidate sections.

Budget Allocation Module

The budget allocation module is run yearly. It takes in the prioritized list of sections from the prioritization module and yields a list of sections to be repaired in that year for a given budget. The advantage of using the modular approach is that the prioritized list is obtained independently of the budget, so changes in proposed budget can be handled easily in the budget allocation module without requiring recalculation in other modules.

Figure 4 shows the module flowchart. The family/state identification associated with the section at the top of the prioritized list is obtained. This is then used to locate the recommended treatment for this family/state combination in the optimal decision file obtained from dynamic programming. The unit cost (cost per square yard) is obtained from the cost file for this repair option and is then multiplied by the section's total area to get the cost of repair.

This repair cost is then subtracted from the allowable budget if the allowable budget is for repair only. If the allowable budget is the total that can be spent on both repair costs and routine maintenance costs for the entire network, however, a different approach is necessary. The do-nothing/routine maintenance module gives the total cost of performing routine maintenance over the network. The surplus between this amount and the amount allocated as budget is the amount available for repair costs.

The section repair cost is subtracted from this figure, and the cost of routine maintenance that would have accrued if repair had not been carried out is added to the repair budget. This whole cycle is repeated until the available repair budget is exhausted. A search is continued until as much of the budget as possible is used up. Thus, a section with a large area and a high potential E/C ratio may be rejected because of insufficient funds. However, another section with a lower E/C ratio but with a smaller area (and, hence, lower total costs) may be chosen because it still is affordable within the available budget.

The output from the budget allocation module is a list of sections to be repaired in the year considered, the type of treatment to be performed on each section, the cost on a section-by-section basis, and the total cost. The expected network PCI to be obtained as a consequence of carrying out this repair schedule can also be computed. The budget allocation process is performed for each year of the 5-year plan being formulated.

Section Prediction

As a part of the analysis performed to obtain PCI prediction curves on a family-by-family basis, deterministic, constrained polynomial curves are fitted to each family's (PCI, age) data, as outlined in other research (*3*). These curves are then used here on a section-level basis to predict the future PCI of each section.

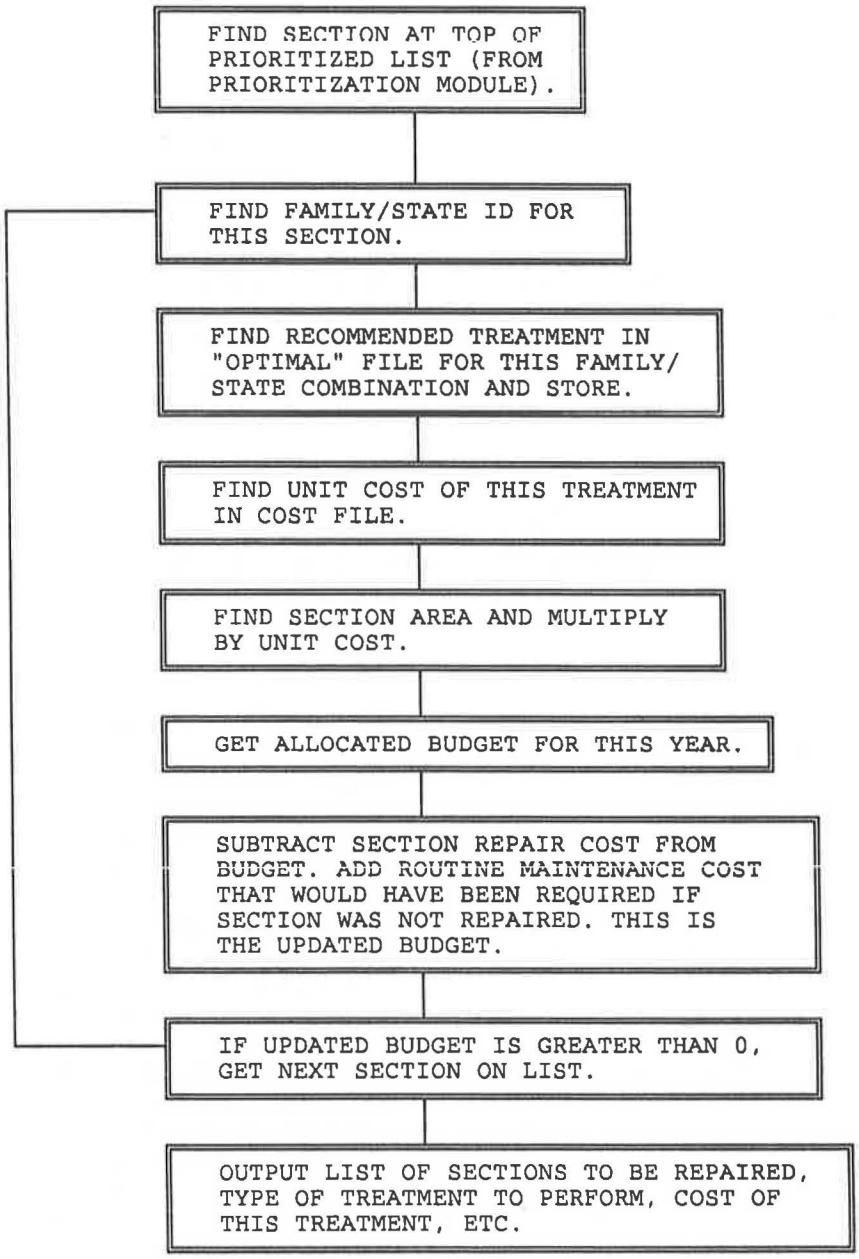

FIGURE 4 Budget allocation module.

If a section is chosen for nonroutine repair in budget allocation, it is assumed that the PCI is returned to 100. If routine maintenance is recommended, the PCI versus age family curves can be used and adjusted directly to predict the section's future PCI in the following year. The flowchart for the section condition in following year module is shown in Figure 5.

PRIORITIZATION EXAMPLE

This section uses a brief example to illustrate the working of the prioritization program. To make it as simple as possible to follow, only five sections in a network are analyzed. The functioning of the program proceeds just as easily, however, when more sections are included. The prioritization program uses the Markov probabilities, costs by state, and dynamic programming outputs described earlier.

Table 1 contains the section information for each of the five sections. These properties were formulated hypothetically. The lowest PCI, 55, occurs in section 5. This relatively high value occurs because it was previously specified in the dynamic programming and simulation routines that the minimum allowable state would be state 5, with PCI values of 50 to 60. It can also be seen from this table that numerous and variable properties are represented among the five sections included.

Table 2 illustrates the weighting factors used in the example. It can be seen that there are four possible surface types: asphalt concrete, surface treatment, thin overlay, and structural overlay. There are three possible branch uses: roadway,

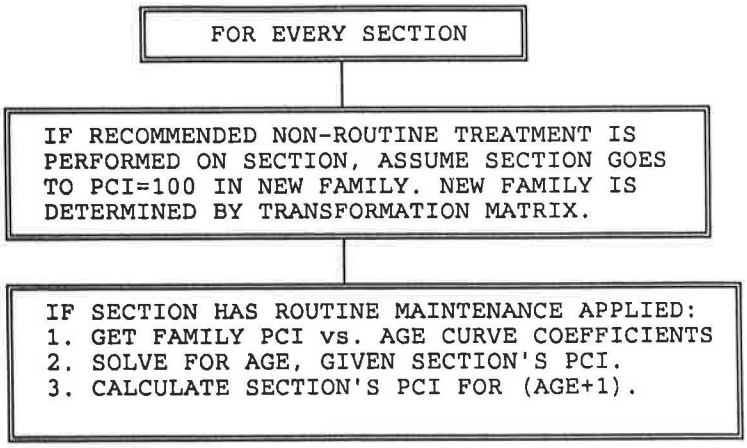

FIGURE 5 Section condition in following year module.

TABLE 1 SECTION INFORMATION

Section Number	Branch Use	Surface Type	Pavement Rank	Cause of Deterioration
1	RO	AC	P	LOAD
2	PA	ST	S	CLIMATE
3	PA	ST	S	LOAD
4	RO	ST	T	CLIMATE
5	RO	TO	S	OTHER

Section Number	PCI	Section Area (sy)	Pavement Family	Rate of Deterioration
1	80	2000	1	2.0
2	65	4000	2	3.0
3	75	5000	3	5.0
4	89	10000	4	5.0
5	55	4500	2	2.5

AC = ASPHALT CONCRETE
ST = SURFACE TREATMENT
TO = THIN OVERLAY
SO = STRUCTURAL OVERLAY

RO = ROADWAY
PA = PARKING

P = PRIMARY
S = SECONDARY
T = TERTIARY

TABLE 2 WEIGHTING FACTORS USED

Category	Surface Type	Branch Use	Pavement Rank	Pavement State
1	.9 (AC)	.6 (RO)	1.0 (P)	.5 (ST 1)
2	.5 (ST)	.7 (PA)	.6 (S)	.6 (ST 2)
3	.7 (SO)	.4 (OTH)	.3 (T)	.7 (ST 3)
4	.3 (TO)			.8 (ST 4)
5				.9 (ST 5)

AC=ASPHALT CONCRETE
ST=SURFACE TREATMENT
TO=THIN OVERLAY
SO=STRUCTURAL OVERLAY

RO=ROADWAY
PA=PARKING
OTH=OTHER

P = PRIMARY
S = SECONDARY
T = TERTIARY

TABLE 3 SAMPLE COSTS ($1/SQ YD)

FAMILY 1

STATE	ROUTINE MAINT.	SURFACE TMT.	THIN OVL.	STRUCT. OVL.	RECONST.
1	0.1	1.1	3.31	4.53	11.8
2	0.1	1.4	3.49	4.68	11.8
3	0.1	1.7	3.67	4.83	11.8
4	0.15	1.86	3.76	4.95	11.8
5	0.2	1.89	3.79	5.05	11.8

FAMILY 2

STATE	ROUTINE MAINT.	SURFACE TMT.	THIN OVL.	STRUCT. OVL.	RECONST.
1	0.05	0.8	3.44	4.5	12
2	0.1	1.2	3.56	4.7	12
3	0.3	1.6	3.68	4.9	12
4	0.4	2.1	4.16	5.45	12
5	1.4	2.7	4.99	6.35	12

FAMILY 3

STATE	ROUTINE MAINT.	SURFACE TMT.	THIN OVL.	STRUCT. OVL.	RECONST.
1	0.05	1.43	3.54	4.59	11.85
2	0.1	1.58	3.66	4.71	11.85
3	0.2	1.73	3.79	4.84	11.85
4	0.3	2.1	4.26	5.24	11.85
5	0.35	2.7	5.09	5.92	11.85

FAMILY 4

STATE	ROUTINE MAINT.	SURFACE TMT.	THIN OVL.	STRUCT. OVL.	RECONST.
1	0.05	1.3	3.15	4.29	11.85
2	0.1	1.5	3.45	4.51	11.85
3	0.2	1.7	3.75	4.74	11.85
4	0.33	2	4.16	5.08	11.85
5	0.6	2.4	4.69	5.53	11.85

FAMILY 5

STATE	ROUTINE MAINT.	SURFACE TMT.	THIN OVL.	STRUCT. OVL.	RECONST.
1	0.1	1.1	3.31	4.53	11.8
2	0.1	1.4	3.49	4.68	11.8
3	0.1	1.7	3.67	4.83	11.8
4	0.15	1.86	3.76	4.95	11.8
5	0.2	1.89	3.79	5.05	11.8

TABLE 4 FAMILY MARKOV PROBABILITIES

FAMILY	STATE 1	STATE 2	STATE 3	STATE 4	STATE 5	STATE 6	STATE 7	STATE 8	STATE 9	STATE 10
1	0.7825	0.8656	0.8717	0.8752	0.0006	0.4144	0.2845	0.6346	0.3548	1
	0.0001	0.5021	0.5015	0.5014	0.0013	0.0001	0	0	0	1
	0.001	0.5	0.4999	0.4999	0.4765	0.1364	0.037	0.0112	0.0025	1
	0.1374	0.6502	0.5021	0.5003	0.0001	0.0361	0.001	0.0001	0.0005	1
2	0.8481	0.407	0.2631	0.4502	0.6058	0.4976	0.5	0.4996	0.859	1
	0.1821	0.4714	0.4736	0.4815	0.0615	0.0029	0.0016	0	0.0442	1
	0	0.5001	0.5	0.5	0.0012	0.0001	0	0	0	1
3	0.7764	0.8579	0.8627	0.8631	0.0007	0.4767	0.5376	0.4954	0.6414	1
	0	0.5	0.5	0.5	0.0001	0.0302	0.0336	0.0008	0.0007	1
	0.6862	0.874	0.6205	0.306	0.001	0.0001	0	0	0	1
4	0.8136	0.7798	0.7829	0.7832	0.0038	0.0001	0.7491	0.2284	0.7604	1
	0.001	0.5	0.4999	0.5	0.0022	0.0006	0.0001	0	0.26	1
	0.9853	0.5002	0.5	0.4999	0.0001	0.0122	0.0327	0.0006	0.0003	1
5	0.7825	0.8656	0.8717	0.8752	0.0006	0.4144	0.2845	0.6346	0.3548	1
	0.0001	0.5021	0.5015	0.5014	0.0013	0.0001	0	0	0	1
	0.001	0.5	0.4999	0.4999	0.4765	0.1364	0.037	0.0112	0.0025	1
	0.1374	0.6502	0.5021	0.5003	0.0001	0.0361	0.001	0.0001	0.0005	1

FAMILY 1: AC PAVEMENTS
FAMILY 2: ST PAVEMENTS
FAMILY 3: AC THIN OVERLAYS
FAMILY 4: AC STRUCTURAL OVERLAYS
FAMILY 5: AC RECONSTRUCTION

YEAR	SECTION NUMBER	MAINT. ALT.	COST	STATE	E/C RATIO
1	1	1	200	2	36.68
	2	2	8400	4	22.95
	3	1	1000	3	20.39
	5	2	12150	5	16.94
	4	1	1000	2	9.34
2	1	1	200	2	34.78
	3	2	10500	4	21.08
	2	1	200	1	19.54
	5	2	5400	2	16.14
	4	1	2000	3	8.21
3	1	1	200	2	32.82
	2	1	200	1	17.96
	3	1	250	1	17.96
	5	1	225	1	15.39
	4	1	2000	3	7.79
4	1	1	200	2	30.82
	2	1	200	1	16.12
	3	1	250	1	16.12
	5	1	225	1	13.82
	4	1	2000	3	7.6
5	1	1	200	2	28.76
	2	1	200	1	16.09
	3	1	250	1	16.09
	5	1	225	1	13.79
	4	1	2000	3	7.33

	YEAR 1	YEAR 2	YEAR 3	YEAR 4	YEAR 5
REQUIRED BUDGET	22750	18300	2875	2875	2875
AVERAGE PCI	81	89	89	89	85
AVG. PCI WEIGHTED BY AREA	79	86	86	86	81

FIGURE 6 Available annual budget of $25,000.

YEAR	SECTION NUMBER	MAINT. ALT.	COST	STATE	E/C RATIO	
1	1	1	200	2	36.68	
	2	1	1600	4	22.95	#
	3	1	1000	3	20.39	
	5	1	6300	5	16.94	#
	4	1	1000	2	9.34	
2	1	1	200	2	34.78	
	2	1	1600	4	21.08	#
	3	1	1500	4	21.08	#
	5	1	6300	5	15.33	#
	4	1	2000	3	8.21	
3	1	1	200	2	32.82	
	2	1	1600	4	19.33	#
	3	1	1500	4	19.33	#
	5	1	6300	5	14.08	#
	4	1	2000	3	7.79	
4	1	1	200	2	30.82	
	2	1	1600	4	17.35	#
	3	1	1500	4	17.07	
	4	1	2000	3	7.6	
	5	1	7650	6	0.02	#

	YEAR 1	YEAR 2	YEAR 3	YEAR 4
REQUIRED BUDGET	10100	11600	11600	12950
AVERAGE PCI	69	69	67	65
AVG. PCI WEIGHTED BY AREA	69	69	67	65

Budget Required in Year 5 is Insufficient
Min. Budget Required is $16950

FIGURE 7 Available annual budget of $15,000.

parking, and other. The three pavement rank categories are primary, secondary, and tertiary, whereas there are five possible pavement states as defined by the ten PCI point brackets. Again, the weighting factors assigned are purely arbitrary. It is envisaged that the user would determine these on a location-specific basis, thus bringing about a customized prioritization. The values used in the example are intended solely to illustrate the working of the program.

It was decided not to weight on the basis of primary cause of deterioration, rate of deterioration, or pavement family for this example. The capacity does exist within the program to deal with weights assigned on the basis of any of these variables. Table 3 contains the repair costs on the dollar-per-square-yard basis used in the example. There are five possible repair options to be considered: routine maintenance, surface treatment, thin overlay, structural overlay, and reconstruction. The costs are given on a state-by-state basis within each pavement family.

Table 4 contains the Markov probability values used in the analysis. The values for all five options are given on a state-by-state basis for states 1 to 10. The Markov zoning approach was used, as detailed elsewhere (*4,7*), and options 1 and 5 had four zones, while options 2, 3, and 4 used three zones to model the deterioration process accurately. The probability values for original AC pavements and reconstructed AC pavements are identical. This is because the usual assumption made in the absence of substantive data is that reconstructed pavements will behave in the same manner as the original AC pavements. The Markov values and cost figures are actually those obtained from the Tulsa database (*9*).

The Tulsa transformation matrix and optimal decision and effectiveness/cost ratio files from dynamic programming were also used in the analysis. It was decided to run the prioritization package for a 5-year analysis period, with output reports in every year. Three sets of budget figures were used: (1) $25,000 available in each year, (2) $15,000 in each year, and (3) $18,000 in the first 2 years and $13,000 in the last 3 years. The figures for option 3 were chosen to total $75,000 for direct comparison with option 2.

The output from the program for these three sets of budgetary inputs is shown in Figures 6, 7, and 8. In Figure 6, it can be seen that sufficient money was available in every year to perform the optimal treatments. Without discounting the expenditures in any year to present worth values, the total money required to be spent over the 5-year period is $49,675. It can be seen that in the last 3 years, relatively little expenditure is required. The PCI for the network after 5 years is 85 compared to an original value of 73 if section PCIs unweighted

by area are used. If the network PCIs weighted by area are compared, there is still a rise from 76 in the present to 81 in 5 years' time.

Figure 7 contains the results for a budget of $15,000 in each of the 5 years. The # signs in the rightmost column indicate that routine maintenance is being performed, even though that is not the optimal alternative for that family/state combination. This is confirmed in referring back to Figure 6, where surface treatments (alternative 2) are chosen for sections 2 and 5. A similar pattern is seen in the succeeding years. In this case, the budget is sufficient to perform routine or holding maintenance only.

By year 5, the section's conditions have deteriorated to such an extent that the $15,000 allotted is not even sufficient to cover the routine and short-term maintenance required; hence, the message output at the bottom of Figure 7. It is interesting to note that a total of $63,200 in undiscounted dollars is required over the 5 years, significantly more than the $49,675 required earlier. Meanwhile, the PCIs after 5 years are much lower, 65 for both unweighted and weighted, compared with 85 and 81 seen in Figure 6.

Figure 8 has the output for the third set of budgetary inputs. Again, some # signs are seen, indicating a deferment of the optimal strategy due to a lack of money. The total expenditure over the 5 years in undiscounted dollars is $48,250. For this outlay, the network PCI remains the same in unweighted terms but drops from 76 to 70 when each section's PCI is weighted by its area in calculating the network average. Note that there is a severe drop in PCI from year 4 to year 5, and if the available budget in year 5 were increased a little over $13,000, the PCI would probably improve appreciably. These are the type of "what if" games it is possible to play easily with this program. Figure 9 illustrates the performance of the network over time under each of the budget scenarios. The program executes almost instantaneously on an IBM AT or compatible.

SUMMARY

A prioritization program that takes the outputs from dynamic programming and combines them with budgetary constraints to produce a prioritized list of sections for repair with the recommended type of treatment and cost has been produced

YEAR	SECTION NUMBER	MAINT. ALT.	COST	STATE	E/C RATIO	
1	1	1	200	2	36.68	
	2	2	8400	4	22.96	
	3	1	1000	3	20.39	
	5	1	6300	5	16.94	#
	4	1	1000	2	9.34	
2	1	1	200	2	34.78	
	3	1	1500	4	21.08	#
	2	1	200	1	19.54	
	5	2	12150	5	15.33	
	4	1	2000	3	8.21	
3	1	1	200	2	32.82	
	3	1	1500	4	19.33	#
	2	1	200	1	17.96	
	5	1	450	2	14.28	
	4	1	2000	3	7.79	
4	1	1	200	2	30.82	
	3	1	1500	4	17.07	
	2	1	200	1	16.12	
	5	1	1350	3	13.98	
	4	1	2000	3	7.6	
5	1	1	200	2	28.76	
	3	1	1500	4	17	#
	2	1	200	1	16.09	
	5	1	1800	4	14.57	#
	4	1	2000	3	7.33	

	YEAR 1	YEAR 2	YEAR 3	YEAR 4	YEAR 5
REQUIRED BUDGET	16900	16050	4350	5250	5700
AVERAGE PCI	75	81	79	77	73
AVG. PCI WEIGHTED BY AREA	73	79	77	75	70

FIGURE 8 Variable available annual budget.

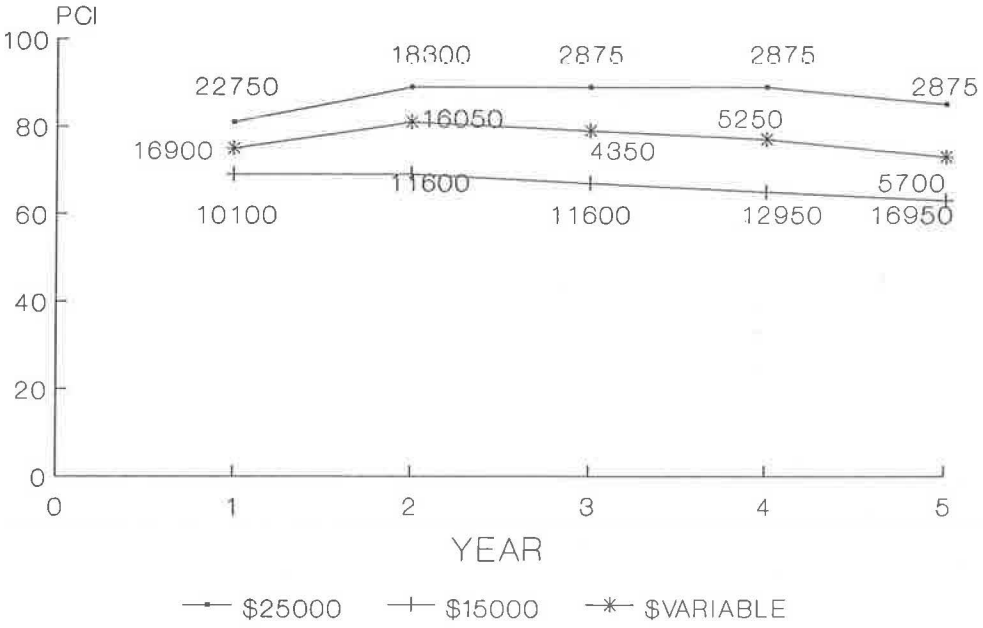

FIGURE 9 Network performance.

for the Micro PAVER pavement management system. The network PCI, calculated both with and without weighting by section area, is also output. It is possible to determine at a glance which sections are being forced to use suboptimal treatments because of budgetary constraints. These programs provide the final link in a chain that goes from extracting raw PCI versus age data out of the Micro PAVER databanks to producing network and semi-project-level recommended maintenance alternatives, costs, and projected network PCI levels within specified budgetary constraints at the microcomputer level.

REFERENCES

1. M. Y. Shahin and S. D. Kohn. *Overview of the "PAVER" Pavement Management System*. Technical Manuscript M-310. USA-CERL, Champaign, Ill., Jan. 1982.
2. M. Y. Shahin, K. A. Cation, and M. R. Broten. *Pavement Maintenance Management: The Micro PAVER System*. DOT/FAA/PM-87/7. USA-CERL, Champaign, Ill., July 1987.
3. M. Y. Shahin, M. M. Nunez, M. R. Broten, S. H. Carpenter, and A. H. Sameh. New Techniques for Modeling Pavement Behavior. In *Transportation Research Record 1123*, TRB, National Research Council, Washington, D.C., 1988, pp. 40–46.
4. A. A. Butt, M. Y. Shahin, K. J. Feighan, and S. H. Carpenter. Pavement Performance Prediction Model Using the Markov Process. In *Transportation Research Record 1123*, TRB, National Research Council, Washington, D.C., 1988, pp. 12–19.
5. K. J. Feighan, M. Y. Shahin, K. C. Sinha, and T. D. White. *An Application of Dynamic Programming and Other Mathematical Techniques to Pavement Management Systems*. Presented at 67th Annual Meeting of the Transportation Research Board, Washington D.C., Jan. 1988.
6. K. J. Feighan, M. Y. Shahin, and K. C. Sinha. A Dynamic Programming Approach to Optimization for Pavement Management Systems. In *Proc., Second North American Conference on Managing Pavements*, Toronto, Ontario, Canada, Nov. 1987.
7. K. J. Feighan. *An Application of Dynamic Programming to Pavement Management Systems*. Ph.D. dissertation, Department of Civil Engineering, Purdue University, West Lafayette, Ind., May 1988.
8. K. J. Feighan, M. Y. Shahin, T. D. White, and K. C. Sinha. *A Sensitivity Analysis of the Application of Dynamic Programming in Pavement Management Systems*. Paper presented at the 68th Annual Meeting of the Transportation Research Board, Washington, D.C., Jan. 1989.
9. E. Reichelt, E. A. Sharaf, K. C. Sinha, and M. Y. Shahin. *The Relationship of Pavement Maintenance Costs to the Pavement Condition Index*. USA-CERL Interim Report M-87/02. Champaign, Ill., Feb. 1987.

Publication of this paper sponsored by Committee on Pavement Management Systems.

A Sensitivity Analysis of the Application of Dynamic Programming to Pavement Management Systems

KIERAN J. FEIGHAN, MOHAMED Y. SHAHIN, KUMARES C. SINHA, AND THOMAS D. WHITE

There has been a concerted research effort to update the prediction and optimization capabilities of the Micro PAVER pavement management system. An approach uniting the Markov probability prediction curves and dynamic programming optimization has been proposed. This paper briefly outlines the background work done on both. It examines the sensitivity of the dynamic programming output to changes in input parameters. Data from three existing databases and a fourth, formulated database are used in the analysis. Output values from dynamic programming are also compared with results obtained from deterministic analysis using best-fit curves for prediction and cost versus condition data. It is concluded that the dynamic programming results are reasonable. A multizone dynamic programming approach was seen to give more consistent results than a one-zone approach. It was found that for life-cycle lengths greater than 15 years, there was little change in optimal decision or cost. Low interest rates favored more expensive, longer-lasting solutions. The minimum Pavement Condition Index (PCI) level specified affected the results appreciably, in general. These results were consistent through all four databases examined. It was concluded that the Markov/dynamic programming approach was functioning satisfactorily, and was suitable and appropriate for use at the microcomputer level.

This paper describes a series of analyses performed on the dynamic programming optimization package developed for the Micro PAVER pavement management system (*1*) in which the sensitivity of the output to changes in input parameters is documented. The outputs are also compared with a "traditional," deterministic life-cycle analysis to determine how well the dynamic programming algorithm is performing. The major advantage in using this dynamic programming approach is that the generation of the output is extremely fast and efficient on a microcomputer. The system is directly applicable to any pavement management system that uses a condition index to indicate overall condition.

This work is part of an overall effort to improve the prediction, optimization, and budget allocation capabilities of Micro PAVER. A necessarily brief background on the Markov process and dynamic programming is included. Further details are available in the literature cited (*2–6*).

K. J. Feighan, ERES International Inc. Champaign, Ill. 61820. M. Y. Shahin, United States Army, Construction Engineering Research Laboratory, Champaign, Ill. 61820. K. C. Sinha and T. D. White, Department of Civil Engineering, Purdue University, West Lafayette, Ind. 47907.

MARKOV PREDICTION MODEL

It is not possible to describe the functioning of the dynamic programming algorithm without first describing the prediction model used. More detailed and comprehensive descriptions have already been published elsewhere (*2,3*). Much of the terminology used in this description also is used in dynamic programming.

The Pavement Condition Index (PCI) range of 0 to 100 is divided into ten states, each state being 10 PCI points wide. A pavement is modeled as beginning its life in near-perfect condition (a PCI of 100 being perfect) and deteriorating as it is subjected to a sequence of duty cycles. A duty cycle is defined as 1 year's imposition of the effects of weather and traffic. A state vector indicates the probability of a pavement section being in each of the ten states in any given year. Figure 1 shows the schematic representation of state, state vector, and duty cycle.

The sections are grouped into families of sections having common characteristics, such as pavement type, traffic, and so forth. All of the sections are grouped into one of the ten states at any age. It is assumed that all of the pavement sections are in state 1 (PCI of 90 to 100) at an age of 0.

It is necessary to identify the Markov probability matrix to model the deterioration process of the pavements. The assumption made is that the pavement condition will not drop by more than one state (10 PCI points) in a single year. Thus, the pavement will either stay in its current state or transit to the next lowest state in 1 year. The probability transition matrix has a diagonal structure as shown in Figure 2.

The state vector for any duty cycle t, $S(t)$, is obtained by multiplying the initial state vector $S(0)$ by the transition matrix P raised to the power of t. Thus

$$S(1) = P * S(0),$$
$$S(2) = P * S(1) = P^2 * S(0), \text{ and}$$
$$S(t) = P * S(t-1) = P^t * S(0).$$

If the transition matrix probabilities can be estimated, the future condition of the road at any duty cycle (age) t can be predicted.

The probabilities are estimated using a nonlinear programming approach. Probability values are found that, when inserted into the Markov chaining process, match the actual (PCI, age) data points as closely as possible. It has been found that this approach can accurately model the pavement deteriora-

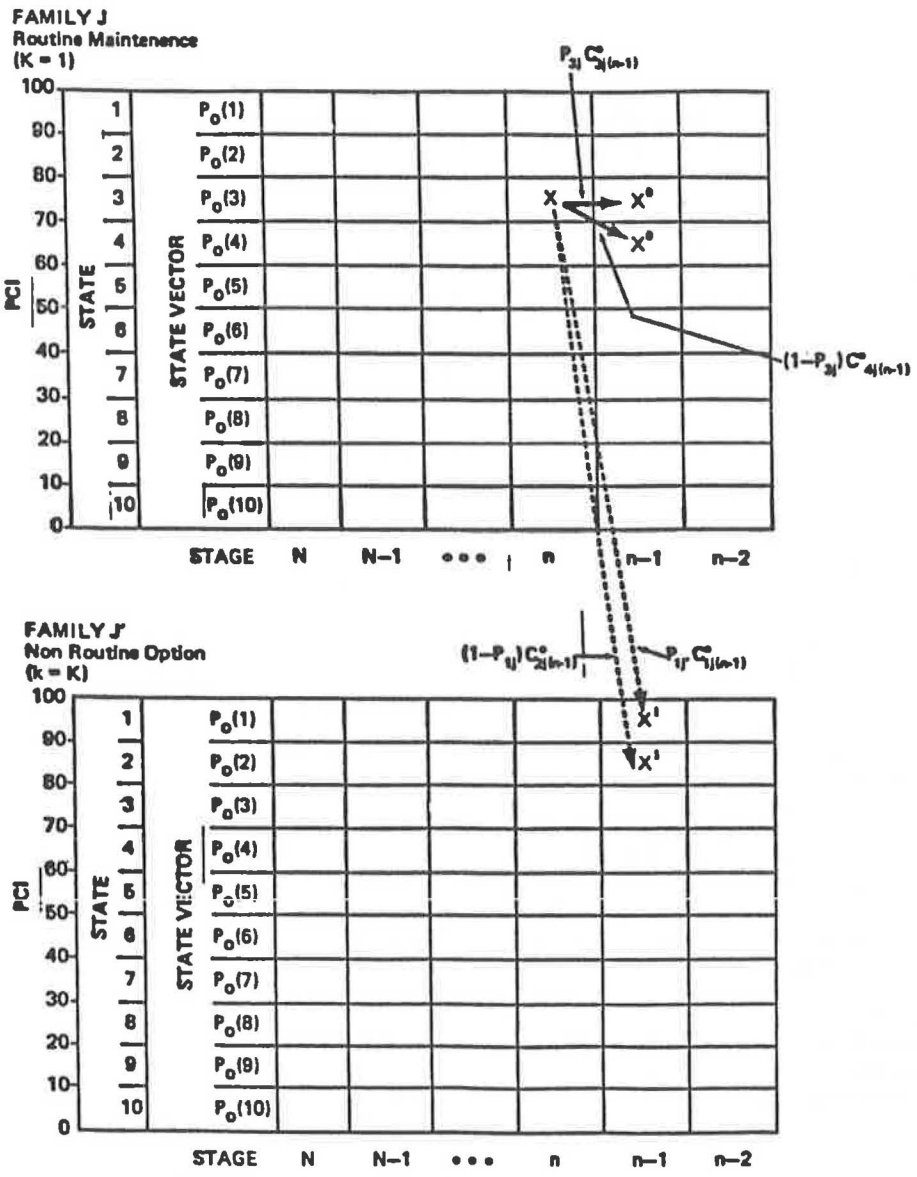

FIGURE 1 Diagram of state, state vector, and duty cycle.

$$P = \begin{bmatrix} p(1) & 1-p(1) & 0 & 0 & 0 & 0 & 0 & 0 & 0 & 0 \\ 0 & p(2) & 1-p(2) & 0 & 0 & 0 & 0 & 0 & 0 & 0 \\ 0 & 0 & p(3) & 1-p(3) & 0 & 0 & 0 & 0 & 0 & 0 \\ 0 & 0 & 0 & p(4) & 1-p(4) & 0 & 0 & 0 & 0 & 0 \\ 0 & 0 & 0 & 0 & p(5) & 1-p(5) & 0 & 0 & 0 & 0 \\ 0 & 0 & 0 & 0 & 0 & p(6) & 1-p(6) & 0 & 0 & 0 \\ 0 & 0 & 0 & 0 & 0 & 0 & p(7) & 1-p(7) & 0 & 0 \\ 0 & 0 & 0 & 0 & 0 & 0 & 0 & p(8) & 1-p(8) & 0 \\ 0 & 0 & 0 & 0 & 0 & 0 & 0 & 0 & p(9) & 1-p(9) \\ 0 & 0 & 0 & 0 & 0 & 0 & 0 & 0 & 0 & 1 \end{bmatrix}$$

FIGURE 2 Probability transition matrix structure.

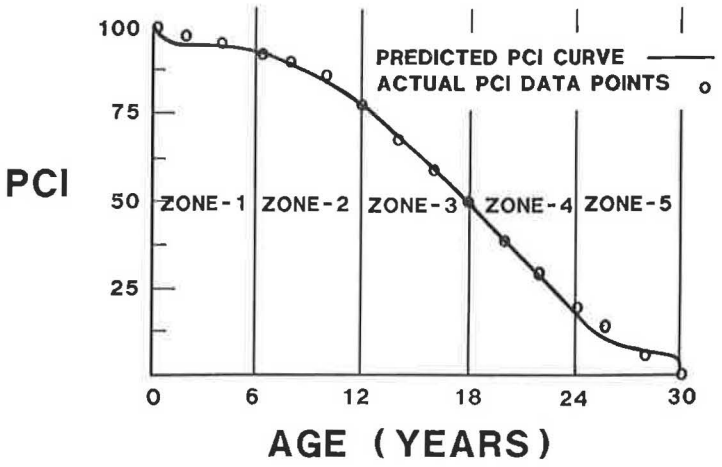

FIGURE 3 Sample Markov prediction curve.

tion over time. A sample output of this program is shown in Figure 3.

INTRODUCTION TO DYNAMIC PROGRAMMING

Dynamic programming is an approach to optimization. It is not based on a well-defined, consistent algorithm such as the simplex algorithm used in linear programming. Instead, it seeks to take a single, complex problem and break it down into a number of smaller constituent problems. It is hoped that the solution of these smaller problems will arrive much faster and require considerably less computational power. If set up properly, dynamic programming is guaranteed to find the global optimal solution(s).

This is a major advantage over almost all classical optimization techniques. A general dynamic programming approach is also extremely robust in that it can handle integrality, negativity, and discreteness of variables very easily. It also, by its nature, produces the solution to all of its constituent subproblems.

The major constraint upon the use of dynamic programming is that the proposed problem to be solved must be able to be formulated in terms of subproblems. If that is possible, however, as in the present case, dynamic programming provides an extremely fast and efficient optimization tool.

Structure of Dynamic Programming

The basic components of dynamic programming are states, stages, decision variables, returns, and transformation or transition functions (*7*). A physical system is considered to progress through a series of consecutive stages. In pavement performance terms, each year is viewed as a stage.

At each stage, the system must be capable of being fully described by the state variables or state vector. In the present case, as described earlier, each state is a 10-PCI bracket for every pavement family, and the condition of the pavement at any year (stage) can be defined as being in one of the ten states.

At each stage, for every possible state, there must be a set of allowable decisions. The decisions being made in the dynamic programming model are *which repair alternative to implement in each state at every stage.*

Finally, there is the transformation or transition function. If a process is in a given state and a feasible decision is made, there must be a function that determines the new state to which the process should move. In general, dynamic programming transformation functions can be deterministic or stochastic. In this particular case, the transition function is defined by the Markov probability matrix derived in the curve-fitting process described earlier and, hence, is a stochastic process.

In summary, the problem set up for this dynamic programming formulation is:

Minimize: Expected cost over a specified life-cycle length subject to keeping all sections above a defined performance standard.

The dynamic programming parameters are:

States: Each bracket of 10 PCI points in a family.
Stages: Each year in the analysis period.
Decision Variables: Which M&R treatment to apply.
Transformation Function: The Markov transition probability matrix defines the transformation.
Return: Expected cost if a particular decision is made in each state at each stage.

Dynamic Programming Output

The output from the dynamic programming program consists of

1. A file containing the optimal maintenance alternative in every year (stage) for every family/state combination;
2. The discounted present worth costs expected to accrue over the life cycle specified if the optimal decisions are implemented;
3. The expected effectiveness accrued as a result of following the optimal decisions calculated for every family/state combination; and

4. The calculated effectiveness/cost ratio for every family/state combination.

INTRODUCTION TO ANALYSIS

The data analysis is made up of two main sections. First, an analysis of the sensitivity of the dynamic programming results to changes in input parameters is performed for four databases. These databases were selected because relevant condition performance and condition/cost data were available.

Second, a comparison of the dynamic programming results with those obtained from a deterministic analysis using best-fit performance curves is performed.

DESCRIPTION OF PARAMETER SETTINGS

The parameters considered in the sensitivity analysis of the dynamic programming solution were

1. Minimum allowable state,
2. Combined zone versus multizone probability values,
3. Effective interest rate, and
4. Length of life-cycle analysis.

The variable levels used in each parameter were as follows:

1. *Minimum allowable state (MAS):* The minimum allowable state, as the name implies, is the worst PCI level that the pavement manager will allow a pavement to reach before it must be repaired. In terms of feasible maintenance alternatives, the implication is that routine maintenance is not allowed in the minimum allowable state; the only feasible alternatives are those that will raise the PCI above the present condition state. It differs from a trigger point in that a nonroutine maintenance action can be taken above the MAS if it is economically advantageous to do so. Thus, with a specified MAS of 5 (minimum PCI of 55), if dynamic programming recommends a surface treatment at a PCI of 75, this nonroutine maintenance action will be taken. Three levels of this parameter were chosen: minimum allowable states of 3, 5, and 7.

2. *Zone approach:* There were two levels for this variable: the combined zone approach and the multizone approach. In the approach used to obtain the Markov probabilities that define the deterioration of condition over time, the life span of each family is divided into a number of zones. A separate set of Markov transition probabilities is obtained for each zone.

The multizone approach uses all of these sets and uses all of the transition probabilities within each set to define the transition from one state to another as a function of time. The combined zone approach identifies the states in which most of the data points of that zone are located. The state transition probabilities corresponding to those states *only* are chosen. Thus, for example, if the majority of the data points in zone 2 are located in the PCI range of 70 to 90, the combined zone approach will take the transition probabilities corresponding only to states 2 and 3 (PCIs of 80 to 90 and 70 to 80, respectively). In this way, a single representative transition probability matrix is compiled for use in the dynamic programming algorithm.

3. *Interest rate:* Two levels of effective interest rates were used in the analysis: 5 percent and 15 percent. The interest rate is used to discount future expenditures to present worth costs, the most equitable basis of comparison for strategies having different expenditures at differing times.

4. *Life-cycle analysis period:* Three analysis periods were investigated: 5, 15, and 25 years.

AVAILABLE DATABASES

Four databases were prepared for use by the dynamic programming programs:

1. Fort Eustis,
2. Tulsa,
3. Great Lakes Naval Center, and
4. A sample formulated database.

Information on cost and performance for the three actual databases was obtained from the CERL report, "The Relationship of Pavement Maintenance Costs to the Pavement Condition Index" (*8*). This report contains detailed cost information and best-fit performance curves for five locations. The three selected have the most complete data and more maintenance alternatives from which to choose.

The formulated database has hypothetical performance and cost relationships. Some of these relationships were chosen specifically to attempt to show how optimal alternatives may change depending upon state, interest rates, life-cycle length, and other factors.

The maintenance alternatives available for each database are shown in Table 1. Sample best-fit constrained least-squares performance curves are shown in Figures 4 and 5 for the Great Lakes base. Markov probability values were obtained to model these curves. Examples are shown in Figures 6 and 7. Some sample PCI/cost relationships are shown in Figures 8 through 10 for both initial cost and routine maintenance cost. In the CERL report, cost values are given for every 20-PCI-point bracket. These values were taken to be centered at the midpoint of the bracket, and a best-fit curve was obtained for the entire PCI range using these points.

PROCEDURE UTILIZED FOR SENSITIVITY ANALYSIS

The basic procedure used follows. For each of the four databases, 12 dynamic programming runs were performed. (This number is made up of two interest rate levels times three minimum allowable state levels times two zone approaches used in estimating Markov probability values.) A life-cycle analysis period of 25 years was always specified. Because of the nature of the dynamic programming formulation, the 25-year solution set also contains the optimal solutions for every year fewer than 25 years; thus the 5- and 15-year optimal decisions and costs are readily obtainable. Forty-eight dynamic programming runs were performed.

TABLE 1 MAINTENANCE ALTERNATIVES FOR EACH DATABASE

	FORT EUSTIS	TULSA	GREAT LAKES	SAMPLE DATA
ROUTINE MAINTENANCE	YES	YES	YES	YES
SURFACE TREATMENT	YES	YES	YES	YES
THIN OVERLAY	YES	YES	YES	YES
THICK OVERLAY	YES	YES	YES	YES
RECONSTRUCTION	NO	YES	NO	YES

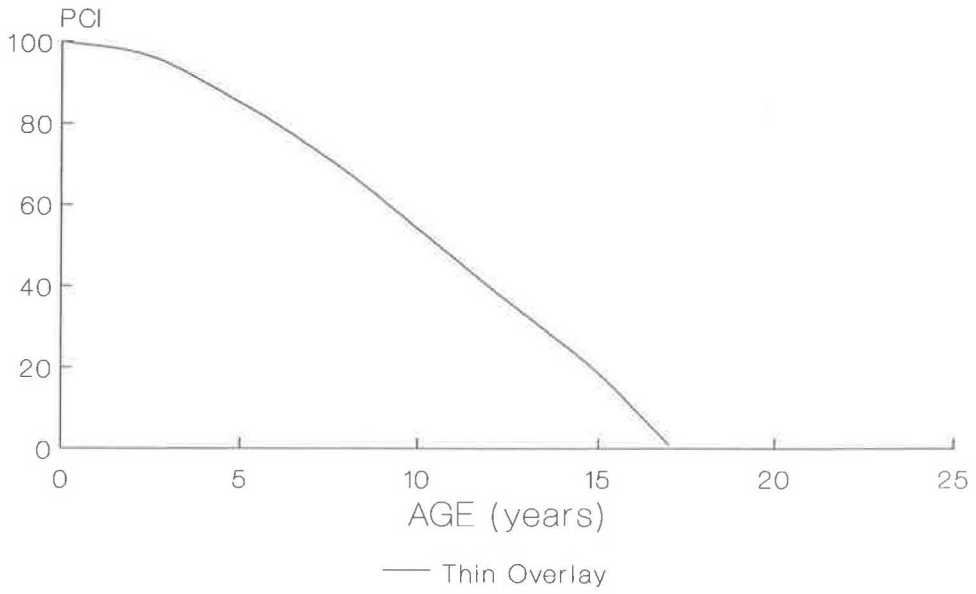

FIGURE 4 Thin overlay at Great Lakes.

It is not possible to obtain the variance of the expected cost from dynamic programming. Consequently, a random simulation was performed after each dynamic programming run. The purpose of this was to obtain a mean estimated cost and variance for each family/state combination. The estimated cost can be compared with the expected cost obtained from dynamic programming. These values will not usually be the same but should be reasonably close in magnitude. Twenty-five simulations were performed for each family/state combination. Thus, the final products for all such combinations were

1. Optimal decisions from dynamic programming,
2. Expected costs from dynamic programming,
3. Estimated mean cost from simulation runs, and
4. Estimated variance of the mean cost from simulation runs.

All of the data were entered into data spreadsheets, one for each database. This was done for ease of data manipulation. Confidence limits were drawn about the mean cost using the estimated variance. An example from the Great Lakes database is shown in Table 2. It can be seen that, in general, these limits are reasonably tight, especially given that a 95 percent confidence level is used. In almost all cases, the

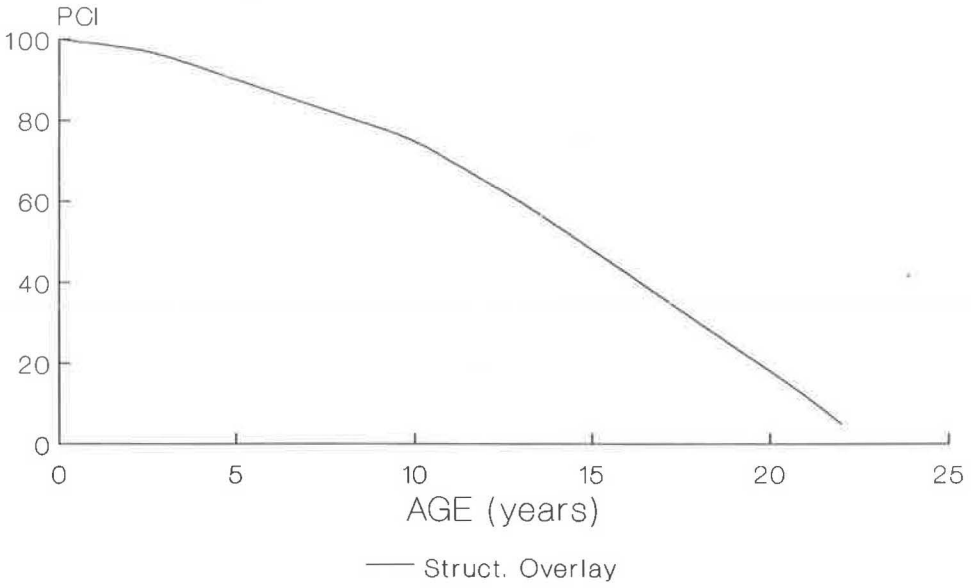

FIGURE 5 Structural overlay at Great Lakes.

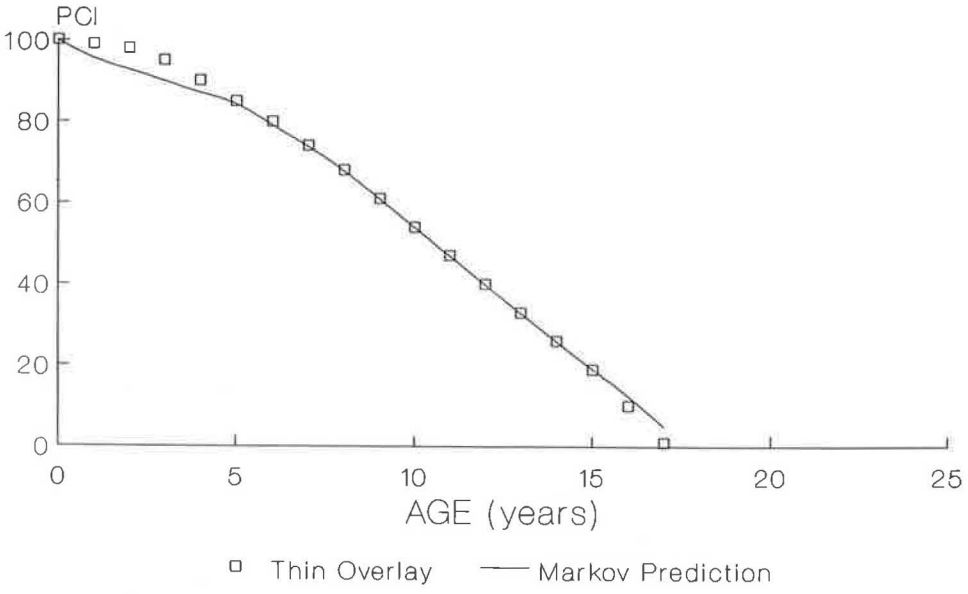

FIGURE 6 Markov prediction for thin overlay.

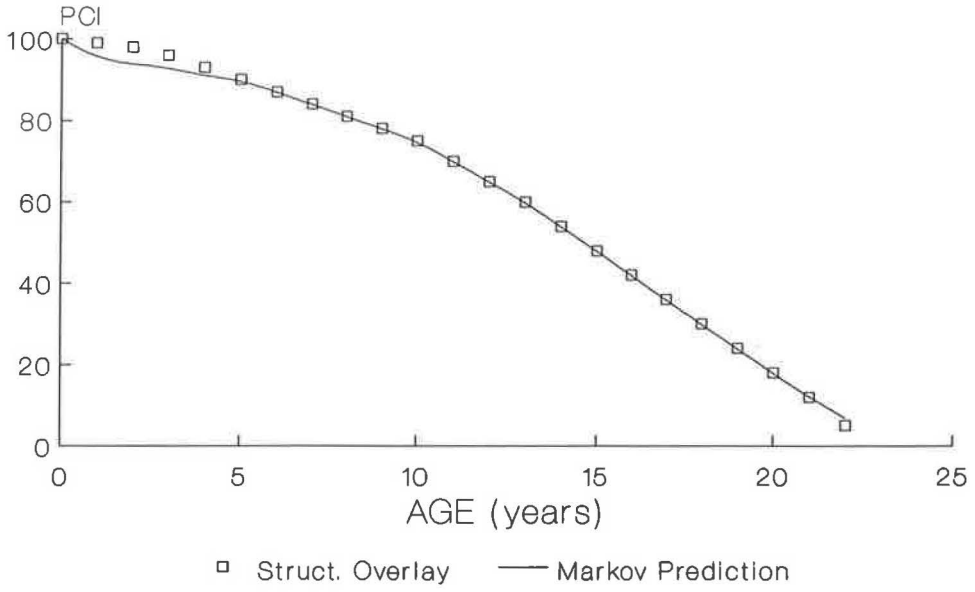

FIGURE 7 Markov prediction for structural overlay.

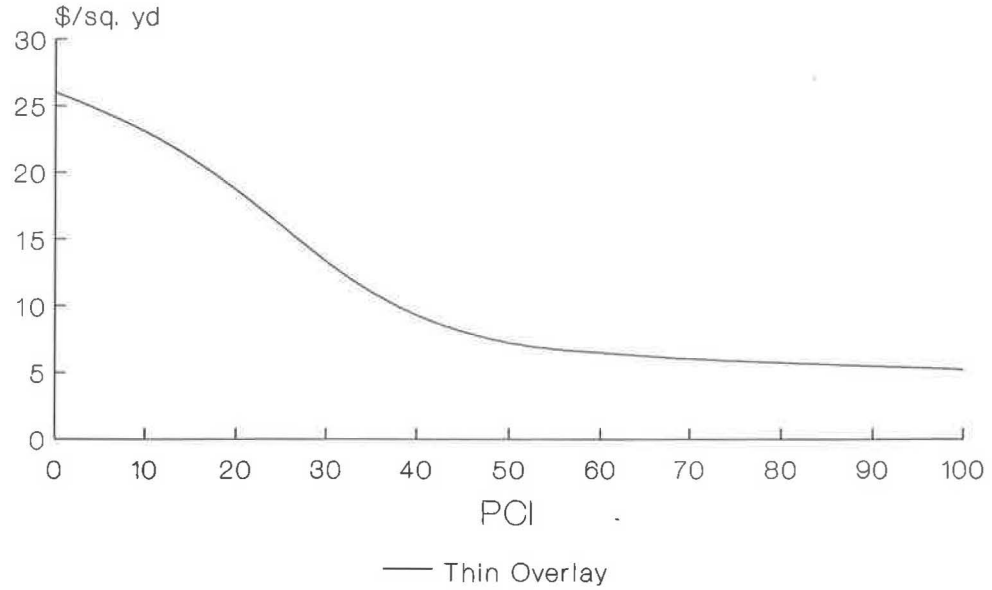

FIGURE 8 Initial cost of thin overlay.

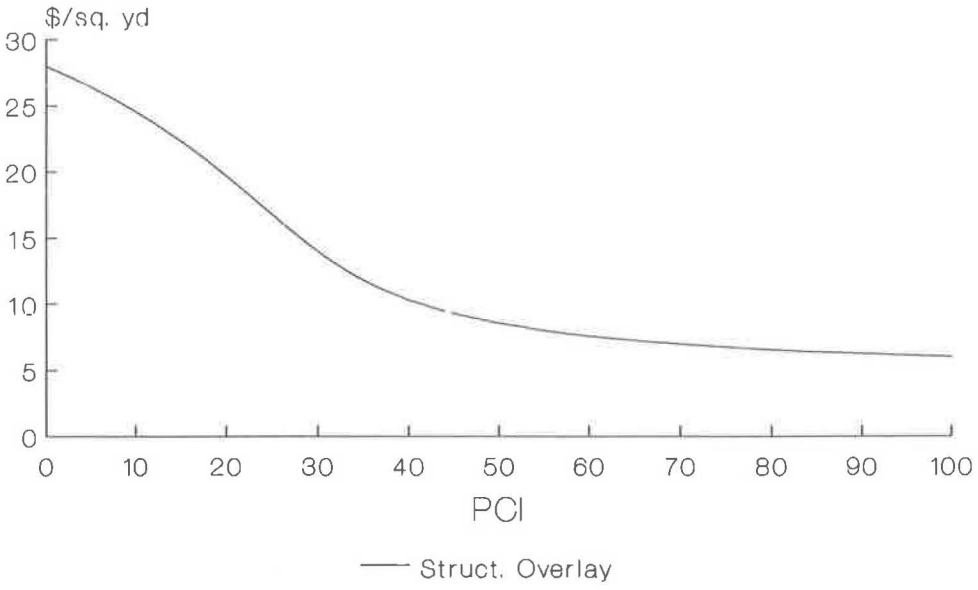

FIGURE 9 Initial cost of structural overlay.

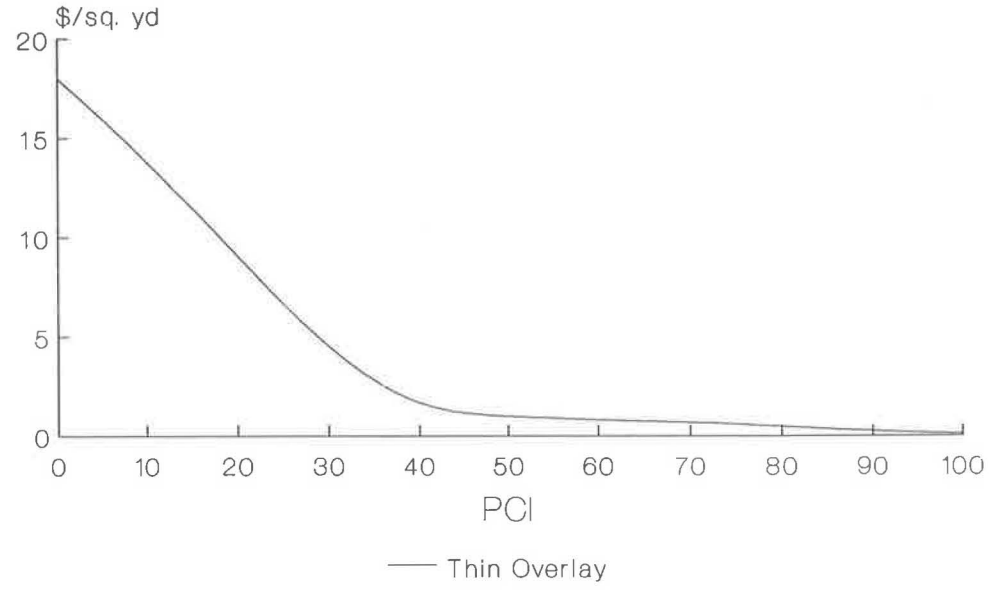

FIGURE 10 Maintenance cost of thin overlay.

TABLE 2 GREAT LAKES EFFECTIVENESS/COST RATIOS

INTEREST RATE: 5%

FAMILY	STATE	STRAT. A	STRAT. B	STRAT. C	STRAT. D	COMB. ZONE	MULTI ZONE
1	1	121.1	118.99	109.08	112.26	200.2	160.6
1	4	81.8	77.99	65.08	87.62	111.8	90.9
1	7	67.46	62.27	59.59	66.67	89.6	71.3
2	7	64.13	59.32	56.71	63.43	149.2	121.5
3	1	115.49	109.68	95.35	106.16	89.6	71.3
3	4	78.15	78.06	64.24	88.57	117.5	90.9
4	1	141.57	113.89	109.62	109.38	252.8	163.3

INTEREST RATE: 15%

FAMILY	STATE	STRAT. A	STRAT. B	STRAT. C	STRAT. D	COMB. ZONE	MULTI ZONE
1	7	93.98	90.64	83.81	91.99	106	94.7
2	1	243.25	219.29	172.59	225.48	294.8	258.3
2	7	87.63	84.52	78.23	85.93	106	94.7
3	1	266.59	259.9	216.55	249.53	326.2	297.6
3	7	92.18	88.91	90.32	82.27	106	94.7

estimated mean cost from simulation falls within a 95 percent confidence bracket around the dynamic programming mean. This is encouraging and indicates that the costs obtained are reasonable and the programs are functioning correctly.

For the purposes of analysis, the data were extracted from the database in a number of structured ways. As there were four parameters of interest, data were extracted so that the effect of changing the parameter level of one variable while holding the others constant could be examined.

SUMMARY OF RESULTS

A brief description of the trends seen in all four databases for each of the input parameters follows.

Interest Rates

The predominant observed trend was that low interest rates tended to favor the alternatives with more expensive initial costs and lower subsequent maintenance costs. This pattern is consistent with basic economic theory. There was an interaction between interest rate and time. As the analysis period was increased, differences between costs using the 5 percent and 15 percent interest rates became more substantial, both in absolute terms and in percentage terms for any family/state combination. This pattern was observed regardless of the minimum allowable state (MAS) specified.

Minimum Allowable State

Costs decreased as the MAS increased. This is again in line with the expected pattern, as specifying an MAS is basically equivalent to putting a constraint on the feasible optimal decisions; and the greater the MAS, the less confining the constraint is. Consequently, the optimal costs would be expected to decrease as the MAS is increased. For any family/state combination, the cost difference between an MAS of 3 and one of 5 was greater than the difference between an MAS of 5 and one of 7. Consequently, it was concluded that the optimal solutions were reaching a steady-state level at about an MAS of 5; and further loosening of the constraint to an MAS of 7 had little further influence.

Varying Zone Analysis

Few consistent patterns were obvious in comparing the optimal decisions and costs for the two zone approaches specified. Generally, it was found that the 5 percent interest rate caused differences in optimal decisions between the two approaches much more than the 15 percent rate did. There were no consistent trends other than this. For any given family/state combination, the optimal decisions and costs varied considerably from database to database. Sometimes the combined zone approach gave higher costs; other times the multizone costs were higher. The analysis later in this paper comparing the dynamic programming results to the deterministic results was used to determine which approach was more realistic.

Varying Life-Cycle Length

The present worth costs always increased with increasing life-cycle length, as expected. In general, when the present worth costs were expressed as equivalent uniform annual costs (EUACs), the EUAC decreased with increased life-cycle

length. This was believed to be because the costlier but longer-lasting M&R alternatives were getting an insufficient length of time to "justify" their cost over the 5-year life-cycle length.

Occasionally, this pattern was reversed in states 1 and 2 when the EUACs for the 5-year life cycle were lowest. Routine maintenance was always the optimal decision in those states when this pattern was observed, and it is believed that this was reflecting the fact that routine maintenance is a short-lived activity that does not require a lengthy life cycle to justify its expenditure.

It was also observed that there was much less of a drop in EUAC from 15 to 25 years than from 5 to 15 years. Again, this was believed to be because the life cycles of most of the M&R alternatives were greater than 5 years but shorter than 25 years. Thus, the 5-year life cycle was not long enough to "prove" the worth of the costlier alternatives, while life-cycle lengths greater than 15 years basically reproduced a repeat of the 15-year optimal decision cycle with little or no further reduction in EUAC.

COMPARISON WITH DETERMINISTIC RESULTS

The dynamic programming algorithm has as its output the optimal maintenance decision to make for every state of every family in each year of the life cycle considered. The costs and benefits associated with this decision are also produced. These results are obtained on a probabilistic basis and represent the mean minimum cost in each case.

Certain simplifying assumptions are made in defining the dynamic programming setup for network-level optimization. The major assumption is in the state definition concept that essentially assumes that all sections in each 10-PCI-point bracket of each family behave in the same way. The Markov assumption hypothesizes that the performance curve for any family can be represented through the Markov transition probability matrix values. Information on both initial cost and routine maintenance cost is used on a state basis, again assuming that all family sections in each 10-PCI-point bracket will have the same maintenance costs.

As a result of these simplified assumptions, there may be some doubt as to the veracity of the "optimal" decisions chosen. To obtain some idea of how good the dynamic programming solutions are, it is necessary to compare the solutions with those obtained from a different analysis of the available data. The alternative analysis used is the "strategy" algorithm, which contains PCI versus age and PCI versus dollar curves into a life-cycle cost analysis. Figure 11 shows the sample strategies considered.

By experimenting with different strategies for a given life cycle and interest rate, it is possible to come close to the optimal combination of alternatives. This program's approach is deterministic, assuming that future condition can be predicted precisely. Thus, it is not connected theoretically or practically with the dynamic programming approach. By comparing the outputs of these programs, it should be possible to

1. Confirm or reject the optimality of the dynamic programming solution,
2. Confirm or reject the validity of the cost and cost/benefit ratios output by dynamic programming (the magnitude of these values should be comparable for both programs), and
3. Investigate the sensitivity of the dynamic programming solution to changes in input values.

ANALYSIS APPROACH USED

It was not realistic to attempt to run the deterministic cost analysis package on every combination of parameter variables for every database, as the number of such combinations is much too large. It was decided to specify certain variable-level combinations and then randomly choose a number of these combinations for analysis.

It was decided to fix the life-cycle analysis length at 25 years, as it was believed that this would yield the most valuable insights into the behavior of the one-zone and multizone dynamic programming approaches. It was decided to examine the results using both the 5 percent and 15 percent effective interest rates. It was further decided that all four families in each database should be candidates for analysis and that all four databases should be examined. Also, it was decided to limit the initial candidate starting states to states 1, 4, and 7.

Thus, for each database, the potential number of combinations of parameters for deterministic analysis is

3 states * 2 interest rates * 4 families = 24 combinations

It was anticipated that there would be four trial strategies run deterministically for each such combination, leading to almost 100 runs for each of the four databases. It was decided to select randomly 12 combinations from the 24 to reduce the number of required runs to a manageable figure.

After random selection, the list of combinations selected was as follows:

1. Family 1, state 1, 5 percent interest rate;
2. Family 1, state 4, 5 percent interest rate;
3. Family 1, state 7, 5 percent interest rate;
4. Family 2, state 7, 5 percent interest rate;
5. Family 3, state 1, 5 percent interest rate;
6. Family 3, state 4, 5 percent interest rate;
7. Family 4, state 1, 5 percent interest rate;
8. Family 1, state 7, 15 percent interest rate;
9. Family 2, state 1, 15 percent interest rate;
10. Family 2, state 7, 15 percent interest rate;
11. Family 3, state 1, 15 percent interest rate; and
12. Family 3, state 7, 15 percent interest rate.

ANALYSIS OF DETERMINISTIC RESULTS

The deterministic analysis cost package was run for each of the family/state combinations chosen in each database. The results, the present worth cost and total effectiveness, were entered on spreadsheets for ease of analysis.

The effectiveness/cost ratio for each of the strategies chosen was tabulated with those predicted by the dynamic programming approaches. These results are given in Tables 3 to 6. The remainder of this analysis is concerned with the examination of these tables in an effort to determine the reason-

STATE 1 OF EACH FAMILY:

A: SURFACE TREATMENT WHEN PCI = 70, REPEAT SURFACE TREATMENT WHENEVER PCI FALLS TO 70.

B: THIN OVERLAY WHEN PCI = 50, REPEAT THIN OVERLAY WHENEVER PCI FALLS TO 50.

C: STRUCTURAL OVERLAY WHEN PCI = 40, REPEAT STRUCTURAL OVERLAY WHENEVER PCI FALLS TO 40.

D: SURFACE TREATMENT WHEN PCI = 70, THEN APPLY THIN OVERLAY WHEN PCI = 50, REPEAT SURFACE TREATMENT WHEN PCI = 70.

STATE 4 OF EACH FAMILY:

A: SURFACE TREATMENT WHEN PCI = 55, REPEAT SURFACE TREATMENT WHENEVER PCI FALLS TO 70.

B: THIN OVERLAY WHEN PCI = 50, REPEAT THIN OVERLAY WHENEVER PCI FALLS TO 50.

C: STRUCTURAL OVERLAY WHEN PCI = 40, REPEAT STRUCTURAL OVERLAY WHENEVER PCI FALLS TO 40.

D: SURFACE TREATMENT WHEN PCI = 65, THEN APPLY THIN OVERLAY WHEN PCI = 50, REPEAT SURFACE TREATMENT WHEN PCI = 70.

STATE 7 OF EACH FAMILY:

A: SURFACE TREATMENT WHEN PCI = 35, REPEAT SURFACE TREATMENT WHENEVER PCI FALLS TO 70.

B: THIN OVERLAY WHEN PCI = 35, THEN APPLY THIN OVERLAY WHENEVER PCI FALLS TO 50.

C: STRUCTURAL OVERLAY WHEN PCI = 35, REPEAT STRUCTURAL OVERLAY WHENEVER PCI FALLS TO 40.

D: SURFACE TREATMENT WHEN PCI = 35, REPEAT SURFACE TREATMENT WHENEVER PCI = 70.

FIGURE 11 Symbol key for database LCCST comparisons.

ableness of the dynamic programming results vis-à-vis the deterministic results, and to establish which of the dynamic programming zone approaches gives more reasonable results.

EFFECTIVENESS/COST RATIO COMPARISONS

In general, the effectiveness/cost (E/C) ratios predicted by the deterministic approach and those given by dynamic programming were certainly comparable in magnitude. It was not anticipated that the figures would be exactly the same since the dynamic programming approach uses cost figures on a state-by-state basis, assigning the same cost for each PCI in each 10-PCI-point bracket. The deterministic approach, on the other hand, is more detailed and can calculate the cost for any PCI point between 0 and 100.

It was also anticipated that, in general, the dynamic programming E/C ratios would be higher as these solutions should be global optimal in comparison with the strategies selected for the deterministic analysis. In fact, in many cases, it was found that the best strategy in the deterministic analysis mirrored the dynamic programming strategy almost completely, leading to almost identical E/C ratios under both analyses.

There are a total of 48 family/state combinations to be analyzed, spread over the four databases of interest. In 37 of the 48 cases, the multizone dynamic programming approach was close to the best deterministic E/C result. In 6 cases, the one-zone and multizone results were equally close to the deterministic results, and in 5 cases, the one-zone dynamic programming results were closer. Of the 37 cases in which multizone was closer, 34 of the E/C ratios were higher than the deterministic values, an expected result in the context of global and local optima.

In the Great Lakes analysis, the multizone results were closer to the deterministic results in 11 of the 12 comparisons. The magnitudes of the results are generally very close, especially for the multizone results. The only obvious difference is in family 2, state 7, under a 5 percent interest rate, where

TABLE 3 TEST EFFECTIVENESS/COST RATIOS

INTEREST RATE: 5%

FAMILY	STATE	STRAT. A	STRAT. B	STRAT. C	STRAT. D	COMB. ZONE	MULTI ZONE
1	1	140.87	145.7	119.98	144.64	242.5	229.8
1	4	67.29	68.8	58.52	63.6	136.2	104.7
1	7	79.35	66.73	86.19	111.68	113.2	90.7
2	7	78.55	66.18	85.54	110.81	113.2	90.7
3	1	120.17	76.58	98.91	95.42	218.3	139.8
3	4	64.84	63.69	59	76.26	136.2	104.7
4	1	167.1	112.63	125.51	134.17	195	178.9

INTEREST RATE: 15%

FAMILY	STATE	STRAT. A	STRAT. B	STRAT. C	STRAT. D	COMB. ZONE	MULTI ZONE
1	7	127.77	113.61	140.99	164.65	158.3	132.3
2	1	243.83	163.27	183.6	198.44	426.5	270.43
2	7	125.72	111.89	139.27	162.56	158.3	132.3
3	1	283.63	203.27	223	239.44	466.6	325.2
3	7	124.57	110.93	138.26	161.34	158.3	132.3

TABLE 4 FORT EUSTIS EFFECTIVENESS/COST RATIOS

INTEREST RATE: 5%

FAMILY	STATE	STRAT. A	STRAT. B	STRAT. C	STRAT. D	COMB. ZONE	MULTI ZONE
1	1	379.32	225.49	150.92	241.33	3066.53	922.3
1	4	126.09	116.88	91.1	127.84	260.7	231.3
1	7	105.19	97.53	92.48	67.92	142.5	134.3
2	7	109.38	104.11	70.07	95.81	111.3	106.6
3	1	257.72	265.69	178.16	240.72	1307	786.3
3	4	144.55	134.83	103.99	133.55	231.3	209
4	1	360.17	256.66	170.58	244.9	2479.9	1020.9

INTEREST RATE: 15%

FAMILY	STATE	STRAT. A	STRAT. B	STRAT. C	STRAT. D	COMB. ZONE	MULTI ZONE
1	7	128.33	126.81	91.83	110.65	151.6	148.3
2	1	563.68	477.1	538.6	407.36	1280.4	860.5
2	7	134.77	133.18	95.79	115.45	116.4	114.9
3	1	704.55	734.48	609.26	700	3324.4	1908.9
3	7	131.4	129.84	93.72	112.94	116.4	114.9

the one-zone and multizone analyses have substantially higher E/C ratios.

In the Fort Eustis analysis, the same pattern is again evident. However, there are more family/state combinations where the dynamic programming E/C results are substantially greater than the deterministic results. Generally, these differences occur in state 1 of the various families, especially with a 5 percent interest rate being used. An examination of present worth costs shows that the dynamic programming costs are much lower than those given by the deterministic analysis.

It is believed that the costs projected through dynamic programming in this case are, in fact, too low. The value is low because the Markov transition probability value selected by the Markov program for state 1 is well above 0.9, thus encouraging a pavement section to be retained in state 1 for longer than it would normally be expected to remain. Naturally, this results in a lower life-cycle cost. Modifications to the Markov program since this analysis was performed have resulted in more reasonable state 1 values being chosen consistently.

The test and Tulsa databases show patterns similar to those

TABLE 5 TULSA EFFECTIVENESS/COST RATIOS

INTEREST RATE: 5%

FAMILY	STATE	STRAT. A	STRAT. B	STRAT. C	STRAT. D	COMB. ZONE	MULTI ZONE
1	1	232.38	185.66	115.16	178.25	472	253.5
1	4	159.23	124.08	87.5	120.46	294	156.3
1	7	122.84	103.25	66.83	108.79	159.1	114.3
2	7	119.77	101.09	65.77	106.6	121.1	92.2
3	1	221.53	140.99	105.76	167.25	484.4	240.9
3	4	149.08	124.07	83.27	120.46	280	160.3
4	1	234.77	174.13	114.05	180.2	472.7	259.2

INTEREST RATE: 15%

FAMILY	STATE	STRAT. A	STRAT. B	STRAT. C	STRAT. D	COMB. ZONE	MULTI ZONE
1	7	165.61	150.47	106.35	140.46	187.6	139.6
2	1	490.99	318.07	230.64	393.68	969.8	456.9
2	7	160.31	145.93	103.69	136.66	134.9	103.9
3	1	483.76	341.69	263.54	387.78	1073.5	528.3
3	7	162.8	148.27	105.06	138.62	139.1	106.9

TABLE 6 COMPARISON OF DYNAMIC PROGRAMMING MEAN WITH SIMULATION MEAN

FAMILY	STATE	DYN. PROG. MEAN	SIMULATION MEAN	UPPER BOUND	LOWER BOUND
1	1	7.7	7.02	8.39	7.01
	2	9.65	10.43	10.65	8.65
	3	12.42	11.55	12.95	11.89
	4	13.01	12.94	13.76	12.26
	5	14.15	14.32	14.96	13.34
	6	15.2	15.48	15.96	14.44
	7	16.7	16.95	17.41	15.99
2	1	9.98	9.74	10.57	9.39
	2	10.92	11.09	11.83	10.01
	3	11.97	11.83	12.57	11.37
	4	13.01	13.18	13.68	12.34
	5	14.15	14.86	14.92	13.38
	6	15.2	15.3	15.89	14.51
	7	16.7	16.62	17.33	16.07
3	1	9.13	8.87	9.8	8.46
	2	10.61	10.49	11.29	9.93
	3	11.86	11.39	12.61	11.11
	4	13.01	13.12	13.68	12.34
	5	14.15	14.34	14.76	13.54
	6	15.2	15.48	15.92	14.48
	7	16.7	17.03	17.41	15.99
4	1	7.66	7.44	8.35	6.97
	2	11.22	11.36	12.01	10.43
	3	12.41	12.28	13.03	11.79
	4	13.23	13.2	13.83	12.63
	5	14.38	14.49	15.16	13.6
	6	15.23	15.56	16.18	14.28
	7	16.18	15.85	16.81	15.55

observed in Great Lakes. In general, the E/C values for the optimal deterministic strategy and the multizone dynamic programming approach are very close, especially considering the differences in exactness of cost estimation and PCI prediction. In the test database, for a 15 percent discount rate, three of the five family/state combinations result in ties between the multizone and one-zone approaches in terms of closeness to the optimal deterministic result.

It is interesting to note that the structural overlay option is found to be most cost-effective in the deterministic approach, as generally the thin overlay option is favored in state 7 for most of the databases. In summary, the E/C ratios predicted by the multizone dynamic programming approach are in good agreement with those predicted by a deterministic approach.

SUMMARY

This paper describes the results of an experimental analysis performed on four databases where condition and cost data were available. The effect of varying parameter-level inputs for these databases was investigated and reported. The effect was measured both in terms of change and expected cost. In general, the anticipated changes were actually reflected in the outputs. How the formulation is sensitive to changes in input values and which parameters in particular affected the results in a substantial way were revealed.

In general, the longer life-cycle analysis periods tended to favor more costly initial alternatives with higher initial cost and greater life expectancy. Lower interest rates also tended to favor these alternatives. Changes in the minimum allowable state produced much greater differences as the state was lowered from 3 to 5 than when it was lowered from 5 to 7. The effect of using the Markov probability values in two different ways in the dynamic programming analysis was also considered.

This was also seen in the latter part of the paper, where the outputs for the two zoning approaches were compared with the results from a deterministic analysis. Based on these comparisons, it was concluded that the approach using all the Markov values in every zone was superior to the alternative of using the Markov values for each state from the zone that contains the deterioration curve in that state. It was also concluded that the dynamic programming and deterministic analysis results were certainly of the same magnitude and selected similar optimal maintenance decisions.

REFERENCES

1. M. Y. Shahin, K. A. Cation, and M. R. Broten. *Pavement Maintenance Management: The Micro PAVER System*. DOT/FAA/PM-87/7. USA-CERL, Champaign, Ill., July 1987.
2. A. A. Butt, M. Y. Shahin, K. J. Feighan, and S. H. Carpenter. Pavement Performance Prediction Model Using the Markov Process. In *Transportation Research Record 1123*, TRB, National Research Council, Washington, D.C., 1988, pp. 12–19.
3. P. I. Keane and M. I. Wu. *An Integrated Decision-Making Methodology for Optimal Maintenance Strategies*. Master's thesis. University of Illinois, Urbana, 1985.
4. K. J. Feighan, M. Y. Shahin, K. C. Sinha, and T. D. White. *An Application of Dynamic Programming and Other Mathematical Techniques to Pavement Management Systems*. Presented at 67th Annual Meeting of the Transportation Research Board, Washington, D.C., 1988.
5. K. J. Feighan, M. Y. Shahin, and K. C. Sinha. A Dynamic Programming Approach to Optimization for Pavement Management Systems. In *Proc., Second North American Conference on Managing Pavements*, Toronto, Ontario, Canada, November 1987.
6. K. J. Feighan. *An Application of Dynamic Programming to Pavement Management Systems*. Ph.D. thesis. Department of Civil Engineering, Purdue University, West Lafayette, Ind., May 1988.
7. L. Cooper and M. W. Cooper. *Introduction to Dynamic Programming*. Pergamon Press, Oxford, United Kingdom, 1981.
8. E. Reichelt, E. A. Sharaf, K. C. Sinha, and, M. Y. Shahin. *The Relationship of Pavement Maintenance Costs to the Pavement Condition Index*. USA-CERL Interim Report M-87/02, Champaign, Ill., February 1987.

Publication of this paper sponsored by Committee on Pavement Management Systems.

Remote Pavement Performance Monitoring

JAMES K. CABLE, D. Y. LEE, F. WAYNE KLAIBER, AND JOHN R. ROHDE

The Iowa State University Civil and Construction Engineering Department has initiated a demonstration of pavement instrumentation with the Federal Highway Administration (FHWA) and the Iowa Department of Transportation. The paper outlines the procedures used to establish the project location, select the software and hardware, and complete the installation of more than 120 sensors in a 40-ft segment of I-80. Moisture and density of the base are measured by nuclear means. Temperature of slab and base, strains in the pavement and on the dowels, and deflections of the pavement are monitored. The entire system is triggered by the use of a piezoelectric weigh-in-motion system. Information from the site will provide the research team with a way to monitor the performance of pavement in the field under actual traffic and environmental conditions. The site is unique in that all the electronic sensors will be controlled from a site some 150 miles away and will utilize microcomputers to perform the controls. The problems and results associated with that installation are described.

The reaction of pavement structures to traffic loads and the environment has been studied in many ways in the laboratory. With the exception of the American Association of State Highway Officials (AASHO) Road Test and other previous tests at test tracks, little has been done to test the performance of pavements under field traffic and environmental conditions. Iowa State University and the Iowa Department of Transportation (DOT) are assisting the Federal Highway Administration (FHWA) in demonstrating the use of pavement instrumentation as a way of obtaining these type of data for possible assistance to the states and the Strategic Highway Research Program. A demonstration project entitled "Pavement Instrumentation" (*1*) is designed to demonstrate state-of-the-art equipment and methods in four states and on two types of pavement. Iowa's involvement in the project is providing an opportunity to achieve a better understanding of the performance of portland cement concrete pavements under actual traffic and environmental conditions.

PROJECT GOALS

This project has both short- and long-range goals.

Short-Range

The short-range goals of this demonstration project are

1. Installation of instruments in a new pavement during paving operations;
2. Development of a data acquisition system, including hardware and software appropriate to the instruments installed;
3. Installation of a communications link for remote monitoring of the site traffic;
4. Sensor response calibration to the known static and dynamic load situations and ranges; and
5. Installation of the moisture/density instrumentation equipment.

Long-Range

The long-range goals of this demonstration project are to

1. Monitor pavement responses to mixed traffic loads during varying base moisture conditions and varying times of the day;
2. Monitor the changes in density and moisture at the interface of the pavement and the base material;
3. Analyze the response frequency and magnitudes to determine the pavement performance in terms of equivalent axle loads;
4. Compare the rate of pavement loadings to that predicted by the pavement design formulas used in construction;
5. Develop relationships between the observed strains and the measured moisture/density at the pavement/base interface; and
6. Define the drainability of the base material and the performance of the longitudinal subdrains.

PROJECT OBJECTIVES

The study has three primary objectives and several secondary objectives to be achieved through the primary research effort. They are

1. Demonstration of portland cement concrete pavement instrumentation, including the following areas:
   (a) Instrument placement,
   (b) Instrument reliability,
   (c) Hardware and software needs,
   (d) Instrumentation costs,
   (e) Potential uses,
   (f) Evaluation of pavement design and performance, and
   (g) Assistance in the development of empirical/mechanistic design procedures;

Department of Civil and Construction Engineering, Iowa State University, Ames, Iowa 50011.

2. Evaluation of dynamic load magnitude and frequency applications to portland cement concrete versus static design loads; and
3. Evaluation of pavement behavior versus various base and subgrade temperature and moisture conditions.

Electronic sensors of the following types were installed at predetermined locations in a 40-ft-long section of I-80 to measure the pavement performance.

1. Concrete strain sensors (locations shown in Figure 1). Measuring 1 in. below the top surface and 1 in. above the bottom surface, sensors were placed longitudinally at midslab in equal transverse spacing increments. Additional sensors were located in an exterior corner on a diagonal. Redundancy of sensor placement was accomplished in two adjacent slabs.
2. Dowel bar strain sensors (locations shown in Figure 2). Measured on selected joint bars under the wheelpaths, centerline, midjoint, and near the slab edges, these sensors were mounted on the bottom of the dowel beneath the proposed saw cut.
3. Temperature sensors (locations shown in Figure 3). Temperature sensors were measured near the top of the pavement, top of the base, and the top of the subgrade. They were rebar mounted near the centerline and 6 in. from pavement edges. Ambient temperature was measured near the control cabinet.
4. Pavement deflection sensors (locations shown in Figure 4 and a cross-sectional view of the gauge housing in Figure 5). Pavement deflection was measured by transducers located in vertical housings in the pavement. Sensors were under wheelpaths and the transverse joint at midslab location. Redundancy was achieved at two consecutive joints and midslab locations.
5. Relative moisture and density sensors. Relative moisture and density were measured by a nuclear density system in pipes at the interface of the pavement and base layers. These elements were measured at three joints and two midslab locations. The sensors were located 6–7 in. below the pavement.
6. Traffic sensors (piezo locations shown in Figures 6 and 7). These sensors measured only single-axle trucks or larger. Axle spacings, vehicle speeds, and axle weights were mea-

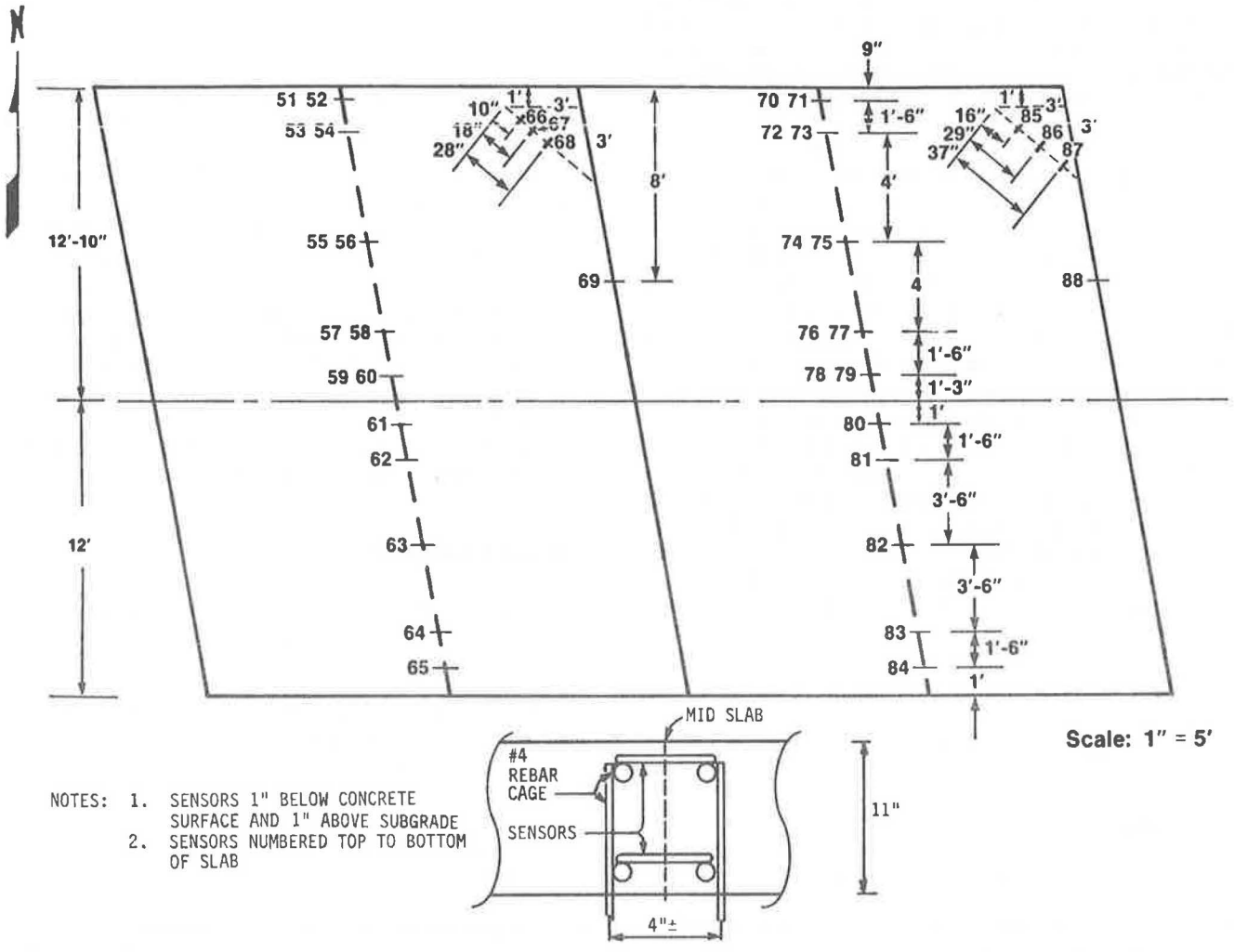

FIGURE 1 Concrete sensor location.

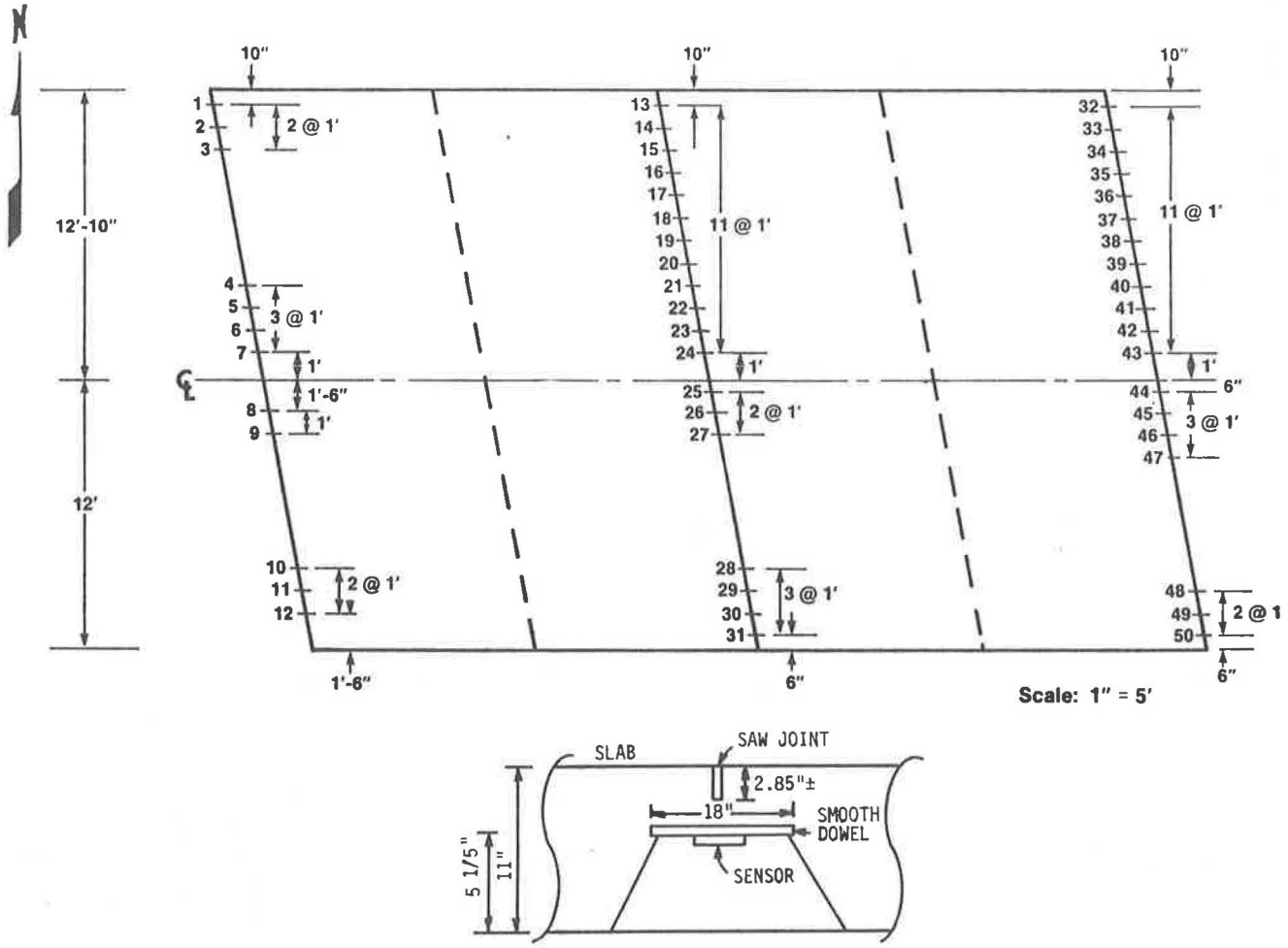

FIGURE 2 Dowel bar sensor location.

sured with piezoelectric cables. Each vehicle was classified by current FHWA classifications. The gross weight of the vehicle and the individual axles were measured with piezo cables.

Initial specifications for the data collection system included the capability of monitoring/scanning each of the gauges or any combination of the gauges in the site at any time at a rate of 1,000 times per second per gauge. Based on cost limitations, a system was selected that provides a rate of 300–400 readings per second per gauge for each of the gauges in two consecutive joints (full pavement width) and the strain gauges in the slab between the joints. The system simultaneously monitors deflection and strain, traffic counting, and classification, temperature, and real time. The data acquisition system is a compromise on account of cost and allows for readings for approximately every 3½ in. of vehicular movement.

The field unit includes a microcomputer, monitor, and storage units with the data collection manager hardware to collect and store data for 1 or more hours of traffic passing the site. The output of the system is in the form of a graphical display and numerical lists of data for each vehicle selected for data collection. It is capable of identifying the strains associated with the loading at any of the individual sensors and of identifying which lane the vehicle is traversing. Data are transmitted via telephone to the central office location in Ames upon demand.

The central office portion of the system serves as the detailed analysis area and includes a microcomputer with plotter and printer to display the analysis results.

Software for data collection and analysis is coming from that provided in the hardware management package subroutines, available spreadsheets, and communications packages. The subroutines to be utilized in the following required programs must be developed by the project staff. They will include:

1. Initiation, completion, and storage of the data from individual vehicles or a series of vehicles in bins with a capacity equal to that of a floppy disk;
2. Conducting a zero reading for each sensor (at predetermined intervals) and collecting temperature data at the same time; and
3. Allowing operator control of sensor selection.

Commercially available communications and spreadsheet software is being used for the majority of data analysis. Other pavement-related software available in pavement design and finite element analysis will be used to verify the pavement design theories.

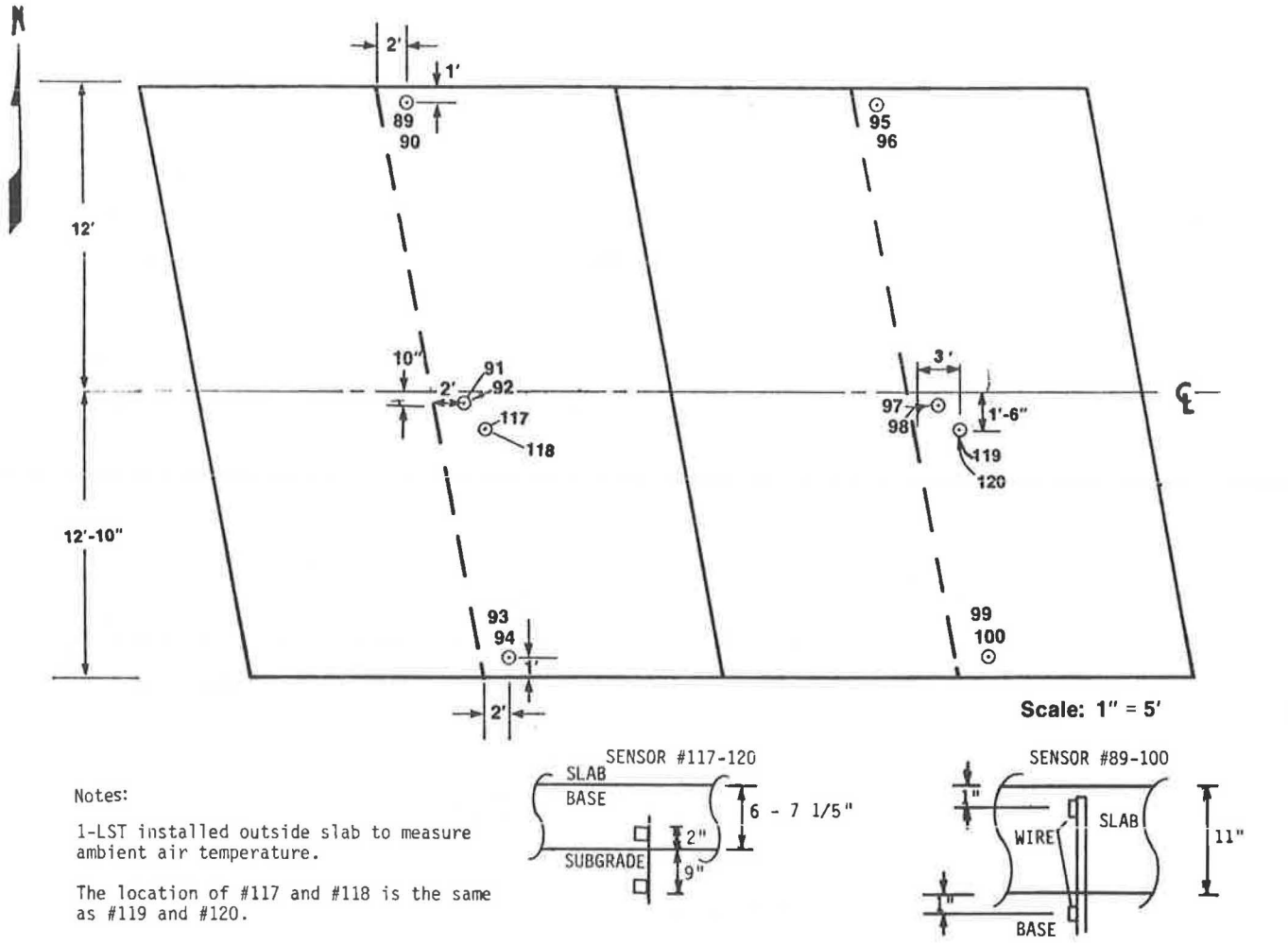

FIGURE 3 Temperature sensor location.

Acquisition equipment can be programmed for data collection rates and times based on the vehicle speed and is triggered by a piezo cable arrangement. Each lane uses a separate piezo cable arrangement. Data will be collected for 3 sec to account for vehicle passage over the test slabs at speeds of 50–90 mph. It also allows for multiples of the 3-sec collection periods for additional vehicles. The piezo cable arrangements are being designed to provide the following accuracies:

- Steering axle—plus or minus 10 percent of static weight on at least 80 percent of the vehicles;
- Other single axles—plus or minus 10 percent of static weight on at least 80 percent of the vehicles;
- Tandem axles—plus or minus 10 percent of static weight on at least 80 percent of the vehicles; and
- Gross weight—plus or minus 10 percent of static weight on at least 80 percent of the vehicles.

Data collected at any given time are limited to the capacity of the floppy disk with 15 percent of the volume left vacant. All information shall be real-time recorded. The field unit will be capable of storing data in increments equal to the noted floppy-disk volume until the total hard disk storage is filled. The unit then waits to be downloaded to the central unit.

The unit will be calibrated with the use of known vehicles and static scales at creep speed, 30 mph, and 55 mph in each lane. Calibration of the piezo cables will use the static scale, and 100 trucks form the traffic stream.

The data collected in the field are to be transferred via modem at 300–1,200 baud using suitable communications software in combination with the appropriate subroutines.

The data collected are to be analyzed to determine the maximum and minimum strains, mean values, areas under the strain curves, and the length and rate of increases and decreases of strain. The zero or null situation will provide for reduction of the data to a standard for analysis. These data will be correlated with the vehicle classification, weight, speed, and location information. They will be used to compare the static and dynamic weights of the vehicles, the weight to strain magnitude, weight to deflection, and frequencies of the strains to the expected pavement damage and what is observed. Use of the moisture/density information will aid in understanding the changes in strain and deflection for given loads over time.

SITE SELECTION

The final site selected for the instrumentation is located in Pottawattamie County in southwestern Iowa in the westbound

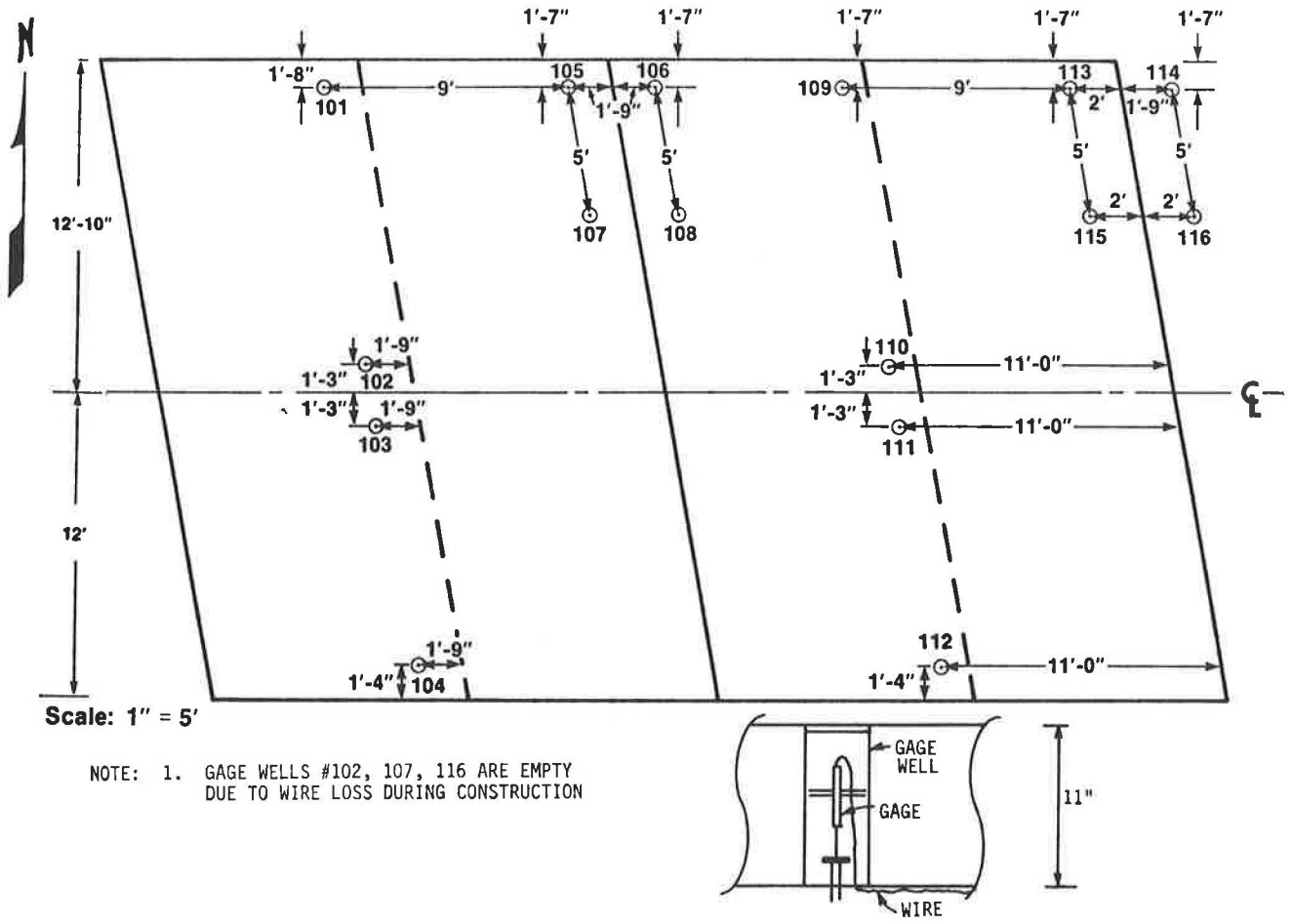

FIGURE 4 Deflection sensor location.

lanes of I-80. The site is part of a 7-mile reconstruction project. The site was selected for the following reasons

1. The pavement was being replaced as part of the reconstruction project. This provided an opportunity for good documentation of the base and pavement characteristics of the reconstruction.
2. The bridge could be used as a weigh-in-motion site for calibrating the sensors in the pavement to known loads. It also could be used for identification of the lateral location and speed of the vehicles entering the test site and crossing the traffic loops. Lane changing by vehicles is reduced on the bridge.
3. This route provided the heavy truck traffic and a mix of truck configurations to test the pavement strain theories adequately.
4. The section is near the low point of a 1,400-ft sag vertical curve, providing a relatively flat grade across the test site. The effects of grade are minimized in the test.
5. The new pavement created a very good chance to obtain a smooth pavement profile at the beginning of the test.
6. A static weight station is located east of the site approximately 15 miles on both the east- and westbound lanes and can be used to check the correlation of weights and strains. A continuous traffic recorder is located in the new pavement approximately 1 mile east of the site in the westbound lanes that can provide ADT counts for pavement wear calculations.

The existing pavement was crushed and returned to the site to be used as a drainable base. The base varied in thickness from 6.5 in. at the median side of the driving surface to 9.5 in. at the outside shoulder. An 11-in.-thick joint reinforced concrete pavement was placed on top of the base. The construction work took place in the summer months of 1986 in stages to meet traffic needs at the various interchanges along the project. Installation was anticipated as early as July but, because of bad weather and other project construction problems, the pavement was placed in this location in September.

The project site is located some 4,000 ft east of both the center of the Minden interchange and all sources of power and telephone. A phone cable and high-voltage power line were buried in a common trench along the north right-of-way line of the interstate highway from a pole at the end of the controlled access in the northeast corner of the Minden interchange. The cable was purchased from the local telephone and power companies and placed using Department of Transportation staff costs.

Aluminum irrigation pipe with a 2-in. inside diameter was installed transversely at each of three joints and two midslabs for nuclear moisture density testing. A common trench

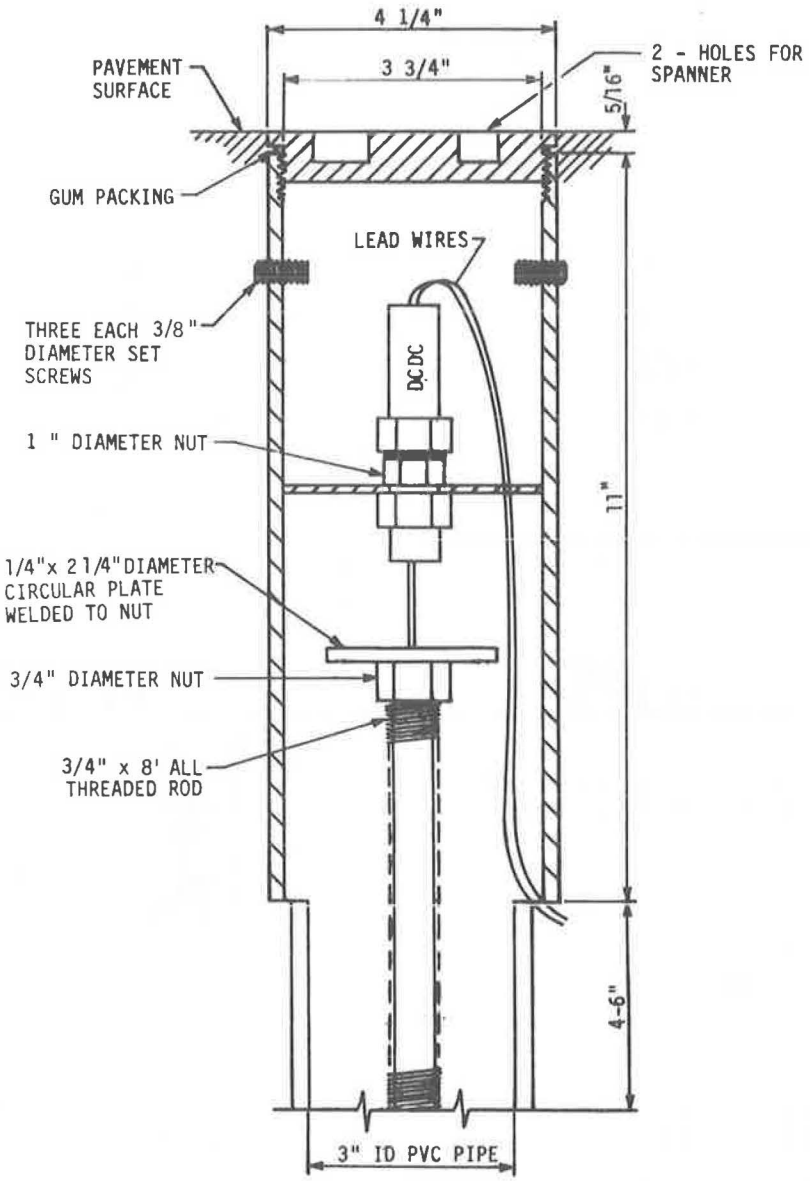

FIGURE 5 Sectional view of the deflection housing.

approximately 6 in. wide was cut longitudinally from the westernmost pavement joint of the test site, easterly on the outside shoulder to the control box site on the wing dike of the Keg Creek Bridge. The control box houses the data collection and storage unit at the field installation.

A soils investigation drill unit was used to drill 5-in.-diameter holes, 5 ft deep, at each of the deflection gauge locations. This was accomplished in the completed base and subgrade prior to the paving operation. A 5-ft section of 3-in.-diameter PVC pipe was inserted in each of the holes. This casing provides protection for the reference rod that was later driven inside the casing. A 1-ft-square section of plywood was used to cover each of the holes during concrete placement. The center of each hole was precisely located by a survey crew for future retrieval purposes. The target plywood section was painted in four colors (red, yellow, green, and blue) and placed in the same color arrangement over each hole. This was done to ensure a way to identify any location changes required in the drilling of the completed concrete to place the housing over the test hole.

INSTRUMENT SELECTION

Costs of purchasing and commercial availability of equipment were the prime considerations in the project. The selection of the concrete and steel strain gauges for this project was based largely on the experience of the ISU Civil Engineering staff. This particular staff has completed similar work on the instrumentation of concrete bridge decks, beams, and railroad subgrades. The particular instruments were selected on the basis of reliability, cost, ease of installation, and durability under field conditions (*2,3,5*). The gauges selected included the following:

- Concrete Strain Measurement: A molded PML-60 gauge

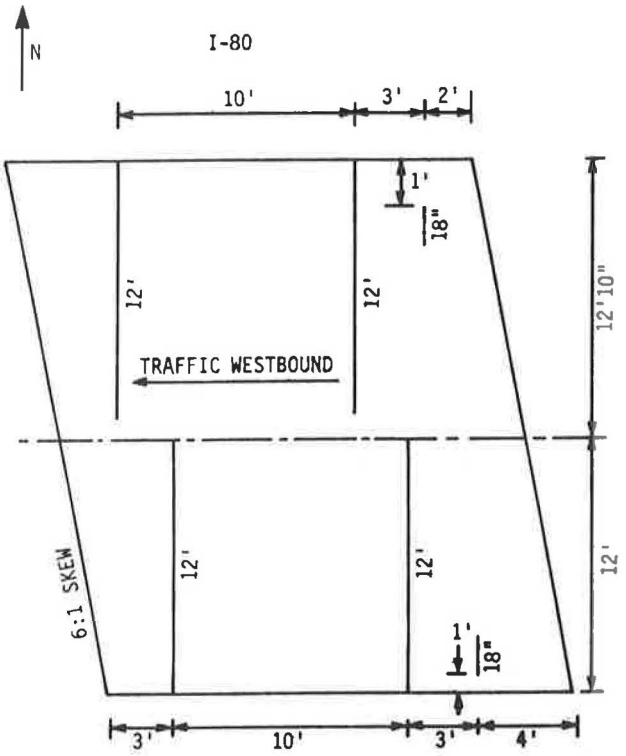

FIGURE 6 Vehicle identification piezo cable configuration.

distributed by the Texas Measurements Inc. Company of College Station, Texas.

- Reinforcing Dowel Strain Measurement: A weldable strain gauge, model LWK-06-W250B-350, made by Micro Measurements Division of Measurements Group.
- Temperature Measurement: A Micro Measurements model WTG-50C grid sensor was used to measure the concrete, air, and base material temperature.
- Deflection Measurement: A Trans-Tek Inc. Displacement Transducer DC-DT series 240-000 was used.
- Moisture and Density Measurement: Troxler density gauge model 1352, with scaler unit and moisture gauge model 3321, with extended probe cables was used for the testing. Special 90- and 100-ft hoses were obtained for the units.

All gauges were prepared for installation in the laboratory at ISU; they were attached to the dowel bar assemblies and tested for continuity and strain registration. The laboratory was used extensively for preparation of the instruments to improve their reliability once installed.

A layout of the site from the construction road plans was established to determine the location of each sensor and the length of wire needed to connect it to the control cabinet. Belden #8723, four-conductor wire in 1,000-ft spools, was used for this purpose because of its insulation and durability features. Some 18,000 ft of wire was required for this project. Each sensor and its connecting wire cable were identified with the cable markers at the control box end. A tag was used to identify the entire unit for placement during installation.

Special housings for the deflection gauges were constructed in the Department of Transportation machine shop from stock materials.

GAUGE INSTALLATION

The goal of the installation was placement of the instruments in the pavement area immediately in front of the paving operation. This required a great deal of coordination with the construction company and the university staff. The fact that the site is some 150 miles from the university added to the coordination problems. Coordination began at the time of highway contract award and continued through the planned July construction date until the installation in September. The entire concrete placement operation was completed at the site in less than an hour with no delay to the contractor.

Several follow-up activities were required to make the site ready for data collection. The first of these were burial of the connecting cables between the site and the control box and construction of the control site. A prefabricated control box was assembled at the site and placed by the department staff. The metal box includes a special electric heater and air conditioner to provide a constant temperature and humidity for the data collection equipment housed in the control box. The box is also insulated, lighted, and equipped with a telephone to provide full field communication and work space. A special transformer and base immediately adjacent to the control box, to step down the 7,000-volt line to the 110/220-volt connections, were required.

The final site work performed prior to opening the road was installation of the deflection gauges using a concrete core drill and the specially built housings.

GAUGE TESTING

On August 10–11, 1987, continuity testing of the instruments was conducted in the field. Completed circuits were found at

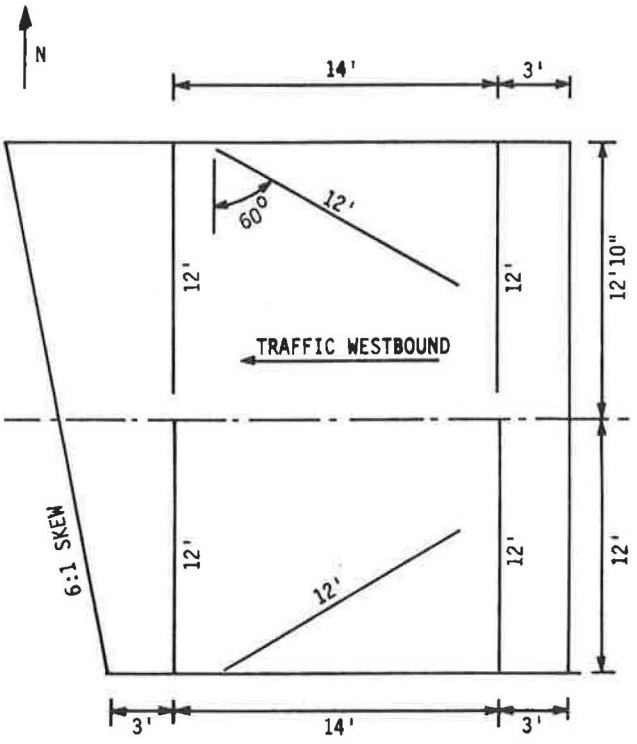

FIGURE 7 Vehicle lateral location piezo cable configuration.

48 of 50 weldable gauges. One gauge provided no circuit, and another showed signs of damage and inconsistent results. Of the 38 concrete strain gauges installed, 3 gave no response and 1 gave intermittent response. All 16 temperature gauges responded positively. Three of the 16 deflection gauges were not installed because of damage to the wiring. Of the remaining 13 gauges, 1 showed signs of fluctuating voltages during testing. This represents a 92.4 percent positive response. This is very good compared with other study results, where a 50 percent failure rate is not uncommon.

EQUIPMENT SELECTION AND PURCHASE

A decision was made in the development of the work plan to provide a form of remote sensing in connection with the project. Equipment was to be selected that would provide on-site collection and analysis of multiple gauge outputs. The results were to be available at the site for calibration and analysis as well as being transmitted over telephone lines to a central Ames location. The original plan called for the field unit to have the ability to scan up to 120 separate gauges at the rate of 1,000 times per second. Compatibility with existing hardware at the Department of Transportation was a consideration, as was the mobility of the equipment to be moved to another site in the future.

Hewlett Packard equipment was selected for the project. The hardware consists of a model 310 series workstation for the central Ames office site and a model 320 series engineering workstation for the field location. The central location microcomputer has a color graphic monitor and associated card, 1 megabyte of RAM, and a 20-megabyte hard disk with the floppy disk. An eight-pen plotter and printer are connected to this unit in a special cabinet for transport between offices. It uses a 2,400-baud modem for communication with the field unit.

The field unit is equipped with a monochrome monitor, 3 megabytes of RAM, and a 40-megabyte hard disk. It is also connected to the central office via the 2,400-baud modem. Each of the units comes with the basic 4.0 operating system.

The heart of the data collection system is a HP 3852A Data Acquisition and Control Unit with two extender units (3853A). Accessories include two 24-channel multiplexers, two 13-bit high-speed voltmeters, a five-channel counter totalizer, data acquisition software routines, a DC power supply, and enough connection devices to monitor forty 120-ohm strain gauges and eighty 350-ohm strain gauges simultaneously.

The equipment was shipped to the Iowa DOT and assembled at the office, rather than at the field location, by the research staff. This proved helpful in assuring delivery and assembly of all parts, as well as aiding staff members' understanding of the operation and development of required software. The units came with the basic operating software and the subroutines to perform the scanning, analysis, and data storage functions.

PROJECT PROBLEMS

As the project developed, problems were noted that can delay an experiment of this type. The distance of more than 150 miles between the office and the site made coordination difficult during installation, calibration, and operation of the remote sensing.

The installation was also delayed some 4 months because of paving construction delays and bad weather. In addition, lack of utilities at the site caused additional time and costs to the project that were not anticipated in the planning phase.

Computer hard disk failures and changes in equipment caused a loss of some 6 months in site installation. Computer software availability and training caused an additional 6 months in preparation for site operation.

The scope and size of the project, which will provide answers to many questions, will also create a similar magnitude of problems in installation and operation. One such problem was that the sensors selected for the project were designed to be relatively inexpensive. They are not designed to last for several years in such a location. Several have failed prior to the collection of any data. This problem reinforces the need to provide redundancy in sensor installation.

RECOMMENDATIONS

Project Planning

Construction of the project presented an evident need for the approach of an interdisciplinary team, including a pavement engineer, a programmer, a research with experience in sensor selection and installation, a computer/communications specialist, and department representatives from the areas of construction, maintenance, and materials.

Site Preparation

Coordination and communication between the project contractor and the research team are a must to assure installation success. These are especially important in

1. Construction scheduling,
2. Storage of construction materials, and
3. Subcontractor and utility activities.

Proper estimation of utility installation and operation costs is also necessary.

Gauge Preparation

Prepare the gauges and lead wiring in the lab, and pretest all gauges prior to field installation.

Gauge Installation

Prepare an installation diagram, and conduct a trial run of the installation at the laboratory. Use an ample amount of trained staff members for the installation.

Data Handling Preparation

Several items of information must be decided in the planning stages of the project to make this portion of the work proceed

smoothly and on time. The project investigators must establish answers to the following questions:

1. What will be measured?
2. How fast will it be measured?
3. What are the limitations of the sensors that the data collection equipment will need to meet?
4. What are the budget limitations on hardware costs?
5. What will the location of data collection and analysis be?
6. What system operation and data analysis software will be used?
7. What software sources are to be used—commercial or in-house?

A literature search also pointed out the strong and weak points of various types of sensors for consideration in obtaining maximum reliability of survival in the concrete situation (*3–5*). The speed of data collection and the number of sensors to be scanned at any one time have a direct bearing on the cost and size of the data collection units. The cost of scanning 120 instruments at the rate of 1,000 times per second per instrument was estimated at between $175,000 and $200,000. By reducing the rate of scan to 300–400 times per second per instrument and scanning some 50–80 instruments at a time, the price was reduced to $60,000.

Delays in the delivery of data collection equipment happened because of the nature of the order. In most cases this is a special order of several parts of subsystems and requires close communication between the investigator, the purchasing agent, and the vendor representative. Cooperation in this case was good, and some equipment had to be returned and replaced owing to incompatibility of parts or changes in the method of handling the data.

The project team chose to use the subroutines provided by the vendor to do some of the data analysis at the field site. In-house programming was used to tie the subroutines together and transmit data to the central office. This work is still under way.

TOTAL SITE COSTS

The following represents a cost estimate of the various parts of the installation as stated in the original proposal.

Item	*Actual/Projected Cost*
Gauges—purchase and installation	$ 58,500
Power and telephone supply to the site	8,000
Monthly service charges for power and phone—2 years at $125 per month	3,000
Consultation travel expense	2,500
Computer hardware	65,500
Software, testing analysis	33,700
Weigh-in-motion materials, equipment, and installation	14,000
Total	$185,200

SUMMARY AND CONCLUSIONS

The instruments have been installed in the pavement during paving operations and exhibit excellent survival rates. The project has the potential to measure deflection and concrete and dowel bar strain at successive joints and to relate this to the loads and the moisture/density changes at the pavement/base interface. It has been shown that arrangements can be made to monitor the information remotely, without the knowledge of the vehicle operator. In the future this will assist the research staff with their ability to monitor vehicle location on the slab, weights, strains, and deflections. It can also be used to calibrate deflection measuring equipment.

The results to date provide information on the costs, problems, and planning steps that should be considered in the establishment of instrumentation sites to answer pavement performance questions. Details of the installation, costs, problems, and conclusions reached during the initial phase of the project are included in FHWA Demonstration Projects Division Report FHWA-EP-88-621-001 (*1*).

Work will continue on calibration of the site to known weights of trucks under both static and dynamic conditions and the collection of data for the next year. Personnel training for computer operation will also continue at both the Iowa Department of Transportation and the university. Additional consideration is being given to a future project to investigate the retrofitting of additional sensors to replace those that have failed to date.

REFERENCES

1. J. K. Cable, J. R. Rohde, D. Y. Lee, and F. W. Klaiber. *Experimental Project No. 621, Pavement Instrumentation*. FHWA-EP-88-621-001, Demonstration Projects Division, FHWA, U.S. Department of Transportation, March 1988.
2. J. T. Christison. In Situ Measurement of Pavement Behavior Under Load. Paper presented at the annual conference of the Roads and Transportation Association of Canada, Sept. 25–29, 1983.
3. B. E. Colley, C. G. Ball, and P. Arriyavat. *Evaluation of Concrete Pavements with Lane Widening, Tied Concrete Shoulders, and Thickened Pavement*. Report prepared for the Minnesota Department of Transportation by the Portland Cement Association Research and Development Construction Technology Laboratories, Skokie, Ill., Sept. 1977.
4. H. Wang. *Comparisons of Solutions for Responses in Jointed Concrete Pavements*. M.S. thesis. Iowa State University, Ames, Sept. 1987.
5. T. D. White. *Instrumentation for Flexible and Rigid Pavements*. Report prepared for the Experimental Application and Evaluation Branch, Demonstration Projects Division, FHWA, U.S. Department of Transportation, June 1985.

Publication of this paper sponsored by Committee on Pavement Monitoring, Evaluation and Data Storage.

Toward an Integrated Nondestructive Pavement Testing Management Information System Using Infrared Thermography

GARY J. WEIL AND LONNIE E. HAEFNER

This paper describes the theoretical basis and practical procedures for use of thermography in detection of pavement distress. It also illustrates the field use of thermography with some recent applications on airport taxiways, bridge decks, and parking garage slabs. It provides an overview of a staged research process under way by the authors to integrate nondestructive pavement testing using infrared thermography with evaluation models that form the basis for an integrated pavement testing, management information system.

The objective of this paper is to illustrate the use of a new, nondestructive testing (NDT) process, infrared thermography, for testing pavements for defects. Applied research case studies demonstrating the equipment, operation, and pavement distress data output are documented. The ultimate integration of the process with transportation systems evaluation models to yield a turnkey pavement testing and management information-capital budgeting system is conceptually presented.

Objectives of the Current Effort

The objectives of the applied research effort are to

1. Review and demonstrate effective mechanics of infrared nondestructive testing;
2. Investigate the testing procedures and state-of-the-art software for integration of data gathering and data interpretation; and
3. Structure, in preliminary form, a long-range program of integration of testing with pavement serviceability indices and capital budgeting algorithms.

Research Work Plan

Conceptually, the synthesis of a research program is shown in Figure 1. Emphasis is on field use of thermographic infrared techniques for assessing pavement and cross-section distress in both asphalt and concrete pavements related to surface cracking, subsurface voids, subgrade voids, and right-of-way drainage voids. The resultant scanner output and color image refinement yield a graphic-colorized interpretation of distress. These data, from the testing regime, can be input with a series of other data related to pavement serviceability variables to yield a basis from which to develop a number of management information system formats.

The inclusion of uncertainty analysis allows a series of "what if" questions with respect to average daily traffic, percent trucks, weather conditions, and other stochastic variables to be formatted into types of modeling often used in resource allocation, such as Markovian decision theory, or decision tree analysis, or dynamic programming–critical path method constructs. In conjunction with the database, an integrated testing–management information system–resource allocation algorithm that prioritizes location by rehabilitation-replacement policies can be built. It should again be pointed out that the preceding is a long-range research goal of the authors. Operable software exists for the information system regime from previous transportation systems evaluation computational research. This paper concentrates on the testing. A second-round paper in the future will concentrate on synthesizing the testing and the management information system evaluation software.

Use of Infrared Thermography

Infrared thermography is a noncontact, noninvasive means of producing visible images from the invisible heat energy emitted from an object. The pictures produced are in the form of a monitor picture with gray scale variations, or different colors, representing various temperatures and temperature ranges.

Thermography has limitations, as do all temperature sensing and measurement techniques. The observed radiometric temperature is affected by such things as the object's absolute temperature, ambient temperature, the objective's emissivity, the emissivity of nearby surroundings, atmospheric filtering of energy, and the distance from the objective to the scanner. Thermographic information can be adjusted for these factors, but training and experience are required to understand when these factors are important, when and where to adjust for them, and how to go about it.

G. J. Weil, EnTech Engineering, Inc., 111 Marine Lane, St. Louis, Mo. 63146. L. E. Haefner, Washington University, St. Louis, Mo. 63130.

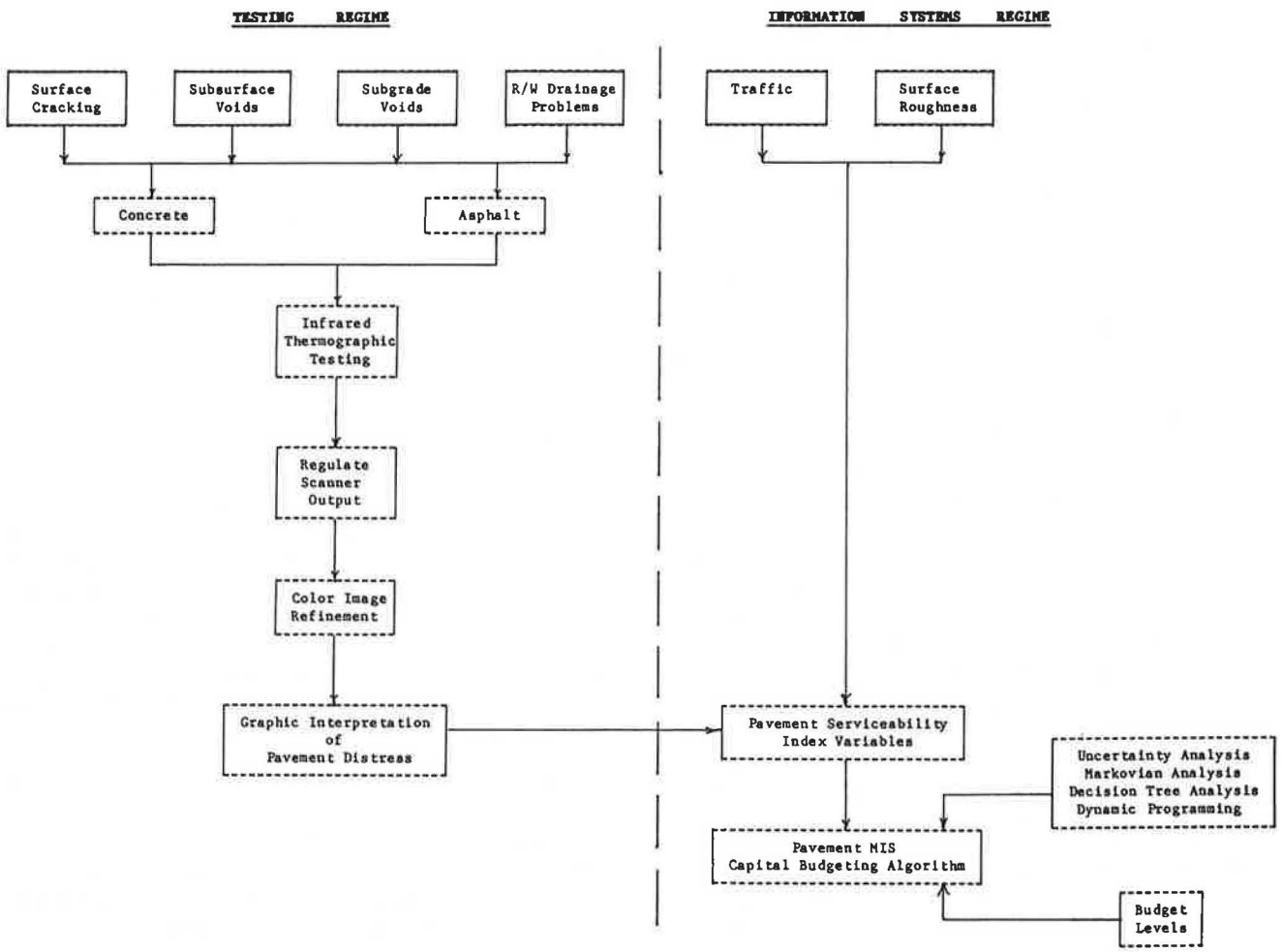

FIGURE 1 Development of an integrated nondestructive testing pavement management system.

Use of the Infrared Scanner

An infrared imaging system consists of an infrared scanner (similar in appearance to a portable video camera) with optics transparent only to infrared radiation and a real-time display monitor (similar to a portable television with a small screen coupled to a microprocessor). The scanner unit converts the radiated heat that is allowed to pass through the optics into an electronic signal. The signal is then turned into a real-time thermal image on the monitor screen of the display unit. The thermal image is composed of a gray scale with continuous tones ranging from black to white. Areas of higher relative temperature appear lighter, and areas of lower relative temperature appear darker. Intermediate shades of gray indicate variations between the extremes of temperature the unit is set to detect. A color monitor and an additional microprocessor can also be used to display the thermal image. A limited number of colors may be employed to show the full range of temperatures in the thermal picture. In this case, each color would represent a particular temperature range.

Defining a Thermogram

A thermogram is a permanent picture of the thermal image produced by the infrared scanner. By the use of special adapters, these images can be recorded on 35-mm film, instant film, or videotape. The thermograms can also be recorded in both black and white or color with the use of special microprocessor equipment. With some systems, actual temperature measurements can be determined from the thermograms. Areas or temperatures of special interest can be highlighted in both the black-and-white and color modes directly on the thermogram for easier identification.

THEORETICAL CONSIDERATIONS

An infrared thermographic scanning system measures surface temperatures only. But the surface temperatures that are measured on a pavement mass are dependent on three subsystems: (1) the subsurface configuration, (2) the surface condition, and (3) the environment.

The subsurface configuration effects are based on the theory that energy flow from warmer to cooler areas cannot be stopped. The flow can only be retarded by the insulating effects of the material through which it is flowing. Various types of construction materials have different insulating capabilities. In addition, various types of pavement defects have different insulating values.

There are three ways of transferring energy: (1) conduction, (2) convection, and (3) radiation. Good pavement should

have the least resistance to conduction of energy, and the convection effects should be negligible. But the various types of problems associated with poor pavement, particularly voids, increase the insulating ability of the pavement by reducing the energy conduction properties without substantially increasing the convection effects. This is due to the presence of voids or dead air spaces, which do not allow the formation of convection currents.

To have an energy flow, one must start with an energy source. Since pavement testing can involve large areas, the heat source should be both inexpensive and capable of giving the pavement surface an even distribution of heat. The sun, which fulfills both of these requirements, will normally supply all the energy needed for areas under test. During nighttime hours, the process may be reversed, with the ground as the heat source and the night sky as the heat sink. For pavement areas not accessible to sunlight, an alternative is to use the heat sinking ability of the earth to draw heat from the pavement under test.

The second critical factor to consider when evaluating pavement for temperature differentials (i.e., anomalies) is the surface condition of the test area. There are three ways to transfer energy. Radiation is the method that has the most profound effect on the ability of the surface to transfer energy. The ability of a material to radiate energy is measured by its emissivity. This is defined as the ability of the material to release energy as compared to that of a perfect blackbody radiator. This is strictly a surface property. It normally exhibits itself in higher values for rough surfaces and lower values for smooth surfaces. For example, rough concrete may have an emissivity of 0.95, while a shiny piece of tinfoil may have an emissivity of only 0.05. In practical terms, this means that inspecting large areas of concrete requires an awareness of differing surface textures caused by such things as broom-roughed spots, tire rubber tracks, oil spots, or loose sand and dirt on the surface.

The final system that affects the temperature measurement of a pavement surface is the environmental system that surrounds the pavement to be measured. Some of the various parameters that affect the surface temperature measurements are as follows:

1. *Solar radiation:* Testing should be performed during times of the day or night when the solar radiation or lack of it would produce the most rapid heating and/or cooling of the pavement surface.
2. *Cloud cover:* Clouds reflect infrared radiation. This has the effect of slowing the process of heat transfer to the sky. Therefore testing should be performed during times of little or no cloud cover to allow the most efficient transfer of energy out of or into the pavement.
3. *Ambient temperatures:* Ambient temperatures should have a negligible effect on the accuracy of the testing since the important consideration is the rapid heating or cooling of the pavement surface. This parameter will affect the length of time (i.e., the window) during which high-contrast temperature measurements can be made.
4. *Wind speed:* High gusts of wind have a definite cooling effect on surface temperatures. Measurements should be taken at wind speeds of less than 15 mph.
5. *Moisture on the ground:* Moisture tends to disperse the surface heat and mask the temperature differences and thus the subsurface anomalies. Tests should not be performed while the ground has standing water or snow.

Once the proper conditions are established for scanning, a relatively large area should be selected for calibration purposes. This area should encompass both good and bad pavement areas (i.e., areas with voids, potential delaminations, cracks, or powdery concrete). Each type of anomaly will display a unique graphic signature depending on the conditions present. Most anomalies will be between 0.1°C and 5°C cooler than the surrounding solid pavement, depending on configuration at night (see Figure 2). A daylight survey will show reversed results.

TESTING EQUIPMENT

To test a pavement for subsurface voids and other types of anomalies, a sensitive contact thermometer is needed. In even the smallest test area, thousands of readings would have to be made simultaneously in order to outline the anomaly precisely. To inspect large areas of pavement efficiently and quickly, it is recommended that a high-resolution infrared thermographic scanner be used. (See Figures 3 and 4.) This type of equipment allows entire areas to be scanned and the resulting data to be displayed as pictures with areas of differing temperatures designated by differing gray tones on a black-and-white image or by various colors in a color image. A wide variety of auxiliary equipment can be used to facilitate the data recording and interpretation.

The actual scanning and analysis system can be divided into four main subsystems. The first is the infrared scanner head and detector that normally can be used with interchangeable lenses. It is similar in appearance to a portable video camera. The scanner's optical system, however, is transparent only to shortwave infrared radiation in the spectrum field of 3 to 5.6 microns or the medium-wave infrared spectrum field of 8 to 12 microns. Normally, the infrared scanner's highly sensitive detector is cooled by liquid nitrogen to a temperature of −196°

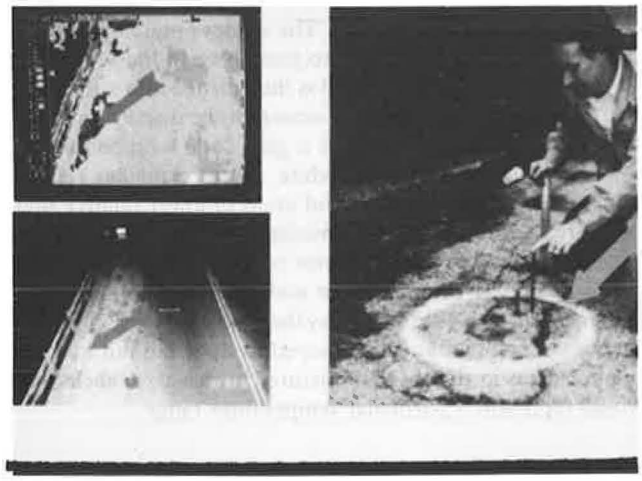

FIGURE 2 Computer-enhanced infrared thermogram (*top left*), visual picture (*bottom left*), and confirmation test (*right*), of defective pavement on the Martin Luther King Jr. Memorial Bridge spanning the Mississippi River at St. Louis, Missouri.

FIGURE 3 Infrared scanner mounted on portable body harness.

C and can detect temperature variations as slight as 0.1° C. Alternative methods of cooling the infrared detectors that use either compressed gases or electric cooling are available. These last two cooling methods may not give the same resolution, since they cannot bring the detector temperatures as low as liquid nitrogen can. In addition, compressed gas cylinders may present safety problems during storage or handling.

The second major component of the infrared scanning system is a real-time microprocessor coupled to a black-and-white display monitor. With this component, cooler items being scanned are normally represented by darker gray tones, while warmer areas are represented by lighter gray tones. To make the images easier to understand for those unfamiliar with interpreting gray-tone images, a color monitor and associated hardware and software may also be installed in the monitoring system. The hardware and software, in conjunction with the color monitor, will quantify the continuous gray-tone energy images into two or more "buckets" of energy levels and assign them contrasting visual colors representing relative thermal energy levels.

The third major component of the infrared scanning system is data acquisition and analysis equipment. It is composed of an analog-to-digital converter, a digital computer with high-resolution color monitor, and storage and analysis software. The computer allows the transfer of moving instrumentation videotape or live images of infrared scenes to single-frame computer images. The images can then be stored individually and later retrieved for enhancement and individual analysis. The computer allows specific analysis standards to be set, based upon destructive sample tests, such as corings, and applies them uniformly to every square inch of pavement. Standard off-the-shelf-type image analysis programs may be used, or custom-written software may be developed.

The fourth major component of the system consists of various types of image recording and retrieving devices. These should be used to record both visual and thermal images. They may be composed of instrumentation videotape recorders, still-frame film cameras with both instant and 35-mm or larger formats, or computer-printed images.

All of the preceding equipment may be carried into the field, or parts of it may be left in the laboratory for additional use. A van may be used to set up and transport the equipment for field testing. This van should include energy supplies to power all the equipment, either batteries and inverter or a small gasoline-driven generator. The van should also include a method to elevate the scanner head and accompanying video camera to allow scanning of the widest pavement area possible, depending on the system optics used.

TESTING PROCEDURES

To initiate an infrared thermographic pavement test, a movement of energy or heat must be established. For testing an open concrete bridge deck surface, the day preceding the test should be dry with substantial sunshine. The test may begin either 2–3 hours after sunrise or 2–3 hours after sunset, both being times of rapid heat transfer. The deck should be cleaned of all debris, and traffic control should be established to prevent vehicles from stopping or standing on the pavement to be tested. The infrared scanner is mounted in a mobile van with the necessary peripheral equipment for data storage and a computer for assistance in data analysis.

The next step is to choose a section of pavement deck and, by coring, establish that it is sound pavement. The reference area is then scanned, and the equipment controls are set to enable an adequate temperature image to be viewed and recorded.

Subsequently, a section of pavement known to be defective by containing a void, delamination, or powdery material is located. This reference area is scanned to assure that the

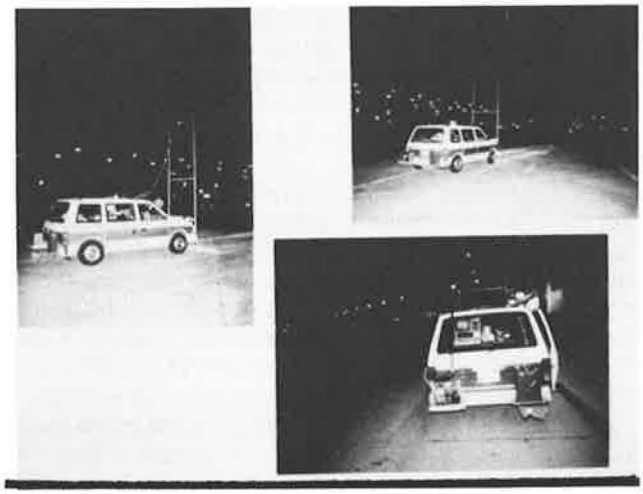

FIGURE 4 Mobile computer-enhanced infrared thermographic scanner, data acquisition, and processing system designed by EnTech Engineering, Inc., in use at the St. Louis International Airport.

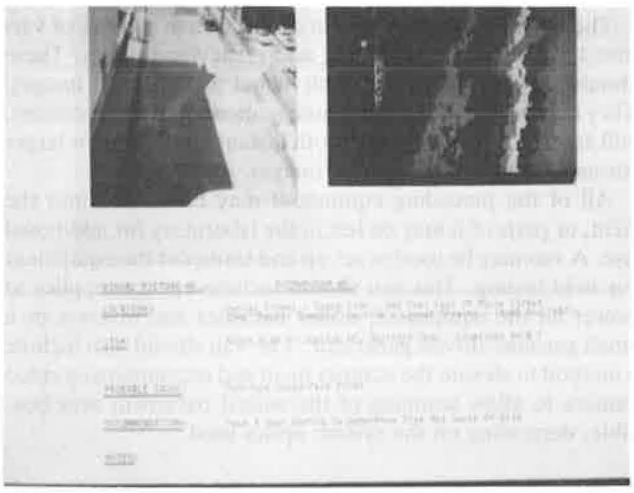

FIGURE 5 Infrared thermographic scan illustrating building shadow-caused temperature differentials.

equipment settings allow viewing of both the good and bad reference areas in the same image with the widest contrast possible. These settings normally reflect a full sensitivity scale of width no greater than 5 degrees.

If a black-and-white monitor is used, better-contrast images are normally produced when the following convention is used: black is defective pavement, and white is sound material. If a color monitor or computer enhancement screen is used, three colors are normally used to designate definite good areas, definite bad areas, and indeterminate areas. When tests are performed during daylight hours, the defective pavement areas usually appear warmer, while during tests performed after dark, defective areas appear cooler.

Once the controls are set and traffic control is in place, the van may be moved forward as rapidly as images can be collected, normally 1–10 mph. If marking the pavement is desired, white or metallic paint may be used to outline the defective deck areas. As an alternative, videotape may be used to document the defective areas, or a scale drawing may be drawn with reference to bridge deck reference points. Production rates of up to 500,000 sq ft per hour (approximately 8 lane-miles) have been attained. During long testing sessions, reinspection of reference areas should be performed approximately every 2 hours, with more scheduled during the early and latter parts of the session when the testing "window" may be opening or closing.

For areas where the sun cannot be used for its heating effects, it may be possible to use the same techniques except for using the ground as a heat sink. The same equipment should be set up in a fashion similar to that described earlier, except that the infrared scanner's sensitivity will have to be increased. This may be accomplished by setting full-scale deflection to 2° C and/or using computer enhancement techniques to bring out detail and to improve image contrast.

Once the data are collected and analyzed, the results should be plotted on scale drawings of the area inspected. Defective areas should be marked clearly so that trends can be observed. Computer enhancements can have varying effects on the accuracy and efficiency of the inspection system. Image contrast enhancements can improve the accuracy of the analysis by bringing out fine details, while automatic plotting and area analysis software can improve the efficiency of the finished, written report.

One note of caution is worthwhile: When inspecting areas that contain shadow-causing elements, such as bridges with superstructures or pavements near buildings, it is preferable to perform the inspection after sundown (see Figure 5). Since the shadows will constantly move, their resulting temperature variations will average out to a uniform level.

CASE HISTORIES

To illustrate the most diverse applications for infrared thermographic pavement testing, three case histories are reviewed in this section:

1. Bridge deck concrete,
2. Airport taxiway concrete, and
3. Garage deck concrete.

Each of these inspections emphasizes a different important feature of this nondestructive, remote sensing evaluation technique.

The first case history reviews the 1985 inspection of a concrete deck on the Martin Luther King Jr. Memorial Bridge spanning the Mississippi River at St. Louis, Missouri (see Figure 6). In this location, weather conditions can quickly change, and conditions can alter from clear sky to fog and rain in a matter of minutes. Therefore it was decided to perform the field inspection in one 8-hour period or less. The deck and its associated ramps were four lanes wide and almost a mile long, and included various sections with and without an overhead superstructure. It was determined to use a mobile lift platform capable of constant movement at up to ¾ mph while simultaneously lifting the infrared equipment, an operator/engineer, and a vehicle driver to heights sufficient to view all four lanes in a single pass (see Figure 7).

Because traffic restrictions prevented the inspection team from fully closing the bridge during inspection, the survey was performed on March 16, 1985, a weekend night between 7:30

FIGURE 6 Martin Luther King Jr. Memorial Bridge spanning the Mississippi River between St. Louis, Missouri, and East St. Louis, Illinois.

FIGURE 7 Self-propelled mobile lift platform used to hold engineer during infrared thermographic inspection of the Martin Luther King Jr. Memorial Bridge.

P.M. and 2:00 A.M. Actual survey time on the bridge deck itself was only 4 hours. The data, both infrared and visual, were recorded on both instrumentation videotape and 35-mm film formats. Before, during, and after the inspection, reference areas were scanned to determine equipment settings that would give the greatest contrast on the infrared imager. The main sensitivity of the equipment was set at 5 degrees for full screen deflection (see Figures 2A and 2B).

After the inspection, a simple technique was used to confirm the infrared data and interpretations to the supervising engineering company; three separate areas were chosen from the void, delamination, and anomaly drawings developed from the infrared data. Then an 8-in. nail was driven into the pavement, and its penetration was determined under a standard blow. The depth of penetration measurements correlated exactly with the test inspection party's determinations (see Figure 2C). Because of the large area of the bridge deck that was found to be defective, savings were realized by curtailing further pavement tests and by immediately initiating a complete bridge rehabilitation program during 1988–1989. Minimum savings in further testing programs were estimated at $80,000, and another estimated $150,000 was saved in unnecessary patching. The cost of the inspection was approximately $8,900.

A second case study involved the inspection of more than 3,125 slabs of reinforced concrete on the taxiway of one of the busiest airports in America, Lambert St. Louis International Airport. This inspection was performed during August 1987, and the field inspection took a total of 5 nights of work.

Owing to the need for no interruptions to air traffic, the decision was made to perform the inspection from 11:00 P.M. to 5:00 A.M. when traffic was slowest. To move the infrared equipment about rapidly, a mobile van was employed for inventory, recording, and analysis (see Figure 4). The van was custom-designed to allow the scanner head and visual cameras to be raised to a 14-ft height during scanning runs to allow the surveying of a 25-ft-wide by 25-ft-long slab in a single view. Production rates, including the activities of the scanning operation, storage of images on computer disks and videotape, 35-mm photographs, and related analysis, approximated 500,000 sq ft of concrete slabs per night.

Prior to the beginning of the inspection, reference and calibration areas were determined for good, solid pavement and for pavement with subsurface voids and delaminations. These areas were rescanned during the inspection window each night at regular intervals to make sure that equipment settings allowed for accurate data collection. This information was fed continuously into a digital computer, and a color monitor was used to assist in the determination and location of anomalies. To speed interpretation, the thermal data presented on the computer monitor were divided into three categories represented by three separate colors: green for solid pavement, yellow for pavement areas with minor temperature deviations most likely caused by minor surface deterioration, and red for pavement areas with serious subsurface cracks/voids. The computer was also used to determine the area designated on each slab by the aforementioned color determinations. These data were used to designate each individual slab for no corrective action, spot repairs, or major replacement.

The results of taxiway pavement inspection showed that approximately one-third of the concrete was in good condition. Another one-third of the area needed only cosmetic rehabilitation, and the remaining one-third needed complete slab replacement. This meant a potential savings in rehabilitation costs of approximately $16 million out of $33 million. This included approximately $11 million saved by not replacing good slabs and $5 million saved by performing surface reconditioning instead of full slab replacement of one-third of the slabs.

The third case history involves inspection of garage concrete and adjacent roadway concrete at the same facility, Lambert St. Louis International Airport. In January 1986, garage facilities and associated roadways were thermographically inspected. The same techniques as described earlier were used, but particular attention was paid to expansion strip areas between concrete slabs. Figure 8 illustrates one of the computer-enhanced thermograms with an expansion strip in mixed condition. The left side of the expansion strip of an elevated roadway shows clearly defined edges on the temperature thermogram, while the right side of the same expansion joint shows ragged edges of the temperature profile. Also perpendicular to the expansion joint is another expansion strip showing ragged edges on the temperature profile. Close inspection of the visual photograph will indicate that some of the areas show surface deterioration (see arrow) while other areas exhibit no surface spalling. All deteriorated areas shown in the thermographs were confirmed and rehabilitated the following year. The circular areas in the thermogram were caused by heat transfer of the circular support columns beneath the elevated roadway.

ADVANTAGES AND LIMITATIONS OF THE METHOD

Nondestructive, thermographic, remote sensing pavement testing techniques for determining pavement subsurface voids, delaminations, and other anomalies have major advantages over destructive tests, such as coring and chloride methods, and other NDT techniques, such as radioactive/nuclear, electrical/magnetic, acoustic, and ground probing radar.

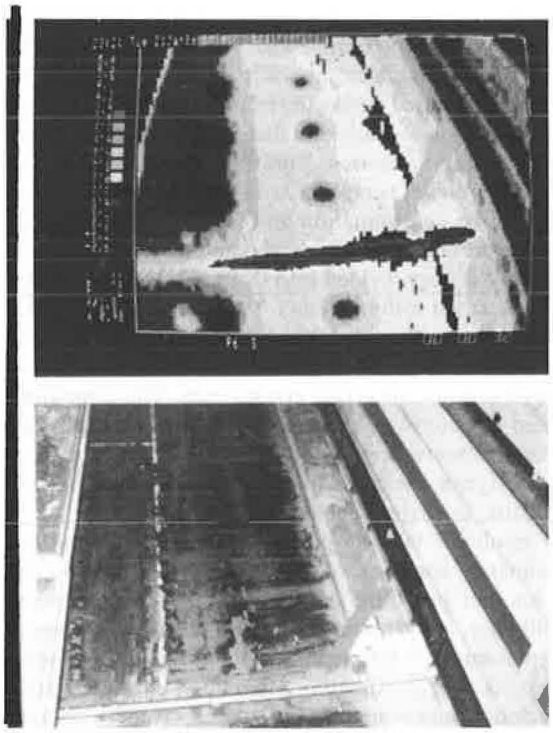

FIGURE 8 (*Top*) Ragged temperature distribution profiles near arrow illustrate areas of pavement deterioration. (*Bottom*) Expansion joint located on elevated roadways at Lambert St. Louis International Airport.

There are several advantages of infrared thermographic analysis compared with the destructive testing methods. No major pavement areas must be destroyed during the testing. Only small-calibration corings must be used. This results in major savings in time, labor, equipment, traffic control, and scheduling problems. In addition, when esthetics are important, no disfiguring of the pavement to be tested occurs. Rapid setup and take-down are also advantages when vandalism is possible. Finally, since no destruction is caused, no concrete dust or debris is generated that could cause health and housekeeping problems.

Further, infrared thermographic equipment is extremely safe. It emits no radiation. It records only thermal radiation that is naturally emitted from the pavement, as well as from all other objects, both living and nonliving. It is similar in function to any normal thermometer, only much more efficient and easier to use.

In comparison, other forms of NDT testing have a variety of inherent problems. Radioactive/nuclear and electrical/magnetic methods emit various types of radiation that can be harmful to people, animals, and other equipment. They may need various forms of licensing for and restriction on use outside of the lab.

Acoustic emission testing and ground probing radar are greatly affected by the type of material to be tested. Such objects as buried water lines and structural steel can distort the test signals and make their interpretation almost impossible. Acoustic emission testing is also affected by the surrounding environment. Noise generated by passing truck and automobile traffic can make the acoustic equipment difficult to use.

It is critical to note that infrared thermography is designed to be used as an area testing technique, while the other methods are all either point- or line-testing methods. A two-dimensional area of various combined lengths and widths may be scanned with images illustrating areas of voids, delaminations, and anomalies displayed on a televisionlike picture of the entire area.

The other methods, including radioactive/nuclear, electrical/magnetic, acoustic, and ground probing radar, are point tests and depend upon a signal propagating downward through the pavement at a discrete point. This gives a reading of the pavement condition at a single spot. If an area is to be tested, then multiple readings must be taken, sometimes numbering in the thousands. Ground probing radar has the advantage over the other point-testing techniques in that the sensor may be mounted on a vehicle and moved in a straight line over pavement materials. This improves efficiency somewhat, but if an area is wide, many line passes would still have to be made. In addition, this could present problems of test mapping alignment.

Infrared thermographic testing has two disadvantages. At this stage of development, it cannot determine the depth or thickness of a void, although the outer dimensions of the void are evident. It cannot determine if a subsurface void is near the surface or farther down, possibly below the enclosed reinforcing bars. A technique such as ground penetrating radar can determine the depth of the void and its thickness but is not as accurate as infrared thermographic testing at determining dimensions and location.

In most testing instances, the thickness of the anomaly is not nearly as important as its other dimensions. In those instances where information on a specific anomaly thickness or depth is needed, however, it is recommended that infrared thermography be used to survey the large areas for problems. Once specific problem locations are found, ground penetrating radar can be used to spot-check the anomaly for its depth and thickness. This combined technique would give the best combination of accuracy, efficiency, economy, and safety.

The second disadvantage of infrared thermography is concerned with the size of the anomaly that can be located. The size of the locatable voids, delaminations, or cracks depends upon the infrared optics, video camera optics, and the speed of the infrared scanner-video system. Cracks as small as 50 mm have been located by stationary systems. However, optics and speeds of data collection must be matched to the type and size of anomalies to be found. The wider the area scanned in a single frame, the less the physical resolution. The faster the motion of the sensor, the greater the image blur.

SUMMARY

1. Infrared thermographic techniques can be used to detect pavement defects, such as subsurface voids, cracks, and changes in density.
2. Infrared thermographic testing techniques are nondestructive.
3. Infrared thermographic pavement anomaly testing techniques are based on the theory that various pavement defects change the rate at which energy flows through normal pavement.

4. Infrared thermographic pavement testing may be performed during both day- and nighttime hours, depending on environmental conditions and what results are desired.
5. Infrared thermographic pavement anomaly testing techniques can distinguish various types of anomalies, although test borings for each type of defect must be made for calibration purposes.
6. Infrared thermographic scanning techniques are more efficient and more accurate than other destructive and nondestructive, manual and electronic methods when testing large pavement areas.
7. Computer analysis of thermal images greatly improves the accuracy and speed of test interpretations.
8. Computer analysis of pavement thermographic data can improve the ability to set repair priorities for areas in a state of change.

FURTHER RESEARCH AGENDA

The long-range research effort will attempt integration of testing activity with data interpretation, storage, and computation of priorities using reasonably robust evaluation modeling formats, employing uncertainty analysis. The operational capability of a turnkey testing and management information system for budget allocation and policy decisions would greatly enhance the highway planning and maintenance process.

Publication of this paper sponsored by Committee on Pavement Monitoring, Evaluation and Data Storage.

Skid Resistance of Adjacent Tangent and Nontangent Sections of Roads

BOHDAN T. KULAKOWSKI AND WOLFGANG E. MEYER

The objective of this study was to compare skid resistance on adjacent tangent and nontangent sections of roadways based on the results of a full-scale field testing program. Test sites were selected in New York State and in Texas to provide data from different climatic regions. It was found that blank-tire skid numbers in both regions are significantly lower on nontangent curved sections than on adjacent tangent straight sections. The ribbed-tire skid number measurements in Texas followed the same pattern; however, no significant difference was found between tangent and nontangent ribbed-tire skid numbers on sites in New York. The absence or presence of winter effects, which stimulate recovery of the pavement microtexture, seem to be responsible for the different observations regarding ribbed-tire data in Texas and New York.

One of the main conditions for safety of a vehicle negotiating a curve is that the level of tire/pavement friction is sufficiently high to counteract the lateral force developed during cornering. If the lateral force at the tire/pavement interface exceeds available lateral friction force, the vehicle will skid off the road. At the same time, as the friction demand is higher, skid resistance on nontangent (curved) sections is expected to be lower than on adjacent tangent (straight) sections because of the more severe polishing action of traffic.

Heavy trucks, which constitute a significant percentage of highway traffic, are primarily responsible for polishing pavement texture. The lateral tire/pavement forces generated by a tractor-semitrailer in a 450-ft (137-m)-radius curve at 40 mph (64 km/h) are approximately ten times higher than the lateral tire/pavement forces generated by a passenger car under the same conditions. The truck lateral forces calculated using the Phase 4 computer program were 800 lb on tractor front axle and 1,500 lb and 1,600 lb on tractor rear axle and trailer axle, respectively. For a typical medium-size sedan the lateral tire/pavement forces calculated using HVOSM program were 195 lb and 120 lb on the front and rear axle tires, respectively. The consequently expected lower skid resistance, combined with increased demands for pavement friction, makes nontangent sections particularly critical for highway safety.

This paper compares skid resistance on tangent and nontangent sections of roadways to find out if, indeed, the skid resistance in curves is significantly lower than in adjacent straight sections.

Department of Mechanical Engineering, The Pennsylvania Transportation Institute, The Pennsylvania State University, University Park, Pa. 16802.

TESTING PROGRAM

The full-scale testing plan developed for this study involved measurements of skid resistance on pairs of adjacent tangent and nontangent sections of roadways. The measurements were conducted using a two-wheel skid tester in accordance with ASTM Method of Test E 274 (*1*).

When a standard two-wheel trailer is operated on a curve in accordance with the ASTM method, some conditions may cause deviations from the specified procedure:

- Lateral inertial forces acting on the trailer may displace it from its normal attitude relative to the towing vehicle.
- As a result of altered trailer attitude, the force component at the tire/road interface will not act in the plane of the skidding test tire.
- Weight transfer across the trailer caused by the lateral acceleration will change the vertical load on the test tire, which may deviate by more than the allowable amount from the nominal normal load.
- For a radius of curvature less than approximately 400 ft (122 m), it is not possible to maintain a speed of 40 mph (64 km/h) without exceeding acceptable lateral acceleration limits.
- The limited length of nontangent sections may make it impossible to obtain five skid tests along a given curve, thus the curve may have to be tested by repeated passes.
- The influence of the lateral acceleration may cause the distribution of the water film across the tire pavement interface to be unacceptable.

In a study conducted at the Texas Transportation Institute (TTI) (*2*), it was determined that, compared with other systems, ASTM Method E 274 provided the best all-round performance in the nontangent mode in spite of the limitations already listed. By conducting a series of controlled track tests supplemented by highway tests, researchers determined the accuracy and limitations of this system operating in the nontangent mode. It was found that the limit of maneuverability of the typical ASTM E 274 test trailer in a locked-wheel test occurs when the lateral inertial force caused by road curvature reaches approximately 0.3 to 0.4 g in the two-wheel trailer's horizontal plane. This limit is imposed by the finite capability of the second trailer wheel, which is rolling freely on dry pavement, to generate the side force necessary to keep the trailer on course. It was also determined that, to obtain accurate measurements in nontangent sections, the trailer must be capable of measuring both the longitudinal traction force and the dynamic vertical load on the test wheel. These forces are then used to compute the skid number. When force transducers capable of measuring these two forces are used, the

TABLE 1 SKID NUMBER MEASUREMENTS FOR NEW YORK SITES, 1986

	May 15		June 18		July 16		August 4		Sept. 11		Oct. 16		Nov. 18	
Site	SNB	SNR	SNB	SNR	SNB	SNR	SNB	SNR	SNB	SNR	SNB	SNR	SNB	SNR
1S	42.3	56.7	44.8	57.7	38.1	58.1	40.0	53.9	42.9	57.0	36.6	52.3	42.2	52.1
1R	40.3	55.3	43.4	55.5	37.7	58.3	40.0	54.4	41.7	57.0	39.7	52.5	39.5	51.8
2S	51.9	54.7	54.5	55.8	61.3	51.2	50.5	52.8	50.9	51.0	49.4	52.4	47.8	50.4
2R	50.2	53.0	51.9	54.1	57.3	51.9	52.8	55.9	49.9	51.7	46.4	49.6	49.8	50.2
3S	36.6	36.8	41.9	40.8	38.5	40.9	38.1	37.6	35.2	34.2	36.5	36.8	37.1	36.0
3L	34.9	41.3	39.0	47.0	35.4	43.1	38.1	41.8	33.2	44.9	34.9	40.8	35.4	41.0
3R	29.2	32.5	35.1	38.8	32.9	37.7	31.0	34.6	28.9	34.1	28.9	33.0	29.7	33.2
4S	21.9	45.1	21.7	45.0	22.0	47.1	22.5	45.1	22.2	39.5	20.9	44.3	24.2	42.2
4R	23.3	48.3	22.7	47.8	23.0	51.4	22.2	47.8	22.6	44.0	22.4	45.0	24.9	45.8
5S	39.1	57.3	40.1	56.8	32.5	60.8	38.6	56.5	40.4	55.1	34.3	57.4	34.3	55.6
5R	29.7	54.3	31.8	57.5	24.2	58.8	28.9	56.6	29.7	54.2	26.2	58.5	28.9	56.7
6S	21.0	39.5	23.5	39.5	23.3	44.0	20.7	36.7	20.5	37.5	20.4	40.2	23.3	37.0
6L	16.8	34.7	19.6	35.6	19.0	42.3	17.4	32.8	16.0	32.6	16.9	35.7	19.1	32.4
7S	22.4	35.5	24.2	34.8	24.9	41.1	22.6	35.1	21.0	34.1	23.0	36.4	21.6	35.2
7R	22.9	36.0	22.8	37.6	24.1	38.9	22.0	35.7	20.5	34.6	25.8	37.7	23.2	36.2

S = tangent section; R = nontangent, right curve; L - nontangent, left curve

SNB = Skid Number with the blank test tire; SNR = Skid Number with the ribbed test tire

errors caused by the inertial forces and load transfer on the trailer are insignificant.

The TTI study concluded that the accuracy of the skid number measurements on nontangent sections is comparable with that of tangent sections, provided the tested curves do not generate lateral accelerations in excess of 0.3 g and the instrumentation system measures both the longitudinal and vertical force components. Moreover, the study recommended that testing on nontangent sections be avoided when the water tank level is low because the water may move away from the water outlet of the tank unless the tank is specially baffled.

The skid tester used in this study was equipped with force transducers measuring the tire/pavement force components in longitudinal and vertical directions. Also, following the TTI recommendations, nontangent test sections with a radius of curvature no less than 450 ft (137 m) were selected. At 40 mph (64 km/h) the maximum lateral acceleration on a curve with a 450-ft (137-m) radius is 0.25 g. Both ribbed and blank standard ASTM test tires were used in the program (*3*, *4*).

Because weather conditions affect the skid resistance of road surfaces (*5*), the testing was conducted on sites in New York State and Texas. Eight pairs of adjacent tangent and nontangent sections were selected in New York State and four pairs in Texas. All curves were "soft," generating lateral accelerations of less than 0.25 g at the test speed of 40 mph (64 km/h). Both bituminous and concrete pavements were tested.

To determine if significant seasonal changes are present in the data, the skid resistance measurements in New York State were repeated at approximately monthly intervals from May through November.

TEST RESULTS

In both New York and Texas ribbed- and blank-tire measurements were made on all sites, following the same wheelpath with both tires. The results of the measurements are given in Tables 1 and 2.

To determine whether a statistically significant difference existed between skid numbers on tangent and nontangent sections of the same roads, the following regression model was used to relate the tangent and nontangent data:

$$SN_T - SN_{NT} = \alpha SN_T \quad (1)$$

where SN_T is a skid number on a tangent section of the road and SN_{NT} is a skid number on an adjacent nontangent section. The values of α for each monthly set of data using linear regression are listed in Table 3. Also given in Table 3 are the *t*-ratios that indicate that the regression coefficient can be considered statistically significant. The results of the computation are shown in Table 3. The values of the parameter α are also plotted in Figure 1 for May through November 1986.

In Texas, four pairs of adjacent tangent and nontangent sections of roads were tested. Only two sets of data were collected, one in July 1985 and the other in November/December 1985, since small seasonal effects were not expected to be a factor under Texas climatological conditions. The model used in the New York data analysis, Equation 1, was applied to relate tangent and nontangent skid numbers for the four Texas sites. The results of the linear regression analysis are shown in Table 4.

TABLE 2 SKID NUMBER MEASUREMENTS FOR TEXAS SITES, 1985

	July		Nov./Dec.	
Site	SNB	SNR	SNB	SNR
1S	40.6	44.9	39.2	38.3
1R	36.7	39.8	35.5	35.3
2S	48.6	51.5	50.9	48.8
2L	46.5	46.9	48.2	43.2
3S	50.9	54.1	53.4	51.0
3L	48.5	49.5	52.2	48.1
4S	11.0	18.4	13.5	21.7
4R	8.5	16.6	11.4	18.9

S = tangent section; R = right curve; L = left curve

SNB = Skid Number with blank tire

SNR = Skid Number with ribbed tire

DISCUSSION OF THE RESULTS

The results obtained with the ribbed and blank tires at the New York sites, as presented in Table 3 and in Figure 1, differ considerably from each other. For the ribbed tire, the param-

TABLE 3 RESULTS OF REGRESSION ANALYSIS OF NEW YORK DATA

		May 15	June 18	July 16	Aug. 14	Sept. 11	Oct. 16	Nov. 18
Ribbed	Parameter α	0.0214	-0.0033	0.0041	-0.0148	-0.0107	-0.0033	-0.0086
Tire	t-ratio	0.83	-0.13	0.22	-0.67	-0.33	-0.13	-0.34
Blank	Parameter α	0.0909	0.0895	0.0886	0.0618	0.0930	0.0693	0.0613
Tire	t-ratio	2.56	3.40	3.13	1.47	2.50	1.56	1.74

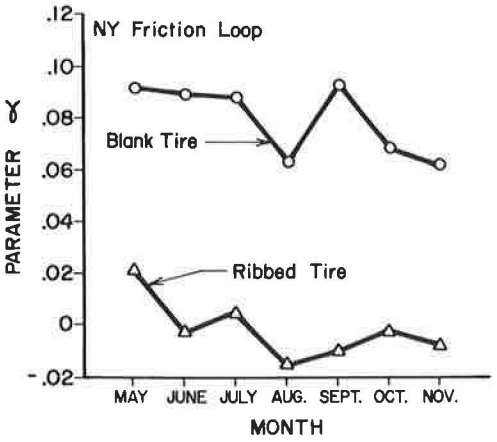

FIGURE 1 Difference between skid resistance on adjacent tangent and nontangent roads in New York in terms of Parameter 2, Equation 1.

eter α was close to zero and the values of the *t*-ratio were also very small, which indicates that there is no significant difference between skid numbers on adjacent tangent and nontangent sections.

The parameter α for the blank tire varied between 0.06 and 0.09, which corresponds to a 6 to 9 percent difference between skid numbers on adjacent tangent and nontangent sections of the same paving project. Furthermore, since the parameter α is always positive, it can be said that the blank-tire skid numbers on tangents are 6 to 9 percent higher than on adjacent curves. The relatively high *t*-ratio values confirm the statistical meaningfulness of the results.

The different results obtained with the two tires indicate that the pavement macrotexture and microtexture are subject to different processes on tangent and nontangent road sections. The limited amount of experimental data collected in this project allows for only a hypothetical explanation. Macrotexture is reduced more by wear and compaction, while microtexture is reduced more by polishing. Both effects seem to be more pronounced on nontangent than on tangent sections of roads, even though the nontangent sections are limited to relative "soft" curves. (The lateral acceleration at 40 mph [64 km/h] does not exceed 0.25 g.) It appears, however, that the microtexture recovers during the winter months so that the ribbed-tire skid numbers show little difference between tangents and curves. The pavement macrotexture, on the other hand, does not recover, or does not recover completely, during the winter; hence, a significant difference is observed between the blank-tire skid numbers on tangent sections and those on nontangent sections.

The magnitude of the difference between the blank-tire skid numbers on tangent and nontangent sections varies among the test sites. This may be explained by considering the long-term changes in skid number on both types of sections. Assuming, as before, that the pavement macrotexture does not recover during the winter, the blank-tire skid numbers on both tangent and nontangent sections will decrease in time; and the rate of the decrease will be higher for the nontangent sections because of the more severe wear and surface compaction by traffic. If the changes of the blank-tire skid numbers have an approximately exponential character, as shown in Figure 2, the difference will change with time, as shown in Figure 3. The curve of Figure 3 starts at zero because the skid numbers are expected to be the same when the pavement is new. With time, and with progressing wear of the surface macrotexture, the difference increases, reaches a maximum, and then decreases, approaching zero when the macrotexture of both tangent and nontangent sections becomes heavily worn. Three stages of pavement wear—none, light to moderate, and heavy—are indicated in Figure 3. Although it is impossible to define the three stages precisely, it can generally be concluded that the difference in the blank-tire skid numbers on tangent and nontangent sections of roads is largest at the stage

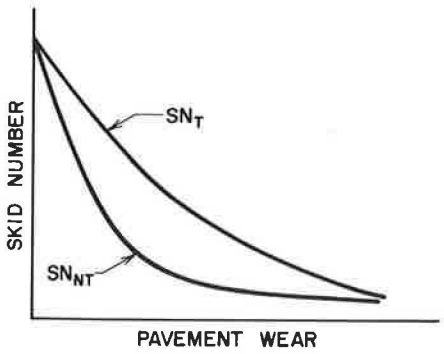

FIGURE 2 Blank-tire skid number of adjacent tangent (SN_T) and nontangent (SN_{NT}) sections versus pavement wear.

TABLE 4 RESULTS OF REGRESSION ANALYSIS OF TEXAS DATA

Tire		July 1985	Nov./Dec. 1985
Ribbed	Parameter α	0.0927	0.0949
	t-ratio	5.37	5.29
Blank	Parameter α	0.0953	0.0958
	t-ratio	6.80	4.62

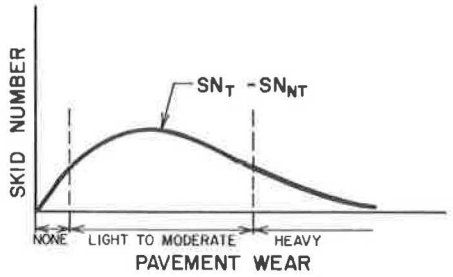

FIGURE 3 Difference between skid numbers on adjacent tangent and nontangent sections versus pavement wear.

of light-to-moderate wear of the pavement macrotexture and is very small on new and on heavily worn pavements.

Figure 4 shows the difference between the measured blank-tire skid numbers for sites in New York and Texas and the blank-tire skid numbers on nontangent test sections, which is here considered a measure of wear of the pavement macrotexture. There is a considerable scatter of data in this plot, but it should be kept in mind that these data points represent a variety of pavement materials, various levels of average daily traffic, and the drastically different climatic conditions of New York and Texas. It should not be expected, therefore, that these data points will form a smooth curve similar to that in Figure 3. Such a smooth curve could be obtained, provided the conceptual explanation offered here is sound, only if all data points represented the same pavement at different stages of wear. Nonetheless, the distribution of the data in Figure 4 suggests that the difference between skid numbers on tangent and nontangent sections is very small if the blank-tire skid number on the nontangent section is greater than 40. A blank-tire skid number of 40 might therefore separate new from lightly to moderately worn pavements. The cutoff between lightly to moderately worn and heavily worn pavements is less obvious, but a value of 20 for the blank-tire skid number can tentatively be considered the borderline. In summary, the difference between the blank-tire skid numbers on tangent and nontangent sections of roads should be expected to be very small if the blank-tire skid number on the nontangent section is either greater than 40 (new pavements) or less than 20 (pavements with heavy wear of the macrotexture.

The ribbed-tire results from the Texas sites are quite different from the New York results. The ribbed-tire skid numbers on nontangent sections are significantly and consistently lower than on tangent sections. Thus, the ribbed-tire data from Texas follow the same pattern as the blank-tire data, which is in accordance with the earlier explanation of the blank-tire results from the New York sites except that in Texas the pavement microtexture does not recover, or does not recover completely, because of the absence of winter effects.

CONCLUSIONS

The level of skid resistance on nontangent sections of roadways is usually lower than on adjacent tangent sections. The decrease in skid resistance combined with increased demand for friction by a vehicle negotiating a turn may create serious safety problems in the curved sections of roadways.

The difference between frictional characteristics of pavements on adjacent tangent and nontangent sections of roads depends on the climatic conditions in the region. At northern latitudes (New York State) no significant difference was found in the pavement microtexture measured by the ribbed-tire skid number. The blank-tire skid number of the same sites, which characterizes pavement macrotexture, was consistently lower, by 6 to 9 percent, on nontangent sections. At southern latitudes (Texas) both ribbed- and blank-tire skid numbers on nontangent sections were lower than on the adjacent tangent sections. The difference in the ribbed-tire skid numbers can be explained by the lack of winter effects that would stimulate recovery of pavement microtexture observed in the northern climate.

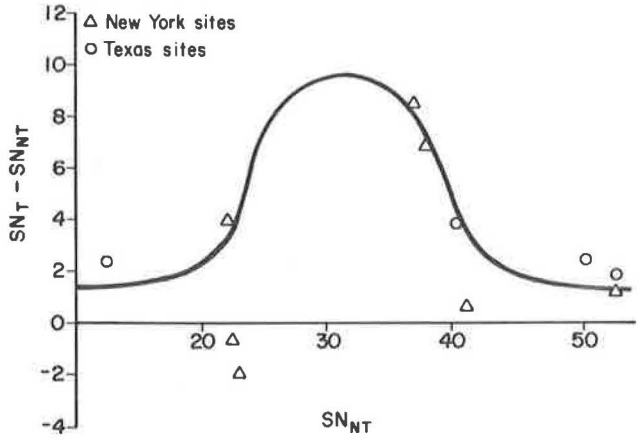

FIGURE 4 Difference between blank-tire skid numbers on adjacent tangent and nontangent sections versus skid numbers on nontangent sections.

ACKNOWLEDGMENT

The work reported in this paper was conducted under the sponsorship of the Federal Highway Administration.

REFERENCES

1. Standard Test Method for Skid Resistance of Paved Surfaces Using a Full Scale Tire, E 274-85. *Annual Book of ASTM Standards*, Section 4, Vol. 04.03, 1987, pp. 755–762.
2. R. A. Zimmer and R. D. Tonda. Pavement Friction Measurements on Nontangent Sections of Roadways. Comprehensive Report FHWA/RD-82/150, Vol. 11. FHWA, U.S. Department of Transportation, 1983.
3. Standard Specification for Standard Tire for Pavement Skid-Resistance Tests, E 501-82. *Annual Book of ASTM Standards*, Section 4, Vol. 04.03, 1987, pp. 777–781.
4. Standard Specification for Smooth-Tread Standard Tire for Special-Purpose Pavement Skid-Resistance Tests, E 524-82. *Annual Book of ASTM Standards*, Section 4, Vol. 04.03, 1987, pp. 790–793.
5. S. H. Dahir and J. J. Henry. Seasonal and Short-Term Variations in Skid Resistance. In *Transportation Research Record 715*, TRB, National Research Council, Washington, D.C., 1979, pp. 69–76.

The findings and conclusions in this paper are those of the authors and do not necessarily represent the views of the Federal Highway Administration.

Publication of this paper sponsored by Committee on Surface Properties—Vehicle Interaction.

Simple Computer Models for Predicting Ride Quality and Pavement Loading for Heavy Trucks

KEVIN B. TODD AND BOHDAN T. KULAKOWSKI

Increasing pavement damage caused by the increasing number of heavy trucks on today's highways has promoted concern about the dynamic pavement loads and the ride quality of trucks. So far, these concerns have been analyzed using only experimental studies and complex computer programs. This paper presents three possible simple truck models—a quarter-truck, a half-single-unit truck, and a half-tractor semitrailer—that can be used on personal computers to predict ride quality and pavement loading. Numerical values for the model parameters are suggested for possible standardization. Sample results are presented in the form of vertical acceleration frequency responses and root mean square vertical acceleration for ride quality and tire force frequency responses and dynamic impact factors for pavement loading. The quarter-truck model overestimated both ride quality and pavement loading when compared to the half-single-unit truck model.

In recent years, the percentage of trucks in the highway traffic stream has increased significantly—up by 30 percent on some highways. As a result of improving brake and engine technology, longer and wider trucks are being constructed to carry heavier loads. In addition to affecting cornering and braking performance, increasing truck size and weight dramatically increases dynamic pavement loading. The resulting increase in pavement roughness and wear has made ride comfort a major concern for truck drivers covering long distances.

Various aspects of truck dynamics are being examined in several current research studies (*1*). Of three types of research methods—analytical, experimental, and computer simulation—only the last two find wide application in those studies. Analytical methods are practically useless in dealing with problems of the complexity associated with mathematical models of heavy trucks. Experimental methods offer the most valuable results; however, they are usually very costly. Moreover, the experimental methods are limited by safety requirements. Probably the most successful approach has been to conduct a limited number of field tests to provide actual truck performance data to validate computer simulation programs. These computer simulation programs are then used to extrapolate the experimental results over the range of test conditions where experimentation would be too dangerous or too expensive.

Department of Mechanical Engineering, Pennsylvania Transportation Institute, The Pennsylvania State University, University Park, Pa. 16802.

Several truck simulation programs have been developed in recent years (*2–4*). In most cases these programs, such as the Phase 4 program (*2*) developed at the University of Michigan Transportation Research Institute, are products of long-term efforts. Although relatively accurate, these programs are very complex and require detailed input and long execution times even for simple problems.

The objectives of this paper are twofold. First, relatively simple mathematical models of truck dynamics are presented. The applicability of the proposed models is limited to those problems involving two-dimensional dynamics. Examples of such problems are dynamic pavement loading and ride quality. Second, possible numerical parameters for the various models are suggested to represent typical trucks. Acceptance of standard truck models similar to those developed for passenger cars (*5*) would allow for comparison of computer sim-

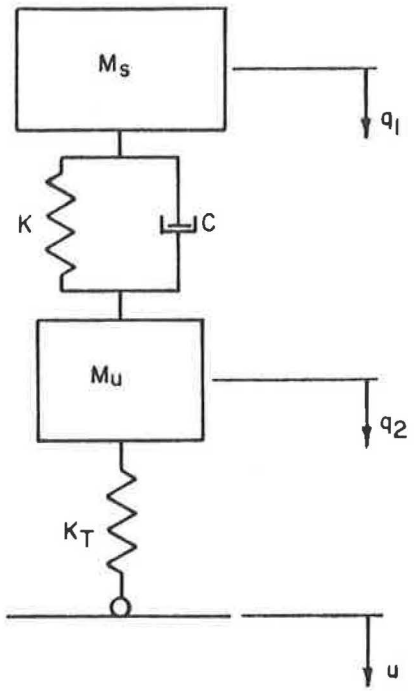

FIGURE 1 Quarter-truck model.

TABLE 1 QUARTER-TRUCK MODEL PARAMETERS

Parameters:

Symbol	Description
M_m	One quarter vehicle sprung mass
M_u	Unsprung mass corresponding to one wheel
K	Suspension spring constant
C	Suspension damping constant
K_t	Tire spring constant

Numerical Values Used:

Symbol	Single Unit Truck Front Axle	Single Unit Truck Rear Axle
M_m	13.975 $lbsec^2/in$	22.9036 $lbsec^2/in$
M_u	1.553 $lbsec^2/in$	2.976 $lbsec^2/in$
K	1132. lb/in	6500. lb/in
C	15. lbsec/in	15. lbsec/in
K_t	4500. lb/in	5000. lb/in

ulation results conducted by different research groups. Sample simulation results are presented to demonstrate the use of these simple truck models and the numerical parameters selected.

MATHEMATICAL MODELS

To develop three mathematical truck models, the following was assumed:

- Constant vehicle velocity,
- No vehicle body or axle roll,
- Rigid vehicle bodies,
- Linear suspension and tire characteristics,
- Point tire to road contact, and
- Small pitch angles.

Quarter-Truck Model

The first model, a quarter-truck, is shown in Figure 1. The parameters are defined in Table 1; the state equations are presented in Table 2. The parameter values for this simple model can be derived in a variety of ways. One possible approach is to use front axle parameters for ride comfort studies and rear axle parameters for pavement loading studies. The quarter-truck model represents only the heave mode of the vehicle.

Transfer functions, listed in Table 3, can be developed easily in the frequency domain for both the tire force and the

TABLE 2 QUARTER-TRUCK STATE EQUATIONS

$$\dot{q}_1 = q_3 \qquad \dot{q}_2 = q_4$$

$$\dot{q}_3 = \{-q_1(K)+q_2(K)-q_3(C)+q_4(C)\}/M_s$$

$$\dot{q}_4 = \{q_1(K)-q_2(K_t+K)+q_3(C)-q_4(C)+u(K_t)\}/M_u$$

where:

q_1 = Vertical displacement of sprung mass

q_2 = Vertical displacement of unsprung mass

q_3 = Vertical velocity of sprung mass

q_4 = Vertical velocity of unsprung mass

u = Vertical displacement of road under wheel

vertical acceleration of the sprung mass. Considerable time can be saved by using the transfer functions instead of the simulation routines to calculate the frequency responses.

Half-Single-Unit Truck Model

The second model, a half-single-unit truck with single axles, is shown in Figure 2. The parameters are defined in Table 4; the state equations are presented in Table 5. This model includes both front and rear axles, resulting in both a pitch and a heave mode of the vehicle body being incorporated in the model.

Although this model is considerably more complicated than the quarter-truck model, the transfer function method could be used to determine specific frequency responses. Computer simulations can be used to determine frequency responses for any combination of the state variables and inputs. In this study, computer simulations are used to determine the half-single-unit truck frequency responses.

Half-Tractor Semitrailer Model

The third model, a half-tractor semitrailer, is shown in Figure 3. The parameters are defined in Table 6; the state equations are presented in Table 7. This model expands the half-single-unit truck model to include double axles and a semitrailer. The fifth wheel connecting the tractor to the semitrailer is modeled with a stiff spring and damper. This makes the fifth wheel appear nearly rigid without complicating the state equations. As with the half-single-unit truck, the pitch angles have been assumed small to make the mathematical model linear.

The complexity of this model makes developing transfer functions in the frequency domain a formidable task. Computer simulations are used to determine all frequency responses for this model.

NUMERICAL PARAMETER VALUES

Because truck sizes and loads vary greatly, it is much more difficult to select representative parameter values for trucks than for passenger cars. The numerical data used in this paper represent a fully loaded, single-unit, single-rear-axle truck and a fully loaded, 18-wheel tractor semitrailer with the payload evenly distributed (*6*). These values could be used with half-truck models to study typical loaded trucks.

Because the load often is unevenly distributed, selecting parameter values for the quarter-truck model is even more difficult. Two possible approaches are presented in this paper—one for ride comfort and one for pavement loading. In both cases the numerical values are based on the single-unit-truck parameter values. The first approach uses the front axle suspension parameters and half of the actual unsprung mass sup-

TABLE 3 QUARTER-TRUCK TRANSFER FUNCTIONS

Transfer Functions:

Vertical acceleration of sprung mass (a_1):

$$\frac{a_1(s)}{u(s)} = \frac{K_t s^2(C_s + K)}{(M_u s^2+Cs+k+K_t)\,(M_s s^2+Cs+K+K_t) - (Cs+K)^2}$$

Vertical tire force (F_t):

$$\frac{F_t(s)}{u(s)} = \frac{K_t^2\,(M_s s^2+C_s+K)}{(M_s s^2+Cs+K)\,(M_u s^2+Cs+k+K_t) - (Cs+k)^2} - K_t$$

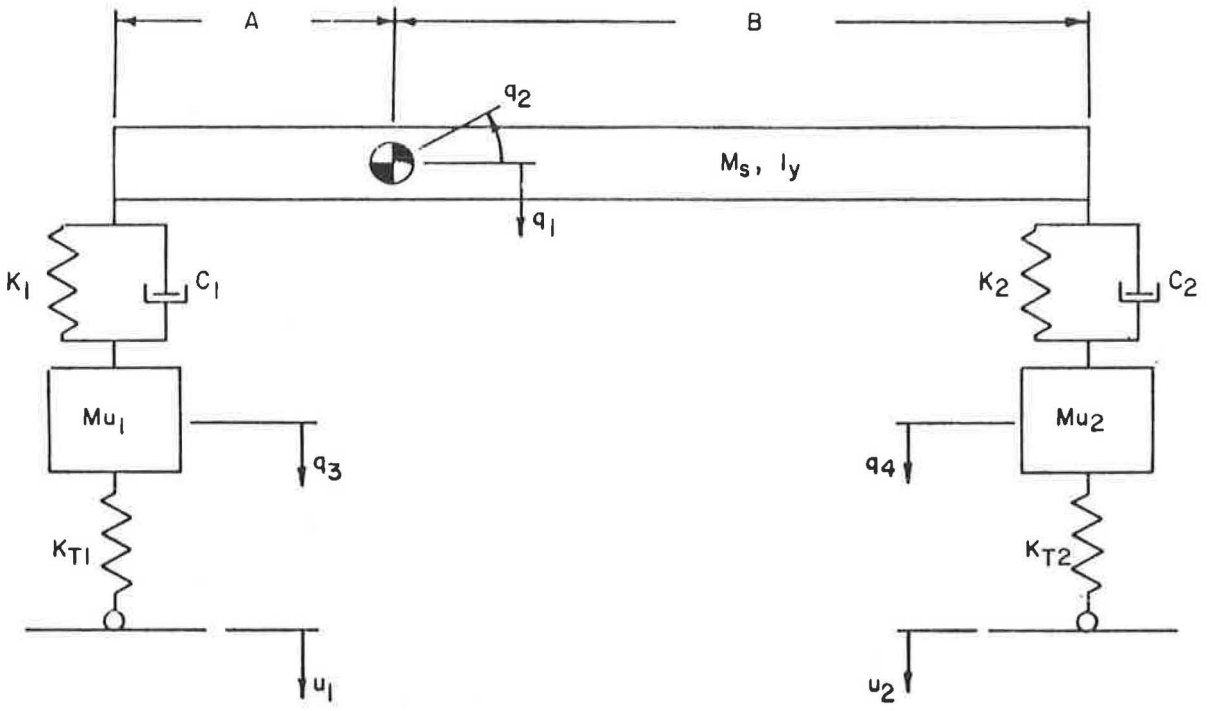

FIGURE 2 Half-single-unit truck model.

TABLE 4 HALF-SINGLE-UNIT TRUCK MODEL PARAMETERS

Parameters:

Symbol	Description	Numerical Value	
M_s	One half vehicle sprung mass	36.8789	$lbsec^2/in$
I_v	One half sprung mass pitch moment	410876.4	$lbsec^2in$
M_{u1}	One half front axle unsprung mass	1.5528	$lbsec^2/in$
M_{u2}	One half rear axle unsprung mass	2.9762	$lbsec^2in$
K_1	Front suspension spring constant	1132.	lb/in
K_2	Rear suspension spring constant	6500.	lb/in
C_1	Front suspension damping constant	15.	lbsec/in
C_2	Rear suspension damping constant	15.	lbsec/in
K_{t1}	Front tire spring constant	4500.	lb/in
K_{t2}	Rear tire spring constant	5000.	lb/in
A	Horizontal distance from front axle to sprung mass center of gravity	149.052	in
B	Horizontal distance from rear axle to sprung mass center of gravity	90.948	in

TABLE 5 HALF-SINGLE-UNIT TRUCK STATE EQUATIONS

$$\dot{q}_1 = q_5 \qquad \dot{q}_2 = q_6 \qquad \dot{q}_3 = q_7 \qquad \dot{q}_4 = q_8$$

$$\dot{q}_5 = \{-q_1(K_1+K_2)+q_2(K_2B-K_1A)+q_3(K_1)+q_4(K_2)-q_5(C_1+C_2)+q_6(C_2B-C_1A) + q_7(C_1)+q_8(C_2)\}/M_s$$

$$\dot{q}_6 = \{-q_1(K_1A+K_2B)+q_2(K_2B^2-K_1A^2)+q_3(K_1A)+q_4(K_2B)-q_5(C_1A+C_2B) + q_6(C_2B^2-C_1A^2)+q_7(C_1A)+q_8(C_2B)\}/I_y$$

$$\dot{q}_7 = \{q_1(K_1)+q_2(K_1A)-q_3(K_1+K_{t1})+q_5(C_1)+q_6(C_1A)-q_7(C_1)+u_1(K_{t1})\}/M_{u1}$$

$$\dot{q}_8 = \{q_1(K_2)-q_2(K_2B)-q_4(K_2+K_{t2})+q_5(C_2)-q_6(C_2B)-q_8(C_2)+u_2(K_{t2})\}/M_{u2}$$

where:

q_1 = Vertical displacement of sprung mass

q_2 = Pitch angular displacement of sprung mass

q_3 = Vertical displacement of front unsprung mass

q_4 = Vertical displacement of rear unsprung mass

q_5 = Vertical velocity of sprung mass

q_6 = Pitch angular velocity of sprung mass

q_7 = Vertical velocity of front unsprung mass

q_8 = Vertical velocity of rear unsprung mass

u_1 = Vertical displacement of road under front wheel

u_2 = Vertical displacement of road under rear wheel

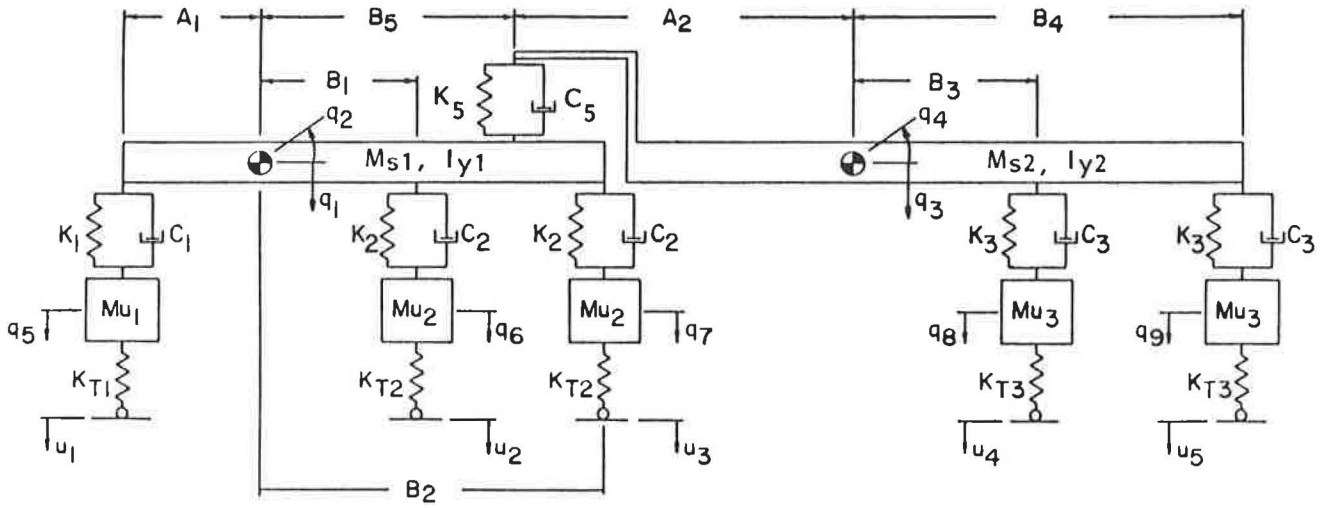

FIGURE 3 Half-tractor trailer model.

TABLE 6 HALF-TRACTOR SEMITRAILER MODEL PARAMETERS

Parameters:

Symbol	Description	Numerical Value	
M_{m1}	One half tractor sprung mass	10.401	$lbsec^2/in$
I_{y1}	One half tractor sprung mass pitch moment	200490.	$lbsec^2in$
M_{u1}	One half front axle unsprung mass	1.5528	$lbsec^2/in$
M_{u2}	One half tractor rear tandem axle unsprung mass (per axle)	2.9782	$lbsec^2in$
K_1	Tractor front suspension spring constant	1132.	lb/in
K_2	Tractor rear suspension spring constant	7200.	lb/in
C_1	Tractor front suspension damping constant	15.	lbsec/in
C_2	Tractor rear suspension damping constant	15.	lbsec/in
K_{t1}	Tractor front tire spring constant	4500.	lb/in
K_{t2}	Tractor rear tire spring constant	9000.	lb/in
A_1	Horizontal distance from front axle to tractor sprung mass center of gravity	60.108	in
B_1	Horizontal distance from leading rear axle to tractor sprung mass center of gravity	126.342	in
B_2	Horizontal distance from fifth wheel to tractor sprung mass center of gravity	177.442	in
B_5	Horizontal distance from fifth wheel to tractor sprung mass center of gravity	118.662	in
M_{s2}	One half trailer sprung mass	81.731	$lbsec^2/in$
I_{y2}	One half trailer spung mass pitch moment	90575.5	$lbsec^2in$
M_{u3}	One half trailer tandem axle unsprung mass (per axle)	1.941	$lbsec^2/in$
K_3	Trailer suspension spring constant	7500.	lb/in
C_3	Trailer suspension damping constant	15	lbsec/in
K_{t3}	Trailer tire spring constant	10000	lb/in
A_2	Horizontal distance from fifth wheel to trailer sprung mass center of gravity	235.581	in
B_3	Horizontal distance from leading rear axle to trailer sprung mass center of gravity	220.419	in
B_4	Horizontal distance from trailing rear axle to trailer sprung mass center of gravity	268.4	in
C_5	Fifth wheel damping constant	1000.	lbsec/in
K_5	Fifth wheel spring constant	100000.	lb/in

TABLE 7 HALF-TRACTOR SEMITRAILER STATE EQUATIONS

$$\dot{q}_1=q_{10} \qquad \dot{q}_2=q_{11} \qquad \dot{q}_3=q_{12} \qquad \dot{q}_4=q_{13} \qquad \dot{q}_5=q_{14}$$

$$\dot{q}_6=q_{15} \qquad \dot{q}_7=q_{16} \qquad \dot{q}_8=q_{17} \qquad \dot{q}_9=q_{18}$$

$$\dot{q}_{10}=\{-q_1(K_1+2K_2+K_5)+q_2(K_5B_5-K_1A_1+K_2(B_1+B_2))+q_3(K_5)+q_4(K_5A_2)$$
$$+q_5(K_1)+q_6(K_2)+q_7(K_2)-q_{10}(C_1+2C_2+C_5)+q_{11}(C_5B_5-C_1A_1+C_2(B_1+B_2))$$
$$+q_{12}(C_5)+q_{13}(C_5A_2)+q_{14}(C_1)+q_{15}(C_2)+q_{16}(C_2)\}/M_{s1}$$

$$\dot{q}_{11}=-\{q_1(K_1A_1-K_2(B_1+B_2)-K_5B_5)+q_2(K_1A_1^2+K_2(B_1^2+B_2^2)+K_5B_5^2)$$
$$+q_3(K_5B_5)+q_4(K_5B_5A_2)-q_5(K_1A_1)+q_6(K_2B_1)-q_7(K_2B_2)$$
$$+q_{10}(C_1A_1-C_2(B_1+B_2)-C_5B_5)+q_{11}(A_1C_1+C_2(B_1^2+B_2^2)+C_5B_5^2)$$
$$+q_{12}(C_5B_5)+q_{13}(C_5B_5A_2)-q_{14}(C_1A_1)+q_{15}(C_2B_1)+q_{16}(C_2B_2)\}/I_{y1}$$

$$\dot{q}_{12}=\{q_1(K_5)-q_2(K_5B_5)-q_3(K_5+2K_3)+q_4(K_3(B_3+B_4)-K_5A_5)+q_8(K_3)$$
$$+q_9(K_3)+q_{10}(C_5)-q_{11}(C_5B_5)-q_{12}(C_5+2C_3)+q_{13}(C_3(B_3+B_4)-C_5A_2)$$
$$+q_{17}(C_3)+q_{18}(C_3)\}/M_{s2}$$

$$\dot{q}_{13}=-\{-q_1(K_5A_2)+q_2(K_5A_2B_5)+q_3(K_5A_2-K_3(B_3+B_4))+q_4(K_5A_2^2$$
$$+K_3(B_3^2+B_4^2))+q_8(K_3B_3)+q_9(K_3B_4)-q_{10}(C_5A_2)+q_{11}(C_5A_2B_5)+q_{12}(C_5A_2$$
$$-C_3(B_3+B_4))+q_{13}(C_5A_2^2+C_3(B_3^2+B_4^2))+q_{17}(C_3B_3)+q_{18}(C_3B_4)\}/I_{y2}$$

$$\dot{q}_{14}=\{q_1K_1+q_2(K_1A_1)-q_5(K_1+K_{t1})+q_{10}C_1+q_{11}(C_1A_1)-q_{14}C_1+u_1K_{t1}\}/M_{u1}$$

$$\dot{q}_{15}=\{q_1K_2-q_2(K_2B_1)-q_6(K_2+K_{t2})+q_{10}C_2-q_{11}(C_2B_1)-q_{15}C_2+u_2K_{t2}\}/M_{u2}$$

$$\dot{q}_{16}=\{q_1K_2-q_2(K_2B_2)-q_7(K_2+K_{t2})+q_{10}C_2-q_{11}(C_2B_2)-q_{16}C_2+u_3K_{t2}\}/M_{u2}$$

$$\dot{q}_{17}=\{q_3K_3-q_4(K_3B_3)-q_8(K_3+K_{t3})+q_{12}C_3-q_{13}(C_3B_3)-q_{17}C_3+u_4K_{t3}\}/M_{u3}$$

where:

q_1 = Vertical displacement of tractor sprung mass

q_2 = Pitch angular displacement of tractor sprung mass

q_3 = Vertical displacement of trailer sprung mass

q_4 = Pitch angular displacement of trailer sprung mass

q_5 = Vertical displacement of tractor front unsprung mass

q_6 = Vertical displacement of tractor leading tandem axle

q_7 = Vertical displacement of tractor trailing tandem axle

q_8 = Vertical displacement of trailer leading tandem axle

(*continued on next page*)

TABLE 7 (*continued*)

q_9 = Vertical displacement of trailer trailing tandem axle
q_{10} = Vertical velocity of tractor sprung mass
q_{11} = Pitch angular velocity of tractor sprung mass
q_{12} = Vertical velocity of trailer sprung mass
q_{13} = Pitch angular velocity of trailer sprung mass
q_{14} = Vertical velocity of tractor front unsprung mass
q_{15} = Vertical velocity of tractor leading tandem axle
q_{16} = Vertical velocity of tractor trailing tandem axle
q_{17} = Vertical velocity of trailer leading tandem axle
q_{18} = Vertical velocity of trailer trailer tandem axle
u_1 = Vertical road displacement under tractor front wheel
u_2 = Vertical road displacement under tractor leading rear wheel
u_3 = Vertical road displacement under tractor trailing rear wheel
u_4 = Vertical road displacement under trailer leading wheel
u_5 = Vertical road displacement under trailer trailing wheel

ported by the front axle. The second approach uses the rear axle suspension parameters and half of the actual unsprung mass supported by the rear axle.

COMPUTER SIMULATIONS

A Fortran simulation routine was written for an IBM XT or compatible personal computer. To perform the different tasks involved in digital simulation, the program was divided into several subroutines. An integration subroutine performed the numerical integration of the state equations. For this study a constant time step, fourth-order, Runga-Kutta algorithm was used (*7*). State equation subroutines were created for each model so that the desired model could be selected when the program was compiled. An input subroutine defined the different road profiles. All subroutines were controlled by a main program that allowed the user to specify the simulation start time, end time, output interval, and time step.

As with any digital computer simulation, the integration time step must be selected carefully. A large time step can cause the results to be inaccurate and often unstable. A small time step causes the simulation program to use excessive computer time. The time step selection involves a compromise between speed and accuracy. The time step also depends on the vehicle parameters and the type of input used. Considerable care must be taken when selecting the time step for a fixed time step integration algorithm. A variable time step can achieve good results with a minimum of computer time.

APPLICATIONS

The primary application of these three truck models is to predict both ride comfort and dynamic pavement loading. Ride comfort is often determined from the vertical acceleration of the sprung mass. Using the models, acceleration frequency response and root mean square (RMS) acceleration can be calculated. Tire force frequency responses and dynamic impact factors (DIFs) can be determined to predict pavement loading.

The truck models were tested using two types of road profiles. A sinusoidal road profile was used to determine frequency responses. Actual road profiles were used to calculate RMS acceleration and DIF.

The sinusoidal road profile used in this study is defined by

$$U_i(t) = (.1 \text{ inch}) \sin (2 \pi f (t - t_{di})) \quad (1)$$

where

U_i = road elevation under wheel i (in.),
f = frequency (Hz),
t = time (sec), and
t_{di} = time delay between axles (sec).

Simulations were run using frequencies between 0 and 25 Hz and a vehicle velocity of 60 ft/sec. The resulting steady-state amplitudes were plotted as a function of frequency to obtain a frequency response plot. Transfer functions were used for the quarter-truck model.

The road profile used in this study is shown in Figure 4.

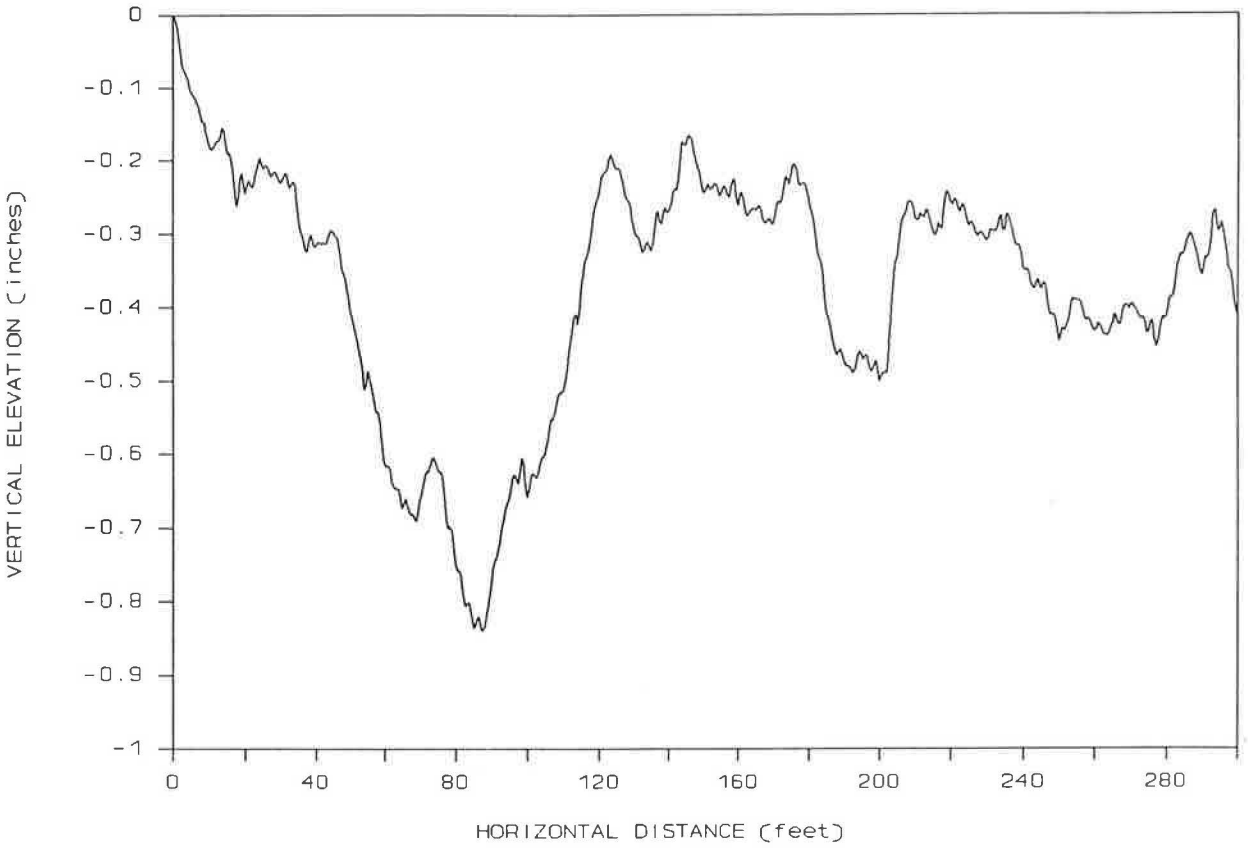

FIGURE 4 Road profile.

This profile is from a medium-roughness road having a quarter-car roughness index of 105 in./mile. The RMS acceleration is calculated from Equation 2. The DIF is calculated from Equation 3.

$$\text{RMS} = \left[\left(\frac{1}{N}\sum_{i=1}^{N} a_i^2\right)\right]^{1/2} \tag{2}$$

where

RMS = root mean square acceleration,
N = total number of data points, and
a_i = acceleration at ith time step.

$$DIF = \left(\{[\sum_{i=1}^{N} (F_i - F)^2]/[(N - 1) * F^2]\}\right)^{1/2} \tag{3}$$

where

DIF = dynamic impact factor,
F_i = tire force at ith time step,
N = total number of data points, and
F = mean tire force.

RESULTS

Ride Comfort

The sprung mass, vertical acceleration frequency responses for each model are shown in Figures 5 through 7. Comparison of Figures 5 and 6 shows the vertical acceleration frequency response of the quarter-truck model using the front axle parameters to be similar to frequency response of the half-single-unit truck model. The resonant peaks predicted by the quarter-truck model occur at similar frequencies but have different amplitudes than those of the half-single-unit truck model.

The RMS vertical accelerations for each model, calculated using the actual road profile, came to 13.35 for the quarter-truck (front axle); 9.01, half-single-unit truck; and 22.36, half-tractor semitrailer. The lower the RMS, the smoother the ride. As might be expected from the frequency responses, the quarter-truck model predicts a higher RMS acceleration.

Pavement Loading

The vertical tire force frequency responses for each axle of each model are shown in Figures 8 through 11. The quarter-truck model using only rear-axle parameters predicts resonant peaks near 2 and 10 Hz. The half-single-unit truck shows similar resonant peaks, but the 2-Hz peak has a larger amplitude than that of the quarter-truck model.

Table 8 lists the DIF for each model determined from the actual road profile. The lower the DIF, the less pavement loading. The quarter-truck model prediction is considerably higher than the DIF predicted by the half-single-unit truck model. Thus, the simpler model overestimates pavement

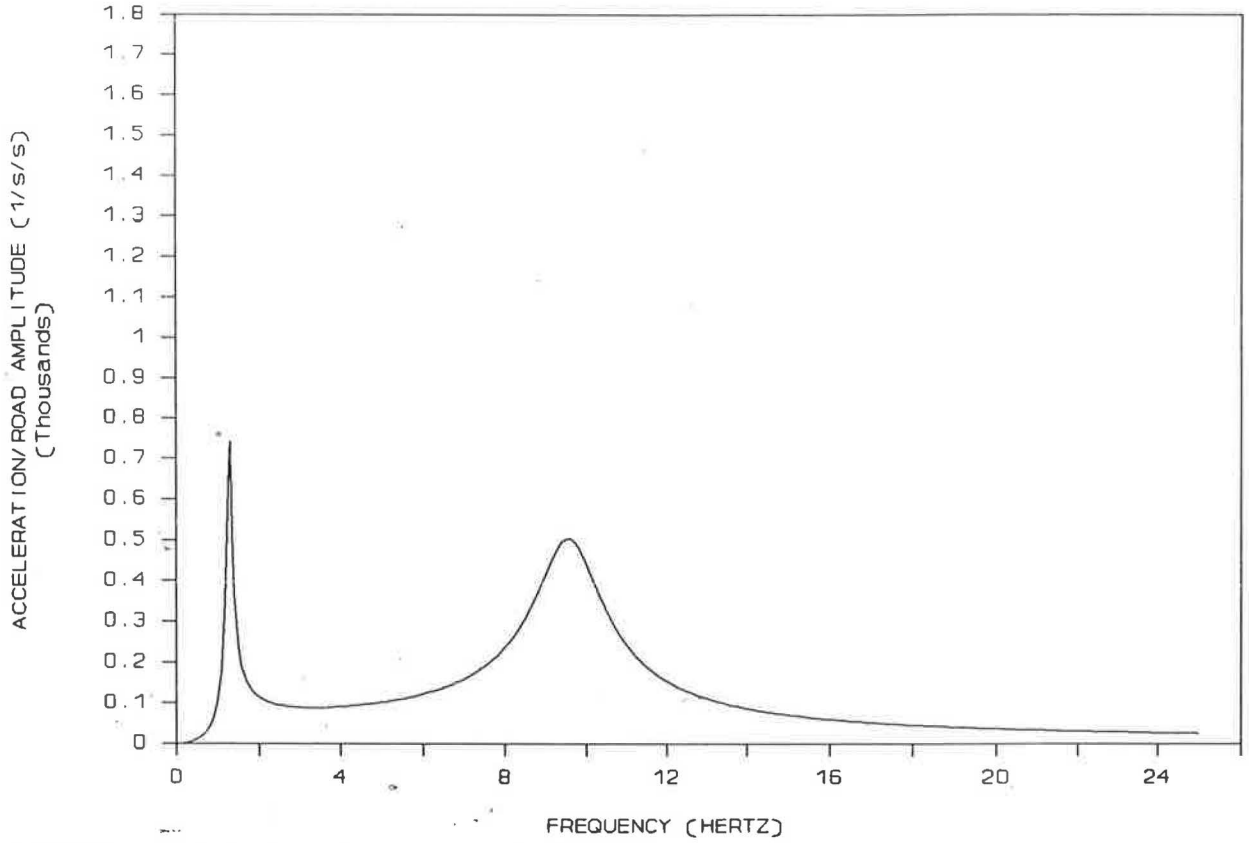

FIGURE 5 Quarter-truck model sprung mass vertical acceleration frequency response using single-unit truck front axle parameters.

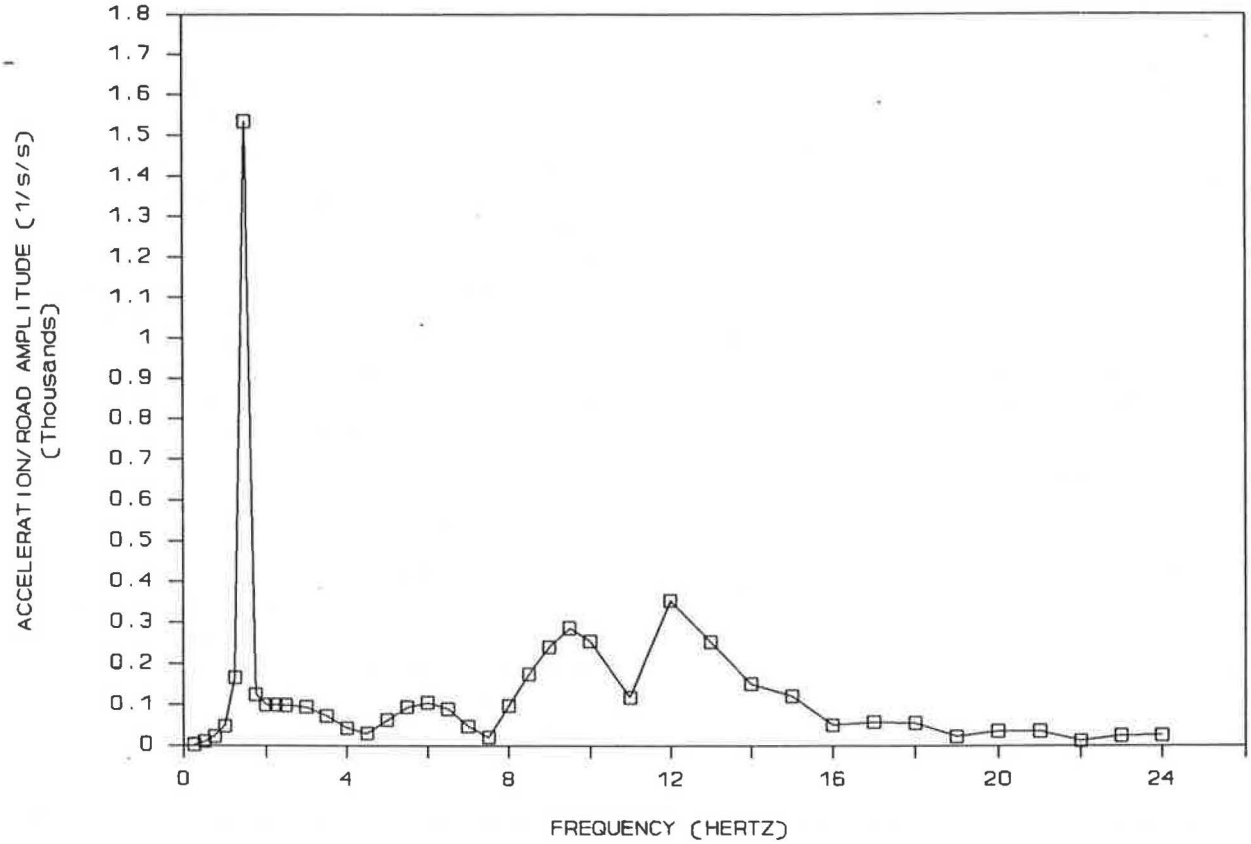

FIGURE 6 Half-single-unit truck model sprung mass vertical acceleration frequency response.

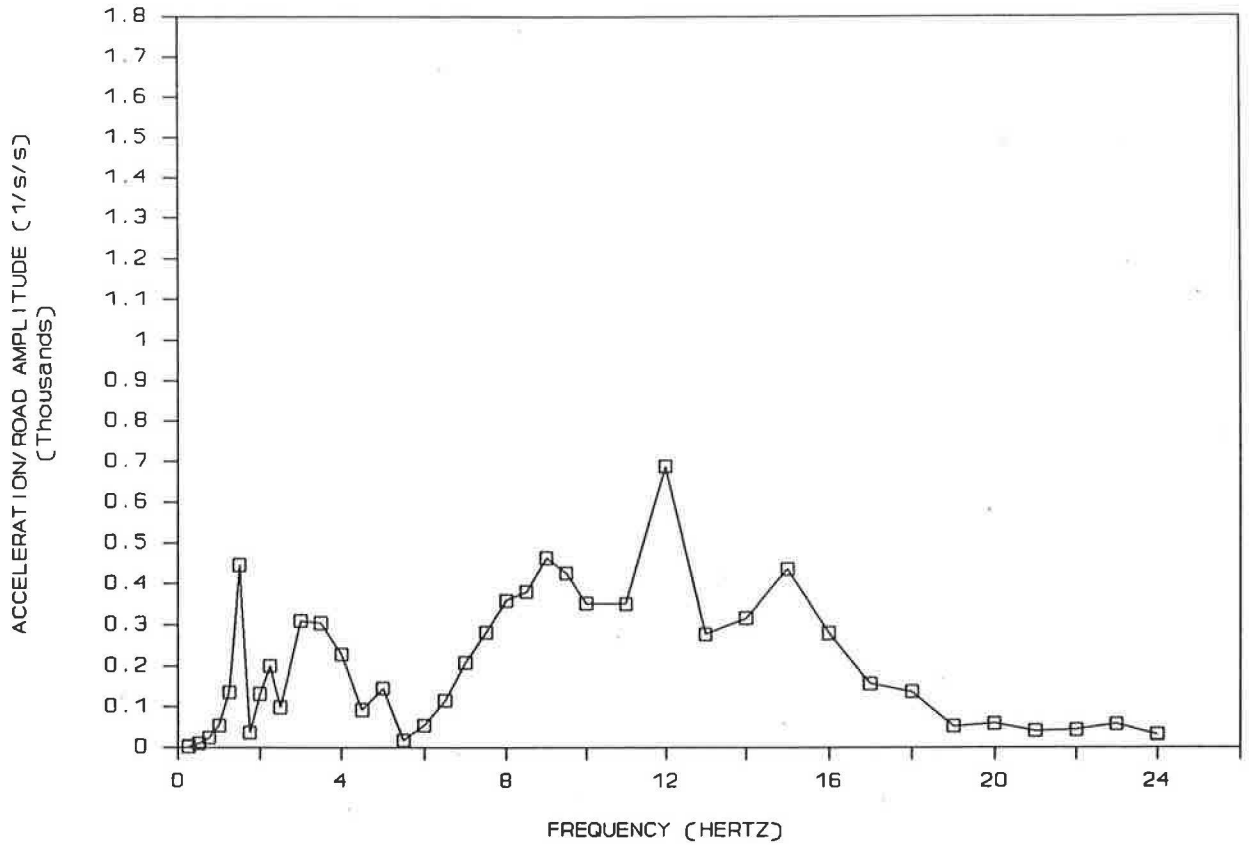

FIGURE 7 Half-tractor semitrailer model tractor sprung mass vertical acceleration frequency response.

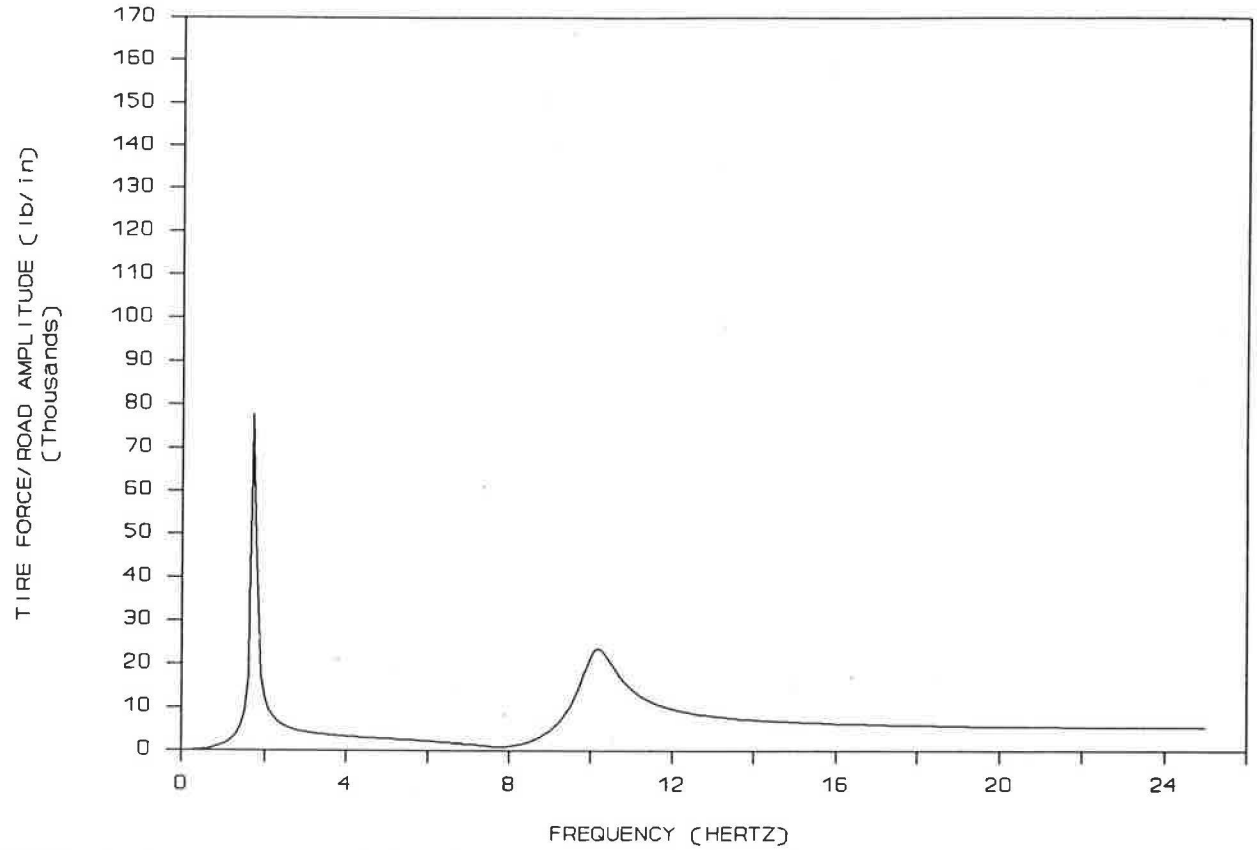

FIGURE 8 Quarter-truck model tire force frequency response using single-unit rear axle parameters.

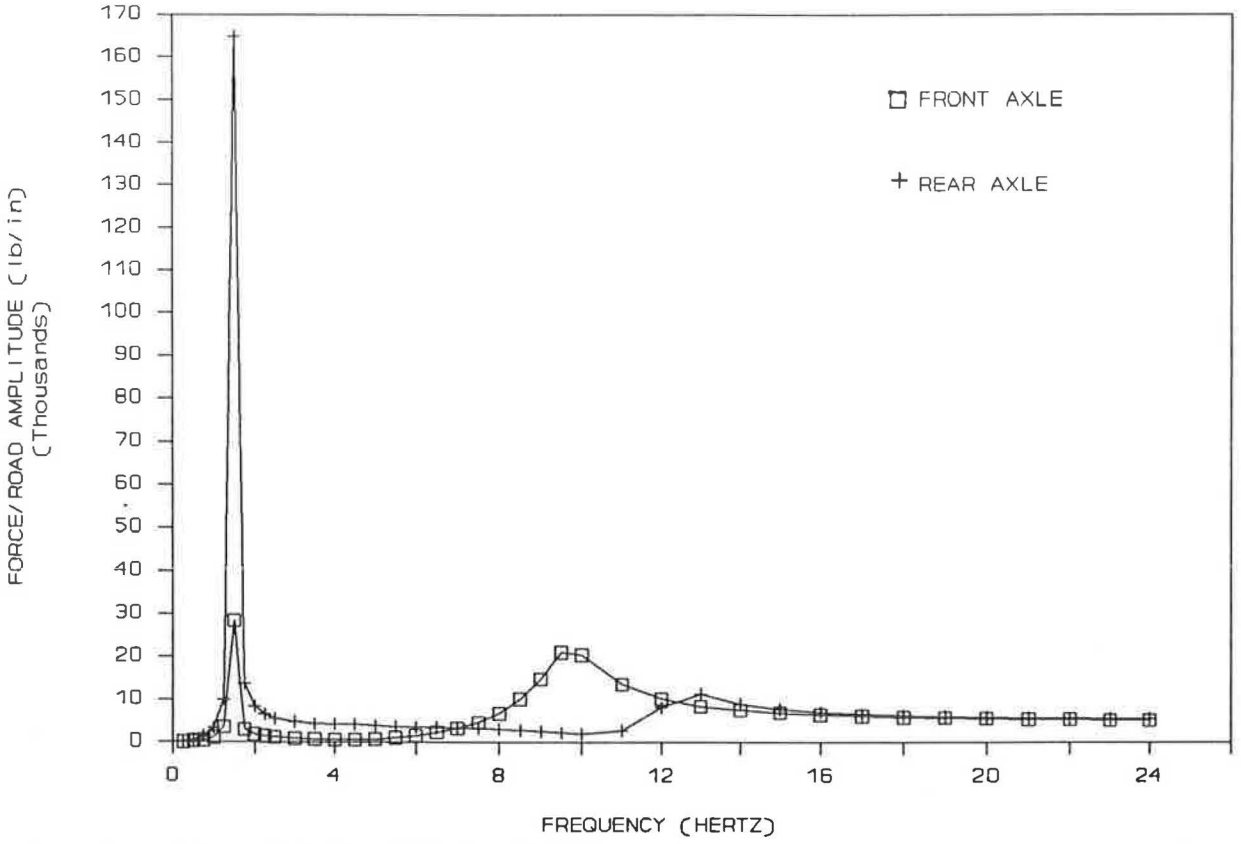

FIGURE 9 Half-single-unit truck model tire force frequency response.

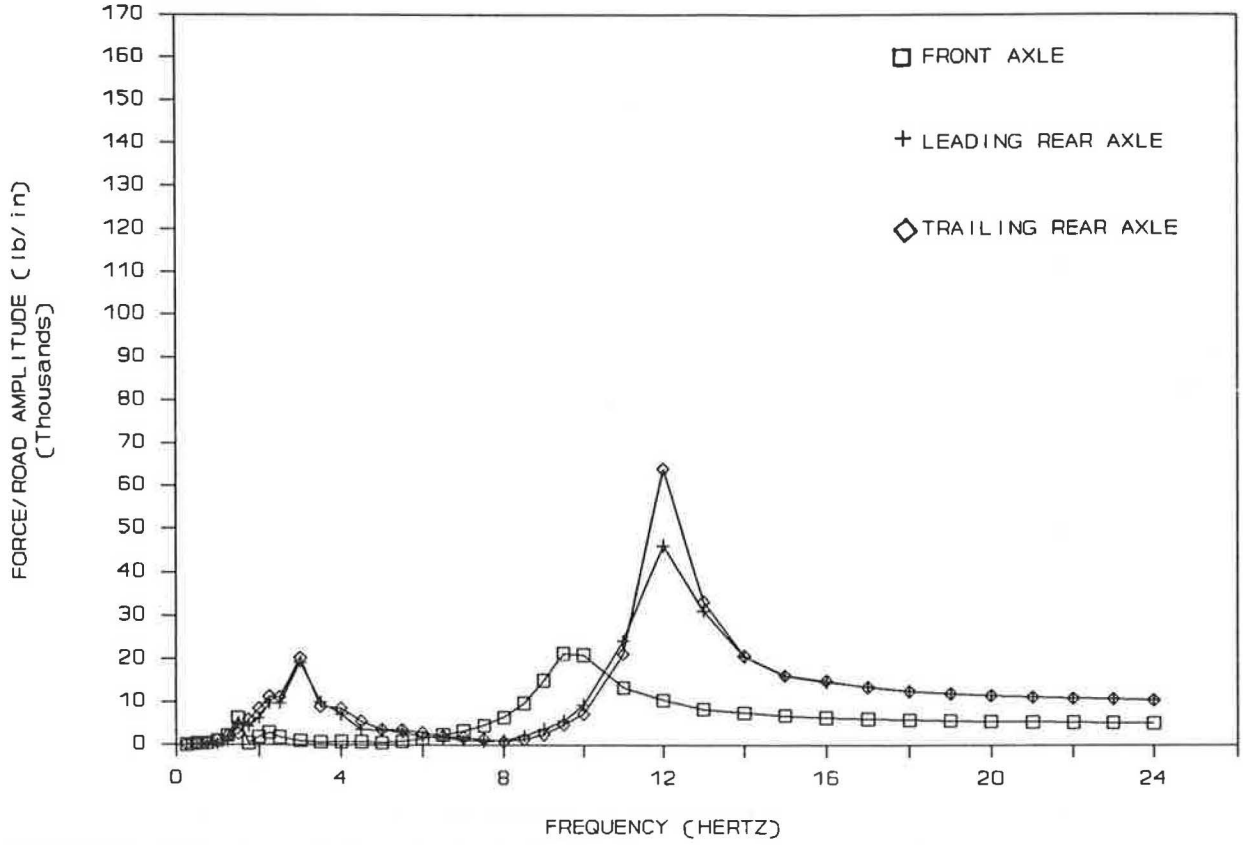

FIGURE 10 Half-tractor semitrailer model tractor tire force frequency responses.

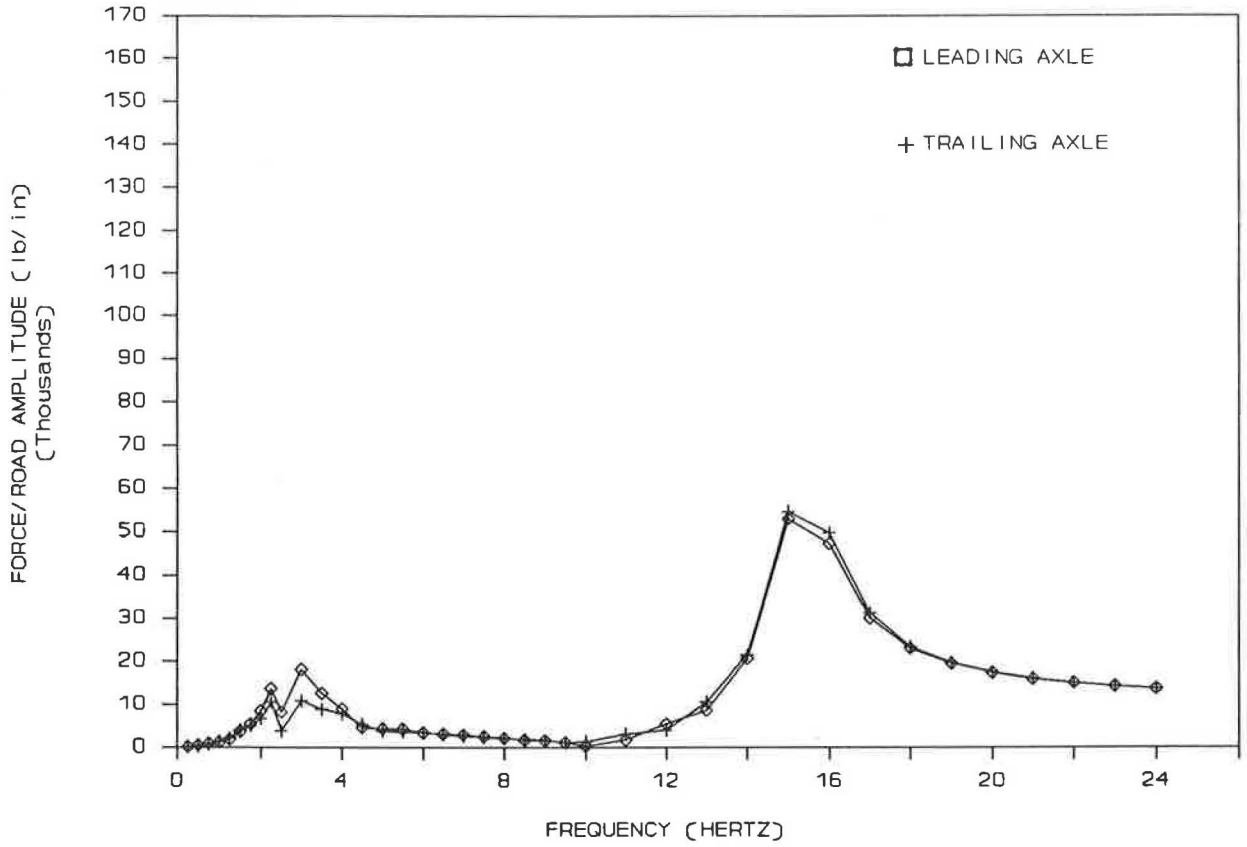

FIGURE 11 Half-tractor semitrailer model trailer tire force frequency responses.

TABLE 8 DYNAMIC IMPACT FACTORS FOR ACTUAL ROAD PROFILE

Axle Number	Quarter-Truck (Rear Axle)	Half-Single Unit Truck	Half-Tractor Semitrailer
1	.142	.030	.029
2	---	.071	.042
3	---	---	.039
4	---	---	.036
5	---	---	.035

--- Not applicable

loading, and a more complex half-truck model has to be used if more accurate results are needed.

CONCLUSIONS

Large complicated simulation programs should not be necessary for most studies concerning the vertical dynamics of heavy trucks. Simple two-dimensional truck models can be used with personal computers to predict ride quality and pavement loading. The quarter-truck model can be used as an initial estimate by selecting the parameters properly. For more accurate results that include pitching motion, the half-single-unit truck and the half-tractor semitrailer models can be used. With standardized parameter values, uniform simulations could be performed by different research groups to allow for comparison of the results of different studies.

REFERENCES

1. R. R. Hegmon. Tire-Pavement Interaction. *Public Roads*, Vol. 51, No. 1, 1987, pp. 5–11.
2. T. D. Gillespie, C. MacAdam, G. T. Hu, J. Bernard, and C. Winkler. *Truck and Tractor-Trailer Dynamic Response Simulation*. FHWA/RD-79-123,124,125,126. University of Michigan, Highway Safety Research Institute, FHWA, U.S. Department of Transportation, Washington, D.C., 1979.
3. G. Rill. Vehicle Dynamics in Real-Time Simulation. In *The Dynamics of Vehicles on Roads and Tracks*, In Proc., 10th IAVSD Symposium, Prague, 1987, pp. 337–347.
4. G. T. Hu. *Truck and Tractor Trailer Dynamic Response Simulation, T3DRS:V1*. UM-HSRI-79-38-2; FHWA/RD-78/126. University of Michigan, Highway Safety Research Institute, FHWA, U.S. Department of Transportation, Washington, D.C., 1979.
5. Standard Practice for Simulating Vehicular Response to Longitudinal Profiles of a Vehicular Traveled Surface. E1170-87. *Annual Book of ASTM Standards*, Section 4, Vol. 04.03, 1988.
6. G. S. Alves. *Computer Simulation of Truck Rollover Performance on Horizontal Curves*. Master's thesis. Pennsylvania State University, University Park, 1988.
7. J. M. Smith. *Mathematical Modeling and Digital Simulation for Engineers and Scientists*, 2nd ed. John Wiley & Sons, New York, 1987.

Publication of this paper sponsored by Committee on Surface Properties—Vehicle Interaction.

Pavement Microtexture and Its Relation to Skid Resistance

STEPHEN W. FORSTER

This paper presents the findings of a study conducted to investigate the quantitative role played by small-scale surface texture (microtexture) in determining the skid resistance of a pavement. Specific objectives were to understand better the microtexture's influence on skid resistance and to determine if optimal dimensions of microtexture exist that should be sought when designing a pavement or selecting aggregate materials. Measurements of microtexture profiles were obtained on a series of pavement cores using a noncontact image analysis system in the laboratory. Correlations were determined between these measurements and British Portable Tester numbers (BPNs), obtained on the same cores. (BPNs are friction measurements believed to be closely related to microtexture.) Finally, the microtexture measurements were combined with estimated tire-contact area measurements (representing macrotexture) and the results correlated with skid resistance measurements taken on the same pavements. Correlation coefficients of up to 0.70 were attained. Examination of the data indicates that some improvement in this correlation may be possible. It is concluded that pavement microtexture can be characterized by one profile parameter. Additionally, pavement macrotexture can be characterized by estimating the percent contact a vehicle tire would have on the pavement surface in question. A combination of these two measurements shows a good correlation with skid measurements and should be further investigated.

The skid resistance (frictional properties) of the surface of a pavement is one of the major factors in determining the overall safety of a highway. The critical aspect of skid resistance is the friction available when a pavement is wet, since almost all pavements have more than adequate friction for safe vehicle maneuvering in dry conditions. Previous studies (*1–3*) have clearly demonstrated that the friction levels developed by a pavement in contact with a given tire are largely dependent on two characteristics: surface macrotexture and surface microtexture. (See ASTM E867, Standard Definitions of Terms Relating to Traveled Surface Characteristics.)

Macrotexture is generally defined as those surface textural features that are greater than 0.5 mm in height and therefore provide a drainage system for water on the pavement surface, thus preventing a buildup of water between the tire and the pavement and resultant hydroplaning. Additionally, the macrotexture provides the hysteresis component of the tire-pavement friction—that is, the energy loss as the tire deforms around the macrotexture asperities.

Microtexture is defined as those surface features less than 0.5 mm in height. Its role in friction development is to penetrate the thin water film present on a wet pavement so that intimate tire-pavement contact is maintained.

Pavements Division, HNR-20, Office of Engineering and Highway Operations R&D, Federal Highway Administration, 6300 Georgetown Pike, McLean, Va. 22101.

This report summarizes work done in the second of two studies investigating the profile measurement and interpretation of aggregate and pavement surface microtexture. In the first study (*4*) microtexture profiles of coarse-sized aggregate particles (as used in British Polishing Wheel specimens) were measured to determine if a correlation exists between the profile characteristics and measurements (initial friction values and polish values [*PVs*]) obtained using the British Portable Tester (BPT). A suite of aggregates ranging from polish-susceptible to polish-resistant was examined both before and after being subjected to the British Polishing Wheel test (ASTM D3319).

The study results indicated the presence of a definite positive correlation between microtexture profiles and friction measurements made with the BPT. The correlation coefficient for all data was 0.73.

The next step in this program was to attempt to correlate microtexture profile measurements on pavement core samples with BPT measurements on those cores and full-scale skid resistance measurements taken on the same pavement section at the same time as the core sample was obtained. This was the objective of the study reported herein. Because of the influence of both scales of texture on skid resistance, the microtexture measurements on the core samples must be combined with a macrotexture measurement in order to attempt a direct correlation with the skid resistance measurements.

This study addressed two specific objectives:

1. To understand better the influence of microtexture in determining a pavement's skid resistance, and
2. To determine if optimal dimensions of microtexture exist that should be sought when choosing an aggregate for a particular application.

DATA COLLECTION

Samples

Samples used in this study were pavement cores either 6 or 8 in. (153 or 204 mm) in diameter. The 8-in. (204-mm) cores were preferred because the necessary slider path length for the BPT measurement was more easily obtained on them. The larger cores also have a greater surface area for making sand patch texture (ASTM E965) measurements. Cores were obtained from Virginia, North Carolina, New Mexico, and Nebraska, and a complete listing of the cores examined is given in Table 1. The pavements sampled included grooved

TABLE 1 PAVEMENT AND CORE INFORMATION

PAVEMENT INFORMATION			CORE INFORMATION					
No.	Description	SN40	No.	BPN	MTD (in)	Microtexture Data Av Hgt (μm)	Av Dens pks/μm	Av S.F.
1	AC overlay, gravel C.A., 3/8 max.	52	1-1	71	.018	54.5	.0025	.14
		57	1-6	77	.030	53.0	.0026	.14
		55	1-4	73	.022	50.4	.0035	.18
		55	1-2	75	.024	57.7	.0029	.17
		56	1-7	75	.031	57.5	.0032	.18
		54	1-3	76	.024	53.2	.0035	.19
2	AC overlay, gravel C.A., 3/8 max.	53	2-5	77	.058	44.9	.0029	.13
		52	2-2	69	.053	57.9	.0029	.17
		57	2-4	74	.058	53.5	.0037	.20
		55	2-7	73	.058	57.5	.0033	.19
		55	2-3	78	.058	59.1	.0032	.19
3	PCC, ungrooved.	33	3-3	65	.009	42.5	.0028	.12
		34	3-2	70	.006	40.5	.0040	.16
4	AC overlay, gravel C.A., 3/8 max.	56	4-7	71	.031	53.1	.0026	.14
		53	4-5	75	.038	53.5	.0029	.16
		55	4-3	68	.034	53.7	.0031	.16
		51	4-6	72	.030	55.8	.0032	.18
		53	4-4	75	.049	55.9	.0032	.18
		51	4-2	73	.036	52.3	.0030	.16
5	AC overlay, cr.limest.C.A. 1/2 max.	32	5-A	62	.047	51.1	.0034	.17
		32	5-B	54	.044	48.0	.0030	.15
6	AC overlay, cr.limest.C.A. 1/2 max.	37	6-1	55	.042	47.9	.0026	.13
		34	6-3	57	.044	46.8	.0026	.12
		39	6-7	59	.034	51.9	.0022	.12
7	AC overlay, cr.granite C.A., 3/8 max.	50	7-1	66	.020	47.7	.0033	.16
		49	7-5	70	.018	49.4	.0030	.15
		44	7-2	70	.017	48.8	.0033	.16
		47	7-4	64	.024	47.4	.0033	.16
		46	7-7	73	.022	47.9	.0033	.16
8	Grooved PCC	39	8-3	61	.035	39.1	.0032	.13
		39	8-2	57	.034	36.0	.0032	.12
		36	8-5	59	.032	35.7	.0034	.12
		34	8-1	56	.034	42.4	.0033	.14
		32	8-4	57	.032	43.4	.0028	.12
9	AC open grad overlay, cr.gneiss C.A.	51	9-4	72	.066	48.9	.0032	.15
		50	9-2	70	.058	46.4	.0031	.14
		52	9-6	75	.055	51.5	.0029	.15
		52	9-5	72	.060	52.0	.0028	.15
		51	9-3	72	.054	56.5	.0027	.15
		51	9-1	64	.060	51.9	.0027	.14
10	AC,cr.gneiss C.A.	45	10-2	69	.010	44.5	.0029	.13
			(79)					
		47	10-4	65	.010	48.2	.0024	.11
		39	10-3	68	.010	49.3	.0037	.18
		43	10-6	68	.010	46.2	.0037	.17
		39	10-2	68	.015	48.2	.0037	.18
			(81)					
11	AC overlay, cr.limest.C.A. 1/2 max.	38	11-4	60	.020	44.2	.0024	.11
		38	11-3	61	.025	41.8	.0030	.13
		34	11-6	63	.029	44.3	.0032	.14
		37	11-2	62	.016	44.6	.0030	.14
		36	11-1	63	.016	46.4	.0023	.13

TABLE 1 (*continued*)

No.	PAVEMENT INFORMATION Description	SN40	CORE INFORMATION No.	BPN	MTD (in)	Microtexture Data Av Hgt (μm)	Av Dens pks/μm	Av S.F.
12	AC cr.limest.	59	B5021B	66	.060	41.8	.0030	.12
13	AC sand asphalt	70	B5022A	78	.015	69.7	.0034	.24
14	AC gravel C.A.	65	B5023B	72	.026	51.7	.0032	.17
15	AC cr.limest.	72	B5024B	71	.060	41.5	.0030	.13
16	AC cr.granite-gneiss	64	B5025C	67	.031	60.9	.0036	.22
17	AC cr.quartzite	71	B5026C	63	.028	46.1	.0037	.17
18	AC cr.granite-gneiss	62	B5027C	70	.044	51.7	.0035	.18
19	AC cr.granite-gneiss	66	B5028B	78	.049	57.7	.0036	.21
20	AC cr.quartzite	62	B5029A	71	.018	60.5	.0033	.20
21	AC cr.quartzite	67	B5030A	86	.049	62.0	.0028	.17
22	AC gravel C.A.	58	B5031A	66	.044	51.6	.0035	.18
23	AC cr.limest.-gravel C.A. 3/4 - 1 max.	41	79-4	52	.016	42.2	.0025	.11
		41	79-1	48	.021	41.5	.0026	.11
		40	79-2	55	.015	43.1	.0030	.13
		44	79-3	50	.021	38.6	.0026	.10
24	AC cr.gravel 3/8 max.	32	90-1	54	.007	44.6	.0030	.14
25	AC cr.limest.-gravel	39	444-4	55	.018	41.5	.0028	.12
26	AC cr.limest.-gravel	50	382-1	61	.047	53.9	.0028	.15
27	AC cr.gravel 3/8 max.	51	x-5-3	69	.009	52.2	.0030	.15
28	AC open graded cr. gravel	52	x-1-1	65	.033	52.0	.0028	.15
29	AC open graded cr. gravel	53	x-3-4	67	.052	47.6	.0027	.13
30	AC cr. gravel 3/8 max.	45	x-1-2	64	.009	44.5	.0030	.14
31	AC open graded cr. gravel	51	x-1-3	61	.022	44.0	.0030	.13
32	AC cr.gravel 3/8 max.	51	85-2	59	.016	53.6	.0031	.16
33	AC open graded cr. gravel	48	183-2	64	.038	47.6	.0032	.15
34	AC open graded cr. gravel	48	x-7-1	64	.042	46.6	.0031	.14

(*continued on next page*)

TABLE 1 (*continued*)

No.	PAVEMENT INFORMATION Description	SN40	CORE INFORMATION No.	BPN	MTD (in)	Microtexture Data Av Hgt (μm)	Av Dens pks/μm	Av S.F.
35	AC cr. gravel 3/8 max.	52	x-6-1	68	.008	38.7	.0035	.14
36	AC cr. gravel 3/8 max.	54	x-5-2	62	.038	44.9	.0028	.13
37	AC open graded cr. limest.	38	x-4-4	49	.034	44.7	.0025	.11
38	AC open graded cr. gravel	55	x-3-2	66	.044	50.3	.0028	.14
39	AC open graded cr. gravel	51	x-2-3	63	.010	46.2	.0031	.15
40	PCC,ungrooved	34	1(30)	69	.008	48.9	.0026	.13
41	AC open graded cr.gravel	48	2(30)	66	.062	46.6	.0033	.15
42	AC open graded cr. gravel	59	3(30)	83	.055	52.8	.0041	.22
43	PCC,ungrooved	43	4(30)	73	.008	48.6	.0025	.12
44	AC open graded cr limest.	28	5(30)	48	.062	44.1	.0021	.09
45	AC cr. gravel 1/2 max.	11	6(30)	48	.010	32.1	.0027	.09

Key to abbreviations:
AC = asphaltic concrete
PCC = portland cement concrete
C.A. = coarse aggregate
cr. = crushed
[3/8] max. = maximum size of coarse aggregate, inches

and ungrooved portland cement concrete (PCC) as well as dense- and open-graded asphaltic pavements. They were of various ages and had been subject to a range of traffic and environmental conditions.

Measurement Procedures

In an initial series of measurements, the microtexture of all features encountered on the test surfaces was measured. To perform these microtexture measurements, the first step is to apply a thin, white opaque coating to the sample surface so that, when the surface is illuminated, the light is uniformly reflected from it and does not penetrate it. The sample is then mounted on the viewing stage, and a semicircle of light is projected onto it at a 45° angle. The straight side of this semicircle is sharply focused on the sample. Where this straight edge hits the sample's surface, it produces a profile that, when viewed from above, duplicates a vertical profile through the sample because of the incidence angle and viewing angle. The profile image is gathered by a microscope attached to a television camera for transmitting the profile to the viewing screen for measurement and analysis (see Figure 1). A typical microtextural profile is shown in Figure 2.

Profile Parameters

The profiles are characterized using those parameters developed in the earlier study (*4*). Two parameters are measured directly, and a third is derived from these two. The average asperity (peak) height is defined as the sum of the vertical heights (above the "valley" immediately to the right of each asperity) of all asperities divided by the total number of asperities (see Figure 3). The average asperity density is the total number of asperities divided by the profile length. The average shape factor (SF), which is the derived parameter, is calculated by multiplying the asperity height by the asperity density. Since asperity density, as defined here, closely approximates the inverse of asperity width, SF approximates

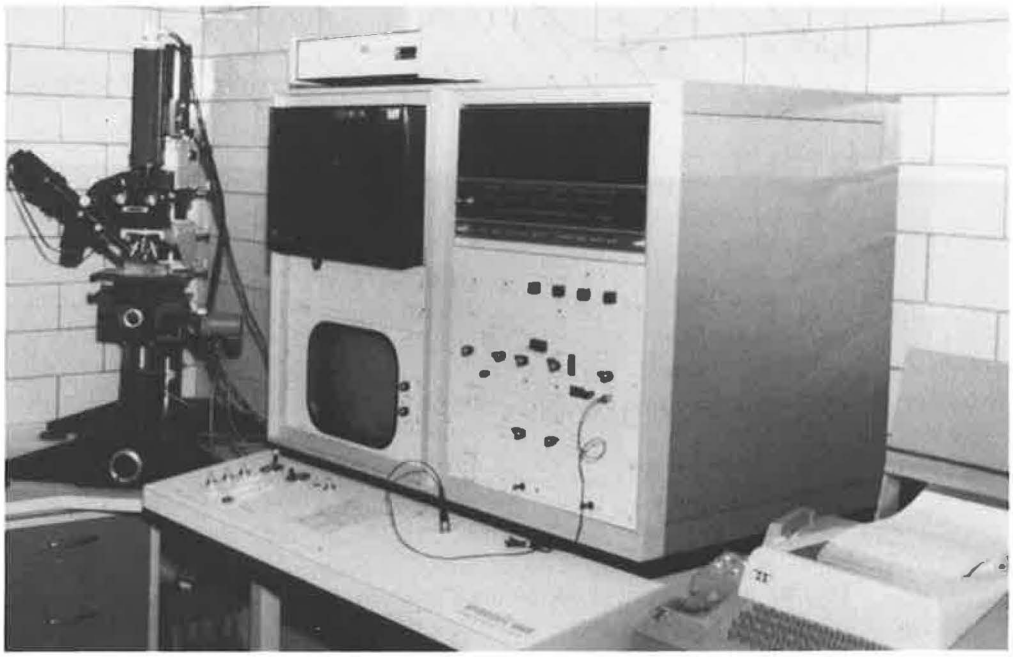

FIGURE 1 Image analysis system used for microtexture measurements.

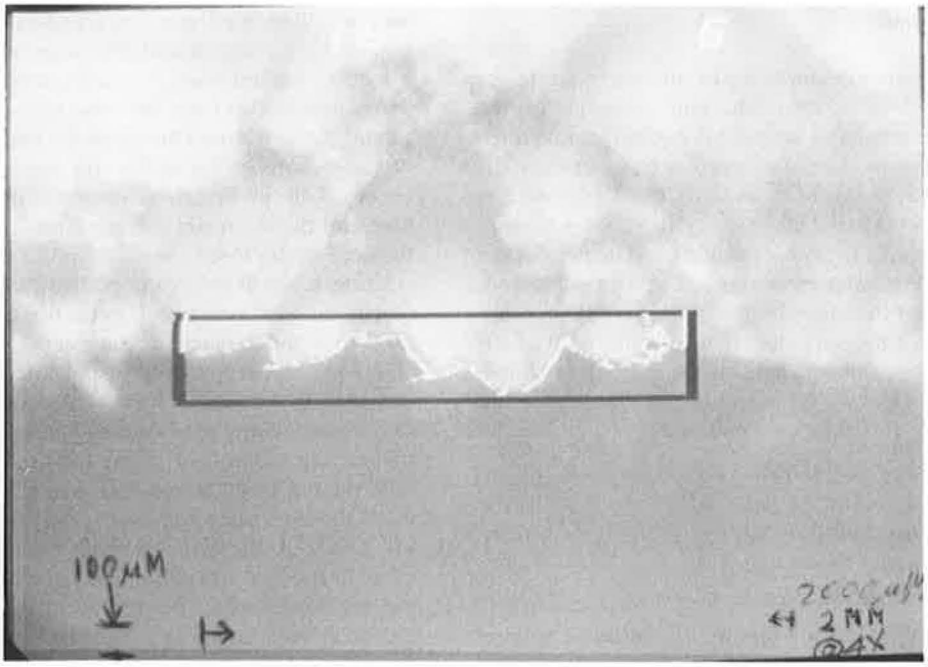

FIGURE 2 Typical microtextural profile on pavement sample.

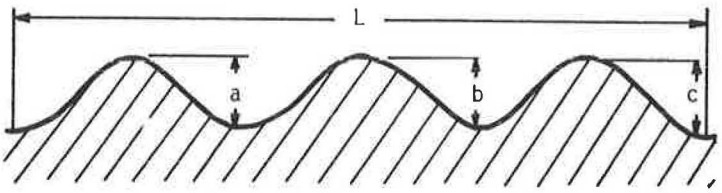

$$\text{Average asperity density} = \frac{\text{count of peaks}}{\text{length of profile}} = \frac{3}{L}$$

$$\text{Average asperity height} = \frac{\text{sum of heights}}{\text{counts}} = \frac{a+b+c}{3}$$

$$\text{Average shape factor} = \frac{\text{average height}}{\text{average width}} = \frac{\frac{a+b+c}{3}}{\frac{L}{3}}$$

FIGURE 3 Definitions of microtextural parameters.

an average height-to-width ratio for the asperities measured. Experimentation indicated that 100 profiles, each approximately 2 mm long, are sufficient to characterize the microtexture of a sample.

Parameter Significance

As already noted, microtextural peaks are necessary under wet conditions for penetration of the thin water film on the surface, thereby maintaining intimate tire-pavement contact. Optimal peak height has been theorized as being in the 0.01- to 0.1-mm range (*2*, p.32). Microasperity density or spacing is also important because it determines the adhesion component of a pavement's frictional properties. The greater the asperity density, the greater the number of contact points and, therefore, the higher the tire adhesion to the pavement. Since the shape factor is a measure of height-to-width ratio of the asperities, larger shape factors indicate sharper, more closely spaced asperities, which in turn tend to promote better tire adhesion to the pavement in wet conditions.

DATA ANALYSIS

Microtexture and BPNs

After the measuring procedure had been finalized, a total of 87 cores were measured for microtexture, macrotexture (sand patch), and British Portable Tester numbers (BPNs). The first correlations investigated were between the average shape factors (SFs) and BPNs, which are believed to indicate the friction of a surface due mainly to microtexture. The plot of these values is shown in Figure 4.

A linear regression fit of these data yielded a correlation coefficient of .68. Compared with the results of the previous study, this coefficient is somewhat low; therefore, reasons were sought for the discrepancy. Since these specimens were all cores from pavement surfaces that were in service, they had been subject to traffic. It was hypothesized that in samples with substantial macrotexture, portions of the surface would never be in contact with the vehicle tires and that these portions would neither have any effect on the microtextural portion of the measured skid resistance of the pavement nor be subject to the polishing action of traffic (see Figure 5). It was therefore theorized that the areas of contact would have measurably lower microtexture than the noncontact areas, because of this polishing. To define the areas that would come in contact with the tire on each specimen, first a typical vehicle load and tire footprint were used to calculate pressure over the area of the footprint.

Using 1,000 lb as a conservative (high) estimate of a passenger car load per wheel and a tire contact area of 48 in.^{2} (.031 m^2), the contact pressure equals approximately 20 psi (137.9 kPa). A rectangular piece of ASTME501 rubber, 3 in. × 1 in. (76 × 25 mm), was used to simulate the tire rubber. The white coating (as described earlier) was applied to the rubber; then, before it dried, the rubber was placed on the core surface being tested and loaded with a 60-lb (27.3-kg) mass, thereby producing 20 psi (137.9 kPa). When the rubber was removed, the areas of contact with the core were delineated by the paint transfer (see Figure 6). Nineteen cores with the contact areas so defined were then used to conduct a second series of microtexture. The results of these measurements were called SF_c (shape factor on contact area) and were plotted versus the BPNs. This plot is shown in Figure 7, and it has a linear regression correlation coefficient of only 0.45. The data points (SF vs. BPN) for these 19 cores from the original 87-point database already discussed had a correlation coefficient of 0.56, as shown in Figure 8. The data for these cores are shown in Table 2. The approach of measuring microtexture only on the contact area therefore unexpectedly

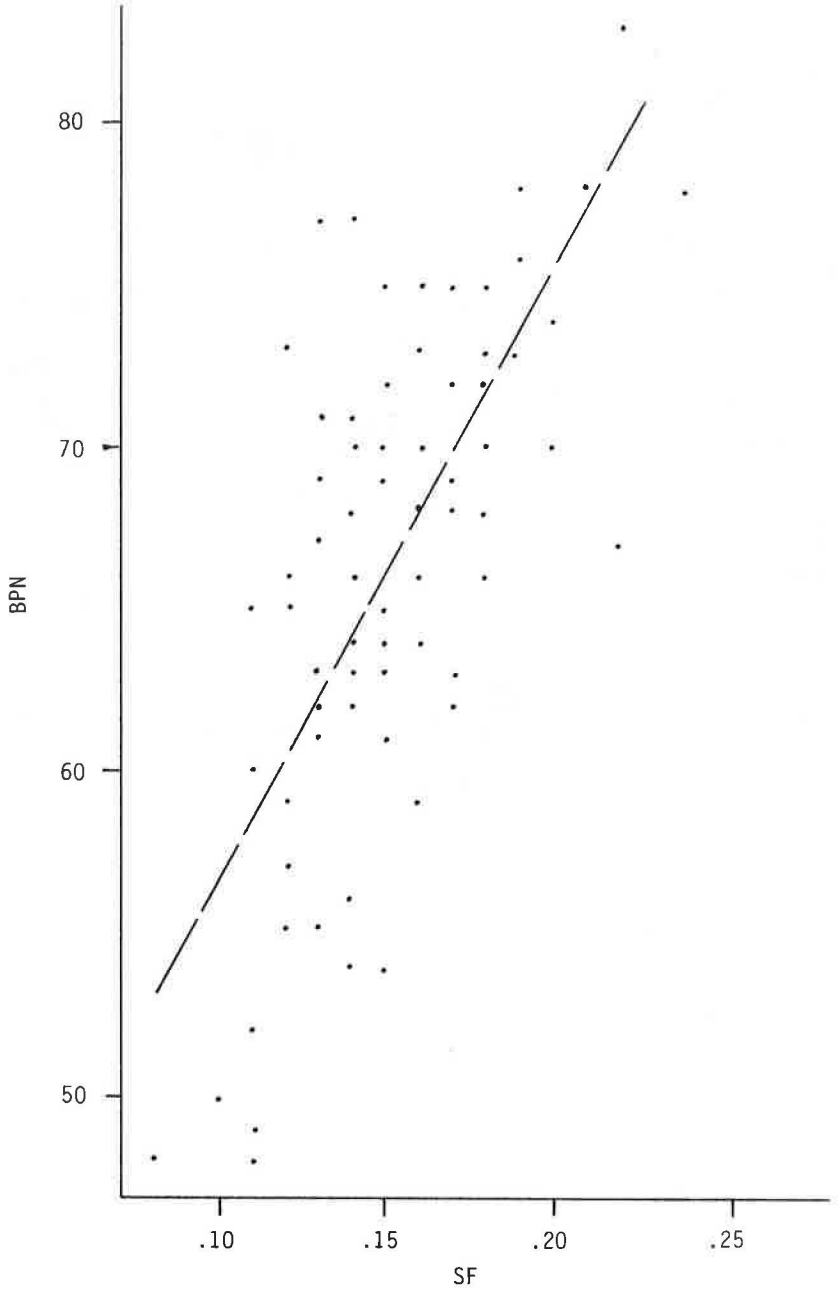

FIGURE 4 Plot of BPN versus SF for eighty-seven cores examined.

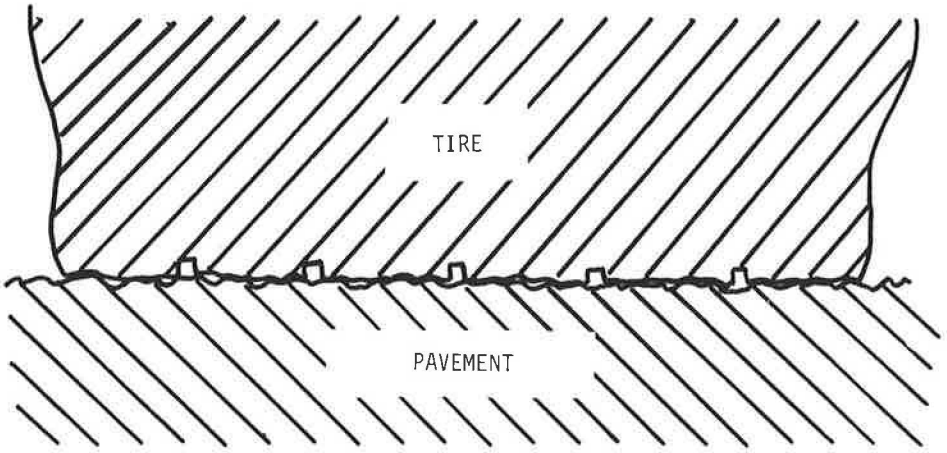

FIGURE 5 Cross section through tire/pavement contact area.

FIGURE 6 Photograph of three cores showing their contact areas.

appeared to worsen the relationship, even though the contact microtexture was, as predicted, in most cases measurably lower than the noncontact microtexture (see Table 2).

Another aspect of the contact area that might influence the correlation between SF and BPNs was therefore considered next. In defining the contact area by means of the coating transfer technique already described, it quickly became obvious that the actual contact area as a percent of the total footprint area could vary over a substantial range. This variation depends directly on the amount of macrotexture present at the pavement surface. It follows that the BPN obtained on the surface (and also the skid resistance) should vary with this variation in contact area.

For asphalt pavements, there are several possible reasons for this macrotexture (and therefore contact area) variation. The first and primary reason is the gradation of the aggregate used in the mix. At one extreme is an open-graded asphalt friction coarse (OGAFC) that has a very open gradation; consequently, the surface consists of nearly all coarse aggregate. At least initially, vehicle tires are riding only on the upper portion of these coarse aggregate particles, leaving some portion of the road surface that never comes in contact with the tires. At the other extreme are the sand-asphalt mixes that have no coarse aggregate and, consequently, virtually no macrotexture. As a result, tire contact is virtually 100 percent. Dense-graded asphalt mixes are all between these two extremes. Their contact area may be nearly as low as an OGAFC or as high as a sand asphalt mix, depending on the particular gradation of the aggregate used as well as the percent asphalt. The contact area may increase with age as the pavement becomes denser under traffic or as the macrotexture is worn away.

For PCC pavements, the situation is quite different. Initial macrotexture (and therefore contact area) is basically dependent on the finish applied to the new concrete, since coarse aggregate is not exposed. This texture is usually a result of some combination of burlap or turf drag plus tining. With time and traffic, this imposed texture wears off, resulting in less macrotexture and greater contact. If surface wear is sufficient to expose the coarse aggregate in the concrete, the macrotexture could conceivably begin to increase again and therefore decrease the contact area. Several rehabilitative methods used on concrete pavements also significantly alter the macrotexture. These are grooving, grinding, and milling. Again, these textures will wear off with time and traffic.

To include contact area percentage in the correlation, the SF_c (obtained on the area of contact) was divided by the percent contact area (CA) and the result multiplied by 1,000. This series of values is plotted in Figure 9 versus the BPNs. The correlation coefficient was improved to 0.62 by this factor.

Since one of the purposes of the study was to attempt correlation of microtexture measurements with skid resistance measurements, that subject was addressed next and no further correlation with BPNs was attempted. That is, the objective was to improve on BPN as a measure of microtexture, not to duplicate it.

Texture vs. Skid Measurements

To estimate skid resistance (as measured in ASTM E274) from texture, it is generally agreed that measures of both microtexture and macrotexture must be included. The SF_c, as described earlier, therefore would have to be combined with some measure of macrotexture before attempting correlation with skid numbers (SNs). In previous research (*2,3*), workers have often suggested combining BPNs (microtexture) and sand

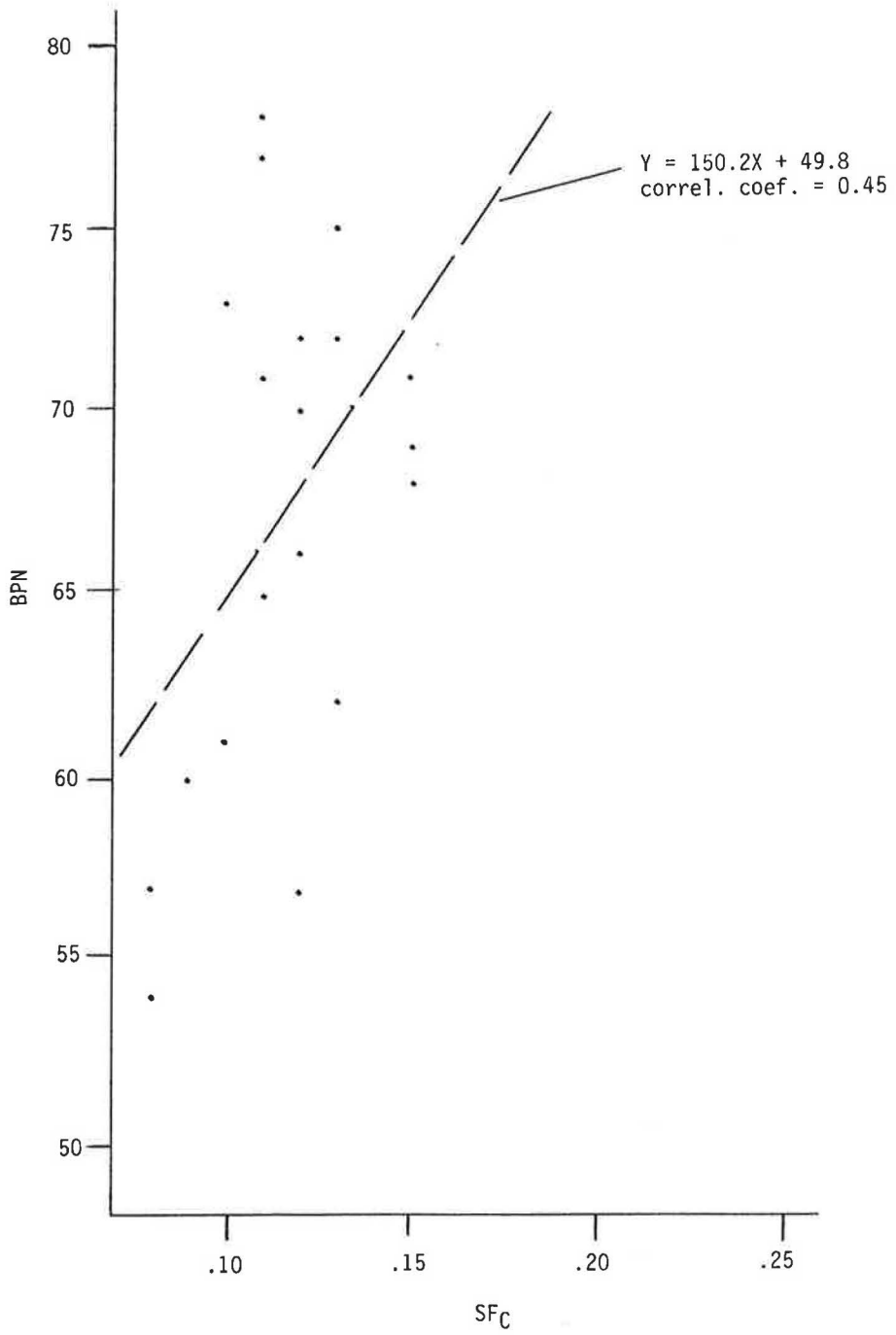

FIGURE 7 Plot of BPN versus SF_c for nineteen cores listed in Table 2.

patch (macrotexture) in an equation to predict SN values. In the course of the comparison study of BPNs and SF_cs, the CAs were compared with mean texture depths (MTDs) as measured by the sand patch method (ASTM E965-83). An inverse relationship was noted, as shown in Figure 10. It was therefore theorized that the SF_c and CA combination might hold promise as a representation of macrotexture and microtexture for correlation with SNs. SN_{40} values were available for the pavements from which the cores used in this study were taken. The schedules of skid tests and coring operations were coordinated to ensure that the surfaces of the cores taken were the same, as nearly as possible, as the surfaces on which the SNs were obtained. Linear regressions were made for SN_{40} values versus various combinations of SF_c and CA for the 19 cores already discussed. The best correlation was obtained between SN_{40} and $(SF_c \times 1{,}000)/CA$. These data are plotted in Figure 11. The resulting correlation coefficient is 0.70. With SN_{40} as the dependent variable, the equation is:

$$SN_{40} = 18.6 \frac{(SF_c \times 1{,}000)}{CA} + 12.6 \quad (1)$$

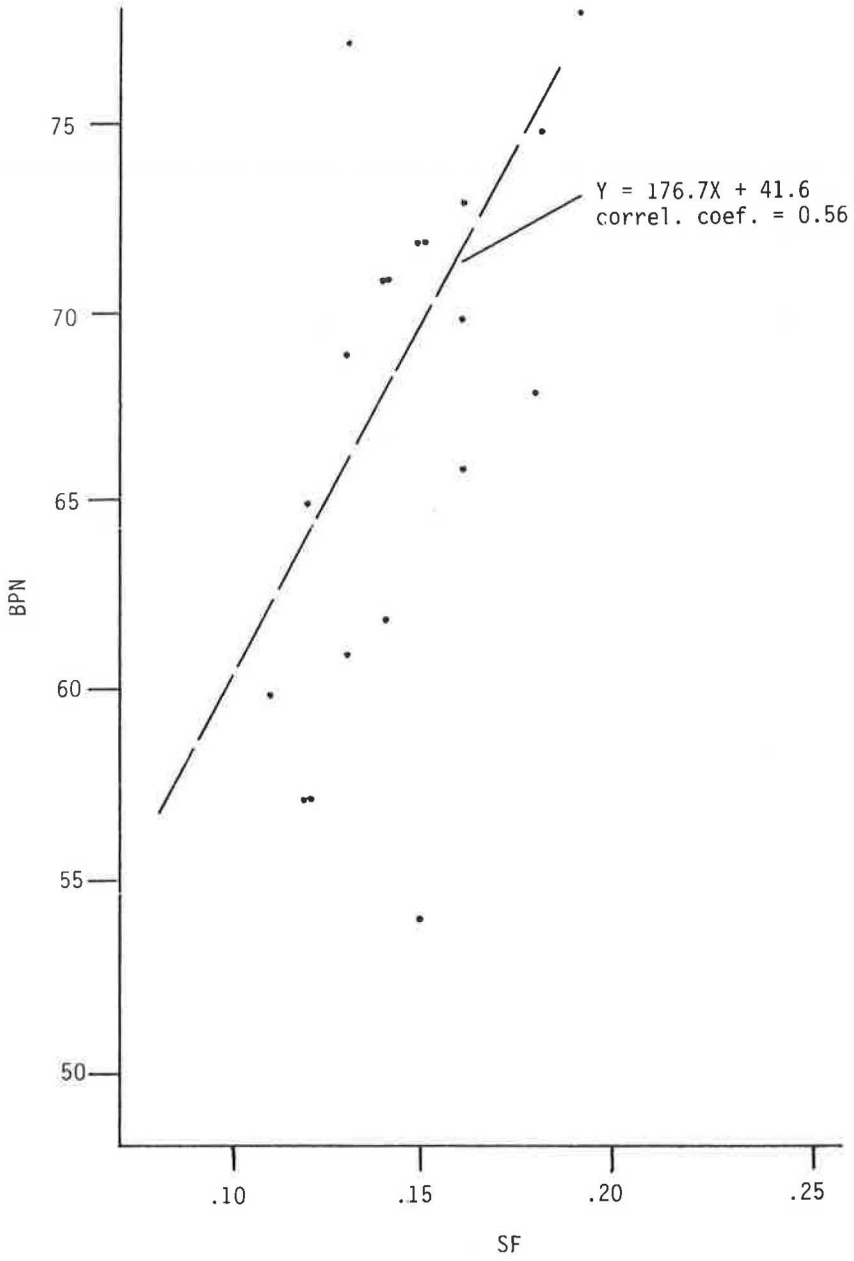

FIGURE 8 Plot of BPN versus SF for nineteen cores listed in Table 2.

Let TXT = overall (microtexture and macrotexture) texture measurement =

$$\frac{SF_c \times 1{,}000}{CA}$$

therefore,

$$SN_{40} = 18.6\ TXT + 12.6 \quad (2)$$

Outliers were examined in an attempt to explain why they did not fit the equation more closely. As can be seen in Figure 11, samples 8-4, 6-3, and 5-B are particularly far off the line. Without these three, the correlation coefficient jumps to 0.89. Sample 8-4 is one of three PCC pavement samples included in this set of 19 (the others being 3-3 and 8-3). The 8-series samples were taken from a longitudinally grooved pavement, 8-3 in November and 8-4 in January. Sample 8-3 is much closer to the best-fit line, mainly because of a higher SN_{40}

Seasonal variation of SN could account for the difference, except that the November core is high (SN_{40} = 39) and the January core is low (SN_{40} = 32), just the opposite of the expected trend. Differences in BPN values (57 vs. 61) and MTD (.032 vs. .035 in.; .81 vs. .89 mm) are not enough to account for the difference in SN_{40}. The TXT value for the two cores varies inversely with the SN_{40} values. The other PCC core, 3-3, like 8-3, is quite close to the best-fit line and is from an ungrooved pavement. Reruns of 8-4 gave results quite close to the first run, which validated the original SF_c

TABLE 2 DATA ON THE SUBJECT OF NINETEEN CORES

Core No.	SN40	Core Measurements					
		BPN	MTD (in)	SF	SFc	C.A. (%)	TXT
5-B	32	54	.044	.15	.08	24	1.83
8-4	32	57	.032	.12	.12	47	1.59
3-3	33	65	.009	.12	.11	77	1.20
6-3	34	57	.044	.12	.08	25	1.79
11-2	37	62	.016	.14	.13	59	1.49
11-4	38	60	.020	.11	.09	46	1.41
8-3	39	61	.035	.13	.10	61	1.27
10-2(81)	39	68	.015	.18	.15	76	1.40
7-2	44	70	.017	.16	.12	51	1.55
10-2(79)	45	69	.010	.13	.15	58	1.60
7-1	50	66	.020	.16	.12	51	1.55
9-4	51	72	.066	.15	.12	32	1.93
4-2	51	73	.036	.16	.10	23	2.07
1-1	52	71	.018	.14	.15	43	1.86
9-5	52	72	.060	.15	.13	34	1.94
2-5	53	77	.058	.13	.11	26	2.04
2-3	55	78	.058	.19	.11	19	2.41
4-7	56	71	.031	.14	.11	30	1.91
1-7	56	75	.031	.18	.13	28	2.16

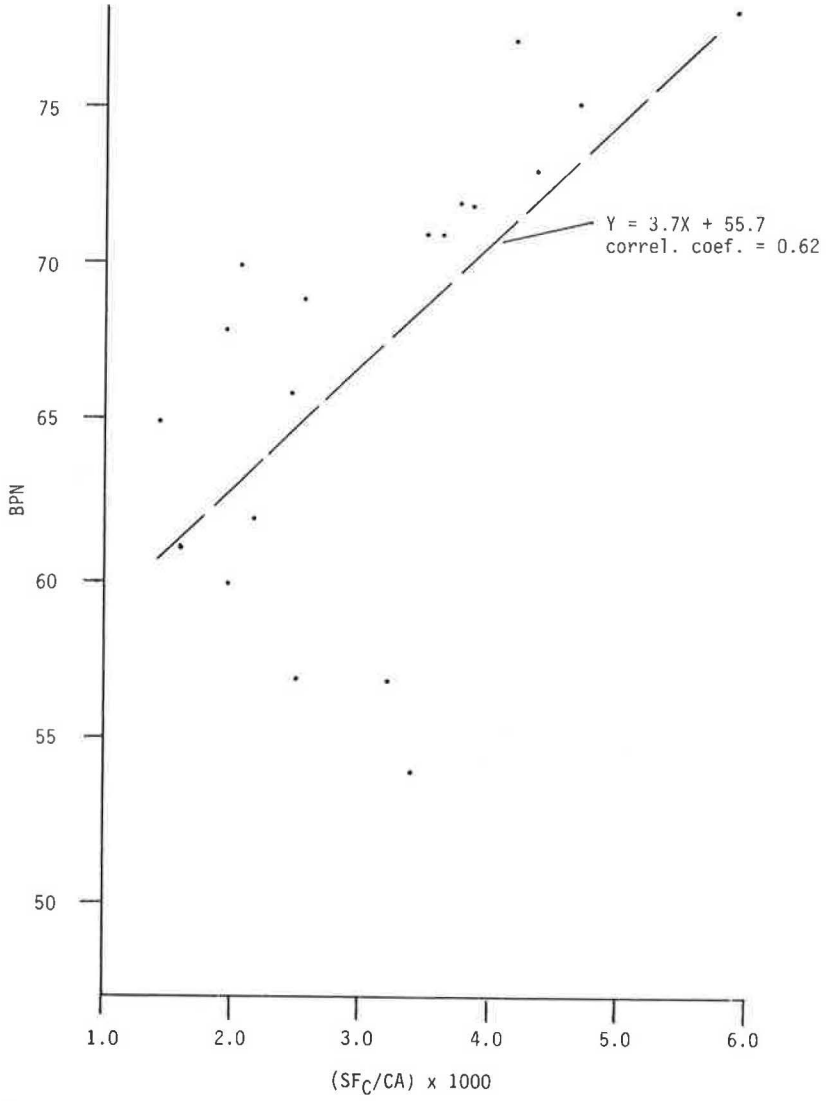

FIGURE 9 Plot of BPN versus $SF_c/CA \times 1{,}000$ for nineteen cores listed in Table 2.

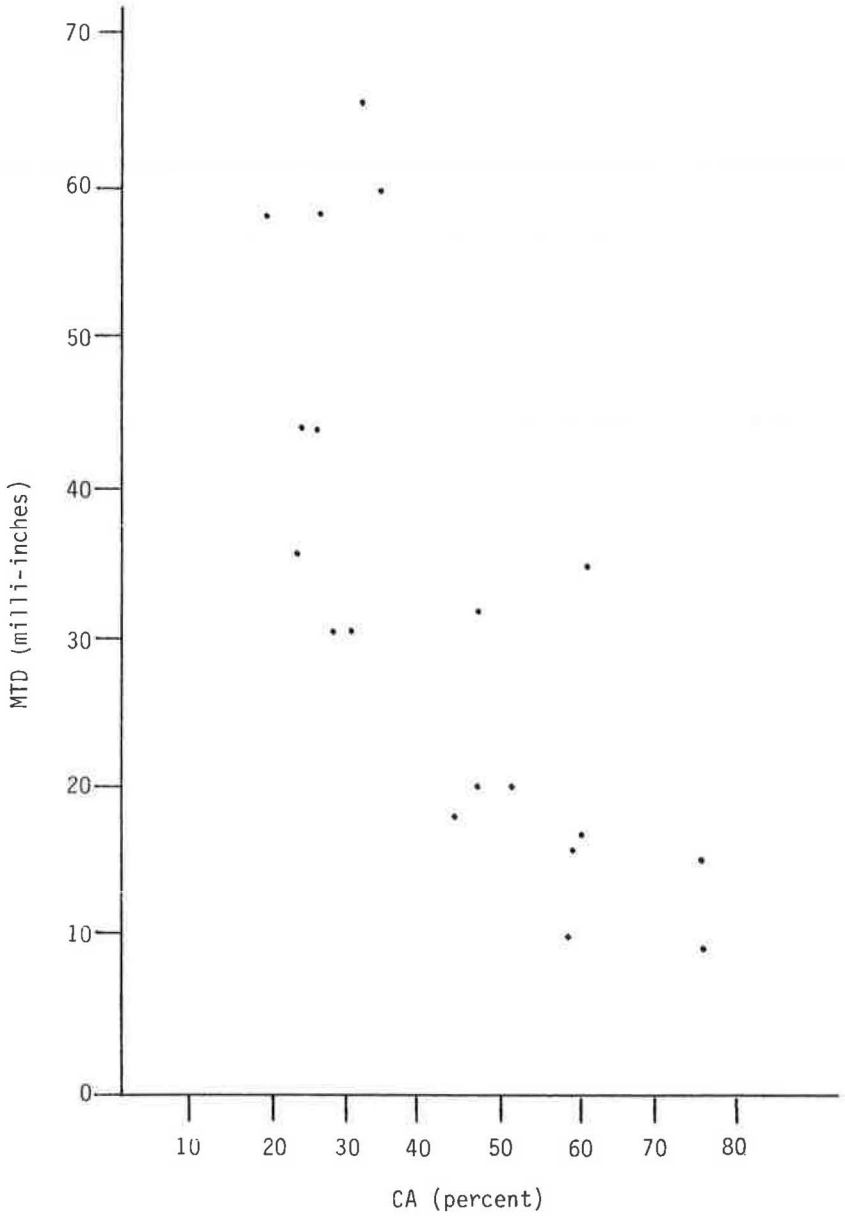

FIGURE 10 Plot of MTD versus CA for nineteen cores listed in Table 2.

and CA measurements. The conclusion from this analysis is that either the SN_{40} value was uncharacteristically low (owing to a long dry spell, for instance) at the time it was measured for 8-4 or there is some other factor influencing skid that is not accounted for by SF_c and CA.

The other outliers, samples 5-B and 6-3, are both from asphalt pavements. Pavement 5 is an asphalt pavement made using crushed limestone aggregate. Pavement 6 has a bituminous surface treatment that was made using limestone screenings. Both pavements were more than 10 years old at the time of testing, so it was expected that SN_{40} values would be low with these aggregates. As shown in Figure 9, pavement 5 had an SN_{40} of 32, and pavement 6 had a value of 34. These figures deviate from the best-fit line, then, probably because of the texture term. The SF_c portion of the term is low, indicating inadequate microtexture (as expected from a polished aggregate). The CA term, however, is also low, indicating that these pavements have a good macrotexture. This may indicate that pavements with a very good macrotexture (open-graded surface, or nearly so) may have to be evaluated separately from dense-graded surfaces. This problem will require future additional work.

SUMMARY

In this study, a microscope-based, automatic image analysis system was used to measure small-scale surface texture (microtexture) on a series of 87 samples from in-service pavements. A range of asphalt and portland cement pavements was included. Based on a previous study, the microtexture was characterized by a single calculated parameter, the shape

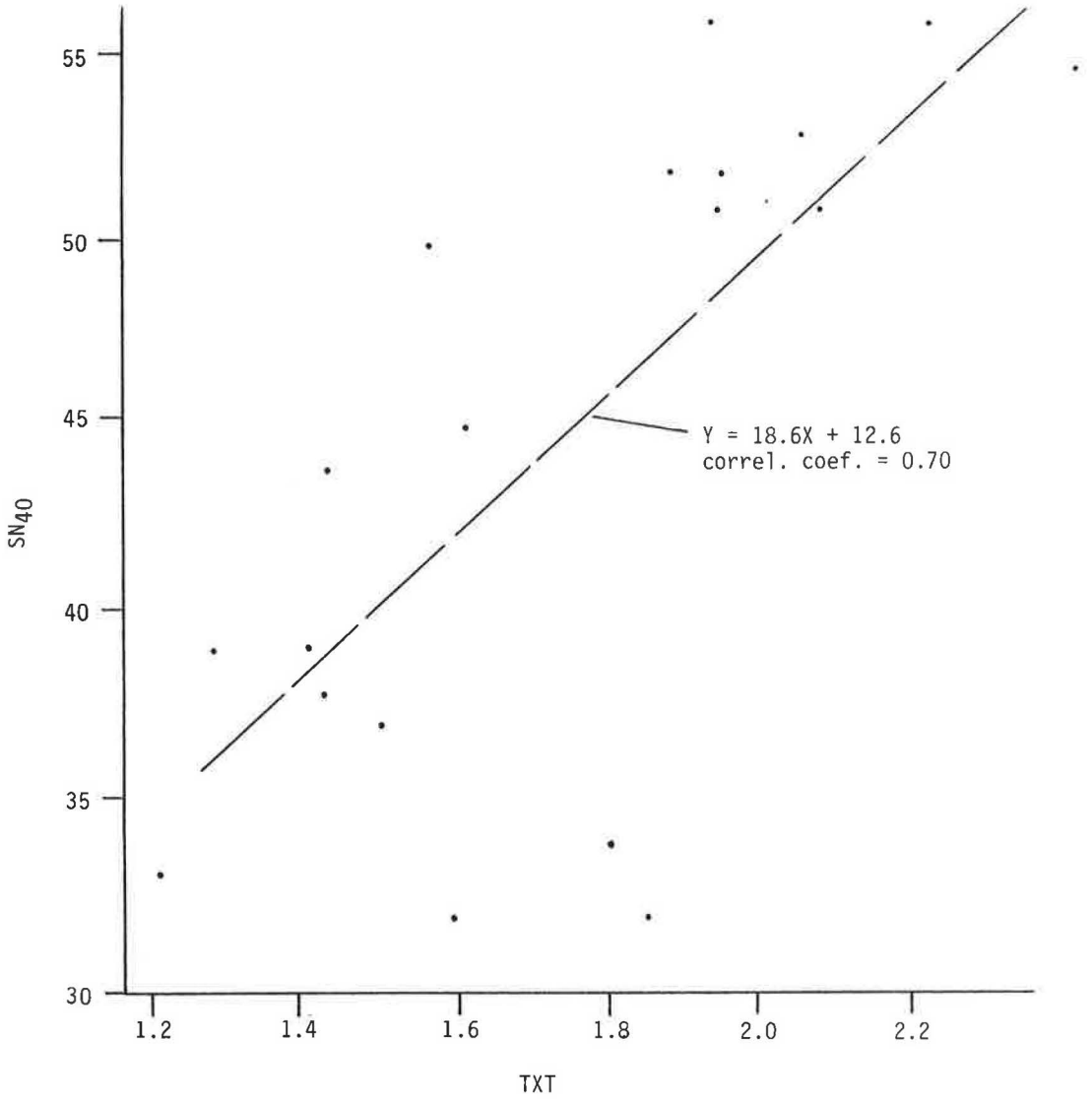

FIGURE 11 Plot of SN_{40} versus TXT for nineteen cores listed in Table 2.

factor (SF). Macrotexture was estimated by measuring contact area percentage (CA). These two texture measurements were combined as the parameter TXT for correlation with skid measurements from ASTM E274 (SN_{40} values) for a subset of 19 samples. The resulting correlation coefficient (0.70) shows promise but also indicates room for improvement. Examination of outliers indicates possible problems with both texture and skid data. Further research may be appropriate to determine if any surface characteristics that affect skid resistance are not adequately accounted for by the texture measurements defined here.

CONCLUSIONS

1. The microtexture of pavement samples can be characterized by a single parameter, the shape factor (SF). SF is a combination of average height and average spacing of the microtexture asperities.
2. Based on comparisons with MTD results from the sand patch test, the macrotexture of the pavements examined could be estimated by simulating and measuring the percentage of contact (CA) within the area of a tire footprint on the pavement surface. Additional testing would verify the universal applicability of this approach.
3. SF_c (shape factor on the contact area) and CA can be combined into an overall texture measurement (TXT) that may be correlated with skid measurements.

EXTENSIONS

1. While TXT has a fairly good correlation with SN_{40} values, additional work is needed to determine if the correlation can be improved by further refinement or the addition of one or more other parameters.
2. Although the pavement microtexture has been successfully quantified, no optimal value for SF_c has been established. For the samples examined, the friction continues to increase with SF_c over the range of values obtained. It may be that

microtexture, as it is measured by SF and as it occurs in pavements, can never attain (or exceed) the optimum. This problem needs further investigation.

3. Aggregate types could be studied and classified according to SF levels. Grouping should include not only initial levels but also ultimate polish or lower limits of SF. The practicality of grouping aggregates according to ultimate SF by general lithology is a possibility worth exploring.

REFERENCES

1. S. H. Dahir, and H. J. Lentz. *Laboratory Evaluation of Pavement Surface Texture Characteristics in Relation to Skid Resistance*. Report FHWA-RD-75-60, FHWA, U.S. Department of Transportation, June 1972.
2. S. H. Dahir and J. J. Henry. *Alternatives for the Optimization of Aggregate and Pavement Properties Related to Friction and Wear Resistance*. Report FHWA-RD-78-209, FHWA, U.S. Department of Transportation, April 1978.
3. W. E. Meyer. *Synthesis of Frictional Requirements Research*. FHWA/RD-81/159, FHWA, U.S. Department of Transportation, June 1982.
4. S. W. Forster. *Aggregate Microtexture: Profile Measurement and Related Frictional Levels*. Report FHWA/RD-81/107, FHWA, U.S. Department of Transportation, Oct. 1981.

Publication of this paper sponsored by Committee on Surface Properties—Vehicle Interaction.

Two Quarter-Car Models for Defining Road Roughness: IRI and HRI

MICHAEL W. SAYERS

There is now a movement in the United States toward standardizing road roughness measurements by using a scale called the International Roughness Index (IRI). The IRI was defined by the World Bank (based on earlier work performed for the NCHRP) and is required by the Federal Highway Administration (FHWA) for the roughness database of the Highway Performance Monitoring System (HPMS). The IRI is defined as a roughness description for a single wheeltrack profile, obtained by using a quarter-car model with certain specified parameter values. A related roughness measure is obtained by using both wheeltrack profiles as inputs to the same computer algorithm used for the IRI. This analysis is mathematically equivalent to a half-car model and produces a roughness measure called the half-car roughness index (HRI). There is currently a mixture of IRI and HRI data being measured in the United States. The two analytic methods are so similar in concept that many practitioners are not aware of the difference between them. As a result, there has been occasional confusion and error when data are reported. The purpose of this paper is to identify and discuss the differences and similarities between IRI and HRI. The paper also summarizes technology used to measure IRI and HRI.

The past few years have seen a rapid expansion of the options available for measuring road roughness and longitudinal road profile. PSI, IN/MI, ARV, ARS, "Golden Car," IRI, RMSVA, M0, QI, RI, and PI are only a few of the names and acronyms that have crept into the literature as new measures are introduced and old measures are better understood. As methods have improved and the transition has begun toward standardization, there has understandably been confusion because the language has lagged behind the technology. For example, many users do not even have a name for their roughness measure; it is referred to simply by units, such as "in./mi."

The bulk of the roughness data collected in the United States is obtained with vehicles that are equipped with roadmeter devices, such as the Mays Ride Meter, the PCA meter, or a generic equivalent. The roadmeter accumulates vibrations as the vehicle responds to road roughness when driven at highway speeds. The measure from the roadmeter can be scaled to approximate an accumulated suspension movement for the vehicle, and then normalized by the distance traveled to obtain a roughness measure with units of slope, such as inches/mile or meters/kilometer. The vehicle and roadmeter together are called a response-type system.

The measures from almost any response-type system can be reported with the same engineering units (e.g., inches/mile), leading to a false sense of standardization among first-time users of these devices. In practice, the "roughness" measures are not highly reproducible when different vehicles, operating conditions, or times are being considered. Several large research programs have addressed this problem and clarified the relationships between alternative measurement methods (*1–3*). The research has shown that measures from dissimilar systems correlate with a variety of numerics that can be computed from measured profiles. Time stability and reproducibility are obtained by calibrating the measures from a response-type system to a rigorously defined mathematical function of profile. The key advantage of this method is that the profile-based reference measure is independent of the particular equipment used to measure the profile.

Profile-based numerics that are highly correlated with measures from response-type systems are now used (1) to calibrate response-type systems so that their measures are converted to a standard scale and (2) as a means for defining roughness for direct measurement using a high-speed profiling system. A review of the high-speed profiling systems that were used in the 1987 Federal Highway Administration (FHWA)/Colorado Profiling Seminar (*4*) indicates that most of the systems report roughness using an analysis based on the IRI. Some of the profiling systems, however, use a nearly identical analysis method that is not the same as IRI; it is called the half-car roughness index (HRI) in this paper.

Currently, a mixture of IRI and HRI data is being measured with existing profiling systems in the United States. The purpose of this paper is to clarify the distinctions and similarities between the IRI analysis, the HRI analysis, and physical response-type systems.

Before delving into details of the analysis methods, several other popular roughness concepts are mentioned in the context of IRI and HRI.

- Present Serviceability Index (PSI) is the name of an estimate of panel rating for data from the original AASHTO experiment (*5*). Although numerous state agencies convert roughness data to units called "PSI" (a scale ranging from 0 to 5) based on correlations linked to the original experiments, no standardized PSI roughness scale is in existence. At the theoretical level, the problem with PSI is that there is no rigorous mathematical definition of PSI that can be used to validate equipment. At the practical level, the problem is that existing versions of "PSI" do not agree; different agencies measuring the same road at the same time have shown differences of more than 1 full PSI unit (*1*). A conversion between IRI and an average of several versions of PSI has been derived from several independent sources by Paterson (*6*) to provide an approximate link to the old PSI concept.

University of Michigan, Transportation Research Institute, Ann Arbor 48109.

- Recent NCHRP research on rideability has resulted in a new roughness statistic called profile index (PI) that has been correlated to panel ratings (*7*). PI is generally not well correlated with measures from response-type systems and, to the author's knowledge, has not yet been used outside of a few research projects.
- Rigid pavements are commonly evaluated immediately after curing with devices called profilographs. The measures from profilographs are also reported with units of slope (typically in./mi). However, the profilograph "in./mi" has little in common with the "in./mi" of the response-type system. Measures from different profilographs are not compatible. The development of calibration practices for these devices is a present research topic.

The preceding roughness measures are mentioned only to note that they are fundamentally different from the IRI and HRI, such that equivalences with the IRI and HRI roughness scales do not exist.

DEFINITIONS OF TERMS

Before discussing the physics of a moving vehicle responding to road roughness, it is important to distinguish between measures and methods, physical systems and mathematical models, and different models.

- A response-type system is a physical, mechanical system consisting of a vehicle that is instrumented with a roadmeter.
- ARS (average rectified slope) is the generic name of a measure that can be obtained from a response-type system or a vehicle model. This numeric is often left nameless, with users calling the measure by the name of the units, such as "in./mi." "ARS" is the name of the numeric, and "in./mi" are the units of ARS. (Of course, ARS could just as well be reported with other units, such as m/km, in./fathom, and so forth.)
- IRI (International Roughness Index) is a roughness scale defined as a specific mathematical property of a longitudinal profile. (The mathematical definition is presented later.) IRI can be obtained directly with a profile measurement system and suitable computer software. Alternatively, IRI can be estimated by transforming the measurement from a response-type system using a valid calibration equation.
- HRI (half-car roughness index) is a roughness scale similar to IRI except that it is defined as a specific mathematical property of a pair of longitudinal profiles.
- A quarter-car model is a mathematical model of a vehicle that represents a body and a single wheel.
- A half-car model is a mathematical model of a vehicle that represents a body and a single axle with two wheels.
- The Golden Car is a set of four parameter values that can be used with either of the preceding two models.
- The IRI analysis is the algorithm used to compute IRI from a longitudinal profile. This analysis produces the ARS from a quarter-car model using the Golden Car parameter values and a simulation speed of 49.7 mph (80.0 km/h).
- The HRI analysis is the algorithm used to compute HRI from two longitudinal profiles. This analysis produces the ARS from a half-car model using the Golden Car parameter values and a simulation speed of 49.7 mi/h (80.0 km/h). It is later shown that HRI is also obtained if the two profiles are first averaged into a single modal profile, which is then used as input to the IRI analysis.

HISTORY OF IRI AND HRI

The quarter-car model underlying the IRI and HRI analyses is widely used by vehicle analysts as a simple means to study alternative vehicle designs. The model also has a long history of use for characterizing road roughness, as summarized below.

In the late 1960s, General Motors (GM) developed a high-speed profiling system that could measure "true profile" over a range of wavelengths affecting vehicle vibrations (*8*). One of the first uses of profile data from that type of system was to use a quarter-car model to replicate the Bureau of Public Roads (BPR) Roughometer, a response-type system (*9*). The BPR Roughometer is a one-wheeled trailer with a roadmeter that represents an early attempt to standardize roughness measurements (*10*). Interestingly, two of the first profiling systems made outside of GM used different vehicle parameter values to describe the BPR Roughometer. Both sets of parameter values were measured in the laboratory for different BPR Roughometers and are listed by Gillespie et al. (*1*). This disparity illustrates the difficulty in standardizing roughness measures by standardizing hardware.

Early commercial versions of the GM-type profiling system included a quarter-car model as a means to summarize roughness of the measured profiles. The model was used with two sets of parameter values: one set for the BPR Roughometer and one set for a 1968 Chevrolet Impala (*11*).

Extensive tests in an NCHRP project using a four-wheel road simulator and a response-type system showed that a half-car model provided as good a reference as more comprehensive vehicle models. Copious computer simulations conducted in that study were used to select a set of parameter values for the model that would maximize the correlation for a variety of response-type systems based on the full spectrum of vehicles available in the United States. This set of parameter values is shown in Figure 1 and has sometimes been called the Golden Car vehicle parameter values. The same set now

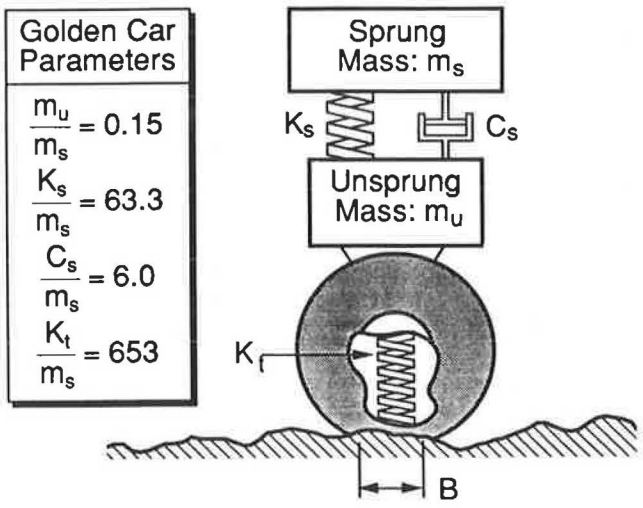

FIGURE 1 Quarter-car model.

appears (ASTM E1170) for a simulated response-type system identified as "Ride-Meter Vehicle-Mounted."

When the half-car model was tested in the NCHRP project with the Golden Car parameter values, the correlations between the profile-based measures and the various response-type systems were better than the correlations between the different response-type systems.

The calibration reference proposed in the NCHRP report is nearly identical to the HRI. The difference is that the NCHRP report did not specify a standard speed. (As defined later in this paper, the HRI applies only for a simulation speed of 49.7 mph (80 km/h).)

The International Road Roughness Experiment (IRRE) was initiated by the World Bank, funded by several countries, and held in Brasilia in 1982 to establish correlation and a calibration standard for roughness measurements (*2*). In this study, it became clear that nearly all roughness measuring equipment throughout the world was capable of producing measures on the same scale, if that scale were suitably selected. Accordingly, the IRI was developed to encourage standardization. The main criteria in designing the IRI were that it be relevant, transportable, and stable with time. To ensure transportability, it must be measurable with a wide range of equipment, including response-type systems. Numerous roughness definitions were considered by applying them to the large amount of test data obtained in the IRRE. The half-car analysis and Golden Car parameters from the NCHRP project were considered a candidate reference. However, some of the instruments measured the roughness in only one wheeltrack; therefore, a quarter-car model (together with the Golden Car parameter values) was also used.

With the half-car model, a single ARS number is obtained that describes both the left- and right-hand wheeltrack profile conditions as seen by a vehicle. With the quarter-car model, an ARS roughness level is determined separately for the left- and right-hand profiles. The ARS values obtained by simulating a quarter-car model over the two wheeltracks are averaged for comparison with the ARS measure obtained from instrumented passenger cars or two-wheeled trailers. Almost identical correlations with the response-type systems were obtained with the quarter-car and half-car models.

After all of the candidate roughness numerics were considered, the best correlations with the response-type systems were obtained with the quarter-car and half-car models, which gave essentially the same level of correlation. The single-track analysis was selected for the IRI, because it was measurable by a much wider range of equipment. The IRI was one of the few profile analyses that was well suited to all profiling methods that were in use at that time, including rod and level, profilometers based on the GM design, and the French APL trailer. (Some high-speed profiling systems do not measure both wheeltrack profiles and, therefore, cannot easily produce HRI.)

As a part of the IRRE, averages of the two IRI numerics for each test section were compared with HRI, as shown in Figure 2. The data showed the correlation between IRI and HRI to be almost perfect. Consequently, the two were equal in performance as a calibration reference for response-type systems.

Fairly complete guidelines were prepared by the World Bank for the calibration and use of road roughness measuring equipment using the IRI scale (*12*). Since then, the IRI has been adopted as a standard in several countries and is currently being evaluated as a candidate standard in many more.

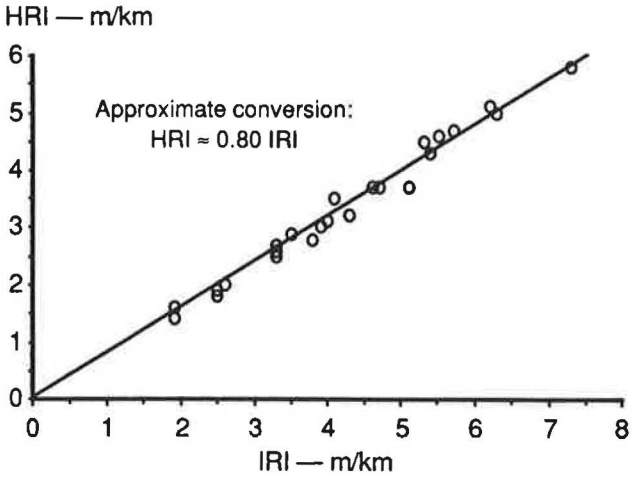

FIGURE 2 HRI—IRI correlation.

In the United States, the IRI has been established by the FHWA as a standard for the Highway Performance Monitoring System (HPMS) database. A condensed (and modified) version of World Bank Guidelines was prepared to help guide states in obtaining valid measures on the IRI scale (*13*). At the time of this writing, several ASTM task groups are incorporating the IRI into ASTM standards involving roughness measurement.

MATHEMATICAL DERIVATIONS

The roughness measure from a response-type system is conventionally divided by the length of the road measured to obtain a measure with units of roadmeter output per units of distance (*1, 14*). For an ideal roadmeter that accumulates displacement perfectly, the accumulation process consists of an integration of the absolute value of the derivative of suspension deflection − deflection velocity. That is, the ARS computed from a vehicle model is defined as

$$\text{ARS} = \frac{1}{L}\int_0^T |\dot{z}_u - \dot{z}_s|\, dt \tag{1}$$

where

ARS = average rectified slope,
T = time duration of test,
L = length of test,
$\dot{z}_u$ = vertical velocity of the unsprung mass (axle), and
$\dot{z}_s$ = vertical velocity of the sprung mass (vehicle body).

Most roadmeters have significant quantization and hysteresis properties that prevent them from measuring the true displacement and the true ARS (*1*). Nonetheless, for the sake of simplicity, the name "ARS" is used here also to describe the measure from a response-type system.

The vehicle models underlying the IRI and HRI roughness scales are defined by differential equations that relate motions of the simulated vehicle to road profile inputs. Even though the equations of motion for these models have been published time and time again, they are derived below to show how the

quarter-car equations are used to simulate a half-car equipped with an idealized roadmeter.

Figure 1 shows a quarter-car model, in which the vertical movements of the body are represented by an element called the unsprung mass. The model includes the major dynamic effects that determine how roughness causes vibrations of the car body. It includes tire compliance, suspension stiffness and damping, and two masses. The equations are derived from Newton's second law, force = mass × acceleration. For the sprung mass, the vertical acceleration is related to vertical forces according to the relationship

$$m_s (\ddot{z}_s - g) = f_{susp} - f_g \quad (2)$$

where

$\ddot{z}_s$ = vertical acceleration (Time derivatives are indicated by dots over a variable. The two dots over z_s indicate a double derivative of the sprung mass position (z_s) with respect to time. The sprung mass velocity is written later as $\dot{z}_s$.);
m_s = sprung mass (portion of mass of car body supported by one wheel);
g = gravitational constant;
f_{susp} = suspension force in addition to static load due to gravity; and
f_g = static load due to gravity = $m_s g$.

The gravitational force and acceleration are constants that can be removed from the equation, leaving

$$m_s \ddot{z}_s = f_{susp} \quad (3)$$

For the simplified mechanical system shown in the figure, the suspension force is the sum of a spring force and damper force. Using simple linear spring and damping components, k_s and c_s, respectively, gives

$$f_{susp} = k_s (z_u - z_s) + c_s (\dot{z}_u - \dot{z}_s) \quad (4)$$

Combining Equations 2 and 3, an equation of motion is obtained:

$$m_s \ddot{z}_s + c_s (\dot{z}_s - \dot{z}_u) + k_s (z_s - z_u) = 0 \quad (5)$$

A similar equation is obtained for the unsprung mass by considering the force from the suspension and also the tire (modeled as a linear spring with rate k_t):

$$m_u \ddot{z}_u + c_s (\dot{z}_u - \dot{z}_s) + k_s (z_u - z_s) = k_t (z_p - z_u) \quad (6)$$

In Equation 6, m_u is the unsprung mass, defined as the mass of the wheel, tire, and half of the axle. Equations 5 and 6 are the equations of motion for the quarter-car model shown in the figure. As input, this model requires wheeltrack elevation as a function of time, designated by the variable z_p. As output, it predicts the displacement, vertical velocity, and vertical acceleration of the sprung and unsprung masses. The actual roughness index is the ARS as defined in Equation 1.

Figure 3 shows a more comprehensive vehicle model in which two inputs are allowed, corresponding to the left- and right- hand sides of the vehicle. With the gravitational terms removed, the vertical forces acting on the sprung and unsprung masses can again be set equal to mass × acceleration, with the results

$$2 m_s \ddot{z}_s + 2 c_s (\dot{z}_s - \dot{z}_u) + 2 k_s (z_s - z_u) = 0 \quad (7)$$

$$2 m_u \ddot{z}_u + 2 c_s (\dot{z}_u - \dot{z}_s) + 2 k_s (z_u - z_s) = k_t (z_{p,right} + z_{p,left} - 2 z_u) \quad (8)$$

where

$z_{p,right}$ = road profile elevation on right-hand side and
$z_{p,left}$ = road profile elevation on left-hand side.

As before, the sprung and unsprung masses correspond to the masses associated with one wheel. Note that the roll angles of the body and axle do not appear in either equation. Newton's second law, applied to a rigid body, involves only the vertical movements of the center of mass points for the two bodies and the vertical forces. This may appear surprising because the left- and right-hand spring, damper, and tire forces are all affected by roll of the vehicle body and axle. Indeed, the roll motions can influence the motions of every point in the bodies except for the center-of-mass points. However, noting that ARS is defined solely from the movements of these two points, it can be seen that Equations 7 and 8 are sufficient for computing the ARS of a half-car.

Note that Equations 7 and 8 (half-car) are nearly identical to Equations 5 and 6 (quarter-car). After canceling the factors of 2 in the half-car model, the equations are made identical

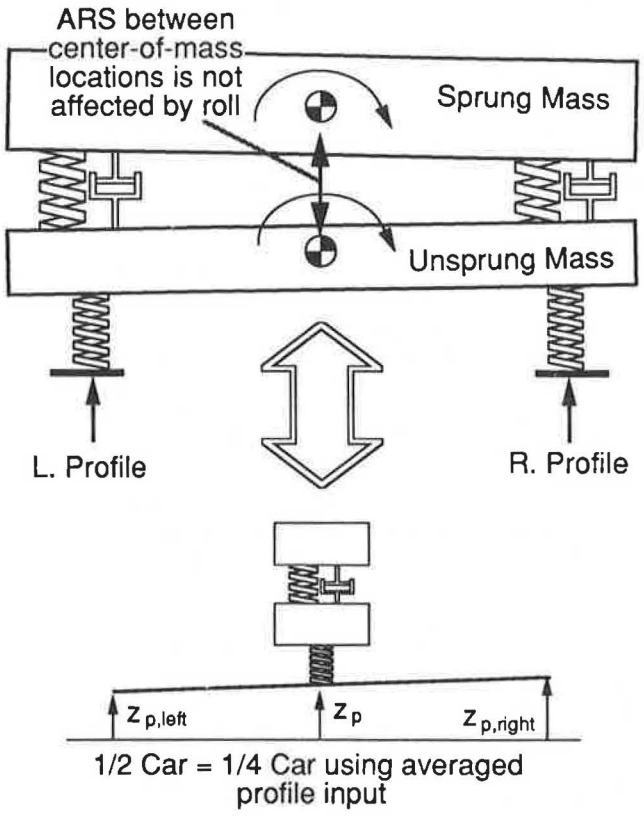

FIGURE 3 Half-car model.

by the substitution

$$z_p \leftarrow \frac{z_{p,\text{right}} + z_{p,\text{left}}}{2} \tag{9}$$

A geometric interpretation of the equivalence of the equations is shown in Figure 3. The prediction of the vertical movements of the center-of-mass locations of the sprung and unsprung masses using the half-car model is exactly the same as would be obtained using a quarter-car model, using as input the point-by-point average of the individual wheeltrack profiles.

The IRI analysis is a special case of the quarter-car model (Equations 5 and 6). It specifies the Golden Car parameter values shown in Figure 1, a simulated travel speed of 49.7 mph (80 km/h), and the ARS averaging (Equation 1). IRI is usually reported with units of m/km = mm/m, or in./mi. (Note: in./mi = m/km × 63.36.)

When the same process is applied to an averaged profile, the resulting ARS value is designated HRI.

To summarize, the IRI and HRI indices are both obtained by using the quarter-car analysis. The distinction is that the IRI is obtained by applying the quarter-car to a single wheeltrack profile (either $z_{p,\text{left}}$ or $z_{p,\text{right}}$), whereas the HRI is obtained by applying the quarter-car to a point-by-point average of two wheeltrack profiles [$z_p = (z_{p,\text{right}} + z_{p,\text{left}})/2$].

DIFFERENCES AND SIMILARITIES

A roughness index can be considered to derive from three considerations. These are listed below, in the context of the IRI and HRI.

1. How is the three-dimensional road surface measured for input to an analysis? Within the scope of this paper, this reduces to two options:
   a. Measure the longitudinal profile for a single wheeltrack, and use that profile as input to the roughness analysis (IRI).
   b. Measure a point-by-point average of the profiles in two traveled wheeltracks, and use that averaged profile as input to the roughness analysis (HRI).
2. How are wavelengths in the profile weighted? In other words, how is the profile spatially filtered? For both the IRI and HRI, the filter is the quarter-car model, using the Golden Car parameter values and a simulation speed of 49.7 mph (80 km/h).
3. What averaging method is used to accumulate the filtered profile to produce a single roughness numeric? For both the IRI and HRI, ARS (Equation 1) is used.

The IRI and HRI analyses differ only in how a profile is defined for input to the quarter-car filter. Ultimately, any similarities and differences between IRI and HRI derive from the similarities and differences in the two types of profiles. A detailed presentation of the relationships between the roughnesses in a single wheeltrack profile is available elsewhere (*15*). A few essential points are repeated below, to establish limits for relationships between the roughness of individual wheeltracks and an averaged profile.

Theoretical Relations Between Averaged Profiles and Wheeltrack Profiles

Profiles can be viewed in the frequency domain, as "amplitude" versus wavenumber (wavenumber = 1/wavelength), using the power spectral density (PSD) function. Correlations between profiles can also be viewed as a function of wavenumber, using the coherence function. When viewed in this way, the correlation between the left- and right-hand wheeltrack profiles changes drastically with wavenumber. For very long wavelengths, there is perfect coherence because the left- and right-hand wheeltracks must go up and down together (in-phase) over hills and valleys. (This hypothesis can be false only for an unrealistic condition in which the elevations of the left- and right-hand wheeltracks differ by several feet or more.) Hence, the average of the two profiles is equal to the individual wheeltrack profiles:

$$G_p(\nu) = G_{p,\text{left}}(\nu) = G_{p,\text{right}}(\nu) \tag{10}$$

valid for very long wavelengths, $\nu \rightarrow 0$

where

G = PSD amplitude at a given wavenumber, and
ν = wavenumber = 1/wavelength.

For very short wavelengths, the coherence approaches zero because the profile features contributing to texture have no point-by-point relationship. That is, they have random phase. (This hypothesis can be false only for the unrealistic condition in which the texture details in one wheeltrack are systematically related to corresponding details in the other wheeltrack. For most types of pavement, when the right-hand profile goes up over a tiny bump in the texture with a length of 0.1 in., the left-hand profile is equally likely to be going up or down.)

The mean-square value for the sum of two uncorrelated, zero-mean random variables is the sum of their variances. To prove this, consider two random variables X_1 and X_2 with variances $\sigma^2_{X_1}$ and $\sigma^2_{X_2}$, mean values of zero, a correlation coefficient $r = 0$, and their sum, Y:

$$Y = X_1 + X_2 \tag{11}$$

The expected value of Y^2, designated by the "expected value" operator, E, is

$$\begin{aligned} E[Y^2] &= E[(X_1 + X_2)^2] = E[X_1^2 + 2X_1X_2 + X_2^2] = E[X_1^2] \\ &+ E[2X_1X_2] + E[X_2^2] \\ &= \sigma^2_{X_1} + 2\cancel{0}\,(\sigma_{X_1}\sigma_{X_2})^{1/2} + \sigma^2_{X_2} \\ &= \sigma^2_{X_1} + \sigma^2_{X_2} \end{aligned} \tag{12}$$

Because the PSD function is a distribution of variance over wavenumber, the same relationship holds for the sum of two random signals whose coherence function is zero. Thus,

$$G_p(\nu) = \frac{1}{4}G_{p,\text{left}}(\nu) + \frac{1}{4}G_{p,\text{right}}(\nu) \tag{13}$$

valid for very short wavelengths, $\nu \rightarrow \infty$

A factor of 4 appears because the averaging involves division by 2, and $2^2 = 4$.

In the case of wheeltrack profiles with the same overall roughness levels (the mean-square values of the two uncor-

related random variables are the same), the mean-square of the sum is twice the mean-square of one side:

$$G_p(\nu) = \frac{1}{2} G_{p,\text{left}}(\nu) = \frac{1}{2} G_{p,\text{right}}(\nu) \quad (14)$$

valid for very short wavelengths, $\nu \rightarrow \infty$

The square roots of the relations of Equations 10 and 14 indicate the limiting relationship between nonsquared roughness values of individual wheeltracks and an averaged profile. For very short wavelengths, the roughness amplitude of the averaged profile is $(1/2)^{1/2} = .707$ of the amplitude of a single wheeltrack profile.

In summary, the limiting relationships between roughness of an averaged profile and individual wheeltrack profiles are:

- For very long wavelengths, the roughness is the same.
- For very short wavelengths, the roughness of the averaged profile is 29 percent lower (0.707) than the roughness of an individual wheeltrack profile.
- Between the "very long" and the "very short" wavelengths, the averaged profile exhibits roughness lower than the average of the roughness values for the individual wheeltrack profiles, by an amount lying between 0 and 29 percent.

Therefore, a bracketing relation is expected between IRI and HRI:

$$.71 \frac{\text{IRI}_{\text{left}} + \text{IRI}_{\text{right}}}{2} < \text{HRI} < \frac{\text{IRI}_{\text{left}} + \text{IRI}_{\text{right}}}{2} \quad (15)$$

Physically, the foregoing results mean that some of the roughness in the left- and right-hand wheeltracks cancels. The roughness that cancels causes roll motions in a vehicle, which are not detected by a roadmeter located at the center.

Relations Between the Two Types of Profile on Real Roads

Virtually all of the wavelengths contributing to IRI and HRI lie between the limits deduced in the preceding theoretical analysis. The exact relationship between the types of profile is itself a property of a road surface. The data collected in the Brazilian experiment (the IRRE) covered asphalt, surface treatment, gravel, and dirt roads. Figure 2 shows that excellent correlation was found for that range of conditions. An empirical relation between the two was derived from paved test sites used for the Brazil experiment:

$$\text{HRI} \approx 0.80 \frac{\text{IRI}_{\text{left}} + \text{IRI}_{\text{right}}}{2} \quad (16)$$

When the unpaved roads are also included, a slightly lower ratio of 0.76 was found (*2*), indicating slightly less coherence between the two wheeltrack profiles.

A similar analysis has not been performed for rigid pavements. Measurements show that the relationships between the two types of profiles are substantially different for PCC roads (*15*). A significant part of the roughness was derived from misalignment at the joints between slabs. This type of roughness tends to appear identically in both the left- and right-hand wheeltrack profiles. Even when the roughness is greater in one wheeltrack, the disturbance occurs in the same place in both, so they are in phase and thus highly correlated. The effect on vehicles is that they receive less roll input for the amount of roughness on PCC roads than on asphalt roads. Consequently, the HRI is closer in amplitude to the average of the two IRI values, and a ratio of approximately 0.90 is expected.

Practical Interpretation of the Differences Between HRI and IRI

The (slight) difference between IRI and HRI is partly derived from seeing roughness from the perspective of different points in a vehicle. The IRI more closely indicates vehicle response at the wheels, while the HRI more closely indicates response of the vehicle at its center. Thus, the IRI could be viewed as a marginally better indicator of vehicle suspension wear, pavement loading, and adhesion utilization, because these measures all depend mainly on the dynamic response of a single wheel. HRI unquestionably offers a better representation of a two-track vehicle (passenger car or two-wheeled trailer) equipped with a roadmeter when the roadmeter is mounted over the center of an axle. It is not clear which is the better indicator of cargo damage and ride quality, as this depends on how the roll dynamics contribute to the vibrations of the sprung mass away from the centerline of the vehicle.

IRI might be viewed as a potentially more useful roughness index simply because it can provide roughness levels separately for left- and right-hand wheeltracks, to show how one side of a lane has deteriorated more than the other. The HRI cannot be used for this purpose; neither, however, can most response-type systems now in use. The potential advantage of the IRI mainly applies to high-speed profiling systems.

The major practical consideration is simply which is more convenient to measure and to relate to other data. Some profiling systems can measure IRI but not HRI; others can measure HRI but not IRI. An agency that has been measuring a reproducible index for the past 5 years will probably prefer to continue using that index unless there is a truly compelling reason to switch.

Automated Profiling Systems

In 1984, a profilometer meeting was held in Ann Arbor, Michigan, for the purpose of determining the performance capabilities of numerous profiling systems in use at that time (*16*). Nearly all of the high-speed profilometers in use in North America participated. At that time, only a few of the systems had software to compute quarter-car numerics routinely. Since then, software options have been added, and other profiling systems have been developed. The situation today is that nearly all of the automated profiling systems used in North America include some form of quarter-car analysis, and they are most commonly used to measure IRI or HRI (*4*). Some of these systems are listed in Table 1 to indicate whether they currently measure IRI and/or HRI.

The table also indicates the principles upon which the systems operate. Reference is made to four designs, which have been used or demonstrated in the United States.

TABLE 1 SUMMARY OF AUTOMATED PROFILING SYSTEMS AND ASSOCIATED QUARTER-CAR ANALYSES

Profiling System	Developer	Design	Quarter-car
APL	French Bridge and Pavement Laboratory (LCPC) and MAP Sarl, Illfurth, France	APL	IRI
Dipstick	Edward W. Face Company Norfolk, VA	Static Level	IRI
ARAN with profile option	Highway Products International Paris, Ontario, Canada	2-accel.	HRI
PURD with profile option	Highway Products International Paris, Ontario, Canada	2-accel.	HRI
690 DNC Profilometer	K. J. Law Engineers, Inc. Farmington Hills, MI	GM	IRI, HRI
8300 Roughness Surveyor	K. J. Law Engineers, Inc. Farmington Hills, MI	GM	IRI
S. Dakota Profiling System	S. Dakota DOT Research Program Pierre, SD	GM	IRI
PRORUT	Univ. of Mich. and FHWA McLean, VA	GM	IRI
Laser Road Surface Tester (RST)	Swedish National Road and Traffic Institute (VTI) and Infrastructure Management Services (IMS), Arlington Heights, IL	GM	IRI

- GM-type inertial profiling system: This is the design developed by Spangler and Kelly at General Motors Research Laboratories around 30 years ago (*8*). In this design, the vertical motions of the moving vehicle are sensed with an accelerometer and processed to obtain the vertical position of the vehicle relative to an inertial reference. The distance between the vehicle and the ground surface is also measured and is subtracted from the inertial height of the vehicle. Originally, vehicle-to-ground distance was measured with an instrumented follower wheel. In most modern systems, this distance is measured with a noncontacting transducer.
- Two-accelerometer inertial profiling system: This design by Sayers and Gillespie (*17*) requires two accelerometers installed in a vehicle with a beam axle. One of the accelerometers is mounted on top of the axle at the center. The second accelerometer is mounted in the body of the vehicle, directly above the center of the axle. The two accelerometer signals are processed to cancel the suspension effects, so that the linear spring properties of the tires are used to sense the vehicle-to-ground distance required to measured profile.
- French APL inertial profiling trailer (*18*): In this design, an isolated rotational pendulum provides an inertial reference. The pendulum is supported by a one-wheeled trailer. Profile is measured directly as a displacement of a linkage relative to the pendulum.
- Proprietary "Dipstick" static leveling method, originally used for measuring floor flatness in constructions.

The GM, APL, and Dipstick designs measure a single profile and are well suited for obtaining IRI measures. To measure HRI, the vehicle-based systems must include separate sets of transducers for the right- and left-hand wheeltracks. The outputs of each set of transducers must be precisely synchronized and averaged at every profile measurement point to obtain HRI. (For the static Dipstick method, HRI would be obtained by measuring the two wheeltrack profiles con-

secutively and using new software to perform the point-by-point averaging of the two profiles.) The two-accelerometer design inherently measures the average of the two profiles traversed by the tires of the test vehicle and is thus well suited for measuring HRI.

SUMMARY AND CONCLUSIONS

Most of the automated profiling systems used in North America include a quarter-car analysis as a means of summarizing roughness. Systems that measure a single wheeltrack profile can measure roughness on the IRI scale. Systems that can measure the point-by-point average of the two traveled wheeltracks can measure roughness on the HRI scale. The HRI from two wheeltrack profiles is always lower than the average of the IRIs from the two wheeltracks, because some of the roughness is canceled in the HRI analysis. Most of the time, the IRI and HRI measures are very highly correlated. Existing data for asphalt roads suggest an approximate relationship:

$$\text{HRI} \approx 0.8\ \text{IRI}$$

There are subtle theoretical differences in how the two are interpreted. The distinctions are so slight, however, that the choice of which to measure should be largely determined by practical considerations.

There has been confusion between the two because of limits in terminology; the name "quarter-car" alone does not distinguish which version is used. (For example, the data from at least one of the profiling systems involved in the 1987 Colorado Profiling Seminar are labeled incorrectly in the final report.) Users of a quarter-car analysis should be aware of which type they are using and should clarify this when reporting roughness data to others. As defined by the World Bank, the name "IRI" refers to ARS as computed with a quarter-car model for a single wheeltrack profile using the "Golden Car" parameter values and a simulation speed of 49.7 mph (80 km/h). The name "HRI" is suggested for use of the same analysis applied to an averaged profile.

REFERENCES

1. T. D. Gillespie, M. Sayers, and L. Segel. *NCHRP Report 228: Calibration of Response-Type Road Roughness Measuring Systems*. TRB, National Research Council, Washington, D.C., Dec. 1980, 88 pp.
2. M. Sayers, T. D. Gillespie, and C. Queiroz. *International Experiment to Establish Correlations and Standard Calibration Methods for Road Roughness Measurements*. World Bank Technical Paper 45. World Bank, Washington D.C., 1986.
3. W. Gulden. *Calibration Procedures for Roadmeters*. Report FHWA-TS-86-201. FHWA, U.S. Department of Transportation, April 1986.
4. D. E. Donnelly, W. Huttler, and J. P. Kiljan. *Pavement Profile Measurement Seminar Proceedings, Ft. Collins, Colo., October 5–8, 1987*. Report FHWA DP-88-072-004, FHWA, U.S. Department of Transportation, April 1988, 3 volumes.
5. W. N. Carey, Jr., and P. E. Irick. The Pavement Serviceability-Performance Concept. *HRIB Bulletin 250*, 1960, pp. 148–158.
6. W. D. Paterson. International Roughness Index: Relationship to Other Measures of Roughness and Riding Quality. In *Transportation Research Record 1084*, TRB, National Research Council, Washington, D.C., 1986, pp. 49–58.
7. M. S. Janoff, J. B. Nick, P. S. Davit, and G. F. Hayhoe. *NCHRP Report 275: Pavement Roughness and Rideability*. TRB, National Research Council, Washington, D.C., 1985.
8. E. B. Spangler and W. J. Kelly. *GMR Road Profilometer: A Method for Measuring Road Profile*. Research Publication GMR-452. General Motors Corp., Warren, Mich., Dec. 1964.
9. J. R. Darlington. *Evaluation and Application Study of the General Motors Corporation Rapid Travel Profilometer*. Research Report R-731. Michigan Department of State Highways, Oct. 1970.
10. J. A. Buchanan and A. L. Catudal. Standardizable Equipment for Evaluating Road Surface Roughness. *Public Roads*, Feb. 1941.
11. J. L. Burchett et al. *Surface Dynamics Profilometer and Quarter-Car Simulator: Description, Evaluation, and Adaptation*. Research Report 465. Kentucky Department of Transportation, Frankfort, 1977.
12. M. Sayers, T. D. Gillespie, and W. D. Paterson. *Guidelines for the Conduct and Calibration of Road Roughness Measurements*. World Bank Technical Paper 46. World Bank, Washington D.C., 1986.
13. *Highway Performance Monitoring System Field Manual for the Continuing Analytical and Statistical Database, Appendix J*. FHWA Order M5600.1A, OMB No. 2125-0028. FHWA, U.S. Department of Transportation, Dec. 1987.
14. *Standard Test Method for Measurement of Vehicular Response to Traveled Surface Roughness*. ASTM E1082. American Society for Testing and Materials, 1987.
15. M. W. Sayers. Characteristic Power Spectral Density Functions for Vertical and Roll Components of Road Roughness. In *Proc., Symposium on Simulation Control of Ground Vehicles and Transportation Systems*, American Society of Mechanical Engineers, Anaheim, Calif., Dec. 1986.
16. M. Sayers and T. D. Gillespie. *The Ann Arbor Road Profilometer Meeting*. Report FHWA/RD-86/100, FHWA, U.S. Department of Transportation, July 1986.
17. M. W. Sayers and T. D. Gillespie. An Overview of Road Meter Operation in Measuring Pavement Roughness, with Suggested Improvements. In *Transportation Research Record 836*, TRB, National Research Council, Washington, D.C., 1981, pp. 29–35.
18. *Analyseur de Profil en Long—APL 72*. Bulletin 1BAC76. Laboratoire Central des Ponts et Chaussées, 58 Boulevard Lefèbvre, 75732 Paris Cedex 15, France.

Publication of this paper sponsored by Committee on Surface Properties–Vehicle Interaction.

A Criterion for Optimizing Surface Characteristics

GUY DESCORNET

Requirements for road pavement performance were long centered on safety but are currently being extended to such concerns as the environment, comfort, and costs. The following aspects must now be considered: (1) for safety: skid resistance, road-holding qualities, splash and spray reduction, and visibility of the road and road markings; (2) for economy: reduction of fuel consumption, tire and vehicle wear, and dynamic extra loads that may shorten the life of road (and engineering) structures; and (3) for user comfort and the environment of roadside residents: reduction of noise and vibrations inside and outside vehicles. Each feature of pavement performance is chiefly or partly determined by surface irregularities on different scales. Traditionally, three ranges of irregularities have been considered: microtexture, macrotexture, and roughness. Recent research into the relations between performance and pavement characteristics has revealed the part played by a hitherto unchecked range of irregularities: the so-called megatexture, with wavelengths between 50 and 500 mm, the adverse effects of which (noise, vibrations, and extra rolling resistance) used to be attributed to macrotexture. Megatexture is out of the measuring range of conventional test methods and devices but can now be checked with the new generation of contactless profilometers, such as laser profilometers. Thus it is possible, in principle, to optimize road pavement performance while meeting most of the requirements, even minor ones, by considering that some surface characteristics must be present (micro- and macrotexture) and that others are undesirable (megatexture and roughness).

Traditionally, road surface requirements and specifications are intended to ensure, first, the safety of road users and, second, their comfort. At present, constantly increasing road traffic has a considerable impact on the environment and the economy. Recent awareness of the influence of surface characteristics has extended the performance requirements for road pavements, resulting in conflicts between apparently contradictory requirements. This paper reviews the main performance requirements for road pavements as well as the surface characteristics that determine performance; it shows that it is possible, in principle, to meet most if not all requirements without compromising any. The key to the problem lies in investigating the part played by a characteristic that the PIARC Technical Committee on Surface Characteristics has termed "megatexture" (*1*).

MEGATEXTURE

Figure 1 shows the deformation of a tire traveling over various road profiles with irregularities of the same amplitude but different wavelengths. This deformation results from two components: a stationary component (broken line), which does not depend on the shape of the profile and corresponds to the deformation that the tire would have undergone on a rectilinear profile (i.e., a flat surface); and an alternate component that varies with the shape of the profile. It can be seen that the second component is maximized on a profile whose wavelength (λ) approaches the footprint length (a) of the tire. More exactly, it can be shown that this critical wavelength equals $a/2$ (*2*), which generally is about 50 to 100 mm, both for passenger cars and for trucks.

Such surface irregularities are bound to cause dynamic effects that generate vibrations inside vehicles, tire/road contact noise inside and outside vehicles, and extra fuel consumption from rolling resistance (*3, 4*). Even though they seem to match the definition of roughness (ASTM E867) and could be thought of as small-scale roughness, this range of irregularities is out of the span of the various roughness measuring devices; and they cannot be detected from sand patch tests, either. Moreover, because of the specific nature of their effects, they should be distinguished from the ranges of irregularities hitherto considered by road engineers. That is why the scale of relevant wavelengths (λ) has now been divided as follows by the PIARC Technical Committee on Surface Characteristics (*1*):

Microtexture: $\lambda < 0.5$ mm,
Macrotexture: 0.5 mm $< \lambda <$ 50 mm,
Megatexture: 50 mm $< \lambda <$ 500 mm, and
Roughness: 0.5 m $< \lambda <$ 50 m.

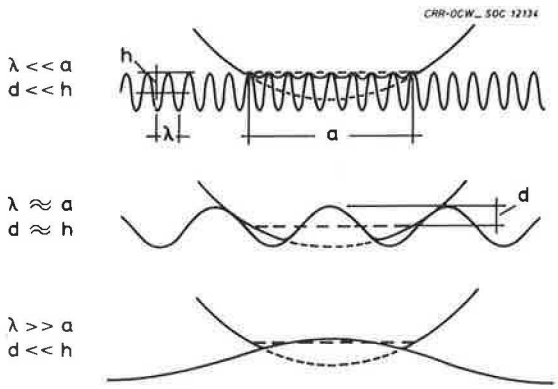

FIGURE 1 Deformation of tire when rolling on a profile with undulations of variable wavelength (*d*: alternate component of tire deformation; *a*: length of tire footprint; *h*: mean profile depth; λ: profile wavelength).

Belgian Road Research Center, Boulevard de la Woluwe, 42, B-1200 Brussels, Belgium.

In that definition, megatexture extends beyond the above-mentioned critical domain and reaches up to the lower wavelength cutoff of the response of the conventional roughness-measuring devices.

Megatexture can be produced by deterioration of the road surface: alligator cracks and spalling, small potholes, plucking, and scabbing. It also exists, however, on roads in good condition or those newly built. It can be a byproduct of the way macrotexture is achieved: a surface dressing with two chipping sizes, a chipped bituminous or cement concrete, or a stripped concrete (a technique for exposing the aggregates) can present the tire with an irregular contact area because of a lack of homogeneity of macrotexture. Or it can originate from the laying process: corrugation and other kinds of "waviness" sometimes show up on top of cement concrete layers and could be due to vibrations of the paving machine, the action of the smoothing beam, and other possible factors or circumstances.

PERFORMANCE FOR SAFETY

Skid Resistance

Wet road skid resistance is achieved (provided there is also good transverse evenness) by the presence of two ranges of surface irregularities (*5*): (1) microtexture, which ensures preservation of a high friction coefficient by breaking the water film on the asperity tips of the pavement that remain in contact with the tire, and (2) macrotexture, which drains away the water at the tire/pavement interface, preventing the buildup of hydrodynamic pressure that may induce aquaplaning. In this way, macrotexture helps keep a high coefficient of friction at high speeds.

When related to profilometric measurements on dozens of road sections with varying pavement characteristics (*2*), sideway force coefficient (SFC) measurements indicate that the drop in SFC between 20 and 80 km/h presents a maximum correlation with the surface irregularities of 20 mm in wavelength (Figure 2). This finding agrees well with the theoretical and experimental study of Bond et al. (*6*), which pointed out that, other things being equal, maximum effectiveness of drainage at tire/pavement contact is achieved where irregularities have wavelengths of 8 to 16 mm.

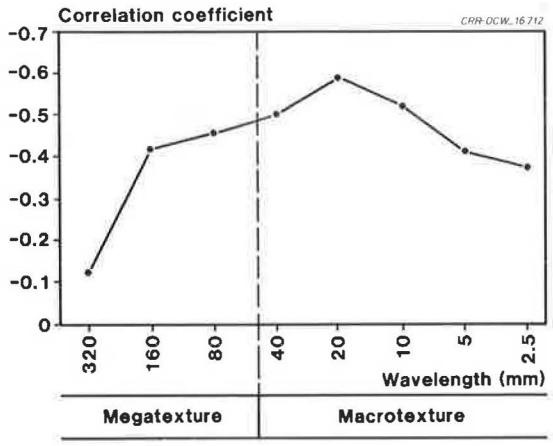

FIGURE 2 Correlation coefficient between drop in SFC from 20 to 80 km/h and amplitude of surface irregularities in relation to their wavelength (number of road sections = 36).

Splash and Spray

Studies have not quantitatively associated splash and spray with a given range of irregularities. Nevertheless, it may reasonably be assumed that splash and spray will be lessened as the surface characteristics of the pavement allow more effective drainage and minimize the thickness of the water film. Apart from cross slope and the absence of ruts, macrotexture should also have a favorable effect.

Optical Properties

The synthesis recently published jointly by the International Commission on Illumination and PIARC (*7*) defines three optical properties of road surfaces beneficial to safety:

1. The average dry-weather luminance coefficient, which must be high to ensure that the road contrasts well with the surrounding landscape both in daylight and under public lighting at night;
2. The luminance coefficient for grazing illumination, which must be high to ensure effective retroreflection of road illumination from car headlights; and
3. The specular factor, which must be as low as possible to avoid glare being produced by the headlights of opposing cars on the wet pavement at night.

These three conditions will be fulfilled all the better as the surface has a marked macrotexture. Moreover, the latter helps to improve the visibility of road markings on wet pavement (*8*).

Road-Hold

To allow maximum tire grip, the vertical action on the wheel must be as constant as possible. Critical frequencies in this respect range from 5 to 20 Hz, which approximately corresponds to the roughness of wavelengths of 0.5 to 8.0 m (*9*). It should be remembered that transverse irregularities (ruts and asymmetry between left- and right-hand longitudinal profiles) must also be avoided.

PERFORMANCE FOR ECONOMY

Dynamic Loads

Irregularities in the road profile subject the sprung and unsprung masses of vehicles to vertical oscillations that cause the loads exerted on the pavement to vary by as much as 10 to 20 percent with respect to their static values. Since the relations between loads and their damaging effects are strongly nonlinear, this fluctuation is equivalent to a 30 to 40 percent increase in the number of equivalent standard axles (*10*) and thus results in accelerated deterioration of the pavement. The ranges of

wavelengths involved are those that correspond to the resonant frequencies of the tires (about 1 Hz) and the body (about 15 Hz) and to medium or high speeds (15 to 30 m/s), which virtually cover the whole range of roughness (1 to 30 m).

Vehicle Wear

Studies conducted by the World Bank in Brazil (*11*) have made it possible to establish significant correlations between the consumption of spare parts and an overall assessment (QI) of the roughness of roads considered in the statistical analysis. Under the worst conditions, maintenance costs may be up to 20 percent higher.

More specific studies on tire wear have shown a strong dependence on texture. For example, tires were found to wear down three times more rapidly on a surface that was both harsh and rough than on another that was merely rough (*12*). Observations clearly point to microtexture as the determining factor (*6*).

Rolling Resistance

Using an apparatus developed at the Belgian Road Research Centre, measurements of rolling resistance were performed on paved roads and related to surface irregularities. Rolling resistance was 47 percent higher on the worst surface than on the best. This amounts to potential fuel savings of up to 9 percent. Various ranges of surface irregularities seem to contribute to the higher rolling resistances observed, but megatexture appears to be the most important factor. The rolling resistance coefficient of a car tire at 50 km/h presents a maximum correlation with the level of the irregularities of 80 mm in wavelength (Figure 3) (*4*).

PERFORMANCE FOR COMFORT AND THE ENVIRONMENT

Traffic Noise

One of the major, often dominant sources of noise emitted by vehicles turns out to be tire/road interaction (*1*). Tire/road contact noise varies greatly (more than 10 dB[A]) with certain surface characteristics. By studying the relations between the spectrum of the profile irregularities of closed-textured pavements and the spectrum of the tire/road contact noise generated by a test car, it has been possible to establish the following (*13, 14*) (see Figure 4):

1. When surface irregularities with wavelengths close to 80 mm increase in amplitude, the level of tire noise increases; this effect is apparent mainly in the low-frequency part (< 1 kHz) of the sound spectrum.
2. On the other hand, when surface irregularities with wavelengths close to 3 mm increase, the level of tire noise decreases; this effect is apparent mainly in the high-frequency part (> 1 kHz) of the sound spectrum.

The first effect results from tire vibrations induced by megatexture. The second is most generally assumed to be connected with suction noise ("air pumping") that can be reduced

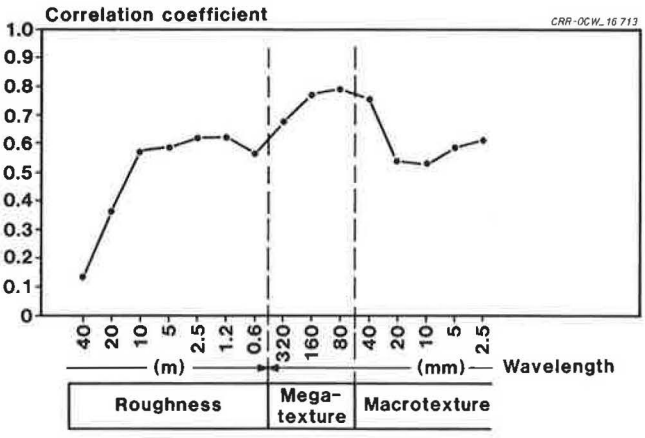

FIGURE 3 Correlation between rolling resistance coefficient and amplitude of surface irregularities in relation to their wavelength (number of road sections = 37).

by the presence of irregularities on the scale of the width of the grooves in the tire tread, which would explain the beneficial effect of a fine macrotexture. This air-pumping abatement effect is also obtained by open-textured surfaces.

Noise Inside Vehicles

Noise inside vehicles not only causes discomfort but also affects safety by contributing to the fatigue of drivers and consequently impairing their performance. Moreover, this aspect may be expected to gain importance with the extension of verbal communication in vehicles (e.g., radio guidance, vocal commands). Noise levels inside medium-sized passenger cars are determined mainly by tire/road contact noise. Variations observed between different pavements may exceed 15 dB(A) (*3*). Studies by the author have revealed the predominant influence of megatexture, as shown in Figure 5.

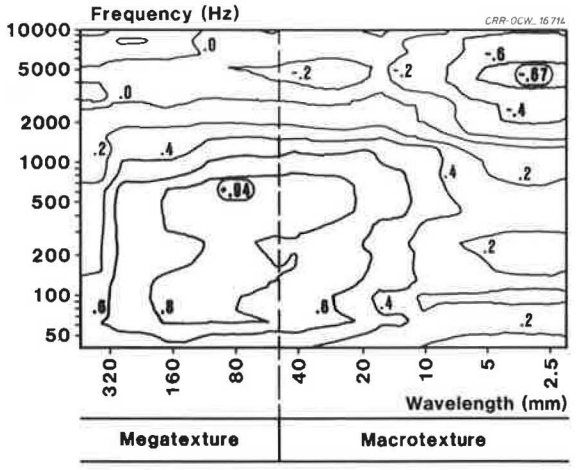

FIGURE 4 Contour lines representing correlation coefficient between spectrum of tire/road contact noise (outside the vehicle) and power spectrum of longitudinal profile of pavement (number of road sections = 33). The two extreme values of the correlation coefficient are denoted by circles.

Vibrations Inside Vehicles

The influence of surface irregularities on comfort levels has been subjectively evaluated by panels of drivers in many studies, which have established the relations between various overall measurements of roughness spanning a wide range of wavelengths approximately contained between 0.5 m and 50 m. A recent investigation (*15*) to define better the wavelengths that are critical in this respect has pointed out, using correlations established between the power spectrum of the road profile and the mean comfort rating by a panel, that short-range roughness ($0.5 < \lambda < 3$ m) is determinant. Below 0.5 m, the drop in the correlation coefficient could either actually reflect a smaller contribution of the shorter wavelengths to the feeling of discomfort or be caused by the proximity of the cutoff frequency of the profilometer used. If it were confirmed that megatexture contributes to the feeling of discomfort, it would be difficult to discriminate between the part of the vibrations and that of the noise, the two phenomena being connected, as shown in some studies published by manufacturers (*16*).

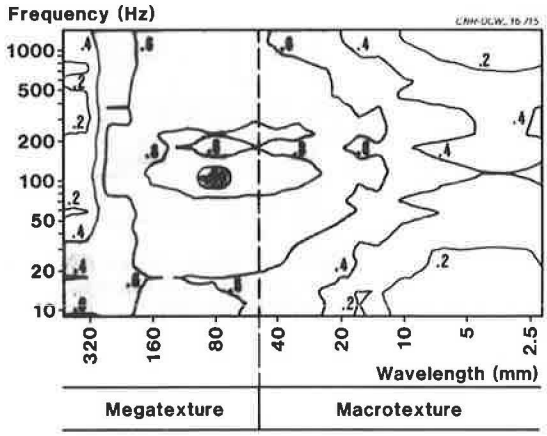

FIGURE 5 Contour lines representing correlation coefficient between spectrum of tire/road contact noise (inside vehicle) and power spectrum of longitudinal profile of pavement (number of road sections = 33). The maximum value of the correlation coefficient is denoted by a circle.

CONCLUSIONS

A review has been presented of various features of road pavement performance that may need to be considered; the critical range of wavelengths of longitudinal profile irregularities that determine these features has been indicated for each. An overview is presented in Figures 6 and 7. This approach is based on the results of recent studies that, using modern profilometric methods and spectrum analysis, have revealed the hitherto ignored role of megatexture. It makes it possible, in principle, to solve apparent conflicts between certain

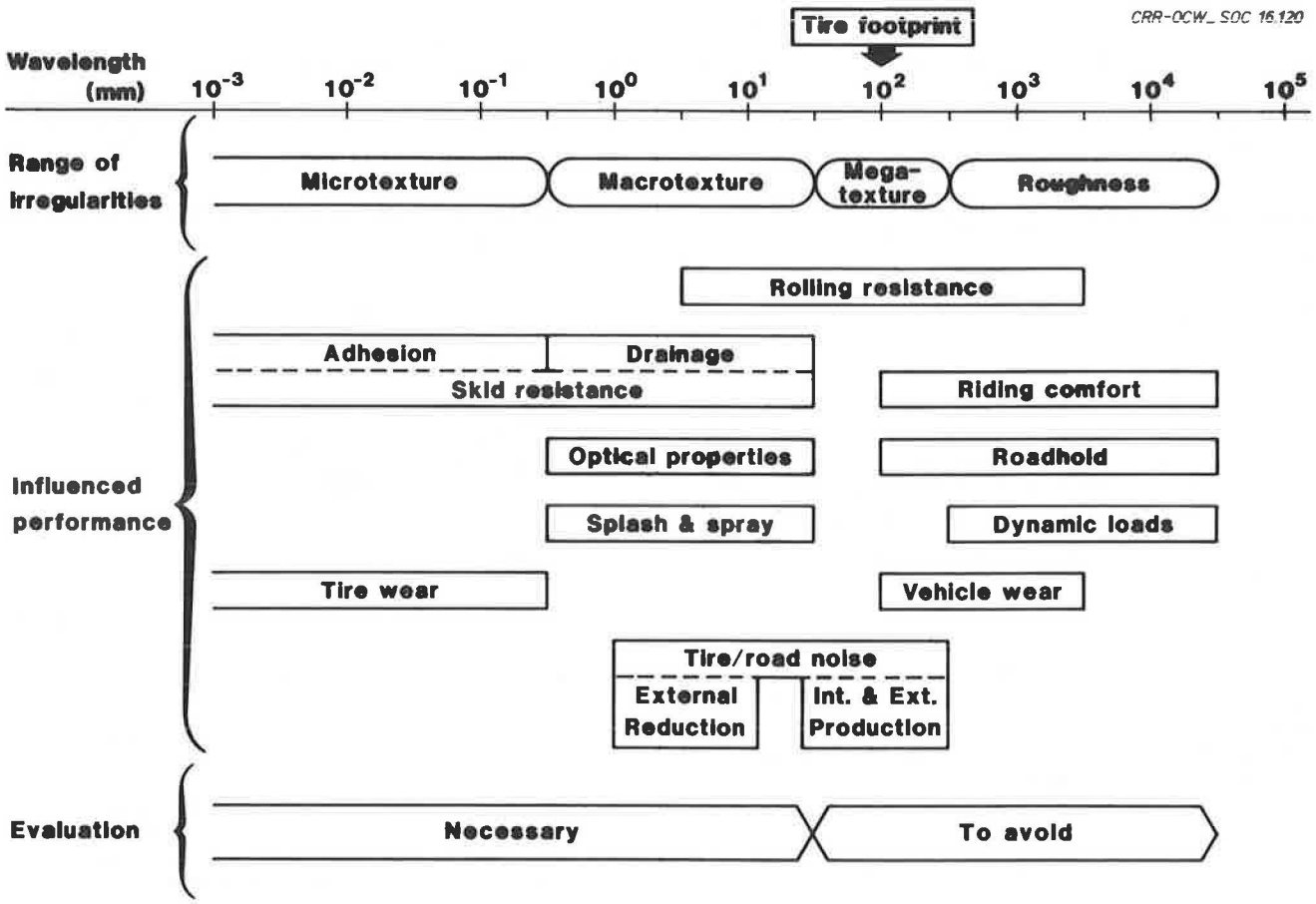

FIGURE 6 Performance features of road pavements against wavelength ranges of surface irregularities that influence them.

	Texture			Roughness
	Micro	Macro	Mega	
Skid resistance	+	+		
Roadhold				−
Splash & Spray		+		
Reflectance		+		
Dynamic loads				−
Vehicle wear				−
Tire wear	−			
Rolling resistance			−	
Vibrations (inside)			−	−
Noise (inside)			−	
Noise (outside)	+	+	−	

FIGURE 7 Relations between performance features and surface characteristics. Beneficial and adverse effects are denoted by + and −, respectively.

requirements, such as skid resistance on one hand and low tire noise and low rolling resistance on the other hand, which seemed to dictate contradictory specifications for macrotexture. Figure 7 shows that the undesirable effects that are often attributed to macrotexture are actually due to megatexture. This clears the way for optimizing surface characteristics by setting a simple criterion that should make it possible to maximize compliance with virtually all performance requirements (even minor ones, with the exception of tire wear) without compromising any. It consists of recognizing that there are two categories of irregularities: one that must be present (micro- and macrotexture) and another whose presence is undesirable (megatexture and roughness). The limit between the two is at approximately 50 mm of wavelength. Porous asphalt surfaces may be included in the overview provided it is considered that the macrotexture function is performed by porosity, which may be viewed as a negative, or inversed, macrotexture.

ACKNOWLEDGMENTS

This work has been financially supported by IRSIA, the Belgian Institute for Encouraging Research in Industry and Agriculture. It owes much to the author's years-long participation in the PIARC Technical Committee on Surface Characteristics, to the members of which he expresses his thanks for their contributions and review work.

REFERENCES

1. P.I.A.R.C. *Report of the Technical Committee on Surface Characteristics*. Presented at XVIIIth World Road Congress, Brussels, Belgium, 1987.
2. G. Descornet. *Tyre/Road Noise Generating Mechanisms*. Internationales Seminar, Reifengeräusch und Strassenbau, ETH Mitteilung nr.57, Zürich, Switzerland, 1984.
3. G. Descornet. *Experimental Study of the Rolling Noise of a Test Car on Various Existing Road Surfaces in Belgium*. Presented at International Tire Noise Conference, Stockholm, Sweden, 1979.
4. G. Descornet. *Influence of Surface Characteristics on Rolling Resistance and Fuel Consumption*. Presented at International Conference, Roads and Road Traffic for the Year 2000, Berlin, Federal Republic of Germany, 1988.
5. P.I.A.R.C. *Report of the Technical Committee on Surface Characteristics*. Presented at XVIth World Road Congress, Vienna, Austria, 1979.
6. Bond, Kathekda, Lees, and Williams. Tyre/Road Surface Interaction. *Journal of the Institution of Highway Engineers*, Nov. 1976.
7. *Common Technical Report*. International Commission on Illumination (C.I.E) and P.I.A.R.C. Road Surfaces and Lighting, Paris, France, 1983.
8. Ph. Léger. Marquage Routier—Visibilité—Rétroréflexion. *Bulletin de Liaison des Laboratoires des Ponts et Chaussées* No. 114, 1981.
9. P.I.A.R.C. *Report of the Technical Committee on Skid Resistance and Roughness*. Presented at XVth World Road Congress, Mexico, 1975.
10. Molenaar and Sweere. *Road Roughness, Its Evaluation and Effect on Riding Comfort and Pavement Life*. Delft University of Technology, The Netherlands, 1981.
11. *Research on the Interrelationships Between Costs of Highway Construction, Maintenance and Utilization*. Final Report. Ministerio dos Transportes (Brasil) and United Nations Development Program (UNDP), 1981.
12. R. W. Lowne. *The Effect of Road Surface Texture on Tyre Wear*. Laboratory Report LR265. Road Research Laboratory Crowthorne, Berks., England, 1969.
13. U. Sandberg and G. Descornet. *Road Surface Influence on Tire/Road Noise (Part I)*. Presented at International Conference on Noise Control Engineering, INTER-NOISE 80, Miami, Fla., 1980.
14. G. Descornet and U. Sandberg. *Road Surface Influence on Tire/Road Noise (Part II)*. Presented at International Conference on Noise Control Engineering, INTER-NOISE 80, Miami, Fla., 1980.
15. M. S. Janoff. Methodology for Computing Pavement Ride Quality from Pavement Roughness Measurements. In *Transportation Research Record 1084*, TRB, National Research Council, Washington, D.C., 1986, pp. 9–17.
16. Yoshida, Suzuki, and Suzuki. *Analysis and Improvement of Vibration and Acoustic Characteristics of Automobiles*. SAE Paper 740950, Society of Automotive Engineers, Warrendale, Pa., 1974.

Publication of this paper sponsored by Committee on Surface Properties—Vehicle Interaction.

A Two-Point Vehicle Classification System

BERNARD C. MCCULLOUGH, JR., SIAMAK A. ARDEKANI, AND LI-REN HUANG

The counting and classification of vehicles is an important part of transportation engineering. In the past 20 years many automated systems have been developed to accomplish that labor-intensive task. Unfortunately, most of those systems are characterized by inaccurate detection systems and/or classification methods that result in many classification errors, thus limiting the accuracy of the system. This report describes the development of a new vehicle classification database and computer program, originally designed for use in the Two-Point-Time-Ratio method of vehicle classification, which greatly improves the accuracy of automated classification systems. The program utilizes information provided by either vehicle detection sensors or the program user to determine the velocity, number of axles, and axle spacings of a passing vehicle. It then matches the axle numbers and spacings with one of thirty-one possible vehicle classifications and prints the vehicle class, speed, and wheelbase lengths. It also tabulates and prints totals and average speeds for each vehicle type. This paper describes the database built and utilized, as well as a roadside experiment conducted to test the accuracy of the database and the classification program, showing the classifications to be highly accurate.

In 1912, the U.S. government realized that a vast network of public roads had to be built and maintained for automobile travel. Today, that network consists of a staggering 3.8 million miles of highways. Unfortunately, that growth has not been able to keep up with the steadily rising number of automobiles in the United States. Thus many urban areas (and even some rural areas) are plagued with congestion problems.

To prevent such problems from occurring, and to alleviate those that do occur, careful planning and monitoring are needed. This is often accomplished through the use of traffic surveillance and control systems or traffic flow data collection systems. Those systems are also used in pavement management and maintenance to estimate pavement loads due to various types of trucks, depending on the axle configuration. Such systems are used in a similar way in bridge maintenance and management. A common feature of such systems is a method of counting and classifying the number of vehicles using the facility. For many years this was commonly done by roadside observers who spent long hours sitting in a vehicle along the facility, manually recording and totaling the number and type of vehicles going by. The job was tedious, and the pay was usually minimum wage; because of the manpower and man-hours required, however, the cost of such a count was often high. To offset such costs, many techniques for the automatic counting, length determination, and classification of vehicles have been developed within the past decade. One popular method, especially in Europe, is the Automatic Length Indication and Classification Equipment method, known as "ALICE," which was introduced by D. D. Nash in 1976 (*1*). This report covers a simpler, more accurate system of vehicle counting and classification and details the development of the classification software that will enable it to surpass previous systems in accuracy.

Although many articles on vehicle classification methods have appeared in transportation journals within the past decade, most have dealt solely with new types, or applications, of vehicle detection systems. For the actual classification of the vehicles detected, most have depended on the classification method developed by D. D. Nash (*1*) for his Automatic Length Indication and Classification Equipment system. Therefore this paper begins with an overview of that system, which is referred to as the ALICE method.

THE ALICE METHOD

In 1974, during a project known as the West London Area Traffic Control Experiment in England, planners encountered a major problem. Owing to the traffic composition changes that occurred at various times, it was determined that the vehicular counts to be utilized in the experiment would have to be weighted by vehicle type. An investigation of the traffic instrumentation equipment available at the time revealed that nothing met the requirements, and thus the planners set out to create such a system. What they created was termed the Automatic Length Indication and Classification Equipment, or ALICE, method. It was introduced in an article by D.D. Nash (*1*).

ALICE utilizes two loop detectors and an axle detector, which are placed in sequence in a short (about 5.5-m) segment of highway (Figure 1).

As a vehicle enters the segment, it is detected by the first loop detector and then by the second loop detector after a short time interval, called $t1$. The axles of the vehicle then trip the axle detector as they pass; and the time interval between axles, called $t2$, is recorded. The time intervals are measured using a rather complex circuit consisting of a crystal oscillator, a comparator, and several counters. The distance between the leading edges of the two loop detectors, called $d1$, is known and is related to $t1$ and the velocity of the vehicle.

B. C. McCullough, Jr., F. R. Harris, Inc. S. A. Ardekani, Virginia Polytechnic Institute and State University, Blacksburg 24061. Current affiliation: University of Texas at Arlington, Arlington 76019. L.-R. Huang, University of Texas at Austin, Austin 78712.

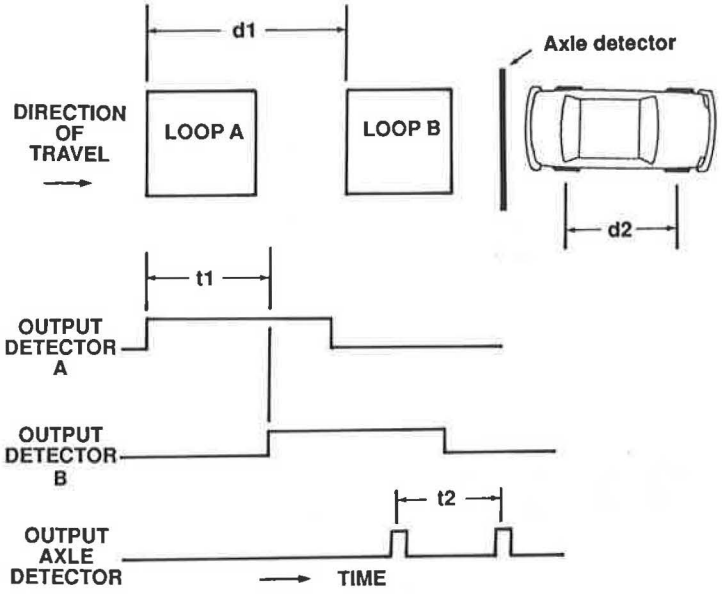

FIGURE 1 Principle of the ALICE method.

Likewise, $t2$ is related to the velocity of the vehicle and the distance between the two axles, termed $d2$. Since this produces two equations with two unknowns, $d2$ can be determined. This calculation is performed within the circuit, which results in the recording of the length, axle spacings, speeds, and gap distance for each vehicle that passes through the segment.

The ALICE system then compares the axle numbers and spacing data of the vehicle with a database, consisting of the axle number and spacing ranges of fourteen vehicle groups, using a logic program. The database includes the following classification groups as termed by ALICE (and as commonly referred to):

1. Motorcycles,
2. Private cars and light vans,
3. Two-axle heavy goods vehicles (two-axle single-unit trucks or vans),
4. Three-axle rigid goods vehicles (three-axle single-unit trucks),
5. Four-axle rigid goods vehicles (four-axle single-unit trucks),
6. Three-axle articulated lorries (three-axle tractor-trailers),
7. Four-axle articulated lorries (two-axle tractors with two-axle trailers),
8. Five-axle articulated lorries (two-axle tractors with three-axle trailers),
9. Four-axle articulated lorries (three-axle tractors with one-axle trailers),
10. Five-axle articulated lorries (three-axle tractors with two-axle trailers),
11. Six-axle articulated lorries (three-axle tractors with three-axle trailers),
12. Road trains (single-unit trucks with trailers),
13. Cars with caravan/trailer, and
14. Buses or coaches.

If the axle data of the vehicle fit within the spacing ranges of one of those groupings (Figure 2), then the vehicle is classified as a member of that group and recorded.

THE TWO-POINT-TIME-RATIO METHOD

The Two-Point-Time-Ratio, hereafter referred to as TPTR, method of vehicle classification is similar to the ALICE method, except that only two vehicle detectors are needed to determine the same data (except for vehicle length, which is not essential for classification purposes); thus, it is more efficient in its use of hardware. The detector sensors are placed in a short section of highway, similar to the ALICE sensors; but more flexibility is offered because in TPTR, unlike ALICE, any combination of passage loop detectors, presence loop detectors, or axle detectors may be utilized. For simplicity the first detector in the sequence is referred to as sensor A and the second detector, as sensor B, as shown in Figure 3.

As a vehicle enters the segment, its front axle is initially detected by sensor A and then by sensor B after a short time interval, which is referred to as $T0$ (and is equivalent to the variable $t1$ in the ALICE method). The time interval(s) between axle detections at sensor A are also determined, with $T1$ representing the interval between the first and second axles, $T2$ representing the interval between the second and third axles, and so on.

As the work progressed on the circuitry necessary to interface the TPTR sensors with a microcomputer, the focus shifted to possible classification programs. The first such program that was considered was one that would utilize the methodology of the ALICE system; it was determined, however, that such a program would not be well suited for use with the TPTR system for several reasons. One of the predominant reasons was the limited number of vehicle classes covered by the ALICE database. Since the database resulted from observations in England in the early 1970s, it was biased toward

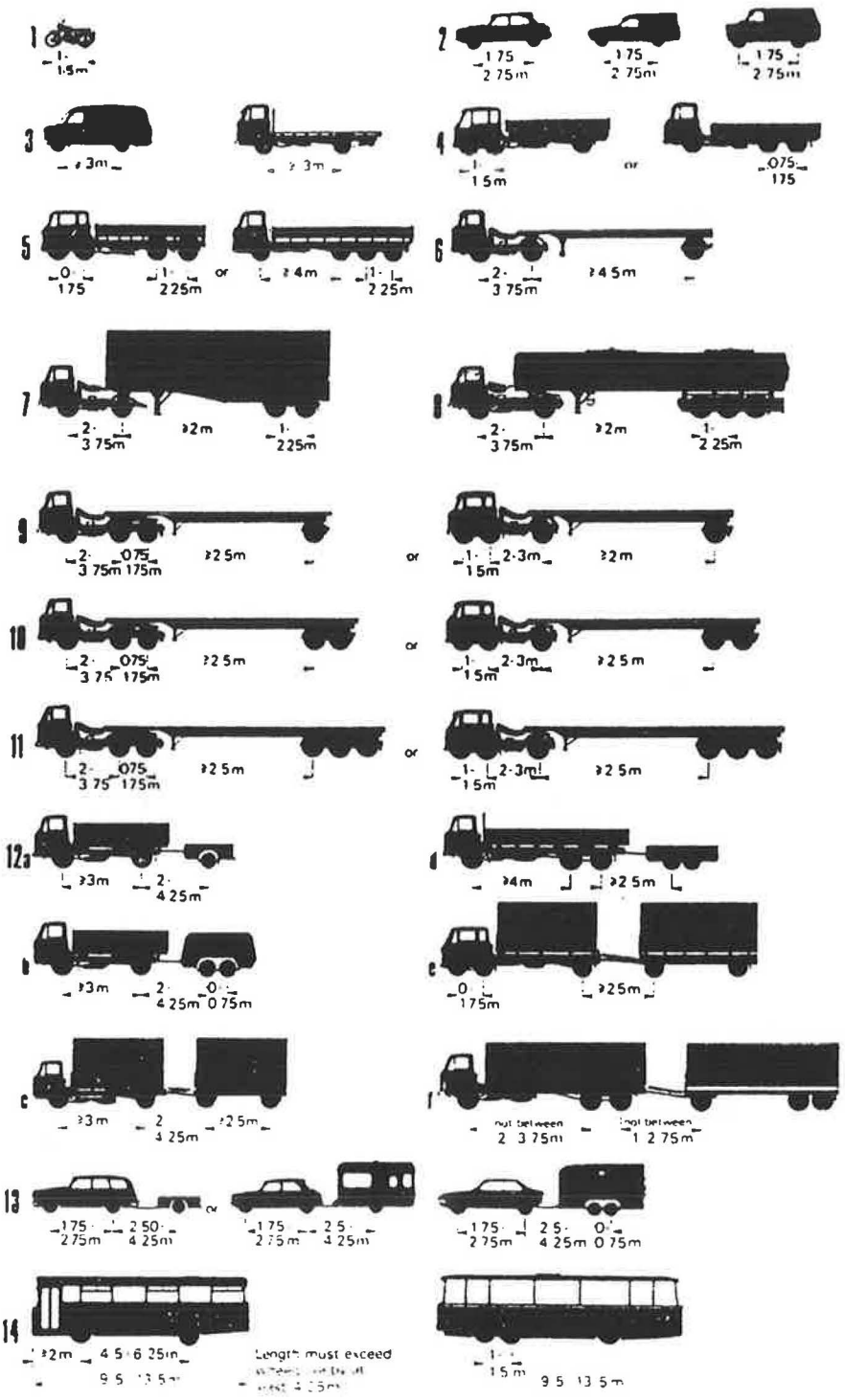

FIGURE 2 ALICE classification groups and ranges.

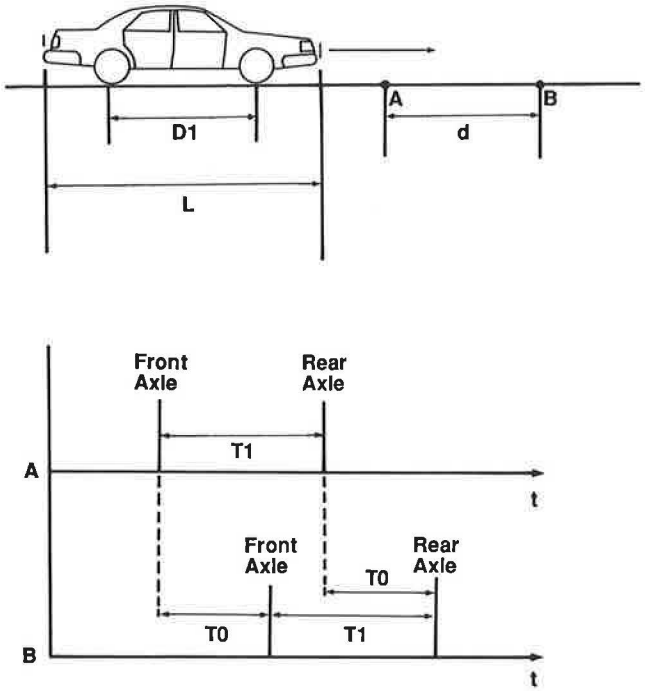

FIGURE 3 Principle of TPTR method.

vehicles of European design, which in some cases are very different from North American designs. For example, a two-axle vehicle with a wheelbase of 10 ft (3.07 m), such as the typical American-made, sedan-type passenger car, would be classified as a two-axle, heavy goods vehicle by a classification system using the ALICE grouping ranges. The ALICE database also contains many axle configurations, such as three-axle full trailers, which are very rarely seen in North America. The database also lacks groupings for vehicles, such as tractor twin-trailers, that have become common in recent years. Therefore it was determined that an updated, and more extensive, classification program was needed for the TPTR system.

The objective therefore was to create a flexible, modern classification program that could be interfaced to operate automatically with the TPTR system, or operated interactively by an individual, and would result in greater accuracy than the ALICE system for the North American vehicle mix.

The Classification Methodology

This classification program was set up so that it could be used in either of two modes. The first mode, referred to as the automatic mode, is for use when the microcomputer is directly interfaced with the field sensors. In that mode data are retrieved directly from the storage file. The second mode, referred to as the interactive mode, is interactive and allows data to be entered from the computer keyboard in either time-interval or wheelbase-spacing form. The classification theory utilized by both modes is the same, and the process can be divided into two steps: speed and wheelbase determination, and vehicle classification.

The theory behind the calculation of speed in this program is simple. Point A and point B (Figure 3), the locations of the two sensors, are a known distance apart. The time taken by the vehicle to travel that distance, $T0$, is also known (one of the time intervals retrieved from data storage or entered by the operator). Therefore, by dividing the distance by the time, the program computes the speed of the vehicle.

The program then uses that speed calculation and the time intervals between axles ($T1$, $T2$ . . .) to compute the axle spacings. $D1$ (the distance between the first two axles) is computed by multiplying $T1$ by the vehicle speed. Likewise, $D2$ can be calculated from $T2$, $D3$ from $T3$, and so forth.

Those simple calculations result in obtaining estimates of the speed of the vehicle and, more important, the axle spacings, which are the basis for the vehicle classification.

The classification methodology on which this program is based rises from the fact that the number and spacing of a vehicle's axles are closely related to the length and use of that vehicle. Because of different designs, manufacturers, and options, very few of the thousands of vehicle models produced are exactly alike in all wheelbase measurements. While no single set of measurements can be used, however, ranges can be developed that will include most, if not all, of the vehicle models that are similar in appearance and function. For example, one vehicle type is the passenger automobile, which is intended for the transport of a small number of people and a low amount of weight. It is characterized by a frame that has two axles, a length of less than 20 ft, and a wheelbase spacing of between 6 and 13 ft. The development of such ranges for all vehicle types is discussed later, in the section entitled "Vehicle Classes." Those ranges are the basis for the computer program used for classification.

In the first step of the classification process, the program retrieves the axle count and proceeds to the section where vehicles with that number of axles are analyzed. The program then retrieves the axle spacing data and compares them to the axle spacing ranges of the most common vehicle class with the same number of axles. If all the axle spacings of the vehicle fit within the ranges of that class, then the vehicle is classified as a member of that class. If not, then the axle data are compared to the ranges of the second most common vehicle, and so on, until the vehicle is classified. If the vehicle data do not fit into any of the class ranges in the database, then the vehicle is classified as an "unknown X-axle vehicle" (where X is the number of axles). This is unlike the ALICE method, which classifies any vehicle that does not fit within any other group into group 12 ("road trains"). Because of the design of the program, it is unlikely for a vehicle to be classified into more than one group; but in those cases where a vehicle's wheelbase can be associated with more than one class, the operator is alerted through an information screen that may be viewed after the classification. That screen lists the most common vehicle in the class, other vehicles within the class, and vehicles of other classes that may be erroneously placed in that class owing to similar axle spacings.

For example, a two-axle vehicle with a 14-in. wheelbase is detected by the sensors. The program shifts to the section for analysis of two-axle vehicles. After unsuccessfully comparing the 14-in. wheelbase with the range for the small and midsize car class (6–9 ft) and the range for the large passenger car class (9–13 ft), it successfully matches that wheelbase to the two-axle, single-unit truck class (13–25 ft). Therefore the vehicle is classified as a two-axle single-unit truck. That classification is displayed on the screen along with the calculated speed of the vehicle (in miles per hour) and the wheelbase.

A quick glance at the information screen, invoked with a response of yes to the next prompt, reveals that the most common vehicle in this class is indeed the two-axle single-unit truck and that recreational vehicles (RVs) and conventional schoolbuses are also included in the class. It also reveals that limousines and crew-cab pickup trucks (both members of the large passenger car class) have wheelbases that may cause them to be incorrectly placed in this class.

The program also tabulates totals as it proceeds. These totals include the number of motorcycles, cars, single-unit trucks, buses, tractor-trailers, and others. The average speed of each of these groups is also tabulated and displayed along with a breakdown of the number of each class within the group.

The method used by this program is important, but the key to its success is the extensive number of vehicle classes covered and the ranges developed for each.

Vehicle Classes

In the early stages of the project, field observations were conducted to determine a list of the predominant vehicle types, or classes. The observations consisted of watching the surrounding traffic for new types of vehicles while driving on several roads and highways in the state of Virginia. The number of axles, along with their configuration and approximate spacings, was noted for many vehicle types, with special attention paid to those types that were not covered within ALICE's classes. Vehicle types common in other areas of North America, but prohibited in Virginia, such as triple-trailer truck units, were included in the list. This continued until it was believed that all of the major, and as many as possible of the minor, types of vehicles had been accounted for in the list. Each of the vehicle types was then given a two-digit class number for identification. The list of vehicle types and their identification classes is shown in Table 1.

The numbering system was developed in research conducted at the University of Texas Center for Transportation Research (*2*). The first digit refers to the number of axles of the vehicle type, and the second digit refers to the axle spacing pattern. Extensive research was then performed to find suitable wheelbase ranges for each of the vehicle types in the list.

The development of the ranges for each class often depended upon the development of ranges for other classes within the same vehicle group. The development of the ranges is dis-

TABLE 1 VEHICLE CLASSES AND DESCRIPTIONS

Class	Vehicle Description
21	Small or midsize passenger car, jeep, small pickups
22	Large passenger car, fullsize pickup truck, vans
23	Two-axle single-unit truck, RV's, schoolbuses
24	Motorcycles or mopeds
25	Two-axle transit bus
31	Three-axle single-unit truck
32	Two-axle tractor with one-axle semitrailer
33	Passenger car with single-axle trailer
34	Motorcycle with trailer
35	Three-axle transit bus or coach
36	Two-axle single-unit truck with one-axle trailer
41	Two-axle tractor with two-axle semitrailer
42	Three-axle tractor with one-axle semitrailer
43	Four-axle single-unit truck
44	Passenger car with two-axle trailer
45	Two-axle single-unit truck with two-axle trailer
46	Three-axle single-unit truck with one-axle trailer
51	Three-axle tractor with two-axle semitrailer
52	Two-axle tractor with two short trailers
53	Three-axle single-unit truck with two-axle trailer
54	Four-axle single-unit truck with one-axle trailer
55	Two-axle tractor with three-axle semitrailer
61	Three-axle tractor with three-axle semitrailer
62	Three-axle tractor with two short trailers
63	Four-axle single-unit truck with two-axle trailer
64	Four-axle tractor with two-axle semitrailer
71	Three-axle tractor with long and short trailers
72	Two-axle tractor with three short trailers
73	Four-axle tractor with three-axle semitrailers
81	Three-axle tractor with three short trailers
91	Three-axle tractor with two long trailers

TABLE 2 WHEELBASE RANGES (IN FEET) BY CLASS

Class	W1	W2	W3	W4	W5	W6	W7	W8
21	6-9							
22	9-12.25							
23	12.25-25							
24	3-6							
26	25-35							
31	8-25	2-6						
32	8-20	20-45						
33	6-12.25	6-20						
34	3-6	3-7						
35	25-35	2-6						
36	12.25-25	6-20						
41	8-20	15-45	2-12.5					
42	8-25	2-6	15-45					
43	8-25	2-6	2-6					
44	6-12.25	6-15	2-6					
45	12.25-25	6-15	2-6					
		6-12	7-20					
46	8-25	2-6	6-15					
51	8-25	2-6	15-45	2-12.5				
52	8-25	11-36	6-20	7-35				
53	8-25	2-6	6-15	2-6				
			6-12	7-20				
54	8-25	2-6	2-6	6-15				
55	8-20	11-42	2.6	2-6				
61	8-25	2-6	11-42	2-6	2-6			
62	8-25	2-6	11-36	6-20	7-35			
63	8-25	2-6	2-6	6-15	2-6			
				6-12	7-20			
64	8-25	2-6	2-6	15-45	2-12.5			
71	8-25	2-6	11-45	2-6	7-15	11-25		
72	8-20	11-45	7-15	11-25	7-15	11-25		
73	8-25	2-6	2-6	11-42	2-6	2-6		
81	8-25	2-6	11-45	7-15	11-25	7-15	11-25	
91	8-25	2-6	11-45	2-12.5	7-15	2-6	11-45	2-12.5

cussed in this section on a group-by-group basis. The ranges obtained are shown in Table 2. In this table, *W*1 represents the distance between the first and second axles, *W*2 represents the distance between the second and third axles, and so on.

Motorcycles

The vehicle type that is most easily identified from its wheelbase is the motorcycle (class 24). Although model lengths have tended to increase in recent years, the motorcycle wheelbase has remained much shorter than that of any other vehicle. The first range considered for this vehicle type was the 1–1.5-m range used by ALICE. Field measurements showed that the lower limit was appropriate but that some models had wheelbases exceeding the upper limit. Therefore the lower limit was converted to the nearest equivalent length in feet, namely 3 ft, and the upper limit was extended to 6 ft, a distance that would include all the models inspected.

Motorcycles with small trailers were also encountered during research and were included in the vehicle list as class 34. These vehicles consist of a cycle with a short single-axle trailer connected to it at the hub of the rear wheel to provide additional luggage or storage space. The vehicles inspected were found to have distances of approximately 3 to 7 ft between the rear cycle axle and the trailer axle. Since these trailers can be used with most cycles, the range used for the distance between the first and second axles, *W*1, was the same as that used for class 24 (3–6 ft).

Passenger Cars

The most common type of highway vehicle is the passenger car, which accounts for more than half of the traffic on a typical highway. Every year, several manufacturers produce millions of these vehicles in a variety of hundreds of models and sizes. These range from tiny, two-door subcompact models to limousines. Naturally, most of those models have different wheelbases, encompassing a wide size range. As an example of the wide range in car wheelbases, consider the 1988 Yugo and the 1988 Cadillac Fleetwood. The Yugo has a wheelbase

of 84.6 in., whereas the Fleetwood has a wheelbase of 134.4 in., a difference of 50 in. in cars produced in the same year (*3*). Research determined that the shortest wheelbase among car models produced in the past 15 years was the 83.0-in. span of Triumphs produced between 1972 and 1980 (*4*). The vehicle with the longest wheelbase within the same period was the 1975 Cadillac Fleetwood, with a span of 151.5 in. (*5*). For most years, however, the longest wheelbase was 145 in. or less. If present trends continue, cars in the future will have shorter wheelbases than those currently seen. Such a trend led to the consideration of the lower limit of 6 ft used by Izadmehr (*2*).

Pickup trucks and vans are also included in the passenger car classes; thus, research was likewise performed to determine the upper limits of their wheelbase ranges. The lower limit was not examined thoroughly because field observations had revealed that limit to be much longer than 83 in. From brochures of various manufacturers, it was determined that most conventional, full-sized pickups had wheelbases of as much as 168 in. (*6*).

Based on those figures, and the fact that a significant number of single-unit trucks had been found to have wheelbases as short as 150 in., the lower and upper limits of the passenger car range were set at 6 ft (72 in.) and 12.25 ft (147 in.). This class was then split into two classes: class 21, for small and midsize cars, Jeeps, Blazers, and small pickups; and class 22, for large cars, vans, and full-size pickups. The point of division was selected as 9 ft, since it resembled figures used by automotive magazines (*3*) for such separation.

Two other classes were created for passenger cars with trailers. Class 33 is for passenger cars, pickups, Jeeps, and Blazers that are pulling a short, single-axle trailer. Class 44 is for such cars pulling a short, two-axle trailer. The range for the first axle spacing in each of these classes is the 6- to 12.25-ft range developed earlier. For the development of the range for the second axle spacing of these classes, other factors had to be considered. The first factor was that three-axle single-unit trucks have a first axle spacing that closely resembles that of larger passenger cars and a second axle spacing of 2 to 6 ft. The second factor was that the first axle spacing of three-axle tractor-trailers is also similar to that of passenger cars. Those tractor-trailers have a second spacing of 11 to 45 ft. From field measurements, it was determined that the distance between the rear passenger car axle and the front trailer axle is usually greater than 6 ft. It was also determined that for a three-axle vehicle with a second axle spacing greater than 20 ft, three-axle tractor-trailers were more common than cars with trailers. But for four-axle vehicles with second axle spacings greater than 15 ft, four-axle tractor-trailers were found to be more common.

Therefore class 33, cars with a one-axle trailer, was given a range of 6 to 20 ft for the spacing between the second and third axles.

Class 44, cars with a two-axle trailer, was given a range of 6 to 15 ft for the second axle spacing and a range of 2 to 6 ft for the third axle spacing, because that is the range of tandem axles.

Single-Unit Trucks

To determine appropriate intervals for the nine classes of single-unit trucks covered by the program, each class was divided into its components. Because of similarities between classes, the task could be reduced to the development of intervals for the five components that make up those nine classes. Those components are two-axle, three-axle, and four-axle single-unit trucks and one-axle and two-axle trailers.

The interval of 11 to 25 ft is suggested by Izadmehr (*2*) for two-axle single-unit trucks, but that interval was found to include many passenger cars and pickups and thus had to be altered. As described earlier in the section on passenger cars, research determined that an appropriate upper limit of the range for the passenger car class would be 12.25 ft, to minimize classification errors between the two classes. Therefore 12.25 ft, inclusive, was decided on as the lower limit for the interval. After research revealed a significant number of two-axle single-unit trucks with wheelbases of 24 ft, the suggested upper limit of 25 ft was adhered to.

Izadmehr (*2*) also suggests an interval of 8 to 26 ft for the first axle spacing and an interval of 2 to 6 ft for the second axle spacing of three-axle single-unit trucks. Since three-axle passenger cars are rare, the same lower limit constraints do not exist for these vehicles. All of the three-axle single-unit trucks observed during research fit within the suggested range, but some transit buses that were observed had 25-ft distances between the first two axles. Thus the ranges within the program for three-axle single-unit trucks were set at 8 to 25 ft and at 2 to 6 ft.

Izadmehr also suggests ranges of 8 to 25 ft and of 2 to 6 ft for the axle spacings of four-axle single-unit trucks. Since all such vehicles observed fit within those ranges, they were adopted into the program.

For the one-axle trailers an interval had to be determined for the distance between the last axle of the preceding truck and the axle of the trailer. As in the previous case with passenger cars, it was determined that ranges that included lengths shorter than 6 ft would result in the classification of the rear axle of some tandem-axle vehicles as a trailer, since some tandem-axle sets have spacings of 6 ft. Likewise, it was determined that ranges with upper limits exceeding 15 ft would result in numerous misclassifications of short tractor-trailer combinations. The interval selected was 6 to 15 ft.

For two-axle trailers, two types were noted. The first type involves a set of tandem axles near the rear of the trailer. The second type, called a full trailer, has a front axle and a rear axle. The range for single-axle trailers (6–15 ft) was chosen, along with the typical tandem-axle spacing of 2 to 6 ft, for the first type. Since few examples of the second type of trailer could be found, the first range used by the ALICE system was adopted, and a second range was created that was thought to typify short full trailers. Those ranges are 6 to 12 ft and 7 to 20 ft, respectively. The axle spacing ranges for each class that result from the preceding component spacings can be seen in Table 2.

Buses

Buses are probably the most difficult type of vehicle to differentiate from vehicles of other classes. This is due to the fact that most buses, especially schoolbuses, are constructed on frames that were designed for single-unit trucks. That results in a range of wheelbases from 12 ft (typical minibus) to more than 30 ft (long transit-type buses). The most common school-

bus, called a conventional type, has a wheelbase of about 22 ft, depending on the manufacturer, and thus cannot be distinguished from a single-unit truck built on the same, or a similar, frame. For that reason schoolbuses were put into the single-unit truck class (class 23). Transit buses and motorcoaches, however, are built on longer frames intended for their purpose.

Transit buses observed during research had wheelbases ranging from 20 ft to well beyond 30 ft. Intercity motorcoaches had first-axle spacings ranging from 25 to 30 ft.

As mentioned in the previous section on single-unit trucks, a significant number of 24-ft-wheelbase trucks were observed; thus the upper limit for class 23 was set at 25 ft. Since trucks far outnumbered buses in the number of vehicles with 20- to 25-ft wheelbases, that limit was not changed. The resulting range for the distance between the front two axles of buses was set at 25 to 35 ft.

Class 25, two-axle transit buses, was therefore given a wheelbase range of 25 to 35 ft. Class 35, three-axle transit buses, was given the same first interval and the typical tandem-axle spacing range, 2 to 6 ft, for the second interval.

Tractor-Trailers

There are fourteen classes of tractor-trailer trucks included within the program. Most of those types are common, while others (such as classes 71, 72, 81, and 91) are allowed only on certain highway sections in some states and may be unfamiliar to most people. Class 71 is a double trailer truck consisting of a three-axle tractor, a tandem-axled semitrailer, and a pup trailer using a single-axle dolly. It is legal in at least twenty states and is commonly referred to as a "Rocky Mountain double." Classes 72 and 81 are triple trailer trucks consisting of a tractor with two axles (class 72) or three axles (class 81), one single-axle semitrailer (or pup trailer), and two pup trailers connected with two single-axle dollies. They are legal on some sections of freeways in a few western states. Class 91 is a double trailer truck consisting of a three-axle tractor and two tandem-axle semitrailers connected using a tandem-axle dolly. It is legal on some sections of highways in at least thirteen states and is commonly referred to as a "turnpike double" (*7*). Classes 64 and 73 include four-axle tractors that, although rarely seen a few years ago, have become more popular in recent years for operations involving very heavy loads, such as construction equipment.

To develop ranges for each of the fourteen types of tractor-trailers in the program, a method similar to that used for single-unit trucks was used. Each class was divided into its components, and the result was three types of tractors (one-axle, two-axle, and three-axle) and two types of dollies (single-axle and tandem-axle). Dollies are the devices used to couple rear trailers in multiple trailer trucks. Izadmehr (*2*) suggests ranges for all of those components.

First, ranges for the distances between tandem-axle sets within those components were all set to the typical tandem range, 2 to 6 ft. That accounted for the ranges between the second and third axles of three-axle and four-axle tractors, the third and fourth axles of four-axle tractors, the axles of tandem dollies, and the axles of two-axle and three-axle trailers.

All of the two-axle tractors observed during research had distances between the first and second axles that fit within the 8- to 20-ft range suggested (*2*). Research also failed to reveal a two-axle tractor in production that would not fit into that range, so it was adopted.

For three-axle tractors, Izadmehr suggests a range of 8 to 25 ft for one of his classes and 8 to 20 ft for the two others. Two three-axle tractors observed during research had axle spacings in the 20- to 25-ft range, thus the larger range was accepted. Since one four-axle tractor was observed with an axle spacing range of about 22 ft the larger range was also adopted for four-axle tractors.

For the distance between the rear axle of a tractor and the front axle of a trailer, Izadmehr suggests a range of 11 to 45 ft for both single-axle and two-axle trailers, 11 to 42 ft for three-axle trailers, and 11 to 25 ft for short trailers of the type seen in twin trailer trucks (hereafter referred to as pups). Owing to favorable research results, all of those ranges were accepted, except for the cases (classes 32, 41, 51, 55, and 64) in which such a range would have interfered with the ranges of single-unit truck with trailer and passenger car with trailer groups. In those cases the lower limit of the range was set at the upper limit of the conflicting range. Later research showed that some two-axle trailers have splits of up to 12.5 ft between axles, and classes with those trailers were changed accordingly.

Izadmehr's ranges for double trailer trucks (8–20, 11–36, 6–20, and 7–35 ft, respectively) were also accepted after research revealed no conflicting data, as was his range of 7 to 15 ft for the distance to the first dolly axle from the preceding trailer axle.

Those ranges were then combined to produce ranges for all fourteen tractor-trailer types and can also be seen in Table 2.

ANALYSIS AND RESULTS

The best method of assessing accuracy would have been to interface vehicle detection sensors with a roadside microcomputer and use the program in the automatic mode. Because of hardware unavailability, financial limitations, and interfacing difficulties, however, another method had to be developed. The resulting method involved videotaping passing traffic and then analyzing the wheelbases of each vehicle taped to determine if the program would properly classify that vehicle.

For the experiment, a video camera was set up at a right angle to Interstate 81 at an elevated location within a rest area near Ironto, Virginia. The date was December 22, 1987. From that location the camera could tape the passing traffic in both the northbound and southbound lanes. A tripod was used to ensure that there would be no camera movement during the duration of the taping, since such movement could cause analysis error. Traffic during the 1-hour period of 1:40 P.M. to 2:40 P.M. was taped.

That tape was then played back using a 13-in. monitor and advanced until a vehicle of known wheelbase appeared in the northbound lane. That vehicle happened to be a 1984 Ford Mustang, which has a 101.5-in. wheelbase. At that point the tape was paused, and the distance on the monitor between the axles was measured. That distance was used to create a scale to measure the axle spacings of all of the northbound vehicles. The same procedure, again using a Ford Mustang, was used to create a similar scale for the southbound lane. The tape was then rewound and the analysis began.

As each vehicle passed across the monitor, the tape was paused and the axle spacings measured. The measured spacings were then compared with the ranges used with the program to determine whether the vehicle would have been classified into the correct class. The result for each vehicle was then recorded as either a correct or an incorrect classification. That procedure was repeated until all of the vehicles on the tape had been classified.

Because of the small screen used and the amount of visual distortion common to video recordings, the spacings could be measured only to within 3 in. (0.25 ft). This was judged to be accurate enough for vehicles where a difference of 3 in. would not have affected classification. In those cases where it would have affected classification, the distance was measured in several consecutive video frames and an average calculated.

The measurements of certain vehicles, such as 1983–1985 Mustangs, were also compared with the actual wheelbases (from *Chilton's Automotive Industries*) throughout the analysis to determine the accuracy of the experiment and to make sure that the camera had not moved.

The results showed the program to be very effective in correctly classifying vehicles of all types, especially passenger cars and tractor-trailers. Those results are shown in Table 3.

Twenty-one of the thirty-one classes covered by the program database were represented within the experimental period. Of those not represented, four were prohibited by law and only one, the motorcycle, could be considered a common vehicle type. The reason that no motorcycles were encountered was probably that the taping day was a cold and windy December day, not suitable for cycle riding. Although only two buses were included in the hour taped, those buses were of the type found to be most common in earlier field experiments; thus, the correct classification of those vehicles was important. The one "other" vehicle was a two-axle single-unit truck with a three-axle trailer, not covered by any of the classes within the program, which would have been classified as an "unknown five-axle vehicle" by the program.

Assuming that the field detectors worked accurately in measuring the number of axles and their spacings, the program would properly have classified 2,474 of the 2,499 vehicles that passed during the taping hour. That classification could also have been performed by one person, in a short period of time, using the classification software described next.

SOFTWARE DESCRIPTION

The classification software program was designed for use with IBM or IBM-compatible microcomputers. It has been tested on IBM (and compatible) ATs, XTs, and PCs and on Zenith "laptop" portables, with favorable results. An 8087 math coprocessor is recommended but not required. Users with RGB monitors will also enjoy the color screens and prompts the program was designed to provide.

The program progresses through a series of screens that direct the user to the mode best suited for the type of data being handled. The first such screen asks the user to select either automatic mode (for use when the computer is directly interfaced with the detection sensors) or interactive mode (for use when data are to be entered by the user via the keyboard).

If the operator selects the automatic mode, prompts will follow asking whether a printout is desired, the distance between the sensors, and the number of vehicles to be classified. The computer then proceeds automatically, obtaining the required vehicle information from the input-output port. The program analyzes these data, displays the class and speed of the vehicle on the computer, and provides a printout of the class and speed if requested earlier.

After the requested number of vehicles has been classified, the user is asked if group and class totals are wanted. If so, screens showing the totals and average speeds of each group

TABLE 3 RESULTS OF CLASSIFICATION ACCURACY EXPERIMENT

Vehicle Type	Number Taped	Correctly Classified	Incorrectly Classified	% Correctly Classified
Motorcycle	0	0	0	0%
Passenger Cars	2169	2154	15	99.3%
Single-Unit Trucks	55	49	6	89.1%
Buses	2	2	0	100%
Cars with Trailer	15	13	2	86.7%
Tractor-Trailers	257	255	2	99.2%
Others	1	1	0	100%
Total	2499	2474	25	99.0%

(car, bus, and so on), along with the totals for each class, are displayed on the monitor and the user is asked if a printout of those totals is desired. The next prompt asks if classification of another set of vehicles is desired. If the user answers yes, the program asks whether the totals are to be reset to zero, and then returns to ask the number to be classified. If the answer is no, then the computer asks the user whether it is desired to change mode or quit. When the user requests a mode change, the computer asks whether totals are to be reset and then asks which mode is desired.

If the operator selects the interactive mode, he or she is then asked to choose either the time-based option (for entry of data in the form of time intervals) or the length-based option (for entry of data in the form of wheelbase distances). Both options begin by asking if a printout is desired.

The time-based option then asks for the distance between the detection sensors, the time interval between the detection of the first axle at the two sensors, the number of axles, and the time interval between the axles at either of the detection sensors.

The length-based option asks for the number of axles, the distances between the axles, and whether a calculation of the speed is required. If so, the user is asked for the distance and time between the two points (or the sensors).

The program then uses that information to classify the vehicle and prints the class, speed (which is "unknown" if speed calculation was not requested in the length-based mode), and wheelbases of the vehicle on the monitor.

The user is also asked if additional information on the class of the vehicle is wanted. If the reply is yes, an information screen is displayed that lists the most common vehicle type in the class, other vehicles within the class, and vehicles of other classes that may accidentally be placed in the class.

The next prompt allows the user to perform one of five options. By selecting "C" (for "continue") the user is returned to the beginning of the previous option, so that data on the next vehicle can be entered. The selection of "T" (for "totals") results in the display of the previously mentioned total screens, showing group totals, group average speeds, and class totals. The user is then asked if he or she wants a printout of the totals, before returning to this prompt. Selecting "R" (for "reset") results in the resetting of the totals to zero and a return to this prompt. Selecting "M" (for "mode change") allows the user to change modes and reset the totals to zero if desired, while selecting "Q" allows the user to "quit."

To operate properly in automatic mode, vehicle detection sensors must be interfaced with the microcomputer so that the axle count (A), the time interval between sensors for the first axle ($T0$), and nine time intervals between axles ($T1$–$T9$) are supplied to the program via the input-output port. Research is currently under way at Virginia Polytechnic Institute to develop such an interfacing system.

SUMMARY AND CONCLUSIONS

This report has described in detail the theoretical similarities and differences between the ALICE and Two-Point-Time-Ratio systems of vehicle classification. It contains a review of the methodology used by the ALICE vehicle classification system and the deficiencies of the database of the program used. The methodology and development of an alternative program, being developed for use with the TPTR system, were then discussed at length, with particular attention focused on the classification ranges used within it. An experiment has been conducted to determine the accuracy of the program, and the results are given. The results prove the program to be highly accurate in the classification of all vehicle groups.

A thorough overview of the software has been given, followed by a discussion of the interfacing required for automatic operation. The uses and possible extensions of the classification system and the program itself have also been discussed.

It is therefore concluded that the Two-Point-Time-Ratio vehicle classification system represents a definite improvement over the popular ALICE system in the field of automated vehicle classification and speed determination. It requires only two detection sensors, covers a broader range of vehicle types, can be used interactively, is more modern, and is more accurate in classification. With an experimentally tested classification logic accuracy of 99.0 percent, the system can be viewed as a major advance in automated vehicle classification systems.

It is also anticipated that other automated classification systems could be greatly improved through use of the classification data bank and program set forth here.

APPLICATIONS

This classification system and its program can be used in many ways. It will provide needed information on the number of each type of vehicle using a portion of highway and will perform traffic counts to monitor the level of service provided. It will also provide information on the axle configurations of vehicles for use in maintenance management and planning, especially in the case of trucks, where those configurations greatly influence the stress and wear on highways and bridges. It also allows for monitoring vehicle speeds.

The program itself can be used in conjunction with other classification systems. As has been shown, the program is flexible enough to be used in the field or in the office. It was also designed with future vehicles in mind. That was done through the study of current trends in automobile design, such as size reduction, and the projection of those trends into the future.

With the inclusion of an axle counter that produces a signal proportional to the weight of a passing axle (such as a piezoelectric cable), this system could be extended to include weight information.

REFERENCES

1. D. D. Nash. ALICE: Automatic Length Indication and Classification Equipment: An Equipment for Automatically Classifying Vehicles and Measuring Their Speed. *Traffic Engineering & Control*, Vol. 17, No. 12, December 1976, pp. 195–201.
2. B. Izadmehr. *Automatic Vehicle Classification System*. Ph.D. dissertation. University of Texas, Austin, 1986, pp. 109–117.
3. Engineering Specifications and Statistics: Motor Vehicles. *Chil-*

ton's Automotive Industries, Vol. 166, No. 3, March 1987, pp. 57–81.
4. Engineering Specifications and Statistics: Motor Vehicles. *Chilton's Automotive Industries*, Vol. 152, No. 7, April 1, 1975, pp. 40–57.
5. Engineering Specifications and Statistics: Motor Vehicles. *Chilton's Automotive Industries*, Vol. 150, No. 7, April 1, 1974, pp. 46–68.
6. *Ford F-Series Pickup*. Brochure 8803. Ford Motor Company, Detroit, Mich., August 1987, p. 19.
7. *Special Report 211: Twin Trailer Trucks*. TRB, National Research Council, Washington, D.C., 1986, pp. 212–219.

Publication of this paper sponsored by Committee on Vehicle Counting, Classification, and Weigh-In-Motion Systems.

Accuracy of Weigh-in-Motion Scales and Piezoelectric Cables

A. T. PAPAGIANNAKIS, W. A. PHANG, J. H. F. WOODROOFFE, A. T. BERGAN, AND R. C. G. HAAS

This paper describes an experimental study comparing the accuracy of Weigh-in-Motion (WIM) scales and piezoelectric cables (PIEZO). The axle loads measured by the WIM and the PIEZO are compared to the dynamic axle load measurements obtained with the instrumented vehicle developed by the Vehicle Dynamics Lab of the National Research Council of Canada. The experiment was carried out in October 1987 at the instrumented pavement site constructed by the Ministry of Transportation of Ontario on Highway 7N north of Toronto. The site is equipped with a variety of sensors, including one conventional, platform-type WIM scale and five piezoelectric sensors. The experiment involved three levels of vehicle speed (40, 60, and 80 km/h), two levels of tire inflation pressure (80 and 100 psi), and two suspension types (air and rubber). Three replicate runs were performed for each combination of variables. The longitudinal placement of the vehicle with respect to the sensors was determined with a laser beam-based axle detector. Analysis of the accuracy of individual sensors revealed that only two of the PIEZO cables were sensitive with respect to tire inflation pressure, while none was sensitive with respect to vehicle speed. The average accuracy of the WIM scale was in the order of 6 percent, while the accuracy of the PIEZO cables ranged from 6 to 12 percent. Paired comparisons of the accuracy of each of the PIEZO cables to the accuracy of the WIM scale revealed that one of the PIEZO cables is comparable to the WIM scale while the other four are less accurate than the WIM scale. Considering the variation involved, however, only one of the PIEZO cables was shown to be significantly less accurate than the WIM scale.

The accuracy of systems weighing vehicles in motion has been a subject of debate since their conception in the early 1950s (*1*). This is mainly because the meaning of "accuracy" has not been properly recognized as "the closeness or nearness of the measurements to the true or actual value of the quantity measured" (*2*, p. 14). Typically, experimental studies have compared scale measurements to the static axle loads of passing vehicles. Findings of recent studies, however, suggest that the axle loads of moving vehicles can be considerably different from their static values (*3–6*). It was shown, for example, that the coefficient of variation of dynamic load ranges from 4 to 20 percent, depending on suspension type, vehicle speed, and level of pavement roughness (*6*). An example of the variation in time of the axle load generated by a leaf-spring suspension is shown in Figure 1, suggesting a frequency of load fluctuation of approximately 3 cycles/sec. Obviously, the "true" dynamic axle load can be considerably different than the static one at any time. Therefore, evaluating the accuracy of weigh-in-motion scales on the basis of static axle loads is conceptually wrong and confuses rather than resolves the problem.

To date, most of the experience with weigh-in-motion scales has been with transducer-based scales (*7, 8*). Recently, there has been a growing interest in the development of piezoelectric sensors as an alternative to the conventional weigh-in-motion scales (*9*). Piezoelectric cables are made of a piezoelectric ceramic material wrapped around a conductive core and covered by a 3-mm-diameter outer sheath. Cables are placed flush with the pavement using a steel channel filled with resin. The cables produce a voltage proportional to the stress level applied and can be calibrated to yield axle load.

The considerably different operational and cost characteristics of conventional weigh-in-motion scales and piezoelectric cables suggest the need for a thorough comparison of their accuracy. This paper addresses this problem by comparing the measurements of these two types of weigh sensors, hereafter referred to as WIM and PIEZO, respectively, to the "true" dynamic axle load obtained with an instrumented vehicle. This vehicle was developed by the National Research Council of Canada (NRCC) for the Roads and Transportation Association of Canada Weights and Dimensions Study (*4, 5*), (Figure 2). The study was undertaken jointly by the Ministry of Transportation of Ontario (MTO) and the Vehicle Dynamics Laboratory of the NRCC. The experiment was conducted at the MTO instrumented pavement site on HW 7N north of Toronto. The MTO instrumented site is equipped with one WIM scale, five PIEZO sensors, and a variety of pavement response sensors (i.e., strain gauges, deflection transducers, and temperature transducers) (Figure 3). The pavement layer thicknesses at the site were measured at 9, 15.6, and 42.8 cm, respectively (i.e., 3.5, 6, and 16.7 in.). The WIM scale is placed on a Portland concrete pad that is typical of this type of installation. The PIEZO sensors were installed as part of a joint program between the MTO and the French Laboratoire Centrale des Ponts et Chaussées. This paper describes the particular objectives, discusses the testing methodology, and presents the results of the study.

A. T. Papagiannakis, Memorial University of Newfoundland, St. John's, Newfoundland A1B 3X5, Canada. W. A. Phang, Pavement Management Systems, 3729 Union Road, Buffalo, N.Y. 14225. J. H. F. Woodrooffe, National Research Council of Canada, 89 Uplands Road, Ottawa, Ontario K1A 0R6, Canada. A. T. Bergan, University of Saskatchewan, Saskatoon, Saskatchewan S7N 0W0, Canada. R. C. G. Haas, University of Waterloo, Waterloo, Ontario A1B 3X5, Canada.

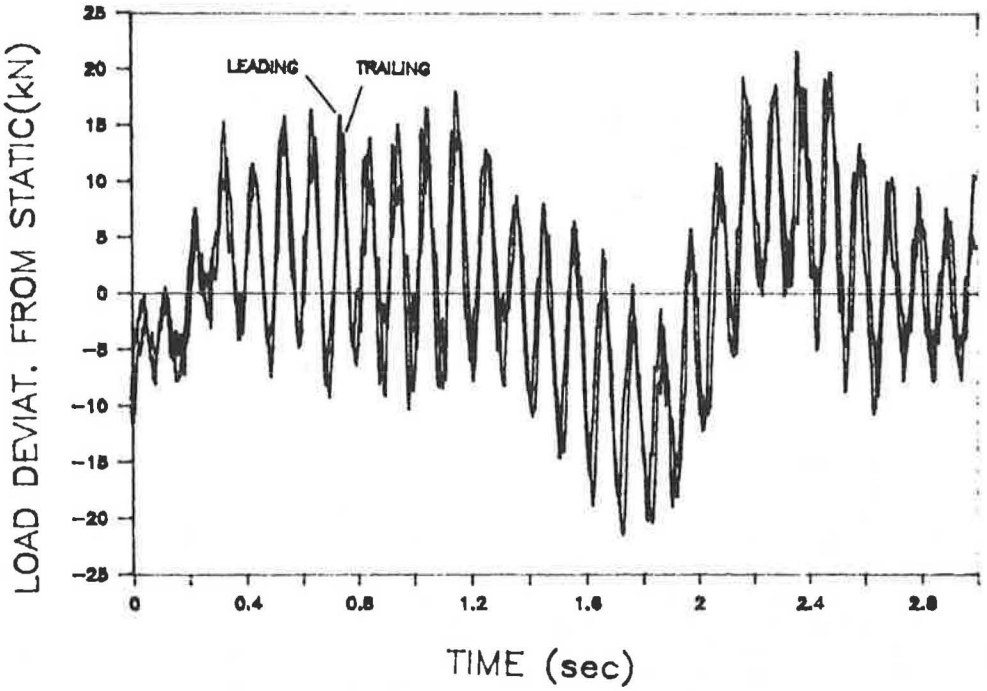

FIGURE 1 Dynamic axle loads of tandem axles on a leaf-spring suspension (*6*).

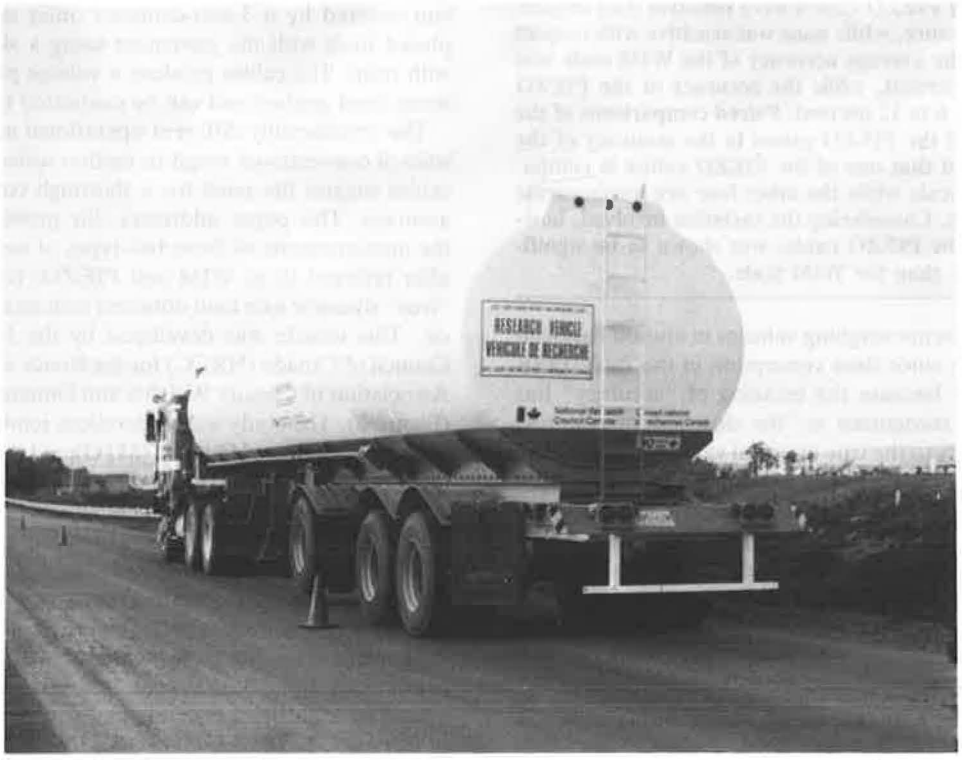

FIGURE 2 Instrumented vehicle developed by NRCC.

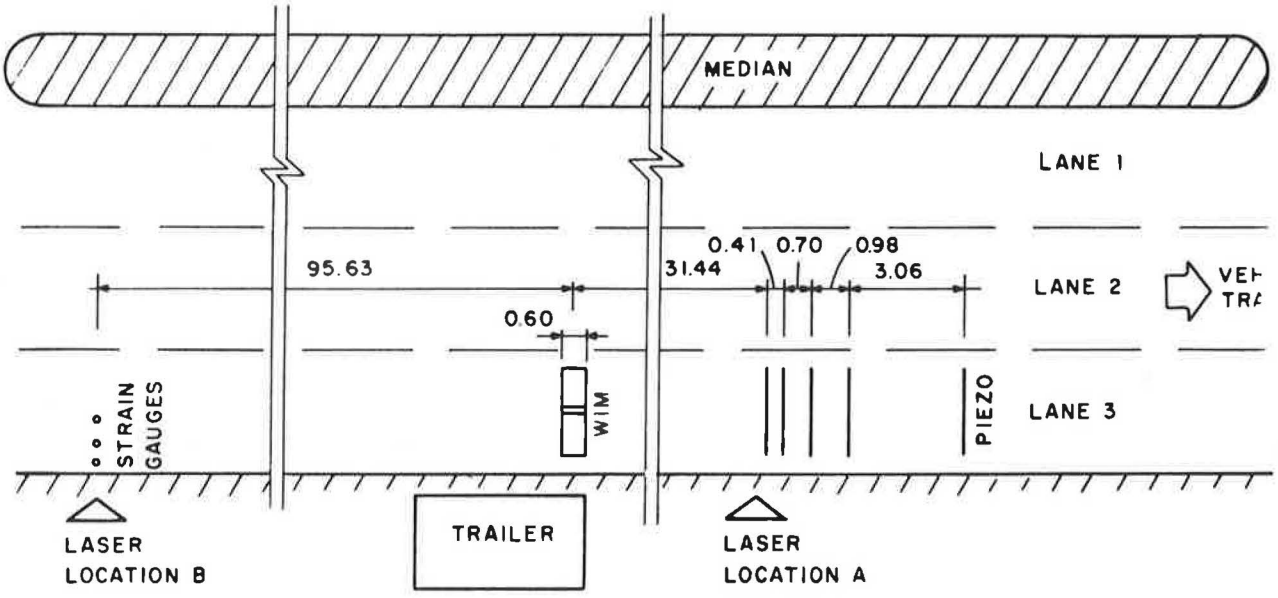

FIGURE 3 Arrangement of WIM and PIEZO sensors at MTO site (i.e., dimensions in meters).

OBJECTIVES

The particular objectives of the study are to

1. Determine the accuracy of WIM and PIEZO sensors under a variety of vehicle and operating conditions (e.g., tire inflation pressure, suspension type, vehicle speed) and
2. Compare the accuracy of each of the PIEZO sensors to the accuracy of the WIM scale over the range of independent variables.

THE EXPERIMENT

The NRCC vehicle was equipped with an air suspension on the drive axles and a rubber suspension on the trailer axles. Study of their dynamic behavior has shown that the rubber suspension can produce considerably higher dynamic loads than the air suspension at high vehicle speeds and/or levels of pavement roughness (*4–6*). It was also shown that the dynamic axle load generated by the right-hand side and the left-hand side of an axle can be substantially different because of vehicle roll and pavement cross slope. On the other hand, for relatively smooth pavements, the inertial load component generated by the acceleration of the tire assemblies is not substantial and can be neglected.

Although the pavement roughness at the MTO site was moderate (Table 1), it was decided to monitor only the right-hand and left-hand strain gauges on each axle of the NRCC vehicle (Table 2). The accelerometers could not be monitored because of the limited number of channels in the data recording system. The output of all the gauges was recorded on an analogue FM tape that was subsequently digitized using a frequency of 100 cycles/sec. The static load of each axle was added to the measured deviation to yield the total dynamic axle load. The static axle weights were obtained using a static weigh scale operated by the MTO for load enforcement purposes (Table 3). The lack of accuracy resulting from neglecting the inertial component of the axle load can be up to 5 percent, as reported by Woodrooffe et al. (*5*). On the other hand, the accuracy of the static weigh scale is in the order of 1 percent, as indicated by the gross vehicle weight measurements obtained for the two positions of the lift axle (Table 4). There is also the possibility that part of this discrepancy may be due to sloshing of the water ballast carried in the tank of the vehicle.

The most crucial aspect of the testing was to relate particular load values of the load output from the NRCC vehicle to sensor measurements on the ground. For this purpose, the longitudinal position and the speed of the NRCC vehicle should be known exactly. This was accomplished with a laser beam-based axle detector that transmitted a signal on the NRCC vehicle every time an axle interrupted the laser beam (*6*). The laser beam was placed across the driving lane directly above the first PIEZO cable. The speed of the vehicle was determined from the time elapsed between the pulses created by two passing axles and their respective distances. The ambient temperature was approximately 15°C (i.e., 59°F), being relatively unchanged over the 2-day period during which the experiment took place.

The methodology followed in selecting particular load values from the output of the NRCC vehicle is illustrated in Figure 4. It shows the dynamic load waveform of the first trailer axle of the NRCC vehicle, the output of the axle detector, and the selected load values corresponding to the location of the WIM scale and the PIEZO cables. It should be noted that, because of the 60-cm width of the WIM scale platform, a number of load values from the vehicle had to be averaged to yield a representative value of the dynamic load.

The experiment was performed over a 3-day period in October 1987. Three independent variables were considered: the tire inflation pressure, the vehicle speed, and the suspension type. Their respective code names and levels are listed in Table 5. It should be noted that the inflation pressure of the tires on the drive axles was not lowered to 80 psi because of

TABLE 1 PAVEMENT ROUGHNESS AT TEST SITE (INTERNATIONAL ROUGHNESS INDEX)

INTERVAL (meters)	AHEAD OF WIM (in/mi)	AFTER WIM (in/mi)
50	70	151
100	96	136
150	87	94
200	79	83
250	78	86
300	149	77
350	173	113
400	144	231
450	99	116
500	126	79
AVERAGE	110	117

Notes: 1. Roughness was measured with a Surface Dynamics Profilometer (10) and IRI was calculated according to (11).

2. 63.36 in/mi IRI = 1 m/km IRI

TABLE 2 DATA RECORDED ON NRCC VEHICLE

RECORDED CHANNEL	FUNCTION	STATUS
1	Voice	OK
2	First Tractor Axle Right Strain Gauge	
3	First Tractor Axle Left Strain Gauge	
4	Second Drive Axle Right Strain Gauge	OK
5	Second Drive Axle Left Strain Gauge	OK
6	Lift Axle Right Strain Gauge	
7	Lift Axle Left Strain Gauge	
8	First Trailer Axle Right Strain Gauge	
9	First Trailer Axle Left Strain Gauge	
10	Second Trailer Axle Right Strain Gauge	OK
11	Second Trailer Axle Left Strain Gauge	
12	Fifth Wheel	
14	Laser-Based Axle Detector	OK

OK indicates a good signal throughout testing

TABLE 3 STATIC AXLE LOADS IN kN (1,000 LB) OF NRCC VEHICLE

AXLE	LIFT AXLE UP		LIFT AXLE DOWN	
Steering	57.5	(12.9)	54.6	(12.3)
First Tractor	104.2	(23.4)	90.1	(20.3)
Second Tractor	103.2	(23.2)	89.7	(20.2)
Lift	-		77.8	(17.5)
First Trailer	100.0	(22.5)	73.1	(16.4)
Second Trailer	102.9	(23.1)	76.3	(17.2)
GROSS VEHICLE WEIGHT	467.8	(105.2)	461.6	(103.8)

TABLE 4 RUN NUMBER DESIGNATION AND LEVEL OF VARIABLES TESTED

RUN	TIRE PRESSURE kPa (psi)	SPEED km/h (mph)	LIFT AXLE
2	689.5 (100)	40 (25)	Down
4	689.5 (100)	40 (25)	Down
5	689.5 (100)	40 (25)	Down
6	689.5 (100)	40 (25)	Up
9	689.5 (100)	60 (37.4)	Down
10	689.5 (100)	60 (37.4)	Up
12	689.5 (100)	80 (50.7)	Down
13	689.5 (100)	40 (25)	Up
14	689.5 (100)	40 (25)	Down
15	689.5 (100)	60 (37.4)	Down
16	689.5 (100)	60 (37.4)	Down
18	689.5 (100)	60 (37.4)	Up
20	689.5 (100)	60 (37.4)	Up
39	551.6 (80)	40 (25)	Up
40	551.6 (80)	40 (25)	Down
41	551.6 (80)	60 (37.4)	Down
42	551.6 (80)	60 (37.4)	Up
43	551.6 (80)	80 (50.7)	Up
44	551.6 (80)	80 (50.7)	Down
45	551.6 (80)	40 (25)	Down
46	551.6 (80)	40 (25)	Up

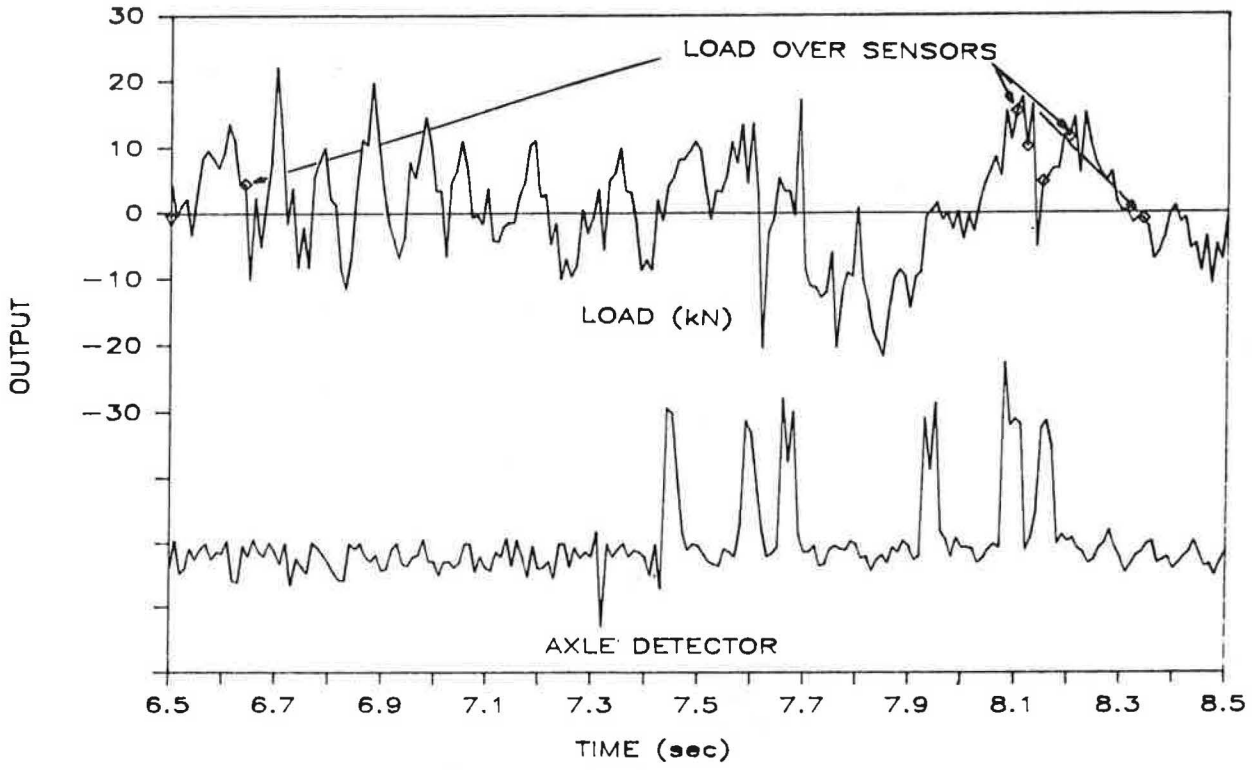

FIGURE 4 Dynamic load values corresponding to sensor locations.

TABLE 5 CODE NAMES AND LEVELS OF VARIABLES TESTED

VARIABLE	CODE	LEVELS
Tire Inflation Pressure	P	689.5, 551.6 kPa, (100, 80 psi)
Vehicle Speed	V	40, 60, 80 km/h, (25,37.4 50.7 mph)
Suspension Type	SU	air, rubber
Sensor	SE	WIM, PIEZO 1, 2... 5

safety considerations (i.e., the tires would rub against each other). Three replicate runs were intended for each combination of the independent variables. Hardware problems, however, compromised the quality of a number of runs, which were not considered for analysis. The vehicle runs analyzed and the variables involved are listed in Table 4.

RESULTS

Data processing revealed that only certain channels on the NRCC vehicle functioned properly during testing. These are indicated by an "OK" status on Table 2. It can be seen that only three strain gauge channels functioned properly, namely, those on the left-hand side and right-hand side of the second drive axle and on the right-hand side of the second trailer axle. To obtain the dynamic axle load of the second trailer axle, the load obtained from the right-hand side strain gauge had to be multiplied by a factor of 2. There is no doubt that this compromises the accuracy of the dynamic load data of the second trailer axle, as discussed earlier. Thus, the evaluation of the accuracy of the WIM scale and the PIEZO cables was based on the dynamic load measurements of the second tractor axle and the second trailer axle.

The results of data processing are presented in Table 6 in the form of the percentage error of the sensor measurement with respect to the dynamic load value obtained by the NRCC vehicle, whereby PA1 designates the first PIEZO, PA2 designates the second PIEZO, and so on.

STATISTICAL ANALYSIS

The objectives of the study were addressed by statistically analyzing the calculated measurement errors. To avoid differentiating between positive and negative errors, the abso-

lute value of the measurement errors shown in Table 6 was analyzed. The microcomputer package SYSTAT was used for the statistical analysis (*12*). The following sections deal with the sensitivity of the individual sensors to the variables tested and paired comparisons of the accuracy of each PIEZO cable to the WIM scale.

Accuracy of Individual Sensors

The first part of the study deals with the accuracy of individual weigh sensors and the variables that affect it. Table 7 shows a summary of the analysis of variance performed on the accuracy of individual sensors; the code names of the variables are listed in Table 5. It can be seen that the suspension type is a statistically significant variable (i.e., at a 90 percent confidence level) for two of the six weigh sensors. There is no reason, however, for the sensitivity of sensor accuracy with respect to the axle of the vehicle used. The observed difference is attributed to the fact that the dynamic axle loads calculated for the second trailer axle of the vehicle differ considerably from the "true" load value. The unexpectedly high errors calculated for the second trailer axle (Table 6) suggest that this is correct.

It can also be seen that two of the five PIEZO cables, namely, cables 1 and 4, are sensitive to tire inflation pressure. On the other hand, none of the weigh sensors seems to be sensitive to vehicle speed.

Comparison of Each PIEZO to the WIM

The second part of the study deals with paired comparisons of the accuracy of each PIEZO cable to the accuracy of the WIM scale. Table 8 summarizes the results of the analysis of variance of these paired comparisons. As expected, the NRCC vehicle axle used as the reference for calculating accuracy was found to be a statistically significant variable. It was decided, as a result, to consider only the data obtained with reference to the second tractor axle for the accuracy comparison. A

TABLE 6 ACCURACY OF INDIVIDUAL SENSORS (PERCENT IS WITH RESPECT TO LOAD OBTAINED BY THE NRCC VEHICLE)

	AIR SUSPENSION						RUBBER SUSPENSION					
	WIM	PA1	PA2	PA3	PA4	PA5	WIM	PA1	PA2	PA3	PA4	PA5
RUN	%	%	%	%	%	%	%	%	%	%	%	%
2	5.3	-1.9	-15.0	5.9	-11.2	-41.8	8.3	-3.6	-17.2	12.0	15.8	-4.7
4	3.0	8.3	-11.5	-8.7	8.8	4.2	7.7	-2.1	-10.5	8.2	13.1	6.8
5	11.8	-3.4	-15.5	2.1	-2.3	-8.3	7.5	-1.2	-16.9	12.5	8.3	-4.8
6	10.3	-15.2	-27.9	-6.6	-13.6	-11.5	8.1	-13.9	-14.9	4.7	-23.4	-13.8
9	7.8	-1.1	-23.9	1.0	0.8	2.7	24.0	1.0	-12.0	25.1	18.6	7.9
10	-0.5	-0.7	-23.7	-10.6	-14.4	-11.4	13.7	1.1	-22.2	-2.6	-15.1	-17.5
12	1.2	-4.5	-9.6	-5.6	-8.4	11.2	-36.3	-8.4	-17.8	-0.9	21.2	54.0
13	8.2	-17.6	-23.9	3.7	-6.3	-4.7	7.8	-14.2	-16.8	10.6	-4.1	1.1
14	10.3	-3.9	-22.4	8.2	7.4	10.9	8.8	-4.3	-7.3	8.0	31.7	19.9
15	4.9	-5.6	-21.5	8.8	-2.9	7.3	20.1	-1.4	-18.6	7.1	34.0	14.7
16	-2.4	-0.2	-14.8	-7.9	9.2	15.9	-1.8	10.0	-10.1	9.3	15.4	11.1
18	-3.5	-4.1	-6.9	-10.3	-9.8	-1.2	13.4	-6.5	-12.7	-3.5	-2.8	-10.6
20	5.6	-15.9	-7.9	-11.8	-5.9	13.5	14.6	-9.2	-8.7	-10.1	-0.3	-3.5
39	11.7	-8.4	-5.5	-5.3	7.3	-8.7	7.9	-26.7	-13.5	-5.0	-8.6	-21.1
40	13.1	-9.1	4.5	13.6	12.5	-5.8	15.9	-10.9	4.4	-2.0	21.6	-16.2
41	-0.4	5.9	1.0	2.7	9.8	2.4	33.0	-4.1	6.0	-1.1	8.6	4.3
42	-1.8	-4.2	-2.4	-10.3	2.7	-1.6	17.9	-21.6	-9.8	-13.0	-2.9	-20.4
43	-10.2	-14.0	-4.5	-13.0	-5.1	7.2	12.3	-32.5	-21.0	-27.4	18.3	7.1
44	-7.8	-3.3	-0.5	-5.9	6.7	14.0	21.5	-0.7	-1.9	-7.3	-2.4	16.9
45	7.9	1.9	0.0	-8.8	9.8	3.2	11.4	-5.8	3.9	1.4	4.3	-10.0
46	7.1	-9.7	-10.8	-7.5	-0.2	-4.6	2.2	-26.7	-12.7	-3.7	-10.8	-18.4

TABLE 7 VARIATION IN ACCURACY OF INDIVIDUAL SENSORS

SENSOR	SOURCE	SUM OF SQUARES	DF	MEAN SQUARE	F-RATIO	PROB.	
WIM	P	8.807	1	8.807	0.186	0.669	
	V	162.268	2	81.134	1.715	0.194	
	SU	398.699	1	398.699	8.426	0.006	*
	ERROR	1750.659	37	47.315			
PIEZO 1	P	435.494	1	435.494	9.064	0.005	*
	V	80.393	2	40.196	0.837	0.441	
	SU	1.693	1	1.693	0.035	0.852	
	ERROR	1777.731	37	48.047			
PIEZO 2	P	106.780	1	106.780	1.915	0.175	
	V	37.002	2	18.501	0.332	0.720	
	SU	33.360	1	33.360	0.598	0.444	
	ERROR	2063.171	37	55.761			
PIEZO 3	P	10.386	1	10.386	0.325	0.572	
	V	53.180	2	26.590	0.833	0.443	
	SU	15.379	1	15.379	0.482	0.492	
	ERROR	1180.628	37	31.909			
PIEZO 4	P	198.388	1	198.388	3.820	0.058	*
	V	38.000	2	19.000	0.366	0.696	
	SU	569.985	1	569.985	10.976	0.002	*
	ERROR	1921.421	37	51.930			
PIEZO 5	P	1.240	1	1.240	0.013	0.911	
	V	374.077	2	187.039	1.924	0.160	
	SU	168.451	1	168.451	1.733	0.196	
	ERROR	3596.216	37	97.195			

P=tire pressure, V=speed, SU=suspension type

* = Significant at 90% confidence level

TABLE 8 COMPARISON OF EACH PIEZO CABLE WITH WIM SCALE

SENSOR	SOURCE	SUM OF SQUARES	DF	MEAN SQUARE	F-RATIO	PROB.	
PIEZO 1	P	284.080	1	284.080	5.636	0.020	*
	V	105.141	2	52.571	1.043	0.357	
	SU	174.217	1	174.217	3.456	0.067	*
	SE	84.900	1	84.900	1.684	0.198	
	ERROR	3931.686	78	50.406			
PIEZO 2	P	27.128	1	27.128	0.481	0.490	
	V	23.475	2	11.737	0.208	0.813	
	SU	331.359	1	331.359	5.873	0.018	*
	SE	81.363	1	81.363	1.442	0.233	
	ERROR	4400.623	78	56.418			
PIEZO 3	P	0.033	1	0.033	0.001	0.978	
	V	198.632	2	99.316	2.410	0.097	*
	SU	285.345	1	285.345	6.923	0.010	*
	SE	107.578	1	107.578	2.610	0.110	
	ERROR	3214.791	78	41.215			
PIEZO 4	P	61.799	1	61.799	1.220	0.273	
	V	96.354	2	48.177	0.951	0.391	
	SU	961.052	1	961.052	18.979	0.000	*
	SE	0.710	1	0.710	0.014	0.906	
	ERROR	3949.660	78	50.637			
PIEZO 5	P	1.719	1	1.719	0.024	0.876	
	V	454.708	2	227.354	3.234	0.045	*
	SU	542.731	1	542.731	7.720	0.007	*
	SE	27.401	1	27.401	0.390	0.534	
	ERROR	5483.707	78	70.304			

P=tire pressure, V=speed, SU=suspension type, SE=sensor

* = Significant at 90% confidence level

summary of the *T*-tests performed is given in Table 9. The average accuracy of the WIM scale is in the order of 6 percent, while the accuracy of the PIEZO cables varies from 6 percent up to 12 percent. One of the PIEZO cables was found to have an accuracy comparable to the WIM platform, while the other four were shown to be less accurate than the WIM platform. Considering the variance in accuracy, however, only one of the PIEZO cables was shown to be significantly less accurate than the WIM platform (i.e., PIEZO cable 2).

CONCLUSIONS

Whereas two of the five PIEZO sensors tested were found to be sensitive with respect to the tire inflation pressure, neither the WIM scale nor the PIEZO cables were found sensitive to vehicle speed.

The average accuracy of the WIM scale was found equal to 6 percent, while the average accuracies of the PIEZO cables ranged from 6 to 12 percent. One of the PIEZO cables was found comparable in accuracy to the WIM scale, while the other four were inferior. Considering the variation in the calculated mean accuracy of the sensors, however, the accuracy of only one PIEZO cable (i.e., PIEZO 2) was found significantly inferior to the accuracy of the WIM scale at a 90 percent confidence level. Future study of the accuracy of PIEZO cables should include more extensive experimentation involving a wider range of operating conditions and a larger number of passes of the instrumented vehicle. Experimentation should consider PIEZO sensors of various manufacturers as well as alternative installation methods to determine the installation that yields the higher accuracy. Finally, it is recommended that the accuracy of dynamic axle load measurements on board similar instrumented vehicles be increased by accounting for the inertial component of the load generated by the bouncing mass of the rims and tires. This can easily be done by recording the acceleration of the axles and applying Newton's second law.

TABLE 9 COMPARISON OF MEAN ACCURACIES BETWEEN EACH PIEZO CABLE AND WIM SCALE

SENSOR	MEAN ACCURACY %	S.D.	COMPARISON	T-VALUE	PROBABILITY
WIM	6.405	3.973			
PIEZO 1	6.602	5.2247	PIEZO 1-WIM	0.137	0.892
PIEZO 2	12.051	8.890	PIEZO 2-WIM	2.657	0.011 *
PIEZO 3	7.527	3.454	PIEZO 3-WIM	0.976	0.335
PIEZO 4	7.385	4.011	PIEZO 4-WIM	0.795	0.431
PIEZO 5	9.143	8.654	PIEZO 5-WIM	1.317	0.195

* = Significant at 90% confidence level

ACKNOWLEDGMENTS

Thanks are extended to the Ministry of Transportation of Ontario for funding the study and to International Road Dynamics Inc. and the Laboratoire Centrale des Ponts et Chaussées for providing the technical support.

REFERENCES

1. O. K. Norman and R. C. Hopkins. Weighing Vehicles in Motion. *Bulletin 50*, HRB, National Research Council, Washington, D.C., 1952.
2. J. B. Kennedy and A. M. Neville. *Basic Statistical Methods for Engineers and Scientists*, 2nd ed. Harper & Row, New York, 1974.
3. P. F. Sweatman. *A Study of Dynamic Wheel Forces in Axle Group Suspensions of Heavy Vehicles*. Special Report No. 27. Australian Road Research Board, Melbourne, 1983.
4. J. H. F. Woodrooffe, P. A. Leblanc, and K. R. LePiane. *Effect of Suspension Variations on the Dynamic Wheel Loads of a Heavy Articulated Vehicle*. Vehicle Weights and Dimensions Study, Technical Report Volume 11. Roads and Transportation Association of Canada, Ottawa, Ontario, July 1986.
5. J. H. F. Woodrooffe and P. A. Leblanc. *The Influence of Suspension Variations on Dynamic Wheel Loads of Heavy Vehicles*. Paper 861973. Society of Automotive Engineers, Warrendale, Pa., Nov. 1986.
6. A. T. Papagiannakis. *Impact of Roughness-Induced Dynamic Load on Flexible Pavement Performance*. Ph.D. dissertation. Department of Civil Engineering, University of Waterloo, Waterloo, Ontario, Canada, 1988.
7. *Dynamic Weigh In Motion Scales*. Roads and Transportation Association of Canada, Ottawa, Ontario, Canada, 1985.
8. C. E. Lee, B. Izadmehr, and R. B. Machemehl. *Demonstration of Weigh-in-Motion Systems for Data Collection and Enforcement*. Research Report 557-1F. Center for Transportation Research, University of Texas, Austin, Dec. 1985.
9. M. Siffert. *Dynamic Weighing by Piezoelectric Sensors*. OECD-TRRL Seminar on Freight Vehicle Overloading and Load Measurement, Paris, France, June 1985.
10. B. C. Butler. *Composite Instrumentation State of the Art Report*. Composite Instrumentation Task Group, ASTM Subcommittee E17.41, Philadelphia, Pa., 1987.
11. M. W. Sayers, T. D. Gillespie, and W. D. O. Paterson. *Guidelines for Conducting and Calibrating Road Roughness Measurements*. World Bank Technical Paper 46. World Bank, Washington, D.C., Jan. 1986.
12. L. Wilkinson. *SYSTAT: The System for Statistics*. SYSTAT Inc., Evanston, Ill., 1986.

Publication of this paper sponsored by Vehicle Counting, Classification, and Weigh-in-Motion Systems.

Crack and Seat Method of Pavement Rehabilitation

AMY M. SCHUTZBACH

This paper describes a research project that evaluated the effectiveness of the crack and seat method of pavement rehabilitation. The process involves cracking a Portland cement concrete pavement into pieces measuring 1½ to 2 ft and firmly seating the pieces into the subgrade prior to overlaying with asphalt concrete. Cracking and seating is designed to reduce or retard reflective cracking by minimizing the movements in the underlying concrete that create stress in the overlay. Six construction sections located throughout the state of Illinois were cracked and seated between 1983 and 1987. The majority of the projects were thickened edge pavements constructed 55 to 65 years ago, with longitudinal edge bars for reinforcement. One pavement did contain reinforcing mesh. The pavements were cracked with either a spring arm or a guillotine hammer and then seated with a heavy rubber tire roller. The desired crack pattern consisted of hairline cracks, thereby maintaining aggregate interlock. Overlay thicknesses ranged from 3 to 7½ in. of asphalt concrete. After construction, the projects were visually surveyed and tested with a Falling Weight Deflectometer biannually. The crack and seat process was beneficial in reducing reflective cracking in overlays on thickened edge pavements containing only edge bar reinforcement. The crack and seat method of rehabilitation is not recommended for use on reinforced pavements. Cracking and seating is possible through existing overlays provided certain precautions are taken. Guillotine-type hammers are recommended for the cracking process. An overlay thickness design procedure based on mechanistic concepts was developed.

The primary system of the state of Illinois has many miles of jointed plain and reinforced, Portland cement concrete pavements in need of some form of rehabilitation. Resurfacing with asphalt concrete is the method of rehabilitation most commonly used in Illinois. In time, however, cracks reflect through the asphalt overlay directly over the joints and cracks in the concrete pavement.

Both horizontal and vertical movements in the underlying Portland cement concrete pavement contribute to the reflective cracking in the asphalt concrete overlay. Horizontal movements are caused by the expansion and contraction of the slab in response to temperature variation. Traffic produces vertical movement at joints and cracks in the underlying pavement. These movements create stresses in the overlay that result in reflective cracking.

Maintaining overlays with reflective cracking can be a costly endeavor. Reducing or retarding reflective cracking can extend the service life of the overlay and ensure a more profitable return on the rehabilitation dollar. Cracking and seating Portland cement concrete pavements prior to resurfacing is one method proposed to reduce or retard reflective cracking.

Cracking and seating seeks to minimize the movement in the underlying concrete pavement. Cracking the slab into small pieces reduces the horizontal movement due to thermal expansion and contraction. Seating the pavement minimizes vertical movement by restoring subgrade support. Minimizing movement in the underlying concrete pavement should, theoretically, reduce the amount of reflective cracking in the bituminous overlay.

The main objective of this study was to evaluate the effectiveness of the crack and seat method of pavement rehabilitation. The primary benefits of favorable crack and seat performance included the extension of life of resurfacing projects and the reduction of future maintenance costs. Six projects were constructed and monitored for the study. The subject pavements were observed prior to and during construction. The projects were visually inspected biannually after construction to monitor the occurrence and progression of reflective cracking. Since crack surveys were not performed prior to cracking and seating, it was not possible to determine the actual percentage of crack reflectance, only its occurrence and progression. In addition, deflection tests were run biannually after construction with a Falling Weight Deflectometer.

Control sections were defined as sections that were not cracked and seated yet received an asphalt overlay. Control sections were monitored in the same manner as the crack and seat sections. Unfortunately, not all the projects had control sections because of lack of input during the design stage. Among the jobs that contained control sections, the overlay thickness in the control section was not always the same as the overlay thickness in the crack and seat section. This problem led to some difficulties in accurately assessing the effectiveness of cracking and seating.

GENERAL INFORMATION

Six projects were evaluated for the study. Figure 1 shows the general location of the projects. The same basic steps were followed on all of the projects, with only minor changes in equipment and procedures.

Two types of equipment were used to crack the concrete pavements. Five of the six test sections were cracked using a hydraulic-powered, spring-arm hammer that could be controlled in both the vertical and horizontal directions. Several blows of the spring-arm hammer were required to crack the

Bureau of Materials and Physical Research, Illinois Department of Transportation, 126 East Ash Street, Springfield, Ill. 62704-4766.

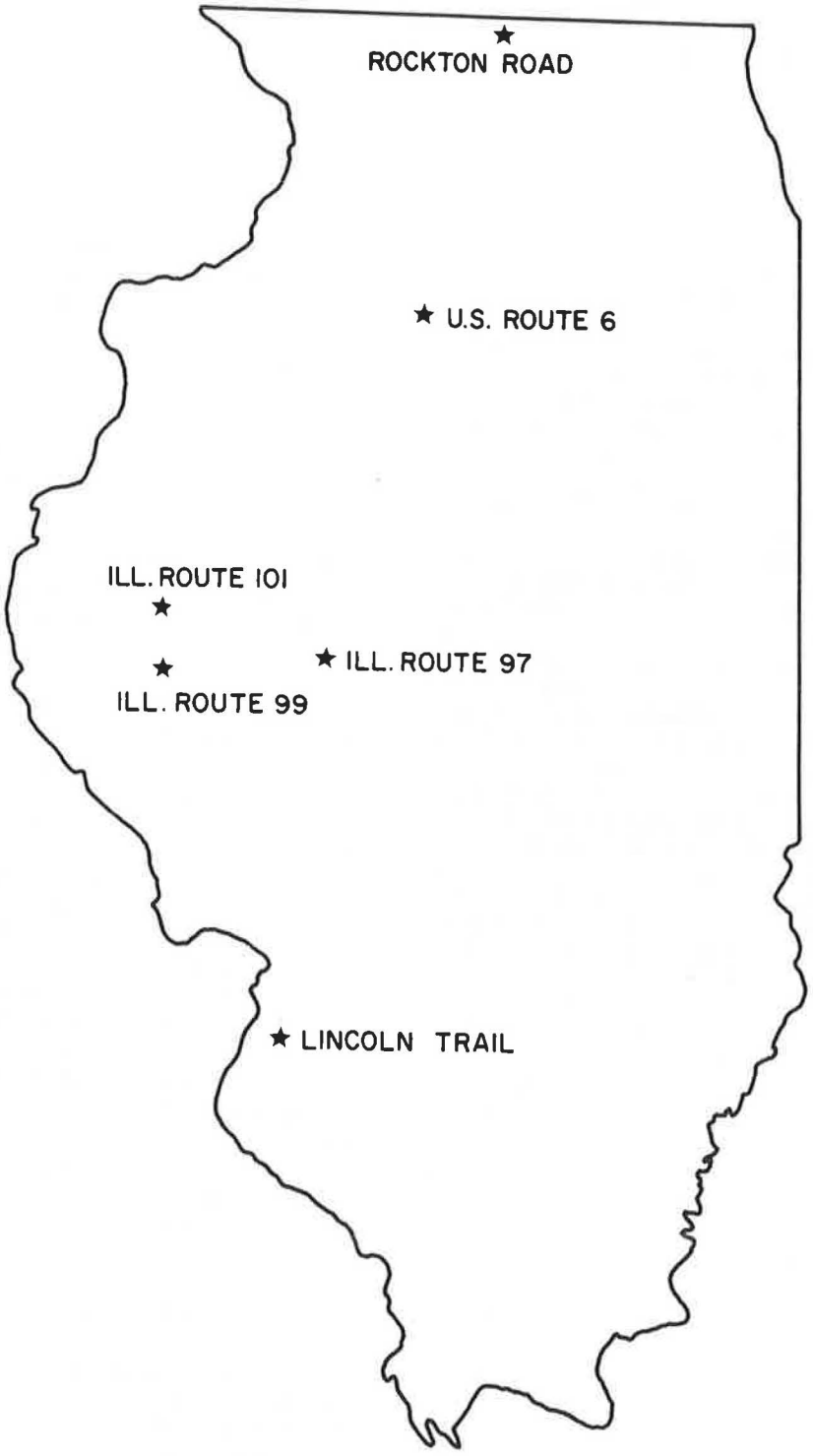

FIGURE 1 Project location map.

full-lane width of the pavement. The remaining test section was cracked with a guillotine hammer, which featured a 12,000-lb, guided free-falling drop weight. The 6-ft guillotine was capable of producing full-lane-width transverse cracking. Neither breaker scattered debris, which made it possible to maintain traffic in the adjacent lane. Since the cracking was not destructive and the test sections were all on two-lane roads, traffic was allowed on the cracked pavement behind the breaker. Some full-depth patching with asphalt concrete was required in soft areas where the breaker broke through the pavement surface.

The size of the cracked pieces ranged from 1½ to 2 ft per side. These dimensions were chosen based on the experience of others (*1–3*). Hammer drop height and spacing were varied in a test section to produce the required crack dimensions. The desired crack pattern consisted of fine, hairline cracks, thereby maintaining aggregate interlock. Since the cracks were so fine, water was sometimes sprayed on the pavement in the test section to highlight the crack pattern. On one job, cores were taken over cracks to ensure that the cracks ran the full depth of the concrete slab. On those pavements that had an asphalt concrete overlay in place, 50-ft full-lane-width test strips were removed at various locations throughout the project. This was done to verify that full-depth cracking was occurring through the overlay. Pavement widening, where scheduled, was completed prior to cracking and seating. Care was taken to minimize damage to the bituminous widening during the breaking operation. Culverts were marked and breaking stopped at 2 ft on either side of the drainage facility to prevent possible structural damage.

The majority of pavements were seated with two or three passes of a 50-ton rubber tire roller. Roller passes were staggered to ensure full coverage of the pavement. Soft spots and areas of pumping evident after rolling were patched to their full depth with asphalt concrete. Traffic was allowed on the pavements prior to seating, after seating, and prior to overlaying. The contractors were required to maintain the pavements for traffic by sweeping and patching as necessary. Care was taken, however, to ensure that the overlays were placed prior to winter.

Overlay thicknesses ranged from 3 to 7½ in. Some overlay thicknesses were basically cost comparisons: if a 2-in. overlay with typical patching quantities cost x dollars, what thickness of overlay could be placed over a cracked and seated pavement with minimal patching for the same x dollars? Other designs assigned a structural coefficient value of 0.28 to the cracked pavement—a value near that of a cement-stabilized aggregate base. During the latter stages of the project, the University of Illinois developed an overlay thickness design procedure in conjunction with a joint Federal Highway Administration (FHWA)/Illinois Department of Transportation (IDOT) study on mechanistic design procedures. This design concept was applied on the sixth experimental section, Illinois Route 99.

PAVEMENT EVALUATION SECTIONS

Original pavement data and crack and seat information on the six sections are summarized in Table 1. A typical pavement cross section is shown in Figure 2.

Lincoln Trail Road

Lincoln Trail Road is located in Fairview Heights, Illinois. This two-lane residential street was cracked and seated in 1983. The 1.73-mile project featured 4,654 ft of cracked and seated pavement with a 4-in. asphalt overlay and 4,500 ft of control section that had a 2-in. asphalt overlay over the patched pavement. Total average daily traffic (ADT) for 1982 was 4,600.

Originally constructed 55 to 65 years ago, Lincoln Trail featured a 9½–7–9½ thickened edge design with 1-in.-diameter edge bars. A 1- to 2-in. asphalt overlay placed in the mid-1950s was badly deteriorated. The overlay remained in place during the cracking operation, but soil adjacent to the pavement was removed at several locations to verify full-depth cracking. A spring-arm hammer was used to crack the pavement. After seating the pavement with two to three passes of a 50-ton rubber tire roller, the few soft spots were marked and patched. Traffic was allowed on the pavement prior to placement of a 4-in. asphalt overlay.

Illinois Route 97

Located between the Mason/Menard County line and the town of Atterberry, Illinois, this 4.9-mile stretch was cracked and seated in 1984. Approximately 4.1 miles received a 4-in. asphalt overlay, while the remaining 0.8 mile received a 3-in. overlay. In addition, two control sections were placed. A 3-in. overlay was placed over 0.4 mile of patched, noncracked, and seated pavement, and a 2-in. overlay was placed over 0.5 mile of patched, noncracked, and seated pavement. The 1985 total ADT was 1,850, with 100 multiunit and 100 single-unit trucks.

The original pavement was constructed in 1939. It was a thickened edge pavement of 9–7–9 design with 50-ft joint spacing. This pavement differed from others in the study because it contained 55 lb of reinforcing steel per 100 sq ft of pavement. Route 97 was bare at the time of cracking and seating, and virtually every joint and the majority of cracks were badly spalled and deteriorated. Cracking was accomplished with a spring-arm hammer and rolling with a 50-ton rubber tire roller. The pavement was watered to check the crack pattern. Rolling produced no soft spots, and therefore no patching was required.

Illinois Route 101

The Illinois Route 101 section is located between the towns of Brooklyn and Littleton. In 1984, 3.2 miles of the section between Illinois Route 99 and Littleton, Illinois, were cracked, seated, and covered with a 4½-in. overlay. A 2-in. asphalt overlay control section was placed through the town of Brooklyn where the pavement was not cracked and seated. Total ADT for 1985 was 700, with approximately 20 multiunit and 50 single-unit trucks.

Illinois Route 101 was built in 1929. It was a 9–6–9 thickened edge pavement with ¾-in.-diameter edge bars. A badly deteriorated, 3-in. asphalt overlay put down in 1960 was left in place, but a number of test strips were removed to verify that full-depth cracking had occurred. A spring-arm hammer was used to crack the pavement, and two passes of a 50-ton rubber tire roller were made to seat the pavement. Approx-

TABLE 1 CRACK AND SEAT SUMMARY INFORMATION

	LINCOLN TRAIL	ILLINOIS ROUTE 97	ILLINOIS ROUTE 101
YEAR CRACKED AND SEATED	1983	1984	1984
SECTION LENGTH	4,654'	25,900'	17,467'
BREAKING EQUIPMENT	SPRING ARM HAMMER	SPRING ARM HAMMER	SPRING ARM HAMMER
SIZE OF CRACKED PIECES	1.5'-2.0'/SIDE	1.5'-2.0'/SIDE	1.5'-2.0'/SIDE
ROLLER	50 TON RUBBER TIRE	50 TON RUBBER TIRE	50 TON RUBBER TIRE
OVERLAY THICKNESS	4"	3", 4"	4 1/2"
CONTROL SECTION	2" OVERLAY	2", 3" OVERLAYS	2" OVERLAY
TRAFFIC (ADT)	4,600 (1982)	1,850 WITH 100 MU'S AND 100 SU'S (1985)	700 WITH 20 MU'S AND 100 SU'S (1985)
ORIGINAL PAVEMENT DATA			
YEAR CONSTRUCTED	1920'S	1939	1929
SLAB THICKNESS	9 1/2"-7"-9 1/2"	9"-7"-9"	9"-6"-9"
REINFORCING	1" Ø EDGE BARS	55 LB. STEEL MESH/100 FT.^{2}	3/4" Ø EDGE BARS
JOINT SPACING	CONSTRUCTION JOINTS	50'	CONSTRUCTION JOINTS
PREVIOUS OVERLAY	1"-2" (1950'S)	NONE	3" (1960)
CONDITION	BADLY DETERIORATED	POOR-JOINTS AND CRACKS DETERIORATED	POOR-OVERLAY DETERIORATED

	ROCKTON ROAD	U. S. ROUTE 6	ILLINOIS ROUTE 99
YEAR CRACKED AND SEATED	1984	1985	1987
SECTION LENGTH	17,524'	6,150'	16,832'
BREAKING EQUIPMENT	SPRING ARM HAMMER	SPRING ARM HAMMER	GUILLOTINE
SIZE OF CRACKED PIECES	1.5'-2.0'/SIDE	1.5'-2.0'/SIDE	1.5'-2.0'/SIDE
ROLLER	50 TON RUBBER TIRE	50 TON RUBBER TIRE	35 TON RUBBER TIRE
OVERLAY THICKNESS	3" 4"	3 1/2", 4"	4 1/2", 5 1/2", 6 1/2", 7 1/2"
CONTROL SECTION	NONE	NONE	4 1/2", 5 1/2", 6 1/2" OVERLAYS
TRAFFIC (ADT)	1,550 with 78 MU'S AND 108 SU'S (1981)	3,300 WITH 75 MU'S AND 75 SU'S (1985)	1,985 WITH 238 MU'S AND 119 SU'S (1985)
ORIGINAL PAVEMENT DATA			
YEAR CONSTRUCTED	1932	1924	1933
SLAB THICKNESS	9"-6"-9"	9"-6"-9"	9"-6"-9"
REINFORCING	3/4" Ø EDGE BARS	3/4" Ø EDGE BARS	3/4" Ø EDGE BARS
JOINT SPACING	30' CONTRACTION, 90' EXPANSION	CONSTRUCTION JOINTS	
PREVIOUS OVERLAY	YES - WAS REMOVED	NONE	3" (1970)
CONDITION	VERY POOR - JOINTS DETERIORATED	CRACKING AND SETTLING	BADLY DETERIORATED

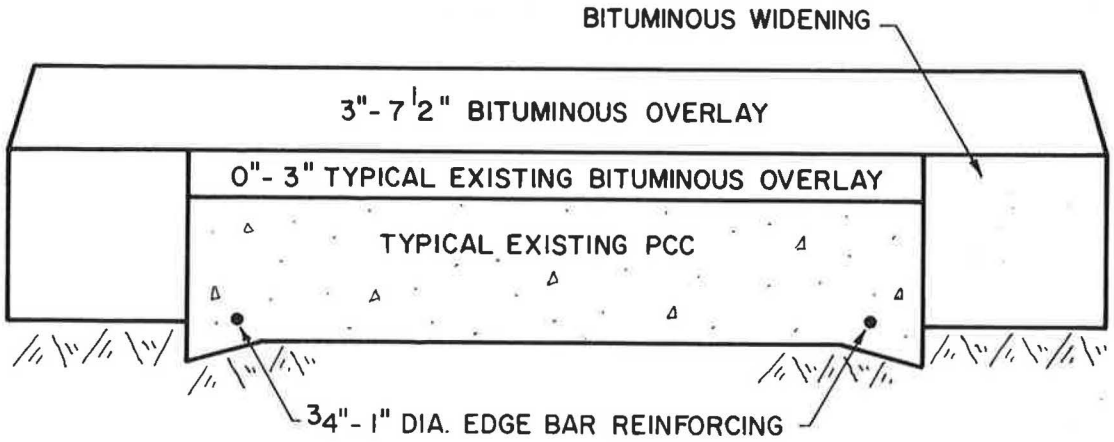

NOTE: ONE TEST SECTION, ILLINOIS ROUTE 97, CONTAINED 55 POUNDS OF REINFORCING MESH PER 100 SQUARE FEET OF PAVEMENT IN LIEU OF THE EDGE BAR REINFORCEMENT.

FIGURE 2 Crack and seat pavement cross section.

imately 2 percent of the pavement required patching after rolling.

Rockton Road

Located in the far northern portion of the state, this 3.3-mile section west of the town of Rockton, Illinois, was cracked and seated in 1984. Two overlay thicknesses were placed: 2.8 miles of 3-in. asphalt concrete and 0.5 mile of 4-in. asphalt concrete. A geotextile fabric was placed full width over the leveling binder in the 4-in. section because the county superintendent had reported a history of water problems. No control sections were constructed at this site. The 1981 total ADT for this section was 1,550, with 78 multiunit and 108 single-unit trucks.

Originally constructed in 1932, Rockton Road was a 9–6–9 thickened edge pavement with ¾-in.-diameter edge bars. Joint spacing was 30 ft, with every third joint an expansion joint and contraction joints between. The existing asphalt overlay was removed prior to cracking and seating, revealing a badly deteriorated pavement in need of patching prior to cracking. This pavement was also cracked with a spring-arm hammer and seated with three passes of a 50-ton rubber tire roller. No pumping or soft spots due to the breaking operation were observed.

U.S. Route 6

Located on the outskirts of Princeton, Illinois, this 1.2-mile section was cracked and seated in 1985. Approximately one-half of the project received a 3½-in. asphalt overlay; the other half had a 4-in. asphalt overlay. A strip of geotextile fabric was placed over the leveling binder on top of the widening joint on both sections as an additional reflective crack control treatment. No control sections were constructed at this site. The total ADT for 1985 was 3,300, with 75 multiunit and 75 single-unit trucks.

Constructed in 1924, this pavement was a 9–6–9 thickened edge design with ¾-in.-diameter edge bars. The pavement was bare at the time of cracking and seating and was badly cracked and settled. The pavement was cracked with a spring-arm hammer and seated with one to two passes of a 50-ton rubber tire roller. Soft spots were patched with asphalt concrete prior to overlaying.

Illinois Route 99

The sixth crack and seat project is located on Illinois Route 99 between the towns of Mt. Sterling and Versailles. Approximately 3.2 miles were cracked and seated in 1987. Four overlay thicknesses were placed: 4½, 5½, 6½, and 7½ in. A strip of geotextile fabric was placed over the first lift of binder on top of the widening joint in the crack and seat sections as an additional reflective crack control treatment. There were also three control sections: 4½-, 5½-, and 6½-in. overlays over non-cracked and seated pavement. The total ADT for 1985 was 1,985, with 238 multiunit and 119 single-unit trucks.

The original pavement was constructed in 1933 and was a 9–6–9 thickened edge pavement with ¾-in.-diameter edge bars. The pavement had been overlaid in 1970 with 3 in. of asphalt concrete. Heavy coal truck traffic had caused serious damage to the pavement. The overlay remained in place, but portions were removed to verify full-depth cracking. Unlike the other sections, this pavement was cracked with a guillotine hammer. The pavement was watered to check the crack pattern. Two passes were made with a 35-ton rubber tire roller to seat the pavement. Rolling produced three soft spots in the 3.2-mile section. The soft areas were removed and patched with asphalt concrete before overlaying.

The Illinois Route 99 section was the result of the learning curve developed on the other five projects. Four overlay thicknesses (4½, 5½, 6½, and 7½ in.) were tested and three control sections (4½, 5½, and 6½ in.) established. Surveys were made prior to construction so that the degree of reflective cracking could be monitored. In addition, this section received the highest level of truck traffic of all the experimental sections. These factors combined to make Illinois Route 99 the most comprehensive test of the cracking and seating process in Illinois.

The overlay design procedure used on Illinois Route 99 was also the product of several years of work. The procedure was developed by Marshall Thompson of the University of Illinois as part of a joint FHWA/IDOT study, "Mechanistic Evaluation of Illinois Flexible Pavement Design Procedures." For a given overlay thickness, the required design inputs are the asphalt concrete modulus (E_{AC}), the resilient subgrade modulus (E_{Ri}), and the "equivalent modulus" of the cracked and seated concrete (E_{cs}). The finite element program ILLI-PAVE was then used to estimate the asphalt concrete bending strain (E_{AC}) for various overlay thicknesses. Transfer functions estimating the number of repetitions to failure for a given bending strain were developed for typical IDOT Class I asphalt concrete mixtures. Failure was defined as cracking in the bottom of the asphalt layer. Figure 3 shows the curve developed for Illinois Route 99 and gives the estimated lives of the four overlay thicknesses that were constructed.

PERFORMANCE OF SECTIONS

The six projects evaluated in this study have been monitored for 1 to 5 years. Variables such as average transverse crack spacing, cumulative lineal feet of longitudinal cracking, and cumulative lineal feet of widening cracking were calculated and compared. Average transverse crack spacing was defined as follows:

$$S = \frac{L_S}{L_T/W} \tag{1}$$

where

S = average transverse crack spacing, feet;
L_S = length of survey section, feet;
L_T = cumulative total length of transverse cracks, feet; and
W = pavement width, feet.

Tables 2 through 7 detail the progression of cracking observed throughout the study, and the transverse crack spacing results are graphically illustrated in Figures 4 and 5.

Lincoln Trail Road

After 5 years in service, the crack and seat section seems to be performing well. While not directly comparable to the

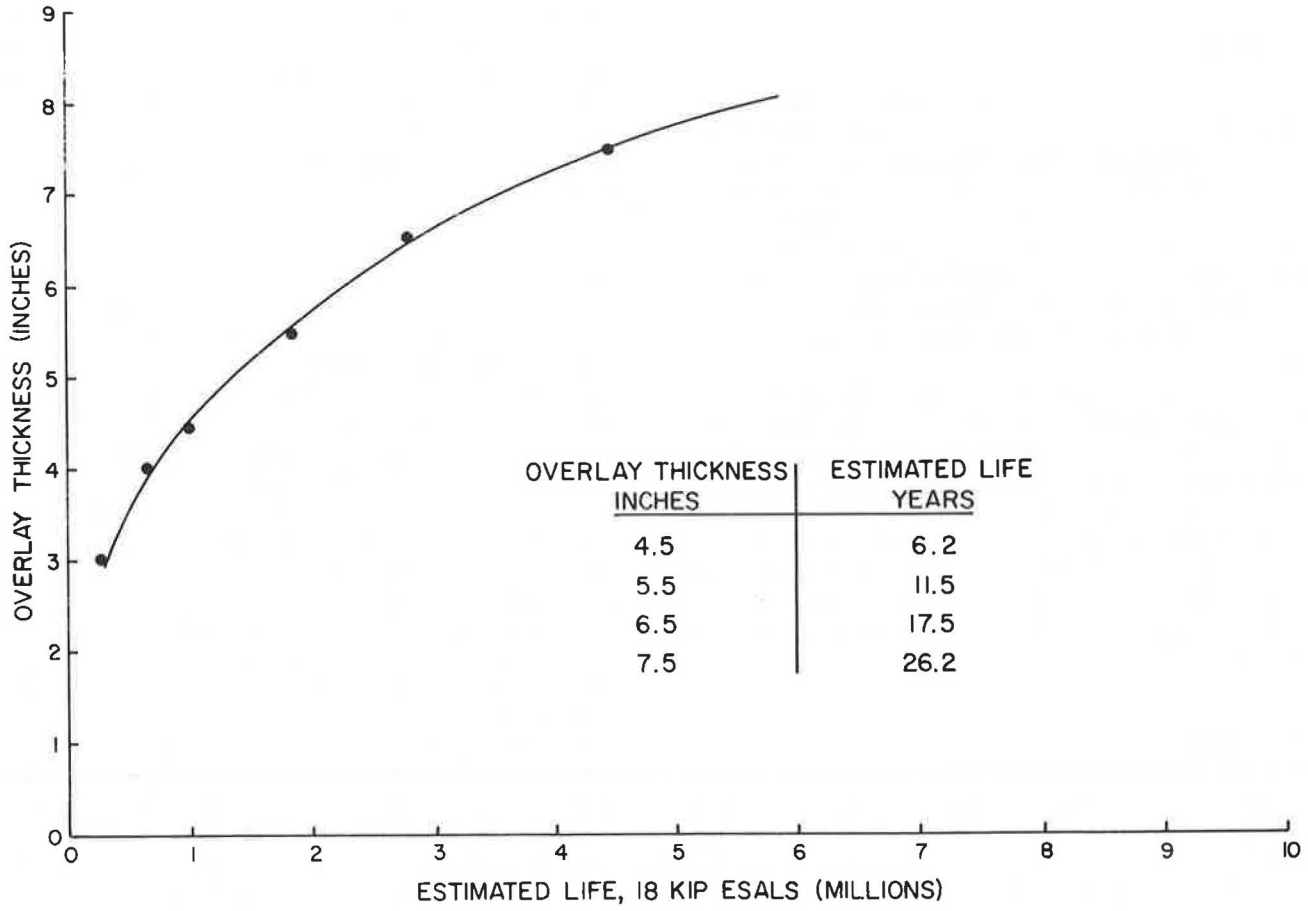

OVERLAY THICKNESS INCHES	ESTIMATED LIFE YEARS
4.5	6.2
5.5	11.5
6.5	17.5
7.5	26.2

FIGURE 3 Mechanistic overlay thickness design curve for Illinois Route 99.

TABLE 2 LINCOLN TRAIL ROAD—REFLECTED CRACK SURVEY DATA

OVERLAY	NUMBER OF MONTHS SINCE CONSTRUCTION	AVERAGE TRANSVERSE CRACK SPACING, FT.	LONGITUDINAL CRACKING, CUMULATIVE LIN. FT.	WIDENING CRACKING, CUMULATIVE LIN. FT.
CRACK AND SEAT	19	3025	6	---
WITH 4 INCHES	28	2420	6	---
(1100 FT. SECTION)	34	1424	6	---
	43	896	8	12
	49	896	8	20
	56	440	54	56
CONVENTIONAL	19	196	---	---
WITH 2 INCHES	28	104	---	---
(500 FT. SECTION)	34	92	11	---
	43	74	11	---
	49	73	13	---
	56	65	13	---

--- DENOTES NONE OBSERVED.

control section because of differences in overlay thickness, cracking and seating did significantly reduce the amount of transverse cracking, as can be seen in Table 2. There was a slight increase in the amount of longitudinal cracking, which may be attributable to the type of pavement breaker used and the crack pattern it produced. Other states have noted that continuous longitudinal cracking should be avoided because of its tendency to reflect through the overlay (*2*). Prior to the last survey, all the cracks had been routed and sealed.

Illinois Route 97

A comparison of Figures 4 and 5 shows Illinois Route 97 to be the most poorly performing section. After 4 years in service, transverse and longitudinal cracking are present in both the crack and seat and control sections. The majority of patches are reflecting through the overlay in the control sections. Table 3 shows that there is less transverse and widening cracking present in the crack and seat sections than in the control sections. While there is more longitudinal midlane cracking in the crack and seat section, it appears to be a result of mix segregation in the paver auger during laydown.

Illinois Route 101

Illinois Route 101, constructed at the same time as Illinois Route 97, is in excellent condition. Forty-three months after construction, the crack and seat section with a 4½-in. overlay shows a transverse crack spacing of 5,500 ft, compared with the 2-in. overlay control section, which has a 60-ft crack spacing. While the two sections are not directly comparable owing to differences in overlay thicknesses, it is evident that the crack and seat section is performing as was expected. Table 4 details the progression of reflective cracking.

Rockton Road

Table 5 contains reflected crack survey data from Rockton Road. As expected, the 4-in. overlay outperformed the 3-in. overlay, at least in terms of transverse crack spacing. As previously noted, the 4-in. overlay section had a history of water problems and frost-susceptible soils. These conditions may explain the increased longitudinal cracking found in the 4-in. overlay section. The geotextile fabric placed at full width over the leveling binder in the 4-in. overlay section did not appear to be beneficial in controlling longitudinal cracking.

U.S. Route 6

Two years after construction, both the 3½-in. and 4-in. crack and seat overlay sections were in excellent condition. After the third year in service, both sections had an increase in transverse cracking, and the 3½-in. overlay experienced a large increase in longitudinal and widening cracking, as illustrated in Table 6. To some extent the increase in cracking can be attributed to segregation in the asphalt concrete overlay mix-

TABLE 3 ILLINOIS ROUTE 97—REFLECTED CRACK SURVEY DATA

OVERLAY	NUMBER OF MONTHS SINCE CONSTRUCTION	AVERAGE TRANSVERSE CRACK SPACING, FT.	LONGITUDINAL CRACKING, CUMULATIVE LIN. FT.	WIDENING CRACKING, CUMULATIVE LIN. FT.
CONVENTIONAL	4	36	---	85
WITH 3 INCHES	10	25	---	98
(400 FT. SECTION, 12 FT. LANES)	16	21	---	150
	24	20	---	244
	28	19	---	279
	34	18	---	304
	44	17	---	316
CONVENTIONAL	4	54	---	21
WITH 2 INCHES	10	36	3	25
(600 FT. SECTION, 12 FT. LANES)	16	33	6	37
	24	28	66	64
	28	27	95	70
	34	26	117	78
	44	25	158	94
CRACK AND SEAT	4	889	---	---
WITH 4 INCHES	10	333	---	---
(1000 FT. SECTION, 12 FT. LANES)	16	238	---	---
	24	198	99	---
	28	137	357	---
	34	117	396	3
	44	77	564	3
CRACK AND SEAT	4	267	---	---
WITH 3 INCHES	10	90	---	---
(1000 FT. SECTION, 12 FT. LANES)	16	56	---	4
	24	44	---	6
	28	38	4	31
	34	35	10	38
	44	30	107	82

--- DENOTES NONE OBSERVED.

TABLE 4 ILLINOIS ROUTE 101—REFLECTED CRACK SURVEY DATA

OVERLAY	NUMBER OF MONTHS SINCE CONSTRUCTION	AVERAGE TRANSVERSE CRACK SPACING, FT.	LONGITUDINAL CRACKING, CUMULATIVE LIN. FT.	WIDENING CRACKING, CUMULATIVE LIN. FT.
CRACK AND SEAT	5	∞	---	---
WITH 4 1/2 INCHES	16	∞	---	---
(1000 FT. SECTION, 11 FT. LANES)	21	∞	---	---
	27	∞	---	---
	33	∞	---	---
	43	5500	---	---
CONVENTIONAL	5	310	---	28
WITH 2 INCHES	16	111	---	54
(1000 FT. SECTION, 11 FT. LANES)	21	86	---	54
	27	77	---	54
	33	74	---	54
	43	60	---	58

--- DENOTES NONE OBSERVED.

TABLE 5 ROCKTON ROAD—REFLECTED CRACK SURVEY DATA

OVERLAY	NUMBER OF MONTHS SINCE CONSTRUCTION	AVERAGE TRANSVERSE CRACK SPACING, FT.	LONGITUDINAL CRACKING, CUMULATIVE LIN. FT.	WIDENING CRACKING, CUMULATIVE LIN. FT.
CRACK AND SEAT	21	558	179	---
WITH 4 INCHES	26	471	221	---
(1000 FT. SECTION, 12 FT. LANES)	34	381	274	2
	44	115	487	5
CRACK AND SEAT	21	157	59	---
WITH 3 INCHES	26	110	127	---
(1000 FT. SECTION, 12 FT. LANES)	34	90	150	---
	44	46	152	---

--- DENOTES NONE OBSERVED.

TABLE 6 U.S. ROUTE 6—REFLECTED CRACK SURVEY DATA

OVERLAY	NUMBER OF MONTHS SINCE CONSTRUCTION	AVERAGE TRANSVERSE CRACK SPACING, FT.	LONGITUDINAL CRACKING, CUMULATIVE LIN. FT.	WIDENING CRACKING, CUMULATIVE LIN. FT.
CRACK AND SEAT	10	∞	---	---
WITH 4 INCHES	15	∞	4	---
(1000 FT. SECTION, 12 FT. LANES)	23	12,000	4	---
	33	212	20	4
CRACK AND SEAT	10	∞	---	---
WITH 3 1/2 INCHES	15	∞	5	---
(1000 FT. SECTION, 12 FT. LANES)	23	4,000	5	---
	33	144	255	79

--- DENOTES NONE OBSERVED.

TABLE 7 ILLINOIS ROUTE 99—REFLECTED CRACK SURVEY DATA

OVERLAY	NUMBER OF MONTHS SINCE CONSTRUCTION	AVERAGE TRANSVERSE CRACK SPACING, FT.	LONGITUDINAL CRACKING, CUMULATIVE LIN. FT.	WIDENING CRACKING, CUMULATIVE LIN. FT.
CRACK AND SEAT (1000 FT. SECTIONS, 12 FT. LANES)				
7 1/2 INCHES	7	∞	---	---
6 1/2 INCHES	7	∞	---	---
5 1/2 INCHES	7	∞	---	---
4 1/2 INCHES	7	∞	---	---
CONVENTIONAL (1000 FT. SECTIONS, 12 FT. LANES)				
6 1/2 INCHES	7	∞	---	---
5 1/2 INCHES	7	∞	---	---
4 1/2 INCHES	7	∞	---	---

--- DENOTES NONE OBSERVED.

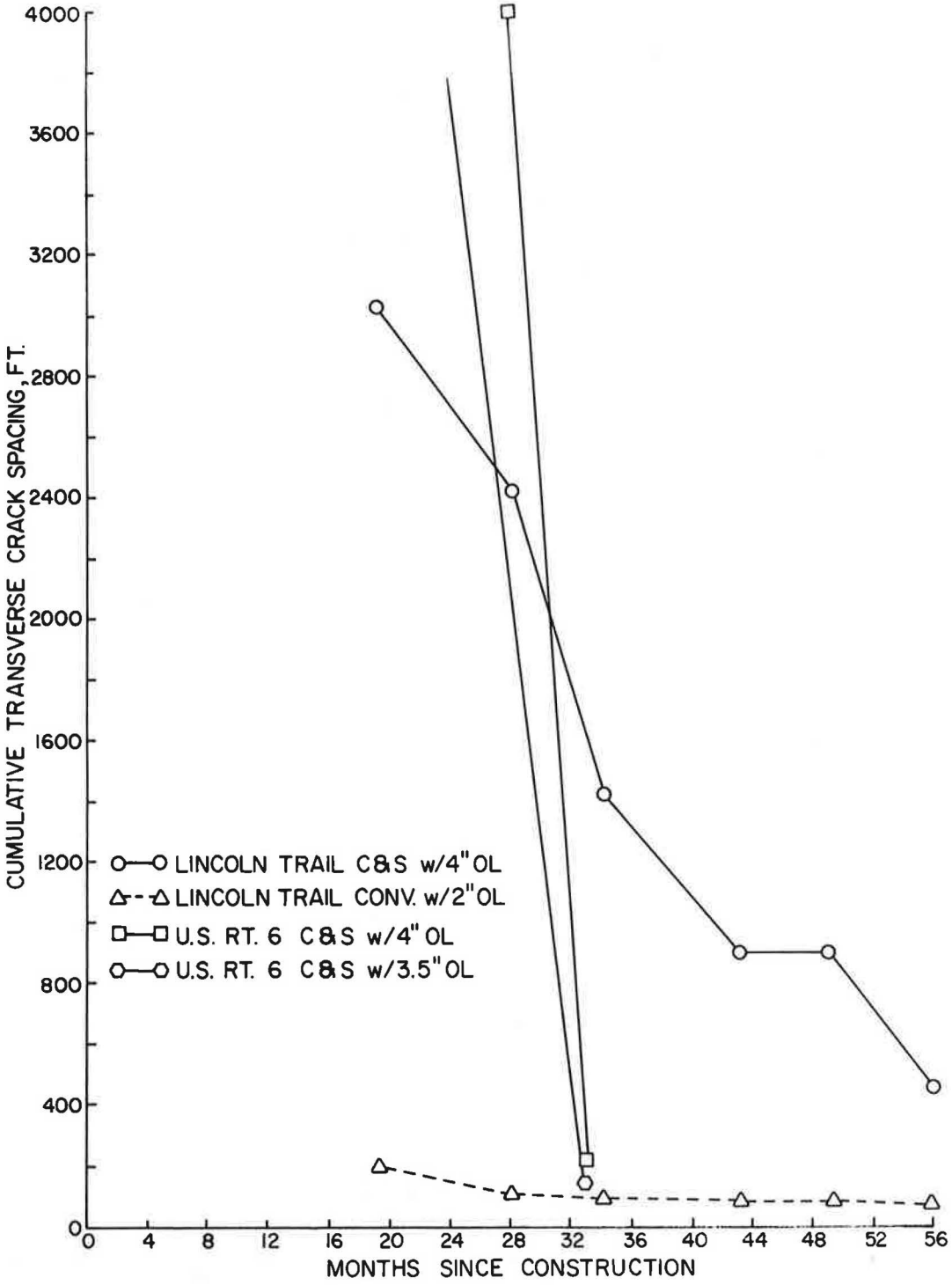

FIGURE 5 Transverse crack spacing versus time for Lincoln Trail and U.S. Route 6.

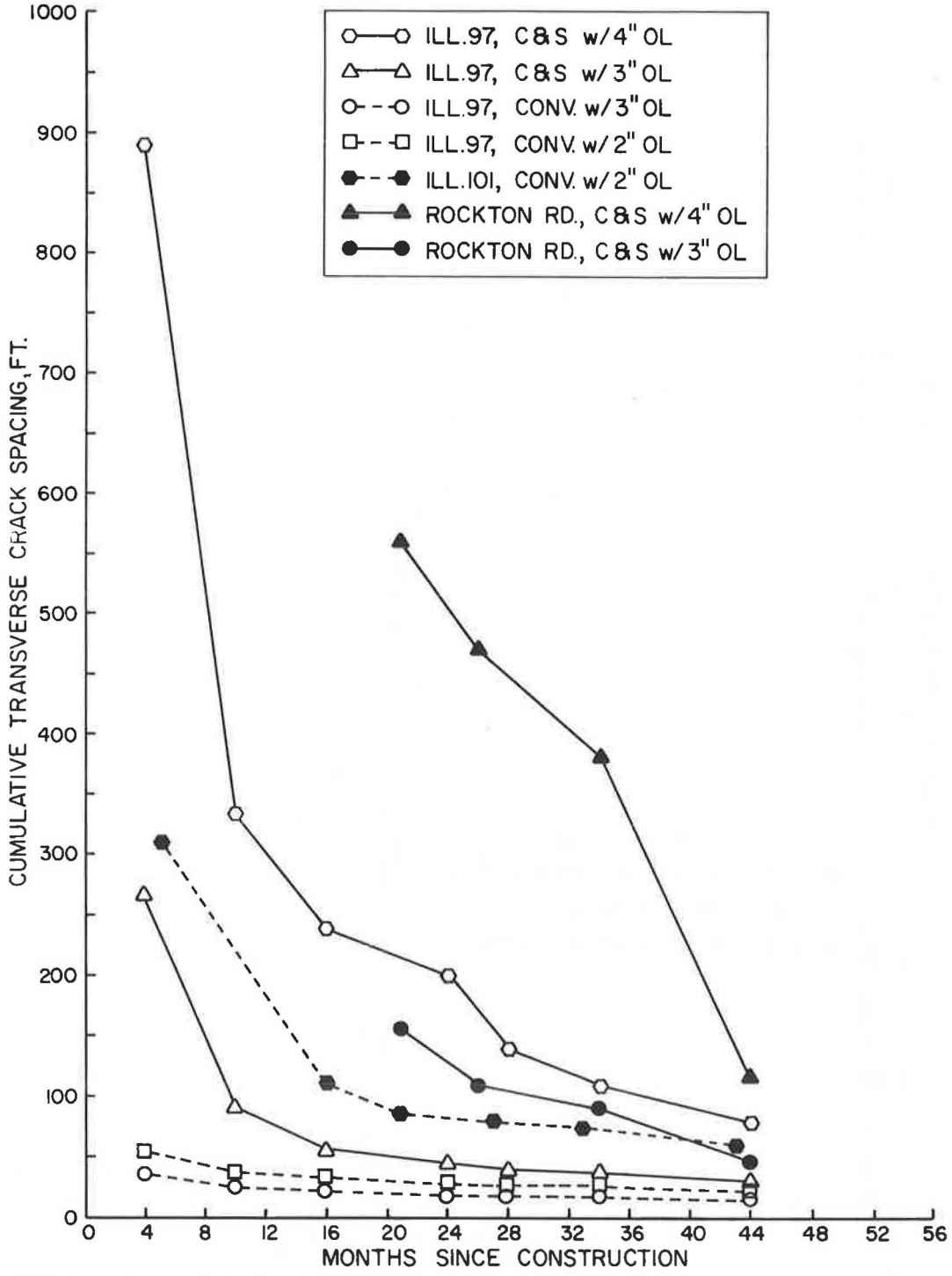

FIGURE 4 Transverse crack spacing versus time for Illinois Routes 97, 101, and Rockton Road.

ture. The open texture of the mix allowed water infiltration and promoted crack formation. The geotextile fabric strip over the longitudinal widening joint appears to be working, as only minimal cracking is evident 3 years after construction.

Illinois Route 99

After 1 year in service, all of the crack and seat and control sections are in excellent condition with no signs of reflective cracking. Table 7 gives the crack survey data for Illinois Route 99.

DISCUSSION AND CONCLUSIONS

Two factors make it difficult to assess accurately the ability of cracking and seating to reduce reflective cracking: lack of traffic and lack of control sections. Five out of the six test sections receive less than 100 multiunits a day. The sixth section, Illinois Route 99, has 238 multiunit and 119 single-unit trucks per day, for a total of 440, 18-kip equivalent single axle loads (ESALs) per day. More important, because of a lack of comparable control sections, it is difficult to tell what absolute benefits are directly derived from the cracking and seating process and which are attributable to the increased overlay thickness. Of the first five projects constructed, only one features a short control section with an overlay thickness equal to the overlay thickness on a cracked and seated section. Conversely, the recently constructed Illinois Route 99 has three control sections that correspond to crack and seat overlay thicknesses. For these reasons, Illinois Route 99 promises to be the most comprehensive test of cracking and seating in Illinois. This section will continue to be monitored to gain further information on the effectiveness of the crack and seat process.

Although the majority of the projects were constructed without proper control sections and on pavements with relatively low traffic volumes, certain observations can still be made. Illinois Route 97 has both a crack and seat section and a control section with a 3-in. overlay. While the crack and seat sections on Illinois Route 97 are performing poorly, they are still in better condition than the control sections. Table 3 indicates that the transverse crack spacing in the crack and seat section with a 3-in. overlay is approximately double that in the control section with a 3-in. overlay. A comparison of the two sections, as shown graphically in Figure 4, shows that for the 3-in. overlay section, cracking and seating delayed the degree of reflective cracking for approximately 3 years.

This raises the question of whether cracking and seating is a cost-effective method of rehabilitation. Various costs for the six projects are shown in Table 8. Cracking and seating costs varied but appeared to be related to contractor experience. Of the three jobs located in close proximity, Illinois Routes 97, 101, and 99, costs fell as the contractors became more familiar with the procedure. If cracking and seating with a 3-in. overlay did indeed retard the degree of reflective cracking for 3 years on Illinois Route 97, then the average annual cost for the rehabilitation amounted to less than $0.19 per square yard per year.

Since patching quantities are reduced when cracking and seating, the process does appear cost-competitive. Current Illinois practice, however, assumes that patching and a 2-in. overlay on distressed roads in the primary system will last 6 to 10 years. The projects in this study are 1 to 5 years old. Therefore, more time is needed to determine the life span of cracking and seating. In the future, cost-effectiveness will need to be evaluated on a project-by-project basis. The extra costs of cracking and seating and additional overlay thickness, if required, and the reduced cost of patching will need to be factored into the decision.

The question of the cost-effectiveness of additional overlay thickness over cracked and seated pavements will probably be best answered in time by the Illinois Route 99 project. However, a comparison of the Rockton Road and Illinois Route 97 crack and seat sections from Figure 4 is still informative. The additional inch of overlay thickness on Rockton Road bought 1½ years of reflective crack prevention. The additional inch of crack and seat overlay thickness on Illinois Route 97 bought more than 2½ years of reflective crack prevention. Based on the price per square yard of asphalt concrete on these jobs, an inch of overlay adds between $0.68 and $1.29 per square yard to the annual cost of the rehabilitation. Again, more time is needed to determine the actual cost-effectiveness of the method and the optimum overlay thickness.

It should be pointed out that determining the effectiveness

TABLE 8 PROJECT COST INFORMATION

PROJECT	CRACK & SEAT COST, $ PER SQUARE YARD	CRACK & SEAT OVERLAY THICKNESS, INCHES	CRACK & SEAT OVERLAY COST, $ PER SQUARE YARD
Lincoln Trail	1.70	4	7.30
Illinois Route 97	0.55	3-4	5.66 - 7.37
Illinois Route 101	1.00	4.5	6.57
Rockton Road	0.55	3-4	5.80 - 7.73
U.S. Route 6	3.00	3.5-4	5.00 - 5.72
Illinois Route 99	0.51	4.5-7.5	5.83 - 9.56

of geotextile fabrics in preventing reflective cracking over the pavement widening joint was outside the scope of this study. The fabric was used on three projects at the district's option. The Illinois Department of Transportation has previously published research on the use of fabrics in pavement rehabilitation (*4*).

Although Illinois Route 97 is the most poorly performing section, it was the only pavement in the study that contained reinforcing steel. Falling Weight Deflectometer tests done on the experimental sections after cracking, seating, and overlaying indicated an average concrete modulus of almost 3,000,000 psi on Illinois Route 97. Concrete moduli values from the other cracked and seated pavements averaged 546,000 psi. These values are listed in Table 9. Such a high modulus value on the Illinois Route 97 project would seem to indicate that the reinforcing steel was not adequately broken during the cracking process. The steel still held the concrete together, and as it expanded and contracted in response to temperature variations, stresses developed in the overlay and resulted in early reflective cracking. Other studies have confirmed that jointed reinforced pavements are not suited to cracking and seating (*5*).

Information provided by Marshall Thompson of the University of Illinois also indicated the importance of adequately breaking the concrete. Willard Airport Road in Savoy, Illinois, is under the jurisdiction of the University of Illinois. This 7-in. plain Portland cement concrete pavement was cracked and seated in 1984. The pavement was cracked with a spring-arm hammer on a very hot day and overlaid with 4 in. of asphalt concrete. Reflective cracking appeared very early. Falling Weight Deflectometer tests performed after cracking, seating, and overlaying indicated an average concrete modulus of 4,050,000 psi, a value similar to that of unbroken concrete. These test data are found in Table 9. The extremely hot conditions put the concrete in compression, and apparently the spring-arm hammer was not able to crack the pavement. Both Illinois Route 97 and Willard Airport Road of the University of Illinois indicate the importance of establishing a test section where the cracking pattern can be varied and full-depth cracking verified.

Both pavements exhibiting early reflective cracking due to insufficient slab cracking were broken with a hydraulic-powered spring-arm hammer. Coring and Falling Weight Deflectometer (FWD) testing on the Illinois Route 99 section, which was cracked with a guillotine hammer, verified full-depth cracking. Based on the results of the FWD testing and the surveys showing early reflective cracking, it appears that a guillotine-type hammer is best suited to provide the desired full-width, full-depth cracking pattern.

The seating process is equally important as the cracked pieces must be firmly seated on the subgrade or they will rock and produce reflective cracking. While both 35-ton and 50-ton rubber tire rollers were used to seat the experimental sections, current practice favors the 35-ton roller, especially

TABLE 9 CRACKED AND SEATED CONCRETE MODULI VALUES

PAVEMENT	TEST DATE	FALLING WEIGHT DEFLECTOMETER[1] 9,000 LB. LOAD DEFLECTION, MILS	CRACKED AND SEATED CONCRETE MODULI,[2] KSI
LINCOLN TRAIL	SUMMER/FALL 1985	7.8	1,080
LINCOLN TRAIL	SPRING 1986	8.4	770
ILLINOIS 97 - 3 IN.	SUMMER/FALL 1985	7.3	3,250
ILLINOIS 97 - 3 IN.	SPRING 1986	7.8	1,850
ILLINOIS 97 - 4 IN.	SUMMER/FALL 1985	8.7	4,000
ILLINOIS 97 - 4 IN.	SPRING 1986	7.3	2,400
ILLINOIS 101	SUMMER/FALL 1985	14.2	420
ILLINOIS 101	SPRING 1986	10.1	600
ROCKTON ROAD	SPRING 1985	14.0	150
ROCKTON ROAD	SPRING 1986	13.7	240
ROCKTON ROAD	SUMMER/FALL 1986	12.3	300
U. S. 6 - 3.5 IN.	SUMMER/FALL 1986	14.7	680
U. S. 6 - 4 IN.	SUMMER/FALL 1986	12.2	670
WILLARD AIRPORT RD.	SUMMER/FALL 1985	7.7	4,100
WILLARD AIRPORT RD.	SPRING 1986	5.3	4,000+

[1] Dynatest 8002 Falling Weight Deflectometer

[2] Cracked and seated concrete moduli back-calculated using the finite-element program ILLIPAVE.

on sections with weak subgrades (*5*). Steel wheel rollers and vibratory rollers are not recommended because they bridge the pieces and do not adequately seat them. Determination of adequate seating is somewhat subjective. In Illinois, an upper limit of five one-way passes per lane is used. The resident engineer then makes a visual inspection of the seating operation and a judgment call regarding the number of roller passes. The roller passes are staggered to ensure full-width coverage. Additional research is needed to develop a more objective method of determining if the cracked pieces are adequately seated.

RECOMMENDATIONS

Based on the observations made on the six experimental sections, the following recommendations are offered:

- A 100-ft test section should be designated on each job. The drop height and spacing of the pavement breaker can be varied to obtain the desired crack pattern. Cores should be taken over a crack to verify that full-depth cracking is taking place.
- A light spray of water should be applied to the test section after cracking to highlight the crack pattern.
- Certain precautions must be taken when cracking through an existing asphalt overlay. Asphalt concrete overlay test strips should be removed in 50-ft lengths to verify that the underlying concrete pavement is being cracked. These test strips should be located along the entire length of the job, as pavement condition and overlay thickness may vary and thus cause the crack pattern to vary.
- Guillotine-type hammers or heavy, guided, free-falling drop weights capable of producing full-width, full-depth cracking are recommended for the cracking process.
- Traffic can safely be maintained adjacent to the pavement breaker. Traffic can also be allowed on the cracked pavement prior to seating and on the cracked and seated pavement prior to overlaying, provided that the pavement is patched and swept as needed. The cracked pavement should be rolled prior to overlaying if it has been open to traffic for a long period of time. Care should be taken to ensure that the cracked pavement is overlaid prior to winter.
- One to five one-way passes per lane with a 35-ton rubber tire roller should be sufficient to seat the cracked pieces onto the subgrade. The passes should overlap to ensure full-lane coverage.
- Use of the crack and seat process on reinforced concrete pavements is not recommended at this time. Thickened edge pavements containing edge bars are suitable for cracking and seating prior to overlaying.
- Overlay thicknesses should be carefully designed on the basis of traffic, subgrade support, and asphalt concrete and cracked and seated concrete moduli values.

A sample specification incorporating these recommendations has been developed (*6*).

ACKNOWLEDGMENTS

This paper is based on the results of the project, "Evaluation of Crack and Seat Method of Resurfacing," which was sponsored by the Illinois Department of Transportation, Division of Highways, and the U.S. Department of Transportation, Federal Highway Administration.

REFERENCES

1. R. A. Eckrose and W. E. Poston, Jr. Asphalt Overlays on Cracked and Seated Concrete Pavements. *National Asphalt Pavement Association Information Series 83*. National Asphalt Pavement Association, Riverdale, Md., July 1982, 16 pp.
2. C. Crawford. Cracking and Seating of PCC Pavements Prior to Overlaying with Hot Mix Asphalt—State-of-the-Art. *National Asphalt Pavement Association Information Series 91*. National Asphalt Pavement Association, Riverdale, Md., March 1985, 10 pp.
3. *Cracking and Seating of PCC Pavements Prior to Asphalt Overlay*. Audio-Visual Program. The Asphalt Institute, College Park, Md., 1984.
4. I. C. Mascunana. *An Evaluation of Engineering Fabric in Pavement Rehabilitation*. Physical Research Report 88. Illinois Department of Transportation, Bureau of Materials and Physical Research, Springfield, March 1981, 41 pp.
5. ERES Consultants, Inc. *Techniques for Pavement Rehabilitation*, 3rd rev. Training Course. U.S. Department of Transportation, Federal Highway Administration, and National Highway Institute, Champaign, Ill., October 1987, pp. 731–760.
6. A. M. Schutzbach. *The Crack and Seat Method of Pavement Rehabilitation*. Physical Research Project 104. Illinois Department of Transportation, Bureau of Materials and Physical Research, Springfield, July 1988, 50 pp.

Publication of this paper sponsored by Committee on Pavement Rehabilitation.

Performance and Structural Evaluation of Cracked and Seated Concrete

R. C. AHLRICH

The benefits derived from rehabilitating Portland cement concrete (PCC) pavements using asphalt concrete (AC) overlays may be minimized because of reflective cracking in the AC overlay. Reflective cracks can cause early deterioration of the asphalt pavement in the form of raveling and spalling adjacent to the joints. One method that has been successful in reducing reflective cracking is known as "cracking and seating." This method involves cracking the existing PCC pavement into smaller interlocking pieces that have aggregate-to-aggregate contact. This cracked PCC pavement is then seated with a heavy pneumatic-tired roller that prevents rocking or movement of the existing pavement. This procedure reduces the potential for reflective cracking by reducing the amount of movement at the joints due to temperature changes. Cracking the existing PCC pavement into smaller pieces reduces the strength of the rigid pavement, but little information has been published on how much loss is expected. This paper addresses the reduction in pavement strength due to the "cracking and seating" method by evaluating the effective modulus. Effective modulus values for the cracked PCC pavement were determined using measured deflection basins obtained by the Falling-Weight Deflectometer (FWD) and comparing these deflection basins to those predicted by the elastic layer theory. The effective modulus values were obtained for the existing PCC pavement before and after the pavement had been cracked and seated. The effective modulus values of the pavement layers were also determined after placing each intermediate course of asphalt concrete (AC) overlay.

Background

The performance of rehabilitated Portland cement concrete (PCC) pavements with asphalt concrete (AC) overlays is often marginal and only a temporary solution. One of the shortcomings of this rehabilitation technique is the eventual occurrence of reflective cracking, which is the development of a crack pattern in the AC pavement similar to the crack pattern in the underlying PCC pavement. Cracks and joints of the PCC pavement eventually propagate up through the new AC overlay, causing early deterioration of the pavement. Rehabilitation techniques that provide improved performance at lower costs are very important to pavement engineers because of the increasing maintenance requirements of rigid pavements.

Reflective cracks are fractures in the AC overlay that result from movement of cracks and joints in the PCC pavement. These differential movements, either horizontal or vertical, cause high stresses in the asphalt concrete that develop fractures in the overlay. Vertical movements that are caused by traffic loads or rocking slabs, and horizontal movements that are caused by temperature and moisture changes must be reduced in order to retard or prevent early deterioration of an AC overlay.

One method that has been used to reduce the potential for reflective cracks in PCC pavements with AC overlays is cracking and seating of the existing PCC pavement prior to the overlay. Cracking and seating the PCC pavement has been used for more than 25 years as a method to prevent reflective cracking. New improvements in equipment and a better understanding of the method, primarily due to experience, have encouraged the use of this technique. Satisfactory results in pavement overlays using this method have been widespread.

The cracking and seating technique involves the breaking up of the existing PCC into small segments that contain interlocking pieces and then seating those pieces with a heavy pneumatic roller. This procedure prevents rocking or moving of the PCC pavement. Once the existing PCC has been cracked, however, the strength of the PCC has been reduced.

Objective

The objective of this study was to perform a structural evaluation of cracked and seated Portland cement concrete pavement with various thicknesses of AC overlays and to analyze the performance and effectiveness of this rehabilitation technique.

Scope

This study was conducted to evaluate the effectiveness of cracking and seating PCC pavements with AC overlays to retard reflective cracking. An investigation was undertaken to obtain information relating to the performance and structural strength of cracked PCC. Three cracking and seating projects were investigated to determine the effectiveness of this method. Construction projects at Rock Island Arsenal, Illinois, and Fort Wainwright, Alaska, were evaluated to determine the performance of cracking and seating. A structural evaluation using nondestructive testing (NDT) equipment was performed on a cracking and seating project at Aberdeen Proving Ground, Maryland. This analysis evaluated the PCC pavement before and after cracking and after

R. C. Ahlrich, U.S. Army Corps of Engineers, Waterways Experiment Station, P.O. Box 631, Vicksburg, Miss. Attn: CEWES-GP-IM.

placing three layers of asphalt concrete. From these investigations, the performance of cracking and seating PCC pavements to prevent reflective cracks and the reduction of PCC pavement strength were determined.

DESCRIPTION OF CRACKING AND SEATING

Cracking and seating of rigid pavements prior to an AC overlay is an accepted method for rehabilitating rigid pavements. This method involves cracking the existing PCC slab into small segments, which reduces movement of the rigid layer. By inducing small hairline cracks in the PCC pavement, the potential for reflective cracks is decreased. Various types of equipment and construction procedures are used to produce satisfactory results.

Cracking Equipment

Cracking the PCC pavement is the most important step of this rehabilitation technique. The cracking pattern must produce hairline cracks that break the PCC into segments that have aggregate particle interlock. The pavement strength is reduced by cracking, but the cracked PCC still functions as a load-carrying medium. Excessive cracking can be detrimental to the pavement structure and turn the PCC into rubble, which is not desired.

Various types of equipment can be used to produce the desired cracking of a PCC pavement. These hammers include the modified pile driver, impact hammer, guillotine hammer, and the whiphammer. Each device can adjust the impact force applied to the pavement, thus producing the desired cracking pattern.

Construction Procedures

Preparation of the existing PCC pavement is essential for the success of the rehabilitation method. The existing joint and crack sealant is removed prior to cracking the slabs. The joint and crack sealing material is removed to prevent any slippage or bleeding of the sealant through the AC overlay. Proper drainage of the pavement is also required prior to cracking the PCC. Drains can prevent water from accumulating under the pavement and can prevent a loss of structural support due to a saturated base.

As previously mentioned, cracking of the PCC pavement is extremely important to the success of cracking and seating. A proper cracking pattern that produces small segments that have aggregate particle interlock is required. Several factors that influence the cracking pattern are (1) type and size of hammer, (2) impact force of hammer, (3) strength and thickness of PCC, and (4) condition of subgrade.

The cracking pattern usually preferred in cracking and seating breaks the slabs into pieces that measure from 18 in. to 36 in. Because of the variables listed in the previous paragraph, a test section is cracked to determine the impact force and spacing of the hammer that will produce the recommended crack pattern. Because of various field conditions, the crack pattern developed in the test section may have to be adjusted. Segments that are cracked into pieces smaller than 12 in. may result in spalling and loss of structural strength.

After the PCC pavement has been cracked as specified, the cracked concrete is seated or embedded into the base with a heavy pneumatic roller. This process ensures that the rigid pavement does not rock or move under traffic loads. The seating of the cracked PCC is accomplished by using a 30- to 50-ton, rubber-tired roller. Generally, three to five coverages of a heavy pneumatic roller are adequate to seat the cracked PCC.

During the cracking and seating operation, areas that are not structurally sound will be evident. Punch-throughs in the PCC and rocking of the PCC slabs indicate that the pavement needs repair. In these weak areas, the affected pavement is removed and replaced. Full-depth asphalt or crushed-base course of adequate strength should be used as a patch prior to the AC overlay.

To complete the rehabilitation of the rigid pavement, an AC overlay is placed. The cracked and seated pavement is prepared by removing all debris and applying a tack coat. To correct the uneven surface caused by cracking and seating, a leveling course is placed prior to the surface course material. The thickness of AC depends on the structural capacity of the existing pavement and the amount of anticipated traffic. The minimum recommended thickness of asphalt concrete for cracking and seating is 4 in. (*1–3*).

PERFORMANCE OF CRACKING AND SEATING

The Waterways Experiment Station (WES) has been actively involved in evaluating the construction procedures and the effectiveness of cracking and seating as a rehabilitation method to prevent reflective cracks of PCC pavements through an AC overlay. Two projects that have been evaluated were located at Rock Island Arsenal, Illinois, and Fort Wainwright, Alaska. The project description, construction, and performance are discussed for each site.

Rock Island Arsenal

The cracking and seating method was used to rehabilitate a PCC parking lot at Rock Island Arsenal, Illinois. This project was conducted as a demonstration under the Facilities Technology Application Test (FTAT) program. This nonreinforced rigid pavement was rough and uneven and presented a constant maintenance problem. Several slabs were excessively cracked and needed replacing. Water accumulation under the slabs also caused support problems throughout the pavement. Rehabilitation using the cracking and seating method was the best alternative for this repair. Prior to cracking the PCC, all existing joint and crack sealing material was removed to a minimal depth of 1 in. below the surface. Slabs that were excessively cracked and structurally unsound were removed and replaced with high-quality base material. Drainage of the subgrade under the parking lot was also corrected by constructing a French drain system along the outside edge of the pavement.

The cracking of the PCC parking lot was accomplished using an impact hammer shown in Figure 1. A cracking pattern was

FIGURE 1 Impact hammer used at Rock Island Arsenal.

FIGURE 2 Fifty-ton pneumatic-tired roller used to seat cracked PCC pavement.

selected to break the existing PCC slabs into pieces with a minimum size of 18 in. and a maximum size of 24 in. After cracking, the PCC pavement was seated using a 50-ton roller shown in Figure 2. A minimum of two passes was required to seat the cracked PCC. After the cracking and seating procedures were completed, a minimum of 4 in. of asphalt concrete was placed.

The rehabilitation project was completed in 1984. Figure 3 shows the finished AC pavement surface. The pavement was inspected in August 1988, and no reflective cracks were observed. The performance to date has been very satisfactory. The cracking and seating method has been successful in preventing reflective cracking for 4 years. The cracking and seating method has been an effective and economical method to reduce reflective cracking of PCC pavement through an AC overlay (*4*).

FIGURE 3 Completed asphalt concrete pavement.

Fort Wainwright

The cracking and seating technique was used to rehabilitate the 6-in. reinforced PCC runway pavement at Fort Wainwright, Alaska. Some of the existing PCC slabs had become severely cracked, and the pavement surface had become so rough and uneven that an asphalt overlay was required. The pavement distress was due primarily to the extreme weather conditions.

There were several objectives in using the crack and seat method to repair the PCC runway. One objective was to locate voids and areas that were structurally unsound and replace them prior to overlaying. Another was to provide a smooth pavement surface at the desired grade. The main objective in using this method was to reduce the amount and degree of reflective cracks that would propagate through the AC overlay.

The specified cracking pattern required the breaking of the PCC pavement into 2-ft squares. An impact hammer was used to produce hairline cracks that penetrated the full thickness of the pavement. A section of PCC was removed to evaluate the total cracking of the pavement. Typical scenes of the construction are shown in Figures 4 through 6.

The cracked concrete was seated with thirty coverages of a 50-ton pneumatic roller. During the proofrolling, areas with

FIGURE 4 Hydraulic impact hammer for cracking PCC slabs.

FIGURE 5 Overall view of cracking pattern.

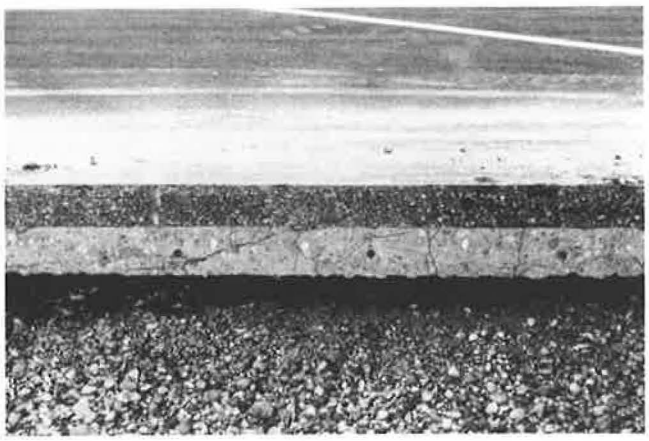

FIGURE 7 Cut-away section of asphalt overlay of cracked and seated pavement.

voids and weak spots were located and repaired prior to the asphalt overlay. After cracking and seating procedures, the pavement was overlaid with 4 to 5 in. of asphalt concrete.

The rehabilitation of this pavement was completed during the summer of 1982. The pavement was evaluated in July 1984 and was in excellent condition. The pavement surface did contain transverse cracks that occurred at 100-ft intervals. These cracks appeared to be caused by thermal stress and not by reflection. In 1983 and 1984, sections of the pavement were removed to inspect its full depth. Several photos were taken to show the effectiveness of the crack and seat method. Figure 7 shows the cracked PCC pavement under the AC pavement with no reflective cracks. Figure 8 shows the AC overlay over a joint in the PCC pavement. Figure 9 shows a typical transverse crack and indicates that the crack is caused by temperature changes and not movement in the cracked PCC.

The runway at Fort Wainwright was inspected again in July 1988, and the pavement was still in good condition. The pavement did have transverse cracks at 60-ft intervals, but these cracks were caused by thermal stresses. These transverse cracks continued across the entire width of the runway into the shoulders, which indicated that these wide cracks (1–2 in.) were caused by earth movement and were not reflecting up from the cracked PCC. The performance to date using cracking and seating has been satisfactory, and no deterioration has occurred adjacent to any cracks (*5*).

STRUCTURAL EVALUATION OF CRACKED AND SEATED PCC

Description

Aberdeen Proving Ground (APG), Maryland, contracted a project to rehabilitate Maryland Boulevard, which is a primary access road to the installation. The existing 40-year-old PCC pavement contained slabs that were structurally sound but had excessive movements over the years, causing a very rough ride. The joints were a tremendous maintenance problem. Medium to severe joint spalling had occurred on a large portion of the roadway. The PCC around many of the joints

FIGURE 6 Close-up view of cut-out section demonstrating full-depth cracking.

FIGURE 8 Cut-away section of asphalt overlay over a PCC pavement joint (ballpoint pen shows scale).

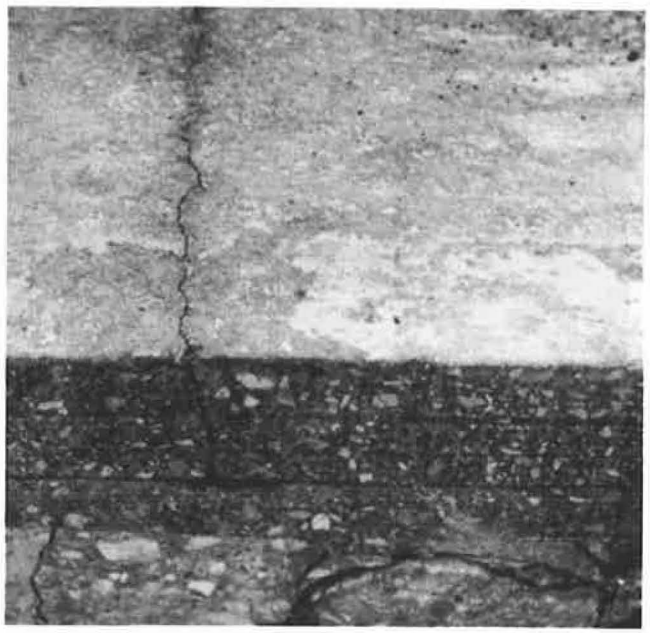

FIGURE 9 Cut-away section of typical transverse crack.

had been removed and replaced with asphalt concrete. Because of the importance of this pavement and the high volume of traffic it served, it was determined that the maintenance procedures being used would not slow the deterioration of the pavement and that some form of resurfacing should be implemented.

The initial plans for reconstruction of Maryland Boulevard included removing and replacing faulty slabs and resurfacing with asphalt concrete. The pavement section designed for this rehabilitation included a 3.5-in. crack relief layer and 4.5 in. of AC overlay. Before construction began, the contractor submitted a comprehensive Value Engineering Change Proposal that included the cracking and seating method. Owing to the uncertainties of this method, APG requested that Waterways Experiment Station (WES) evaluate the proposal and provide technical assistance in all phases of the project.

The proposal generated a cost savings of approximately 30 percent, which is substantial since the total project was bid at more than $3 million. The new proposal deleted any removal and repair of existing PCC slabs and implemented the cracking and seating procedures. The AC overlay thickness was determined using the National Asphalt Pavement Association (NAPA) guidelines. The total overlay thickness recommended was 8 in. This thickness was checked using Corps of Engineers (COE) thickness design AC overlays and was considered adequate.

Construction

The construction of this rehabilitation project began in late September 1986. Several areas of the roadway had to be prepared prior to cracking and seating the PCC pavement. Excessive crack and joint sealing material was removed using a small grinder. Extensive grading was done to improve water runoff and drainage along the roadway. Edge drains were also installed in some areas of Maryland Boulevard to improve subsurface drainage.

The 8-in. nonreinforced PCC slabs were broken using a whiphammer (Figure 10). It was recommended that the slabs be broken into segments approximately 2 ft square. To break up the 12 ft by 15 ft slabs in the desired cracking pattern, the whiphammer had to impact the slabs at 2-ft intervals in the transverse direction. The trial section was dampened to show the hairline cracks that were produced by the cracking operation (Figure 11). Cores were also taken to ensure the cracks penetrated the full depth of the pavement.

Immediately after cracking the PCC slabs, the cracked pavement was seated with a heavy pneumatic roller. The 50-ton roller made three passes over the pavement to ensure the slabs were embedded in the subgrade to prevent any rocking of the slabs. No excessive movement was noticed during any of the seating operations.

The project was separated into three segments for ease in construction and traffic control. Once all four lanes of a segment were cracked and seated, a leveling course using a surface mixture was placed over the cracked PCC and the asphalt shoulders. This produced a good riding surface until the remaining lifts could be placed and also protected the base from harsh weather conditions. Two intermediate courses, each 2.75 in. thick, were placed on Maryland Boulevard, making the total AC thickness approximately 6.0 in. The final surface course was placed in October 1987.

FIGURE 10 Whiphammer used at Aberdeen Proving Ground.

FIGURE 11 Close-up view of cracked PCC pavement.

Nondestructive Testing

As previously mentioned, cracking and seating PCC pavements reduces the structural strength of the pavement. To determine the extent of this reduction in pavement strength, the layered elastic model using nondestructive test data was used to evaluate the effective modulus for the cracked concrete and the remaining pavement layers. This project evaluated the structural strength of the pavement before and after cracking and after placing 4- and 6-in. asphalt concrete.

The effective modulus values for the cracked PCC pavement were determined using measured deflection basins obtained by the Falling Weight Deflectometer (FWD) shown in Figure 12. This FWD uses a weight dropped on a steel plate to produce an impulse load to the pavement that causes the pavement to deflect. Four drop heights were available to vary the impact load, which ranges between 8,000 and 26,000 lb. For these deflection readings, the maximum load was used for each slab. The actual load applied to the slab was measured by a load cell. Velocity transducers that are spaced at 0, 12, 24, 36, 48, 60, and 72 in. from the center of the plate were used to measure surface deflections (Figure 13).

The deflection basins measured by the FWD were used to determine modulus values for the pavement layers, subgrade, concrete, and asphalt concrete. The effective modulus values were determined by matching the measured deflection basin with the calculated deflection basin. The calculated deflections were determined using the layered elastic model solved with the BISAR computer code. To match the measured and calculated deflection basins as closely as possible, several iterations were done using the computer programs BISDEF and COMDEF.

Deflection basins were measured at the center of fifty slabs on Maryland Boulevard. It is general practice to measure deflections in the center of the slab so that conditions of continuous, homogeneous, linearly elastic layers assumed in the analytical model are as valid as possible. For each case, before and after cracking and after placing each intermediate course of asphalt concrete, deflection basins were measured to be used to determine modulus values for each pavement layer. The average predicted effective modulus values for each case are shown in Table 1.

FIGURE 12 Dynatest Falling Weight Deflectometer.

FIGURE 13 Close-up view of velocity transducers.

ANALYSIS OF DATA

Although the cracking and seating rehabilitation technique has been accepted and had widespread use, the effect of its use on the pavement structure has not been quantified. Evaluation of each pavement layer with the FWD during each phase of construction was considered the best method of assessing the technique. A comparison of each pavement layer was made for each phase of construction, before cracking, after cracking, and after placing asphalt concrete overlays.

With the data from the nondestructive testing and the use of the computer programs BISAR, BISDEF, and COMDEF, the effective modulus values for the subgrade, concrete, and asphalt concrete were predicted. The average predicted modulus values for each case are shown in Table 1. The computer modeling of these field data was excellent; the computed deflection values matched the deflection value measured by the FWD. Because of low percent errors in matching the deflection basins, the confidence level of the predicted modulus was high.

The predicted modulus values computed using the measured deflection basins showed that the effective subgrade modulus was stress-dependent. The average predicted subgrade modulus was 22,618 psi for the existing PCC pavement. After cracking and seating the PCC, the average predicted subgrade modulus decreased to 12,106 psi. This indicated that the subgrade after cracking and seating was carrying an additional load and a higher stress was being applied to the top of the subgrade because of the reduced strength of PCC. The subgrade modulus then increased with each additional asphalt overlay, which corresponds to a lower stress on the subgrade. The

TABLE 1 PREDICTED MODULUS VALUES

Case	Subgrade (PSI)	Concrete (PSI)	Asphalt Concrete (PSI)
Before cracking	21,618	5,896,165	–
After cracking	12,106	1,143,948	–
4-in. AC	15,642	1,276,666	271,885
6-in. AC	17,598	1,541,334	361,063

TABLE 2 SUMMARY OF STRESS ANALYSIS

Case	Maximum Vertical Stress (PSI)
Before cracking	2.02
After cracking	3.77
4-in. AC	2.97
6-in. AC	2.33

subgrade modulus for 4 to 6 in. of asphalt concrete was 15,642 psi and 17,598 psi, respectively.

The measurement of the reduction in PCC pavement strength was a primary objective of this investigation. The predicted modulus values for the PCC before and after cracking were used to evaluate the reduction in strength. The modulus value for the PCC prior to cracking and seating was 5,896,165 psi, which is a reasonable value for a 40-year-old PCC pavement. Once the PCC was cracked and seated, the predicted modulus value decreased to 1,143,948 psi, an 80 percent decrease. The modulus value did not vary much with the addition of asphalt overlays. The approximate modulus value of the cracked concrete after the AC overlays was 1,500,000 psi. Although there was a significant reduction in PCC stiffness, the modulus values predicted for the cracked concrete are much higher than typical modulus values for base courses. Typical modulus values for base courses range from 30,000 psi to 100,000 psi.

An additional stress analysis was computed on the pavement layers using the computed modulus values. For each phase of construction, the maximum vertical stress was computed in the top of the subgrade. The standard 18,000-lb, single-axle dual wheel (SADW) loading was used in all calculations. Table 2 lists the value for stress calculated by the BISAR computer programs.

The computed stress values in the top of the subgrade indicated that the subgrade modulus value is stress-dependent; as stress decreases, the effective modulus value increases. The computed stress on the top of the subgrade for the existing pavement was 2.02 psi. After cracking and seating the PCC, the stress increased by 86 percent to 3.77 psi. The stress on the subgrade decreased with each additional asphalt overlay. Approximately 6 to 7 in. of asphalt concrete was needed after the concrete was cracked and seated to result in the same stress on top of the subgrade as in the PCC pavement prior to cracking and seating.

CONCLUSIONS AND RECOMMENDATIONS

Conclusions

Cracking and seating of jointed PCC pavements is a viable rehabilitation alternative. This rehabilitation technique can reduce and retard cracks and joints from reflecting upward when the existing pavement is properly cracked and seated and when an adequate thickness of asphalt concrete is used. The pavement strength is reduced by the cracking and seating, but the cracked PCC layer still functions as a load-carrying medium.

Based on the data obtained in this investigation, the following conclusions can be made concerning the cracking and seating rehabilitation technique:

1. Cracking and seating of PCC pavements does significantly reduce the stiffness of the PCC.
2. Joints and cracks reflecting through the asphalt concrete overlay are reduced.
3. Flexural fatigue of asphalt concrete should not be a problem if slabs are broken into pieces 2 ft by 2 ft.
4. Approximately 6–7 in. of asphalt concrete was needed after the concrete was cracked and seated to result in the same stress on top of the subgrade as in the PCC pavement prior to cracking and seating.

Recommendations

1. Sealer material should be removed from cracks and joints prior to cracking and seating to prevent bleeding and slippage of the asphalt concrete overlay.
2. Proofrolling is required to seat the cracked PCC pavement but can damage the subgrade if there is excessive proofrolling.

REFERENCES

1. C. Crawford. *Cracking and Seating of PCC Pavements Prior to Overlaying with Hot Mix Asphalt*. National Asphalt Pavement Association Information Series 91. National Asphalt Pavement Association, Riverdale, Md., 1985.
2. C. V. Densen, A. B. Webb, Jr., and R. A. Welke. Cracking and Seating of Jointed Portland Cement Concrete Pavements in Michigan. In *Proc., Association of Asphalt Paving Technologists*, St. Paul, Minn., Vol. 53, 1984, pp. 51–79.
3. E. O. Lukanen and E. L. Skok. Structural Evaluation of Crack and Seat Overlay Pavements. In *Proc., Association of Asphalt Paving Technologists*, St. Paul, Minn., Vol. 56, 1987, pp. 720–732.
4. L. N. Godwin. *Cracking and Seating of Portland Cement Concrete Pavement Prior to Asphalt Concrete Overlay*. Miscellaneous Paper GL-8603. U.S. Army Engineer Waterways Experiment Station, Vicksburg, Miss., 1986.
5. E. R. Brown, J. W. Hall, and T. W. Vollor. *Improved Technique for Overlaying PCC Pavement*. U.S. Army Engineer Waterways Experiment Station, Vicksburg, Miss., 1984.

Publication of this paper sponsored by Committee on Pavement Rehabilitation.

Field Performance of Crack and Seat Projects

SAMUEL H. CARPENTER AND MICHAEL I. DARTER

Crack and seat rehabilitation on concrete pavements is the process whereby the existing concrete pavement is cracked to destroy the integrity of the slab. This cracking reduces the slab length, which reduces the thermal effect on joint movement. The seating operation is required to ensure that the pieces of slab are firmly seated into the underlying foundation material to eliminate vertical movement. Both of these are contributing factors in the development of reflection cracking. Reduction in the amount and severity of reflection cracking in an asphalt concrete overlay is the sole design requirement of the crack and seat procedure on a rigid pavement. This paper presents the results of an analysis of seventy crack and seat projects from twelve states throughout the United States. These data were collected as part of a study funded by the Federal Highway Administration (FHWA) of rehabilitation techniques to evaluate the parameters that affect their performance. By regression analysis of the database, models were developed that demonstrate general tendencies evident from the data concerning the performance of the crack and seat sections. This evaluation will provide the information to develop guidelines and recommendations for construction to improve their performance.

To date there has been one nationwide documentation of the performance of the crack and seat technique (*1*). However, a uniformly recognized standard for construction procedures has not been developed for this overlay technique. General guidelines have been proposed by several agencies, relying on their local experience, but they have not been verified with a comprehensive field survey of performance. The National Asphalt Pavement Association has published two reports on the performance of crack and seat projects in the Midwest (*2, 3*). Recently the Federal Highway Administration (FHWA) released the results of their survey of crack and seat projects in the United States, which provides some indications of performance variables but with no specific recommendations concerning design procedures (*1*). In 1984 the FHWA initiated the study "Rehabilitation Techniques for Rigid Pavements" to establish performance and design recommendations for several rehabilitation techniques.

DATA COLLECTION

To obtain specific indications regarding design of crack and seat rehabilitation projects, the development of an extensive database containing information on the original pavement design, asphalt concrete overlay design, traffic, environmental conditions, and performance of existing overlays was developed. The projects surveyed for inclusion in the database represent a cross section of the crack and seat projects in the United States. These pavements were surveyed between June 1985 and July 1986.

There are five basic data types necessary for the development of life prediction models and for analysis to develop and improve design and construction procedures.

1. Field condition data;
2. Original pavement structural design, in situ conditions, and historical improvement data;
3. Rehabilitation design factors;
4. Historical traffic values, classifications, and accumulated 18-kip equivalent single-axle loadings; and
5. Environmental data.

The database contains as many projects as were available or that could be included, given available resources, to provide a valid range of design parameters. Figure 1 shows the general location of the crack and seat and asphalt concrete overlay projects.

Variables

Figures 2 and 3 show the distribution of age and thickness for the crack and seat projects in the database. These parameters are broken out based on whether the original concrete pavement was plain or reinforced. The presence of reinforcing steel has long been felt to be a major factor influencing the performance of crack and seat rehabilitation. It is seen from the figures that the reinforced pavements have received thicker overlays and are generally not much older than the plain pavements.

There are no "overlay design" variables for crack and seat as there is no design procedure for this rehabilitation strategy outside of assuming a structural layer coefficient for the cracked concrete slab and designing the overlay based on this coefficient. Variables that are felt to be significant to the performance of a crack and seat project are listed in Table 1.

The severity levels employed in describing distresses are those defined in the FHWA distress manual (*4*). For example, low-severity cracking describes hairline cracking, medium-severity describes working cracks, and high-severity describes a badly spalled and faulted crack needing immediate repair.

Distress Present

Data on the condition of the existing pavements prior to the crack and seat rehabilitation were not available. Therefore,

Department of Civil Engineering, University of Illinois, Urbana.

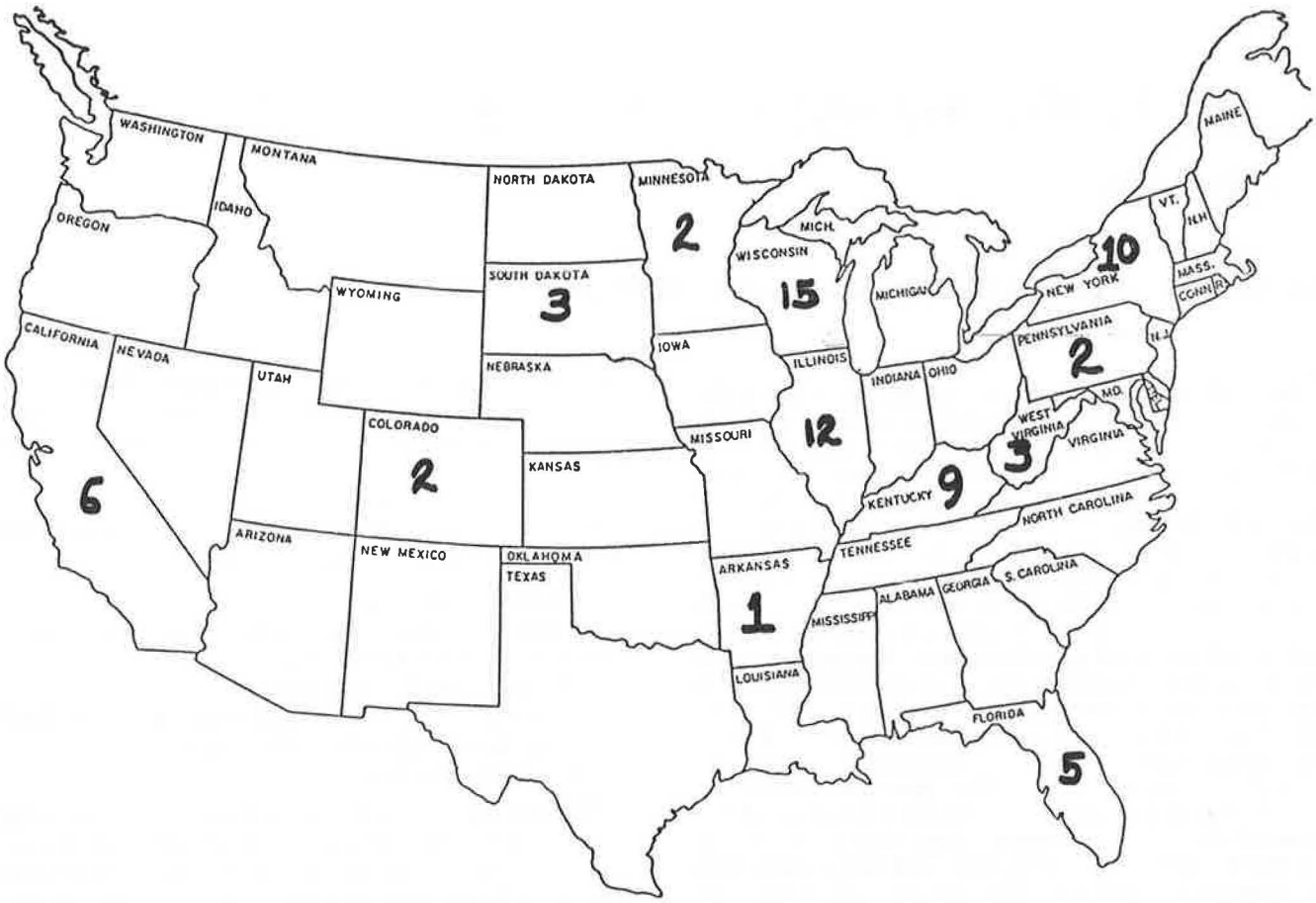

FIGURE 1 Distribution of crack and seat projects in the United States.

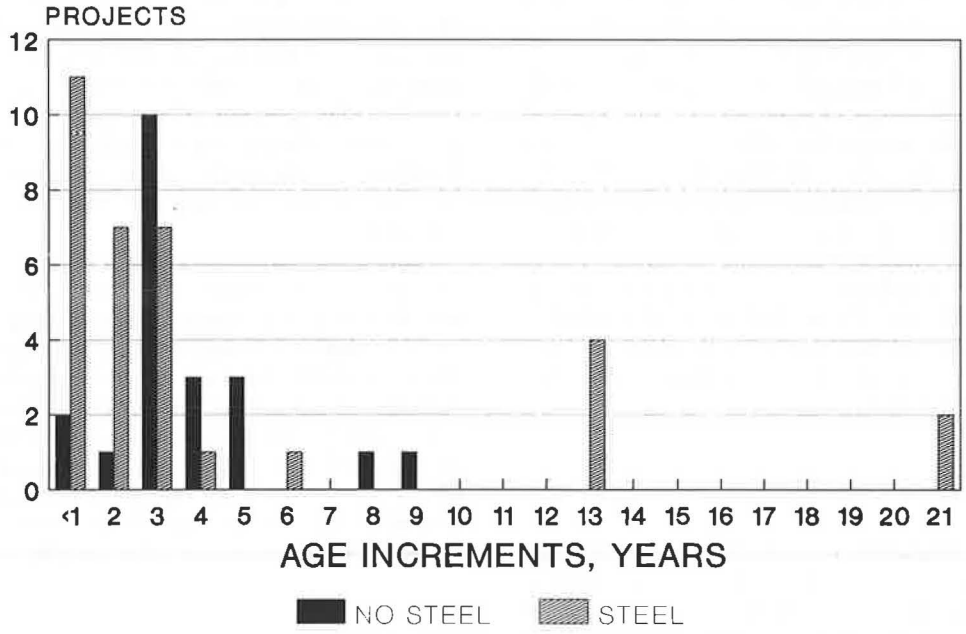

FIGURE 2 Age comparisons for the crack and seat projects in the database.

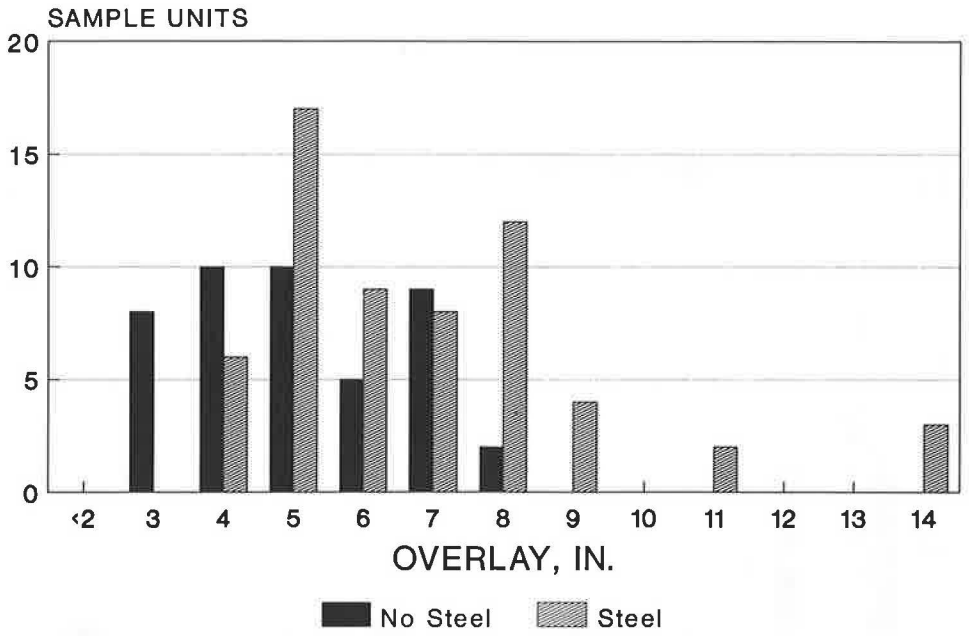

FIGURE 3 Thickness comparisons for crack and seat projects in the database.

TABLE 1 CRACK AND SEAT OVERLAY DESIGN VARIABLES

Project Identification Number
Sample Unit
Presence of "D" Cracking on Existing Pavement
Original Slab Repair
Pavement Breaker Type
Average PCC Breakage Size -- Width
Average PCC Breakage Size -- Length
Wire Mesh Cut or Broken
Seating Roller Type
Seating Roller Weight
Broken Pavement Exposure to Traffic
Sample Unit
Sample Unit Length
Present Serviceability Rating
Foundation of Sample Unit
Condition of Drainage Ditches
Subsurface Drainage Functional

DISTRESS DATA
Outer Lane, Inner Lane
Centerline Longitudinal Cracking
Transverse Cracking
Joint Reflective Cracking
Longitudinal Cracking
Lane Edge Cracking
Pumping
Alligator Cracking
Block Cracking
Raveling/Weathering
Bleeding
Rutting, Inner Wheelpath
Rutting, Outer Wheelpath

a mapping process to illustrate the time development of reflection cracking on each project could not be conducted, and the distress data represent one time-sequence data point. Reflection cracking is the major distress in an asphalt concrete overlay of a concrete pavement. Because the crack and seat process produces a more "flexible" base layer compared with a concrete slab, the development of fatigue cracking may be a distress that develops that would not develop in an asphalt concrete overlay of an uncracked concrete slab.

The percentage of projects containing lengths of cracking (ft/1,000 ft) of low, medium, and high severity are shown in Figures 4 and 5. These figures indicate, for example, that 100 percent of the projects exhibited no high-severity cracking for the plain pavements, and 96 percent of the reinforced pavements had no high-severity cracking. These figures are separated to demonstrate any differences caused by the presence of reinforcing steel in the concrete slab, as this is felt to be a significant variable in the performance of crack and seat rehabilitation.

Figures 4 and 5 show that the reinforced pavements develop more high- and medium-severity cracking than the plain pavements. The plain pavements exhibit much more low-severity cracking, as demonstrated by the greater length of cracking found on the plain sections, which may be a function of shorter joint spacings not allowing the reflection crack to deteriorate.

There is not a great amount of high-severity reflection cracking in any of the sections, even though some of these projects are quite old. The development of medium- to high-severity reflection cracking on the crack and seat projects should be compared to that in conventional overlay projects

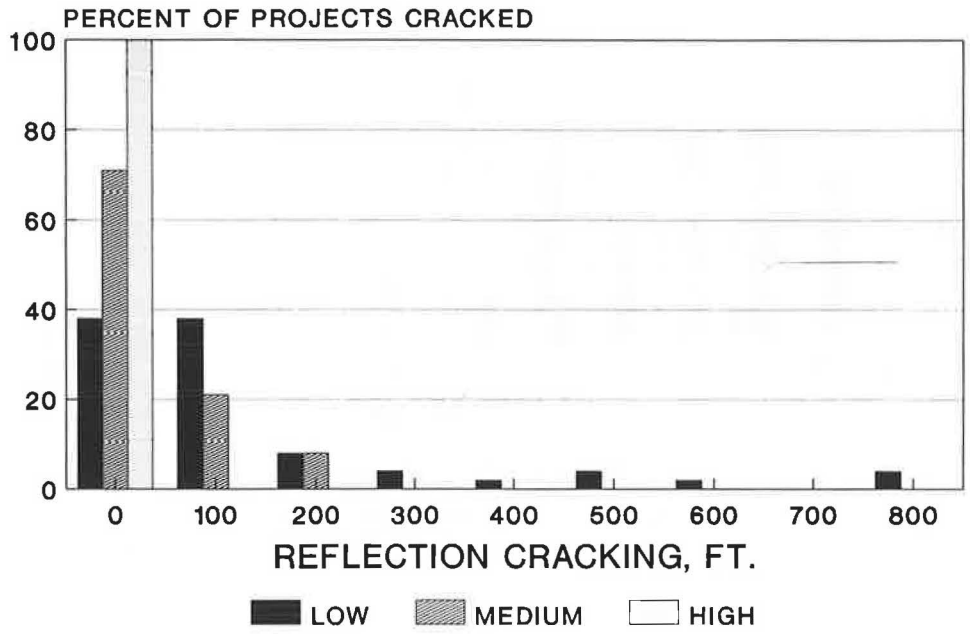

FIGURE 4 Amount and severity of reflection cracking present on crack and seat projects with no reinforcing steel.

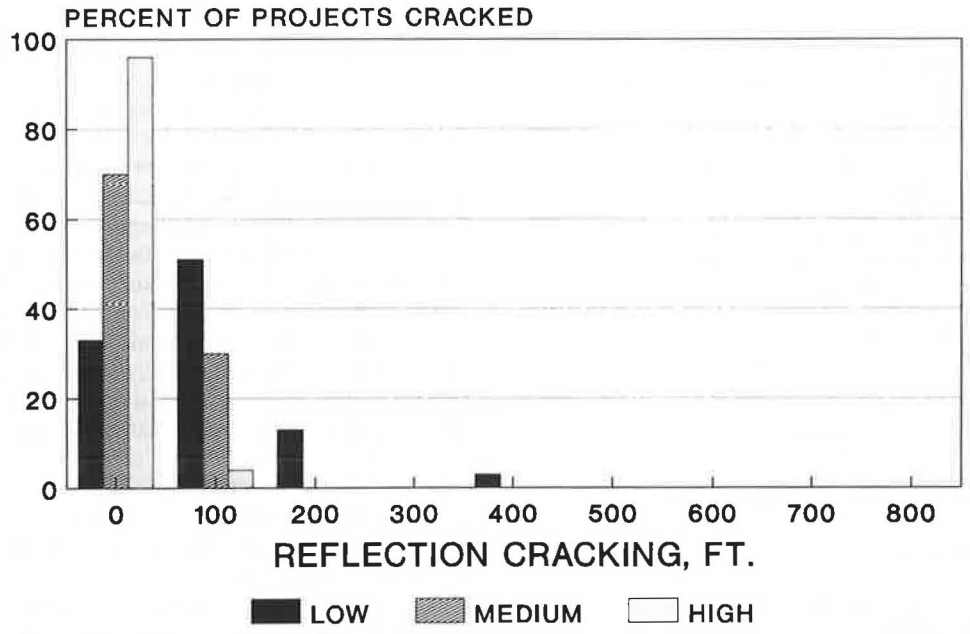

FIGURE 5 Amount and severity of reflection cracking present on crack and seat projects with reinforcing steel.

to determine if the rehabilitation reduces the severity, if not the amount, of the reflection cracking. The small occurrence of the high- and medium-severity cracking was primarily on the reinforced pavements. This may indicate that on plain concrete pavements the severity is being reduced, although the age and traffic may be other factors that must be included in the comparison.

PAVEMENT PROJECT CHARACTERISTICS

Overlay Thickness

The thickness of the overlay has a critical role in the development of reflection cracking, particularly when the overlay is below approximately 6 in. thick. Figure 3 shows the distribution of overlay thicknesses broken out by pavement type. The average overlay thickness for the plain pavements was 4.25 in., while the average overlay thickness for the reinforced pavements was 6.25 in. Thicker overlays retard the appearance of reflection cracking and should produce a lower-severity crack, significantly reducing the development of high-severity cracking. The thicker overlays are indicating a higher potential for medium-severity reflection cracking, which may indicate that the presence of reinforcing steel, joint spacing, and other factors may be significant in the performance of the overlay on a crack and seat project.

Age and Traffic

The average age of the reinforced pavements was 4.7 years, while the age for the plain pavement sections was 4.0 years. The thicker overlays have been in place longer, and they have been subjected to more traffic. The accumulated 18-kip equivalent single-axle loads (ESALs) since overlay for the plain pavements is 1.3 million ESALs while for the reinforced pavements it is 1.9 million ESALs. The percentage of trucks in the traffic stream was also higher for the reinforced pavements (24 percent) compared with the plain pavements (18 percent). The actual values of ESALs varied from approximately 0.08 to 8.3 million ESALs for all projects.

Serviceability

Present Serviceability Rating (PSR) information was available from a small cross section of the crack and seat projects (twenty-seven projects). The PSR curve for the crack and seat sections is shown in Figure 6. There is no tendency for the better performing pavements to have thicker overlays. The best performing projects were in the milder climates (California and Florida, with relatively thin overlays and mixed traffic levels).

This serviceability loss, which begins around 3 million ESALs, can be attributed to cracking, rutting, and possibly roughness induced by slab motion under traffic. The average rut depth for these projects was 0.15 in., with the maximum rut depth measured at 0.42 in., which may contribute to roughness on a few of the sections. In general, the higher rutting did not occur on the projects with lower PSR values, indicating that some design variable in the crack and seat procedure may be contributing to the development of the roughness. Similar correlations with the various forms of cracking also showed no direct relationship between the severity or amount of cracking and the roughness, further lending credence to the feeling that a design variable in the crack and seat process may be responsible.

These differences indicate that the performance of plain and reinforced pavements cannot be made on a direct comparison of visual survey data taken from a distress survey

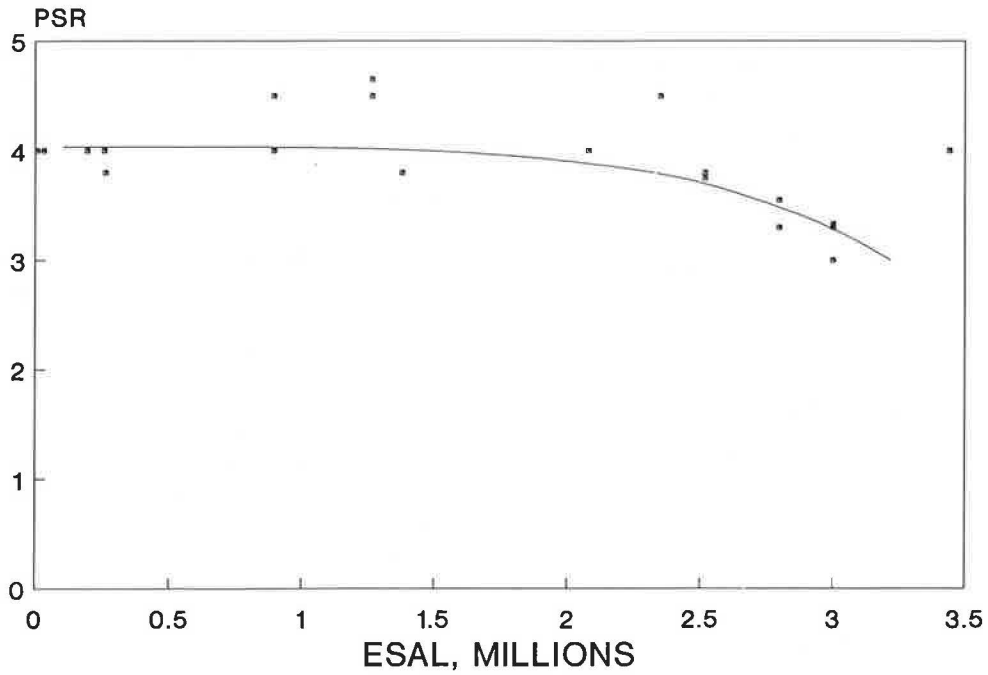

FIGURE 6 Serviceability rating (PSR) for the crack and seat projects.

without knowing the causative factors that may produce different levels of cracking on the surface. In this case, similar performance has developed on projects with very different design considerations of thickness, age, and traffic, which indicates that one set of overlays, those over crack and seated reinforced pavements, are not performing as well as those over plain pavements.

PERFORMANCE MODELS

Model Development

Predictive models were developed for significant distress variables using the regression techniques as included in the Shazam statistical package (*5*). Models for rutting and reflective cracking were developed from the database (*6*), but only the reflection cracking models are discussed here.

As a first step in analyzing the data, all independent variables that were considered to have meaningful and significant influence on the performance of the crack and seat overlays were identified. These variables were then considered in the development of the models with linear regression. Separate models were developed for each severity level (low, medium, and high) of reflection cracking. This was done to illustrate the different factors that are important in the development of cracking and the progression of cracking from low to medium and high. The individual models are not used to predict overall performance primarily because of the lack of sample units in certain distress categories. Because only 4 sample units out of the 107 surveyed contained any high-severity distress, fewer inferences could be drawn from the inadequate models developed. The models for low-severity and for a combined medium- and high-severity are presented here.

Medium- and High-Severity Combination

There were 44 sample units of the 107 surveyed that exhibited some medium-severity reflection cracking. The model developed using data from all 107 sample units was

$$\begin{aligned} RFLCMH = {} & 14.0523 + 2.928(AGE) + 0.04158(FI) \\ & - 10.677(TPCC) - 0.5853(SWR) \\ & - 13.583(WDT) - 6.555(LT) \\ & + 3.236(AREA) + 2.1345(ANNPREC) \\ & - 0.003928[0.14263(ANNAVGT) \\ & - 0.12123(ANNPREC) \\ & + 0.1955(ANNRNG) - 5.9531](ESAL) \end{aligned}$$

R^2, correlation coefficient = 0.61;
SEE, standard error of estimate = 32.7; and
N, number of sample units = 107.

where

RFLCMH = high-severity reflection cracking (ft/1,000 ft);
AGE = age of overlay in years;
TPCC = thickness of original slab (in.);
FI = Freezing Index;
SWR = seating weight of roller in tons;
WDT = width of crack pattern (ft);
LT = length of crack pattern (ft);
AREA = area of the cracked slab pattern (sq ft);
ANNPREC = annual precipitation (in.);
ANNAVGT = average annual temperature (°F);
AVGRNG = average monthly temperature range; and
ESAL = total 18-kip equivalent single-axle loads since overlay (in millions).

Low Severity

There were 71 sample units of the 107 analyzed that exhibited some amount of low-severity reflection cracking. The model developed for low-severity distress with the data from all 107 sample units is

$$\begin{aligned} RFLCL = {} & 87.396 - 1.7074(JTS) + 3.3215(SWR) \\ & + 33.596(LT) - 1.5298(AREA) \\ & - 47.438(SOIL) - 4.6739(ANNPREC) \\ & + 2.5865(ESAL) \times [0.14263(ANNAVGT) \\ & - 0.12123(ANNPREC) \\ & + 0.1955(AVGRNG) \\ & - 5.9531] \end{aligned}$$

$R^2 = 0.41$,
SEE, standard error of estimate = 111.2, and
N = 107

where the variables are as previously defined with the addition of SOIL = subgrade soil type, 1—coarse, 0—fine grained; and JTS = joint spacing (ft).

Model Discussion

These models provide insight into potential areas where performance of crack and seat rehabilitation projects can be improved through control of variables. The development of medium-severity cracking is affected by age and environment, variables that are slightly less influential in the development of low-severity cracking. The original pavement variables and construction procedures are more significant in the development of low-severity cracking and not as significant in the development of medium- or high-severity, with the exception of the cracking pattern and thickness of the original pavement slab.

The analysis of these individual equations tends to indicate that low-severity cracking will occur regardless of environment and traffic, and that construction variables influence the amount of low-severity reflection cracking and its progression. The progression of low-severity cracking into medium- and high-severity cracking is more dependent on the environment in which the project is constructed and the traffic levels on the project.

Application Limits

The use of data outside those present in the database has the potential to produce predicted amounts of reflection cracking

that are not typical of a pavement with the variables chosen. Further, there are certain combinations of variables that should be noted and not used because they were not present in the database, and may or may not be present in another pavement not included in this analysis. The range of variables should be determined (*6*) before using these models on pavements that could be unique. As an example, climatic parameters must be selected in a combination representative of the actual values common to an area. A check is to use the following equation:

$$\text{ZONE} = [0.14263(\text{AVGTMP}) - 0.12123(\text{ANNPREC}) + 0.1955(\text{ANNRNG}) - 5.9531]$$

The result *must* be between 0.5 and 9.5, preferably between 1 and 9, numbers that correspond to the nine environmental zones for FHWA classifications (*7*). When this equation is calculated outside the limits, the combination is not representative of a naturally occurring climatic area of the country, and the input variables should be examined.

Model Performance

The models clearly show that several variables are missing that many have intuitively felt should be influential on the performance of crack and seat and overlay rehabilitation. These variables were either determined to be statistically insignificant in characterizing the noted performance of the overlays or were not present with sufficient variability in the database to allow a true indication of their actual effect. Future refinement of the models as the database is expanded should address the proper inclusion of the following:

1. Thickness of the overlay,
2. Pre-crack and seat and overlay repair techniques employed,
3. Reinforced versus plain concrete,
4. Mechanistic data, such as elastic moduli from FWD deflection testing, that indicate cracking efficiency, and
5. Overlay asphalt mixture properties.

Sensitivity comparisons developed from the models are given in Figures 7 through 13. The separate straight-line portions with different slopes on each graph show the separate influence of low- and medium-high-severity cracking that makes up the total reflection cracking. The following discussions can be drawn from these figures.

Area

Analysis of the area of the cracked sections shows that large areas should be avoided. The area shown on Figure 7 is calculated from length and width. The length-to-width ratio of the cracking pattern also influences the development of reflection cracking. The pattern should be kept nearly square as elongated pieces crack more readily.

Freezing Index

More total reflection cracking can be expected in areas with higher Freezing Index (FI) values up to a certain age, as shown in Figure 8. The FI value relates directly to the amount of thermal activity that produces movement in the joint, propagating the reflection crack.

Thickness

The thickness of the original Portland cement concrete (PCC) slab affects medium- and high-severity cracking but does not alter the development of low-severity cracking, as shown in Figure 9.

Roller Weight

Heavier rollers to seat the cracked sections will produce more low-severity reflection cracking while it reduces the development of medium- and high-severity cracking, as shown in Figure 10. The use of heavy rollers may alter the cracking effectiveness and change the development of low-severity cracking. The effectiveness of the cracking is a critical element in the performance of crack and seat; it cannot be evaluated from distress surveys and thus cannot be included in this analysis. The use of the heavier roller to seat the cracked sections delays the progression from low- to medium- or high-severity and may thus be beneficial.

Joint Spacing

Longer joint spacings produce less total length of cracking in the overlay than do short joint spacings, as shown in Figure 11. This is due partly to the fact that there are fewer joints in a long jointed pavement. An examination of cracking as a percent of joints may be warranted as a better indicator of the performance of the procedure.

Subgrade

The presence of a coarse-grained subgrade soil greatly reduces the amount of low-severity cracking but has no effect on the development of medium- or high-severity cracking, as shown in Figure 12. Better subgrade support allows slightly larger cracked pieces to be produced in the cracking operation, although no correlation is available to relate an optimum size to a subgrade support factor. Poor subgrades generally indicate the need for drainage prior to the crack and seat operation. A thorough evaluation should be performed.

Age and Axle Loadings

The interaction of age and ESALs is unique. Low-severity cracking increases with increasing axle loadings, with no direct relation to age of the overlay. This implies that the same amount of cracking can develop in different time periods, as long as the number of axle loadings is the same. The age of the overlay appears as a factor in the development of medium- and high-severity cracking, in addition to the effect of the axle loadings that accumulate during the year.

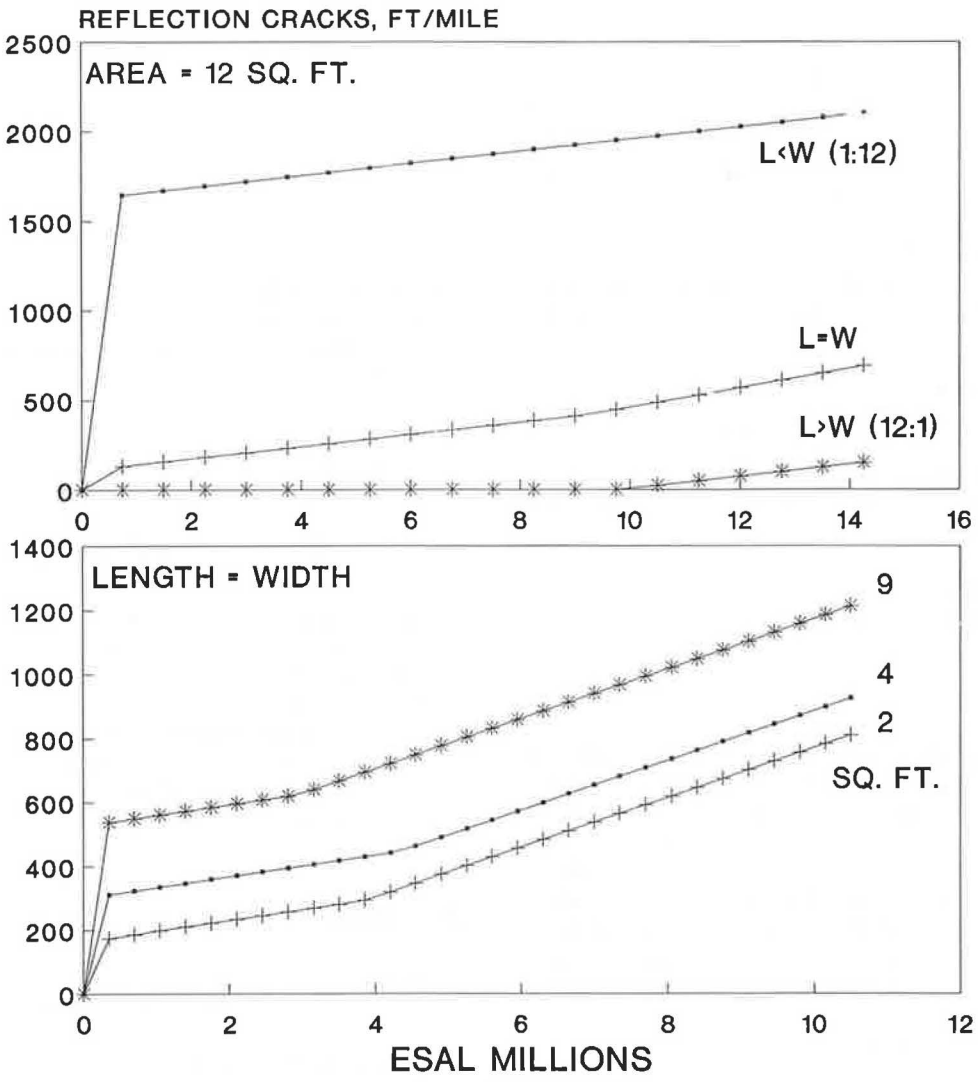

FIGURE 7 Influence of cracking pattern on reflection cracking.

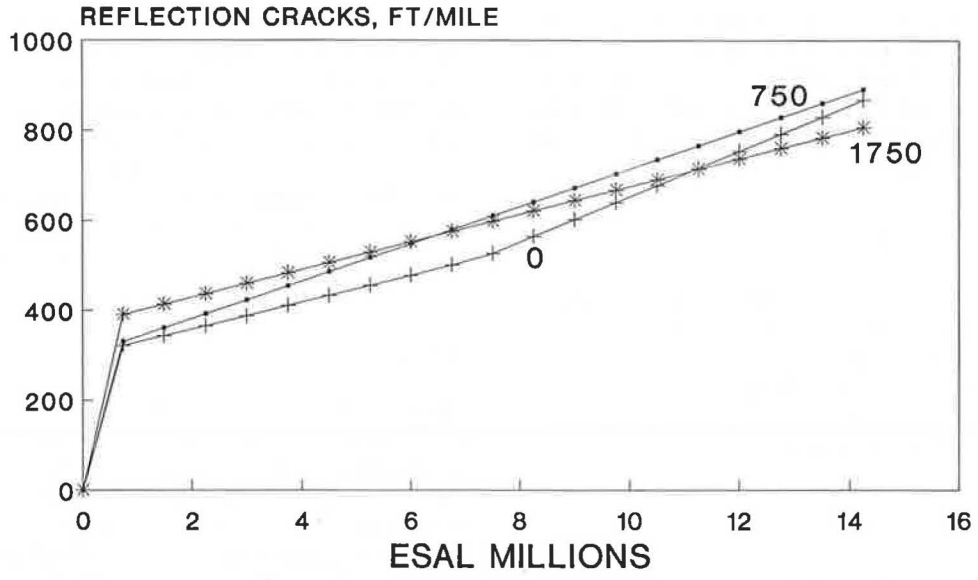

FIGURE 8 Influence of Freezing Index on reflection cracking.

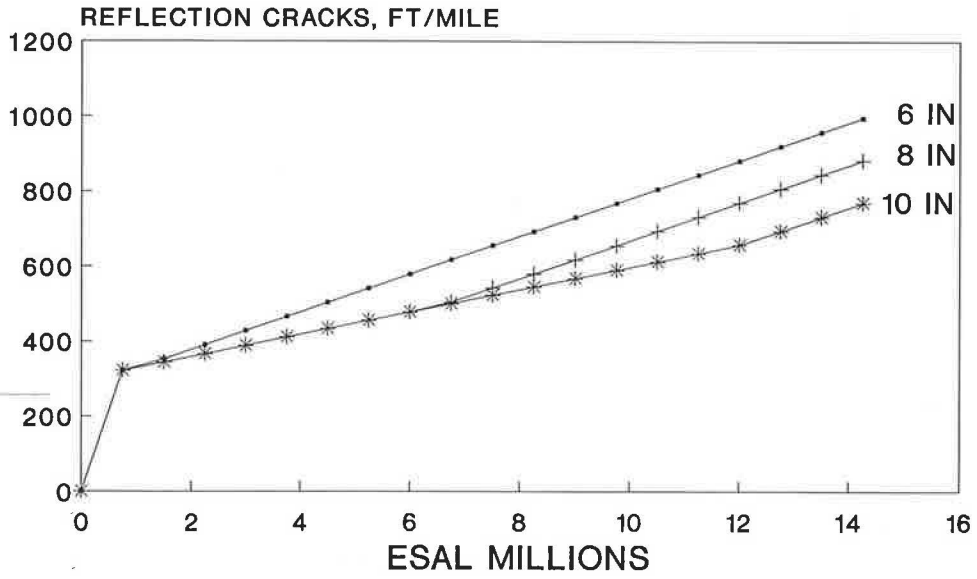

FIGURE 9 Influence of original concrete pavement thickness on reflection cracking.

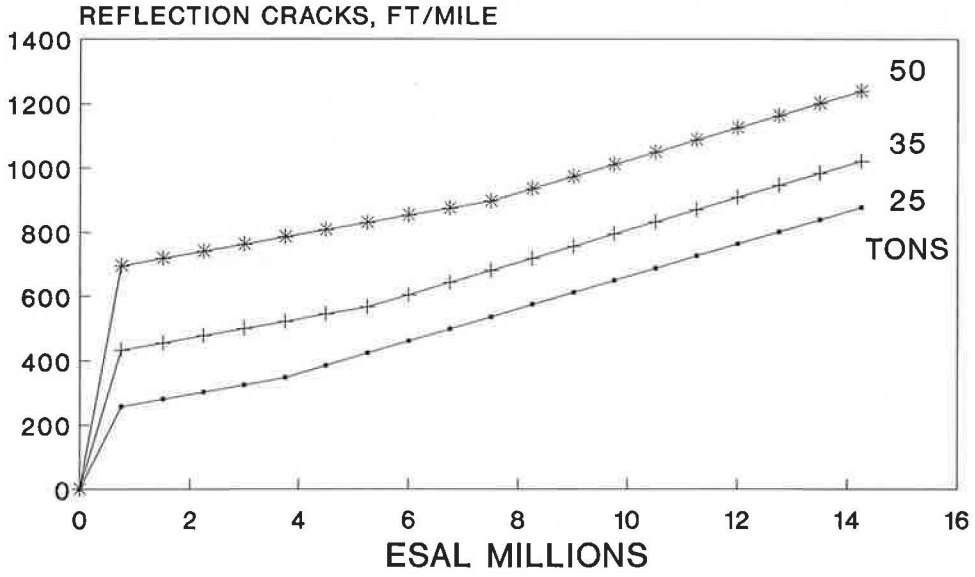

FIGURE 10 Influence of seating roller weight on reflection cracking.

Climate

The climatic variables illustrate the impact of environment on reflection cracking performance. Areas with larger annual rainfall showed lower amounts of low-severity cracking, while the development of medium- and high-severity cracking is greater in these same areas, as shown in Figure 13. Medium- and high-severity cracking develops over time, and higher annual rainfall may produce a lower support in the subgrade that accelerates breakdown of existing cracks. The higher amount of low-severity cracking in areas having low rainfall may be due to greater temperature variations. The combined effects of the climatic factors cannot be totally separated and investigated independently. The annual average temperature and monthly average temperature range combine with the annual precipitation to describe the general climate in the area. Generally, the areas with warmer annual temperatures and a smaller temperature range performed better.

CONSTRUCTION GUIDELINES

The placement of an asphalt concrete overlay over a jointed PCC pavement typically is done to restore smoothness and/or structural adequacy to the overall pavement structure. There are design procedures to select the thickness of asphalt con-

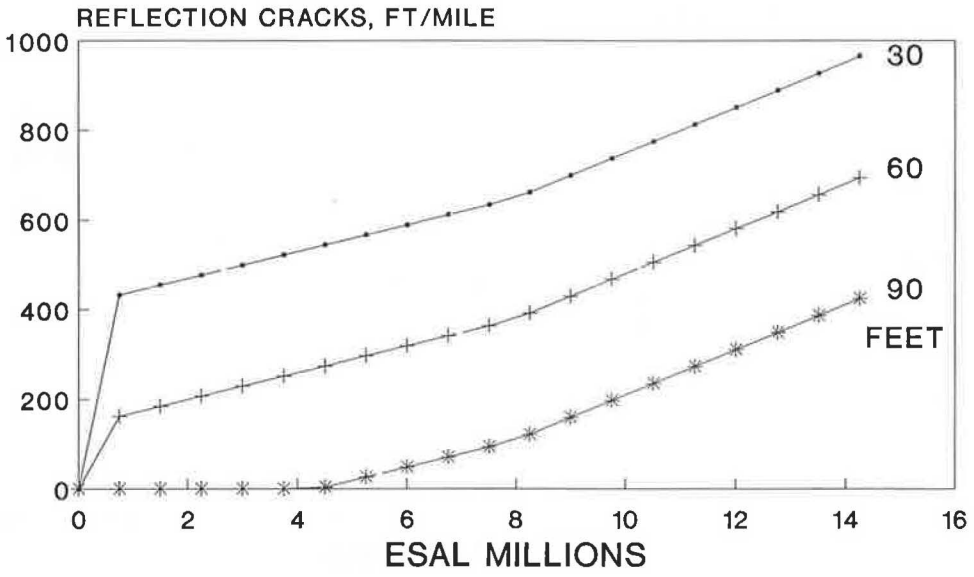

FIGURE 11 Influence of joint spacing on reflection cracking.

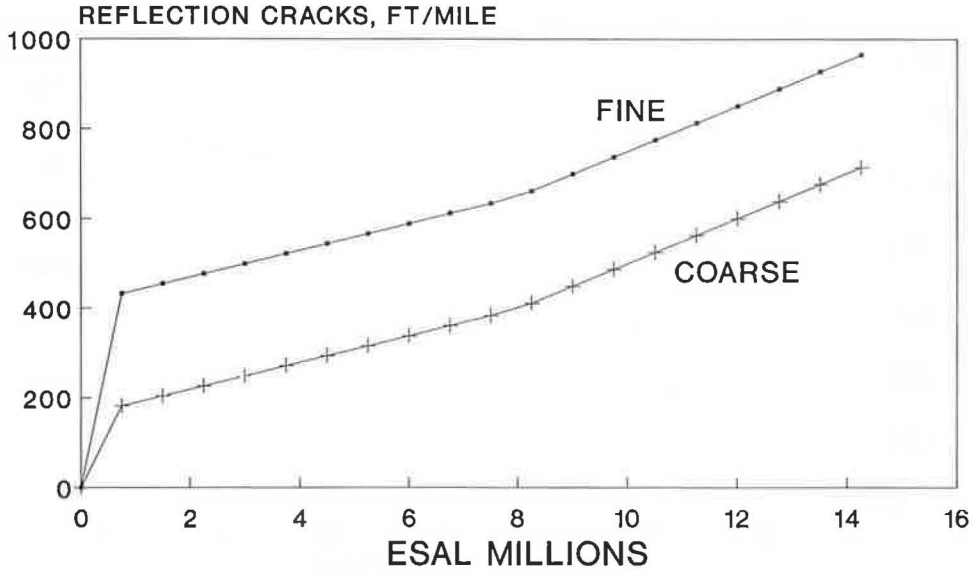

FIGURE 12 Influence of subgrade type on reflection cracking.

crete to carry the predicted traffic (*8*). The design procedures for crack and seat overlays are currently in the formative stages (*9*), and the field data represented by the models developed here provide an excellent initial indication of construction procedures that should be followed.

Selection

This rehabilitation scheme is cost-effective for pavements that do not require extensive slab replacement. A large number of severely deteriorated slabs that normally require replacement may indicate very poor foundation support, and this pavement could not be considered a prime candidate for crack and seat. The crack and seat process does not lend any extra structure to the pavement and actually produces a layer with less structural adequacy than the original concrete slab (*10, 11*). Severely deteriorated and spalled joints and cracks may require repair to the same extent as would be required for a standard asphalt concrete overlay to minimize deterioration once the overlay cracks. The cracking process must not worsen the crack; the crack must be tight and closed for good performance. Slabs exhibiting excessive fatigue damage may indicate that there is a foundation problem that may hinder the provision of sufficient support to the crack and seat section. Further, a fatigued concrete slab may produce a very different crack pattern than a sound slab, and damage to the fatigued slab may be easier, therefore requiring closer control of the cracking equipment and monitoring of the crack pattern to achieve the best performance.

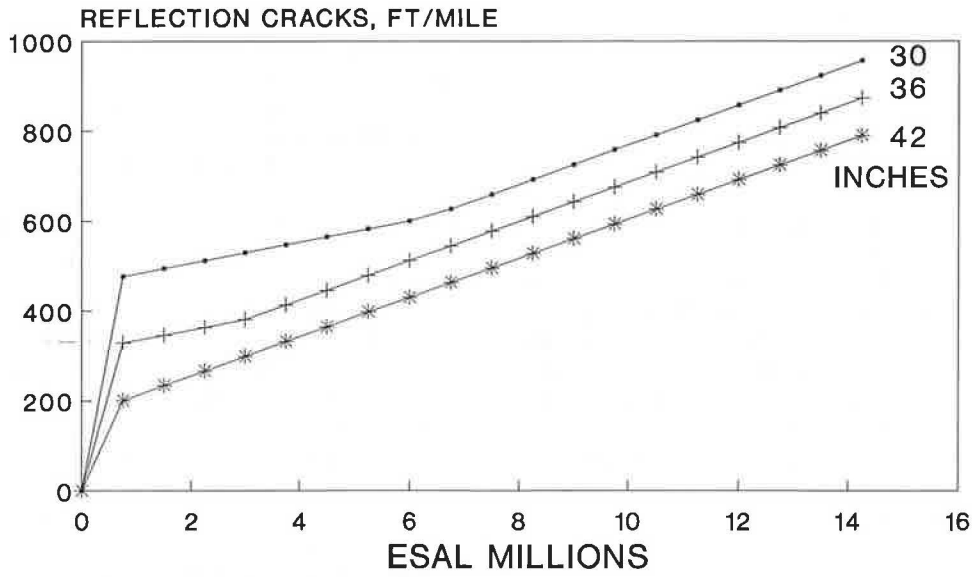

FIGURE 13 Influence of annual precipitation in inches on reflection cracking.

Drainage Considerations

When there is a drainage problem and moisture-susceptible materials are in the pavement structure, drainage should be considered and installed prior to the crack and seat operation. This requires careful evaluation of the pavement to ensure that drainage will improve the performance of the materials.

Subgrade Quality

Subgrade support is influential on performance of the crack and seat overlay. Better subgrade support will provide better support for the seated pieces and better resistance to movements. Pavements with poor subgrades are not the best candidates for crack and seat rehabilitation; when poor support is expected, the seating operation should not use the heaviest roller since this definitely causes nonuniform or excessive movement in the pieces.

Cracked Pattern

It is good practice to specify the cracking pattern desired. To ensure that the specified cracking is obtained, it is recommended that test sections be constructed prior to production. This allows the contractor to investigate various combinations of equipment and striking patterns that will guarantee the desired result. Spalling along the cracks and shattering of the pieces during the cracking operation should be avoided. The cracking pattern should be validated and recorded for comparison during the progress of the crack and seat operation.

Cracking Equipment

If the steel is not ruptured, the integrity of the slab is not broken and the slab will continue to move as an integral unit, propagating reflection cracks. Conversely, the breakdown of the concrete when overcracked may be so extreme that aggregate interlock is lost between the shattered pieces, producing pieces that are capable of moving independently under traffic, accelerating the development of reflection cracks.

Devices that demonstrate the ability to produce the desired cracking pattern should be allowed on the job with the exception of free-fall devices, such as headache balls. Pile drivers and guillotine hammers are the most common devices, generally used with modified striking plates shaped to produce the desired cracking pattern. Sharp striking plates or small striking areas should be avoided as these will tend to spall or penetrate the surface. It is recommended that the cracking not be done any closer than 10 in. to a joint or crack in the original slab.

The whiphammer and the resonant breaker are two newer pieces of equipment that have been investigated for use on crack and seat operations. Further work with these devices is needed to define their operating characteristics (*1*).

Seating

Recent studies indicate that excessively heavy rollers may do more damage than good. A report from Indiana (*12*) indicates that a 50-ton pneumatic roller increased deflections in the cracked pieces after each pass of the roller. These increased deflections indicate less strength in the pavement section, producing a reduced load-carrying capacity. Two projects in California (*13*) with a 13-ton roller gave results indicating that the cracking procedure reduced deflections at 92 percent of the joints, while subsequent rolling increased the deflection at 40 percent of the joints. These studies indicate that rolling may not be beneficial from a structural adequacy standpoint. It is done to seat the pieces to reduce their potential to move under traffic and propagate another crack.

It is recommended that a means of measuring deflections in the broken pieces be implemented to determine the most efficient roller weight and the optimum number of roller passes

before the pieces start to unseat. This can be a simple procedure using a Benkelman beam and a loaded dump truck that is run over the project periodically.

Maintenance of Traffic

Several states allow traffic to use the cracked and seated pavement prior to overlay. It is recommended that traffic not be allowed unlimited access to a project where subgrade support may be low, since the potential for unseating the pieces is higher for this pavement. Where foundation support is good and the base is strong, traffic can be allowed for a limited time. It is good practice to begin placing the overlay within 2 to 3 days following cracking and seating to prevent breakdown of the aggregate interlock and unseating of the pieces. If an excessive delay is encountered, it may be advisable to reseat the pieces immediately prior to overlay.

Utilities, Culverts, Curbs, and Gutters

Cracking operations directly over utilities, culverts, curbs, and gutters should be avoided. This will require accurate marking of the locations of these appurtenances. The Direct Federal Division of FHWA has a specification that does not permit cracking and seating operations within 5 ft of subsurface utilities and structures. The contractor should be required to repair all damage to these installations, which might require a survey prior to crack and seat to determine the preconstruction condition.

Reflection Cracking Treatments

There are many reflection crack treatments (*14*). At present it is not felt that reflection crack treatments such as fabrics should routinely be used in conjunction with crack and seat. The reason for this is principally the cost involved and the inability to predict the effectiveness of fabric installations in general. There are no data to indicate the performance of fabrics in a crack and seat job. If a state has good experience with fabrics for reflection crack reduction, they may be used, and the projects should be studied to determine whether the fabric provides an advantage.

Cracking of a Composite-Asphalt Overlaid Pavement

Cracking can be done through an asphalt overlay. The problem with the operation is that the extent of the cracking cannot accurately be verified without removing the asphalt concrete for visual inspection. It is recommended that the existing asphalt be removed by an appropriate means, and considered for recycling, before the cracking operation.

CONCLUSIONS AND RECOMMENDATIONS

Crack and seat rehabilitation with overlay has been done since the mid-1940s and has recently received increased attention with the increased need for rehabilitation of concrete pavements to reduce reflection cracking in the overlay. The crack and seat operation has as its primary goal the reduction of reflection cracking in the overlay.

A total of seventy projects were surveyed in twelve states for inclusion in the database. Where the projects were long enough, two sample units were surveyed. This resulted in 107 sample units in the final database. These projects represent a cross section of projects constructed in the United States in recent years.

Previous surveys have indicated that crack and seat overlays can reduce reflection cracking, particularly in the early years of the overlay's life. There is some evidence that after a specific number of years, the effectiveness of the crack and seat operation may diminish.

The projects surveyed in this study exhibited good performance in general, with only one section exhibiting high-severity reflection cracking and approximately one-third exhibiting medium-severity reflection cracking of limited extent.

The design and construction of crack and seat overlays require special considerations to reduce the effective slab length to minimize cracking and to seat the cracked sections so they will not move under traffic. Overall conclusions and recommendations from this research study are as follows:

1. The presence of reinforcing steel has a significant influence on the effectiveness of the crack and seat operation. If the cracking operation does not rupture the steel, the slab length will not be reduced. The major difference is in the extra precautions that must be taken in the cracking operation on reinforced pavements. The database analysis did not show a difference in the performance with or without steel, primarily because of other interactions.
2. Without deflection testing of the completed project, there is no way to evaluate the effectiveness of the cracking operation beyond a recognition of the size of the cracked pieces. At present there is no acceptable procedure for evaluating the cracking effectiveness on the concrete slab prior to overlay.
3. The crack and seat overlays develop low-severity reflection cracking relatively quickly, and this development appears to be influenced more by the variables in the crack and seat operation than the original pavement design or environment. The progression of low-severity cracking to medium- and high-severity cracking is more a function of environment, age, original pavement design, and traffic and less a function of the crack and seat construction variables.
4. The seating roller weight has a dual action on reflection cracking. Heavier rollers cause more low-severity cracking to develop initially, while reducing the rate at which the low-severity cracks progress to medium- and high-severity cracking. The impact of heavier rollers is related to foundation quality, and heavy rollers should not be used on weak foundations. The use of a heavy roller does not guarantee improved performance.
5. Cracking pattern is more complicated then merely investigating the area of the cracked pieces. The area should be minimized to the range of 4 to 6 sq ft, and the ratio of length to width should also be controlled. When the length of the cracked piece (length is measured along the longitudinal direction of the pavement) is less than the width (width is measured transversely across the pavement), more cracking will result

than if the length and width are equal or the length is greater than the width. For construction it is recommended that the dimensions be kept equal, and if variation should occur, attempts should be made to control this toward producing a pattern with a slightly greater length than width.

6. Overlay thickness did not show an influence on reflection cracking, which may be due to an interaction effect with the reinforcing steel. The reinforced pavements generally had a thicker overlay, had been in place longer, and had higher traffic levels than the plain concrete sections. The performance of the reinforced and plain sections was so similar that the effect of steel and thickness did not enter the predictive relationships. In general, thicker overlays will perform better for a longer period than thinner overlays placed over the same crack and seat sections.

7. The quality of the asphalt concrete mixture has a significant impact on the performance of an overlay in resisting reflection cracking. The data in the database contained no indication of the mix quality in the individual projects. The rutting performance of these sections was typical of conventional overlays, which indicates the mix quality could be considered typical. Any comparisons of the performance of individual sections should be made with the realization that variability in mix quality can alter reflection cracking.

8. The environment showed an effect on the progression of cracking to the medium- and high-severity levels. In general the milder climates showed the best performance. High monthly temperature extremes and low monthly average temperatures produce more medium- and high-severity cracking. This interaction is shown in the decreased cracking with lower Freezing Index and the decreased cracking with higher precipitation. Higher precipitation generally occurs in areas with a more moderate climate without extreme swings in temperature.

9. Regression models were developed for low-severity and a combination of medium- and high-severity reflection cracking. The ability to model medium- and high-severity cracking is essential to planning rehabilitation, as these levels generally trigger the decision to overlay again. While these initial equations are not refined enough at present to use in designing rehabilitation projects, they provide a means of investigating the variables in a pavement rehabilitation project that have an impact on the development of reflection cracking. These relationships can assist the design and construction engineer in planning a crack and seat operation to provide the highest degree of reliability possible. As crack and seat projects are applied in more states with differing climates and designs, these initial models can be revised to include more variables and wider ranges of applicability to overcome some of the limitations of the database mentioned earlier.

ACKNOWLEDGMENTS

The information contained in this paper is part of a study entitled "Determination of Rigid Pavement Rehabilitation Methods for Rigid Pavements" being conducted for the Federal Highway Administration by the Civil Engineering Department of the University of Illinois at Urbana-Champaign. The authors wish to express their appreciation to Stephen Forster of the Federal Highway Administration and to the states that participated in this study.

REFERENCES

1. *Crack and Seat Performance.* Review report. Demonstration Projects Division and Pavement Division, FHWA, U.S. Department of Transportation, April 1987.
2. *Structural Evaluation of Crack and Seat Overlay Pavements.* Midwest Pavement Management, Inc., September 1986.
3. R. A. Eckrose and W. E. Poston. *Asphalt Overlays on Cracked and Seated Concrete Pavements.* National Asphalt Pavement Association Information Series 83. National Asphalt Pavement Association, Riverdale, Md., January 1983.
4. R. E. Smith, M. I. Darter, and S. M. Herrin. *Highway Pavement Distress Identification Manual.* FHWA, U.S. Department of Transportation, 1979.
5. K. J. White and N. G. Horsman. *Shazam—The Econometrics Computer Program*, Version 5 Users Manual, 1985.
6. G. F. Voigt, S. H. Carpenter, and M. I. Darter. *Rehabilitation of Concrete Pavements, Volume 3—Overlay Rehabilitation Techniques.* Report FHWA/RD-88/073. FHWA, U.S. Department of Transportation, December 1988.
7. S. H. Carpenter, M. I. Darter, and B. J. Dempsey. *A Pavement Moisture Accelerated Distress (MAD) Identification System.* Vol. I, FHWA/RD-81/079; Vol. II, FHWA/RD-81/080. FHWA, U.S. Department of Transportation, September 1981.
8. *Guide for Design of Pavement Structures.* American Association of State Highway and Transportation Officials, Washington, D.C., 1986.
9. *NCHRP Synthesis of Highway Practice 144: Breaking/Cracking and Seating Concrete Pavements.* TRB, National Research Council, Washington, D.C., in preparation.
10. C. Crawford. *Cracking and Seating of PCC Pavements Prior to Overlaying With Hot Mix Asphalt.* National Asphalt Pavement Association Information Series 91. National Asphalt Pavement Association, Riverdale, Md., March 1985.
11. *The Big Crackup.* Workshop Proceedings, National Asphalt Pavement Association, 28th Annual Convention, Phoenix, Ariz., 1983.
12. *Initial Construction and Interim Performance Report.* Division of Research and Training, Indiana Department of Highways, West Lafayette, Ind. September 1986.
13. *Effects of Slab Breaking and Seating on Differential Vertical Movement at PCC Slab Joints and Cracks.* Memorandum, report of construction. California Department of Transportation, undated.
14. *NCHRP Synthesis of Highway Practice 92: Minimizing Reflection Cracking of Pavement Overlays.* TRB, National Research Council, Washington, D.C., 1982.

Publication of this paper sponsored by Committee on Pavement Rehabilitation.

Evaluation of Concrete Pavement Restoration Techniques on I-65

A. SAMY NOURELDIN AND REBECCA S. MCDANIEL

Construction of asphalt overlay layers on top of old concrete pavements is considered an efficient pavement rehabilitation strategy. These asphalt overlay layers, however, are usually subject to reflection cracking and high tensile and shear stresses related to movement of the old concrete slab and the resulting composite nature of the new pavement section (flexible/rigid section). In addition, these asphalt overlay layers are usually vulnerable to rutting-type distresses, which may be occurring more frequently with the recent increases in trucks carrying extremely heavy gross weights (more than 100,000 lb) and frequently reported high tire pressures (more than 120 psi). Concrete (rigid) pavements have the advantage of being rut-resistant compared to asphalt (flexible) pavements. The jointed reinforced concrete pavement (JRCP) has been very successful in Indiana's highway network. The pavement life span between major maintenances was proven to be considerably long (15–20 years). The purpose of this study is to evaluate concrete pavement restoration (CPR) techniques as viable alternatives to the placement of bituminous overlay layers. Statistical inferences were obtained for the effect of these CPR techniques on the improvement in ride comfort (represented by roughness measurements) and safety against skidding (represented by skid resistance or friction measurements). In addition, applying CPR techniques and then resurfacing (adding overlay layers) were compared against two consecutive resurfacing applications. This comparison was made to evaluate the CPR techniques in case future resurfacing is warranted to increase the pavement structural capacity. It was concluded that the CPR techniques have improved the ride comfort and friction (skid resistance) numbers significantly. Cost-effectiveness of CPR techniques may be doubtful, however, especially when the structural value of the rehabilitated pavement is marginal and needs to be increased with overlays.

An adequate pavement evaluation is essential to the ultimate selection of reliable and cost-effective rehabilitation techniques. The evaluation procedure usually involves problem definition through a determination of the cause and extent of the existing deterioration. Data necessary for adequate pavement evaluation generally include distress types, pavement materials, existing structural design, traffic loadings, climatic information, and deflection, roughness, and friction measurements.

This report presents evaluation procedures conducted for a medium-severity, deteriorated concrete pavement surface that was restored utilizing common concrete pavement restoration (CPR) techniques. The original pavement was jointed reinforced concrete pavement (JRCP) with a slab length of 40 ft, width of 12 ft, and thickness of 10 in. The old pavement remained sound for 18–20 years. However, some typical functional distresses were noted.

These distresses were described as corner, diagonal, longitudinal, and transverse cracking and some faulted, spalled, and broken-up joints. The pavement was subject to heavy traffic usage on I-65 (6,000 trucks per day). The deteriorated surface resulted in a rough ride represented by a roughness number of 1,200. Friction values also decreased considerably to hazardously low values (friction number <30).

The restoration techniques used were as follows:

1. Concrete slabs were undersealed with asphalt material to improve the subbase support at the joints.
2. Full-depth patches were used to replace sections of severe pavement breakups.
3. Partial-depth patches were used to repair minor surface distresses.
4. Joints and minor cracks were routed and resealed.
5. Diamond grinding was employed to repair and/or remove faulting at joints and cracks in addition to restoring the smooth riding quality and increasing the skid resistance.

ORIGINAL PAVEMENT CONDITION

A pavement "condition survey" was conducted in the initial stage of the study (1985). The jointed reinforced concrete pavement (JRCP) was sustaining 6,000 trucks per day. It consisted of a 10-in.-thick, reinforced concrete slab over an 8-in.-thick subbase. Slab dimensions were length, 40 ft, and width, 12 ft. The pavement was constructed in 1968 (17 years old at the time of condition survey). The condition survey was performed over the portion of I-65 between 2 miles north of SR-114 and US-231 at Crown Point. The north- and southbound lanes of I-65 (Indiana) between mile markers 217 and 247 (30 miles) were surveyed. The condition survey involved visual inspection, roughness measurements, friction measurements, and deflection measurements.

Visual Inspection

The 30-mile portion of I-65 (two lanes per direction) under study has 7,920 slabs in the northbound (NB) direction and 7,920 slabs in the southbound (SB) direction. Defects were present in 10.7 percent of the SB slabs (848 slabs) and 6.5 percent of the NB slabs (511 slabs). The major type of distress noted was the presence of "transverse cracks" near the mid-slab for a large number of slabs. Some other corner breaks,

Division of Research, Indiana Department of Highways (IDOH), West Lafayette.

FIGURE 1 Major distresses noted on I-65 portion under study. (top) Faulted crack. (bottom) Broken-up slab.

minor surface imperfections, and faulted and broken-up joints were noted (Figure 1). A rough ride and near slippery conditions were experienced when traveling at speeds higher than 55 mph during rainfall.

Roughness Measurements

A response-type PCA roadmeter roughness measuring system, typically used by the Indiana Department of Highways, was used for this study. Average roughness numbers (RNs) of 1,155 and 1,272 (in ⅛ in. per mile) were obtained (Table 1) for the northbound and southbound directions, respectively. These RNs correspond to predicted serviceability indices (PSI) of 3.1 and 2.9, respectively (*1*). The testing vehicle was operating at 50 mph.

Friction Measurements

The standard towed trailer with ribbed, locked wheel torque measuring, friction testing system (ASTM E274) was used to obtain information about friction (skid resistance). This equipment is also typically used by Indiana Department of Highways.

Average friction numbers (FNs) of 31 and 29 at 50 mph were obtained for the northbound and southbound directions, respectively (Table 2). These average friction numbers (average skid numbers) correspond to coefficients of wet pavement friction of 0.31 and 0.29, respectively. These FNs indicate that the pavement was very near the terminal friction life and that the occurrence of a hazardous situation when traveling at the speed limit (55 mph) was more likely.

Deflection Measurements

Tables 3, 4, and 5 show the average deflection measurements near joints, cracks, and midslab points as measured by the Dynaflect. Average readings of sensors 1 and 5, together with the range, are included. It is important to note that sensor 1 is located between the two loading wheels of the Dynaflect; sensors 2, 3, 4, and 5 are spaced at 1-ft increments from sensor 1 with sensor 5 at the greatest distance (4 ft from sensor 1).

The Indiana Department of Highways pavement evaluation practice makes use of the sensor 1 measurement as an indicator of slab stiffness and the sensor 5 measurement as an indicator of the pavement support stiffness (base or subbase). Readings of $50 * 10^{-5}$ in. or less by sensor 1 and $30 * 10^{-5}$ or less by sensor 5 are indicators of adequate pavement conditions and good pavement support, respectively. These values are frequently obtained from measurements of new pavements. Larger deflection values were obtained at the joints and cracks than at midslab points. This was expected since the joints are designed to move more freely. In general, average deflection values at (or near) either joints or midslab points were less than $50 * 10^{-5}$ in., indicating acceptable pavement structural conditions.

CONCRETE PAVEMENT RESTORATION (CPR) TECHNIQUES APPLIED

The CPR techniques applied in the summer of 1985 to restore this jointed reinforced concrete pavement (JRCP) were undersealing, full-depth patches, partial-depth patches, resealing of cracks and joints, and diamond grinding.

Undersealing

Concrete slabs were undersealed with oxidized asphalt to improve the subbase support and eliminate faulting at joints and cracks and to obtain more uniform support for concrete slabs. The Indiana undersealing method has been used successfully throughout the state and proven to be cost-effective in providing good pavement support under concrete pavement slabs. The method simply employs incremental Dynaflect measurements (each 100 ft) to detect locations of poor pavement support. Oxidized asphalt (20–30 penetration) is pumped into these locations, resulting in uniform pavement support and well-seated slab.

Full-Depth Patches

Full-depth patches (Figures 2 through 4) were used to replace sections of severe pavement breakups, for midslab repairs,

TABLE 1 COMBINED AVERAGE ROUGHNESS NUMBERS AND PREDICTED SERVICEABILITY INDEX (PSI)

Year	NB	SB	Average	PSI
1985 (Before CPR)	1155	1272	1214	3.0
1985 (After CPR)	215	247	231	5.0
1986	401	399	400	4.4
1987	426	408	417	4.3
1988	510	498	504	4.1

Note: *Predicted serviceability index values are based on the regression equation:

$PSI = 11.73 - 2.83364 \log (RN)$, $R^2 = 0.68$, Reference No. 1

*Testing vehicle speed was 50 mph.

*Roughness numbers are in 1/8 inch per mile.

TABLE 2 COMBINED AVERAGE FRICTION NUMBERS

Year	NB	SB	Average
1985 (Before CPR)	31	29	30
1985 (After CPR)	40	44	42
1986	49	45	47
1987	40	42	41
1988	34	34	34

*FN of 30 corresponds to a coefficient of wet pavement friction 0.3.

TABLE 3 AVERAGE DYNAFLECT MEASUREMENTS AT JOINTS (IN 10^{-5} IN.) FOR NORTH- AND SOUTHBOUND DIRECTIONS

	Sensor #1				Sensor #5			
Year	NB	SB	Average	Range	NB	SB	Average	Range
1985 Before CPR	38	39	39	35-45	20	20	20	15-25
1985 After CPR	40	40	40	35-45	20	20	20	17-23
1986	45	45	45	40-50	19	20	20	17-23
1987	51	52	52	45-60	21	20	21	15-25
1988	59	60	60	52-70	21	22	22	15-25

NOTE: Measurements are for travelling lanes, no significant differences were found between the various sections of the 30 mile portion of I-65.

TABLE 4 AVERAGE DYNAFLECT MEASUREMENTS AT CRACKS (IN 10^{-5} IN.) FOR NORTH- AND SOUTHBOUND DIRECTIONS

	Sensor #1				Sensor #5			
Year	NB	SB	Average	Range	NB	SB	Average	Range
1985 Before CPR	38	40	39	34-44	19	19	19	15-22
1985 After CPR	40	38	39	34-44	20	20	20	15-23
1986	46	49	48	40-55	23	18	22	16-24
1987	54	52	53	45-60	24	21	23	18-25
1988	60	62	61	50-70	25	23	24	22-28

TABLE 5 AVERAGE DYNAFLECT MEASUREMENTS AT MIDSLABS (IN 10^{-5} IN.) FOR NORTH- AND SOUTHBOUND DIRECTIONS

	Sensor #1				Sensor #5			
Year	NB	SB	Average	Range	NB	SB	Average	Range
1985 Before CPR	28	31	30	25-35	18	18	18	14-22
1985 After CPR	30	34	32	25-35	20	20	20	15-25
1986	40	42	41	34-48	23	24	24	18-30
1987	45	47	46	36-50	24	24	24	18-30
1988	50	50	50	40-55	24	24	24	18-30

and at severely broken up joints and cracks. Three types of patches were employed:

1. An inverted "T" patch (midslab repairs);
2. A doweled patch (midslab repairs); and
3. An inverted "T" patch with a doweled contraction joint (at all replaced joints).

All full-depth patches were at least 8 ft long and 12 ft (lane) wide, meeting IDOH Standard Specifications and NCHRP recommendations (*2, 3*) for full-depth patches (6 ft minimum length and 12 ft width).

The inverted "T" patch was constructed by cutting up and lifting broken old slab pieces and removing the existing subbase beneath the deteriorated slabs and underneath the edge of the adjacent slabs (Figure 4). No problems were noted during removal of deteriorated sections or pouring of the fresh concrete. The subbase was not removed for the doweled patches (Figure 3). Dowel bars were used to provide load transfer to the adjacent slabs. Inverted "T" patches with dowel basket assemblies in the center were used at replaced joints. Figure 4 illustrates the construction of this type of patch.

Partial-Depth Patches

Partial-depth patches (Figure 5) were used to repair minor surface distresses, shallow defects, other surface imperfections, and slab corner breaks (distresses less than ½ ft deep).

Resealing Cracks and Joints

Midslab cracks were routed and resealed (Figure 6). Cracks and joints were resealed to inhibit intrusion of surface water and to avoid possible pumping resulting from water penetration. In addition, an open graded paving layer (#5 base, IDOH Standard Specification) was constructed as an edge drainage treatment between the concrete pavement edge and the existing trench drains in locations needing improved drainage.

Diamond Grinding

After all patches were constructed, diamond grinding was employed on the whole project to obtain a smoother riding

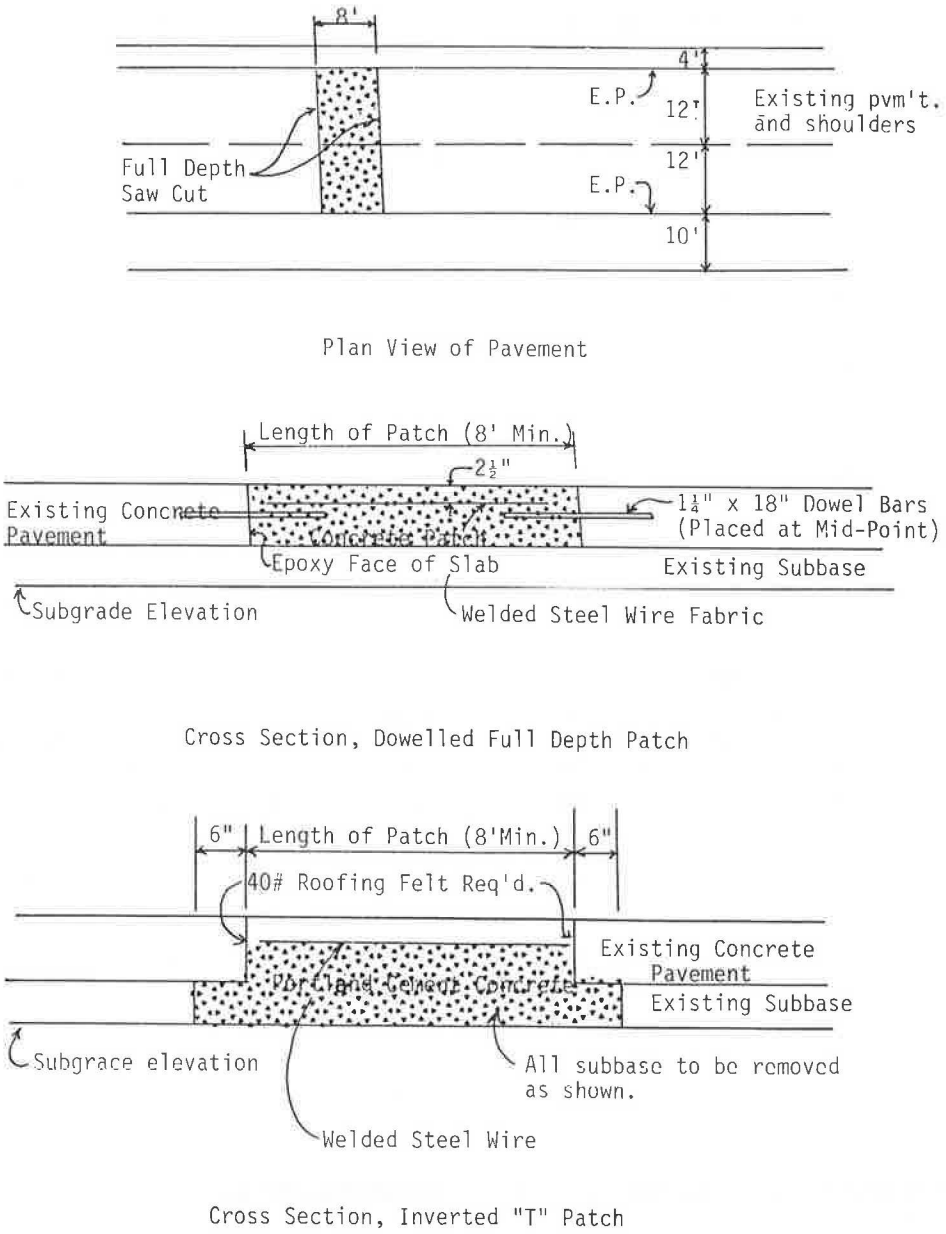

FIGURE 2 Concrete patch details.

quality, eliminate minor faulting at joints and cracks, and improve skid resistance. Figure 7 shows the concrete pavement surface texture after diamond grinding.

Detailed construction specifications for all CPR techniques are available from the authors (appendices) and can be forwarded upon request.

EFFECT OF CPR TECHNIQUES ON PAVEMENT CONDITION

A 3-year "evaluation survey" was conducted on the I-65 portion under study. The evaluation survey was applied annually (summers of 1985, 1986, 1987, and 1988), and pavement conditions were compared to those obtained during the "condition survey" (spring 1985).

The evaluation survey involved visual inspection, roughness measurements, friction measurements, and deflection measurements. The process of preparing the condition survey procedures included review of the literature (*4–12*).

Visual Inspection

Neither faulting nor spalling was observed at the joints. However, many of the routed and resealed cracks faulted about 1/16 in. down in the direction of traffic (measured using a straight edge). These faulted cracks remained almost the same during the 3-year evaluation period, but smaller hairline cracks have developed around them and eventually spalled out under the effect of heavy traffic on I-65 (Figure 6).

Some of the inverted "T," full-depth patches also had about

FIGURE 3 Construction of doweled full-depth patches. (top) Drilling dowel holes for doweled full-depth patch. (bottom) Pouring concrete in doweled full-depth patch.

1/16-in. faults at the last joints (in traffic direction). This may possibly be caused by incomplete concrete consolidation in the undercut areas of the inverted "T" patches.

Partial-depth patches placed adjacent to cracks and joints were spalling and broken up. Repairs were required just 1 year after rehabilitation (Figure 8). These distresses were frequently noted throughout the 3-year study period and may have been caused by poor load transfer and differential slab movement across the crack and through the partial-depth patch. In addition, all partial-depth patches that were placed over a crack had cracked (Figure 8). Furthermore, some partial-depth patches were responsible for creating new midslab cracks. This could be attributed to the weakness of the concrete slab due to the reduction of moment of inertia associated with the discontinuity and stress concentration occurring when partial-depth patches are constructed.

It is recommended that the use of partial-depth patches be limited as much as possible and that they be replaced with full-depth patches or bituminous patches; alternatively, it should be accepted that they must be rehabilitated annually.

Riding comfort and pavement texture have improved directly after the application of diamond grinding. No slippery conditions were experienced when traveling at 55 mph on the wet pavement. No significant declines in these qualities were noted during the 3-year evaluation period.

Roughness Measurements

Table 1 gives the combined average roughness numbers (traveling lane) for the northbound (NB) and southbound (SB) directions before employing CPR (1985) and after employing CPR (1985, 1986, 1987, and 1988) for the 3-year evaluation survey period.

The original data were collected by dividing the 30-mile portion of I-65 into six sections, two directions per section (NB and SB) and two lanes per direction (traveling lane and passing lane). The statistical analysis of variance indicated that the effects of section and direction were not significant; hence, the roughness numbers were combined as shown in Table 1. Roughness numbers for the passing lane were significantly lower than those for the traveling lane, as may be expected, owing to the heavy traffic usage of the traveling lane.

Predicted serviceability index (PSI) is also included in Table 1 for comparison purposes. It can be concluded that CPR is

FIGURE 4 Construction of inverted T full-depth patches. (top) Excavation for full-depth inverted "T" patch. (bottom) Pouring concrete for inverted "T," full-depth joint replacement patch.

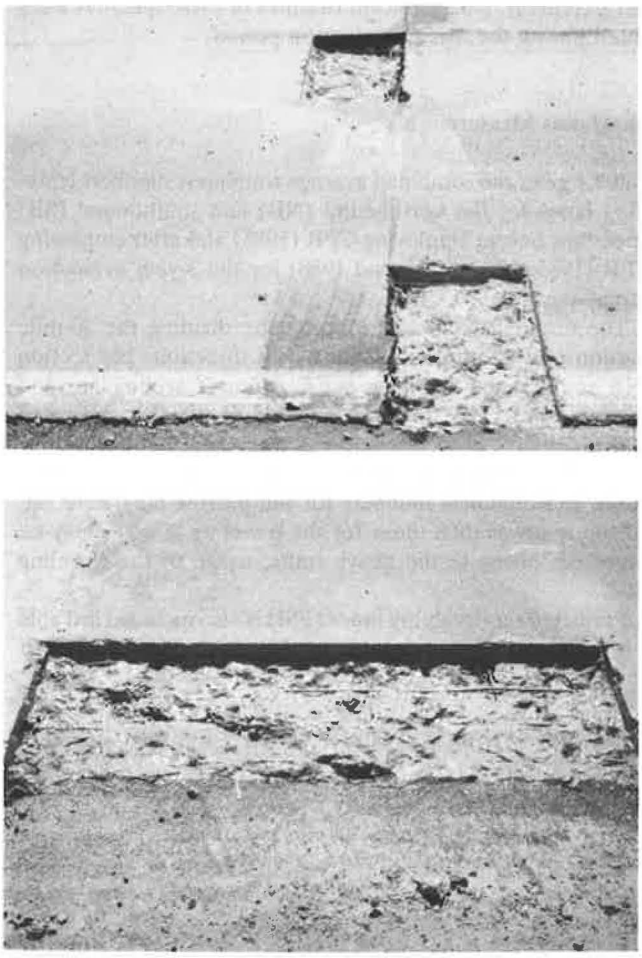

FIGURE 5 Construction of partial-depth patch. (top) Prepared partial-depth patches. (bottom) Epoxy coating on slides of a prepared partial-depth patch.

very successful in improving riding comfort and level of service, as indicated by the RN and PSI values. In addition, this improvement was sustained for a period of 3 years and may remain acceptable for a 6-year period (predicted from Figure 9).

Friction Measurements

Table 2 gives the combined average friction numbers (traveling lane) for the northbound and southbound directions before employing CPR and after employing CPR (1985 through 1988) for the 3-year evaluation survey period. Data were combined for the same reasons given earlier for combining roughness data. Passing lane friction numbers were significantly higher than those for the traveling lane.

CPR techniques (diamond grinding) have improved the friction numbers significantly (Table 2, Figure 10). The improvement in skid resistance, however, was predicted to remain for only 4 years (Figure 10), and another rehabilitation should be required to improve the pavement condition after those 4 years.

Deflection Measurements

Joints, Cracks, and Midslab

Tables 3, 4, and 5 give the average deflection values (traveling lane) before and after employing CPR. The traveling lane was considered to be more critical because it carries heavy truck traffic more frequently. The passing lane was eliminated from computing averages and had significantly lower deflection values than the traveling lane. Average deflection values were also combined for the six sections (covering the entire 30-mile portion) for the same reasons, explained earlier, that roughness and friction measurements were combined.

CPR techniques absolutely did not improve the slab structural capacity (as indicated by the increase in deflection values from 1985 through 1988, Tables 3, 4, and 5). This is attributed to the fact that all the CPR techniques used were only repairs of functional failures.

Undersealing maintained the subbase support for the 3-year evaluation period (see sensor 5 readings, Tables 3, 4, and 5). The increase in slab deflection (sensor 1 readings) is probably related to the cumulative effect of heavy traffic repetitions on I-65 during the study period. Predicted deflection values in 1989 (Figure 11) exceed $50 * 10^{-5}$ significantly, indicating the need for adding overlay layers on top of the concrete slabs by 1989.

Load Transfer Testing

Load transfer across the joints and cracks was evaluated 1 year after employing CPR (1986). Deflection was measured ½ ft before the joint or crack (by sensor 1) and ½ ft after the joint or crack (by sensor 2). The IDOH rigid pavement evaluation practice makes use of the deflection ratio (sensor 2/sensor 1) as an indicator of load transfer across joints and cracks. Ratios of 0.90 or more usually reflect a frozen joint. Ratios of 0.75 to 0.90 indicate good load transfer; values of 0.50 to 0.75 indicate fair load transfer; and ratios of less than 0.50 indicate poor load transfer.

Table 6 gives the load transfer coefficients at joints, cracks, and midslab points (the value shown for midslab is to indicate only that when continuity exists the coefficient is very close to 1.0). Load transfer efficiency across resealed joints was relatively good, while at resealed cracks it was only fair.

Load transfer efficiency was also tested at joints for doweled patches and "T" inverted patches (Table 6). Joints of doweled patches had good load transfer. Load transfer at joints of "T" inverted patches was relatively low, probably because of the lack of grain interlock caused by sawed face joints.

Along Patches

Figure 12 illustrates deflection distribution along the patches (doweled and inverted "T"). Lower deflection values were obtained for inverted "T," full-depth patches, which gained more structural capacity by removal of the subbase and its replacement with concrete. Deflection values along the patch were less than $50 * 10^{-5}$, except at joints where they exceeded this value.

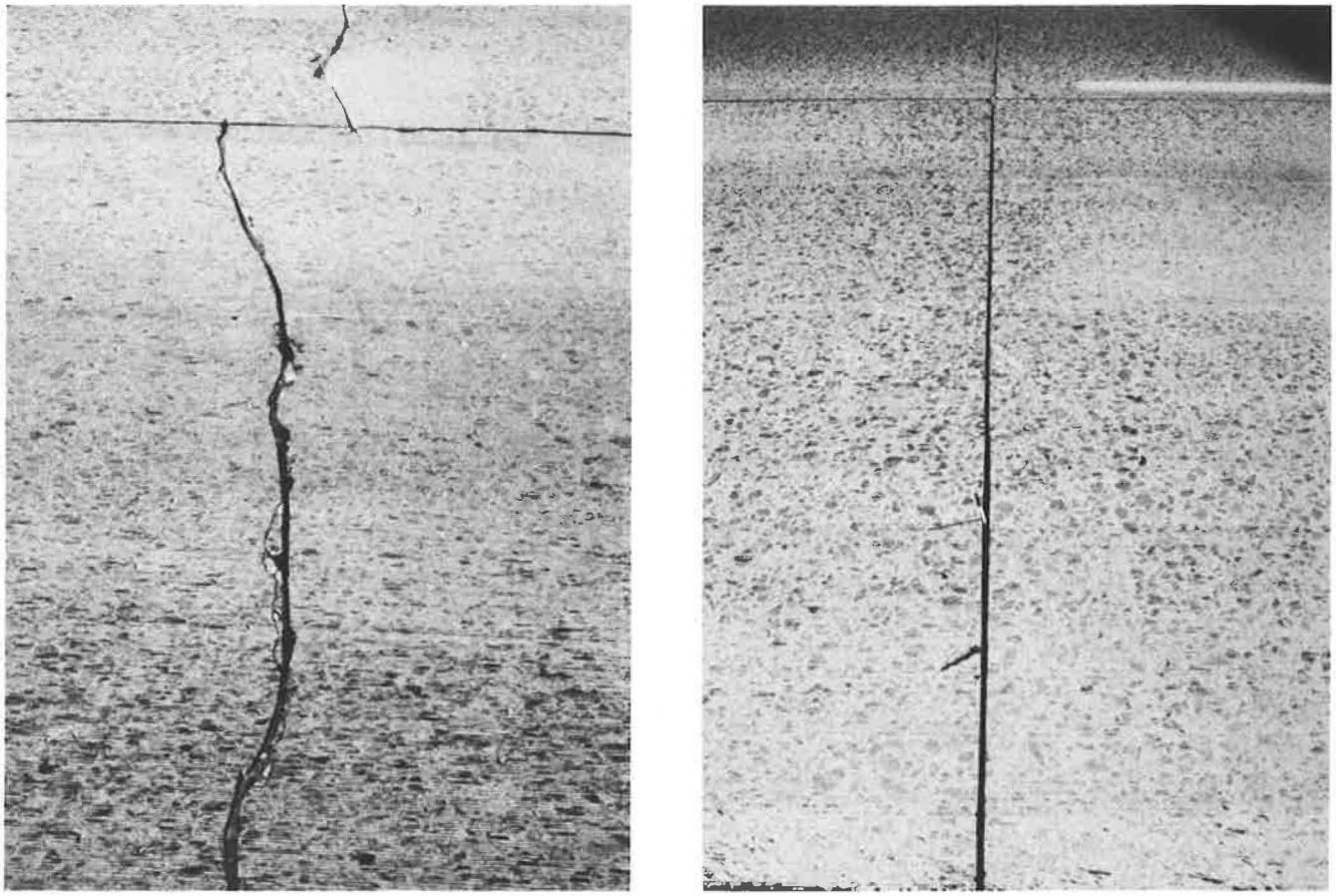

FIGURE 6 Sealing of joints and midslab cracks. (left) Routed and sealed crack. (right) Resealed joint.

COST ANALYSIS

Typical low bid prices on CPR contracts utilizing the three types of full-depth patches considered in this study appear in Table 7. The doweled patches are less expensive than the inverted "T" patches. The lower cost of the doweled patch was probably due to the smaller depth of patch required, since the subbase was not excavated and replaced with concrete.

The inverted "T" patch containing a doweled contraction joint cost approximately $125 more than the same-sized, inverted "T" patch with no contraction joint. The cost per square yard of the partial-depth patch was almost twice as much as for the full-depth patch, even though the partial-depth patch had only a fraction of the depth of the full-depth patch. It should be noted that the minimum patch size of the full-depth patches was 12 ft by 8 ft. No minimum patch size existed for the partial-depth patches. Therefore, the partial-depth patches required more labor-intensive hole preparation covering a smaller area than the full-depth patches did. The cost of diamond grinding concrete surfaces was about $3 per square yard. Typical low bid prices for other interstate rehabilitation projects using a conventional 4-in. overlay also appear in Table 7. The conventional 4-in. asphalt overlay cost is around $5 per square yard. The overlay cost is almost twice as much as that of the diamond grinding treatment; that is, diamond grinding costs the equivalent of a 2½-in. asphalt overlay, although it adds nothing to the structural capacity of the pavement.

The cost comparison presented in Tables 7 and 8 indicates that CPR is more cost-effective than using a 4-in. asphalt overlay. However, values presented are based on the assumption that CPR will restore the pavement for a period of 10 years. This was not true for the I-65 portion under study. Analysis of data indicated that the pavement will need to be overlaid after a period of 4 to 6 years to increase the structural capacity. Data presented in Table 7 are for the I-65 portion under study (CPR, 30 miles) and for another portion of I-65 resurfaced by a 4-in. asphalt layer (7 miles). Although the comparison between these two projects indicates that CPR techniques are more cost-effective (20-year design period), it is not predicted that the CPR techniques will last for the first 10 years of the design period.

SUMMARY OF RESULTS

This study investigated a number of concrete pavement restoration (CPR) techniques. CPR was employed on a 30-mile portion of jointed concrete pavement on I-65 between mile markers 217 and 247 in Indiana in 1985. Three types of full-depth patches (doweled, inverted "T," and inverted "T" with a doweled contraction joint), partial-depth patches, diamond grinding the pavement surface, resealing joints, slab undersealing, and routing and resealing cracks were investigated. The main findings can be summarized as follows:

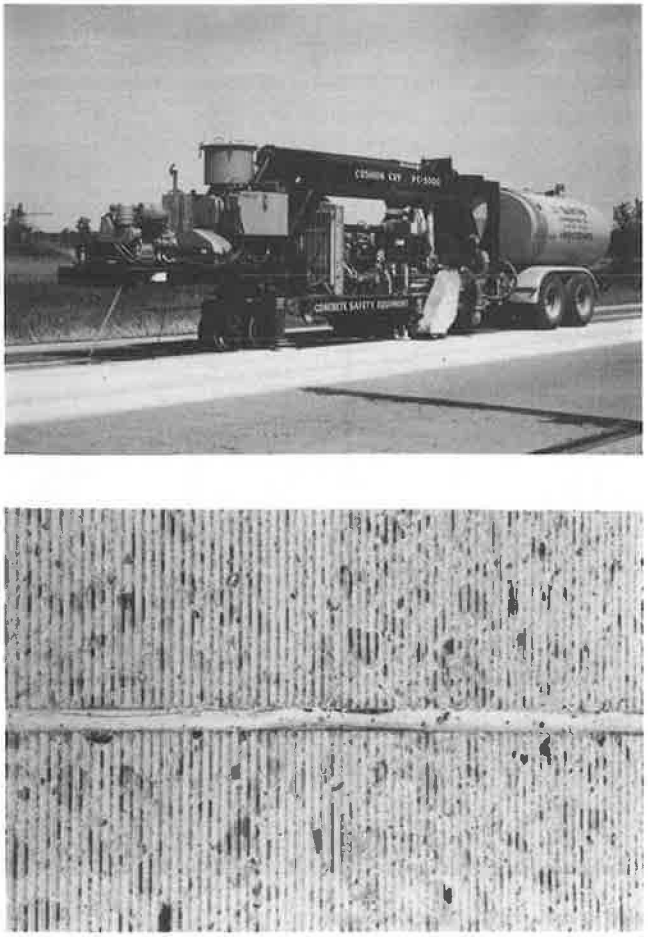

FIGURE 7 Diamond grinding operation. (top) Diamond grinding equipment. (bottom) Concrete surface texture after diamond grinding.

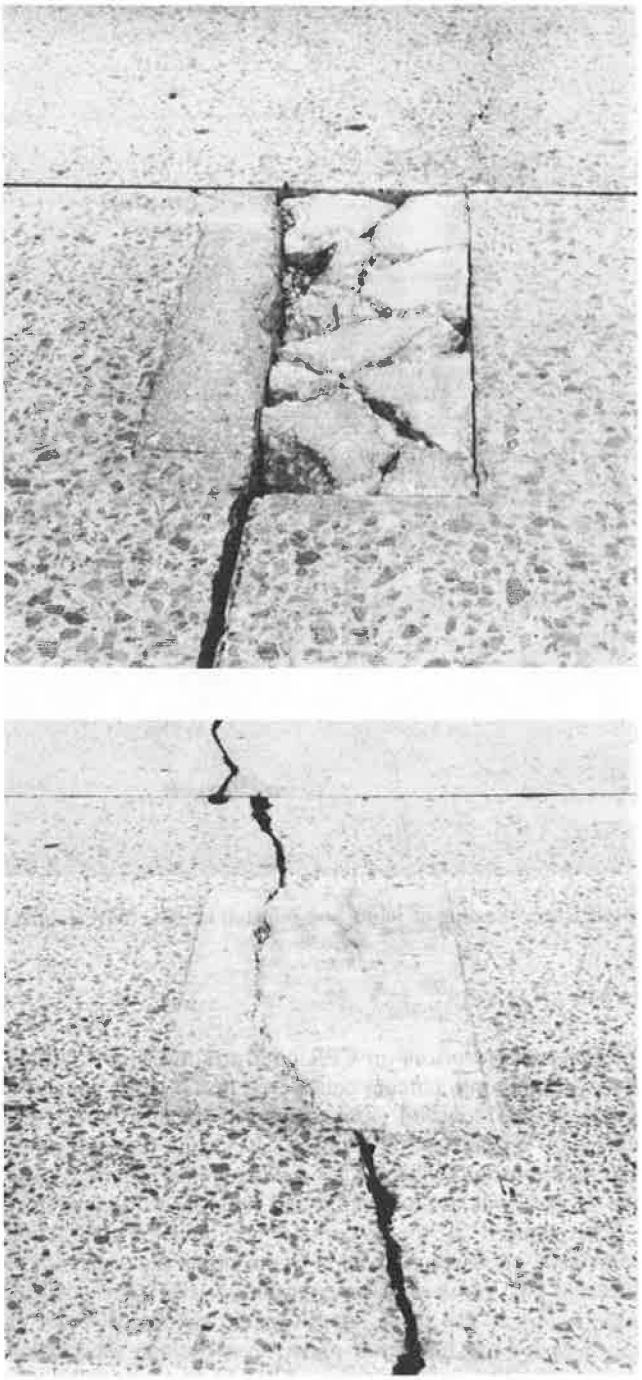

FIGURE 8 Performance problems of shallow-depth patches. (top) Cracking and breakup of shallow-depth patch adjacent to crack. (bottom) Cracking through a partial-depth patch.

1. A condition survey before applying CPR indicated low roadway serviceability (high roughness numbers), hazardously low friction numbers, and some typical functional distresses (transverse cracking, corner breaks, and faulted, broken-up joints). The pavement structural capacity was relatively sound (as evaluated by Dynaflect measurements).
2. Annual evaluation surveys (for 3 years) indicated a significant improvement in serviceability and friction after employing CPR.
3. The pavement life span after using CPR techniques is expected to be between 4 and 6 years (predicted from roughness, friction, and deflection measurements).
4. Slab undersealing helped the slab support (subbase) to remain structurally sound during the 3-year evaluation period. No significant drop in subbase structural condition was noted (according to sensor 5 measurements of the Dynaflect).
5. All full-depth patches performed properly. Doweled full-depth patches have better load transfer at their joint with the pavement, while inverted "T" full-depth patches have better structural capacity.
6. Partial-depth patches performed poorly. This technique has been proven to damage adjacent sound concrete. It is recommended that the use of these patches be limited as much as possible.
7. Diamond grinding provided a smoother ride and improved the surface friction significantly.
8. Structural capacity of concrete slabs was not improved by the CPR techniques used. Deflection values continued to increase annually owing to the increase in heavy truck traffic on I-65.

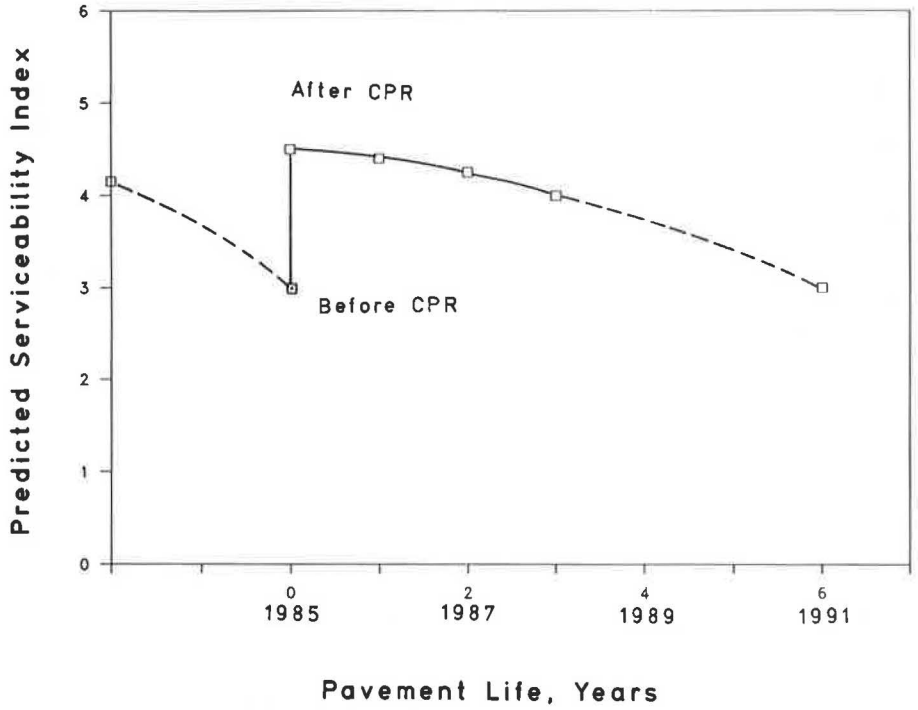

FIGURE 9 Effect of CPR techniques and time on pavement condition (present serviceability index).

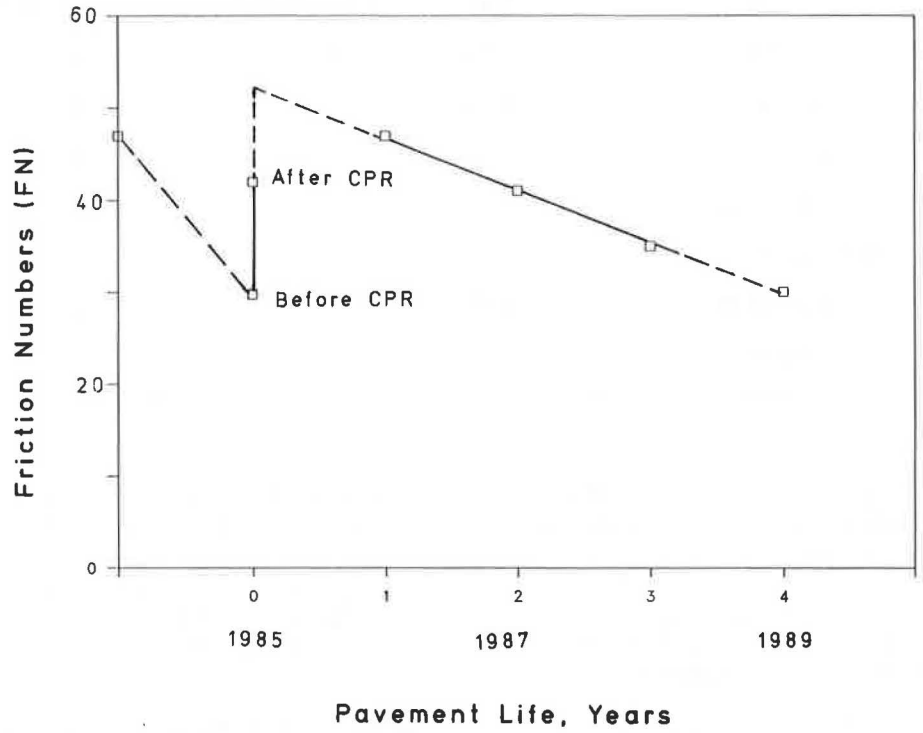

FIGURE 10 Effect of CPR techniques (diamond grinding) and time on pavement condition (skid resistance).

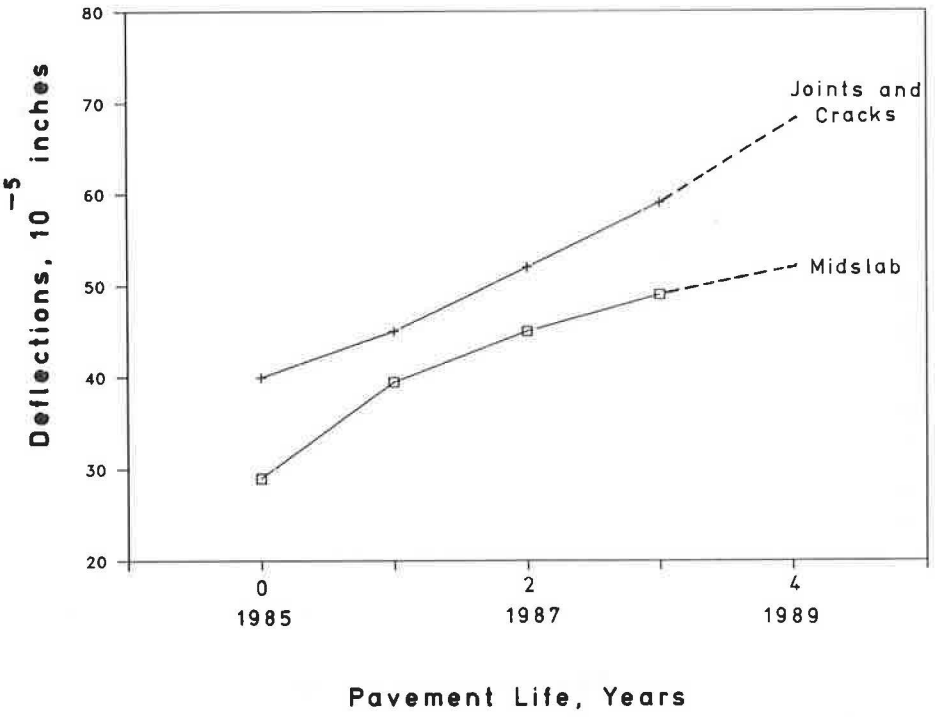

FIGURE 11 Deflection measurements during the 3-year evaluation period.

TABLE 6 LOAD TRANSFER COEFFICIENTS AT DIFFERENT FEATURES (SENSOR 2 READING, SENSOR 1 READING)

Feature	Mean	Standard Dev.	No. of Tests
Midslab	0.96	0.02	10
Joints	0.80	0.10	10
Cracks	0.69	0.21	10
Joints at Dowelled patch	0.80	0.18	20
Joints at Inverted T patch	0.64	0.19	30

9. A comparison between two projects on I-65 (for a design period of 20 years) indicated that employing CPR and then adding a 4-in. asphalt overlay layer after 10 years are more cost-effective than adding a 4-in. asphalt overlay layer and then resurfacing with another 4-in. overlay layer after 10 years. CPR techniques employed in this study, however, are not predicted to keep the pavement structurally sound for 10 years, as was planned.

10. It is recommended that specifications be set for diamond grinding based on resulting improvement in ride comfort (measured by roughness roadmeter) and skid resistance. Financial penalties should be enforced for failure to meet these specifications.

11. Concrete pavements with high deflection measurements at or near maximum tolerable deflection values should be overlaid to increase structural capacity.

12. In general, the CPR techniques employed in this study were effective for 5 years but may not sustain the heavy truck traffic on I-65 for 10 years.

ACKNOWLEDGMENTS

The research described in this paper was carried out at the Indiana Department of Highways, Division of Research. The authors are grateful to Keith J. Kercher (Pavement Research

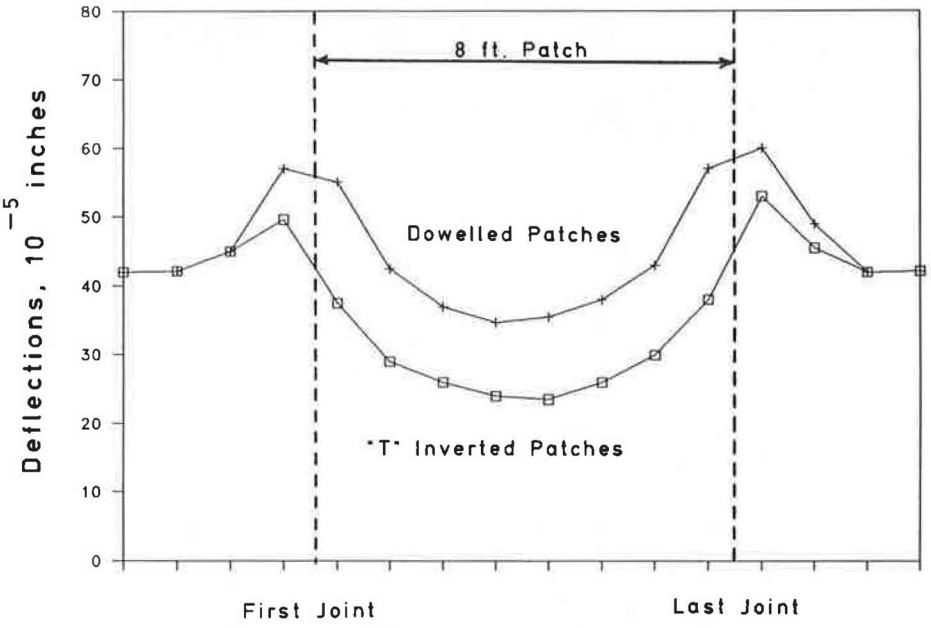

FIGURE 12 Deflection distribution along full-depth patches.

TABLE 7 AVERAGE LOW BID UNIT PRICES FOR RESTORATION TECHNIQUES IN 1985 AND 1986

	Unit Cost	Overall Cost	No. of Low Bids Averaged
Inverted T Full Depth Patch	$79.18/sq.yd.	$845/patch	12
Dowelled Full Depth Patch	$54.47/sq.yd.	$613/patch	4
Inverted T with Dowelled Contraction Joint Patch	$10.39/ft.+ $79.18/sq.yd.	$970/patch	7
Partial Depth Patch	$120/sq.yd.	Variable	4
Diamond Grinding	$ 3.00/sq.yd.		8
4 in. Asphalt Overlay	$ 5.01/sq.yd.		9
250 lb./sq.yd.Base	$ 2.42/sq.yd.		
150 lb./sq.yd.Binder	$ 1.54/sq.yd.		
70 lb./sq.yd.Sand Surface	$ 1.05/sq.yd.		
Joints & Crack Sealing	$ 1.86/sq.yd.		9

Present Worth of Costs (i = 7%)

*CPR and later resurfacing after 10 years = $376,738 per interstate mile.

*Resurfacing and later resurfacing after 10 years = $426,385 per interstate mile.

*Cost savings (20 years design period) = $49,647 per interstate mile.

Figures courtesy of the Indiana Department of Highways

TABLE 8 CPR WITH DIAMOND GRINDING VERSUS ASPHALT OVERLAY

SOUTH CAROLINA — SAMPLE REHABILITATION COST

CPR With Diamond Grinding

I-20; 6.031 miles (Georgia State Line to East of US 25); Project IR-20-1(56), Bid Prices.

	Quantity	Unit Price
Full-depth Patching	750 sq yd	$60/sq yd
Removal & Disposal of Existing Concrete	750 sq yd	$50/sq yd
Partial-depth Patching	1,000 sq ft	$24/sq ft
Grinding (4 lanes)	217,621 sq yd	$2.48/sq yd
Hole Drilling	12,240 holes	$4/hole
Pressure Grouting	4,080 bags	$22/bag
Clean & Reseal Longitudinal Joints	92,150 LF	$1.53/LF
Clean & Reseal Transverse Joints	78,161 LF	$1.53/LF
		Total Cost

CPR Cost Per Interstate Mile (2-lanes *each* direction) = $\frac{\$1,045,496}{6.031 \text{ miles}}$ = **$173,354***

Asphalt Overlay Over Concrete

I-26; 2.005 miles in Lexington and Richland Counties; 2-lanes in one direction; Project IR-26-2(124), Bid Prices.

	Quantity	Unit Price
Pavement Binder #2	3,528 tons	$16.35/ton
Pavement Surface Type 1	1,468 tons	$16/ton
Pavement Binder Asphalt (4.8%)	265 tons	$158/ton
Pavement Surface Asphalt (6.0%)	88 tons	$158/ton
Clean & Reseal Transverse Joints	9,120 LF	$1.36/LF
Shoulder Binder #2	3,116 tons	$16.35/ton
Shoulder Surface Type 1	1,346 tons	$16/ton
Shoulder Binder Asphalt (4.8%)	150 tons	$158/ton
Shoulder Surface Asphalt (6.0%)	81 tons	$158/ton
		Total Cost

Cost Per Interstate Mile (2-lanes *one* direction) = $\frac{\$258,329}{2.005 \text{ miles}}$ = $128,842

Asphalt Overlay Cost Per Interstate Mile = $128,842 × 2 = $257,684**
(2-lanes *each* direction)

*Items not related to restoration of roadway or shoulders not shown.
**Cost of 3½ inch overlay including shoulders which *must* be done when overlaying.
Figures courtesy of American Concrete Pavement Association and its members.

GEORGIA — SAMPLE REHABILITATION COSTS*

CPR With Diamond Grinding
(Actual Prices)

	Project A (11.6 miles)	Project B (11.942 miles)	Average
Slab Removal & Replacement	$ 26,532	$ 14,146	$ 20,339
Spall Repair	$ 50,916	$ 1,000	$ 25,958
Undersealing	$ 2,686	$ 6,232	$ 4,459
Sawing & Resealing Joints	$ 16,509	$ 24,128	$ 20,318
Grinding	$ 91,683	$ 67,632	$ 79,658
Total Cost	$188,326	$113,138	$150,732

CPR Average Cost Per Interstate Mile = $150,732
(2-lanes *each* direction)

Asphalt Overlay
(4-inch overlay, Actual Prices)

	Project C (5.402 miles)	Project D (23.57 miles)	Project E (14.049 miles)	Average
Slab Removal & Replacement	$ 6,009	$ 1,005	$ 5,478	$ 4,164
Undersealing	$ 4,751	$ 5,579	$ 5,719	$ 5,350
Waterproof & Reseal Joints	$ 14,890	$ 20,200	$ 18,888	$ 17,993
Asphalt Overlay	$199,834	$256,844	$222,301	$226,326
Total Cost	$225,484	$283,628	$252,386	$253,833

Asphalt Overlay Average Cost Per Interstate Mile = $253,833
(2-lanes *each* direction)

*Items not related to restoration of roadway or shoulders not shown.
Figures courtesy of American Concrete Pavement Association and its members.

Evaluation Section Manager) and Joseph J. Sudol (Research and Special Projects Section Engineer) for their technical guidance during the course of the study.

REFERENCES

1. K. Trezos and S. Gulen. *Correlation of Roadmeter Roughness Numbers with P.S.I.* Final Report. Division of Research, Indiana Department of Highways, West Lafayette, July 1983.
2. *Standard Specifications.* Indiana Department of Highways, Indianapolis, 1982.
3. *NCHRP Report 281: Joint Repair Methods for Portland Cement Concrete Pavements.* TRB, National Research Council, Washington, D.C., 1985.
4. *Portland Cement Concrete Pavement Restoration.* Demonstration Project 69. FHWA, U.S. Department of Transportation, October 1984.
5. M.D. Harness. *An Evaluation of Concrete Pavement Restoration Techniques on I-65.* Initial construction report. Division of Research, Indiana Department of Highways, West Lafayette, February 1987.
6. *Guide Procedures for Concrete Pavement AR Operations.* AASHTO-AGC-ARTBA, Joint Committee, Task Force 23. American Association of State Highway and Transportation Officials, Washington, D.C., 1985.
7. *Construction Handbook on PCC Pavement Rehabilitation.* FHWA, U.S. Department of Transportation, January 1984.
8. *Pavement Deflection Improvement Due to Asphalt Undersealing.* Final Report. Division of Research, Indiana Department of Highways, West Lafayette, 1983.
9. J. P. Hallin, D. M. Mathis, and R. L. Lee. Performance Review of Concrete Pavement Restoration. In *Transportation Research Record 1186*, TRB, National Research Council, Washington, D.C., 1988, pp. 1–15.
10. J. L. Brown. Concrete Pavement Rehabilitation for the Texas State Department of Highways and Public Transportation. In *Transportation Research Record 1196*, TRB, National Research Council, Washington, D.C., 1988, pp. 306–312.
11. J. L. Guinard, J. L. Nissoux, and P. Orsat. Concrete Pavement Restoration: French Maintenance Strategy and Load Transfer Device. In *Transportation Research Record 1183*, TRB, National Research Council, Washington, D.C., 1988, pp. 35–45.
12. K. Majidzadeh and V. Kumar. *Manual of Operation and Use of Dynaflect for Pavement Evaluation.* Resource International Inc.; Ohio Department of Transportation; FHWA, U.S. Department of Transportation, October 1983.

Publication of this paper sponsored by Committee on Pavement Rehabilitation.

Cyclic Shear Load Testing of Dowels in PCC Pavement Repairs

MARK B. SNYDER

There is a critical need to identify and develop reliable designs and construction techniques for full-depth repair load transfer systems. To address this need, a laboratory study was designed and performed to estimate the effects of several dowel load transfer system design and construction variables on dowel deflection and the development of dowel looseness. The laboratory study involved the application of 600,000 or more bidirectional, 3,000-lb (13.4-kN) shear loads to single dowels anchored in holes drilled in concrete specimens. Test variables included dowel diameter, drill diameter and impact energy, anchor material, and dowel embedment. A thin nylon disk was placed around each of these dowels at the face of the concrete to retain the anchor material in the drilled hole until it could harden. Tests were also conducted using cast-in-place dowels, hollow stainless steel dowels, and dowels installed in very tight holes. Applied load and dowel deflection data were collected and analyzed to produce models for dowel deflection and looseness as functions of the test variables. One key finding of this study is that the dowel must be anchored firmly and supported uniformly to perform well. This can be accomplished by using thin, snug-fitting disks to retain the anchor material in the drilled hole during curing. This type of device should be used for all field installations to improve the performance of properly designed and constructed repairs.

The construction of full-depth repairs of Portland cement concrete (PCC) pavements has become a major part of pavement rehabilitation programs throughout the United States. Unfortunately, while many repairs have performed satisfactorily, many others have performed poorly. Many of these repair failures are directly related to the failure of the repair load transfer system. In 1985, the University of Illinois Department of Civil Engineering contracted with the Federal Highway Administration (FHWA) to conduct extensive field, laboratory, and analytical studies concerning the evaluation and rehabilitation of concrete pavements. This study included repeated shear load testing of dowels installed in concrete and surveys of more than 2,000 in-service, full-depth repairs with various load transfer system designs. This paper describes the design, conduct, results, and conclusions of the laboratory experiment.

DESIGN OF THE LABORATORY EXPERIMENT

This study involved the application of repeated shear loads to dowels anchored in holes drilled in concrete specimens. Data collection and analysis focused on the relationship between applied load and dowel deflection. The purpose of the laboratory study was to estimate the effects of several design and construction variables on the performance of dowels that are anchored into existing PCC slabs during the placement of full-depth repairs. Five design and construction variables were included in the main test matrix: dowel diameter, annular gap (the width of the void to be filled with anchor material when the dowel is placed in the exact center of the drilled hole), anchor material, embedment length, and drill type (varying drill impact energy). Two test levels, one "high" and one "low" (based on the current range of design and construction practice), were selected for each variable except for drill type, for which three types were selected. Table 1 summarizes the test values that were used for each variable.

Tests were also conducted on a number of "special" specimens, including two specimens with dowels cast in place in the lab (rather than drilled), two specimens with dowels turned on a lathe to provide a very tight friction fit, and one specimen with a large-diameter, hollow, stainless steel dowel. These tests were conducted for comparison purposes and to indicate future research needs. A replicated half-fraction, factorial experimental design was employed to provide a sound statistical basis for determining the main effects and interaction effects of the five variables under consideration. A detailed discussion of the experimental design is presented elsewhere (*1, 2*).

PREPARATION OF TEST SPECIMENS

Portland cement concrete slabs were obtained from Interstate 70 near Effingham, Illinois, for the fabrication of test specimens. This pavement was constructed in 1962 using 10-in. (25-cm) reinforced PCC pavement with contraction joints at 100-ft (30.5-m) intervals. It had accommodated approximately 13.8 million, 18-kip (80-kN) ESALs in the design (outside) lane by the date of specimen removal.

In July 1985, 4-ft (1.2-m)-wide asphalt concrete pressure relief joints/repairs were placed near midslab at 1,000-ft (305-m) intervals (*3*). Four undamaged slabs (4 ft by 12 ft [1.2 m by 3.6 m]) were lifted out and transported to the University of Illinois, where they were cut into 18-in. by 12-in. (31-cm by 46-cm) test specimens. The specimen bases were capped with cement mortar to provide a stable base for testing.

A steel drilling frame was assembled to hold the specimens and drill rigs, ensuring that the holes were drilled perpendicular to and centered within one of the 12-in. (31-cm) faces of each test specimen.

M. B. Snyder, Department of Civil and Environmental Engineering, Michigan State University, 347A Engineering Building, East Lansing, Mich. 48824-1226.

TABLE 1 LABORATORY TEST PROGRAM

Variable	Low Value	Intermediate	High Value
Dowel diameter	1 in. (25 mm)		1.5 in. (38 mm)
Annular gap	1/32 in. (0.80 mm)		1/8 in. (3.2 mm)
Anchor material	Cement grout (Dayton Superior Sure-Grip—"flowable" mix)		Epoxy resin (Hilti HIT C-10)
Embedment length	7 in. (178 mm)		9 in. (229 mm)
Drill type; impact energy	Standard pneumatic; ~100 ft-lbs (~135 N-m)	Hydraulic percussion (TAMROCK); 25.2 ft-lbs (35.1 N-m)	Electropneumatic (Hilti, Inc.); 6.35 ft-lbs (8.6 N-m)

Anchor materials were prepared just prior to installation of the noncoated steel dowels. A two-cylinder caulking-gun arrangement provided by the manufacturer dispensed the epoxy mortar. This arrangement provided consistent "on-demand" proportioning and mixing of the mortar and hardener. The cement grout was mixed in accordance with the manufacturer's recommendations for achieving a "flowable" mix. Grout consistency was not measured quantitatively. Cement grout batches were sized to install three to five dowels in a 5- to 10-min period. A vinyl bag was filled with the grout and squeezed to force the grout through an attached nozzle into the drilled hole. This delivery system was recommended by Lippert (*4*). In each case, sufficient anchor material was injected to the backs of the drilled holes to produce some extrusion when the dowels were inserted.

A tight-fitting, hard nylon disk, 2 in. larger than the dowel diameter and approximately 3/32 in. (2.4 mm) thick (see Figure 1), was fixed on each dowel at a distance equal to the embedment length from one end of the dowel. These disks were used to prevent the anchor material from flowing out of the holes and creating voids around the dowels. They also forced the anchor material to fill spalls near the dowel hole on the concrete face caused by the drill.

The dowels were inserted up to the nylon disks using a back-and-forth twisting action to ensure complete and uniform coverage of the dowel and filling of the annular gap with the anchor material. The dowels were allowed to settle or tip in the holes as the anchor material cured. A doweled test specimen (with grout retention disk intact) is shown in Figure 2. The nylon disks were removed after 24 hours.

Two specimens were prepared using 1-in. (25-mm)-diameter dowels cast in fresh concrete with 9 in. (229 mm) of embedment. The concrete mix was designed to produce a 3,000-psi (20.7-MPa) mix using Portland Cement Association procedures (*5*). These specimens were cured for 24 hours, subjected to 5,000 load cycles (to simulate early opening of the repair), cured for an additional 27 days, and subjected to an additional 595,000 load cycles. The purpose of these specimens was to set a standard of deflection performance against which to compare the anchored dowels, and to simulate the conditions imposed on the end of the dowel embedded in the repair.

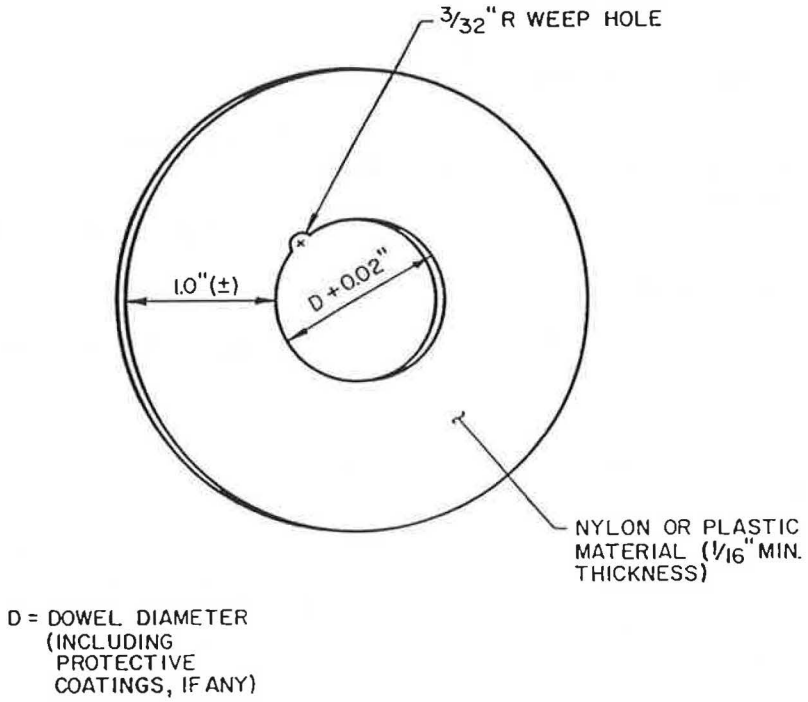

FIGURE 1 Illustration of grout retention disk used in laboratory study.

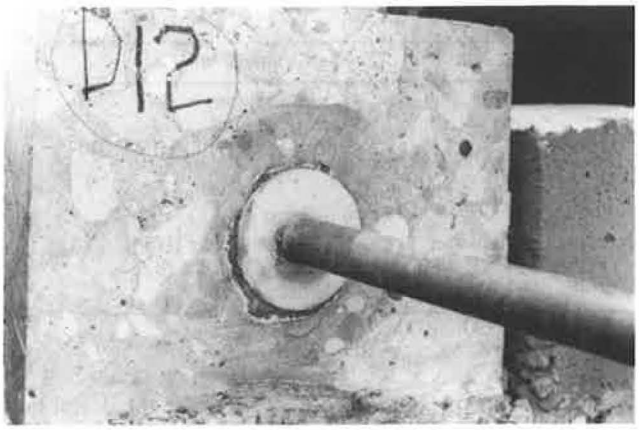

FIGURE 2 Photo of grout retention disk installed on test specimen.

Two specimens were also prepared to test the performance of dowels installed in close-fitting holes. Dowels were turned on a metal lathe to achieve dowel diameters 0.02 in. (0.5 mm) less than the smallest diameter measured in each hole. The finished dowels were 1.06 and 1.10 in. (27 and 28 mm) in diameter. The dowels were inserted to a depth of 9 in. (229 mm) in holes drilled with 1 1/16-in. (27-mm) nominal diameter drill steels. The smaller of the two bars was loose enough to be moved slightly in any direction. Some epoxy mortar was placed around this dowel at the concrete face. The larger bar could not be inserted to full depth by hand. It was forcibly inserted without anchor material using a large hammer.

Specimens fabricated using cement grout were allowed to cure in the lab for 7 to 14 days prior to testing. Specimens prepared using epoxy mortar were cured for 24 hours to 7 days.

A more detailed discussion of test specimen preparation is included elsewhere (*1, 2*).

TEST EQUIPMENT, INSTRUMENTATION, AND RECORDING OF DATA

Repeated bidirectional vertical shear loads were applied to the dowels installed in the test specimens. Several load waveforms (simulating the passage of 36-kip [160-kN] tandem axles) were tried during preliminary tests. Specimen response was found to be relatively insensitive to the waveforms being considered. Thus, a continuous sinusoidal form with a peak magnitude of ±3,000 lb (13.4 kN) and a frequency of 6 Hz was ultimately selected. This resulted in the application of nearly 520,000 load cycles per day, or about a year's worth of heavy traffic loads daily.

Loads were generated hydraulically using an MTS Model 661 ram with an 11-kip (50-kN) capacity. The load was applied to the dowel through a specially fabricated, high-strength steel loading collar that allowed vertical deflection and associated angular dowel movement about a lateral axis.

A linear variable differential transducer (LVDT) was mounted on an aluminum bracket attached to the face of each specimen and connected to the load collar using a small, threaded nylon rod. This device was used to measure electronically the movement of the load collar and dowel relative to the PCC specimen. The MTS load cell data were also collected for analysis and to assist in computer control of the test program.

Deflection and load data were collected during ten load cycles immediately following completion of 1, 2,000, 5,000, 20,000, 100,000, 300,000, and 600,000 load cycles. Extended test data were also collected after 1,200,000, 2,000,000, and 4,000,000 load cycles for certain specimens.

Data collection was accomplished automatically using an IBM Personal Computer (PC) and a Data Translations DT-2801A Analog/Digital (A/D) board. Each data channel was sampled 400 times per second.

Further information concerning the test equipment, instrumentation, and data recording is presented elsewhere (*1, 2*).

TEST PROCEDURE

The entire test operation was controlled by the previously described PC and A/D board. The controlling program was written in BASIC using the PCLAB library of A/D board control subroutines (*6*). Execution of the test control program initiates a series of prompts requesting specimen information and test parameters. The program also includes provisions for (re-)zeroing and (re-)calibrating the data collection channels, test interruption, and test parameter modification.

A data reduction program was written and used to process the raw test data. This program identified average peak loads and computed average theoretical dowel looseness for each set of ten load cycles that comprised a data sample. The reduced and summarized data were loaded into an SPSS (*7*) database and a Lotus 1-2-3 (*8*) spreadsheet for analysis, production of graphs, and so forth.

Detailed descriptions of the test procedure, data reduction programs, summaries of the laboratory test data, load-deflection hysteresis loops, and dowel looseness envelopes are included elsewhere (*1, 2*).

PRELIMINARY RESULTS AND OBSERVATIONS

Effect of Drill Impact Energy on Spalling

Drills that impart high-impact energy produce more spalling on the concrete face near the drilled hole than drills using low-impact energy. The hydraulic drills produced significantly less spalling than the pneumatic drills, and the electric-pneumatic drills produced very little spalling at all.

Even relatively minor spalling around the drilled hole can result in a loss of dowel support. If the spall is not filled with dowel anchor material or PCC repair material, the effective joint width increases in the vicinity of the dowel, causing increased pavement and dowel deflections and increased bearing stresses. Since flat nylon rings were used to retain the anchor material in the drilled holes and spalled areas, the effect of spalling on dowel deflection could not be determined directly. However, increased deflections were recorded where the anchor material did not completely fill the dowel hole or the spalled area.

Consistency of Dowel Anchor Materials

The installation of dowels using cement grout was often difficult. Specimens prepared immediately after the grout was mixed received a grout that was almost "pourable," and grout retention was difficult, even using the nylon rings. Large voids were often observed around these dowels prior to testing (see Figure 3), and they exhibited large deflections. Specimens prepared 5 min after the grout was mixed received a grout that was of the desired consistency, and were found to have no voids (or only very small voids); these specimens performed well. Specimens that were prepared 10 min or more after the grout was mixed often received a very stiff grout that compacted at the back of the hole, preventing proper installation of the dowels. These specimens had to be cleaned out and grouted again.

The wide variation in grout consistency over a relatively short period of time in a controlled laboratory environment brings into question the use of the same material in the field. It is possible that the larger batches typically used in field applications exhibit a different fresh-state behavior and may not be as sensitive to time as were the laboratory batches. Field conditions can be harsh, however, and quality control often takes a position secondary to that of production; a reliable, easy-to-use anchor material is needed for these situations. The cement grout did not consistently meet these requirements in the laboratory.

The epoxy mortar and delivery system used in the lab almost always proportioned, mixed, and delivered a mortar that was of the desired consistency. The mortar "set up" in about 5 min, which was more than enough time for dowel installation. Curing was complete in about 24 hours (according to the manufacturer), although the dowels could not be moved or removed by any means after about an hour of curing.

Although the cost of the epoxy mortar is currently substantially higher than the cost of the cement grout (*4*), the reliability and the uniform consistency of the epoxy should make it the preferred material.

It should be noted that not all epoxy mortar materials are suitable for pavement repair applications. Additional testing should be accomplished before using any unproven material.

FIGURE 3 Photo of void above dowel anchored using fluid cement grout.

Dowel Failures

Five of the specimens with 1-in. (25-mm)-diameter dowels experienced brittle fatigue failures at locations 0.75 to 1.5 in. (19 to 38 mm) inside the face of the PCC specimens. This location corresponds approximately to the predicted point of maximum moment in the dowel (0.75 in. [19 mm] inside the face), as presented by Friberg (*9*) based on the work of Timoshenko and Lessels (*10*). Some of these failures occurred after as few as 40,000 load cycles, while others occurred after nearly 600,000 load cycles.

Four of the failed dowels were anchored using cement grout, while one was anchored using epoxy mortar. Large voids were visible above three of the four grouted dowels prior to testing. These observations indicate the variability of quality of the cement grout anchor material (in spite of the use of the nylon grout retaining rings) and demonstrate the importance of providing void-free, uniform dowel support in pavement joints.

Effectiveness of Grout Retention Rings

The grout retention rings were clearly very effective in reducing the outflow of anchor materials from the drilled holes and ensuring more uniform dowel support. They also forced excess anchor material into the spalled area created by drilling, effectively repairing the spall and reducing dowel deflections.

The effectiveness of the rings was highly dependent on the fluidity of the anchor material being used. Very fluid cement grouts were difficult to work with and were not retained well, even with the rings. Excellent results were obtained using materials that were "flowable" (i.e., the cement grout about 5 min after mixing or the epoxy mortar, as delivered), because they were fluid enough to be moved into the voids, yet viscous enough not to flow appreciably under gravity alone. A smooth, void-free face was produced when material of this consistency was used with the grout retention rings (see Figure 4).

FACTORS AFFECTING DOWEL DEFLECTION AND LOOSENESS

In this paper, "dowel deflection" refers to the deflection (under an applied shear load of ±3,000 lb [13.4 kN]) measured using the LVDT attached to the load collar at a point approximately ½ in. (13 mm) from the face of the specimen. Dowel looseness was estimated by plotting measured dowel deflection versus shear load and projecting the slopes of the loading and reverse loading portions of the load-deflection curve at ±3,000 lb (13.4 kN) back to intercept the deflection axis. This technique was conceptualized by Teller and Cashell (*11*) and is shown in Figure 5.

The halt-fraction, factorial experimental design employed in the lab tests allowed direct identification of significant effects through analysis of variance (ANOVA) techniques. The details of this analysis are presented elsewhere (*1, 2*), but the results are summarized herein.

Most of the main variables were found to affect significantly sensor deflection and the development of dowel looseness. These effects are summarized below:

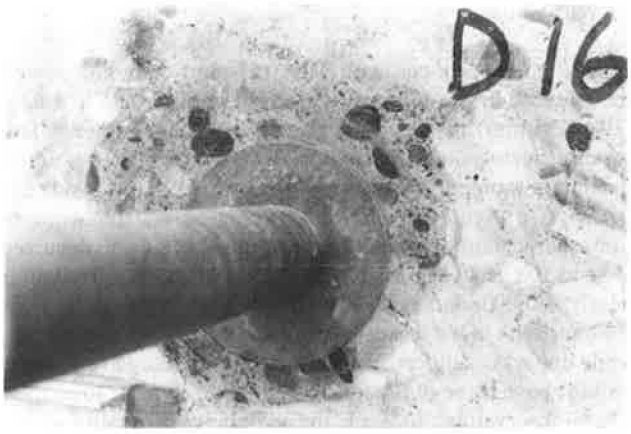

FIGURE 4 Photo of dowel anchored using epoxy mortar and grout retention disk.

Variable Changed	*Effect on Deflection/Looseness*
Increasing dowel diameter	Large decrease
Increasing dowel embedment	Very small decrease
Epoxy anchor material (instead of cement grout)	Small increase
Increase load repetitions	Increase (magnitude varies with other design parameters)

Several significant two-factor interactions were also noted, including anchor material and annular gap, anchor material and dowel diameter (bearing stress), and anchor material and drill impact energy. Additional analyses clarified these relationships, as described below.

Because the epoxy mortar was a softer material than either the cement grout or the concrete specimen, the deflections of bars embedded in this material were more sensitive to dowel diameter (bearing stress) and embedment. Increases in either lead to decreased deflections. As annular gap increased, deflections generally increased owing to the use of larger volumes of softer material. Because the epoxy mortar was always delivered at a uniform consistency that allowed easy insertion of the dowels, there was no apparent need (for installation purposes) for a large annular gap. Therefore, it may be appropriate to use epoxy mortar with the smallest annular gap that will allow dowel installation without excessive force. Voids and spalls would then be filled with a minimum thickness of the softer mortar, allowing the bar to be supported directly by the concrete in many other places.

Since the cement grout was more rigid than the epoxy mortar that was used, the effects (and interaction effects) of dowel diameter and embedment on dowel deflection are reduced for this material. Furthermore, it appears that a larger annular gap generally produces better results for cement grout, presumably because this facilitates dowel installation in a stiffer grout, resulting in more uniform dowel support.

LOAD-DEFLECTION PROFILES AND DOWEL LOOSENESS ENVELOPES

Some of the lab study results are illustrated in Figures 6 through 11, which present dowel "looseness" envelopes (illustrating the development of looseness over time) for several representative specimens. In these figures the "upstroke looseness" (data plotted as × signs) is the component of total looseness computed from the reverse loading curve, "downstroke looseness" (data plotted as diamonds) is the component of total looseness computed from the normal loading curve, and the

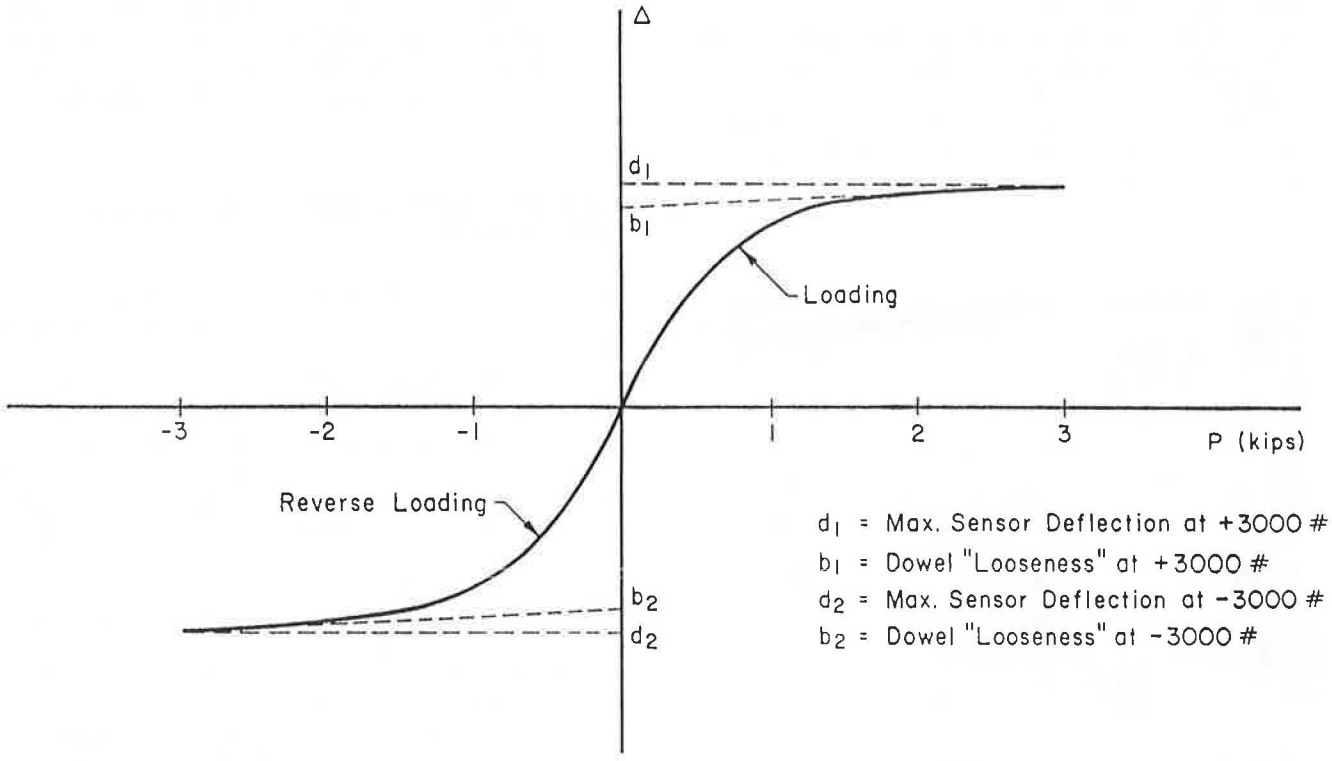

FIGURE 5 Graphic estimation of dowel "looseness."

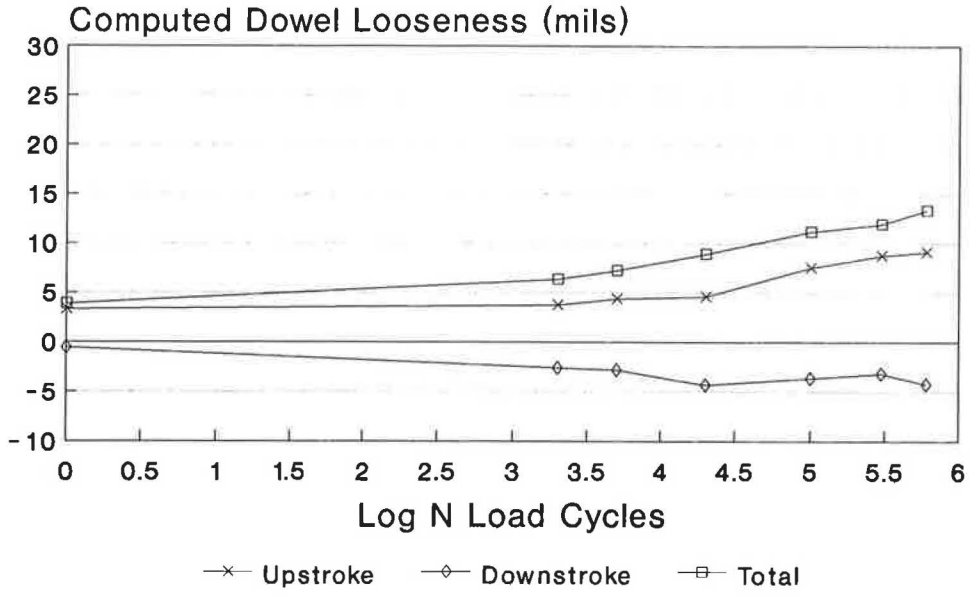

FIGURE 6 Dowel looseness envelope: 1-in. dowel diameter, 1 1/16-in. hole, 9-in. embedment, electric drill, epoxy mortar (Specimen D10R).

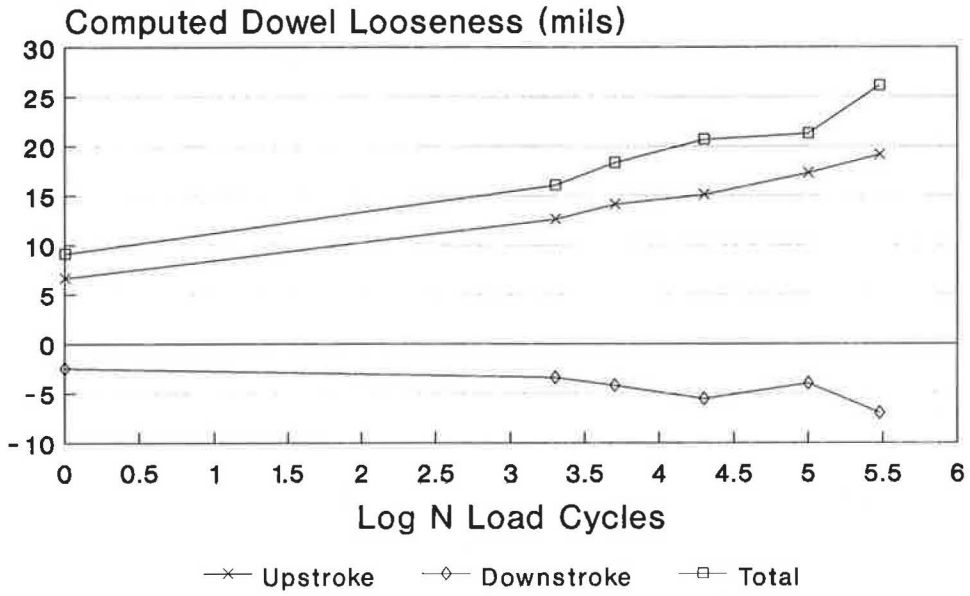

FIGURE 7 Dowel looseness envelope: 1-in. dowel diameter, 1¼-in. hole, 9-in. embedment, electric drill, epoxy mortar (Specimen D6).

"total looseness" (plotted as squares) is the distance between the other two curves.

A comparison of Figures 6 and 7 illustrates the increase in dowel deflection/looseness that accompanied increases in annular gap when the epoxy anchor material was used. These figures also illustrate that the reverse loading mode typically produced higher deflections than normal loading. This is presumably due to settlement of the dowel during curing, which results in the dowel bearing on a very thin layer of anchor material on the bottom with a thicker layer on top. Since deflections are partially dependent on the deformation of the supporting layer, the thicker layer of softer material on top allows more deflection in reverse loading.

Comparing Figures 7 and 8 illustrates that dowels properly installed using cement grout typically exhibited lower deflections than those installed in the same size holes using the epoxy mortar. It must be emphasized, however, that it was often difficult to obtain good anchoring using cement grout due to the extreme variability of grout consistency over short periods of time.

A comparison of Figures 8 and 9 shows the tremendous reduction in deflection (~75 percent) that typically accom-

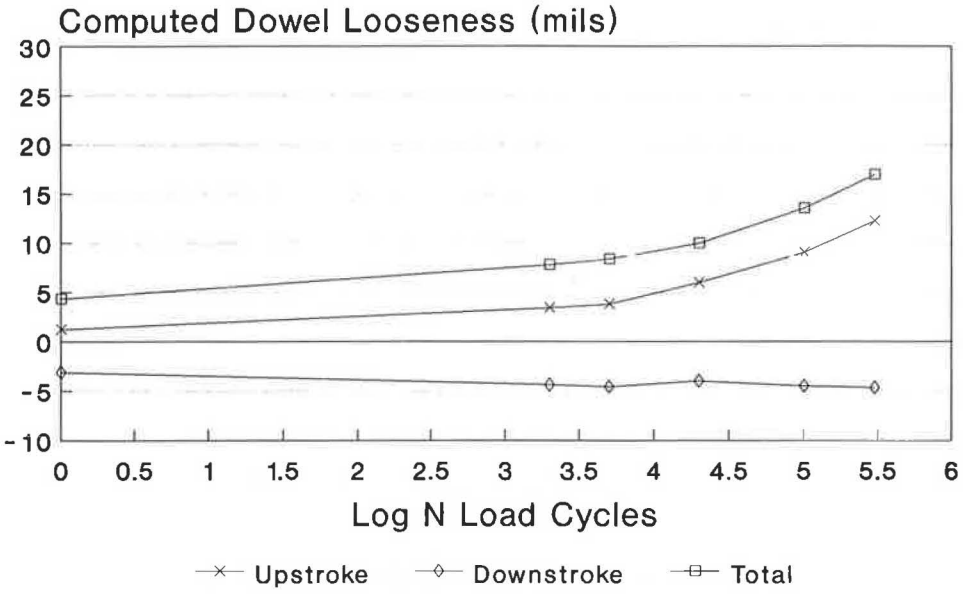

FIGURE 8 Dowel looseness envelope: 1-in. dowel diameter, 1¼-in. hole, 9-in. embedment, electric drill, cement grout (Specimen A8R).

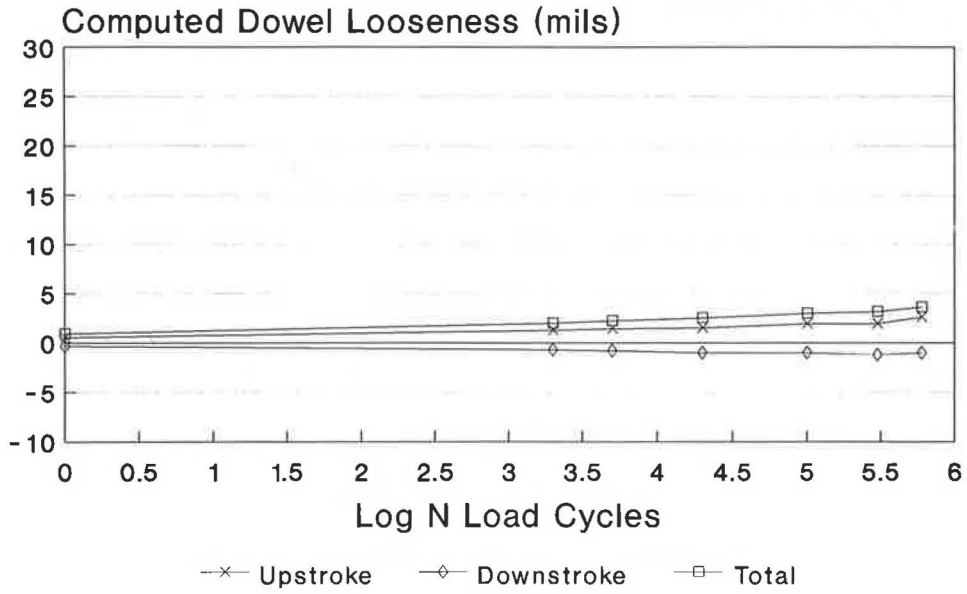

FIGURE 9 Dowel looseness envelope: 1.5-in. dowel diameter, 1¾-in. hole, 9-in. embedment, electric drill, cement grout (Specimen B18).

panied an increase in dowel diameter from 1 in. to 1.5 in. (25 mm to 38 mm).

Figures 10 and 11 illustrate that the effect of dowel embedment on dowel deflection was typically very small for the range of embedments tested (7 to 9 in. [18 to 23 cm]). This confirms other studies that have suggested that embedment lengths of 6–7 in. are adequate for the dowel sizes currently used in highway applications. The effect of embedment on dowel deflection would probably have been larger if grout retention rings had not been used to ensure uniform dowel support.

Figure 12 presents the deflection profile obtained from one of the specimens that was prepared by casting a 1-in. (25-mm)-diameter dowel (embedded 9 in. [23 cm]) in a block of concrete, curing it 24 hours, applying 5,000 load cycles, curing an additional 27 days, and applying an additional 295,000 load cycles. It was believed that a properly prepared, cast-in-place specimen would represent the best possible support that could be provided a dowel and would be a "yardstick" against which to compare the performance of similar specimens. The relatively flat deflection profile indicates that no real looseness existed at the time of testing and confirms the use of such

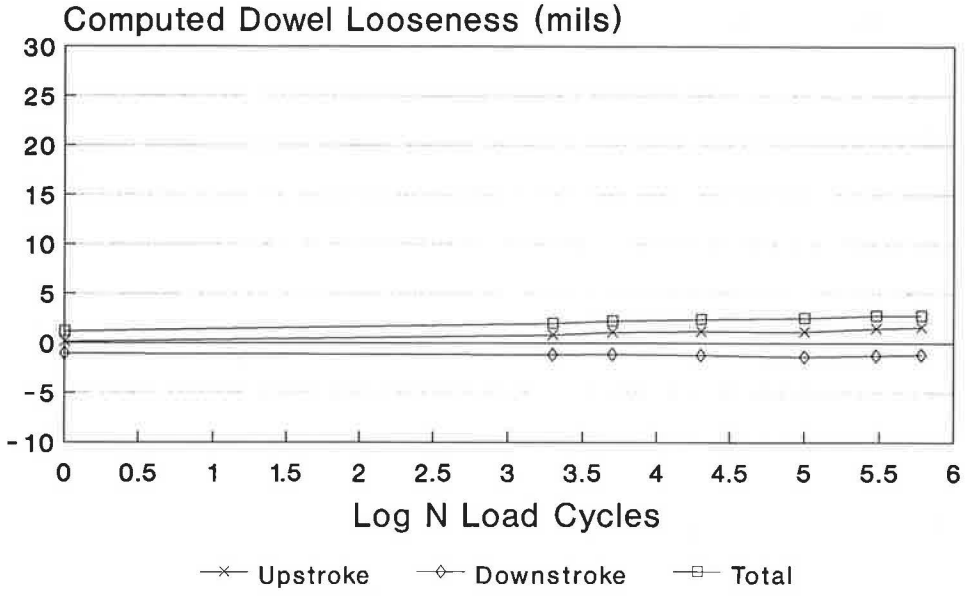

FIGURE 10 Dowel looseness envelope: 1.5-in. dowel diameter, 1¾-in. hole, 9-in. embedment, pneumatic drill, cement grout (Specimen D20).

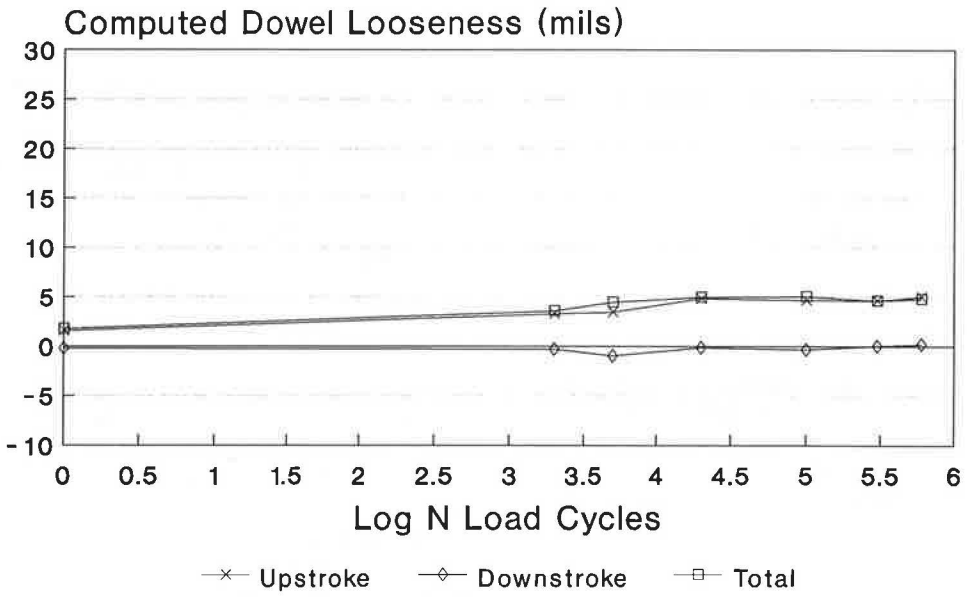

FIGURE 11 Dowel looseness envelope: 1.5-in. dowel diameter, 1¾-in. hole, 7-in. embedment, electric drill, cement grout (Specimen A10).

specimens as idealized dowel installations. A comparison of this profile to those of other 1-in. (25-mm) doweled specimens suggested that the cement grout specimens have the potential to approach this level of dowel support most closely, particularly when longer embedment lengths and good grout installations are present. By comparison, the epoxy mortar specimens performed well when the annular gap was small and the embedment length was 9 in. (23 cm). The "looseness" history of the cast-in-place specimen also suggested excellent performance.

The 1⅝-in. (41-mm) O.D. hollow stainless steel dowel was installed using the epoxy mortar to a depth of 7 in. (18 cm) in a 1¾-in. (44-mm) nominal diameter hole. Its performance was similar to that of a 1-in. (25-mm)-diameter solid dowel with a slightly thicker supporting layer of epoxy mortar. A solid bar (or a tube with thicker walls) would probably have provided better performance. In addition, the stainless steel did not bond to the epoxy mortar, allowing the bar to be twisted freely after testing, although the bar was not necessarily loose.

The two specimens that were prepared using "close-fitting holes" rapidly developed deflections that were beyond the capability of the sensor to measure (>0.05 in. [1.27 mm] in either direction). Neither could be tested to the full 600,000

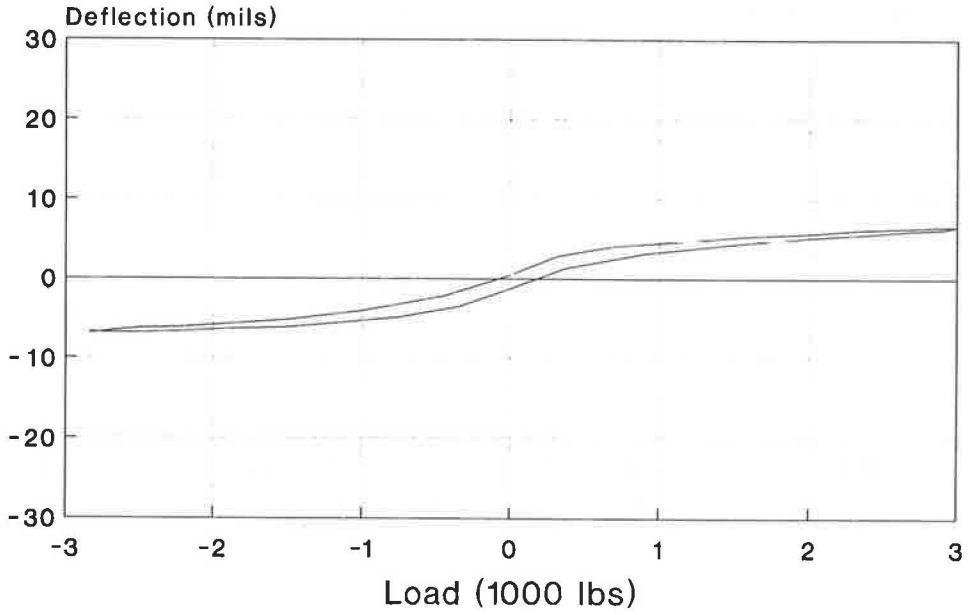

FIGURE 12 Load-deflection profile for cast-in-place specimen after 300,000 load cycles (1-in. dowel).

load repetitions because of possible damage to the test equipment. One of the specimens failed after fewer than 60,000 load cycles.

DOWEL DEFLECTION AND LOOSENESS MODELS

The data sets for each anchor material type were used to develop predictive models for sensor deflection and dowel looseness. Although many factors and interactions appear to affect these performance measures, their inclusion often made the models much more complex without significantly improving their accuracy. Satisfactory models were often obtained using nonlinear regression techniques and including only main effects.

The models developed for the epoxy mortar anchor material are presented below:

$$B_{maxmin} = [34840(AG) + 1167(CT)^{1.058} - 9.899(EB)^{1.160} + 1.079(BS) - 0.6912(EN)^{1.831} + 8380]/1000$$

$R^2 = 0.594$ C.O.V. = 36.9 percent $n = 178$

$$D_{maxmin} = [54210(AG) + 643.3(CT) - 2117(EB) + 2.031(BS) - 8.822(EB)(EN) + 21210]/1000$$

$R^2 = 0.584$ C.O.V. = 28.7 percent $n = 178$

where

B_{maxmin} = total dowel looseness (as defined previously) (mils) (1 mil = 0.0254 mm);
D_{maxmin} = total sensor deflection (as defined previously) (mils);
AG = annular gap = (nominal diameter of drilled hole − nominal dowel diameter)(in.) (1 in. = 25.4 mm);
CT = natural log of number of complete load cycle applications;
EB = dowel embedment (in.);
BS = Friberg's bearing stress (psi) (1 psi = 6.8947 kPa); and
EN = estimated drill impact energy, ft-lb/blow (1 ft-lb = 6.5782 N-m).

Figures 13 through 15 illustrate the sensitivity of the deflection model to the input parameters. The sensitivity of the "looseness" model is similar.

Figure 13 illustrates the relatively large effect of annular gap and the comparatively small effect of the number of load applications on dowel deflection for epoxy mortar installations. This confirms that the epoxy mortar is flexible (when compared to the surrounding concrete) and that thin supporting layers (sufficient to fill drilling voids) are best. It also shows that the material is very resistant to fatigue and undergoes very little permanent deformation or deterioration after many repeated load applications.

Figure 14 further defines the response of the epoxy mortar to applied loads by showing the expected total vertical dowel movement for combinations of bearing stress and annular gap values tested. The predicted behavior is linear because only two levels of bearing stress were examined. Additional data may produce a nonlinear relationship, but the overall effect is likely to be similar. This model predicts dowel deflection increases of 60 to 100 percent for bearing stress increases from 1,000 psi to 5,000 psi (6,900 to 34,000 kPa).

Figure 15 shows that the flexibility of the epoxy mortar makes it sensitive to dowel embedment length. The increase

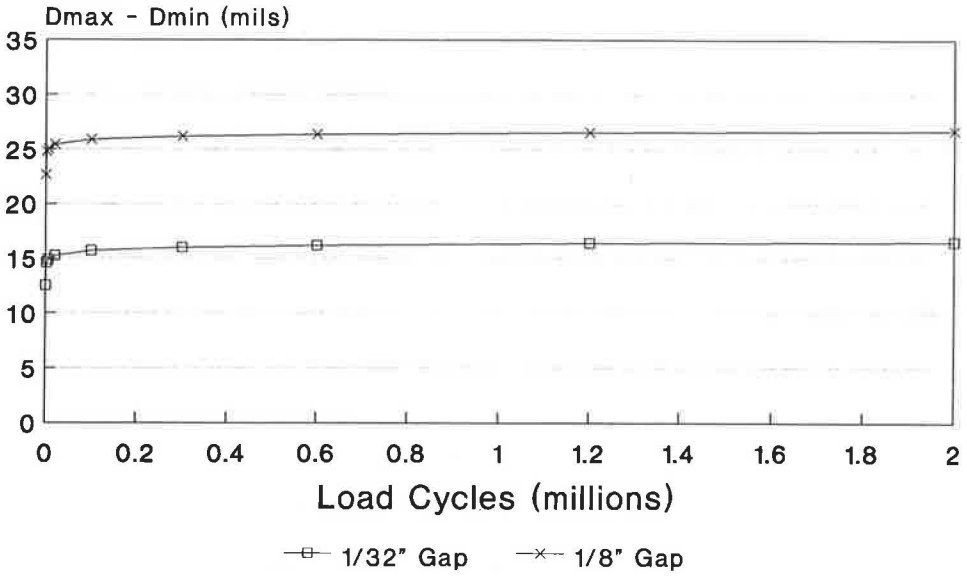

FIGURE 13 Predicted effect of annular gap and load cycles on deflection for epoxy mortar specimens (9-in. embed, 1-in. dowel, medium-energy drill).

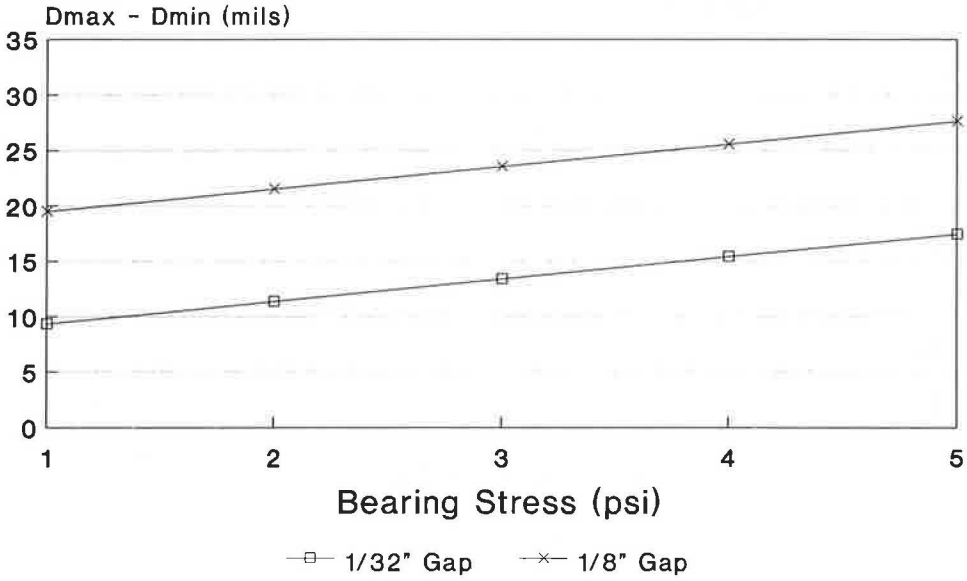

FIGURE 14 Predicted effect of annular gap and bearing stress on deflection of epoxy mortar specimens (N = 600,000, 9-in. embed, medium-energy drill).

in deflection that results from decreasing embedment length from 9 in. to 7 in. (23 cm to 18 cm) is approximately 10 percent and is not considered significant.

The models developed for the cement grout anchor system are presented below:

$$B_{\text{maxmin}} = ((\text{CT})(-2347 + (\text{BS})((0.762 + 2.604/\text{EN})) + 3883)/1000$$

$R^2 = 0.647$ C.O.V. = 61.2 percent $n = 109$

$$D_{\text{maxmin}} = (6.072(\text{BS}) - 66.96(\text{EN}) + 13900(\text{AG}) + 572.7(\text{CT}) - 8946)/1000$$

$R^2 = 0.663$ C.O.V. = 43.3 percent $n = 110$

where all variables are defined as described previously.

It should be noted that these models were developed using only those data that were obtained before deflections exceeded the capability of the measuring device. Some cement grout specimens exhibited excessive deflections after relatively few load applications, and data could be collected only for low numbers of load applications. Thus, the cement grout models may tend to underestimate dowel deflection and looseness after many load applications.

Figure 16 shows the sensitivity of the dowel deflection model to bearing stress and annular gap. The sensitivity of the "looseness" model is similar. The large effect of bearing stress on performance is clear and suggests that the bearing stresses that result from the use of 1-in. (25-mm) dowels (2,500–4,000

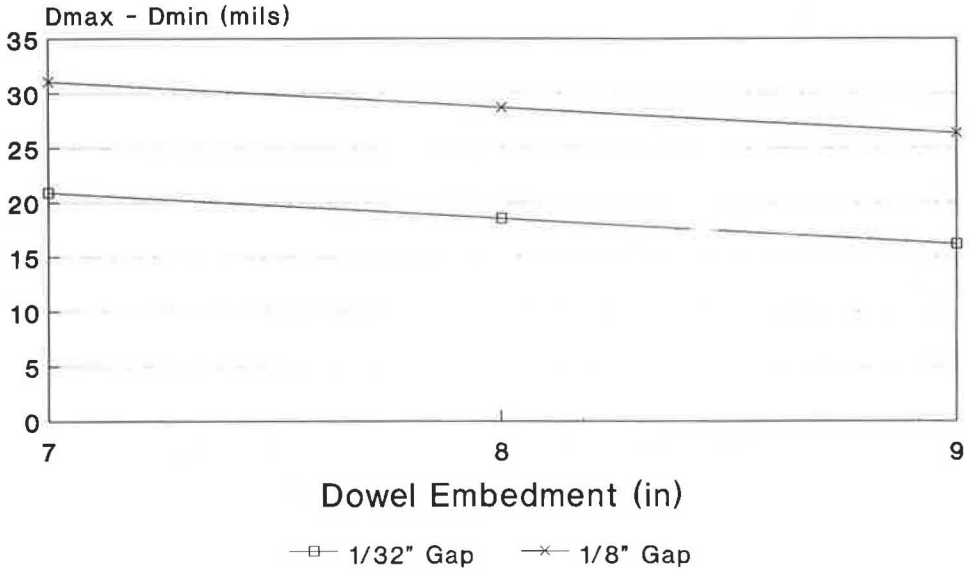

FIGURE 15 Predicted effect of annular gap and embedment length on deflection for epoxy mortar specimens (N = 600,000, 1-in. dowel, medium-energy drill).

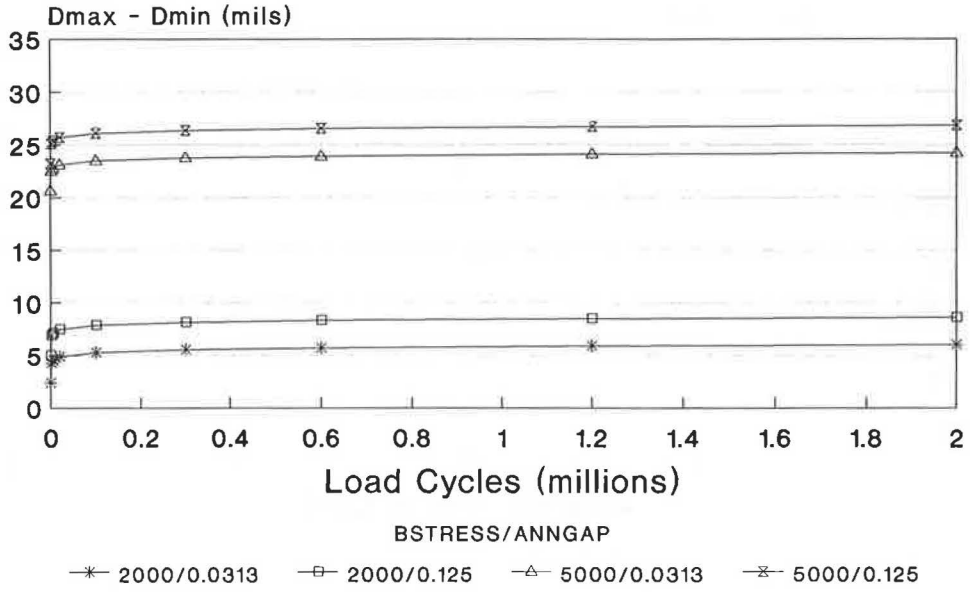

FIGURE 16 Predicted effect of annular gap and bearing stress on deflection for cement grout specimens (medium-energy drill).

psi [17,500–28,000 kPa]) result in deterioration of the anchor material at the joint face. The 1.5-in. (38-mm) dowels (1,000–2,000 psi [7,000–14,000 kPa]) are represented by the lowest curves, which suggest acceptable performance.

The effect of increased heavy load repetitions is also presented in this figure. When good installations are achieved, rapid initial increases in deflection occur as the dowel becomes "seated"; subsequent increases are generally small. Poor installations (characterized by large voids at the joint face) were observed to have excessive deflections from the start; these deflections increased as the dowel repeatedly contacted the supporting material, causing it to deteriorate.

CONCLUSIONS AND RECOMMENDATIONS

The following conclusions and observations were drawn from the analysis of the laboratory experiment results:

1. The use of grout retention disks is essential to achieve the potential performance of any anchored dowel installation. The disks should fit the dowels snugly and have "weep holes" to allow excess anchor material to escape. Excess anchor material should be used to fill spalls surrounding the drilled hole. These disks should be specified for all doweled, full-depth repair construction projects to ensure good bearing support around the dowel.

2. The epoxy mortar anchoring material was easier to use and produced more consistent results than the cement grout. Dowel deflections and computed "looseness" were lower when cement grout was properly installed (i.e., when no voids were present and uniform support was provided). The potential of the cement grout was difficult to achieve, however, because the consistency of the grout typically changed rapidly over very short periods of time.

3. The use of larger diameter dowels significantly reduces concrete bearing stresses, dowel deflections, and dowel "looseness" when all other factors are held constant.

4. Increasing the size of the annular gap (drilled hole radius minus dowel radius) from 1/32 in. to 1/8 in. (0.8 mm to 3.2 mm) improved the performance of dowels anchored in cement grout, apparently because better distribution of stiff grout could be achieved. Very fluid grouts performed poorly, regardless of the annular gap.

5. Small annular gaps improved the performance of dowels anchored in epoxy mortar because thinner supporting layers of epoxy mortar, which was softer than the concrete specimens, deformed less than thick layers. The consistency of the material was such that good support and filling of the voids were achieved regardless of the annular gap.

6. Reducing dowel embedment resulted in very small increases in dowel deflection and "looseness" when epoxy mortar was used. Even smaller increases resulted when good cement grout specimens were tested.

7. Close-fitting holes probably offer promise when used with good anchor materials, quality control, and grout retention disks. Cement grout and "no-grout" applications may experience poor performance due to nonuniform support of the dowel and drill-induced spalling at the joint face.

8. The hollow stainless steel dowel performed adequately, although it did not bond with the epoxy mortar that was used. Concurrent testing by the FHWA has demonstrated the need to fill hollow dowels with concrete or some other stiff material to reduce deformation of the dowel at the joint face (*12*).

9. It appears that the following design and construction parameters would provide excellent field performance on primary and Interstate installations:

- 1½-in.-diameter (nominal), corrosion-resistant solid steel dowels;
- 1 9/16-in.-diameter (nominal), guided drills for epoxy mortar anchor materials; 1 3/4-in.-diameter (nominal), guided drills for cement grout anchor materials;
- 7-in. or greater dowel embedment;
- Use of rapid-curing, consistent, easy-to-use anchor material (reduction of the emphasis on using the cheapest materials when they are difficult to install adequately); and
- Use of grout retention disks during curing of the anchor materials. Field testing of these recommendations should be accomplished prior to widespread installation.

ACKNOWLEDGMENTS

This paper describes a portion of a research study entitled "Determination of Rehabilitation Techniques," which was conducted by the University of Illinois Department of Civil Engineering and funded by the Federal Highway Administration (FHWA). The author gratefully acknowledges the input and assistance of the University of Illinois project team and the FHWA contract staff. Note: The work described herein was performed at the University of Illinois at Urbana-Champaign in partial fulfillment of the requirements for the Ph.D. degree.

REFERENCES

1. M. B. Snyder. *Dowel Load Transfer Systems for Full-Depth Repairs of Jointed Portland Cement Concrete Pavements*. Ph.D. dissertation. University of Illinois at Urbana-Champaign, Urbana, 1989.
2. M. B. Snyder, M. J. Reiter, K. T. Hall, and M. I. Darter. *Rehabilitation of Concrete Pavements, Volume I—Repair Rehabilitation Techniques*. Final Report, FHWA Contract DTFH61-85-C00004. Department of Civil Engineering, University of Illinois, Urbana, December 1987.
3. K. D. Smith, M. B. Snyder, M. I. Darter, M. J. Reiter, and K. T. Hall. *Pressure Relief and Other Joint Rehabilitation Techniques*. Final Report, FHWA Contract DTFH61-83-C00111. ERES Consultants, Savoy, Ill., February 1987.
4. D. L. Lippert. Performance Evaluation of Jointed Concrete Pavement Rehabilitation Without Resurfacing. In *Transportation Research Record 1109*, TRB, National Research Council, Washington, D.C., 1987, pp. 42–55.
5. *Design and Control of Concrete Mixtures*, 12th ed. Portland Cement Association, Skokie, Ill., 1979.
6. *User Manual for PCLAB Machine Language Routine Library*, Version 2.00. Data Translation, Inc., Marlborough, Mass., 1985.
7. N. H. Nie, C. H. Hull, J. G. Jenkins, K. Steinbrenner, and D. H. Bent. *Statistical Package for the Social Sciences*, 2nd ed. McGraw-Hill, New York, 1975.
8. *Lotus 1-2-3 Reference Manual, Version 2.00*. Lotus Development Corp., Cambridge, Mass., 1985.
9. B. F. Friberg. Load and Deflection Characteristics of Dowels in Transverse Joints of Concrete Pavements. *Proc., 18th Annual Meeting of the Highway Research Board*, Washington, D.C., 1938.
10. S. Timoshenko and J. M. Lessels. *Applied Elasticity*. Westinghouse Technical Night School Press, Pittsburgh, Pa., 1925.
11. L. W. Teller and H. D. Cashell. Performance of Doweled Joints Under Repetitive Loading. *Bulletin 217*, HRB, National Research Council, Washington, D.C., 1959.
12. K. N. Black, R. M. Larson, and L. R. Staunton. Evaluation of Stainless Steel Pipes for Use as Dowel Bars. *Public Roads*, Vol. 52, No. 2, September 1988, pp. 37–43.

Publication of this paper sponsored by Committee on Pavement Rehabilitation.

Evaluation of Pressure Relief Joint Installations

MARK B. SNYDER, KURT D. SMITH, AND MICHAEL I. DARTER

Pressure relief joints are used to reduce compressive stresses in concrete pavements and thereby to reduce pressure-related damage. In recent years, their use has become so commonplace that they are frequently overused or used inappropriately. To evaluate the effectiveness of pressure relief joints, representative pressure relief joint installations around the United States were reviewed to identify, define, and document the criteria for the use of these joints. These installations included several climatic zones, placement in both short- and long-jointed concrete pavements, relief joints that were placed prior to overlay, wide joints filled with asphalt concrete, narrow joints filled with foam, and other factors of interest. It was determined that the use of pressure relief joints was often unwarranted and that good contraction joint maintenance programs would have prevented the development of pressure-related problems. The unnecessary or excessive use of pressure relief joints was found to cause damage that was more costly to repair than the damage that would have resulted without the relief joints. Where appropriate, pressure relief joints were found to close rapidly during their first year and to be effective in preventing pressure damage for 3 to 7 years.

Net increases in concrete pavement length are often caused by such factors as the intrusion of incompressibles into poorly sealed joints, the pumping of base materials into joints, and/or the expansion of reactive aggregates in the concrete. If left untreated, these increases in length create compressive forces in the concrete pavement and result in blowups and/or bridge pushing. One means of addressing this problem is through the use of pressure relief joints, the function of which is to relieve compressive stresses in the concrete pavement and thereby to prevent blowups, shattered slabs, severe joint spalling, and damage to secondary structures.

In 1983, a research study entitled "Pressure Relief and Other Joint Rehabilitation Techniques" was sponsored by the Federal Highway Administration (FHWA). Primary objectives of this study included the identification of criteria for the use of pressure relief joints and the development of a set of guidelines for the design and installation of pressure relief joints (*1*). To fulfill these objectives, a field survey of thirty-six rehabilitated projects was conducted in 1985 and 1986; extensive condition, design, traffic, and other data were collected. Twenty-five of these projects, listed in Table 1, included pressure relief joint installations. Detailed, comprehensive project evaluation reports were prepared for each of these projects.

M. B. Snyder, Department of Civil and Environmental Engineering, Michigan State University, A347 Engineering Building, East Lansing, Mich. 48824-1226. K. D. Smith and M. I. Darter, ERES Consultants, Inc., 1401 Regency Drive East, Savoy, Ill. 61874.

The performance information obtained from these in-service projects was supplemented with the knowledge and expertise of an advisory panel of state highway engineers. The resulting information was used to assist in the development of decision trees, improved design guidelines, and guide specifications for the use and construction of the selected joint rehabilitation techniques (*1, 2*). Those projects that provide the most insight regarding the use and performance of pressure relief joints are presented here.

PRESSURE RELIEF JOINTS (PRJs) IN JOINTED CONCRETE PAVEMENT

Louisiana, I-55, Milepost 32

The original pavement was a 10-in., jointed reinforced concrete pavement (JRCP) with 58.5-ft contraction joints, constructed and opened to traffic in 1966. Four-inch wide, cellular plastic-filled, pressure relief joints were installed in the northbound lanes in 1980 at 0.5-mile intervals to relieve expansive pressures and eliminate blowups. The southbound lanes served as a "control" section in which no relief joints were placed. This rehabilitation project was constructed to evaluate the performance of relief joints and analyze the economics of using them (*3*).

By 1985, the pressure relief joints had sustained about 2.7 million, 18-kip, equivalent single-axle loads (ESALs) in the outer lane. The condition surveys conducted in 1985 revealed some low-severity, transverse slab cracking in both directions and one full-depth repair in the southbound sample where a blowup had occurred at a joint. The Louisiana Department of Transportation and Development (LDOTD) reported a total of fifteen blowups in the southbound lane over the 25-mile section, while none occurred in the northbound lane where the pressure relief joints were placed (*3*).

Forty-five percent of the southbound lane original contraction joints and 39 percent of the northbound lane original contraction joints exhibited medium-severity transverse joint and corner spalling; a few displayed high-severity spalling. No significant difference in joint faulting was noted between the two sections. Pavement Serviceability Index (PSI) values determined in 1983 by LDOTD were 3.7 and 3.4 for the northbound and southbound lanes, respectively.

The pressure relief joints had closed to an average width of 1.5 in. and had faulted an average of 0.13 in. The filler was generally absent from these joints, and the joints were full of foreign materials. The contraction joints adjacent to the

TABLE 1 SUMMARY OF PRESSURE RELIEF JOINT INSTALLATIONS

	ORIGINAL PAVEMENT			PRESSURE RELIEF JOINT			
State/Location	Year Built	Pavement Type	Jt Spacing	Year	Width	Filler	Spacing
IL I-55, mp 98	1963	10-in JRCP	100-ft	1973	4-in	Foam	1320-ft
IL I-55, mp 102	1963	10-in JRCP	100-ft	1973	4-in	Foam	1320-ft
IL I-55, mp 252	1956	10-in JRCP	100-ft	1975	4-in	Foam	1500-ft
IL I-72, mp 67	1970	7-in CRCP	- -	1983	4-ft	AC	1000-ft
IL I-80, mp 105	1960	10-in JRCP	100-ft	1984	4-in	Foam	1320-ft
IN I-69, mp 64	1964	10-in JRCP	40-ft	1975	3-ft	AC	40/500/1000-ft
IA US 30, mp 156	1964	10-in JPCP	20-ft	1980	4-in	Foam	1000-ft
IA I-35, mp 86	1965	10-in JRCP	76-ft	1980	4-in	Foam	1000-ft
KY I-65, mp 12	1966	10-in JRCP	50-ft	1982	6-in	Foam	1000-ft
LA I-55, mp 32	1966	10-in JRCP	58-ft	1980	4-in	Foam	2640-ft
OH I-70, mp 66	1969	8-in CRCP	- -	1970	2-ft	AC	2640-ft
OH I-71, mp 210	1959	10-in JRCP	60-ft	1973	2-ft	AC	2640-ft
OH I-270, mp 29	1969	8-in CRCP	- -	1973	4-in	AC	2000-ft
OH I-270, mp 31	1969	8-in CRCP	- -	1983	4-in	AC	2000-ft
MI US 127	1956	9-in JRCP	99-ft	1972	4-in	Foam	200-1200 ft
NE I-80, mp 189	1965	9-in JRCP	46-ft	1981	4.5-in	Foam	2000-ft
NE I-80, mp 210	1964	9-in JRCP	46-ft	1980	4.5-in	Foam	2000-ft
NE I-80, mp 256	1963	9-in JRCP	46-ft	1980	4.5-in	Foam	2000-ft
NE I-80, mp 279	1964	9-in JRCP	46-ft	1980	4.5-in	Foam	2000-ft
NE I-80, mp 382	1962	9-in JRCP	46-ft	1982	4.5-in	Foam	5280-ft
VA SR 44, mp 0	1967	9-in JRCP	61-ft	1984	4-in	Foam	1000-ft
VA I-64, mp 202	1965	9-in JRCP	61-ft	1982	4-in	Foam	1000-ft
VA I-64, mp 279	1967	9-in JRCP	61-ft	1981	4-in	Foam	1000-ft
VA I-64, mp 284	1968	9-in JRCP	61-ft	1978	4-in	Foam	1000-ft
VA I-81, mp 148	1965	9-in JRCP	61-ft	1976	4-in	Foam	1000-ft

relief joints had opened to an average width of 0.8 in., and most of these adjacent joints were also filled with incompressibles.

Figure 1 is a typical plot of contraction joint width versus station for the northbound section and shows that contraction joint widths tended to increase in the vicinity of the relief joints. Figure 2 provides a similar picture for the southbound section where relief joints were not provided but a blowup occurred. Contraction joints were very wide near the blowup location and then became narrower as the distance from the blowup increased.

Analysis

The LDOTD monitored the performance of this project as part of their own research project. Two conclusions reached by LDOTD were that pressure relief joints are effective in eliminating blowups, thereby saving the cost of blowup repair and eliminating a hazard to the motoring public, and that pressure relief joints are effective in prolonging the life of PCC pavements by reducing premature pavement distress due to contraction joint failure (*3*). However, the results of the 1985 field surveys support only the first conclusion. The pressure relief joints installed in the northbound lanes did indeed prevent blowups, but recall that the joint spalling was approximately the same for the lanes in each direction. This could be attributed to the fact that the adjacent regular contraction joints near the relief joints have opened and are often filled with incompressibles.

It is doubtful that the pavement expansion problem would have developed had a good joint maintenance program been in place. Cleaning the incompressibles from the joints and resealing prior to the occurrence of blowups would significantly have reduced the deterioration of this pavement and resulted in a higher overall level of serviceability.

Michigan, U.S. 127, South of Lansing

The original pavement was a 9-in. JRCP with 99-ft contraction joints that was constructed and opened to traffic in 1956. In 1972, this pavement was selected by the Michigan Department of Transportation (MDOT) to serve as an experimental project for evaluating the merit of preventive maintenance of concrete joints (*4*).

Pressure relief joints were installed in the southbound lanes using diamond saws. The northbound lanes served as a "control" section where no relief joints were installed. Full-depth repairs with 2-in.-wide, nondoweled expansion joints were placed in both lanes just prior to installation of the relief joints to repair existing joint distress. They were also placed in the northbound lanes on an annual basis to repair new joint distress as it developed.

The 4-in.-wide, polyethylene-filled, pressure relief joints

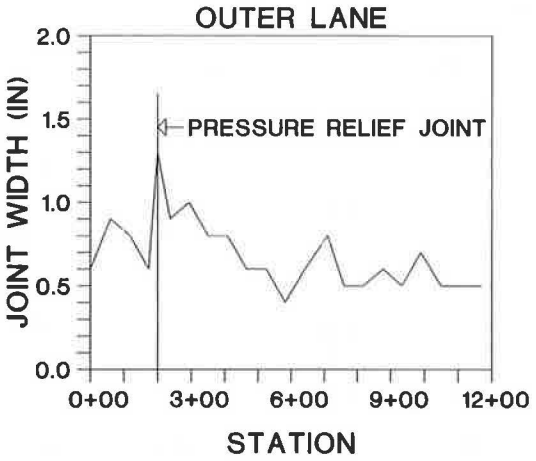

FIGURE 1 Plot of joint width versus station for the northbound outer lane of I-55 in Louisiana (*1*).

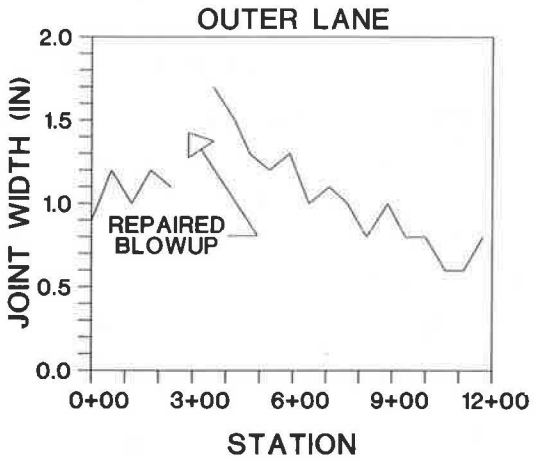

FIGURE 2 Plot of joint width versus station for the southbound outer lane of I-55 in Louisiana (*1*).

were placed at intervals so that each was a minimum of 200 ft and a maximum of 1,200 ft from the nearest full-depth repairs, which were assumed to relieve compressive stresses locally. The relief joints were also placed 6 ft away from the nearest contraction joint. By 1985, the pressure relief joints had sustained about 2.8 million, 18-kip ESALs in the outer lane.

The condition surveys conducted in 1985 revealed all levels of transverse slab cracking in both directions. However, the density and severity of cracking found in the southbound (relieved) lanes were much higher than that found in the northbound (control) lanes, as shown in Table 2.

The contraction joints contained incompressibles and consistently exhibited medium-severity joint and corner spalling throughout all of the surveyed sections. Figure 3 shows the average length of transverse joint spalling observed at each contraction joint for the years 1972–1979, as measured by MDOT. The figure indicates that joint spalling continued to increase in both the relieved and nonrelieved lanes after the relief joint placement. The rate of increase appears to be slightly lower for the relieved lanes, although the spalls observed from the 1985 condition surveys were more severe (deeper and longer over a given width) in the northbound lanes. Comparing the location and severity of the spalls in the two directions suggests that, although the average length of spalling at the joints is approximately equal, the northbound spalls are more pressure-related than the southbound spalls.

Contraction joint faulting was generally about twice as high in the northbound (nonrelieved and more damaged) lanes as in the southbound lanes (0.11 in. versus 0.05 in.). The largest faults and joint widths in either direction were often found near relief joints or full-depth repairs.

The pressure relief joints had closed from 4 in. to an average width of 0.55 in. and had faulted an average of 0.27 in. The joint filler was still intact and was keeping incompressibles from entering. Transverse joint and corner spalling was not exhibited in or along any of the relief joints.

Summer and winter measurements of the relief joints made by MDOT during each year between 1973 and 1979 as part of their own research study are summarized in Figure 4 (*4*). This figure shows that the largest amount of relief joint closure generally took place in the first year after installation. It also indicates that the period of effectiveness of these relief joints ranged from about 3 to 7 years, as indicated by the constant joint openings observed after this period.

Analysis

The pressure relief joints installed in 1972 were apparently an effective means of preventing blowups and pressure-related

TABLE 2 TRANSVERSE CRACKING ON U.S. 127 IN MICHIGAN (*1*)

	AVG. NO. OF CRACKS/MILE (AVG. NO. OF CRACKS/SLAB)			
	SOUTHBOUND		NORTHBOUND	
Crack Severity	Outer	Inner	Outer	Inner
Low (hairline)	134 (2.52)	53 (0.99)	79 (1.49)	41 (0.77)
Medium (working)	57 (1.06)	75 (1.41)	18 (0.33)	18 (0.33)
High (badly spalled)	34 (0.64)	34 (0.64)	9 (0.17)	6 (0.11)
TOTAL	225 (4.22)	162 (3.04)	106 (1.99)	65 (1.21)

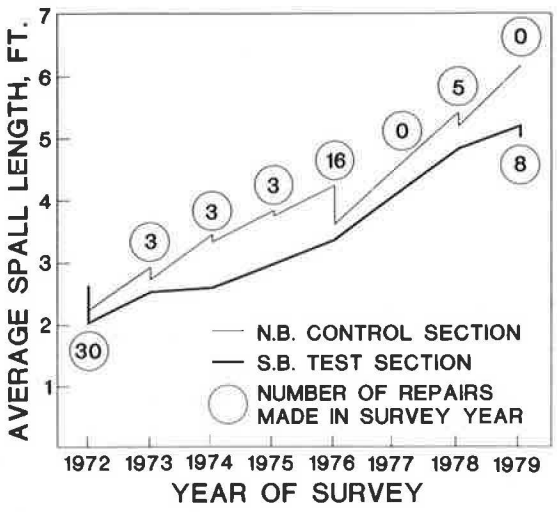

FIGURE 3 Average joint spall length from 1972 to 1979 before and after repair for U.S. 127, Michigan (*4*).

joint damage from occurring in the southbound lanes. Fifty percent of the joints in the southbound lanes were deteriorated, compared with 77 percent in the northbound lanes.

The relief joints have allowed the transverse cracks to deteriorate to the point where the relieved southbound lanes require more repair than the nonrelieved northbound lanes. Successful rehabilitation of the northbound lanes would require full-depth joint repairs, installation of subdrains, and diamond grinding, whereas the southbound lanes would require extensive slab and joint repairs, a structural overlay, or total reconstruction.

This project presents evidence that the installation of relief joints should be kept to a minimum when well-developed transverse cracks are present. An alternative to the installation of pressure relief joints in this case would have been to clean and reseal thoroughly the transverse joints and working cracks. The placement of full-depth repairs with load transfer devices and without expansion joints would have relieved any built-up pressure without allowing the adjacent cracks to open further. Where pressure relief joints were used, additional separation from full-depth repairs might have been desirable.

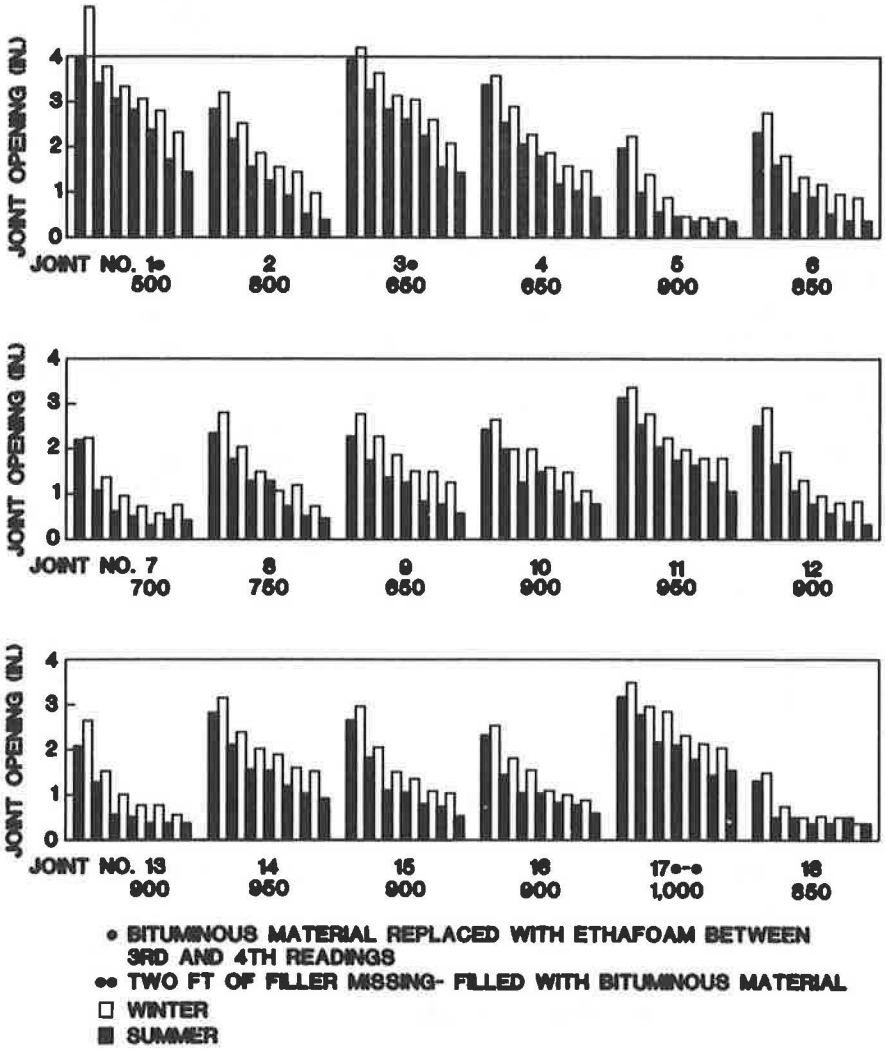

FIGURE 4 Summer/winter relief joint opening from 1973 to 1979 for U.S 127, Michigan (numbers below each joint indicate pavement length in feet contributing to joint closure) (*4*).

Nebraska, I-80, Milepost 189

The original pavement was a 9-in. JRCP with 46.5-ft contraction joints that was constructed and opened to traffic in 1965. Pressure relief joints 4.5 in. wide and filled with a preformed cellular joint filler were installed in 1981 at 2,000-ft intervals to reduce expansive pressures caused by reactive aggregate.

By 1985, the pressure relief joints had sustained about 4 million, 18-kip ESALs in the outer lane. The condition surveys conducted in 1985 showed extensive reactive aggregate distress, low- and medium-severity transverse cracking, poor joint sealant conditions, and medium-severity transverse joint and corner spalling. The remaining transverse contraction joints were faulted an average of 0.02 in. and were open an average of 0.3 in. An average Roughness Index of 120 (fair-good) was obtained by the Nebraska Department of Roads in 1985 using a Mays Ride Meter.

The pressure relief joints had closed to an average width of 0.8 in. and had faulted an average of 0.09 in., more than four times the contraction joint average faulting. The filler was still intact, and only low-severity spalling was observed. The adjacent contraction joints had not opened appreciably wider than the project average joint width. Figure 5 illustrates the closure of the pressure relief joints on this project over time, as measured by the Nebraska Department of Roads.

Analysis

The pressure relief joints were an appropriate measure taken to combat the compressive stresses caused by the reactive aggregate. This need for relief was evidenced by the amount of closure of the relief joints (average amount of closure, 3.7 in.). It is interesting, however, that the average amount of closure is approximately equal to the total amount that the intermediate contraction joints have opened (0.1-in. opening $\times$ 45 joints = 4.5 in.).

Overall, this rehabilitation project was considered successful. The pressure relief joints were probably an appropriate effort to reduce pressure damage caused by the reactive aggregate included in the original pavement. It should be noted, however, that the pressure relief joints did fault rapidly after placement and served to open adjacent contraction joints slightly.

Nebraska, I-80, Milepost 382

The original pavement was a 9-in. JRCP with 46.5-ft contraction joints. It was constructed and opened to traffic in 1962. Pressure relief joints 4.5 in. wide were installed in 1982 at 1-mile intervals to reduce the expansive pressures caused by reactive aggregate. A preformed cellular plastic filler was used to fill the joint. Several other rehabilitation techniques, including full- and partial-depth repairs and joint resealing, were applied concurrently.

By 1985, the pressure relief joints had sustained approximately 5 million, 18-kip ESALs in the outer lane. The condition surveys conducted in 1985 found low- and medium-severity transverse cracks at approximately 15- to 20-ft intervals, although some localized areas displayed transverse cracks at much closer intervals. Low-severity reactive aggregate distress was consistently identified throughout the condition surveys.

Incompressibles were observed in several of the original contraction joints; as a result, medium-severity transverse joint spalling and corner spalling were frequently found in both sections of the project. The average faulting and joint width measurements for the original contraction joints were 0.14 in. and 0.68 in., respectively, in the outer lane. An average Roughness Index of 191 (fair) was obtained in 1985 by the Nebraska Department of Roads using a Mays Ride Meter.

The pressure relief joints had closed to an average width of 1.3 in. and had faulted an average of 0.16 in. The filler was still partially intact in the relief joints; where it was absent, however, the joints contained incompressibles and spalling was observed. Contraction joints adjacent to the relief joints had opened little more than the average observed width of 0.68 in. Figure 6 presents a plot of the relief joint closure over time as measured by the Nebraska Department of Roads.

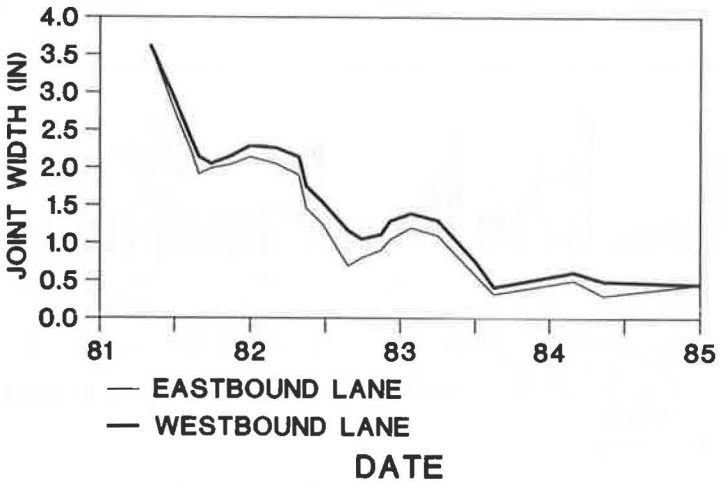

FIGURE 5 Pressure relief joint closure over time on I-80 in Nebraska (milepost 189) (*1*).

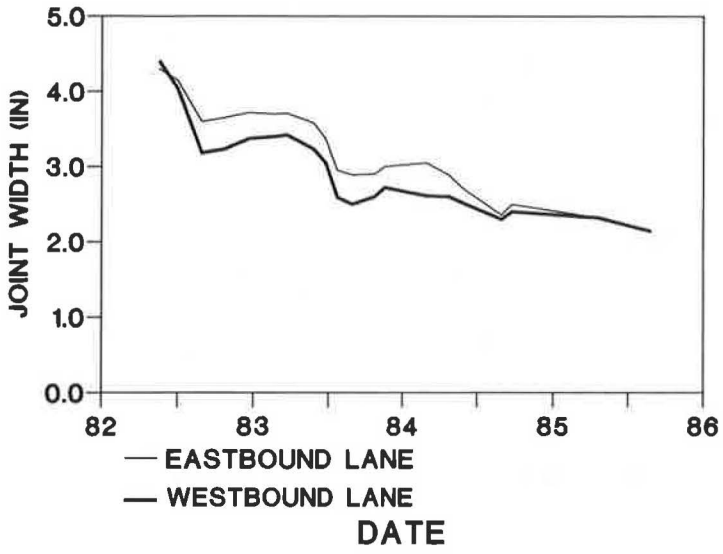

FIGURE 6 Pressure relief joint closure over time on I-80 in Nebraska (milepost 382) (*1*).

Analysis

The pressure relief joints that were installed on this project may not have been necessary. Although the aggregate used in the original pavement was somewhat reactive, it was not the highly reactive North Platte River gravel that had produced problems on other concrete pavements in Nebraska. In addition, any built-up pressure would have been relieved during placement of the full-depth repairs. Much higher rates of relief joint closure were observed on other Nebraska projects (e.g., at milepost 189, as previously described) where full-depth repairs were not placed concurrently with the relief joints.

While the use of relief joints on this project may have been questionable, their presence had apparently not affected the project adversely. The faulting and opening of adjacent contraction joints were average, and nearby slabs exhibited typical types and amounts of distress.

PRJs IN CONTINUOUSLY REINFORCED CONCRETE PAVEMENT

Ohio, I-270, Milepost 29

The original pavement was an 8-in., continuously reinforced concrete pavement (CRCP), constructed and opened to traffic in 1968. Asphalt concrete-filled pressure relief joints 4 in. wide were installed in 1983 at 2,000-ft intervals because of perceived pressure problems.

By 1985, the pressure relief joints had sustained about 1 million, 18-kip ESALs in the outer lane. A few edge punchouts and deteriorated transverse cracks were observed in the original pavement. A Roughness Index (GM Profilometer) of 112 (fair) and a Present Serviceability Index of 3.0 were computed by the Ohio Department of Transportation (ODOT) in 1984.

The pressure relief joints exhibited extensive joint spalling. Transverse cracks adjacent to the pressure relief joints had deteriorated from tight, nonworking cracks to spalled, working cracks. Punchouts were frequently located near the pressure relief joints.

Analysis

The installation of pressure relief joints on this project was inappropriate because any excessive compressive stresses in the pavement had probably been relieved by the blowups that had occurred. When CRCP is repaired, it appears unlikely that there will be a further buildup of stresses since tight cracks do not permit the infiltration of incompressibles. Further, the interruption of the continuous reinforcing steel resulted in premature deterioration of adjacent transverse cracks. If pressure relief was necessary, a better approach might have been to remove pavement sections for the placement of traditional CRCP repairs and leave these areas open for 24–72 hours. A properly constructed repair could then have been installed by carrying the steel through the repair to keep the cracks tight. This would also have reduced the possibility of loss of support caused by allowing water to enter a wide relief joint.

PRJs IN ASPHALT CONCRETE OVERLAID CONCRETE PAVEMENT

Kentucky I-65, Milepost 12

The original pavement was a 10-in. JRCP with 50.0-ft contraction joints, constructed and opened to traffic in 1966. Skewed pressure relief joints 6 in. wide were installed in 1982 at 1,000-ft intervals and filled with asphalt concrete. They were installed because blowups had previously occurred and additional pressure problems were anticipated. In addition, the original aggregate was known to be expansive. Six-inch perpendicular relief joints were also incorporated as approach or leave joints in some of the full-depth repairs that were placed as part of the preoverlay repair. The entire rehabili-

tation project received a 4.0-in. asphalt concrete overlay after the placement of the repairs.

By 1985, the relief joints had sustained approximately 4.5 million, 18-kip ESALs in the outer lane. About one-half of the original contraction joints had reflected through the overlay, whereas very few of the repair joints had reflected through. Rutting measurements in the outer lane averaged 0.13 in.

The condition surveys revealed that the pressure relief joints had reflected through the overlay and the overlay was "humped" above the relief joints, although the hump over one of the relief joints had been milled off. Only one of the three sections surveyed appeared to indicate a relationship between pressure relief joint location and the location of reflective cracks above contraction joints. In this section, more cracks of higher severity were observed near the relief joint than away from it. Overall, the rehabilitated pavement had performed well except for the roughness where the overlay had "humped."

Analysis

The pressure relief joints were probably appropriate for this project since many blowups had previously occurred and were expected to continue owing to the presence of expansive aggregate. It is possible, however, that the construction of full-depth repairs at blowup locations would have provided equal or better service without the localized roughness and risk of more rapid joint and overlay deterioration that often accompanies pressure relief joints.

Illinois I-55, Milepost 252

The original pavement was a 10-in. JRCP with 100-ft contraction joints, constructed and opened to traffic in 1956. Special "heavy-duty" expansion joints with dowels for load transfer were constructed in 1975 at 1500-ft intervals because blowups had occurred previously and future pressure damage was anticipated. The relief joints were 6-ft minimum length, full-depth concrete repairs, tied to the existing slab, that contained a 4-in. formed pressure relief joint incorporating dowel bars (see Figure 7). The repair/relief joint was constructed higher than the existing pavement so that the new asphalt concrete overlay could be constructed flush with the repair. A 3.5-in. asphalt concrete binder course was placed in late 1975, followed with a 1.5-in. asphalt concrete surface course in 1976.

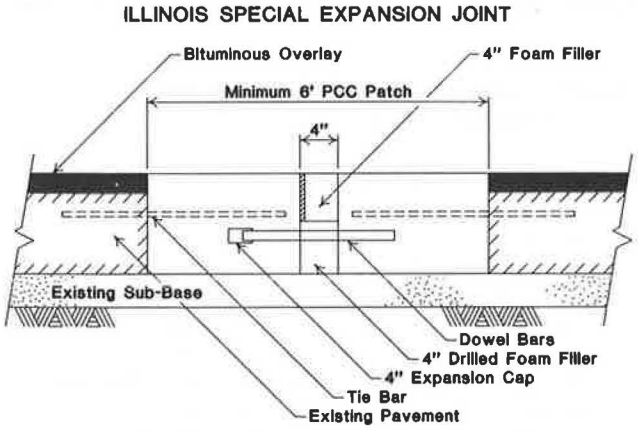

FIGURE 7 Illinois Department of Transportation heavy-duty pressure relief joint design (*1*).

The condition surveys performed on the project revealed medium-severity longitudinal cracking, transverse reflection cracking, and an average rut depth of 0.34 in. A Roughness Index of 75 (smooth) was obtained by the Illinois Department of Transportation in 1985 using a BPR Roughometer.

By 1985, the relief joints had sustained about 10 million, 18-kip ESALs in the outer lane. They had closed to an average width of 2.2 in. and had faulted an average of 0.08 in. While the relief joints themselves were not extremely rough, a significant bump could be felt when driving across the joint between the overlay and the concrete repair. The overlay had shoved and rutted at this location, significantly contributing to the overall pavement roughness.

Analysis

These "heavy-duty" pressure relief joints have performed well. They have withstood 10 years and approximately 10 million, 18-kip ESALs without exhibiting excessive faulting or significant spalling. While this relief joint design is expensive, it does allow a structural overlay of the pavement using asphalt concrete without the humping of the surface and loss of load transfer that often occur when more traditional relief joint designs are used. This relief joint design could also be used for nonoverlaid concrete pavements where relief joint load transfer is desired.

The need for pressure relief joints on this project was questionable since the relief joints had closed only 2.0 in. over 10 years. The placement of full-depth repairs probably relieved any pressure problems that existed at the time of overlay. The use of relief joints where they were not required may have resulted in premature reflection of the contraction and repair joints as they opened in response to the available expansion capacity of the pavement. In spite of this, the relief joints have performed very satisfactorily, and it cannot be determined that they have adversely affected the performance of the adjacent joints.

Indiana, I-69, Milepost 64

The original pavement was a 10-in. JRCP with 40-ft joint spacing, constructed and opened to traffic in 1964. Three-foot wide, asphalt concrete-filled pressure relief joints were installed in 1975 in five experimental sections using three different relief joint spacings: 1,000 ft, 500 ft, and 40 ft. One 0.5-mile section served as a control and contained no relief joints. The relief joints were installed because of bridge pushing, in anticipation of pressure buildup problems, and as part of state policy to prevent blowups of overlaid D-cracked pavements. A 4.25-in. asphalt concrete overlay was placed after the installation of the relief joints.

By 1985, the overlay and repairs had sustained approximately 6.1 million, 18-kip ESALs in the outer lane. All of the relief joints had reflected through the overlay, and many of these reflective cracks had begun to spall, particularly in the section with the short relief joint spacing (40 ft). It was

TABLE 3 "HUMPING" OF AC OVERLAY AT PRESSURE RELIEF JOINT LOCATIONS ALONG I-69 IN INDIANA (*1*)

	INNER LANE			OUTER LANE	
Section	Left Wheelpath Hump, in	Right Wheelpath Hump, in	Center Line Hump, in	Left Wheelpath Hump, in	Right Wheelpath Hump, in
01*	1.00	----	----	0.60	0.40
01	0.50	1.10	0.60	0.80	0.70
02	0.75	0.90	0.80	0.50	0.50
02	0.80	0.80	0.60	0.60	0.50
02	0.70	0.60	0.60	0.50	0.60
03	NO APPRECIABLE HUMPING OF PRESSURE RELIEF JOINTS				
Avg	0.75	0.85	0.65	0.60	0.54
Std. Dev.	0.18	0.18	0.10	0.12	0.11

*This relief joint had been milled off once.

also noted that there were more medium-severity transverse cracks in the vicinity of the relief joints, and these cracks were wider than those located farther away. This is indicative of the movement of the underlying pavement into the relief joints.

The asphalt overlay above the relief joints was generally humped as a result of the expansion of the pavement into the relief joint area. Table 3 summarizes the measured relief joint humping. Sections utilizing different relief joint spacings had different performance characteristics. Section 01 (1,000-ft relief joint spacing) had large "hump" measurements and slightly opened adjacent cracks. Section 02 (500-ft relief joint spacing) had slightly smaller "hump" measurements, but adjacent cracks were wider and spalled slightly. Both of these sections caused a fairly rough ride. Section 03 (40-ft relief joint spacing) was not humped, and the ride was noticeably smoother. However, the transverse reflective cracks above the relief joints had spalled rather severely, and there were many more deteriorated transverse cracks. The control section was not extensively cracked and performed relatively well.

Analysis

The use of pressure relief joints on this project resulted in varying degrees of pavement roughness due to "humping," reflective cracking, and deterioration of the overlay near the cracks. Deterioration of the overlay was most severe where the D-cracking of the original pavement had reflected through the overlay.

The placement of full-depth repairs would probably have reduced any pressure buildup in the pavement. Since the pavement was to be overlaid, however, it is likely that "D" cracking would rapidly have redeveloped outside of any full-depth concrete repairs, causing the overlay to deteriorate. Thus, the asphalt concrete overlay of this severely D-cracked pavement could be expected to provide good serviceability for only a short period of time, regardless of the preoverlay rehabilitation.

CONCLUSIONS

The following conclusions were drawn from the twenty-five individual pressure relief project summary reports (*1*).

1. The use of pressure relief joints was unwarranted on most of the projects surveyed and often caused more distress than would have been prevented.
2. The use of pressure relief joints was generally warranted on projects that included reactive aggregates in the concrete.
3. The unnecessary or excessive use of pressure relief joints often results in the excessive opening of adjacent cracks and contraction joints, the shearing of longitudinal joint ties, the premature failure of load transfer shear devices and of adjacent contraction joint sealant (particularly preformed compression seals), and the loss of load transfer and pavement support, resulting in increased pumping, faulting, corner breaks, and punchouts.
4. Pressure relief joints are not likely to be as detrimental to pavement performance when the existing pavement is free of working transverse cracks and only low volumes of heavy truck traffic are present.
5. The installation of full-depth repairs provides relief of built-up pressure and decreases the need for pressure relief joints in the vicinity of the repair.
6. Where used and constructed appropriately, pressure relief joints have been found to be effective in preventing the development of pressure damage for 3 to 7 years. New or additional joints must be considered when the old ones become ineffective.
7. The largest portion of relief joint closure occurs within the first year after installation.
8. Relief and expansion joints near secondary structures may provide relief as far as 2,000 ft away. Adjacent contraction joints exhibited greater widths and faults and higher incidences of sealant failure than more distant joints.
9. Pressure relief joints placed without load transfer devices fault rapidly.

10. The placement of a joint sealant material over the relief joint filler material improves retention of the filler material.

11. Blowups have about the same effect as pressure relief joints on the total movements at adjacent contraction joints.

12. Wide asphalt concrete-filled pressure relief joints installed in concrete pavements that are to be overlaid can result in "humping" of the overlay over the relief joint, deterioration of adjacent cracks and joints, and increased incidence and severity of reflection cracking. Larger relief joint spacings tend to produce less joint and crack deterioration and reflection cracking but larger "humps." Shorter spacings produce little "humping" but very high densities and severities of reflection cracking, including at the relief joint.

13. Foam-filled pressure relief joints installed in concrete pavements that are to be overlaid can result in deterioration of the overlay directly over the relief joint since the filler material provides no support to the overlay.

14. Overlays placed over pressure relief joints that have been in place for several years may perform well since much of the pavement movement will already have taken place.

15. Illinois DOT's "heavy-duty" pressure relief joints have performed well under heavy traffic, although excessive rutting produces considerable roughness at the transition between the asphalt concrete overlay and the concrete surface.

RECOMMENDATIONS

The following recommendations were developed based on the preceding findings and on the professional experience of the advisory panel members (*1, 2*).

1. In general, the installation of pressure relief joints is recommended only where reactive aggregates are present and a pressure buildup problem exists, or where an asphalt concrete overlay is to be placed over a concrete pavement that is expected to develop pressure buildup problems.

2. The installation of pressure relief joints in continuously reinforced concrete pavements is not recommended.

3. The installation of pressure relief joints is not recommended for pavements with short joint spacing except for protection of secondary structures.

4. The continued use of pressure relief and expansion joints to protect bridges is recommended for all pavement types.

5. Where blowups have occurred recently (not due to expansive or reactive aggregate), thus relieving pressure, joint cleaning and resealing should be considered as an alternative to pressure relief joint installation.

6. The use of pressure relief joints in pavements that are about to be overlaid is not generally recommended. However, it may occasionally be desirable to provide pressure relief joints in concrete pavements prior to placing asphalt concrete overlays. Candidate projects include those with long joint spacings and joints filled with incompressibles when the built-up pressure has not been relieved by blowups, repairs, or other pressure-relieving features. Asphalt concrete is recommended as the joint filler material for relief joints that are constructed in concrete pavements that will be overlaid.

7. Pressure relief joint placement (where appropriate) must consider the rate of pavement growth and the location and effectiveness of other pressure-relieving features.

8. Most new pressure relief joint widths should be limited to 1 to 2 in. to reduce the possibility and severity of over-relief of the pavement. New pressure relief joints should be placed at least 1,000 ft from active pressure-relieving features. Pavements with reactive aggregates may require greater relief joint widths or more frequent relief joint installations.

9. Sealant caps should be placed over the relief joint filler material in all narrow relief joints to help retain the filler and to keep incompressibles from infiltrating. The sealant cap should be recessed appropriately so that it does not extrude as the pavement closes.

10. Deep cleaning of joints and cracks with high-pressure water to remove trapped incompressibles followed by joint resealing should be tried on an experimental basis to relieve pressure buildup.

11. An alternative to the installation of nondoweled pressure relief joints is the placement of doweled full-depth repairs. Pressure relief might be accomplished either by leaving the repair open for 24 hours or by incorporating a narrow (1-in.) expansion joint at one repair joint.

12. An alternate approach to pressure relief in CRCP that could be tried experimentally is to remove small sections of the pavement (at typical relief joint intervals) and leave the repair hole open for 24 hours or more to allow the pavement to expand slightly before placement of a concrete repair.

13. The reservoir dimensions and sealant material properties of adjacent contraction joints should be checked prior to the installation of pressure relief joints to ensure that the expected movement of the joint will not cause the sealant to fail.

14. On an experimental basis, dowels placed in slots across a pressure relief joint may be tried to evaluate the performance and cost-effectiveness of providing load transfer across such a joint.

ACKNOWLEDGMENTS

This paper describes the results of a research study funded by the Federal Highway Administration. Many thanks are extended to the state highway engineers who served on the advisory panel: Emmitt Chastain of Illinois, Eugene B. Drake of Kentucky, Roger L. Green of Ohio, Vernon J. Marks of Iowa, Ken McGhee of Virginia, William Ramsey of Nebraska, Gary Robson of West Virginia, and Joseph Sudol of Indiana. Gratitude is also expressed for the assistance provided by the following state highway engineers: David Lippert of Illinois, Masood Rasoulian of Louisiana, Larry Scofield of Arizona, and Jens Simonsen of Michigan. Special thanks are also due to Michael Reiter and Kathleen Hall for their assistance in the data collection, evaluation, and report-writing activities.

Peter Kopac of the Federal Highway Administration served as contract manager on this project. The project team is grateful for his help in facilitating contacts with the advisory panel, reviewing volumes of material, and providing guidance and general assistance to the project.

REFERENCES

1. K. D. Smith, M. B. Snyder, M. I. Darter, M. J. Reiter, and K. T. Hall. *Pressure Relief and Other Joint Rehabilitation Techniques*. Final Report. ERES Consultants, Savoy, Ill.; FHWA, U.S. Department of Transportation, February 1987.

2. K. D. Smith, M. B. Snyder, M. I. Darter, M. J. Reiter, and K. T. Hall. *Pressure Relief and Other Joint Rehabilitation Techniques—Design and Construction Guidelines and Guide Specifications*. Appendix to Final Report. ERES Consultants, Savoy, Ill.; FHWA, U.S. Department of Transportation, February 1987.
3. M. Rasoulian and C. Burnett. *Evaluation of Relief Joints—Brush Fire C-51*. Research and Development Section, Louisiana Department of Transportation and Development, Baton Rouge, 1983.
4. J. E. Simonsen. *Preventive Maintenance of Concrete Pavements—U.S. 127*. Final Report No. R-1141. Michigan Department of Transportation, Lansing, 1980.

This paper is based on research performed under contract by the FHWA, U.S. Department of Transportation. The contents of this report reflect the views of the authors, who are responsible for the facts and accuracy of the data presented herein. The contents do not necessarily reflect the official view or policy of the Department of Transportation or the Federal Highway Administration. This paper does not constitute a standard, specification, or regulation.

Publication of this paper sponsored by Committee on Pavement Rehabilitation.

Rehabilitation Performance and Cost-Effectiveness: 10-Year Case Study

KATHLEEN T. HALL AND MICHAEL I. DARTER

This paper documents a 10-year case study of pavement rehabilitation performance conducted by the Illinois Department of Transportation. The pavement section, an 8-in., continuously reinforced concrete pavement on Interstate 57 south of Chicago, Illinois, was rehabilitated in 1978. Full-depth repair, epoxy crack sealing, undersealing, and underdrain installation were performed prior to placement of an asphalt concrete overlay. Combinations of these rehabilitation techniques were applied to six test sections on the project. The rehabilitation work was thoroughly documented, and the performance of the project over the past 10 years has been carefully monitored through visual surveys, nondestructive deflection testing, and photographs. The successes and failures of the rehabilitation techniques are described in this paper. A three-part analysis of the cost-effectiveness of rehabilitation was also conducted. Cost-effective rehabilitation is defined as appropriate and adequate repair performed at the appropriate time in the life of a pavement. The analysis investigates three components of this definition as it relates to this project: (1) what rehabilitation is appropriate, (2) how much preoverlay repair is adequate, and (3) the most appropriate time to place an overlay. The results indicate that, although the rehabilitation work performed on this project was appropriate and successful, it may not have been the most appropriate (i.e., most cost-effective) rehabilitation that could have been performed.

"Pay me now, or pay me, much more, later" has been stated many times to emphasize the cost-effectiveness of properly repairing and maintaining everything from automobiles to houses. The cost-effectiveness of keeping any engineering system in operation depends on performing appropriate repair at the right time. However, many highway and airfield pavements have been overlaid with little if any repair done to the existing pavement. This practice has been identified as the primary cause of the premature failure of many overlays. Many other pavements have received too little attention too late, going without repair long past the point at which rehabilitation can significantly extend their lives.

Reasons commonly given for these practices are lack of adequate funds and insufficient evidence that more extensive rehabilitation will significantly improve overlay performance. Very few well-documented studies exist to show clearly the long-term benefits of appropriate and timely rehabilitation.

This paper documents a case study conducted by the Illinois Department of Transportation (IDOT) over a 10-year period on a section of continuously reinforced concrete pavement (CRCP) located on Interstate 57 south of Chicago. This section was repaired and overlaid in 1978 (*1*). Several experimental techniques were included in the rehabilitation work, including epoxying deteriorated cracks, full-depth repairs of various designs (tied, welded, no reinforcement, and bituminous), and subsealing with cement grout and asphalt cement. Some cracks in various stages of deterioration were left unrepaired. An asphalt concrete (AC) overlay was placed after all repairs were made. The preoverlay condition and rehabilitation work performed have been thoroughly documented, and the performance of the project over the past 10 years has been carefully monitored through visual surveys, deflection testing, and photographs.

This paper describes the successes and failures of the rehabilitation effort. The results show the excellent performance of the overlay in areas where adequate preoverlay repair was performed, and the equally poor performance of the overlay in areas where insufficient preoverlay repair was performed. The performance results and cost analysis demonstrate both the importance of careful long-term monitoring of rehabilitation projects and the cost-effectiveness of timely, thorough rehabilitation.

Department of Civil Engineering, University of Illinois at Urbana-Champaign.

PROJECT DESCRIPTION

The project examined in this case study is a 6.6-mile section of four-lane rural Interstate 57 in northeastern Illinois. The project location and limits are shown in Figure 1. The section is an 8-in. CRCP with AC shoulders on a 4-in. cement aggregate mixture (CAM) subbase. The subgrade soil is a silty clay (A-6).

This section of I-57 was constructed in 1965 and opened to traffic in 1968; it was designed for 4.8 million, 18-kip equivalent single-axle loads (ESALs) over 20 years (two lanes, one direction). By 1978, it had carried approximately 5.2 million ESALs; that is, its actual traffic had exceeded its design traffic in less than half of its projected life. Not surprisingly, the pavement was showing considerable structural distress by this time, as shown by the following data:

	Northbound		*Southbound*	
Failures	*In 6.6 Mi*	*Per Mi*	*In 6.6 Mi*	*Per Mi*
Punchouts	10	1.5	6	0.9
Patches	46	7.0	33	5.0
Wide cracks	77	11.7	54	8.2
Total	133	20.2	93	14.1

The total number of failures per mile is very high in both directions and higher in the northbound than in the southbound lanes. Survey records show that the existing patches placed by maintenance crews were generally in very good

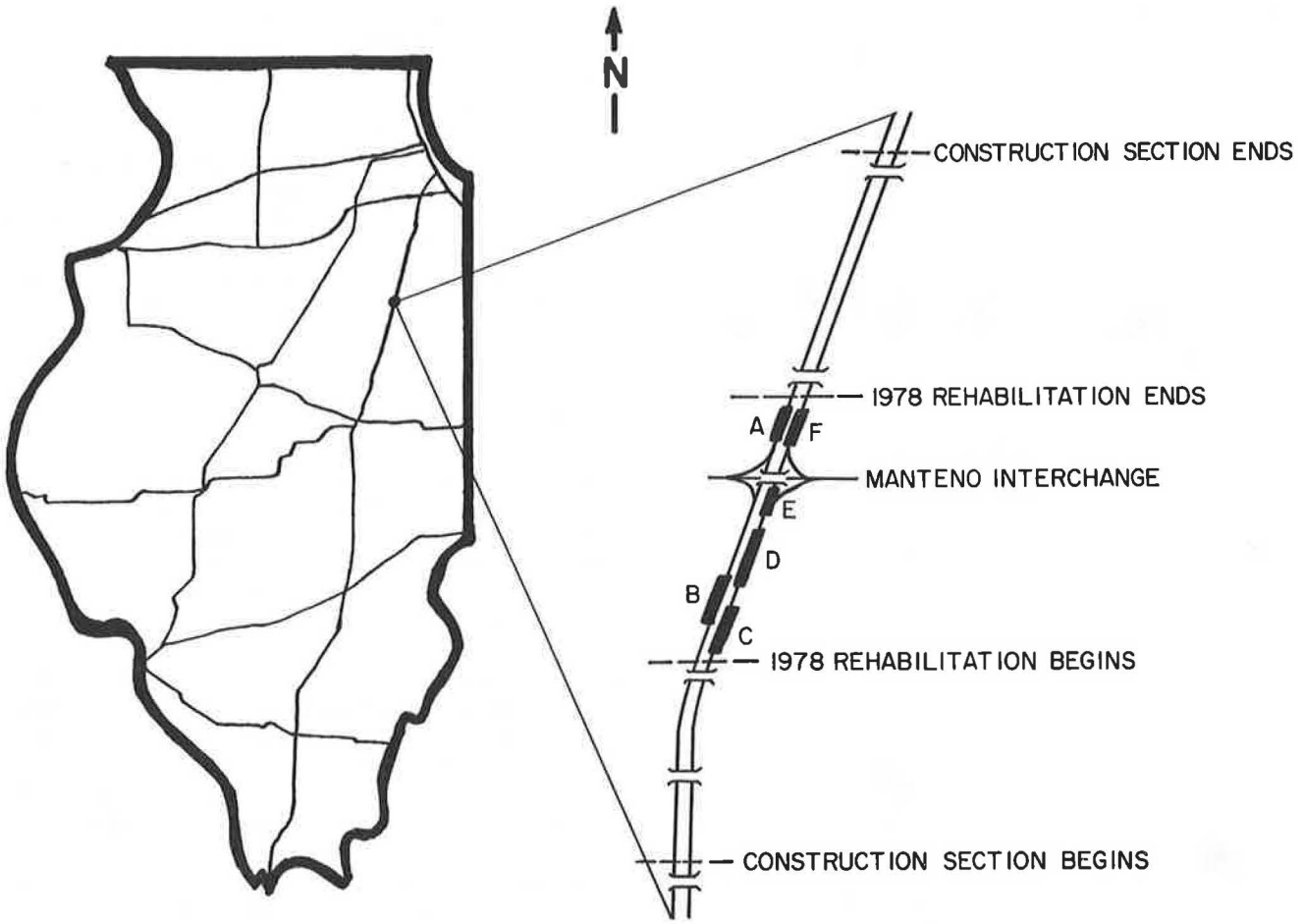

FIGURE 1 Location of I-57 Manteno rehabilitation project and test sections.

condition, although deterioration of the CRCP had occurred adjacent to many of them, requiring additional patching. Aside from the extent of structural damage evident in the preceding numbers, the quantity of unrepaired failures (punchouts plus wide cracks) gives an indication of the pavement's poor ride quality: 87 and 60 failures in the northbound and southbound lanes, respectively, or 13.2 and 9.1 failures per mile. Serviceability of CRCP tends to be poor when the number of unrepaired failures exceeds about 10 per mile.

Not included in the aforegoing quantities are failures in the CRCP adjacent to joints in the JRCP ramps. Such failures appear to be due to joints in the ramps opening and forcing otherwise tight cracks in the CRCP to open. Although not caused strictly by load, the cracks deteriorate rapidly under traffic. This distress is difficult to repair: often when such failures are patched, the ramp joint forces a crack in the patch. Failures adjacent to ramp joints have been frequent occurrences on many CRCP sections of the Illinois Interstate system built before 1967, when design specifications permitted CRCP to be built with either JRCP or CRCP ramps. Around 1967, the specification was changed to restrict ramps for mainline CRCP to be CRCP also (*2*). This section of I-57 at Manteno, however, was constructed prior to that time. During the 1978 distress survey, twenty failures adjacent to ramp joints were observed in the northbound lanes and nine in the southbound lanes.

The other major distress observed during the 1978 distress survey was pumping, which was rated as extensive in both directions. The pavement was not originally constructed with underdrains. The pumping, as well as the variability in condition along the project and between directions, suggests generally poor and possibly variable support, which is typical for the topography and soil of the area.

PREOVERLAY REPAIR AND AC OVERLAY

Based on the 1978 survey results, the Manteno section was selected to be among the first CRCP rehabilitation projects conducted in Illinois. Sufficient funds to repair the entire 6.6 miles of the project were not available, however, so the rehabilitation was limited to the middle 3.1 miles of the project in the vicinity of the Manteno interchange. Figure 2 illustrates that the majority of the distress was located in these middle 3.1 miles. The rehabilitation techniques applied are briefly described in this paper. Complete details are given elsewhere (*1*).

Test Sections

Within the rehabilitation project limits, six test sections were established to evaluate combinations of the techniques. The

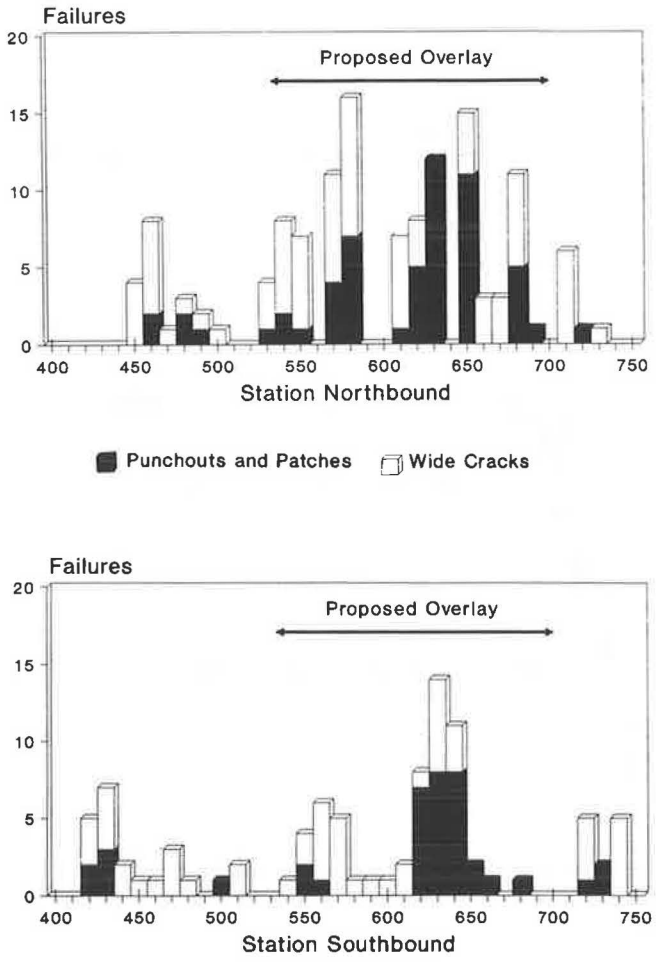

FIGURE 2 Distribution of distress along length of I-57 Manteno project.

locations of the test sections are shown in Figure 1. The length of each section and its condition before rehabilitation follow:

Section	*Direction*	*Length (ft)*	*Existing Failures*	*Existing Failures/Mile*
A	South	2,000	0	0.0
B	South	2,250	16	37.5
C	North	2,800	25	47.1
D	North	2,100	27	67.9
E	North	2,000	7	18.5
F	North	2,600	13	26.4
Total:			88	

Since the sections are of different lengths, failures per mile are given for comparison. Except for section A, which was chosen as a control section, the number of failures per mile is very high for all of the test sections, considerably higher than the average distress levels over the project reported before. This is a reflection of the earlier statement that the middle portion of the project that was rehabilitated was in much worse condition than the two end portions. Note also that the sections vary widely in condition, which is a reflection of the variability in condition even within the rehabilitation project limits. Section D, for example, has almost four times as many failures per mile as section E.

Deflections were measured within the test sections before rehabilitation with IDOT's heavy-load Road Rater. A statistical analysis of the deflection data showed that failure occurrence within a test section was not well correlated with mean deflection but was strongly correlated with the coefficient of variation of deflections (*1*). This was explained by way of the analogy of a chain being only as strong as its weakest link. High variability in deflections within a test section indicates that many localized areas have deflections considerably higher and considerably lower than the section average. Localized areas with unusually high deflections are prime locations for structural failure.

Full-Depth Repairs

The standard IDOT design for CRCP full-depth repair in 1978 was PCC with reinforcing steel tied into the existing slab with 36-in. laps on each side. The specified minimum repair length was 10 ft. Design details are shown in Figure 3. Several such repairs, placed by maintenance crews, were already in place on the project.

Two experimental, full-depth repair designs were developed and tested on this project. The first design used 20-in. tied laps, and the second used two 4-in. welded laps, together with a 16-in. tied center lap. Details for the two experimental repair designs are shown in Figure 4. The purpose of both designs was to reduce the cost of a repair by reducing repair size and lap length. The specified minimum length for the 20-in. tied-lap repair was 5 ft, and the minimum for the 4-in. welded-lap repair was 3 ft. The shorter repair lengths reduce the material costs for the repairs. More important, however, is that the shorter lap lengths greatly reduce the length of concrete that must be broken out by hand around the existing reinforcing steel. That process is a very labor-intensive and time-consuming task that adds quite a bit to the cost of full-depth repair for CRCP.

Two less expensive repair designs were also used in a few locations. One was PCC in which the repair itself contained no reinforcement, although the reinforcement in the existing slab extended about 10 in. into the repair area on both sides. Partial extension of the reinforcement into the repair area contributes to load transfer across the repair joints; since the steel is not carried through the repair, however, continuity of the CRCP is not restored, and repair or repair-adjacent distress is more likely. This repair design is not well suited for

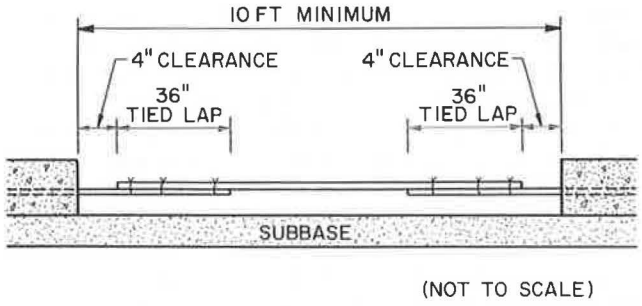

FIGURE 3 Design details for IDOT's old standard CRCP repair with 36-in. tied laps.

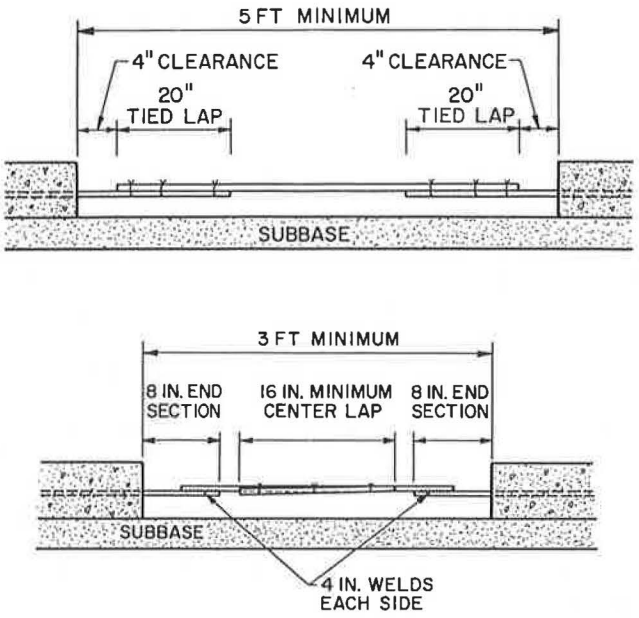

FIGURE 4 Design details for experimental CRCP repairs with 20-in. tied and 4-in. welded laps.

CRCP except for short-term use, as in the case of a severely deteriorated pavement that will be replaced within a few years. The Illinois DOT has placed a number of these unreinforced PCC repairs on CRCP under these circumstances with satisfactory results (*3*).

The second type of inexpensive repair used was full-depth AC. This repair design provides neither continuity nor load transfer and is therefore highly susceptible to repair or repair-adjacent distress. Furthermore, expansion of the CRCP into the repair area in hot weather can compress the AC and create a sizeable hump, which reduces serviceability and may even pose a safety hazard. Full-depth AC is not well suited for repair of CRCP, except for temporary use, as in the case of a blowup (*3*).

Of the 88 repairs placed on the project, 45 were located within the test sections: 30 welded repairs, 10 tied repairs, 2 unreinforced repairs, and 3 full-depth AC repairs. The test sections also included 11 old (36-in. tied-lap) repairs placed by maintenance crews. Welded repairs were placed in test sections B, C, and D; and tied repairs were placed in sections E and F. No repairs were placed in section A. Repair locations are given in Table 1.

Epoxied Cracks

Since funds for this project were limited, full-depth repairs were placed only at punchouts and at high-severity, deteriorated transverse cracks. The remaining deteriorated cracks were repaired with epoxy. The intent of the epoxy treatment was to bond the sides of the cracks back together and restore continuity to the slab at a much lower cost than that of full-depth repair.

Cracks were prepared for epoxy sealing by airblasting. The epoxy was a two-component, high-modulus, moisture-insensitive material, mixed in small quantities at the locations where it was used. It was applied to the cracks in two steps. The

TABLE 1 SUMMARY OF REHABILITATION WORK DONE IN TEST SECTIONS

	A	B	C	D	E	F	Total
Welded FDRs	0	8	15	7	0	0	30
Tied FDRs	0	0	0	0	1*	9	10
AC FDRs	0	0	1	1	1	0	3
No-steel FDRs	0	1	0	0	1	0	2
Existing FDRs	0	0	1	6	4	1	11
Epoxied Cracks	0	7	8	17	5	6	43
Unrepaired Cracks	0	0	1	1	0	0	2
Undersealing	NO	NO	CG	AS	CG	AS	
AC Overlay	YES	YES	YES	YES	YES	YES	

* Four tied repairs placed adjacent to ramp joints are not included.

** CG = cement grout undersealing
AS = asphalt cement undersealing

first application was epoxy alone, to coat the crack walls. For the second application, the epoxy was mixed with an oven-dry silica filler to fill up the cracks.

Undersealing

Undersealing was done in both lanes to fill voids under the pavement that were indicated by pumping and located by deflection testing. Two materials were used for undersealing: cement grout and asphalt cement. Blanket undersealing was performed in areas in poor condition overall. Selective undersealing was performed in areas in better condition, at specific locations identified by observed pumping and high deflections.

Underdrains and AC Overlay

After the preoverlay repair work was completed, pipe underdrains were placed on both sides of the pavement throughout the length of the project, and a 4-in. AC overlay was placed on the lanes and shoulders.

10-YEAR PERFORMANCE RESULTS

Five sets of data have been collected on the condition of the project at different times: in 1978 just before and just after the overlay was placed, at 10 months (1979), at 5 years (1983), and at 10 years (1988). Visual condition surveys were performed, and all distresses observed within the test sections were mapped and photographed. Strip maps showing test section limits, stationing, and exact locations of all full-depth repairs and epoxied cracks were used for mapping distresses and recording the locations of all photographs taken. Nondestructive deflection testing was performed by IDOT personnel with the IDOT Road Rater, at locations marked out by the project team. Deflections were typically taken at 50-ft intervals to coincide with stations along the project length. In several selected locations of interest (e.g., in the vicinity of a full-depth repair or epoxied crack showing significant distress) a series of closely spaced deflections was taken.

Performance of Full-Depth Repairs

The welded and tied repairs have both given excellent performance. Only two welded repairs and one tied repair have failed (as evidenced by high-severity reflective cracking) at the present time and need to be replaced. The only other reflective cracking associated with the repairs is of low severity. The performance of the various types of repairs is summarized in Table 2.

The performance of the welded repairs is illustrated by the series of photos in Figure 5. The first photo was taken in 1978 at a deteriorated construction joint. The pavement had actually blown up in the inner lane and been temporarily patched with AC. The next two photos were taken at the same location just after welded repairs P30 and P31 had been placed. The last photo was taken in 1988.

These photos illustrate the excellent performance of the welded repairs. The performance of the tied repairs has also been excellent. Throughout the test sections, 80 percent of the welded repairs (24 of 30) and 70 percent of the tied repairs (7 of 10) have not reflected through at all in 10 years. Likewise, 91 percent (10 of 11) of the old tied repairs, which are all more than 10 years old, have not reflected through. This clearly demonstrates that tied or welded repairs can be placed on CRCP without causing subsequent reflective cracking in an AC overlay.

The less expensive repairs have not performed well. Two of the three full-depth AC repairs have experienced rutting and shoving as well as reflective cracking. Figure 6 provides a series of photos taken where full-depth AC repair P60 was placed. The first photo shows a working crack to be repaired. The newly placed AC repair is shown in the second photo, taken in 1978. The third and fourth photos were taken during the 1983 and 1988 surveys.

One of the unreinforced PCC repairs is intact and exhibits no distress at this time, but the other one has caused a medium-severity reflective crack at one joint. This is better perfor-

TABLE 2 PERFORMANCE OF FULL-DEPTH REPAIRS IN TEST SECTIONS

	DISTRESS SEVERITY				
REPAIR TYPE	NONE	LOW	MEDIUM	HIGH	TOTAL
36-inch tied PCC	10	1	0	0	11
20-inch tied PCC	7	2	0	1	10
4-inch welded PCC	24	4	0	2	30
Unreinforced PCC	1	0	1	0	2
Full-depth AC	1	0	0	2	3

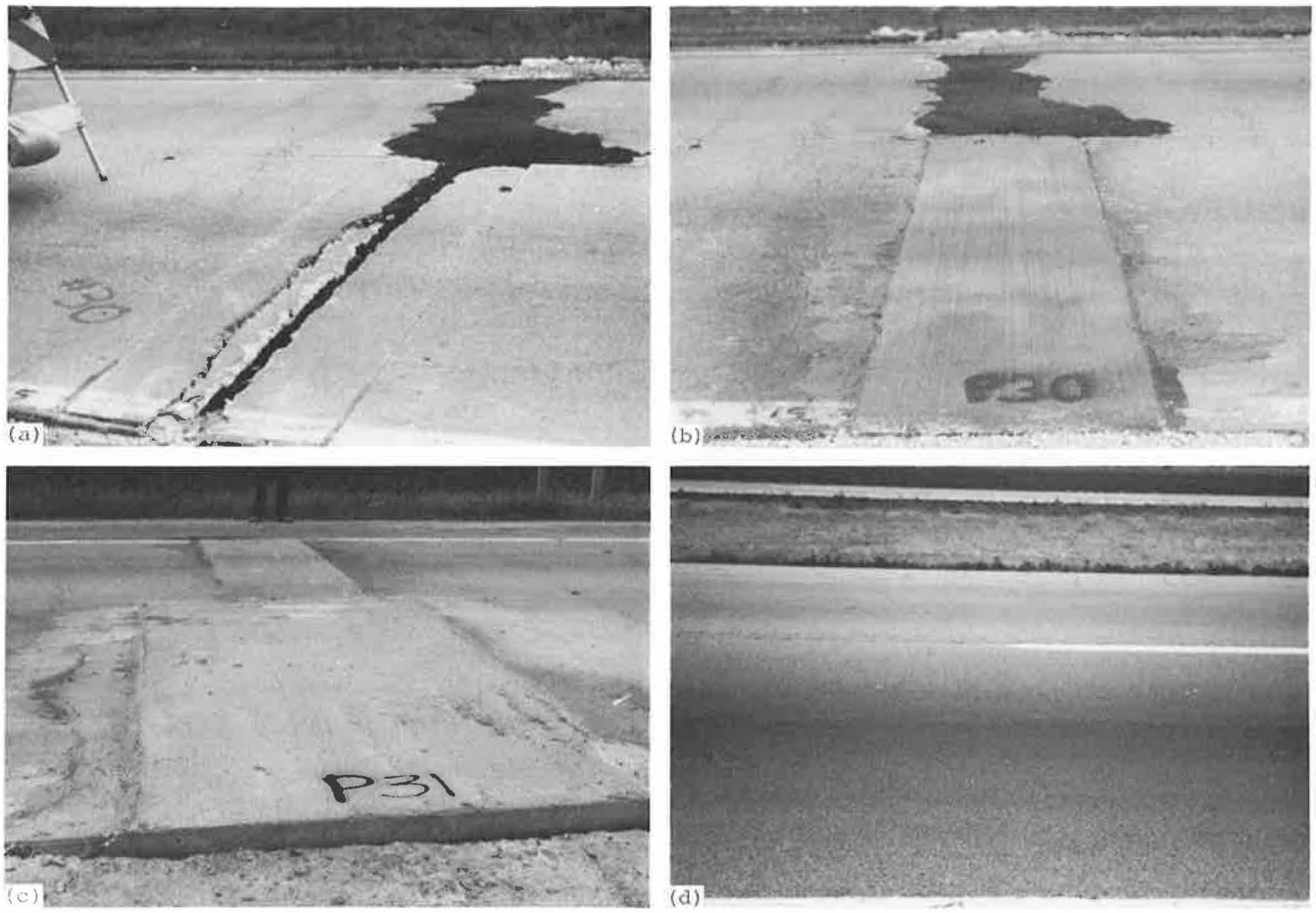

FIGURE 5 Performance of welded full-depth repairs. (a) Deteriorated construction joint before repair. (b) Welded repair P30 placed in outer lane. (c) Welded repair P31 placed in inner lane. (d) No reflection cracking in overlay in 1988.

mance than was expected from the unreinforced PCC repairs but still is not satisfactory.

Performance of Epoxied Cracks

The crack-epoxying treatment did not perform as intended. Even before the overlay was placed in 1978, observers noted that the epoxy bond had failed at many of the cracks within 2 days to 3 weeks after treatment. Some had failed at the epoxy-concrete interface, which may have been due to insufficient cleaning of the sides of the cracks. Many others, however, had failed within the epoxy, suggesting it was not capable of withstanding the large horizontal movements resulting from daily temperature cycling in the CRC slab. Figure 7 shows a series of photos taken at epoxied crack E4. The first photo was taken in 1978 before the crack was filled. The second photo was taken during the 1979 survey (10 months after the overlay was placed) and shows the low-severity reflected crack that had already come through the overlay. The third and fourth photos, which were taken during the 1983 and 1988 surveys, show the progression of the reflected crack to medium and high severity.

The AC overlay reduced deflections at the epoxied cracks, but the deflections have gradually increased as the cracks have reflected through, as illustrated by the deflection profile for a typical epoxied crack shown in Figure 8. The rate at which the epoxied cracks have reflected through the overlay is illustrated in Figure 9.

Effect of AC Overlay on Deflections

The 4-in. AC overlay reduced mean deflections in the six test sections to an average of 55 percent of their preoverlay levels. The mean deflections have gradually increased over time, however, as illustrated in Figure 10, and are now, on average, at 88 percent of their preoverlay levels. The following is a comparison by test section of preoverlay deflections and 1988 deflections:

Section	*Mean Deflection Before Overlay*	*Mean Deflection in 1988*	*Percent of Preoverlay Deflection*
A	7.74	5.43	70
B	10.05	6.16	61
C	7.82	6.80	87
D	6.17	6.55	106
E	5.50	5.09	92
F	7.02	7.90	113

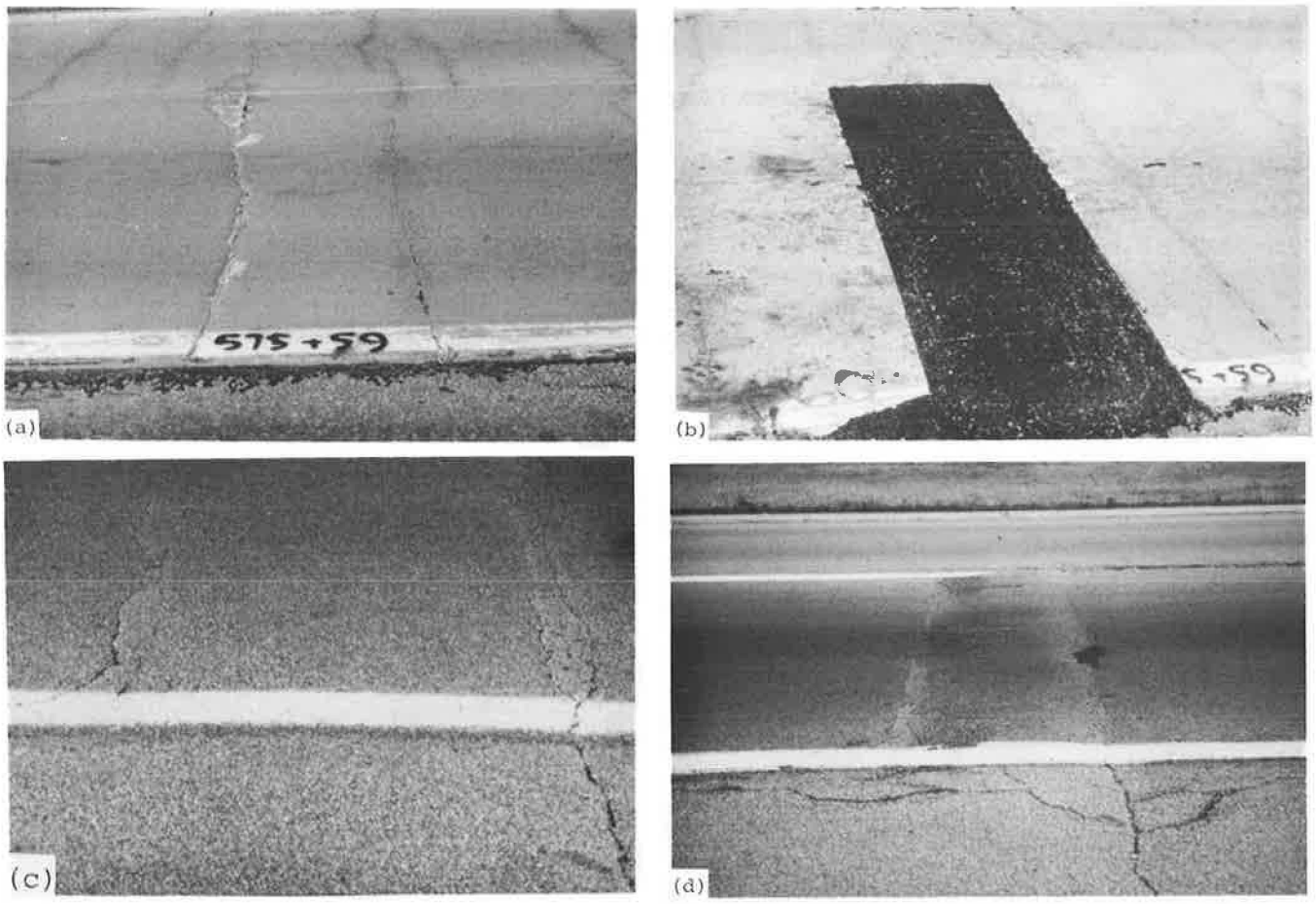

FIGURE 6 Performance of full-depth AC repair. (a) Wide transverse crack before repair. (b) Full-depth AC repair P60 placed in outer lane. (c) Reflection cracking in 1983. (d) Reflection cracking in 1988.

Mean deflections (reported in mils) were taken at 50-ft intervals with the IDOT Road Rater using a 5-kip, 15-Hz load.

Averaging the results from the six test sections together, deflections have steadily increased since 1978, which suggests that progressive deterioration of the overlay and/or underlying concrete slab is taking place. However, the pavement does not appear to have experienced any "new failures" since the overlay was placed. After 5 years (1983), 15 medium- and high-severity reflective cracks not associated with underlying full-depth repairs or epoxy crack treatments were observed in the six test sections, but only those same fifteen cracks were rated at medium or high severity during the 1988 survey. It is likely, therefore, that those cracks were low- to medium-severity cracks that were not repaired in 1978 before the overlay was placed. Despite the nearly 5 million ESALs applied to the pavement between 1983 and 1988, fatigue damage has not yet been manifested in any additional cracking.

Reflective Crack Occurrence

An examination of the data by test section shows that reflective crack occurrence on the overlay after 10 years of service is a function of (1) the number of high-severity failures full-depth repaired prior to overlay, (2) the number of low- to medium-severity cracks not repaired prior to overlay, and (3) whether or not undersealing was performed.

Section	*Preoverlay Full-Depth Repairs/Mi*	*Preoverlay Unrepaired Failures/Mi*	*Undersealed*	*Reflective Cracks/Mi After 10 Yr*
A	0.0	0.0	No	0.0
B	3.4	3.4	No	7.2
C	8.5	5.3	Yes	2.6
D	5.2	7.2	Yes	1.6
E	1.9	2.3	Yes	0.8
F	4.4	3.0	Yes	1.0

The relationship among these factors is expressed by the following multiple regression equation:

$$\text{REFCRK} = 2.18 + 0.42\,\text{FDR} + 0.42\,\text{CRACKS} - 4.67\,\text{UNDERSEAL}$$

where

REFCRK = deteriorated reflection cracks per mile in AC overlay;
FDR = number of full-depth repairs placed per mile;
CRACKS = number of previously unrepaired cracks per mile;

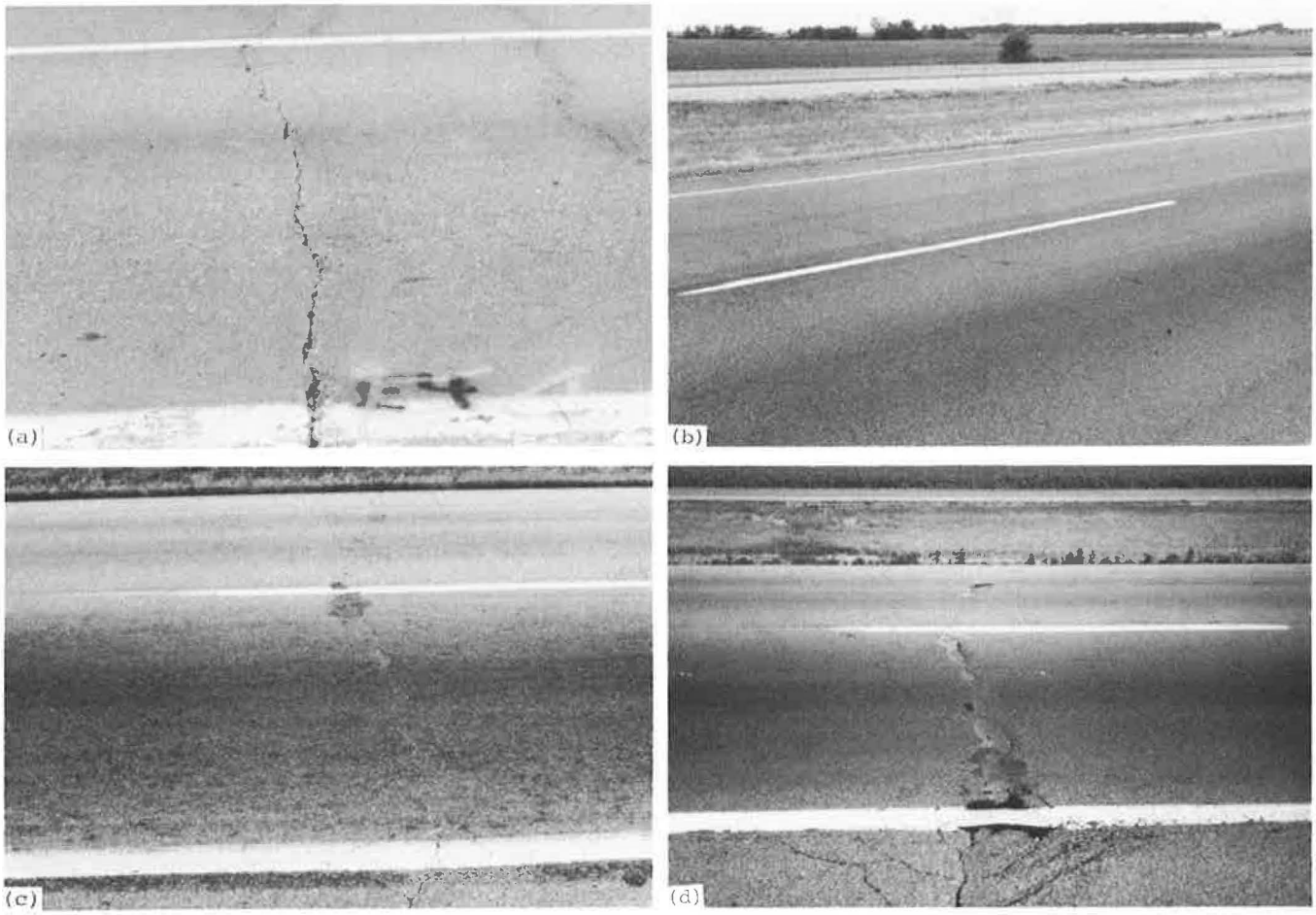

FIGURE 7 Performance of epoxied cracks. (a) Wide transverse crack before repair. (b) Reflection cracking at epoxied crack E4 after 10 months. (c) Reflection cracking at E4 in 1983. (d) Reflection cracking at E4 in 1988.

UNDERSEAL = 0 if no cement grout or asphalt undersealing done and = 1 if cement grout or asphalt undersealing done;
R^2 = 0.60; and
SEE = 2.6 failures/mile.

Effect of Undersealing

The regression equation demonstrates that undersealing had a substantial impact on the occurrence of reflective cracking in the overlay. Type of undersealing did not enter significantly into the regression analysis; that is, no significant difference was found in terms of reflection cracking between cement grout undersealing and asphalt undersealing.

Asphalt undersealing in test sections D and F was found in the 1978 preoverlay survey actually to increase rather than decrease deflections. This was attributed to pumping too much asphalt, which resulted in lifting of the slab and may have created new voids or enlarged existing ones. Regardless of this effect of asphalt undersealing on preoverlay deflections, however, a statistical analysis of preoverlay versus postoverlay deflections was dominated by the substantial reduction in deflections achieved by the AC overlay (*1*). After the overlay was placed, there was no significant difference between the reduction in deflections for control sections and asphalt undersealed sections.

The cement grout undersealing performed in sections C and E was found in the 1978 preoverlay survey to reduce above-average deflections in the vicinity of failures but had little or no effect on average and below-average deflections. This was taken as evidence that blanket undersealing is not as cost-effective as selective undersealing of areas with particularly poor support. As with the asphalt undersealed sections, the substantial reduction in deflections resulting from the AC overlay was not significantly different in the cement grout undersealed sections than in the control sections (*1*).

Effect of Underdrains

Because underdrains were placed throughout the entire rehabilitation project length, including the control sections, it is not possible to compare the actual performance of the rehabilitated pavement with drains to what it would have been without drains. Visual observations, however, attest to

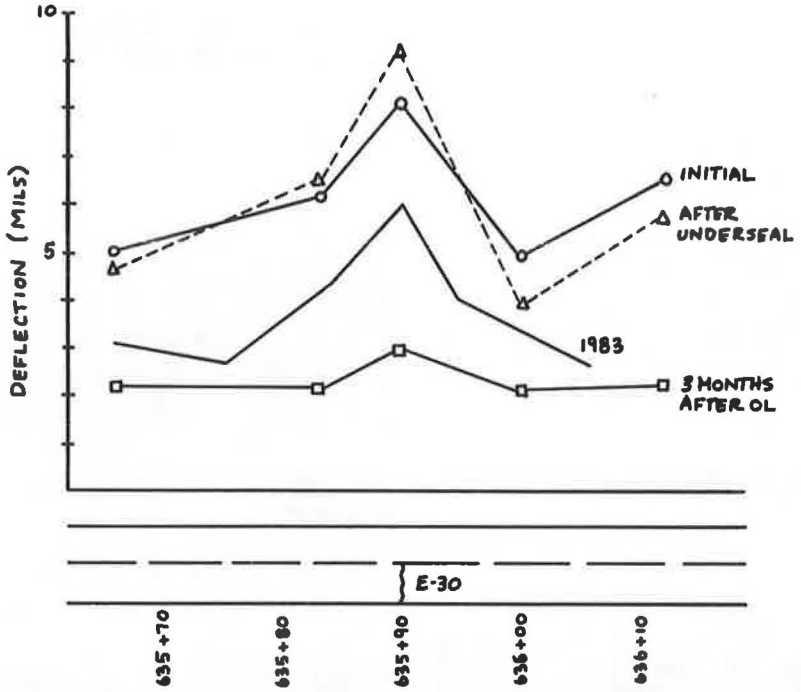

FIGURE 8 Deflection profiles at epoxied crack.

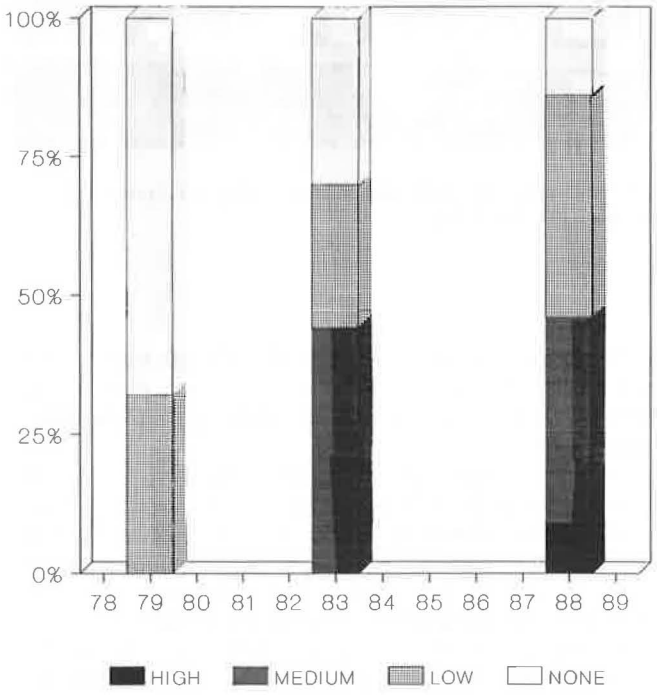

FIGURE 9 Reflective cracking of epoxied cracks.

improved drainage conditions. Immediately after the underdrains were installed, water was observed flowing from the drainage outlets. The drains were observed to be functioning during the 1988 survey, although the need for cleaning some outlets was noted.

More significantly, extensive pumping was observed on the project during the initial distress survey of the project in 1978, but no visible evidence of pumping was noted during the 1988 survey. The fact that this pavement had experienced extensive pumping for the first 10 years of its life before rehabilitation, but that no pumping was observed 10 years after the pavement was rehabilitated, demonstrates that the rehabilitation arrested most of the erosion that was occurring before. However, whether the erosion would have been halted by the undersealing and AC overlay alone, had the drains not been placed, is impossible to say.

COST-EFFECTIVENESS OF REHABILITATION

The cost-effectiveness of rehabilitation depends on performing appropriate and adequate rehabilitation at the appropriate time in the life of the pavement. This raises the following questions:

1. How does repair plus an overlay compare in cost-effectiveness with repair only?
2. What quantity of preoverlay repair is most cost-effective?
3. What is the most appropriate time to perform rehabilitation to maximize cost-effectiveness?

A quantitative comparison of the relative cost-effectiveness of different rehabilitation alternatives requires the selection of an analysis period to serve as a frame of reference. The results of such a comparison are necessarily dependent upon the length of time arbitrarily selected for that analysis period. The analysis period selected for this study was 20 years, from 1978 to 1998. A discount rate (interest minus inflation) of 3 percent was used in the analysis. This value was selected after consulting a recent *NCHRP Synthesis* on life-cycle cost analysis (*4*).

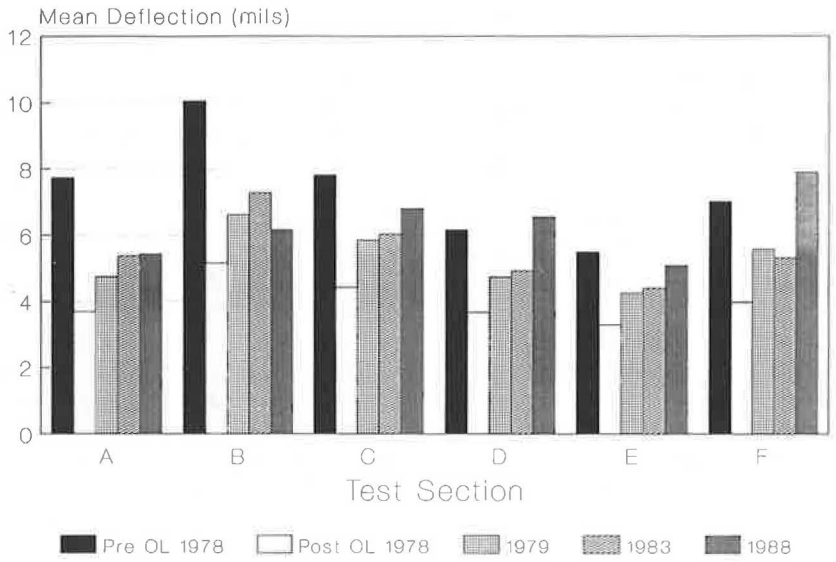

FIGURE 10 Effect of AC overlay on mean deflections in test sections.

Cost-Effectiveness of Overlay Versus Full-Depth Repair

The first of the three questions addressed is the relative cost-effectiveness of repair alone versus the repair plus overlay actually performed.

In 1978, maintenance records were examined to determine how much full-depth repair had been performed on the project in each year since its construction (*1*). The relationship of cumulative area repaired to cumulative 18-kip ESALs was found to follow closely a log-normal distribution, as shown in Figure 11. This is not surprising, since the full-depth repair requirements reflect the rate of deterioration, which accelerates as fatigue damage accumulates.

In 1983, the projected rate of deterioration was verified by determining the percent area repaired in the two end sections of the original project that had not yet been overlaid. These sections have since been overlaid, unfortunately, so it was impossible to check the actual versus the predicted percent area repaired during the 1988 survey. The good fit of the curve to the data through 1983, as shown in Figure 11, is considered to be sufficient for validation.

On the basis of this deterioration curve, it is possible to project the future hypothetical repair needs (in square yards) through 1998 for the middle portion of the project if a repair-only strategy had been adopted. These repair requirements can be translated into repair costs. The actual unit cost of CRCP full-depth repair in 1978 was $100 per square yard. Using a discount rate of 3 percent, all repair expenditures up to 1978 were converted to equivalent 1978 costs. Then, using the log-normal deterioration curve, predicted repair needs for each year through 1998 were computed and their costs converted to equivalent 1978 costs. Based on IDOT's prior experience with tied repairs on nonoverlaid CRC pavements, the life of a full-depth repair was assumed to be 5 years.

The cumulative total of the full-depth repair costs incurred over the analysis period is given by the 1978 present worth (PW) of the repair-only alternative, which can also be expressed

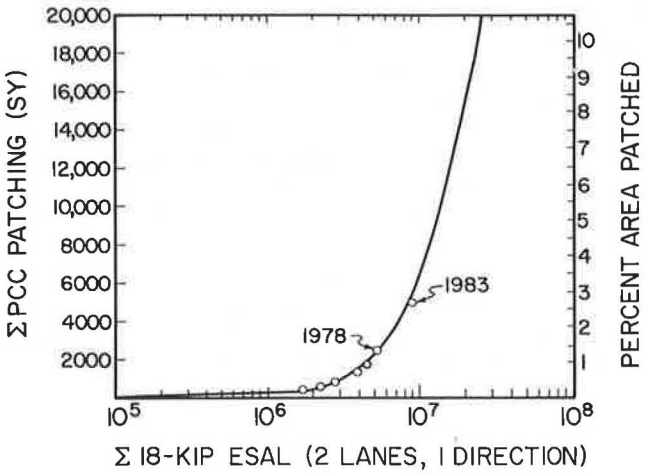

FIGURE 11 Log-normal relationship of cumulative repair requirements to cumulative traffic.

as an equivalent uniform annual cost (EUAC) over the analysis period, as shown below:

Alternative	*Repair Only*
1978 PW	$ 1,030,684
20-yr EUAC	$ 69,278

The repair-plus-overlay alternative had the same cumulative cost up to 1977 as the repair-only alternative. The techniques performed in the rehabilitation effort had the following 1978 costs:

Activity	*Cost* ($)
AC overlay	699,926
Underdrains	137,738
Full-depth repair	67,814
Cement undersealing	32,600
Asphalt undersealing	14,220
Epoxy cracks	5,892
Total	958,190

No rehabilitation work was performed on the project between 1978 and 1988. The 1988 survey showed that the project had an immediate need for 790 yd^2 of full-depth repair to repair medium- and high-severity, reflective cracking caused by repair deterioration, failed epoxied cracks, and previously unrepaired failures. The unit cost of full-depth repair now that the 4-in. overlay is in place was assumed to be increased by 20 percent over the cost of repairing bare 8-in. CRCP.

The future repair needs through 1998 can be estimated by drawing some inferences from the observed performance through 1988. With respect to the repairs that currently show no reflective cracking (after 10 or more years of service and approximately 5 million ESALs), the following assumption is made: since these repairs appear to have been completely successful at restoring the continuity of the CRC slab, they are not expected to exhibit any reflective cracking over the remainder of the analysis period. The repairs that are exhibiting reflective cracking were unsuccessful in completely restoring slab continuity and load transfer. The repairs that currently have low-severity reflective cracking may progress to medium and high levels of cracking but at a rate that is uncertain. They do not warrant repair now, but it is difficult to imagine them withstanding 10 more years of traffic before reaching medium- to high-severity levels of cracking. For purposes of this analysis, it was assumed that they would require repair in 1993, or halfway through the time remaining in the analysis period. Likewise, it was assumed that the epoxied cracks that currently exhibit low-severity reflection cracking will need to be repaired in 1993. As Figure 9 illustrates, 14 percent of the epoxied cracks still have not reflected through in 10 years. Most of these were at the outer edge of the traffic lane and were typically less than 6 ft long. These are not expected to reflect through before 1998.

The third potential need for future repair is new failures (not associated with existing repairs, epoxied cracks, or currently unrepaired cracks) that may arise from fatigue damage in the CRC slab. It is evident from the 10-year performance results that the AC overlay substantially reduced deflections and slowed the rate of failure. Of course, fatigue damage is still accumulating in the pavement, and the rate of development of new failures will likely accelerate in the same manner as (albeit much more gradually than) deterioration of the original slab accelerated from construction through 1978. As described previously, no new failures appear to have occurred in the 10 years since the rehabilitation was done. If a relationship does exist between new failures after overlay and traffic or time, it evidently has a very flat slope as of 1988. It is not anticipated that any significant quantity of full-depth repair due to new failures will be needed between now and the end of the analysis period.

The costs of full-depth repair in 1988 and 1993 were converted to equivalent 1978 costs and added to the cumulative total cost of this alternative. The 1978 present worth (PW) and equivalent uniform annual cost (EUAC) of the repair-plus-AC overlay alternative are shown below:

Alternative	*Repair + Overlay*
1978 PW	$1,156,061
20-yr EUAC	$77,705

Over the 20-year analysis period, the repair-plus-overlay alternative (EUAC = $77,705) appears to be less cost-effective from an agency cost standpoint than the repair-only alternative (EUAC = $69,278). This is illustrated by the accumulation of costs associated with the two alternatives shown in Figure 12. Several points must be made, however, before drawing any conclusions about the relative cost-effectiveness of the two alternatives.

- The overlay is in good condition with respect to reflective cracking but may or may not last the remainder of the analysis period. Rutting of the overlay is currently between ¼ and ⅜ in. and may reach an unacceptable level (½ in.) before 1998. The possible need for a second overlay or a milling operation in the future is not included in this analysis.
- Because the repair-only alternative was not actually done, its performance, in terms of years of pavement life extension

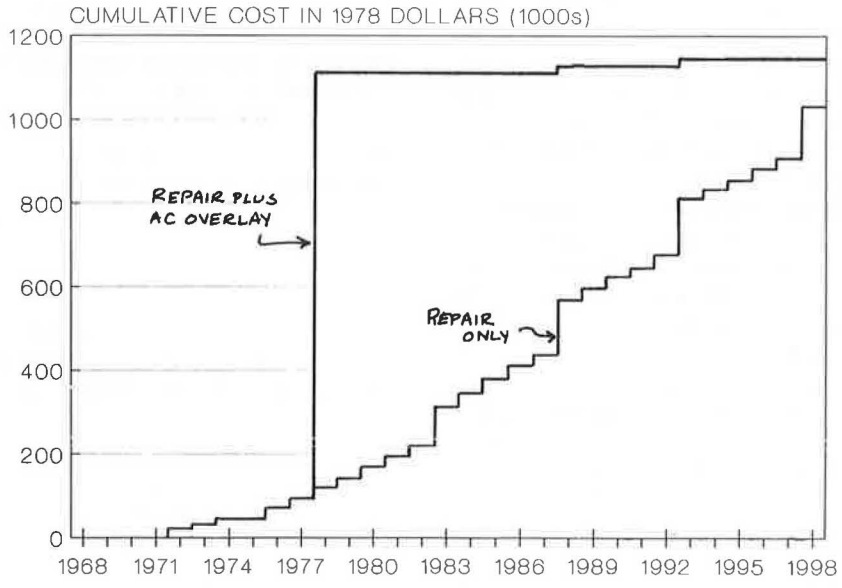

FIGURE 12 Cumulative costs of repair-plus-overlay and repair-only alternatives (in 1978 dollars).

provided before additional major rehabilitation would have been needed, is difficult to assess. Continual patching of a deteriorating pavement without placement of an overlay will at some point result in an unacceptably rough pavement surface. This point might well have occurred before the end of the 20-year analysis period, had this alternative actually been selected.

- This is an analysis of agency costs only, not a cost-benefit analysis, and does not consider some important factors in addition to agency expenditures, such as user costs associated with lane closure time, roughness, and accidents.

Whenever two hypothetical alternatives are equal in *cost*, the one that has kept the pavement condition at the highest average level provides the greater *benefit* to the traveling public. For this project, the repair-plus-overlay alternative probably provided greater benefit to the agency, as well as lower user costs, than the repair-only alternative could have provided. It is not known, however, whether this difference in benefit and user costs, if quantified, would offset the difference in the alternatives' annual costs shown earlier.

Cost-Effectiveness of Preoverlay Repair

The second question addressed is what quantity of preoverlay repair is most cost-effective. On this project, funding limitations prevented the repair of all of the distress present in 1978. In fact, the full-depth repairs placed at all high-severity and some medium-severity distress locations repaired only 55 percent of all the failures present. The remaining failures (45 percent), which were all of medium severity, were treated with epoxy or left untreated. Although the rehabilitated pavement has performed well and 55 percent repair of the worst areas appears to have been, in one sense of the word, "adequate," it would be interesting to know whether it would have been more cost-effective in the long run to perform more repairs.

On this project 100 percent repair would have included all the repairs that were placed, plus repairs for the cracks that were epoxied, plus the cracks not repaired (the 15 failures that reflected through by 1983). This increase in the cost of full-depth repair ($64,600) minus the cost savings without the epoxy ($5,892) would have raised the total cost of the rehabilitation by $58,708, or about 6 percent, to $1,016,898.

If construction quality for the additional repairs were the same as for the repairs actually placed, the same proportion of them would have to be replaced in 1988 and in 1993. There should be no other costs associated with this alternative over the analysis period. The 1978 PW and EUAC of the two preoverlay repair alternatives are shown below:

	Alternative Cost	
	1978 PW	*20-Year EUAC*
Overlay with 55 percent repair	$1,156,061	$77,705
Overlay with 100 percent repair	$1,148,477	$77,196

The surprising result is that the two alternatives have very similar agency costs; 100 percent repair is actually slightly cheaper. Although both alternatives involve performing repairs at the same three times (1978, 1988, and 1993), longer lane closure times might be expected with the 55 percent repair alternative, since there would be more deterioration to repair. From an agency cost standpoint, the two alternatives are essentially equal, although maintenance costs would be lower with the 100 percent repair approach.

Optimal Timing of Rehabilitation

The third issue addressed in rehabilitation planning is the optimal timing of rehabilitation. Highway agencies need to know when in the pavement's life rehabilitation will be most cost-effective and, if adequate funding is not available at that time, what the consequences of delaying the rehabilitation will be. Although the answers to these questions are different for each project, the data available from the Manteno project can be used to illustrate how such an analysis may be conducted.

For this analysis, the repair quantities and costs associated with the 100 percent repair-plus-overlay alternative were used as a starting point. The repair-only alternative was extended 1 year at a time beyond 1978. The repair quantity required for each year of delay was determined using the log-normal deterioration curve shown in Figure 11. The total cost of all other rehabilitation work actually performed in 1978 except full-depth repair was deferred 1 year at a time. It was assumed that future full-depth repair replacements would be done at the same time intervals as before, 10 and 15 years after placement of the overlay. All the deferred costs were discounted 3 percent per year to convert them to equivalent 1978 dollars. The analysis period was kept at 20 years, from 1978 to 1998. The following results were obtained:

Year to Place Overlay	*1978 Present Worth ($)*	*20-Year EUAC Cost ($)*
1978	1,148,477	77,196
1979	1,118,526	75,182
1980	1,111,483	74,709
1981	1,111,244	74,693
1982	1,107,781	74,462
1983	1,100,035	74,447

Delaying the overlay provides a diminishing return in savings: the savings achieved by deferring the overlay is mostly offset by the costs of keeping up with full-depth repairs, with the result that smaller reductions are achieved every year. The annual cost appears to be approaching a minimum somewhere around $74,000, which is still more than the annual cost of continual repair only ($69,278). Rehabilitating the pavement in 1978 appears in retrospect to have been more cost-effective than delaying rehabilitation would have been. Agency maintenance costs associated with rehabilitating in 1978 would also have been lower than if the rehabilitation had been delayed.

Again, this cost analysis does not take into account user costs, which would be higher for the repair-only alternative and would increase, as pavement roughness increased, every year that the overlay was delayed. It may be true that if user costs were included in the analysis, the gap in costs between 1978 rehabilitation and delayed rehabilitation might narrow more quickly. Without user cost data available, however, it is impossible to say.

These findings are reinforced by the log-normal deterioration curve shown in Figure 11. Recall that this pavement was designed for 4.8 million ESALs, a traffic level that Fig-

ure 11 shows was reached around 1977. The point on the curve corresponding to 1978 is very close to the elbow between the relatively flat portion and the steeply sloped portion of the curve. Repair requirements, which are a reflection of structural damage, accelerate dramatically beyond this point. In fact, examination of Figure 11 raises the question of whether repairing and overlaying the pavement a year or two earlier might not have been even more cost-effective. This question was not addressed in the analysis reported in this paper but could easily be investigated with the cost and performance data available.

CONCLUSIONS AND RECOMMENDATIONS

This paper documents a case study of rehabilitation performance and cost-effectiveness conducted over a 10-year period. The project represents one of the oldest rehabilitated CRC pavements in Illinois. The performance of this project provides a great deal of valuable information about the performance and cost-effectiveness of rehabilitation.

Rehabilitation Performance

1. The experimental tied and welded full-depth repairs placed before the overlay have performed extremely well. The vast majority of these repairs have not even reflected through the overlay after 10 years of service and traffic of nearly 8 million ESALs. The data from this project suggest that, for CRCP at least, a well-constructed concrete repair that fully restores the continuity of the slab and the reinforcing steel can perform for 10 years or more beneath an AC overlay without causing any reflective cracking, even in a cold climate under heavy traffic.
2. The cost of CRCP full-depth repair can be significantly reduced with no sacrifice in repair performance by using shorter overall repair lengths and shorter lap lengths. The experimental repair designs with shorter tied laps (20 in.) and welded laps (4 in.) were almost 50 percent less expensive than the then-standard IDOT repairs (36-in. tied laps) and performed the same.
3. Full-depth AC repairs and unreinforced PCC repairs performed very poorly. After 10 years, nearly all of these repairs must be replaced. Full-depth AC and unreinforced PCC are both unsuitable for permanent repair of CRCP, and are not used for this purpose by IDOT. Their performance on this project shows that they also perform poorly even under an AC overlay.
4. Crack epoxying was not successful. Many of the epoxied cracks failed rapidly, even before the overlay was placed, and reflected through the overlay within a year. After 10 years nearly half of them need to be repaired again. Crack epoxying is not recommended for repair of wide cracks that extend across the full lane width of CRCP. The epoxy cannot withstand the large crack openings caused by thermal cycling in the pavement. Crack epoxying may be useful in slowing the rate of propagation of partial-lane-width cracks when at least some of the reinforcing steel across the width of the pavement is still intact.
5. Undersealing with cement grout or asphalt cement reduced deflections before overlay and reduced reflective cracking in the overlay. Sections that were undersealed had about 50 percent fewer medium- to high-severity reflection cracks than sections that were not undersealed, despite the fact that the undersealed sections had many more failures prior to rehabilitation. Blanket undersealing did not prove to be cost-effective. Selective undersealing at locations of poor support, as indicated by deflection testing, was more effective.
6. The 4-in. AC overlay reduced deflections to 55 percent of their preoverlay levels. After 10 years, deflections have increased to 88 percent of their preoverlay levels, indicating that some deterioration is taking place. The overlay is in good condition with respect to cracking, although a thin overlay or milling may be warranted sometime in the next several years to correct rutting. Tied and welded full-depth repairs of the CRCP resulted in practically no reflection cracks in the overlay after 10 years. Deteriorated cracks that were not adequately repaired have reflected through the overlay and now require full-depth repair.
7. Underdrains continually drained water from the pavement section over the 10 years of service. No pumping was evident after 10 years. Although a comparison of performance with and without drains is not possible since drains were placed through the entire project length, the elimination of pumping and the absence of any new failures attest to the improved drainage and support conditions.

Rehabilitation Cost-Effectiveness

1. Analysis of the hypothetical repair-only alternative versus the actual repair-plus-overlay alternative showed that, from the standpoint of agency rehabilitation costs, it would have been more cost-effective to continue the full-depth repair option for several years. The repair-only alternative would have higher maintenance costs, however, as well as higher user delay and accident costs resulting from the frequent lane closures. Pavement roughness would also be significantly greater with the repair-only alternative. A more detailed cost analysis that quantified these factors might show that the lower maintenance costs and user costs associated with repair plus overlay offset the higher agency costs.
2. The amount of preoverlay repair done determines the amount of repair needed after overlay. Repairing the worst 55 percent of the deteriorated areas was about as cost-effective as 100 percent repair would have been. Again, consideration of maintenance costs and user costs might favor the 100 percent repair alternative.
3. Delaying the overlay a few years beyond 1978 would have made it more cost-effective, from an agency cost standpoint, but apparently not enough to offset the maintenance costs of continued full-depth repair, which would have increased every year that the overlay was delayed. Consideration of user costs may change the results and reduce the cost difference. Performance data that illustrate the rate of deterioration with respect to traffic can be very valuable in determining the best time to perform major rehabilitation. Structural deterioration accelerates rapidly beyond the point at which the pavement's fatigue life is consumed, and as deterioration accelerates, so do the annual expenditures for full-depth repair. It is doubtful whether delaying a structural improvement significantly beyond the end of a pavement's structural life can

compete in cost-effectiveness with applying the structural improvement within the flat portion of the deterioration curve.

None of the conclusions contained in this paper concerning performance of rehabilitation techniques or cost-effectiveness of various alternatives should be construed as criticism of the rehabilitation work actually performed by the Illinois DOT on this project. The analyses described in this paper were conducted with the benefit of 10 years of detailed performance data. No such performance data were available to IDOT at the time the rehabilitation was done, since this was among the first full-scale CRCP rehabilitation projects ever undertaken in the state. The Illinois DOT is to be commended for its efforts in planning and executing this rehabilitation project and closely monitoring its performance.

Furthermore, it must be emphasized that this is only one project monitored over 10 years and these results apply only under these specific field conditions. Long-term monitoring of rehabilitation projects, collection of cost and performance data, and careful analysis of data are all greatly needed to improve rehabilitation planning decisions. User costs are an important part of life-cycle cost analysis and should be considered if possible. It is not impossible to conduct a cost analysis without information on user costs, but it requires that decision makers make qualitative judgments about the relative benefits of various rehabilitation alternatives to users.

ACKNOWLEDGMENT

The authors gratefully acknowledge the cooperation and assistance of the Illinois DOT in the field monitoring of the Manteno project. The 5-year (1983) survey and performance report was conducted by Ronald J. Roman of ERES Consultants, Inc., whose contributions to this study are also gratefully acknowledged.

REFERENCES

1. T. L. Barnett, M. I. Darter, and N. R. Laybourne. *Evaluation of Maintenance/Rehabilitation Alternatives for CRCP*. Report FHWA/IL/UI-185. Illinois Cooperative Highway Research Program, University of Illinois, Urbana, 1981.
2. S. A. LaCoursiere, M. I. Darter, and S. A. Smiley. *Performance of Continuously Reinforced Concrete Pavement in Illinois*. Report FHWA/IL/UI-172. Illinois Cooperative Highway Research Program, University of Illinois, Urbana, 1978.
3. M. I. Darter, T. L. Barnett, and D. J. Morrill. *Repair and Preventative Maintenance Procedures for Continuously Reinforced Concrete Pavement*. Report FHWA/IL/UI-191. Illinois Cooperative Highway Research Program, University of Illinois, Urbana, 1982.
4. D. E. Peterson. *NCHRP Synthesis of Highway Practice 122: Life-Cycle Cost Analysis of Pavements*. TRB, National Research Council, Washington, D.C., 1985.

Publication of this paper sponsored by Committee on Pavement Rehabilitation.

Evaluating Alternative Solutions to Reflective Cracking Through Asphalt Overlays

PONNIAH E. JOSEPH AND RALPH HAAS

The problem of reflection cracking through asphalt overlays can be approached from the design perspective of the factors or mechanisms involved, the alternative treatments available, and the analyses and testing required to evaluate the treatments. Then, a selection of the best alternative, provided it satisfies economic criteria, can be made and implemented. This paper concentrates on evaluation and first illustrates how an analytical method, based on a wide-crack band theory in finite element formulation, can effectively be used for the first step of the process. Then, it illustrates how the most promising alternative treatments can be experimentally evaluated. Test procedures and example results are used for this purpose, and relationships between induced stress, or strain energy, and cycles to failure are presented. Selection, installation, and follow-up considerations are briefly discussed. It is pointed out that even with the most technically and economically feasible alternative, proper laydown and construction are important to realizing success. Follow-up monitoring would primarily involve periodic crack surveys. The major conclusions of the paper are that both analytical and experimental evaluations should be performed to screen potential crack reflection treatments, and that proper construction is essential after the best treatment has been selected.

Asphalt concrete overlays are the most commonly used method for rehabilitating deteriorated pavements. However, they often do not perform as satisfactorily as is desirable because of existing cracks that propagate through the newly constructed overlay within a short period of time. This problem of "reflection cracking" is widespread and was in fact considered the most dominant existing pavement problem in a recent Canadian study (*1*).

Reflection cracking is caused by one or more cycles of thermal contraction, by repeated traffic loads, or by a combination of these two mechanisms. Existing methods of design do not generally provide crack reflection criteria. In efforts to minimize or delay occurrence of the problem, however, alternatives such as increase of the thickness of overlay, modification of asphalt properties, and placement of stress-relieving interlayers have been attempted. The degree of success has usually been limited.

There is a need to approach the reflection cracking problem from a perspective that includes a consideration of both of the following questions: (1) If the problem exists, what are the factors or mechanisms and what are the alternatives available? (2) How can the alternatives be screened or evaluated to find the best solution, and how should it be implemented? Figure 1 provides a schematic of the key elements involved in this total perspective or process.

This paper concentrates on the second aspect, evaluation and implementation, after briefly considering the first aspect. More specifically, it has the following objectives:

1. To provide a summary of the factors and mechanisms involved in reflection cracking and the basic alternative treatments available;
2. To present a review of the available analytical evaluation methods, with an example to illustrate how the alternative treatments may be screened;
3. To discuss experimental evaluation methods, as a necessary complement to analytical evaluation, and to provide examples; and
4. To consider some of the key aspects of laydown, construction, and monitoring follow-up.

FACTORS AND MECHANISMS

The basic factors that lead to reflection cracking are (1) repeated traffic loading, (2) thermally induced stresses or strains, and (3) a combination of both. In addition, the temperature-dependent stiffness of the materials and flaws in the overlay (i.e., built-in cracks during construction) can have a major effect.

Thermally induced stresses or strains, with low cyclic frequency, are thought to be the major factor in most cases. Two basic mechanisms can exist for this situation: (1) cracking initiates at both the top and bottom of the overlay, and propagates toward the middle, under very cold conditions; and (2) cracking initiates at the bottom of the overlay, owing to stress concentration around the old crack in the existing pavement, and propagates up under thermal cycling.

A possible third mechanism has been postulated by Abdelhalim et al. (*2*), whereby cracks built in during construction may subsequently propagate through the depth of the overlay with thermal cycling.

The mechanisms of cracking are directly related to the type of displacement induced. Figure 2 shows that this consists of three distinct modes: (1) normal tension, in the case of ther-

P. E. Joseph, Bituminous Branch, Ministry of Transportation, Ontario, 1201 Wilson Avenue, Downsview, Ontario, Canada M3M 1J8. R. Haas, Department of Civil Engineering, University of Waterloo, 200 University Avenue, Waterloo, Ontario, Canada N2L 3G1.

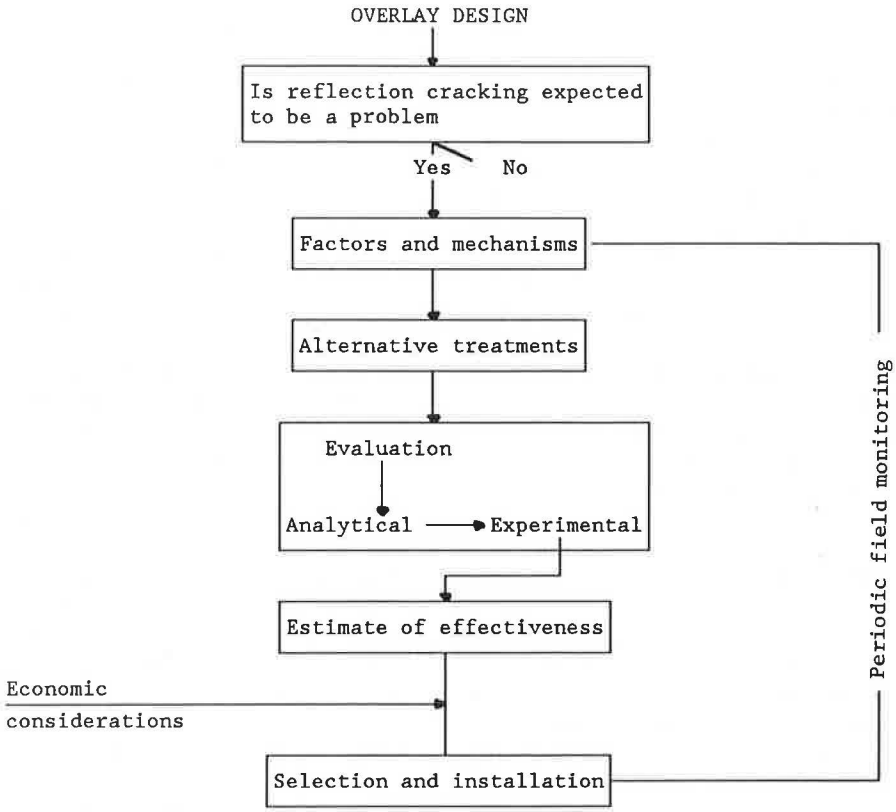

FIGURE 1 Key elements in the total process of handling the reflection cracking problem.

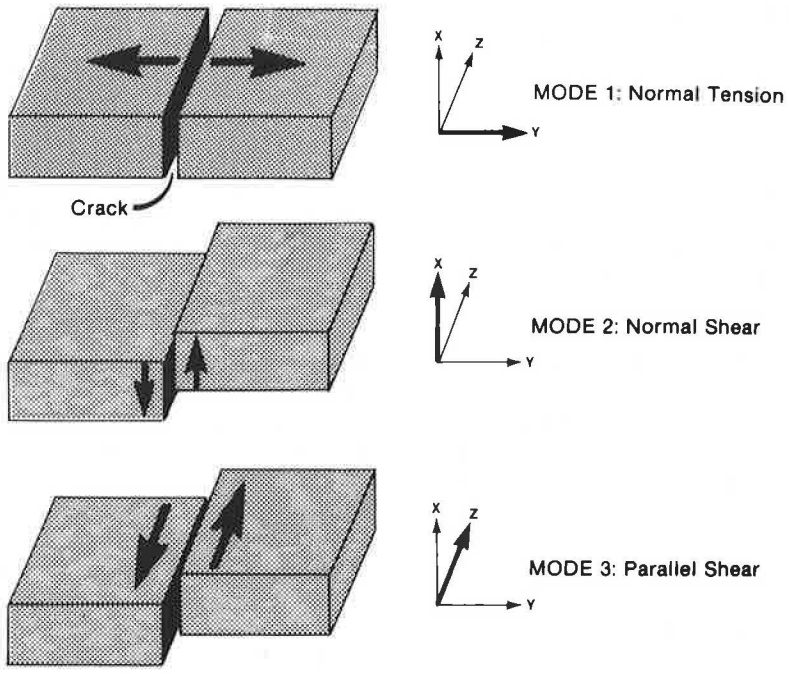

FIGURE 2 Modes of crack displacement.

mally induced displacements; (2) normal shear, usually associated with traffic or differential volume changes; and (3) parallel shear, which may occur only infrequently, for example, under lateral displacement due to instability.

A number of studies have been conducted to calculate the stress distribution in the overlay for Modes 1 and 2. For example, Cheetham and Haas (*3*) have shown how thermal stresses vary through the depth of the overlay for Mode 1, while Luther et al. (*4*) developed a finite element-based method for calculating stress distribution for Mode 2. Joseph (*5*) has shown how tensile and compressive stresses vary through the depth of the overlay under a combination of Modes 1 and 2.

The actual mechanism of crack initiation and propagation involves fracture of the overlay when the tensile stresses exceed tensile strength, under the particular conditions. A considerable amount of attention has been directed to the analysis of these mechanisms, as subsequently discussed.

ALTERNATIVE TREATMENTS

Various treatments have been tried in the past to control reflective cracking through asphaltic concrete overlays. These include the use of low-modulus, stress-relieving interlayers, geogrids, and fabrics. Other alternatives would include modifying the asphalt concrete overlay properties and pulverizing the existing pavement. While the latter can be successful, it is actually a form of reconstruction. Consequently, the following discussion focuses on the first three types of treatment.

Low-Modulus Interlayer

Fracture mechanics suggests that any attempt to reduce reflection cracking must be centered on reducing the stress concentration at the crack front. It has theoretically been established that provision of a lower-modulus, stress-relieving medium above the existing crack can reduce the rate of crack growth (*6*).

Geogrid or Fabric Reinforcement

The use of fabric or geogrid reinforcement has the potential to control crack propagation. The major types of geogrids used for this purpose are polymer-based, or glass grids. Wire meshes have been attempted in the past but are prone to corrosion. A large variety of fabrics is marketed for overlay application.

It is difficult to quantify adequately on an analytical basis the ability of grid or fabric reinforcement to control crack growth after initiation of the crack. Thus, it is important to supplement such analytical evaluation with experimental studies.

A Composite Stress-Relieving Interlayer

As a potential solution to the reflection-cracking problem, the use of a composite interlayer has been suggested (*3*). It involves a combination of low-modulus material with geogrid reinforcement placed on the existing cracked pavement. The expectation is that the low-modulus layer will act as a stress attenuator between the existing pavement and the overlay and that the reinforcement will carry any remaining stress.

ANALYTICAL EVALUATION METHODS

It is logical first to evaluate or screen any potential reflection cracking treatments on an analytical basis so that the experimental evaluation can be made more efficient.

Reflection cracking treatments can be evaluated analytically using a finite element technique. For example, Coetzee (*7*) carried out a limited finite element analysis to evaluate the effect of soft interlayers on asphalt overlay cracking due to low temperature. Also, attempts have been made (*4*) to model the effect of traffic load on reflection cracking using the finite element method.

The principal intent of this section is fourfold: (1) to present very briefly some of the existing analytical methodologies; (2) to provide the basis for selecting a suitable criterion for the analysis of reflection cracking; (3) to present a new approach using a blunt or smeared-crack band concept; and (4) to present some examples of analytical results.

Available Analytical Methodologies

Some of the methodologies that have been used for analyses of the reflection cracking problem include those developed by Majidzadeh and Suharieh (*8*), Hung-Sun et al. (*9*), and Monismith and Coetzee (*10*).

A design methodology for the opening mode, low-temperature reflection cracking of an asphalt overlay on concrete pavement was developed by Majidzadeh and Suharieh (*8*). They assumed that cracking initiates at the surface of an overlay because of contraction and curling of the underlying old pavement surface. Stresses due to horizontal joint movements were estimated using a finite element analysis. Subsequently, they established nomographs to estimate the tensile stress in the overlays.

A design process to arrive at an overlay resistant to environmental reflection cracking has been developed using linear elastic and viscoelastic stress analysis and fracture mechanics at Texas A & M University (*9*). Initially, thermal stresses in the overlay and old asphalt surface were calculated using viscoelastic theory. A crack propagation model was then proposed for the pavement material subjected to these thermal stresses using an empirical relationship developed by Paris and Erdogan (*11*). The stress-intensity factors necessary for this analysis are calculated using a finite element technique with special crack tip elements. Because of the anisotropic and heterogeneous nature of the overlaid pavement, however, the question exists as to whether stress-intensity factor is the best characterization to use.

Monismith and Coetzee (*10*) used finite element analyses, with effective stress as the criterion, to study the stress distribution around the crack (with and without a rubber asphalt membrane interlayer) due to traffic load and thermally induced stresses. They concluded that a softer interlayer has the potential to attenuate the stress concentration around the crack front. They also found that variables such as thickness and stiffness of both the rubber asphalt layers and the asphalt

concrete overlay, and stiffness of the existing cracked layer, have some influence on the stress distribution for any load application.

Monismith and Coetzee suggested that design charts should be developed where stresses or strains could be utilized with an appropriate fatigue relationship to define cumulative damage. They also suggested that future experiments should consider the use of a relatively large slab to which a horizontal displacement can be applied to simulate cracking behavior.

Fracture Criteria

Fracture mechanics provide the following criteria for modeling of fracture: (1) stress-intensity factor, (2) critical strain energy, and (3) maximum stress.

The stress-intensity factor is very difficult to estimate for pavement overlays with underlying cracks because the material is anisotropic and nonhomogeneous. Also, the existing crack is not well represented by the typical mathematical formulations used in the application of fracture mechanics.

An energy criterion is very useful for modeling of fracture, particularly for the study of crack propagation. It represents the global characteristics of the system and does not depend on the detailed distribution of stress and strain near the fracture front. Therefore, it follows that the choice of element size around the crack tip in a finite element analysis will not have any significant effect on the results. Hence, a predictive model relating the energy criterion to the number of cycles required for complete fracture should be useful.

The strength criterion represents the local characteristics of the system and can be used to identify the critical section that is likely to initiate cracking. It could indicate whether or not a crack is likely to initiate at the top or bottom of the overlay, so that any potential treatment can be effectively evaluated. The main disadvantage is that it depends on the chosen mesh size in the elastic finite element analysis of cracking. This problem, however, can be circumvented by maintaining the same type and size of elements for evaluation of all potential treatments.

Joseph (*5*) has concluded that both the strength and energy criteria should be used—that is, the strength criterion for an initial analytical screening and determination of effective potential treatments, and the energy criterion to develop design charts on the basis of experimental results.

Blunt-Crack Band Theory

Fracture of a heterogeneous aggregate material such as concrete has been modeled in large finite element programs as systems of parallel cracks that are densely distributed (smeared) over the finite element. This was originally proposed by Rashid (*12*) and is known as the "blunt-crack band theory."

A detailed account of the analytical development and subsequent implementation of this theory in finite element analyses can be found in Bazant and Oh (*13*) and Joseph (*5*). Only some typical results and the relevant assumptions made in the analyses are presented in the following discussion.

Finite Element Modeling Using Crack Band Theory

A sample application involves the use of (1) low-modulus interlayer, (2) geogrid reinforcement, and (3) composite interlayer. The three-dimensional pavement structure has been simplified into a two-dimensional plane strain problem. The reason for considering plane strain is that the Poisson contraction in the z-direction can be neglected in view of sufficiently large pavement dimensions. More specifically, the following assumptions are made in the finite element analysis.

1. The average spacing of transverse cracks in the old pavement is assumed to be 12 m, based on field observations;
2. Perfect, uniform bonding is assumed between the overlay and the old pavement;
3. Adhesive strength between the overlay and the old pavement is greater than the "strength" of the overlay;
4. Coefficient of thermal shrinkage is the same for all layers and is equal to 27×10^{-6}°C (*3*);
5. Crack band width of 30 mm is assumed (Figure 3) based on the energy criterion (*5*, *13*); and
6. The linear thermoelastic stress-strain relationship is represented by the following equation:

$$\varepsilon_{ij} = \frac{(1 + \nu)\sigma_{ij}}{E} - \frac{\nu}{E}\delta_{ij}\sigma_{kk} + \alpha\Delta T\delta_{ij}$$

where

ε = strain in the element,
σ = induced stress,
E = elastic modulus of the layer,
ν = Poisson's ratio,
α = coefficient of thermal contraction,
ΔT = change in temperature, and
δ_{ij} = 1 for $i = j$, and = 0 for $i \neq j$.

Induced thermal stresses are estimated initially for two different boundary conditions: first, free horizontal movement between the existing, old pavement and the base course material; and second, the horizontal movement is completely restrained. The actual field situation would lie somewhere between these extremes. For evaluation of potential treatments only, the upper-bound situation is considered, that is, free movement between old pavement and the base course.

A typical finite element representation is shown in Figure 4. Temperature drop in each element corresponds to observed field data from the Ste. Anne Road Test (*14*). These input data are required for the finite element program SP23B (*15*).

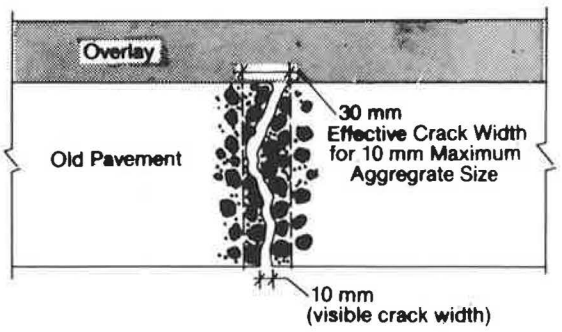

FIGURE 3 Effective width of existing crack.

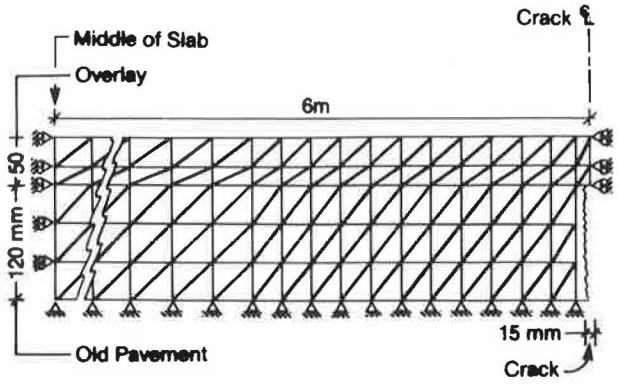

FIGURE 4 Finite element representation.

The material properties and temperature gradient used in the analysis are given in Tables 1 and 2 (compiled from Ste. Anne Road Test temperature measurements for low-temperature cycle, December 17, 1967 to January 11, 1968).

For the analysis of reinforced pavement overlays, additional discrete bar elements are used to represent reinforcement in the pavement section (Figure 5). Bar-element data include the cross-sectional area and the elastic modulus. It is assumed that bars are attached to the asphaltic concrete in nodes of the mesh.

Results of the analysis are given in Figure 6 through 10. In summary, they indicate the following:

1. A stress concentration exists around the crack front, because of the existing crack in the underlying pavement (Figures 6 and 7). The noticeable difference of stress values between two extreme boundary conditions indicates that the stress concentration can be reduced significantly by preventing movement of the underlying pavement. The only method available at the present time, however, is breaking up or pulverizing existing pavements. Figures 6 and 7 further indicate that the vertical section above the crack front is rather critical. This suggests that potential treatments for reflection cracking can be evaluated on the basis of the induced thermal stress distribution across the pavement overlay above the crack front. Figures 8 and 9 give the vertical stress distribution for treated and untreated pavement overlays.

2. The best location for the reinforcement is at the interface (Figure 8). Even though this reduces the induced stress by only approximately 15 to 20 percent, it has been observed that a 2 percent reduction in stress can lead to a 30 percent increase in life, illustrating the importance of stress amplitude in fatigue (*16*).

3. In a comparison of various treatments Figure 9 indicates that the composite interlayer (stress-absorbing membrane interlayer, "SAMI" reinforced with tensar geogrid) with 30-mm overlay thickness produces the same result as that of the SAMI alone with a 50-mm overlay thickness.

4. Figure 10 considers the gradual formation of microcracks leading to a macrocrack ahead of the existing flaw in the old pavement. During this process it is assumed that the stiffness modulus of the material represented by the crack band will gradually decrease to zero. The stress ahead of the crack band (point A) with and without the reinforcement is computed for three different stages of crack formation, with the stiffness modulus of the material changing from 100 percent (no crack) to 50 percent (microcracks), and finally to 0 percent (macrocracks) of the original value. It can be seen from Figure 10 that the reinforcement becomes increasingly effective as the crack propagates. This suggests that reinforcement can have a good potential to retard subsequent crack propagation after initial crack formation.

Analytical evaluation such as the foregoing is valuable in screening alternative treatments. In this example, for the conditions analyzed, all three treatments appear to have a potential for retarding reflection cracking. However, experimental

TABLE 1 MATERIAL PROPERTIES

Material	Elastic Modulus (MPa)	Poisson's Ratio	Thermal Coefficient (°C)
Old Pavement	6,894	0.4	27×10^{-6}
Overlay	2,069	0.4	27×10^{-6}
Softlayer	138	0.4	27×10^{-6}
Geogrid (Tensar)	15,000	0.4	27×10^{-6}
Fibreglass (Glass Grid)	76,000	0.4	27×10^{-6}

TABLE 2 TEMPERATURE GRADIENT FOR AN AMBIENT TEMPERATURE OF −32°C

Depth (mm)	Pavement Temperature (°C)	Depth (mm)	Pavement Temperature (°C)
0	-28.5	77	-21.6
10	-27.8	103	-18.0
20	-27.0	117	-16.2
37	-26.0	143	-12.6
43	-25.6	157	-10.8
63	-23.4		

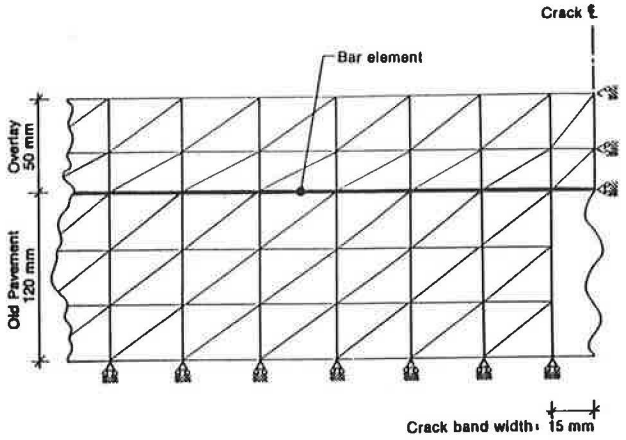

FIGURE 5 Finite element model representation using bar elements.

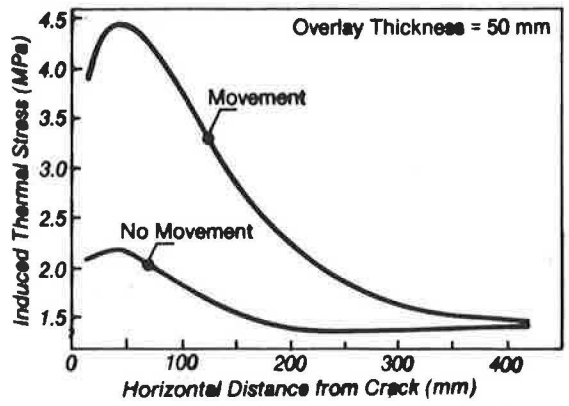

FIGURE 6 Stress distribution in the top of the asphalt overlay for different conditions.

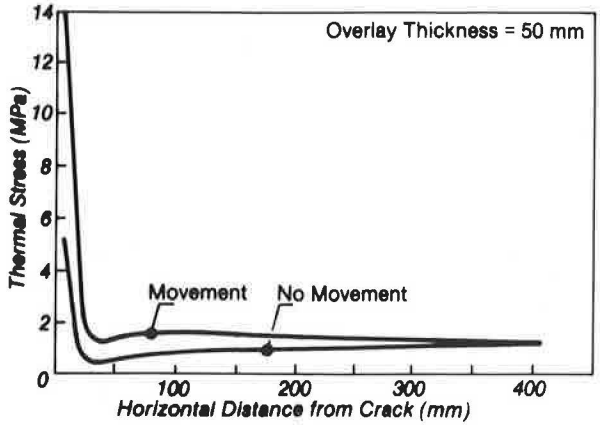

FIGURE 7 Stress distribution in the bottom of the asphalt overlay for different boundary conditions.

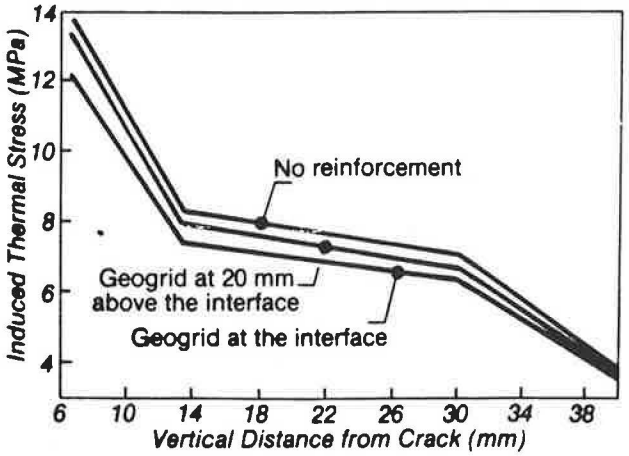

FIGURE 8 Effect of geogrid reinforcement on induced thermal stress.

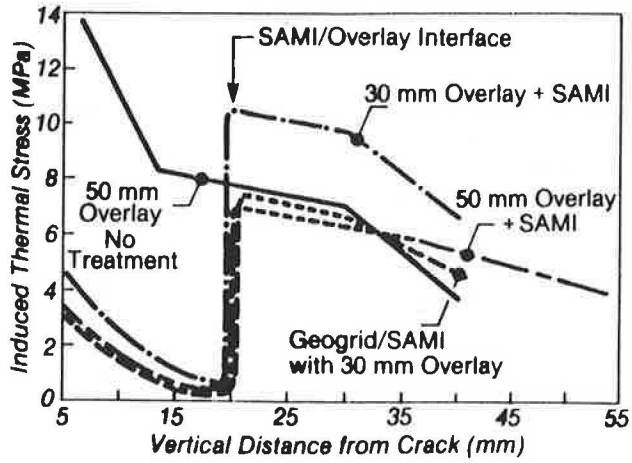

FIGURE 9 Comparative effect of various treatments.

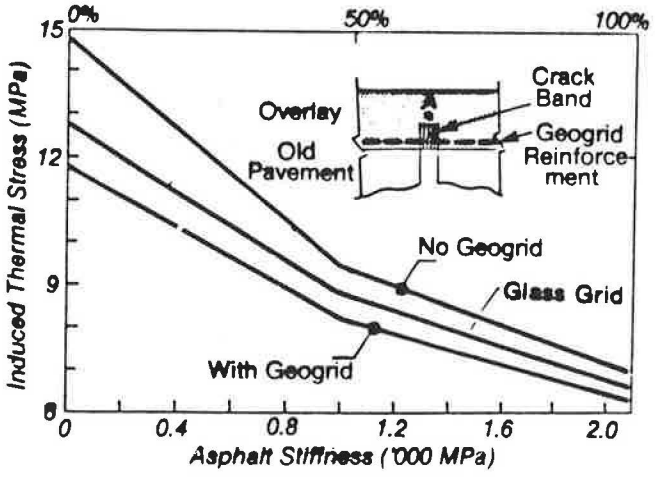

FIGURE 10 Comparative effects of glass-grid and geogrid reinforcements on crack growth for stiffness in the crack band 100 percent, 50 percent, and 0 percent.

evaluation should be used to provide confirmation and to give a better basis for final selection and actual field implementation. An example is given in the next section.

EXPERIMENTAL EVALUATION METHODS

The main objective of an experimental evaluation should be to evaluate potential treatments screened by analytical study and to develop a suitable design methodology. This would ideally involve laboratory tests that completely simulate field conditions. However, it is difficult to reproduce all field conditions, such as temperature gradients, interface conditions, and so forth.

An example experimental program involving two of the treatments (geogrid and glass grid) to follow the analytical evaluation previously described is summarized in the following discussion.

Major Variables

The variables that might be considered include initial crack-width opening, rate of movement of the underlying pavement or rate of drop in temperature, temperature gradient, overlay thickness, temperature and number of cycles, traffic loads and number of cycles, combination of thermal stress and wheel loading, type and location of treatment, and overlay mix type or design.

The most important variable is temperature. When the surrounding temperature drops significantly, thermal stresses are induced in the overlay, and movement of the underlying pavement occurs because of thermal shrinkage. This effect can be simulated mechanically, as illustrated by Joseph et al. (*17*). They developed a large-scale piece of equipment designed for both thermal and traffic load simulation. Their initial investigation, however, considered only thermally associated loads, and the example in this section is based on that work.

Experimental Equipment and Tests

A key part of Joseph et al.'s equipment consists of two steel plates, one fixed and the other horizontally movable on rollers with the aid of ball end bearings. The movable plate is linked to a mechanism designed to move the plate back and forth at variable, very slow rates equivalent to the crack opening or closing in an underlying old pavement. A cooling chamber is built into the system and is capable of maintaining a temperature as low as −40°C.

The equipment was used to test overlay slabs (approximately 450 mm long by 225 mm wide) sawed from constructed field pavements involving control plus reinforced sections, as described in detail by Joseph (*5*). It was felt that building such field sections to provide samples for testing, using standard construction techniques and equipment, would be more desirable than laboratory fabrication, particularly for the reinforcement treatments.

Figure 11 shows the factorial arrangement used for the testing program. Actual testing of each specimen included the following major steps:

Treatment Type / Induced Displacement / Number of Replicates	Control			Geogrid Reinforcement			Glass-grid Reinforcement		
	Low	Med.	High	Low	Med.	High	Low	Med.	High
1	•	•	•	•	•	•	•	•	•
2	•	•	•	•	•	•	•	•	•
Average	•	•	•	•	•	•	•	•	•

NOTE: • = number of cycles to complete fracture

FIGURE 11 Factorial arrangement for the reinforced overlay test program (test temperature −30°C).

1. Cooling the specimen to −30° ± 2°C, until the temperature gradient reached a steady state; and
2. Subjecting the specimen to a uniform cyclic load at a predetermined displacement level, under controlled strain, until fracture propagates through the full depth. Three displacement levels (Figure 11) were chosen to cover the anticipated range of movements of old pavements in the field. A single displacement rate (.0399 mm/min) was used.

Example Results

Crack growth rates for the control and reinforced overlay samples are given in Figure 12. The effectiveness of both types of reinforcement in retarding crack growth at the low level of displacement (0.21 mm) is obvious. Even though a crack up to about 30 percent of the thickness developed after only 3 cycles, subsequent propagation was very slow and did not reach the full depth until after 200 cycles. Only 5 cycles at this displacement level were required to propagate a full-depth crack in the control sample.

At a higher level of induced displacement (0.26 mm) the glass grid reinforced section cracked to full depth in less than 10 cycles, while the geogrid reinforced sample took 25 cycles. Moreover, the glass grid reinforced samples showed some separation of matrix from the reinforcement.

The foregoing results suggest that glass grid and geogrid have potential in retarding crack growth rate. What remains to be seen in the field is whether they would provide effective "crack control" (i.e., keep the crack closed) after full-depth propagation.

The test results can also be presented in the form shown in Figures 13 and 14. These effectively become design charts corresponding to cyclic temperature variation between 0°C and −30°C.

To develop comprehensive thermal fatigue curves for asphalt overlays, it would be necessary to have a larger number of observations, including high cycle fatigue tests under different cyclic temperature variations. However, Figures 13 and 14 demonstrate that the experimental technique used can provide good relationships between stress or strain energy and fracture lives even with a limited number of observations.

In reality, of course, pavement structures are subjected to complex, fluctuating-temperature environments. The development of accurate fatigue-life prediction procedures for overlays requires characterization of the variable-amplitude, cycle-temperature fluctuations. This may best be done through

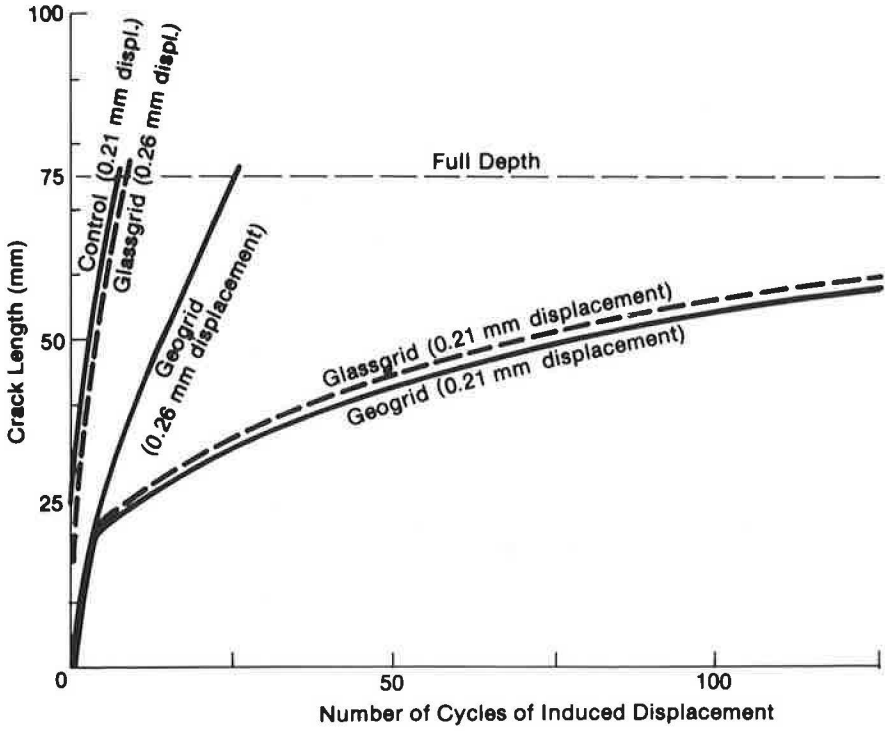

FIGURE 12 Crack growth curves for various overlay treatments.

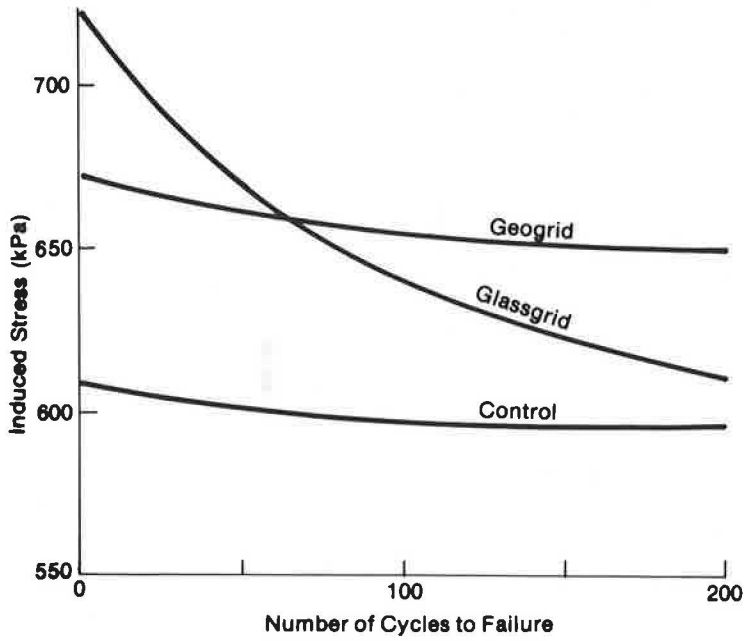

FIGURE 13 S-N curves for various overlay treatments.

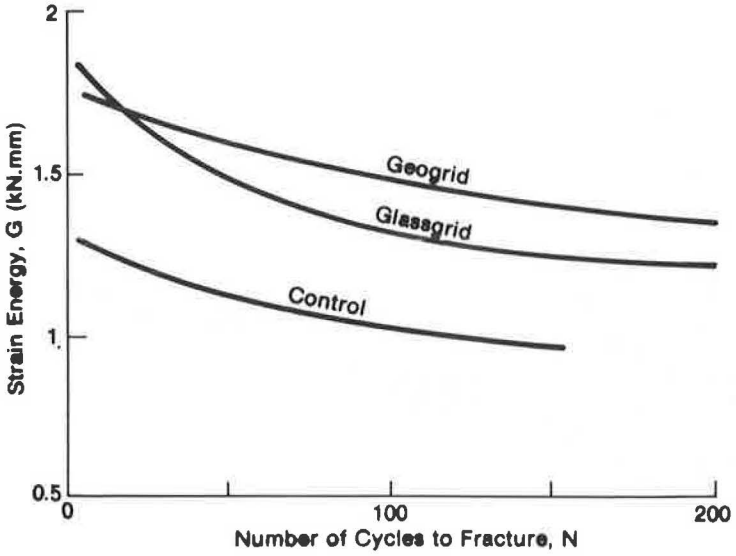

FIGURE 14 G-N curves for various overlay treatments.

the use of probability-density curves applied to the temperature history for a particular region. Then a cumulative damage approach, such as Miner's rule (*18*), could be used to represent the range of conditions.

SELECTION, INSTALLATION, AND FOLLOW-UP

The foregoing analytical and experimental screening or evaluation suggests that both the geogrid and the glass grid showed good potential for retarding reflection cracking in the conditions considered. If the displacement level of 0.21 mm is one of the applicable conditions, then both types of reinforced overlay should be able to withstand 200 very cold (−30°C) temperature cycles. This could cover several winters, depending on the variations at the particular location.

Economic considerations (Figure 1) are also important with regard to selection. The extra costs of geogrid or glass grid purchase and installation would have to be offset by longer service life of the reinforced overlay. Unfortunately, the technology of reflection cracking, including feedback from field observations of behavior and performance, is not yet sufficiently developed to allow for proper life-cycle economic evaluations to be performed.

Assuming that such an economic evaluation were favorable, certain construction or laydown considerations also apply to crack reflection treatments. These include the following:

1. Placement around sharp curves (except for SAMI treatments). Proper tensioning, particularly of geogrids, can also be difficult.
2. Proper bonding between the treatment and the old pavement. If this is insufficient, high traction forces from the paver can dislodge the material, and/or delamination can subsequently occur in service.
3. Roughness or undulations in the old pavement. If this is severe enough, a leveling course may have to be placed first before a treatment can be effectively applied (particularly fabrics, geogrid, or glass grid).
4. Proper bonding or interlocking between the overlay material and the treatment. This is important for fabrics and grids.
5. Temperature of the overlay mix during construction. In the case of polymer geogrids, this can, if too high, cause severe distortion.

Behavior and performance of the installed treatment can be evaluated in several ways. Perhaps the most important is simply to perform periodic crack surveys to determine what percentage of cracks has reflected through the overlay compared with the control or nontreated section. Also, condition or severity of the cracks can be assessed, which is important where a treatment has not prevented cracking but is effective in keeping the cracks closed. In this case the treatment would have more strain capability than the overlay material; that is, it would not have ruptured.

CONCLUSIONS

The problem of reflection cracking through overlays is widespread. It can be approached from the perspective of the factors or mechanisms involved and the alternatives available, combined with an analytical plus experimental evaluation to determine the best alternative for implementation.

This paper has concentrated on the latter aspect, evaluation, and one of the major conclusions is that a crack band theory in the finite element analysis can effectively be used to analyze treatment alternatives for minimizing or controlling reflection cracking. Also, the method allows for the analysis of alternative treatments at various stages of crack propagation without changing the mesh configuration and nodal points.

A further conclusion is that such analytical screening is valuable but not sufficient. Experimental evaluation should also be carried out. Testing procedures and sample results in the paper indicate how the potential success of the most promising treatments can be estimated. Relationships between induced stress and cycles to failure, and strain energy and cycles to failure, are used for this purpose. Such relationships

can also be used to develop suitable design criteria so that reflection cracking can be minimized and/or effectiveness can be estimated in terms of life expectancy.

Finally, it is concluded that economic viability is important and, if this exists for the best alternative, then certain laydown and construction considerations are also important to realizing success.

REFERENCES

1. R. Haas, E. Thompson, F. Meyer, and G. R. Robert Tessier. *Study of Asphalt Cement Additives and Extenders.* Report prepared for Roads and Transportation Association of Canada, Ottawa, Ontario, 1983.
2. A. O. Abdelhalim, W. A. Phang, and R. Haas. Realising Structural Design Objectives Through Minimization of Construction Induced Cracking. In *Proc., Sixth International Conference on Structural Design of Asphalt Pavement,* University of Michigan, Ann Arbor, 1987.
3. A. Cheetham and R. C. G. Haas. *Initial Design Analysis for Elimination of Pavement Reflection Cracking Through Overlays by Use of a Composite Interlayer.* Report prepared for Ontario Joint Transportation and Communication Research Program, Pavement Management Systems Ltd., Cambridge, Ontario, Canada, 1981.
4. M. W. Luther, K. Majidzadeh, and C. Chang. Mechanistic Investigation of Reflection Cracking of Asphalt Overlays. In *Transportation Research Record 572,* TRB, National Research Council, Washington, D.C., 1976, pp. 111–122.
5. P. Joseph. *Low Temperature Reflection Cracking Through Asphalt Overlays.* Ph.D. thesis. University of Waterloo, Waterloo, Ontario, Canada, 1987.
6. E. Orowan. Energy Criteria of Fracture. *Welding Journal Research Supplement,* 1955, pp. 157–160.
7. N. F. Coetzee. *Some Considerations on Reflection Cracking in Asphalt Concrete Overlay Pavements.* Ph.D. dissertation. University of California, Berkeley, 1979.
8. K. Majidzadeh and G. Sucharieh. *The Study of Pavement Overlay Design.* Final Report. Ohio State University, Columbus, 1977.
9. C. Hung-Sun, R. L. Lytton, and H. Samuel. *Prediction of Thermal Reflection Cracking in West Texas.* RR 18-3, Study 2-8-73-18. Texas A&M University, College Station, 1976.
10. C. L. Monismith and N. F. Coetzee. Reflection Cracking: Analysis, Laboratory Studies, and Design Considerations. *Proc., Association of Asphalt Paving Technologists,* Vol. 49, 1980, pp. 268–313.
11. P. C. Paris and F. Erdogan. A Critical Analysis of Crack Propagation Laws. *Journal of Basic Engineering, Transactions of the American Society of Mechanical Engineers,* Vol. 85, 1963, pp. 528–534.
12. Y. R. Rashid. *ASCE State-of-the-Art Report on Finite Element Analysis of Reinforced Concrete.* American Society of Civil Engineers, New York, 1982.
13. Z. P. Bazant and B. H. Oh. *Crack Band Theory for Fracture of Concrete, Materials and Structures,* Vol. 16. RILEM, Paris, 1983, pp. 115–177.
14. F. D. Young, I. Deme, R. A. Burgess, and O. Kopvillem. Ste Anne Test Road—A Field Study of Transverse Crack Development in Asphalt Pavements. In *Construction Summary and Performance After Two Years Service, Proc., Canadian Technical Asphalt Association,* Edmonton, Alberta, Canada, 1969.
15. W. H. Bowes and L. T. Russel. *Stress Analysis for Practicing Engineers.* Lexington Books, Lexington, Mass., 1975.
16. D. C. Drucker and J. J. Gilman, eds. *Fracture of Solids.* Metallurgical Society Conferences, Vol. 20, 1962.
17. P. Joseph, R. Haas, and W. A. Phang. Thermally Associated Fatigue Crack Growth Through Asphalt Overlays: An Experimental Investigation. *Proc., Paving in Cold Areas Workshop 3,* Ottawa, Ontario, Canada, 1987.
18. C. L. Monismith. *Asphalt-Mixture Behavior in Repeated Flexure.* Report No. TE 66-6. University of California, Berkeley, 1966.

The contents of this paper do not necessarily reflect the official views or policies of the Ministry of Transportation of Ontario.

Publication of this paper sponsored by Committee on Pavement Rehabilitation.

Functional and Structural Flexible Pavement Overlay Design for Indiana To Overcome a Deficiency in the 1986 AASHTO Guide

JAY K. LINDLY AND THOMAS D. WHITE

A procedure for designing the thickness of asphaltic concrete overlays of flexible pavements in Indiana was developed. In analyzing the research data collected, a deficiency in the 1986 AASHTO Guide became apparent: the overlay design procedure addresses only structural overlays and ignores functional overlays. Many miles of asphalt pavement in Indiana are overlaid for functional rather than for structural reasons. The research included testing on 30 flexible pavement test sections statistically selected to be representative of flexible pavements in Indiana. Two approaches were taken: an empirical approach that calculates the overlay thickness required to provide functional performance (ride quality) over the life of the pavement and a structural overlay method. Flexible overlay design Method 2 of the 1986 *AASHTO Guide for the Design of Pavement Structures* was selected for structural capacity design. Method 2 uses nondestructive test (NDT) deflection data to calculate overlay thickness. If found, a negative value for overlay thickness indicates that sufficient structural capacity is present without adding an overlay. The functional performance approach used Indiana flexible pavement historical data to produce a regression equation relating overlay thickness to anticipated future traffic, overlay design life, pavement condition at design life end, and CBR. Simultaneous use of the two design methods was recommended to IDOH.

In 1985, Purdue University was asked by the Indiana Department of Highways (IDOH) to perform a Highway Planning and Research (HPR) Part II study titled "Development of an Overlay Design Procedure for Flexible Pavements in Indiana." Currently, the IDOH is using an overlay thickness design based on the *AASHTO Interim Guide for the Design of Flexible Pavement Structures* (*1*). A typical overlay design involves calculating several overlay thicknesses that vary depending on the magnitude of the layer coefficient assigned to the existing pavement layers. One recent design example provided possible overlay thicknesses ranging from 0.5 in. to 4.25 in.; the designer was required to select a design thickness within that range.

The first step of the study was to conduct a survey of the Federal-Aid Primary (FAP) roads in Indiana. As a result of this survey, approximately 3,180 lane-miles of flexible pavement (no Portland cement concrete) were identified. That mileage is represented in 431 pavements of varying cross sections whose lengths may range from less than 0.25 mile to more than 10 miles. In many cases these 431 sections have been overlaid several times. For example, almost 75 percent of the sections have been overlaid at least three times since initial construction, and more than 25 percent have been overlaid five or more times (Figure 1).

The road system described is a "mature" system, developed mainly from roads first paved in the 1930s and 1940s. The high percentage of pavements with multiple overlays (which increase the total asphalt thickness with each overlay) has created the opportunity for many of the pavements to exceed the asphalt thickness required to avoid structural failure at current traffic loads. For those pavements, when an overlay is required, it is added to provide functional performance (ride quality) rather than to provide structural performance (the ability to carry load).

The researchers investigated nondestructive test (NDT)-based overlay design procedures in the 1986 *AASHTO Guide for Design of Pavement Structures* (*2*) for use as a new overlay design procedure for Indiana. While the 1986 AASHTO Guide advocates considering both structural and functional performance, however, it provides only a structural overlay design method. Thus, a functional design procedure specific to Indiana flexible pavements was developed, and both the functional procedure and the 1986 AASHTO Guide structural procedure are used in the final design procedure.

OVERVIEW OF RESEARCH

The first step in this research was to develop an inventory of all the flexible pavement sections in the FAP road system from paper records maintained by the IDOH. The FAP system contains about 55 percent of the pavements maintained by the IDOH, including state roads, U.S. highways, and Interstates. During the inventory, the following data were stored in a computer database for each flexible pavement section: pavement cross section, traffic, climate zone, and overlay age. Other data, such as subgrade type and layer strength data, would have been excellent additions to the database, but they were not readily available at that time.

To collect the necessary field data for developing the overlay design procedure, an extensive field testing and evaluation

J. K. Lindly, Civil Engineering Department, University of Alabama, P.O. Box 870205, Tuscaloosa, Al. 35487-0205. T. D. White, School of Civil Engineering, Purdue University, West Lafayette, Ind. 47907.

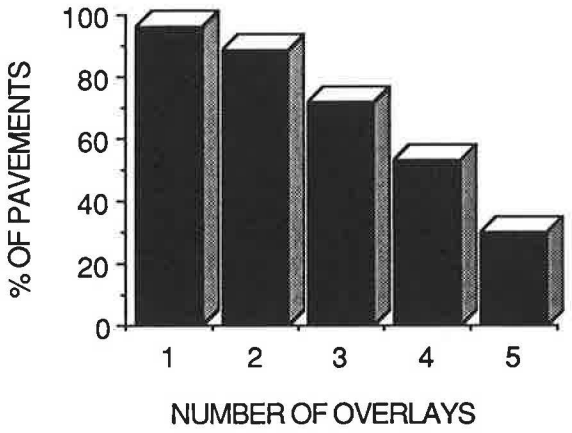

FIGURE 1 Overlays on Indiana flexible pavements.

program was planned. A statistically based design of experiment reduces the number of pavements that must be field tested while maintaining the significance of the results. Thus, statistical design of experiment techniques was used to select thirty 1,250-ft-long pavement test sections that were representative of the FAP flexible pavement sections throughout the state.

The first part of test section selection and experiment design was to choose factors that most affect overlay life. Test sections were then chosen that represent the range of variability of these factors. The following four factors were selected from the available computer database:

1. Most recent overlay thickness;
2. Thickness of asphalt beneath most recent overlay;
3. Traffic to which the most recent overlay has been subjected; and
4. Climate zone location of the sections: based on previous research, a north zone and a south zone have been identified in Indiana.

In each climate zone, a three-factor, three-level composite design was developed that contained low, medium, and high levels of the other three factors. The composite design required 15 test sections in both climate zones, for a total of 30 test sections.

Values for pavement serviceability index (PSI) were obtained for each test section from the IDOH, and the researchers calculated values for pavement condition index (PCI) based on a field survey of the types, severities, and extents of surface distresses (*3*).

The IDOH Division of Materials and Tests obtained one sample of subgrade material in each of the 1,250-ft-long test sections. After coring through the asphalt layers and the subbase, 4 ft of 3-in.-diameter Shelby tube was pushed. The resulting subgrade samples were tested by AASHTO standards for liquid limit, plastic limit, density, moisture content, and particle size distribution. From these data, the subgrades were classified by the AASHTO and Unified soil classification systems and assigned estimated CBR values from published tables (*4*). The limited soils investigation was dictated by financial and time considerations.

Nondestructive testing (NDT) was conducted in both the spring and fall of 1986 so that seasonal differences in NDT results could be considered. A dynamic load of approximately 14,000 lb was applied to the pavement with a Dynatest Falling Weight Deflectometer (FWD). Deflections were recorded directly beneath the load and 1, 2, 3, and 4 ft from the load. These deflections were measured at six sites in each test section. The sites were normally 120 to 180 ft apart and were located in the outside wheelpath of the outside lane. During the spring test period, each site was marked with yellow highway paint so that the exact site could be retested in the summer.

During spring testing, deflections were also taken 5 ft and 7 ft from the load at site 5. The reason these deflections were taken only at site 5 is that a manual procedure was necessary to reset two sensors at those distances to obtain deflection readings. In the summer test period, deflections 5 ft and 7 ft from the NDT load were taken at three sites within each test section: at sites 1, 3, and 5.

The spring series of test results was obtained during a 5-week period in the early spring (March 17 to April 25, 1986) when pavement deflections tend to peak because of pavement layer and subgrade thaw. Climatological data (*5*) from the National Oceanic and Atmospheric Administration (NOAA) indicated that the southern portion of Indiana begins spring thaw approximately 2 weeks before northern Indiana. Therefore, testing began in the south portion of the state and moved north. The summer test period was completed from August 5 to September 5, 1986.

Five-day temperature history and pavement surface temperature during testing were obtained for all NDT testing. These temperature data were utilized to normalize deflections to a common temperature.

The accumulated data were analyzed both by an empirical method (which produced the functional overlay design procedure) and by a structural overlay design method. In the empirical method, regression analysis was applied to the data to determine "what overlay thickness has worked in the past" and under what conditions. In the structural method, the NDT data were analyzed using flexible pavement overlay design Method 2 from the 1986 AASHTO Guide (*2*).

EMPIRICAL DATA ANALYSIS

As previously noted, both pavement serviceability index (PSI) and pavement condition index (PCI) values were determined for each test section. The condition survey results for the 10 out of 30 sections that were at or near terminal serviceability ($PSI \leq 2.5$) showed very little significant alligator cracking (a prime indicator of structural failure). This finding indicated that functional failure, rather than structural failure, often dictates the addition of an overlay. Thus, a relationship was sought between overlay thickness and the functional life of overlays in Indiana in order to derive an overlay design for functional performance.

In the empirical data analysis (which produced the functional overlay design procedure), statistical analysis techniques were used to obtain regression relationships between the most recent overlay thickness (the dependent variable) and a variety of independent variables for the 30 flexible pavement test sections studied. Such regression relationships (equations) can be used to predict required thicknesses for

future overlays for pavements within the factors and their levels represented by the 30 test sections. After a large number of regression analyses were performed, the most appropriate equation was selected for use in the functional overlay design procedure.

A list of the independent variables considered in the regression analyses follows:

- Climate zone of the pavement section (Indiana was divided into north and south climate zones based upon the work of Yoder and Colucci-Rios [6]);
- "Base asphalt" thickness, the asphalt thickness beneath the most recent overlay (in.);
- Truck traffic applied to the most recent overlay (trucks/day);
- Most recent overlay age (years);
- Subbase thickness (in.) (In this research, "subbase" describes all aggregate between the bituminous layer and the subgrade);
- Equivalent asphalt thickness of base asphalt plus subbase (in.) (For this research, 3 in. of subbase was selected as the "equivalent" of 1 in. of base asphalt);
- Total pavement thickness (from top of pavement to the subgrade) (in.);
- Estimated CBR (percent);
- Maximum NDT deflection reading (from "sensor 0" directly under the load) for both spring and summer (mils);
- Pavement serviceability index (PSI); and
- Pavement condition index (PCI).

The following regression equation was selected for empirical design:

$$\text{olay} = 0.7592 + 0.00145(\text{tottrk})^2 + 0.00379(\text{age})^2 + 0.000162(\text{pci})^2 - 0.000429(\text{cbr})^2 \quad (1)$$

where

olay = calculated thickness of required, new overlay (in.);
tottrk = anticipated future traffic: (trucks/day) (365) (age)/365,000;
age = design life of new overlay (years);
pci = desired PCI value at the end of the design life of the new overlay; and
cbr = estimated subgrade CBR (percent).

The equation has been verified for the following range of design values:

- Design life of new overlay: 5–20 years;
- Anticipated future daily trucks: 50–3,000;
- Tottrk: less than 32.2 (Note: tottrk is future traffic defined as (trucks/day) (365) (overlay age) /365,000. The value 32.2 is the highest value for tottrk observed in the thirty test sections. Thus, if tottrk exceeds 32.2, the calculated overlay value may exceed the thickest overlay typically found on Indiana pavements: 3.0 in.);
- PCI: PCI is normally specified as 35, which approximates to a PSI value of 2.5 for the test sections studied in Indiana; and
- cbr: 0–40 percent.

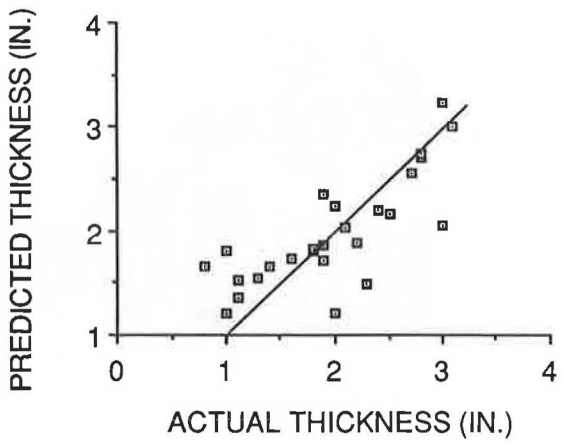

FIGURE 2 Agreement of actual with predicted values.

Figure 2 shows the degree to which Equation 1 predicts the overlay thicknesses measured from core samples taken from the 30 test sections. The coefficient of determination (r^2) is a measure of how well a regression equation fits the observed data. The possible range of values for r^2 is 0 to 1, with 1 indicating perfect fit. The r^2 value for the regression line in Figure 2 is 0.60, which is not high. However, for field experimental work (as opposed to results from highly controlled laboratory experiments), the value is acceptable.

Regression Equation 1 predicts the mean of the distribution of overlay thickness. Most individual outcomes deviate from the mean, and the "reliability" concept accounts for the deviation. "Reliability" refers to the probability that the predicted overlay will be successful in providing acceptable service through the overlay design life. A 95 percent reliability indicates that, on the average, 95 times in 100 the predicted overlay will be successful. Equation 1 provides a 50 percent reliability.

Through the determination of confidence intervals, the computer output for Equation 1 provided the 95 percent reliability overlay thickness value for each of the test sections. For a 95 percent reliability, each value is approximately 0.9 in. thicker than the mean value calculated by Equation 1, and that value must be added to any predicted thickness from Equation 1 to achieve 95 percent reliability. Similarly, other thickness increments were calculated to reach other reliability levels, and the results are presented in Table 1.

Use of the thickness increments in Table 1 would produce some overlay thicknesses that have not been verified through previous service in Indiana. For example, consider a high-traffic pavement for which Equation 1 calculates an overlay thickness of 2.9 in. To reach 95 percent reliability, 0.9 in. of overlay must be added to the 2.9 in. The 3.8-in. total exceeds the typical maximum overlay thickness in Indiana of 3.0 in. Because the reliability-based design concept, as represented by the values in Table 1, is untested in Indiana, its adoption was not recommended at this time. However, the concept is one that deserves further attention.

Equation 1 was used to calculate overlay thicknesses for the 10 out of 30 pavement test sections with a PSI less than 2.7 (sections at or near minimum acceptable serviceability). The calculations were based on a 10-year design life, a terminal PCI of 35 (the equivalent of a PSI of 2.5), estimated CBR values from soil-boring evaluations, and initial truck traffic data from 1986 with a yearly 2 percent traffic growth

TABLE 1 THICKNESS INCREMENTS TO REACH RELIABILITY

Reliability (%)	Thickness (in.)
95	0.9
90	0.7
85	0.6
75	0.4

factor. The results presented in Table 2 reflect expected overlay thicknesses for the input conditions. Sections F13 and V7 represent the extremes of the thickness calculations. The F13 value is less than 1 in., largely owing to the effect of a high CBR subgrade. The 2.2-in. overlay thickness value of V7 reflects the effect that higher traffic has on Equation 1.

1986 AASHTO GUIDE METHOD 2

Two NDT-based methods for designing structural overlay requirements for flexible pavements are provided in the 1986 AASHTO Guide. Method 1 relies on pavement layer modulus values backcalculated from NDT tests. However, the 1986 AASHTO Guide does not specify a method for determining backcalculated layer moduli.

Much controversy surrounds the selection and use of backcalculation routines. The researchers applied two backcalculation computer programs to the collected NDT data. Results were not encouraging. Consequently, use of Method 1 was discontinued. A reliable backcalculation procedure is needed, however, and this area was marked for continued research.

Subsequently, structural overlay design Method 2 was evaluated. Method 2 requires the use of two NDT deflections: temperature-adjusted deflection directly under load and unadjusted deflection from "an outer geophone." An outer geophone is one located far enough from the load that it detects deflection only in the subgrade, not from the other pavement layers. For this research, data from the sensor 7 ft from the load were used.

The 1986 AASHTO Guide presents detailed instructions for the use of Method 2. Following these instructions, the researchers calculated overlay thickness values within the typical range. Moreover, the calculated overlay values made sense when evaluated with engineering judgment. Thus, Method 2 was selected for calculating structural overlay thicknesses for the research.

Method 2 was used to calculate the required structural overlays for the same 10 pavements whose functional overlay requirements were determined in the previous section. Structural calculations were made on the same basis as the functional calculations so that a comparison of the results could be made: 10-year design life, terminal PSI of 2.5, and initial truck traffic from 1986 with an annual 2 percent traffic growth factor. Other inputs specific to AASHTO Guide Method 2 follow:

- Reliability that design life will be met or exceeded: 0.85 (per range provided by 1986 AASHTO Guide);
- Standard deviation: 0.35 (per AASHTO Guide sample calculations);
- Asphalt layer coefficient: 0.34 (per IDOH);
- Aggregate layer coefficient: 0.14 (per IDOH);
- NDT deflections (and temperature adjustment factors) from the previously described field investigation; and
- Initial PSI: 4.5.

Structural overlay calculation results are presented in Table 3, which shows that five out of the ten test sections (those with negative overlays) do not require additional structural overlay during the next 10 years. These results are quite reasonable for the traffic levels and present asphalt thicknesses considered. Two sections (L13 and L14) already have quite thick asphalt layers but carry only average traffic. The other three sections (F13, F16, S16) have average existing asphalt thicknesses but carry low traffic.

Results for four of the sections (L14, F13, F16, S16) indicate that modest reductions in asphalt thickness (0 in. to 1.2 in.) would be acceptable, suggesting that the increase in pavement asphalt thickness over time has been greater than required for structural capacity. The calculation for L13 indicates that 11.5 in. of the existing 12.7 in. of asphalt could be removed. Such action should not be taken. However, the L13 pavement cross section is 12.7 in. of asphalt above 25 in. of subbase over a sandy subgrade (estimated CBR of 28). The asphalt thickness buildup over time on such a strong foundation does appear excessive for the relatively low traffic volume, but removal of 11.5 in. of the existing asphalt is not indicated.

Four of the other five results in Table 3 indicate that moderate (1.3 in. to 2.1 in.) structural overlays are required for future traffic. The value for the fifth remaining section (L11) specifies a 5.3-in. structural overlay. Indiana experience has shown that a 3-in. maximum overlay is usually appropriate,

TABLE 2 FUNCTIONAL EQUATION OVERLAY THICKNESS RESULTS

Section Number	Functional Equation Overlay (in.)	Trucks/ Day	Estimated CBR (%)
L-10	1.3	398	14
L-11	1.4	443	3
L-13	1.0	577	28
L-14	1.3	686	12
L-15	1.2	196	18
L-16	1.1	863	37
F-13	0.8	438	38
F-16	1.5	549	11
S-16	1.3	177	10
V-07	2.2	1989	16

TABLE 3 AASHTO OVERLAY THICKNESS RESULTS

Section Number	AASHTO Overlay (in.)	Trucks/ Day	Current Total Asph. Thickness (in.)	Estimated CBR (%)
L-10	1.6	398	5.9	14
L-11	5.3	443	7.9	3
L-13	-11.5	577	12.7	28
L-14	-0.2	686	11.6	12
L-15	1.3	196	8.1	18
L-16	2.1	863	7.1	37
F-13	-1.1	438	7.5	38
F-16	-0.0	549	6.4	11
S-16	-0.6	177	8.0	10
V-07	1.4	1989	11.2	16

so 5.3 in. is probably excessive. However, the AASHTO calculation for L11 was greatly affected by an unusual circumstance: a peat subgrade. In this situation, if L11 has been performing satisfactorily with thinner, previous overlays and if no alligator cracking is present, the 5.3-in. value should be discounted and a thinner overlay accepted based on a functional evaluation.

The two sections of uncommon cross section (L13 and L11) that produced extreme overlay values demonstrate that engineering judgment and knowledge of local conditions must be used with the 1986 AASHTO Guide procedure when selecting overlay thicknesses for unusual situations.

CONTRASTING FUNCTIONAL AND STRUCTURAL OVERLAYS

Table 4 contrasts the overlay thickness determined using the functional method and the structural method. The functional calculation always adds overlay thickness. In Table 4, the functional thickness values range between 0.8 and 2.2 in., which are typical values for Indiana. The buildup of pavement thickness appears to have produced excess structural capacity in a significant proportion of flexible, primary highway system pavements in Indiana. In many cases, the overlays appear to have been applied as a consequence of functional requirements. Three findings support this statement:

- Very little significant alligator cracking (indicating structural failure) was observed in the test sections;
- Pavement cores from many of the test sections showed thick pavements associated with relatively low traffic (Table 4); and
- AASHTO overlay calculations in Table 4 indicate that five of the ten test sections have excess structural capacity.

Use of the functional and structural design methods together will produce a more effective and economical overlay design procedure than that currently used. The functional method calculates the thickness of newly laid overlay required for rider satisfaction. The AASHTO overlay method calculates required additional structural capacity. If both values are positive, the larger value can be used for the overlay. If the structural value is negative, a thickness equal to the functional overlay may be milled and then an equal thickness of new or recycled material returned to the pavement (satisfying functional performance requirements).

Milling and recycling may also be performed if the required structural overlay is positive but smaller than the functional overlay. In this case, the milled thickness is limited to the functional thickness minus the structural thickness, and an overlay of new and/or recycled material equal to the functional thickness must be added.

It may also be acceptable to mill a thickness greater than the functional overlay before recycling if significant excess structural capacity exists. In this case, the recycle thickness need be only the functional thickness. Engineering judgment should be used when setting the depth of the milling operation.

A pavement requiring rehabilitation should not be milled without a subsequent overlay or seal. This action will expose a cracked surface to the elements and traffic. Such a pavement may deteriorate rapidly.

CONCLUSIONS AND RECOMMENDATIONS

The work reported is based on an example of how the design of experiment concepts can successfully be applied to engineering research. Experiment design factors were selected for their significance. Levels of those factors were adopted to

TABLE 4 AASHTO VERSUS FUNCTIONAL EQUATION OVERLAY THICKNESS RESULTS

Section Number	AASHTO Overlay (in.)	Functional Equation Overlay (in.)	Trucks/ Day	Current Total Asph. Thickness (in.)
L-10	1.6	1.3	398	5.9
L-11	5.3	1.4	443	7.9
L-13	-11.5	1.0	577	12.7
L-14	-0.2	1.3	686	11.6
L-15	1.3	1.2	196	8.1
L-16	2.1	1.1	863	7.1
F-13	-1.1	0.8	438	7.5
F-16	-0.0	1.5	549	6.4
S-16	-0.6	1.3	177	8.0
V-07	1.4	2.2	1989	11.2

ensure that observations and measurements would allow a rational analysis of influences on performance of an engineering system (i.e., overlaid pavements). Analysis of the database so constructed clearly revealed the factors influencing overlay performance. In addition, the deficiency of the 1986 AASHTO Guide in treating overlay design only as a structural problem was identified.

This research has resulted in an overlay design procedure for flexible Indiana pavements that addresses both structural performance and functional performance (ride quality). When flexible pavements are identified for overlay, two calculations should be performed:

- For functional performance, use Equation 1:

$$\text{olay} = 0.7592 + 0.00145\,(\text{tottrk})^2 + 0.00379\,(\text{age})^2 + 0.00162\,(\text{pci})^2 - 0.000429\,(\text{cbr})^2 \quad (1)$$

where:

olay = calculated thickness of required, new overlay (in.);
tottrk = anticipated future traffic: (trucks/day) (365) (age)/ 365,000;
age = design life of new overlay (years);
pci = desired PCI value at the end of the design life of the new overlay (usually 35); and
cbr = estimated subgrade CBR.

- For structural capacity, use the 1986 AASHTO Guide overlay Method 2, which calculates overlay thickness based on NDT deflection measurements.

Both calculations should be considered in overlay thickness selection.

1. If both values are positive, the larger may be specified as the design thickness.
2. If the structural value is negative, a thickness equal to the functional overlay may be milled and an overlay of new and/or recycled material equal to the functional thickness returned to the pavement.
3. Increased milling may be considered if significant excess structural capacity exists. In this case, an overlay of new and/or recycled material equal to the functional requirement thickness should be applied to the pavement.
4. Milling may also be performed if the required structural overlay is positive but smaller than the functional overlay. The milled thickness will be limited to the functional thickness minus the structural thickness, and an overlay equal to the functional thickness must then be added.

ACKNOWLEDGMENTS

Thanks go to the Indiana Department of Highways and the Federal Highway Administration for funding the research effort. Appreciation goes to the U.S. Army Engineers Waterways Experiment Station for the use of their test equipment.

REFERENCES

1. *AASHTO Interim Guide for the Design of Flexible Pavement Structures*. AASHTO Committee on Design, American Association of

State Highway and Transportation Officials, Washington, D.C., October 1961.
2. *Guide for the Design of Pavement Structures*. American Association of State Highway and Transportation Officials, Washington, D.C., 1986.
3. M. Y. Shahin and S. D. Kohn. *Pavement Maintenance Management for Roads and Parking Lots*. Technical Report M-294. U.S. Army Construction Engineering Research Laboratory, Champaign, Ill., October 1981.
4. *Thickness Design for Concrete Highway and Street Pavements*. Portland Cement Association, Skokie, Ill., 1984.
5. *Climatological Data Indiana*. National Oceanic and Atmospheric Administration, U.S. Department of Commerce, Vol. 90, No. 3, March 1985.
6. E. J. Yoder and B. Colucci-Rios. Truck Size and Weight Issues. *Proc., 66th Purdue Road School*. Purdue University, West Lafayette, Ind., March 1980.

Publication of this paper sponsored by Committee on Pavement Rehabilitation.

Evaluation of the 1986 AASHTO Overlay Design Method

HAIPING ZHOU, R. G. HICKS, AND I. J. HUDDLESTON

The 1986 AASHTO Guide for Design of Pavement Structures is currently being evaluated in Oregon for use in the design of overlays. This newly revised guide presents two nondestructive methods for determining the strength of existing pavement structures so that the remaining life of the pavement can be evaluated. In the evaluation of the AASHTO overlay design procedure, five project sites around Oregon were selected, including four flexible pavements and one rigid pavement. Deflection measurements were taken using both the Falling Weight Deflectometer and Dynaflect. Cores were also tested to aid in evaluating paving materials. Three backcalculation programs (BISDEF, ELSDEF, MODCOMP2) were used to compute the moduli of the pavements, and the results were used to perform the overlay design. These results were compared with the current ODOT procedure, which is based on tolerable maximum deflection; and considerable inconsistency was observed. Generally, the AASHTO method provided a thinner overlay than the ODOT procedure. The results of this study show that the guide has an important advantage in that pavement strength for each layer can be quantified (NDT method 1) and remaining life may be taken into account. However, further investigation is still required to verify the method of determining existing pavement strength from backcalculation programs and the remaining life of the existing pavement. Therefore, the guide should be used with caution at the present time.

Problem Statement

Currently, the Oregon Department of Transportation (ODOT) uses the California Transportation Department (Caltrans) Procedure with some modifications to design flexible overlays over distressed highway pavements (*1*). The Portland Cement Association (PCA) and American Association of State Highway and Transportation Officials (AASHTO) methods are employed for Portland cement overlays (*2, 3*). Currently, either the Dynaflect or the Falling Weight Deflectometer (FWD) are used to obtain deflections for the flexible overlay design procedure. The maximum surface deflection obtained using the FWD or Dynaflect (converted to an equivalent Benkelman beam deflection) is used in the modified Caltrans method (*4*). For Portland cement concrete overlays, the overlay thickness is determined by subtracting the new design from the effective thickness of the existing pavement (PCA and AASHTO methods).

In both instances, the data generated are insufficient to define accurately the structural adequacy of the existing pavement. In addition, the current procedures do not take into account the remaining life of the existing pavement. To enable designers to make better evaluations on the remaining life of the pavement and provide for more efficient utilization of paving materials, a new overlay design method is needed. The development and use of this new procedure should assist in determining the structural capacity and remaining life.

H. Zhou and R. G. Hicks, Department of Civil Engineering, Oregon State University, Corvallis 97331. I. J. Huddleston, Oregon Department of Transportation, Salem, 97310.

Purpose

The purpose of this paper is to present an evaluation of the use of the 1986 AASHTO Guidelines (*5*) on selected projects in Oregon. This has included the following steps:

1. Selecting typical project sites for deflection measurements and materials sampling;
2. Laboratory testing materials sampled from each project;
3. Analyzing deflection basin data and developing overlay design recommendations;
4. Discussing results; and
5. Developing appropriate conclusions and recommendations.

1986 AASHTO OVERLAY DESIGN METHOD

Concept

This overlay design procedure is based on the serviceability—traffic and structural capacity—traffic relationships developed at the AASHTO Road Test. Determination of an overlay is accomplished by using a deficiency approach; Figure 1 illustrates seven steps that are generally involved. Of these steps, materials characterization and effective structural capacity analysis require the most effort. Two nondestructive test (NDT) methods are presented in the guide and can be used to analyze the existing pavement structure. They are (1) determination of pavement layer moduli (NDT method 1) and (2) determination of the total structural capacity (NDT method 2). Both methods rely on the use of deflection data generated from a nondestructive testing device.

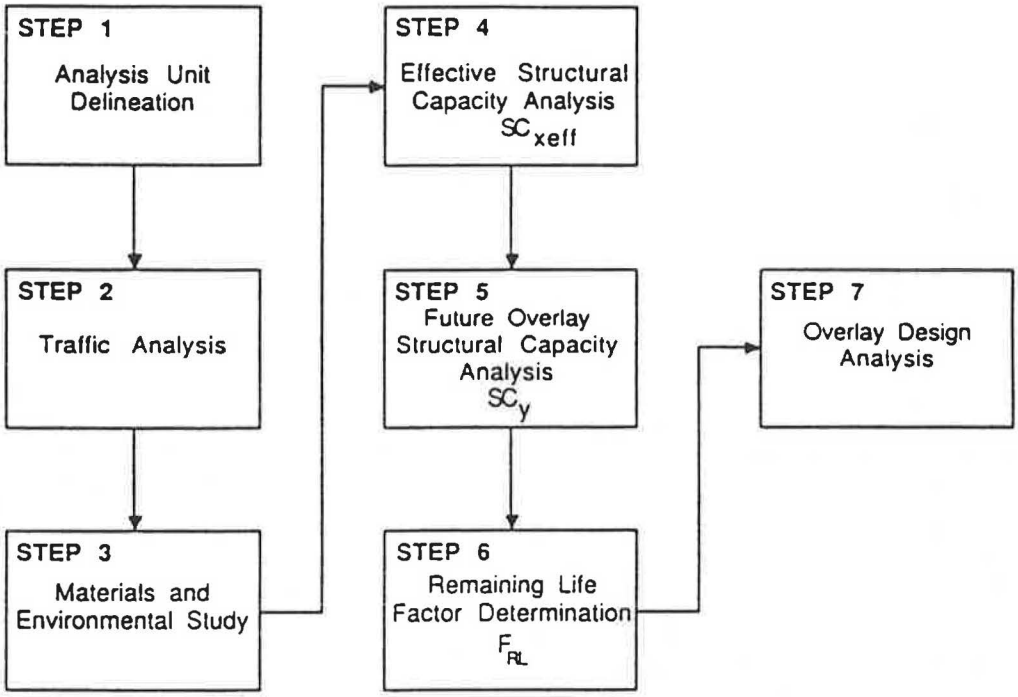

FIGURE 1 Required overlay design steps.

NDT Method 1

NDT method 1 is a technique used to determine the structural capacity of an existing pavement. This technique uses measured deflection basin data from an NDT device to backcalculate the in situ layer elastic moduli, and it is applicable to both flexible and rigid pavements. The fundamental premise of this solution is that a unique set of layer moduli exist such that the theoretically predicted deflection basin is equivalent to the measured deflection basin. To implement this technique, a computer program that backcalculates the elastic modulus for each pavement layer is necessary. The obtained moduli are related to layer coefficients using various charts given in the guide. The structural number is then determined using the equation

$$SN = \Sigma a_i h_i$$

where a_i equals the layer coefficient for each layer and h_i equals the thickness of each layer above subgrade.

NDT Method 2

NDT method 2 is based upon the maximum measured deflection from the dynamic NDT equipment and, as such, does not require a computerized model to backcalculate layer moduli (E_i). With NDT method 2, the maximum measured deflection is used to determine effective pavement structural number (SN_{xeff}) from Burmister's two-layer deflection theory. For a particular pavement structure, the SN_{xeff} value can be determined by a trial-and-error process. This is done by assuming an SN_{xeff} and computing the deflection d_o. If the calculated d_o does not agree with the maximum measured deflection (temperature adjusted), a new SN_{xeff} is assigned. The process is repeated until the calculated deflection matches the maximum measured deflection. A computer program has been developed to solve these equations (*6*).

PROJECTS EVALUATED

Project Descriptions

Field data were collected in the spring of 1987 at five project sites on existing highways in the state of Oregon. Four of the project sites were flexible pavements, and one was a rigid pavement. The age of the projects ranged from 10 to 25 years. Figure 2 shows the location of the project sites, and Figure 3 shows the typical cross sections.

For each of the project sites, data were collected on past and current traffic volumes. The new AASHTO overlay design traffic analysis suggests that two types of data be collected: the cumulative 18k ESAL repetitions until an overlay is placed and the cumulative 18k ESAL expected in the future for the overlay. However, the historic traffic is required only if the traffic method of determining remaining life is used. Table 1 includes a summary of traffic information obtained for each project.

The existing pavement conditions for the five sites varied considerably from one to the other. Two of the test sites (King's Valley Highway and Salem Parkway) did not show any signs of pavement surface distress. The Lancaster Drive site had been overlaid the previous year and, at the time its surface was tested, was in an excellent condition. The Willamina-Salem Highway site showed a considerable amount of cracking, both alligator and longitudinal. The PCC site (Wilsonville-Hubbard Highway) showed a fair amount of cracking in most slabs.

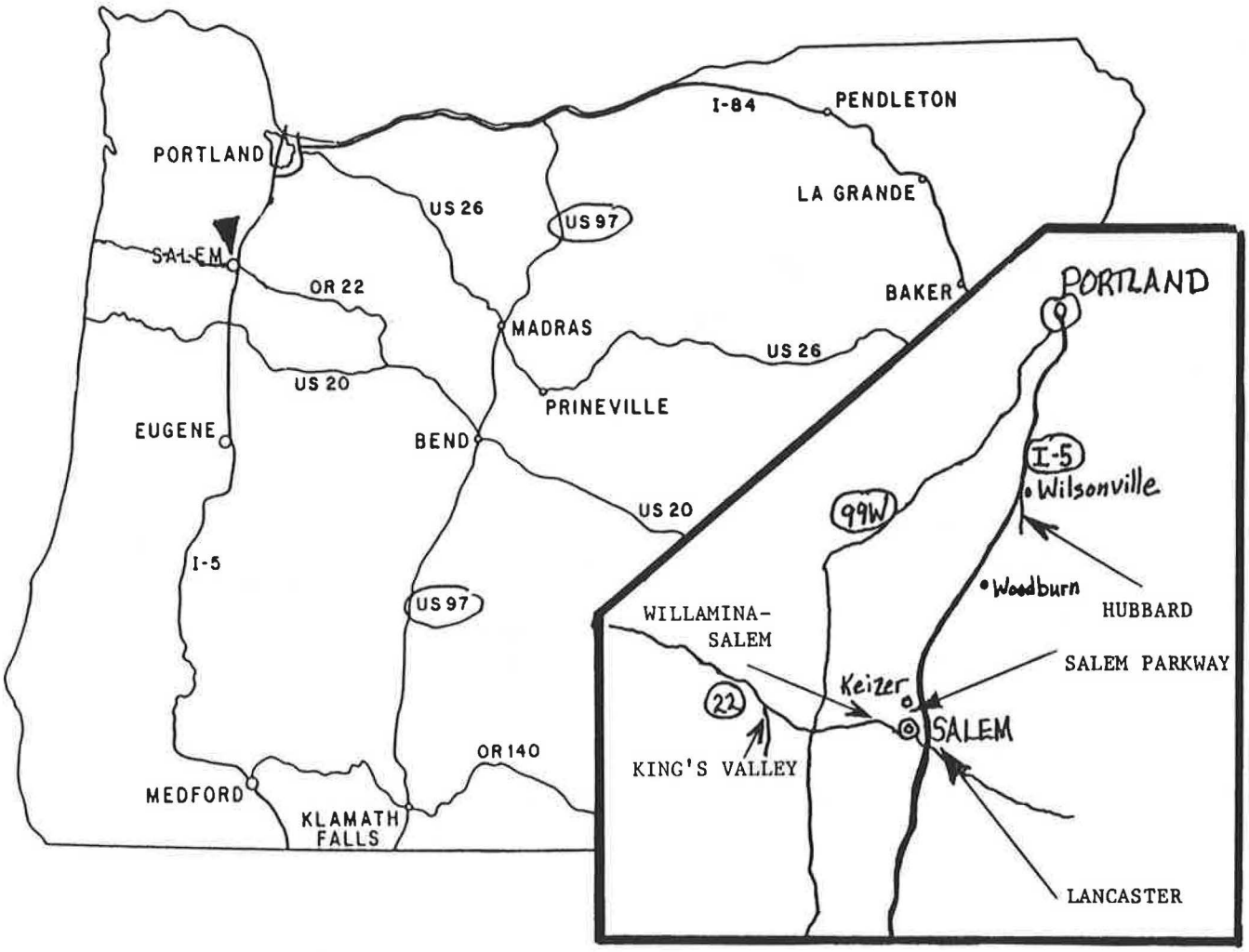

FIGURE 2 Location map of the project sites.

Pavement Deflection Measurements

Pavement surface deflections were measured at 50-ft intervals for 1,000-ft sections for each project. The measurements were taken with the KUAB Falling Weight Deflectometer (FWD) and the Dynaflect, both owned and operated by ODOT. For each site, deflection basin measurements were taken in the outer wheelpath. The FWD data were taken at three load levels and converted to a 9,000-lb load level by simple linear interpolation. The Dynaflect data were measured at a 1,000-lb cyclic load and at a frequency of 8 Hz. The Dynaflect and FWD tests were conducted at the same locations so direct comparisons could be made.

The Dynaflect employs two counter-rotating masses to apply a peak-to-peak dynamic force of 1,000 lb (4.4 kN) at a fixed frequency of 8 Hz. The force is applied to the pavement through the use of two steel wheels 20 in. (50.8 cm) apart, and the deflection basin is measured using five sensors. The spacing of the sensors on this equipment is 1 ft. The ODOT-owned KUAB Falling Weight Deflectometer is trailer-mounted and towed by a ¾-ton van. The impulse force is created by dropping a set of two weights from different heights. By varying the drop height, the load at the pavement surface was varied from 4,900 to 11,300 lb. The two-mass system is used to create a smooth load pulse similar to that created by a moving wheel load (*7, 8*). Surface deflections were measured with four seismic transducers (seismometers) that are lowered automatically with the loading plate and spaced 12 in. apart. Since the FWD can apply a load pulse similar to that produced by a loaded truck, there is no need to correct the determined in situ moduli for stress sensitivity. The load configurations for both the FWD and Dynaflect are shown in Figure 4.

Deflection Results

For each analysis section, the mean and standard deviations of the maximum measured deflection were calculated. Those basins with a maximum deflection that varied by less than the mean or more than 1.5 standard deviations from the mean were discarded. Of the remaining basins, five were randomly selected for further analysis.

In Table 2, the 9,000-lb load level is for the FWD and the 1,000-lb load level, for the Dynaflect. The deflection basins for the FWD were obtained at the 9,000-lb load level by linearly interpolating between the two adjacent load levels.

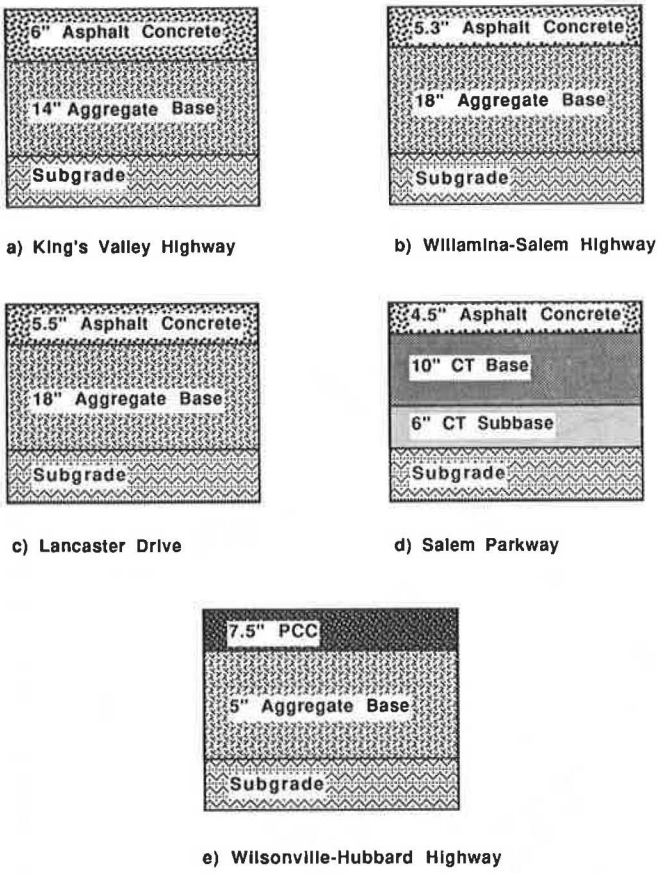

FIGURE 3 Cross sections of pavements analyzed.

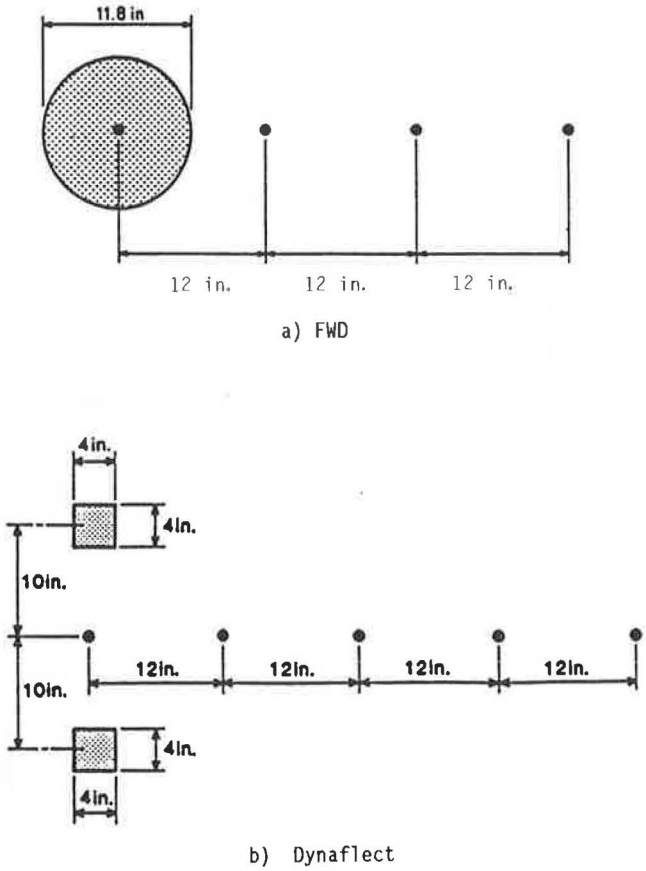

FIGURE 4 Load configuration for both NDT test units.

TABLE 1 SUMMARY OF PROJECT DATA

Project	Cross-Section	Traffic	Pavement Condition
King's Valley Highway	6.0" AC 14.0" Agg. Base Subgrade	4500 ESAL/yr 10 yr TC = 6.0 Cumulative ESAL = $5x10^4$ Future traffic = 33,200	Good surface condition Drainage adequate
Willamina-Salem Highway	5.3" AC 18.0" Agg. Base Subgrade	Current = 173,200 ESAL/yr 10 yr TC = 9.7 Cumulative ESAL = $2x10^6$ Future traffic = 1,876,600	Fair to Poor Longitudinal and alligator cracking in all lanes Evidence of rutting on outside lanes
Lancaster Drive	5.5" AC 18.0" Agg. Base Subgrade	Total Accum. 15 years ~40,000 ESAL/yr 20 yr Future traffic = 1,000,000	Surface condition very good Drainage good
Salem Parkway	4.5" AC 10.0" CTB 6.0" CTS Subgrade	Current = 135,000 ESAL/yr Accumulative = 420,000 ESAL 20 yr Future traffic = 3,200,000	Surface condition and drainage very good
Wilsonville-Hubbard Highway	7.5" PCC 5.0" Agg. Base Subgrade	Current = 115,000 ESAL/yr 10 yr TC = 9.1 Future traffic = 1,097,300	Good to Poor Cracking of slab Erosion of shoulders

Note: TC = Traffic Coefficient = $9.0 \left[\frac{18 \text{ kip EAL's}}{10^6}\right]^{0.119}$

TABLE 2 DEFLECTION VALUES FOR THE PROJECTS EVALUATED

Reading Number	Equipment	Load (lbs)	Sensors ($\times 10^{-3}$) in.				
			1	2	3	4	5
King's Valley Highway							
1	FWD	9000	20.9	16.1	10.6	6.31	
	Dynaflect	1000	1.02	0.76	0.47	0.27	0.16
2	FWD	9000	20.76	16.14	10.67	6.25	
	Dynaflect	1000	1.12	0.81	0.49	0.28	0.16
3	FWD	9000	22.17	16.79	10.52	5.72	
	Dynaflect	1000	1.26	0.90	0.51	0.28	0.17
4	FWD	9000	22.19	16.97	10.47	5.77	
	Dynaflect	1000	0.95	0.74	0.47	0.29	0.17
5	FWD	9000	22.27	16.39	9.88	5.02	
	Dynaflect	1000	1.09	0.77	0.43	0.24	0.14
Willamina-Salem Highway							
1	FWD	9000	36.57	22.65	10.39	4.47	
	Dynaflect	1000	1.76	0.98	0.42	0.20	0.12
2	FWD	9000	42.35	25.12	10.62	3.98	
	Dynaflect	1000	2.27	1.17	0.45	0.20	0.10
3	FWD	9000	43.82	27.36	11.18	3.69	
	Dynaflect	1000	2.39	1.09	0.37	0.16	0.10
4	FWD	9000	36.77	22.22	9.50	3.32	
	Dynaflect	1000	1.84	1.03	0.43	0.17	0.08
5	FWD	9000	39.80	24.70	8.95	3.76	
	Dynaflect	1000	1.90	1.07	0.47	0.23	0.14
Lancaster Drive							
1	FWD	9000	26.17	19.80	11.10	7.70	
	Dynaflect	1000	1.55	1.11	0.71	0.46	0.31
2	FWD	9000	27.30	20.30	12.08	7.23	
	Dynaflect	1000	1.65	1.16	0.72	0.44	0.31
3	FWD	9000	26.39	21.13	12.62	7.94	
	Dynaflect	1000	1.65	1.22	0.78	0.47	0.33
4	FWD	9000	26.06	19.86	12.08	7.59	
	Dynaflect	1000	1.36	0.97	0.62	0.39	0.26
5	FWD	9000	27.12	20.72	13.36	8.75	
	Dynaflect	1000	1.44	1.11	0.76	0.51	0.37
Salem Parkway							
1	FWD	9000	5.22	4.47	3.26	3.11	
	Dynaflect	1000	0.41	0.31	0.26	0.21	0.17
2	FWD	9000	4.47	3.36	2.81	2.4	
	Dynaflect	1000	0.35	0.29	0.26	0.27	0.15
3	FWD	9000	5.04	4.09	3.11	2.65	
	Dynaflect	1000	0.39	0.32	0.26	0.21	0.17
4	FWD	9000	5.78	3.99	3.42	2.83	
	Dynaflect	1000	0.46	0.37	0.30	0.23	0.19
5	FWD	9000	4.90	3.77	2.90	2.27	
	Dynaflect	1000	0.47	0.39	0.32	0.27	0.23
Wilsonville-Hubbard Highway							
1	FWD	9000	16.6	13.81	10.96	9.20	
	Dynaflect	1000	0.98	0.91	0.79	0.66	0.54
2	FWD	9000	16.76	13.48	10.47	8.58	
	Dynaflect	1000	1.21	1.14	1.03	0.89	0.76
3	FWD	9000	15.69	13.74	11.25	10.19	
	Dynaflect	1000	1.09	1.06	0.97	0.85	0.72
4	FWD	9000	15.43	12.62	9.64	8.00	
	Dynaflect	1000	1.15	1.12	1.02	0.89	0.75
5	FWD	9000	17.49	15.46	12.43	10.50	
	Dynaflect	1000	1.29	1.20	1.05	0.90	0.74

TABLE 3 RESILIENT MODULUS OF ASPHALT AND PORTLAND CEMENT CONCRETE CORES

Project	M_R @ 74°F (psi)		M_R @ 50°F (psi)	
King's Valley Highway	608,000	T*	1,758,000	
	451,000			
AC	375,000	M* Av = 568,000	1,409,000	Av = 1,652,000
	732,000			
	673,000	B*	1,791,000	
Willamina–Salem Highway	320,000	**	1,162,000	
	307,000			
	396,000	** Av = 346,000	1,369,000	Av = 1,272,000
AC	334,000			
	306,000	**	1,286,000	
Lancaster Drive	264,000	T*	1,045,000	
	275,000			
AC	336,000	M* Av = 403,000	801,000	Av = 1,242,000
	297,000			
	843,000	B*	1,881,000	
Salem Parkway	217,000	**	760,000	
	200,000			
AC		Av = 231,750		Av = 1,149,000
	257,000			
	253,000	**	1,538,000	
Wilsonville–Hubbard Highway	5,891,300			
	4,064,700	Av = 4,977,000		N/A
PCC				

*T = Top; B = Bottom; M = Middle.

**Samples tested at two strain levels.

The 9,000-lb load was selected to correspond to the standard axle of 18,000 lb commonly used in the United States.

LABORATORY TESTS

Test Procedures

Resilient modulus laboratory tests (ASTM D4123) were performed on representative asphalt concrete core samples (4-in. diameter). Sample preparation consisted of trimming the cores to a height of approximately 2.5 in. The resilient modulus was determined at test temperatures of 50°F and 74°F using a tensile strain value ranging from 75 to 125 microstrain.

The Portland cement concrete modulus tests were performed on 8-in.-high cylinders with a 4-in. diameter at 74°F. The 4-in. cylinders were tested in compression using three strain gauges attached to the side of the specimen. A strain meter was used to detect the change in strain from changes in electrical resistance in the wire gauges. Strain values were recorded at several levels of load.

Results

The laboratory test results are presented in Table 3. The average modulus obtained was the result of testing the top (T), middle (M), and bottom (B) parts of the AC layer. Figure 5 shows the plot of modulus versus temperature for each of the flexible pavements evaluated.

DETERMINING THE EXISTING PAVEMENT STRENGTH

The structural capacity of the existing pavements was estimated using NDT methods 1 and 2 of the AASHTO Guide (*5*). Three backcalculation programs (BISDEF, ELSDEF, and MODCOMP2) were utilized for NDT method 1. For NDT method 2, calculations were performed by following the procedures described in the AASHTO Guide.

Backcalculation Methods

BISDEF

This computer program was developed by the U.S. Army Corps of Engineers, Waterways Experiment Station (*9, 10*). It uses the deflection basin from NDT results to predict the elastic moduli of up to four pavement layers. This is accomplished by matching a calculated deflection basin to the measured deflection basin.

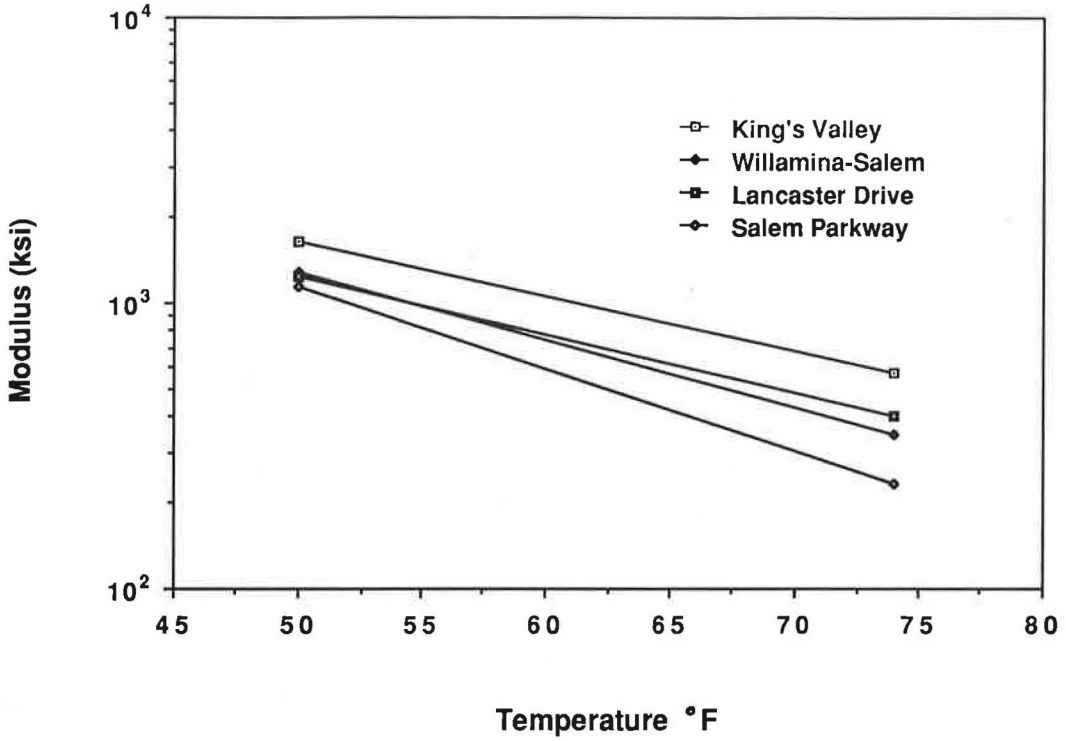

FIGURE 5 Plot of modulus vs. temperature.

To determine the layer moduli, the basic inputs include initial estimates of the elastic layer pavement characteristics as well as deflection basin values. Inputs for each layer include layer thickness, probable modulus range, initial estimate of modulus, and Poisson's ratio. For the deflection basin, the required inputs are load and load radius of an NDT device, deflections at a number of sensor locations, and a maximum acceptable error in deflection matching.

The modulus of any layer may be assigned or computed. If assigned, the value is based on the properties of the material at the time of deflection testing. The number of layers with unknown modulus values cannot exceed the number of measured deflections.

The program is solved using an iterative process that provides the best fit between measured deflection and computed deflection basins. This is done by determining the set of moduli that minimizes the error sum between the computed deflection and measured deflections. BISDEF uses the BISAR program as a subroutine for stress and deflection computations and is capable of handling multiple wheel loads and variable interface friction. BISDEF supports the 8087 or 80287 math coprocessor and runs on IBM-compatible microcomputers.

ELSDEF

This program is a modification of the program BISDEF (*11*). The modification was performed by Brent Rauhut Engineers and uses the computer program (ELSYM5) developed at the University of California at Berkeley (*12*). The input data and output results are basically the same as those of the BISDEF program.

ELSDEF has been compiled with the Microsoft FORTRAN Compiler to run on IBM-compatible microcomputers. Two versions are available: the standard version and an 8087 math coprocessor chip version.

MODCOMP2

This program was developed by Irwin (*13*) of Cornell University. The program utilizes the Chevron elastic layer computer program for determining the stresses, strains, and deflections in the pavement system. As in BISDEF and ELSDEF, there is no closed-form solution for determining layer moduli from surface deflection data. Thus, an iterative approach is used that requires an input of initial or estimated moduli for each layer. The basic iterative process is repeated for each layer (beginning at the bottom) until the agreement between the calculated and measured deflections is within the specified tolerance or until the maximum number of iterations has been reached.

Backcalculation Results

Tables 4 to 8 show the backcalculation results using both the FWD and Dynaflect data on all five project sites. The backcalculation was carried out using the preceding three programs with three different procedures in an attempt to obtain consistent results. Procedure 1 used a fixed surface layer modulus for each project site to determine moduli of the base and subgrade. The surface layer modulus was based on the laboratory test results. Procedure 2 used both a fixed surface

TABLE 4 BACKCALCULATED MODULI (psi) FOR KING'S VALLEY HIGHWAY

a) Procedure 1 - Fixed Surface Modulus

Location Identification	Layer*	FWD			Dynaflect		
		BISDEF	ELSDEF	MODCOMP2	BISDEF	ELSDEF	MODCOMP2
3	Base	1,000	1,100	N/S**	10,200	9,400	20,700
	Subgrade	60,000	60,000		36,600	32,900	27,600
4	Base	1,000	1,000	3,000	7,400	5,700	10,100
	Subgrade	60,000	60,000	12,000	39,400	40,800	33,100
5	Base	1,000	1,000	N/S	5,300	3,800	6,300
	Subgrade	60,000	60,000		39,500	53,200	41,500
8	Base	1,000	1,000	N/S	14,200	13,600	28,500
	Subgrade	60,000	60,000		32,300	27,500	25,500
18	Base	1,000	1,000	N/S	7,300	5,500	9,500
	Subgrade	60,000	60,000		46,700	51,200	41,500

*Surfacing layer modulus = 1,200,000 psi, determined at 60°F from laboratory tests (Fig. 5).
**N/S = no solution
Value 1,000 is low limit of modulus range for base while 60,000 is high limit for subgrade.

b) Procedure 2 - Fixed Surface and Subgrade Modulus

Location Identification	Layer*	FWD			Dynaflect		
		BISDEF	ELSDEF	MODCOMP2	BISDEF	ELSDEF	MODCOMP2
3	Base	9,600	2,700	N/S***	12,300	8,500	N/S
	Subgrade**	10,600	10,600		35,000	35,000	
4	Base	9,300	2,700	N/S	9,800	7,200	N/S
	Subgrade	10,700	10,700		35,000	35,000	
5	Base	6,100	2,300	N/S	8,500	6,100	N/S
	Subgrade	11,700	11,700		32,900	32,900	
8	Base	6,100	2,300	N/S	15,600	9,900	N/S
	Subgrade	11,600	11,600		32,900	32,900	
18	Base	5,000	2,300	N/S	10,000	7,700	N/S
	Subgrade	13,400	13,400		39,900	39,900	

*Surfacing layer modulus = 1,200,000 psi, determined at 60°F from laboratory tests (Fig. 5).
**Subgrade modulus was determined using the equation: $E_{sg} = PS_f)/(rd_r)$.
***N/S = no solution.

c) Procedure 3 - Fixed Subgrade Modulus

Location Identification	Layer*	FWD			Dynaflect		
		BISDEF	ELSDEF	MODCOMP2	BISDEF	ELSDEF	MODCOMP2
3	Surface	472,000	842,300	668,800	1,032,500	1,125,300	3,500,500
	Base	24,700	3,900	8,600	12,200	9,000	4,200
	Subgrade	10,600	10,600	10,600	35,000	35,000	35,000
4	Surface	489,700	853,700	719,400	913,800	973,500	3,228,500
	Base	23,100	3,800	7,600	10,300	8,100	3,400
	Subgrade	10,700	10,700	10,700	35,000	35,000	35,000
5	Surface	427,800	677,400	619,400	687,800	948,100	2,829,900
	Base	16,500	3,800	6,000	9,800	6,800	3,400
	Subgrade	11,700	11,700	11,700	32,900	32,900	32,900
8	Surface	426,100	673,900	655,400	1,225,500	1,465,000	3,717,300
	Base	16,600	3,900	5,500	13,800	8,500	4,600
	Subgrade	11,600	11,600	11,600	32,900	32,900	32,900
18	Surface	379,600	597,100	554,800	756,500	1,062,300	3,250,300
	Base	14,200	3,900	5,600	13,400	8,000	3,700
	Subgrade	13,400	13,400	13,400	39,900	39,900	39,900

*Subgrade modulus was determined using the equation: $E_{sg} = (PS_f)/(rd_r)$.

TABLE 5 BACKCALCULATED MODULI (psi) FOR WILLAMINA-SALEM HIGHWAY

a) Procedure 1 - Fixed Surface Modulus

Location Identification	Layer*	FWD			Dynaflect		
		BISDEF	ELSDEF	MODCOMP2	BISDEF	ELSDEF	MODCOMP2
4	Base	1,000	1,100	N/S**	8,600	5,200	N/S
	Subgrade*	60,000	60,000		46,100	60,000	
7	Base	1,000	1,000	N/S	5,700	3,800	N/S
	Subgrade	60,000	60,000		34,900	60,000	
8	Base	1,000	1,000	N/S	6,400	3,200	N/S
	Subgrade	60,000	60,000		60,000	60,000	
12	Base	1,000	1,000	N/S	7,100	5,600	N/S
	Subgrade	60,000	60,000		59,000	60,000	
16	Base	1,000	1,000	N/S	7,700	4,300	N/S
	Subgrade	60,000	60,000		41,300	60,000	

*Surfacing layer modulus = 600,000 psi, determined at 68°F from laboratory tests (Fig. 5).
**N/S = no solution
Value 1,000 is low limit of modulus range for base while 60,000 is high limit for subgrade.

b) Procedure 2 - Fixed Surface and Subgrade Modulus

Location Identification	Layer*	FWD			Dynaflect		
		BISDEF	ELSDEF	MODCOMP2	BISDEF	ELSDEF	MODCOMP2
4	Base	4,700	2,800	2,800	8,700	6,200	7,300
	Subgrade**	15,000	15,000	15,000	46,600	46,600	46,600
7	Base	3,600	2,300	2,000	6,500	4,400	7,200
	Subgrade	16,900	16,900	16,900	56,000	56,000	56,000
8	Base	3,200	2,100	1,600	6,500	5,300	8,200
	Subgrade	18,200	18,200	18,200	56,000	56,000	56,000
12	Base	4,200	2,700	2,400	6,800	4,900	8,300
	Subgrade	20,200	20,200	20,200	69,900	69,900	69,000
16	Base	4,100	2,600	2,100	8,100	5,700	10,200
	Subgrade	17,900	17,900	17,900	40,000	40,000	40,000

*Surfacing layer modulus = 600,000 psi, determined at 68°F from laboratory tests (Fig. 5).
**Subgrade modulus was determined using the equation: $E_{sg} = PS_f)/(rd_r)$.

c) Procedure 3 - Fixed Subgrade Modulus

Location Identification	Layer*	FWD			Dynaflect		
		BISDEF	ELSDEF	MODCOMP2	BISDEF	ELSDEF	MODCOMP2
4	Surface	199,600	284,300	241,400	203,500	392,600	2,555,600
	Base	8,000	4,000	4,800	10,300	7,300	4,300
	Subgrade	15,000	15,000	15,000	46,600	46,600	46,600
7	Surface	168,500	219,000	214,100	147,500	307,500	1,965,600
	Base	5,900	3,300	2,600	5,100	5,100	3,300
	Subgrade	16,900	16,900	16,900	56,200	56,000	56,000
8	Surface	174,900	215,300	224,200	121,000	251,200	1,706,500
	Base	4,900	2,900	3,400	6,000	7,000	4,300
	Subgrade	18,200	18,200	18,200	56,000	56,000	56,000
12	Surface	203,000	259,600	235,100	279,700	359,700	2,557,000
	Base	6,400	3,600	4,200	8,400	5,700	3,200
	Subgrade	20,200	20,200	20,200	69,900	69,900	69,900
16	Surface	165,900	211,100	236,700	194,900	381,300	2,378,000
	Base	6,500	3,700	3,600	9,900	6,700	4,000
	Subgrade	17,900	17,900	17,900	40,000	40,000	40,000

*Subgrade modulus was determined using the equation: $E_{sg} = (PS_f)/(rd_r)$.

TABLE 6 BACKCALCULATED MODULI (psi) FOR LANCASTER DRIVE

a) Procedure 1 – Fixed Surface Modulus

Location Identification	Layer*	FWD			Dynaflect		
		BISDEF	ELSDEF	MODCOMP2	BISDEF	ELSDEF	MODCOMP2
2	Base	2,100	1,900	2,000	11,700	17,900	17,800
	Subgrade*	20,800	20,600	19,800	20,400	4,000	17,500
3	Base	1,700	1,400	1,300	9,300	11,700	13,400
	Subgrade	60,000	51,200	86,400	21,800	4,000	19,100
14	Base	1,800	1,500	N/S**	9,300	11,700	13,300
	Subgrade	33,700	30,100		20,100	4,400	17,500
17	Base	2,100	1,800	1,800	14,400	25,600	22,600
	Subgrade	31,600	21,700	22,900	23,300	4,100	19,700
19	Base	2,500	2,300	2,300	18,800	21,400	25,100
	Subgrade	17,400	10,800	13,300	16,500	12,800	14,700

*Surfacing layer modulus = 1,000,000 psi, determined at 57°F from laboratory tests (Fig. 5).
**N/S = no solution; Value 60,000 is high limit of modulus range for subgrade.

b) Procedure 2 – Fixed Surface and Subgrade Modulus

Location Identification	Layer*	FWD			Dynaflect		
		BISDEF	ELSDEF	MODCOMP2	BISDEF	ELSDEF	MODCOMP2
2	Base	10,600	4,200	5,100	14,500	10,400	N/S***
	Subgrade**	8,700	8,700	8,700	18,100	18,100	
3	Base	7,400	3,400	4,100	12,700	9,400	N/S
	Subgrade	9,300	9,300	9,300	18,100	18,100	
14	Base	8,600	3,400	4,100	12,500	9,000	N/S
	Subgrade	8,500	8,500	8,500	17,000	17,000	
17	Base	9,400	3,900	5,000	16,400	12,300	N/S
	Subgrade	8,800	8,800	8,800	21,500	21,500	
19	Base	10,000	3,800	5,600	23,100	14,500	N/S
	Subgrade	7,700	7,700	7,700	15,100	15,100	

*Surfacing layer modulus = 1,000,000 psi, determined at 57°F from laboratory tests (Fig. 5).
**Subgrade modulus was determined using the equation: $E_{sg} = PS_f)/(rd_r)$.
***N/S = no solution

c) Procedure 3 – Fixed Subgrade Modulus

Location Identification	Layer*	FWD			Dynaflect		
		BISDEF	ELSDEF	MODCOMP2	BISDEF	ELSDEF	MODCOMP2
2	Surface	287,000	647,100	585,300	383,400	987,300	N/S**
	Base	26,500	6,200	8,300	22,000	10,400	
	Subgrade*	8,700	8,700	8,700	18,100	18,100	
3	Surface	312,000	635,900	537,200	249,300	1,139,600	N/S
	Base	19,300	4,900	7,100	21,700	8,700	
	Subgrade	9,300	9,300	9,300	18,100	18,100	
14	Surface	405,300	765,100	865,000	477,200	882,500	N/S
	Base	18,700	4,600	4,800	17,500	9,600	
	Subgrade	8,500	8,500	8,500	17,000	17,000	
17	Surface	335,800	734,200	621,900	490,200	1,077,000	N/S
	Base	23,200	5,100	7,700	22,200	11,600	
	Subgrade	8,800	8,800	8,800	21,500	21,500	
19	Surface	390,800	834,800	567,500	692,600	1,398,500	N/S
	Base	21,600	4,300	9,200	33,700	11,700	
	Subgrade	7,700	7,700	7,700	15,100	15,100	

*Subgrade modulus was determined using the equation: $E_{sg} = (PS_f)/(rd_r)$.
**N/S = no solution

TABLE 7 BACKCALCULATED MODULI (psi) FOR SALEM PARKWAY

a) Procedure 1 – Fixed Surface Modulus

Location Identification	Layer*	FWD			Dynaflect		
		BISDEF	ELSDEF	MODCOMP2	BISDEF	ELSDEF	MODCOMP2
7	CT Base/Subbase	1,020,000	501,200	365,300	523,000	1,497,300	183,000
	Subgrade*	18,600	15,300	19,100	34,300	14,100	35,600
9	CT Base/Subbase	690,900	681,800	255,400	439,600	981,200	154,100
	Subgrade	23,400	16,500	31,300	35,100	14,600	36,300
12	CT Base/Subbase	805,200	508,700	299,300	543,900	1,035,500	222,700
	Subgrade	24,600	12,300	23,400	35,000	14,400	34,800
15	CT Base/Subbase	727,700	409,600	459,400	400,800	896,100	194,900
	Subgrade	19,700	14,500	20,800	31,300	14,800	29,900
17	CT Base/Subbase	697,400	491,800	250,600	564,400	1,240,600	200,300
	Subgrade	27,200	13,700	28,200	25,800	10,100	27,700

*Surfacing layer modulus = 500,000 psi, determined at 67°F from laboratory tests (Fig. 5).

b) Procedure 2 – Fixed Surface and Subgrade Modulus

Location Identification	Layer*	FWD			Dynaflect		
		BISDEF	ELSDEF	MODCOMP2	BISDEF	ELSDEF	MODCOMP2
7	CT Base/Subbase	751,300	239,000	260,800	585,600	420,100	214,600
	Subgrade*	21,600	21,600	21,600	32,900	32,900	32,900
9	CT Base/Subbase	577,000	207,100	229,800	516,000	375,900	184,400
	Subgrade	32,600	32,600	32,600	33,000	33,000	33,000
12	CT Base/Subbase	671,500	223,700	240,000	604,700	404,400	249,700
	Subgrade	25,400	25,400	25,400	33,000	33,000	33,000
15	CT Base/Subbase	581,800	189,600	314,000	463,800	299,200	200,900
	Subgrade	23,800	23,800	23,800	29,500	29,500	29,500
17	CT Base/Subbase	600,400	212,600	220,400	663,300	340,500	262,300
	Subgrade	29,600	29,600	29,600	24,400	24,400	24,400

*Surfacing layer modulus = 500,000 psi, determined at 67°F from laboratory tests (Fig. 5).
**Subgrade modulus was determined using the equation: $E_{sg} = PS_f)/(rd_r)$.

c) Procedure 3 – Fixed Subgrade Modulus

Location Identification	Layer*	FWD			Dynaflect		
		BISDEF	ELSDEF	MODCOMP2	BISDEF	ELSDEF	MODCOMP2
7	Surface	5,813,400	7,420,300	8,224,900	3,459,500	9,201,800	6,264,500
	CT Base/Subbase	273,400	100,000	130,200	405,600	100,000	125,000
	Subgrade*	21,600	21,600	21,600	32,900	32,900	32,900
9	Surface	919,500	3,387,000	1,762,400	2,549,700	8,157,200	6,360,600
	CT Base/Subbase	476,600	100,000	190,900	370,800	100,000	102,100
	Subgrade	32,600	32,600	32,600	33,000	33,000	33,000
12	Surface	5,127,600	4,224,000	4,807,000	590,117	9,467,400	6,378,500
	CT Base/Subbase	252,800	100,000	153,900	925,800	100,000	147,800
	Subgrade	25,400	25,400	25,400	33,000	33,000	33,000
15	Surface	510,400	3,111,700	526,900	1,030,600	9,246,700	6,673,100
	CT Base/Subbase	556,100	100,000	311,100	609,900	109,000	109,100
	Subgrade	23,800	23,800	23,800	29,500	29,500	29,500
17	Surface	4,408,300	3,722,200	3,234,500	1,673,100	9,186,500	4,106,600
	CT Base/Subbase	230,100	100,000	162,300	608,400	100,000	174,000
	Subgrade	29,600	29,600	29,600	24,400	24,400	24,400

*Subgrade modulus was determined using the equation: $E_{sg} = PS_f)/(rd_r)$.
Value 100,000 is the low limit of modulus range for the CT base/subbase.

TABLE 8 BACKCALCULATED MODULI (psi) FOR WILSONVILLE-HUBBARD HIGHWAY

a) Procedure 1 - Fixed Surface Modulus

Location Identification	Layer*	FWD			Dynaflect		
		BISDEF	ELSDEF	MODCOMP2	BISDEF	ELSDEF	MODCOMP2
1	Base	1,000	1,000	N/S**	1,000	106,900	N/S
	Subgrade	5,900	3,900		11,100	6,200	
2	Base	1,000	1,000	N/S	1,000	128,600	N/S
	Subgrade	6,400	3,900		7,700	4,000	
7	Base	1,000	1,000	N/S	2,600	215,000	N/S
	Subgrade	5,700	3,800		7,900	4,100	
13	Base	1,000	1,000	N/S	1,000	185,700	24,200
	Subgrade	6,900	4,500		8,100	3,900	7,100
14	Base	1,000	1,000	N/S	1,000	130,100	N/S
	Subgrade	5,000	3,200		7,600	4,800	

*Surfacing layer modulus = 4,977,000 psi, determined from laboratory test.
**N/S = no solution; Value 1,000 is low limit of modulus range for base.

b) Procedure 2 - Fixed Surface and Subgrade Modulus

Location Identification	Layer*	FWD			Dynaflect		
		BISDEF	ELSDEF	MODCOMP2	BISDEF	ELSDEF	MODCOMP2
1	Base	1,000	1,000	N/S***	2,700	1,000	1,600
	Subgrade**	7,300	7,300		10,400	10,400	10,400
2	Base	1,000	1,000	<1,000	2,100	1,000	<1,000
	Subgrade	7,800	7,800	7,800	7,400	7,400	7,400
7	Base	1,000	1,000	<1,000	1,000	1,000	4,900
	Subgrade	6,600	6,600	6,600	7,800	7,800	7,800
13	Base	1,000	1,000	<1,000	1,000	1,000	2,200
	Subgrade	8,400	8,400	8,400	7,500	7,500	7,500
14	Base	1,000	1,000	N/S	1,000	1,000	<1,000
	Subgrade	6,400	6,400		7,600	7,600	7,600

*Surfacing layer modulus = 4,977,000 psi, determined from laboratory test.
**Subgrade modulus was determined using the equation: $E_{sg} = PS_f)/(rd_r)$.
***N/S = no solution; Value of 1,000 is low limit of modulus range for base

c) Procedure 3 - Fixed Subgrade Modulus

Location Identification	Layer	FWD			Dynaflect		
		BISDEF	ELSDEF	MODCOMP2	BISDEF	ELSDEF	MODCOMP2
1	Surface	424,100	1,634,700	389,000	1,944,000	4,436,400	1,255,700
	Base	354,200	1,000	343,700	242,900	1,000	502,000
	Subgrade*	7,300	7,300	7,300	10,400	10,400	10,400
2	Surface	171,500	1,548,700	297,600	3,237,100	3,598,900	817,900
	Base	1,028,600	1,000	390,700	21,000	1,000	735,600
	Subgrade	7,800	7,800	7,800	7,400	7,400	7,400
7	Surface	595,700	1,979,200	676,300	4,982,600	4,056,400	906,500
	Base	272,600	1,000	340,900	2,200	1,000	1,124,200
	Subgrade	6,600	6,600	6,600	7,800	7,800	7,800
13	Surface	345,700	1,733,800	393,700	3,750,100	3,757,200	877,900
	Base	582,000	1,000	314,200	3,400	1,000	479,500
	Subgrade	8,400	8,400	8,400	7,500	7,500	7,500
14	Surface	810,900	1,547,700	858,200	2,631,800	3,167,700	872,900
	Base	159,000	1,000	131,600	24,100	1,000	466,000
	Subgrade	6,400	6,400	6,400	7,600	7,600	7,600

*Subgrade modulus was determined using the equation: $E_{sg} = (PS_f)/(rd_r)$.

layer modulus and a preestimated subgrade modulus to solve for the modulus of the base layer. The subgrade modulus was determined using the following AASHTO equation (5):

$$E_{sg} = (PS_f)/(d_r r)$$

where

E_{sg} = in situ subgrade modulus of elasticity (psi);
P = dynamic load of NDT device;
d_r = measured NDT deflection (mils) at a radial distance (r) from the plate load center;
r = radial distance (in.) from the plate load center; and
S_f = subgrade modulus prediction factor, which is a function of radius of NDT load plate, Poisson's ratio, and effective thickness of the pavement.

Procedure 3 used the preestimated subgrade modulus alone to solve for the surface and base layer moduli. Procedure 4 used no fixed value. With this procedure, all layers were considered as unknowns for the program to determine moduli. Since three variables were involved, the computing time was significantly increased and the calculated moduli were also subject to variation with the seed moduli. Because of inconsistent results obtained using this procedure, no further discussion is presented.

Procedure 1

Using this procedure, the surfacing modulus for each project was determined from laboratory tests and used as a fixed value in the backcalculation. For Salem Parkway, base and subbase were treated as one layer, thus eliminating one variable for determining modulus. The results from three programs using FWD data indicate that the King's Valley Highway, Willamina-Salem Highway, and Lancaster Drive sites have a weak base layer. On the other hand, using Dynaflect data, a consistently higher modulus for the base layer was found. Results from BISDEF and ELSDEF are relatively close using both FWD and Dynaflect data. MODCOMP2 provided no solution in several cases. Results from three programs using the same NDT device are generally close.

Salem Parkway has a cement-treated base/subbase. Results from three programs reflect this fact. However, the backcalculated modulus values vary for each program. With FWD data, results from BISDEF are higher than those of both ELSDEF and MODCOMP2. With Dynaflect data, ELSDEF presents the highest modulus values among three programs. In all cases, MODCOMP2 provides the lowest values. Subgrade modulus values calculated from BISDEF and MODCOMP2 are relatively close for each NDT testing device, while ELSDEF gives a consistent lower modulus value using both FWD and Dynaflect data.

Wilsonville-Hubbard Highway is a PCC pavement. Its surfacing layer modulus is about 5 million psi as tested in the laboratory. When fixing this value and backcalculating the other two layer moduli, the program BISDEF predicts a very weak base using both FWD and Dynaflect data; ELSDEF gives different solutions using different NDT device data; and MODCOMP2 fails to provide answers in most cases.

Procedure 2

This procedure used two known moduli to determine the third unknown modulus. The surfacing modulus was determined from the laboratory test, while the subgrade modulus was estimated using the AASHTO equation. Since only one variable (base) is defined, the difference, that of backcalculated moduli using different programs, can easily be seen. For all four flexible pavements, the program BISDEF presents a consistently higher modulus than ELSDEF and MODCOMP2. The results of this method show many similarities with those of procedure 1. A weak base at the King's Valley Highway, Willamina-Salem Highway, and Lancaster Drive project sites is indicated. A similar trend at Salem Parkway is also noted. For the PCC pavement at Wilsonville-Hubbard Highway, a very weak base layer is identified by all three programs using both FWD and Dynaflect data. Again, MODCOMP2 failed to give a solution in some test locations.

Procedure 3

The third procedure used an estimated subgrade modulus as a fixed input to solve for surface and base moduli. The results are presented in Tables 4c to 8c. Although the backcalculated moduli vary for each program, the results from each individual program are fairly close for the projects at King's Valley Highway, Willamina-Salem Highway, and Lancaster Drive. As would be expected, Willamina-Salem Highway would have the lowest modulus values since it had the highest measured deflection at NDT device load center, and King's Valley Highway would have high modulus because of its smaller deflection readings, while Lancaster Drive would stand in among these three project sites. The backcalculated results reflect this phenomenon very well. For Willamina-Salem Highway using BISDEF results, the average modulus for the surface is about 180 ksi. The average surface modulus for King's Valley Highway is close to 440 ksi and, for Lancaster Drive, approximately 350 ksi. The backcalculated moduli for the base layers also seem reasonable. Values are generally uniform, with BISDEF giving a little higher modulus. For the cement-treated base/subbase project at Salem Parkway, the three programs give inconsistent results, as can be seen in Table 7c. This fact is also reflected in the Wilsonville-Hubbard Highway, which is a PCC pavement. It is therefore difficult to make a general prediction of pavement strength on these two projects based on the backcalculated moduli using procedure 3.

Existing Pavement Structural Capacity

The structural capacity of the existing pavements was determined using the backcalculation results. For NDT method 1, the SN_{xeff} values for each test location were computed for both the FWD and Dynaflect using the backcalculated results from the BISDEF program. For King's Valley Highway, Willamina-Salem Highway, and Lancaster Drive, backcalculated moduli from procedure 3 were used to determine the SN_{xeff} since they seemed more reasonable compared with the other two procedures. For Salem-Parkway and Wilsonville-Hubbard Highway, procedure 1 results were used because of

TABLE 9 CALCULATED SN_{xeff} USING BISDEF RESULTS

Project Site	Layer	FWD NDT #1 M_R (ksi)*	FWD NDT #1 SC_{xeff}	FWD NDT #2 M_R	FWD NDT #2 SC_{xeff}	Dynaflect NDT #1 M_R	Dynaflect NDT #1 SC_{xeff}	Dynaflect NDT #2 M_R	Dynaflect NDT #2 SC_{xeff}
King's Valley Highway	Surface	439.0	3.84	–	3.70	923.2	3.17	–	8.15
	Base	19.0		–		11.9		–	
	Subgrade	11.6		11.6		35.1		35.1	
Willamina-Salem Highway	Surface	182.4	1.67	–	2.92	189.3	1.75	–	7.26
	Base	6.3		–		7.9		–	
	Subgrade	17.6		17.6		53.7		53.7	
Lancaster Drive	Surface	346.2	3.96	–	3.99	458.5	4.33	–	8.12
	Base	21.9		–		23.4		–	
	Subgrade	8.6		8.6		18.0		18.0	
Salem Parkway	Surface	500.0	5.34	–	6.95	500.0	3.80	–	12.46
	Base	788.2		–		494.3		–	
	Subgrade	22.7		26.3		32.3		30.2	
Wilsonville-Hubbard Highway	Surface	4977.0	6.00	–	6.00**	4977.0	6.00	–	6.00
	Base	1.0		–		1.3		–	
	Subgrade	6.0		7.3		8.5		8.1	

*Average values
**NDT method 2 is not applicable for the evaluation of rigid pavement systems. With this method, structural capacity is expressed in terms of the PCC layer and not the other layers.

inconsistent results of procedure 3 and a good agreement between procedures 1 and 2. The layer coefficients for the surface and base were determined based on the modulus values from the backcalculation.

For NDT method 2, the SN_{xeff} values were determined using the procedures described previously, while the subgrade modulus was estimated using the AASHTO equation. The results for both methods are presented in Table 9.

The results generally indicate the following:

1. A fair agreement in calculating SN_{xeff} between NDT methods 1 and 2 was found using FWD data.
2. While using Dynaflect data, the NDT method 2 results in much higher SN_{xeff} values than NDT method 1 and also higher than those obtained using FWD data.
3. A maximum surface layer coefficient of 0.44 was used for asphalt concrete pavements. This may not reflect the true structural capacity of those surface layers with high modulus.

OVERLAY DESIGN

AASHTO Method

With the AASHTO method, overlay design was performed based upon the existing pavement structural capacity (SN_{xeff}) and future traffic applications (W_{18}). For each project, SN_{xeff} values determined previously were used to estimate the remaining life of the existing pavement and, consequently, the thickness design. In determining the future overlay structural capacity (SC_y), a 90 percent reliability level (R) was chosen for the Willamina-Salem Highway and Salem Parkway projects. An 80 percent reliability was selected for King's Valley Highway, Lancaster Drive, and Wilsonville-Hubbard Highway. The overall standard deviation (S_o) was selected to be 0.35 for all five projects. The design serviceability loss (DSL) was set at 2.0 (4.2–2.2). The selection of the preceding values was primarily based on the functional class and location of the facility and the projected level of usage.

Knowing the future traffic (W_{18}), reliability level (R), overall standard deviation (S_o), design serviceability loss (DSL), and subgrade modulus (M_R), the structural number (SN_y) was determined.

The remaining life of the existing pavement (R_{LX}) was estimated using the NDT approach. The advantage of this method is that historical traffic data are not required. Using this approach, the existing pavement condition is related to its initial structural capacity by a condition factor, C_x. R_{LX} is a function of the value for C_x. The remaining life of overlaid pavements (R_{LY}) was calculated based upon the projected future traffic applications and the ultimate number of repetitions to failure. The failure serviceability level (P_f) was set at 2.0 for all five projects. After determining both R_{LX} and R_{LY}, the remaining life factor, F_{RL}, was estimated.

The required flexible overlay structural number, SN_{OL}, is a function of the structural capacity of the existing pavement (SN_{xeff}), the overlaid pavement (SN_y), and the remaining life factor (F_{RL}). If this value is less than or equal to zero, no overlay is required. The thickness of an overlay is determined by dividing the SN_{OL} by the layer coefficient of the surfacing material. For the five projects, the thickness of a flexible overlay was determined assuming a layer coefficient of 0.44 for the asphalt concrete. Summaries for both NDT method 1 and NDT method 2 are presented in Table 10.

TABLE 10 OVERLAY THICKNESS USING AASHTO PROCEDURE

Project	E^*_{sg}	SN_{xeff}	SN_y	R_{LX}	R_{LY}	F_{RL}	T_{AC}
NDT Method 1							
		a) FWD					
King's Valley Highway	11,600	3.84	1.47	1.00	0.01	1.00	0.0
Willamina–Salem Highway	17,600	1.67	2.61	0.00	0.05	0.67	3.4
Lancaster Drive	8,600	3.96	2.90	1.00	0.07	1.00	0.0
Salem Parkway	22,700	5.34	2.58	1.00	0.05	1.00	0.0
Wilsonville–Hubbard Highway	6,000	6.00	3.35	1.00	0.10	1.00	0.0
		b) Dynaflect					
King's Valley Highway	35,100	3.17	0.87	0.46	0.00	0.63	0.0
Willamina–Salem Highway	53,700	1.75	1.70	0.00	0.01	0.71	1.0
Lancaster Drive	18,000	4.33	2.21	1.00	0.03	1.00	0.0
Salem Parkway	32,300	3.80	2.26	0.29	0.03	0.53	0.0
Wilsonville–Hubbard Highway	8,500	6.00	2.96	1.00	0.07	1.00	0.0
NDT Method 2							
		a) FWD					
King's Valley Highway	11,600	3.70	1.47	1.00	0.01	1.00	0.0
Willamina–Salem Highway	17,600	2.92	2.61	0.30	0.05	0.58	2.1
Lancaster Drive	8,600	3.99	2.90	1.00	0.07	1.00	0.0
Salem Parkway	26,300	6.95	2.45	1.00	0.04	1.00	0.0
Wilsonville–Hubbard Highway	7,300	6.00	3.12	1.00	0.08	1.00	0.0
		b) Dynaflect					
King's Valley Highway	35,100	8.15	0.87	1.00	0.00	1.00	0.0
Willamina–Salem Highway	53,700	7.26	1.70	1.00	0.01	1.00	0.0
Lancaster Drive	18,000	8.12	1.43	1.00	0.01	1.00	0.0
Salem Parkway	30,200	12.46	2.32	1.00	0.04	1.00	0.0
Wilsonville–Hubbard Highway	8,100	6.00	3.01	1.00	0.08	1.00	0.0

*Average Values

ODOT Method

The Oregon Department of Transportation (ODOT) employs the Caltrans deflection method with some modifications to design flexible overlays over flexible pavements (*1*). Deflection measurements are taken with the Dynaflect or FWD equipment, and the maximum deflection values are converted to equivalent Benkelman beam deflections for the Dynaflect and 9,000-lb load for the FWD. In the ODOT method, the highest 80th percentile deflection value is used in the evaluation in the following equation:

$$D_{80} = \overline{X} + 0.84\,S$$

where

D_{80} = design deflection value (80th percentile deflection);
$\overline{X}$ = mean deflection; and
S = standard deviation.

The representative deflection for a particular project length is then compared with a tolerable deflection that is a function of equivalent axle load repetition and thickness of the in-place pavement that has remaining fatigue life. For pavements that are substantially or wholly failed in fatigue, the tolerable deflection is based on the proposed overlay thickness only. An iterative procedure is then used to find the overlay thickness. If the representative deflection is less than the tolerable deflection, then an overlay is not needed. If the representative deflection is greater than the tolerable deflection, then the percent reduction in deflection is calculated as follows:

$$\text{percent reduction} = 100 * (D_{80} - D_t)/D_{80}$$

where D_t equals tolerable deflection.

The value of percent reduction is used to determine the gravel equivalency factor, which means that 1 in. thick of asphalt concrete is equivalent to certain inches thick of gravel

(*4*). The equivalent factor ranges from 1.52 to 2.5. A factor of 2.0 is used for this study.

A summary of the results for the ODOT method for the flexible pavement sites at King's Valley Highway, Willamina-Salem Highway, Lancaster Drive, and Salem Parkway is presented in Table 11.

DISCUSSION OF FINDINGS

The following discussion covers backcalculation procedures, NDT devices, determination of existing pavement structural capacity, and overlay design methods, since they are believed to be crucial to the implementation of the AASHTO Guide on overlay design.

Backcalculation Procedures

Backcalculation plays an important role in determining the strength of a pavement nondestructively. The result would influence the determination of the existing pavement structural capacity and, consequently, the overlay design. In this study, three backcalculation programs were used. With BISDEF and ELSDEF, a maximum of three iterations with a tolerance of 10 percent were specified. The modulus range and seed modulus were selected to be the same for each test location. With MODCOMP2, a maximum of twenty iterations with a tolerance of 0.15 percent were used. This tight tolerance range could be a reason for no solutions. The seed modulus used as an initial value to start the backcalculation was the same as those used in BISDEF and ELSDEF. The modulus range is not required for this program. Experience obtained from using these backcalculation programs shows that the predicted moduli may vary for each program. It is therefore necessary to use engineering judgment to ensure the calculated moduli are reasonable.

For conventional pavement structures, procedure 3 seems to work best and is recommended for backcalculation analysis. For other types of pavement structures, such as PCC and an AC surface with cement-treated base, laboratory tests on cores may be necessary, and the test result may be used to aid in determining other layers' moduli.

For a distressed PCC pavement, the NDT testing at slab center may not pick up problems at the joint. This is because of strength discontinuity between distressed slabs. For such cases, the NDT test should be performed at both the center and joint of the slab and the results evaluated separately.

NDT Devices

The backcalculated moduli, the existing pavement structural capacity (SN_{xeff}), and, consequently, the overlay thicknesses vary with the type of NDT device used. In this study, the deflection data from the Dynaflect result in a higher subgrade modulus. This is especially true for the NDT method 2. This may be because of the smaller deflection generated by the Dynaflect load and the stress sensitivity of subgrade material property. For NDT method 1, the value of the subgrade modulus has no effect on the determination of the existing pavement structural capacity (SN_{xeff}). However, in NDT method 2, this value can influence SN_{xeff}.

It is also noted that deflection values generated from FWD and Dynaflect are not linearly correlated. For instance, a 9,000-lb FWD load results in a deflection 20.76 mils at plate center (refer to Table 2, reading number 2 of King's Valley Highway), while a 1,000-lb Dynaflect load would have a 1.12-mil deformation at the same test point. The load ratio is 9, while the deflection ratio is 18, twice as high as the load ratio. Generally, for the three conventional types of pavement structure, the deflection ratio ranges from 16 to 22. For the cement-treated base/subbase project at Salem Parkway, the deflection ratio is about the same as the load ratio. For the PCC pavement at Wilsonville-Hubbard Highway, a deflection ratio ranging from 8 to 14 is identified. Because of these differences, it is difficult to tell which NDT device would provide a better indication of the pavement response. Based on the available data only, it is found that the deflection data from different NDT devices do have considerable influence on the backcalculated moduli, which in turn affect the resulting overlay design thickness.

The sensor space setting is an important factor to consider before taking deflection measurements. It is necessary to ensure that the last sensor be far enough away to obtain the pavement response purely from the subgrade. In this study, the last sensor location was 36 in. for FWD and 48 in. for Dynaflect. These configurations may not be appropriate for a good estimate of the subgrade modulus.

TABLE 11 OVERLAY THICKNESS USING ODOT PROCEDURE

	FWD			Dynaflect		
Project	D_{80}*	D_t	T_{AC} (in.)	D_{80}**	D_t	T_{AC} (in.)
King's Valley Highway	22	23	0	18	23	0
Willamina-Salem Highway	40	14	7.8	42	14	8.1
Lancaster Drive	28	16	1.0	28	16	1.0
Salem Parkway	6	19	0	5	19	0

*Deflection in mils.
**Converted to Benkelman beam value using the equation $BB = 15D^{1.3}$

Determination of SN_{xeff}

The existing structural capacity (SN_{xeff}) of a pavement can be determined using either NDT method 1 or NDT method 2, although the background of these two methods differs. For NDT method 1, the determination of SN_{xeff} relies on deflection basin data, methods of estimating the modulus of each pavement layer, and the relationship between layer modulus and layer coefficient. For NDT method 2, SN_{xeff} is determined from the maximum deflection as well as the in situ subgrade modulus. Ideally, these two methods should provide similar solutions. The results in this study (Table 9) show that the calculated SN_{xeff} using FWD data seems to give good correlation, while the SN_{xeff} values are less related when Dynaflect data are used. It should be noted that for NDT method 1, the layer coefficient for AC is restricted to a maximum value of 0.44; any modulus higher than 500 ksi would not contribute to the SN_{xeff} value. For NDT method 2, there is no such restriction; the SN_{xeff} is determined from the matching of the maximum deflection.

Overlay Design Methods

The overlay thicknesses determined from the two design methods, AASHTO and ODOT, are summarized in Table 12. As can be seen from the table, the King's Valley Highway and Salem Parkway projects have no need of an overlay. However, both procedures indicate that the Willamina-Salem Highway requires an overlay. The thickness of the required overlay varies for each method: the AASHTO NDT methods 1 and 2 require an overlay thickness ranging from 1 to 3.4 in., while an overlay thickness of about 8 in. is required by the ODOT method. For the Lancaster Drive site, no overlay is required using both NDT methods 1 and 2, while results from the ODOT method show that an overlay of 1 in. is required. Since Lancaster Drive had been overlaid the previous year (1986), it would seem that the AASHTO procedure provided a more reasonable estimate. The Wilsonville-Hubbard Highway is a PCC pavement. The structural capacity of this pavement is good, and no overlay is needed, as calculated using the AASHTO method. The pavement condition is bad, however, and cracking of slabs was found during the condition survey. It is possible that the determination of the SN_{xeff} was not right. The existence of the slab cracking seems difficult to identify using the AASHTO method.

Preliminary analysis of these results seems to lead to either one of the following conclusions: the ODOT method provides an overdesign of the overlay thickness and the AASHTO method(s) provide a more reasonable result; or the ODOT method provides a reasonable design and the AASHTO method(s) provide an underdesign. Further large-scale investigation on typical asphalt concrete and PCC pavements is needed to verify the conclusions reached thus far.

CONCLUSIONS AND RECOMMENDATIONS

Conclusions

Preliminary conclusions made from the data analyzed include:

1. The AASHTO method is based on the concept of reliability of design as well as the remaining life of the pavement; the ODOT method is based on the highest 80th percentile deflection value while the remaining life of the pavement is ignored.
2. A reliable backcalculation program is critical to implement NDT method 1. The study in this paper shows that the three backcalculation programs seem to work relatively well for the conventional pavement sections analyzed.
3. Good correlation was found between NDT methods 1 and 2 in determining the structural capacity using the FWD data. However, significant differences were also noted while using Dynaflect data.
4. The deflection data collected using FWD or Dynaflect can result in different overlay design. This conclusion is applied to both AASHTO and ODOT methods.

TABLE 12 COMPARISON OF TWO OVERLAY DESIGN METHODS

	AASHTO					
	NDT Method 1		NDT Method 2		ODOT	
Project Site	FWD	Dynaflect	FWD	Dynaflect	FWD	Dynaflect
King's Valley Highway*	0	0	0	0	0	0
Willamina-Salem Highway	3.4	1.0	2.1	0	7.8	8.1
Lancaster Drive	0	0	0	0	1.0	1.0
Salem Parkway	0	0	0	0	0	0
Wilsonville-Hubbard Highway**	0	0	0	0	N/A	

*This pavement would probably require a chip seal to prevent water infiltration. Its structural capacity is good.
**This is a PCC pavement. The structural capacity of this pavement is good; the thickness of the overlay would be controlled by reflection cracking.
N/A = not applicable.

Recommendations for Implementation

The following recommendations are based upon the results of this study:

1. Although the backcalculation program may produce a set of moduli for a pavement structure, laboratory tests may still be necessary for providing an estimate and/or verification of the backcalculated values. In some cases, the laboratory results should be used in the program as a fixed input to determine the moduli of the other layers. For conventional pavements, subgrade modulus may be estimated using the AASHTO equation and used as a fixed input to solve for other layers' moduli.
2. Engineering judgment must be made in selecting the layer coefficients. This is particularly difficult when extremely high and low moduli are involved.
3. A comparison of the two design procedures (AASHTO and ODOT) reveals significant differences between the calculated overlay designs. The reason for these differences needs to be understood before the 1986 AASHTO procedure can be applied to routine design work.

ACKNOWLEDGMENTS

The work presented in this report was conducted as a part of a Highway Planning and Research (HP&R) project funded by the U.S. Department of Transportation, Federal Highway Administration (FHWA), and Oregon Department of Transportation (ODOT). The authors are grateful for the support of the Surfacing Design Unit (ODOT) for collecting the data contained in the report. They are also grateful to the Department of Civil Engineering, Oregon State University (OSU), for providing the laboratory and computer facilities required to complete the needed work. Laurie Dockendorf and Peggy Offutt of OSU's Engineering Experiment Station typed the paper.

REFERENCES

1. *Flexible Pavement Design Procedure.* Oregon State Highway Division, Salem, 1956.
2. *Thickness Design for Concrete Highway and Street Pavements.* Portland Cement Association, Skokie, Ill., 1984.
3. *AASHTO Interim Guide for Design of Pavement Structures.* American Association of State Highway and Transportation Officials, Washington, D.C., 1981.
4. *Asphalt Concrete Overlay Design Manual.* California Department of Transportation, Sacramento, 1979.
5. *AASHTO Guide for Design of Pavement Structures.* American Association of State Highway and Transportation Officials, Washington, D.C., 1986.
6. H. Zhou, R. G. Hicks, and R. Noble. *Development of an Improved Overlay Design Procedure for Oregon: Vol. III—Field Manual.* FHWA-OR-RD-88-03C. FHWA, U.S. Department of Transportation, November 1987.
7. O. Tholen. *Falling Weight Deflectometer, A Device for Bearing Capacity Measurements: Properties and Performance.* Department of Highway Engineering, Royal Institute of Technology, Stockholm, Sweden, 1980.
8. O. Tholen, J. Sharma, and R. Terrel. Comparison of Falling Weight Deflectometer with Other Deflection Testing Devices. In *Transportation Research Record 1007,* TRB, National Research Council, Washington, D.C., 1985, pp. 20–26.
9. A. J. Bush and D. R. Alexander. Pavement Evaluation Using Deflection Basin Measurement and Layered Theory. In *Transportation Research Record 1022,* TRB, National Research Council, Washington, D.C., 1985, pp. 16–25.
10. A. J. Bush III. *Nondestructive Testing for Light Aircraft Pavements: Phase II—Development of Nondestructive Evaluation Methodology.* Final Report FAA-RD-80-9-II. FAA, U.S. Department of Transportation, November 1980.
11. R. L. Lytton, F. L. Roberts, and S. Stoffels. *Determination of Asphaltic Concrete Pavement Structural Properties by Nondestructive Testing.* Final Report, NCHRP, Project 10-27. TRB, National Research Council, Washington, D.C., 1986.
12. R. G. Hicks and R. L. McHattie. *Use of Layered Theory in the Design and Evaluation of Pavement Systems.* Report FHWA-AK-RD-83-8. FHWA, U.S. Department of Transportation, July 1982.
13. L. H. Irwin. *User's Guide to MODCOMP2, Version 2.1.* Local Roads Program, Cornell University, Ithaca, N.Y., November 1983.

The opinions expressed in this paper are those of the authors and not necessarily those of FHWA or Oregon DOT.

Publication of this paper sponsored by Committee on Pavement Rehabilitation.